THE DEVELOPMENT, MANUFACTURE AND EVALUATION OF SUSTAINED RELEASE GASTRIC-RESISTANT ISONIAZID AND GASTRORETENTIVE MICROPOROUS RIFAMPICIN MICROSPHERES

A Thesis Submitted to Rhodes University in

Fulfilment of the Requirements for the Degree of

DOCTOR OF PHILOSOPHY
in
Pharmaceutics

By

Chiluba Mwila

January 2018

Faculty of Pharmacy

Rhodes University

Grahamstown

South Africa

ABSTRACT

According to the World Health Organization Global Tuberculosis (TB) 2017 Report, there were an estimated 10.4 million new TB cases worldwide of which, in 2016, 65 % occurred in men, 28.1 % in women and 6.9 % in children. TB is the ninth leading cause of death globally and is the leading cause due to an infectious organism surpassing HIV/AIDS. Treatment is long-term and the use of a combination of medicines is required for success. The concern related to the use of fixed dose combination products for the treatment of TB is the issue of low bioavailability of rifampicin observed from a number of fixed dose combination (FDC) formulations. The hydrolysis of rifampicin, in acidic media, to form insoluble 3-formyl rifamycin SV contributes to poor bioavailability of rifampicin. The degradation of rifampicin to form this poorly absorbed compound is accelerated in the presence of isoniazid via the reversible formation of isonicotinyl hydrazone is a further factor contributing to the poor bioavailability of rifampicin. Therefore, the development of a novel drug delivery technology that prevents interactions between rifampicin and isoniazid in an acidic medium is required.

A Box Behnken design was successfully used for the optimisation of a rapid and accurate stability-indicating gradient elution RP-HPLC method for the simultaneous analysis of isoniazid, pyrazinamide and rifampicin. The method was validated using ICH guidelines and the results indicate it can be used for the rapid analysis of commercially available TB FDC formulations containing the active pharmaceutical ingredients, API. The method is precise, sensitive and has the necessary selectivity for use during formulation development and optimisation studies for a combination of rifampicin, isoniazid and pyrazinamide.

Initially formulation activities were undertaken with rifampicin and isoniazid for the development of an approach to enhance the effective delivery of these compounds. The characterisation of rifampicin and isoniazid was undertaken using spectroscopic, thermal and microscopic analysis. The studies revealed that the compounds are crystalline and exhibit distinct characteristic sharp peaks in X-ray diffractograms and Differential Scanning Calorimetry thermograms. The thermograms, ^{13}C Nuclear Magnetic Resonance and Fourier Transform Infrared spectroscopy results identified that rifampicin occurs as the form II polymorph however, as there are no significant biopharmaceutic differences between the polymorphic forms of rifampicin this information was used for identification purposes only. The results were

used as baseline data for comparative purposes to monitor changes that may occur when rifampicin and isoniazid are used in formulation development, dosage form manufacture and characterisation activities for a FDC technology designed to deliver both compounds simultaneously.

Hydroxypropylmethylcellulose acetate succinate (HPMC-AS) and Eudragit® L100 polymers were successfully used for manufacture of isoniazid loaded gastric-resistant sustained release microspheres using an o/o solvent emulsification and evaporation approach. A Hybrid experimental design was used to investigate the influence of input variables viz., homogenisation speed and amount of HPMC-AS and Eudragit® L100 on gastric-resistance, INH release and encapsulation efficiency. The approach of using coating polymers viz., HPMC-AS and Eudragit® L100, to manufacture gastric resistant sustained release microspheres of isoniazid is unique and was efficient for preventing the release of isoniazid in an acidic environment. Only 0.523 % isoniazid was released from the optimised formulation after 2 h exposure to pH 1.2 0.1 M HCl suggesting there is also the possibility of minimising the accelerated degradation of rifampicin that occurs in the presence of isoniazid in acidic media. The microspheres also exhibited sustained release properties without burst release in pH 6.8 0.1 M phosphate buffer as < 5 % isoniazid was released at 0.5 h and only 11 % isoniazid was released at 2 h. The release of isoniazid was sustained over the entire period of dissolution testing with > 85 % isoniazid released at 24 h, implying that the majority of encapsulated isoniazid would be available for absorption. The manufacturing process resulted in the production of hard spherical particles and particle size analysis revealed that the microspheres ranged between 415.76 ± 76.93 µm and 903.35 ± 197.10 µm in diameter. The microspheres exhibited excellent flow properties attributed to the spherical nature of particles. Carr‟s index (CI) was 4.934 ± 0.775 % and the Hausner ratio (HR) was 1.148 ± 0.033 indicating good packability of the microspheres that would help in achieving weight and content uniformity of capsule dosage units. The manufacturing process however produced a low % yield suggesting that scale up difficulties may be encountered. However the high encapsulation efficiency observed may counter the challenges associated with the low yield. The DSC thermograms and FT Raman spectra of 1:1 mixtures of isoniazid, excipients and the microspheres did not reveal any potential detrimental interactions.

Microporous floating sustained release microspheres for the delivery of rifampicin in the stomach have been successfully manufactured using emulsification and a diffusion/evaporation process. A novel approach using solvent mixture of acetone and dichloromethane that has not been reported for the manufacture of rifampicin microspheres was successfully used and resulted in the formation of a stable emulsion and the manufacture of rifampicin-loaded microspheres with uniform characteristics. In addition the manufacturing process was shorter than most other reported methods. A Box-Behnken experimental design was successfully used to study the influence of ethylcellulose, Eudragit® RLPO and d-glucose content on the floating properties, encapsulation efficiency and % yield of microspheres. The optimised formulation did not yield desired floating characteristics as the % buoyancy was low and floating lag times were high. The optimised formulation was modified by addition of NaHCO3 to increase the % buoyancy and reduce the floating lag time. Rifampicin release from the microspheres of the modified batch was 87.10 % at 12 h and the microspheres exhibited a % buoyancy of 87.66 ± 1.28 % (n = 6) and floating lag time of 15 ± 3.2 (n = 6) seconds. The microspheres remained buoyant for up to 12 h and an encapsulation efficiency of 88.26 ± 1.25 % was achieved. SEM images of microspheres following exposure to dissolution fluid revealed that the microspheres had numerous pores on their surface. The mean particle size distribution ranged between 423.19 ± 121.86 µm to 620.07 ± 102.67 µm. The microspheres exhibited similar flow characteristics to isoniazid microspheres with a CI of 1.422 ± 0.074 %, and HR of 1.034 ± 0.002. The excellent flow characteristics indicate that filling of the microspheres into hard gelatin capsules was unlikely to pose a challenge in respect of producing a product with uniform content. Rifampicin-excipient compatibility studies did not reveal any potential or significant interactions suggesting that the excipients used for the manufacture of the microspheres were compatible, although long term stability studies would be required to ascertain this is, indeed the case. The microporous floating sustained release microspheres manufactured in these studies has the potential to increase the bioavailability of rifampicin as they may be retained in the stomach where the solubility of rifampicin is high and from which absorption is best achieved.

The degradation of rifampicin after 12 h dissolution testing in pH 1.2 0.1 M HCl in the presence of isoniazid gastric-resistant sustained release microspheres was only 4.44%. These results indicate that the degradation of rifampicin in the presence of isoniazid in acidic media can be overcome by encapsulation of both active pharmaceutical ingredients in a manner that ensure

release in different segments of the gastrointestinal tract. The use of sustained release microporous gastroretentive rifampicin microspheres in combination with sustained release isoniazid gastric-resistant microspheres revealed that accelerated degradation of rifampicin in the presence of isoniazid is reduced significantly when using this approach and a FDC of rifampicin and isoniazid microspheres has the potential to improve the bioavailability of rifampicin thereby enhancing therapeutic outcomes. *In vivo* studies would be required to confirm the potential benefits of using this approach to deliver rifampicin in combination with isoniazid.

ACKNOWLEDGEMENTS

I would like to express my sincere gratitude to the following people:

My supervisor Professor Roderick B. Walker, for the guidance, patience, moral and material support throughout the course of the research and thesis writing. I cannot find perfect words that that fully express how grateful I am to have been part of his research group,

The Rhodes University Postgraduate Funding Office for funding my studies through Henderson Prestigious Scholarship, without the financial assistance it would not have been possible.

Dr. S. M. M. Khamanga for the support during my studies

Mr. Christian Isalomboto Nkanga, from the Department of Chemistry Laboratory for all the help.

My lovely wife Elizabeth Mutale, for the unwavering support and patience during the entire course of my studies. Without your support and understanding, things would have been more difficult.

My daughter Bwalya Rosemary Mwila and my son Chiluba Mwila Junior, I know you have missed playing with me during my time of absence, I hope you will understand when you grow older that I did all this for you. I love you.

My dad Mr. Edward Mwila, for the support and encouragement.

My brothers and sisters: Gilgrest, Chisanga, Mulinda, Chewe, Mwelwa, Mulenga and Chinyimba for the support and understanding during the period of my studies.

My colleagues in the Biopharmaceutics Research Laboratory: Mellisa Chikukwa, Bwalya Angel Witika, Paschal Ntemi, Fadzai Naomi Mungoshi, Tanyaradzwa Musakana, Grace Govere, Tsitsi Mudyahoto, Siyabonga Malemane, Omolola Oridota, Kudzai Makoni, Amanda Mudyahoto, Arthur Manda and Hariska Naidu. Thank you very much for the great support and friendship.

Mr Khazike C. Sakala for accommodating me in his house when I was completing writing the thesis. What a friend!!!

Mr. Niall Borland, Collin Noynti and Mr. Thando Fleck for technical assistance.

Professor. Watkins for allowing me to use the DSC, and FTIR Spectrophotometer in the Chemistry Department.
Dr. Britton for helping me with FT Raman spectroscopy and XRD experiments.
The staff at the electron microscopy unit I would like to thank you all.

This thesis is dedicated to my late mother Rosemary Bwalya Tondwe who went to be with the lord on 24th October 2014. May Her Soul Rest in Eternal Peace.

I would like to give thanks to the almighty God for everything he has done in my life and making the seemingly impossible things possible.

STUDY OBJECTIVES

The WHO recommends that TB therapy include multi-drug therapy comprising of an initial intensive phase of treatment with rifampicin, isoniazid, pyrazinamide and ethambutol administered daily for two months followed by a continuation phase of therapy with rifampicin and isoniazid. Although highly effective treatment for TB is available, cure rates remain low since anti-TB medicines are inconvenient to administer and patients do not adhere to prescribed regimens for sufficient lengths of time to achieve a cure.

A major concern when using fixed dose combination when treating TB is the issue of low bioavailability of rifampicin observed from a number of products. Degradation of rifampicin in the acidic gastric compartment has been estimated to be 8.5 - 50 % over the time corresponding to gastric residence of 15 - 150 minutes for most dosage units in humans. The hydrolysis of rifampicin in acidic media contributes to the poor bioavailability of the compound. The accelerated degradation of rifampicin in the presence of isoniazid is a further compounding factor for the poor bioavailability of the molecule. Therefore there is an urgent need to develop a formulation from which rifampicin and isoniazid are not released simultaneously in the acidic environment of the stomach to maximize the bioavailability of rifampicin.

The specific objectives of this research study were:

1. To use Design of Experiments and Response Surface Methodology to develop, optimise and validate a RP-HPLC method for the simultaneous analysis of rifampicin, isoniazid and pyrazinamide,
2. To use thermo-analytical and spectroscopic techniques to characterize rifampicin and isoniazid,
3. To develop and manufacture sustained release gastric-resistant isoniazid microspheres using polymers used for coating of dosage forms,
4. To develop and manufacture microporous gastroretentive sustained release rifampicin microspheres,
5. To study the dissolution kinetics and release mechanisms of isoniazid and rifampicin from microspheres, and
6. To assess the effectiveness of sustained release gastric-resistant isoniazid microspheres in improving the stability of rifampicin when delivered from micro-porous gastroretentive sustained release F microspheres in pH 1.2 0.1 M HCl.

TABLE OF CONTENTS

LIST OF TABLES

LIST OF FIGURES

CHAPTER ONE

LITERATURE REVIEW

1.0 INTRODUCTION

Tuberculosis (TB) is an infectious disease caused by *Mycobacterium tuberculosis* [1]. According to the World Health Organization (WHO) Global Tuberculosis 2017 Report [2] there were an estimated 10.4 million new (incident) TB cases worldwide of which 65 % were in men, 28.1 % in women and 6.9 % children in 2016. People living with human immunodeficiency virus (HIV) accounted for 10 % (74 % in Africa) of all new TB cases. In the same year, there were an estimated 600 000 new cases reported of resistance to rifampicin, of which 490 000 presented with multidrug-resistant TB (MDR-TB). TB is the ninth leading cause of death worldwide and the leading cause due to a single infectious agent, ranking above HIV/AIDS. There were an estimated 1.3 million TB deaths in 2016 and an additional 374 000 deaths resulting from TB in patients living with HIV.

1.1 TREATMENT OF TUBERCULOSIS

The main goal of treatment of tuberculosis is to ensure that a cure, without relapse, is achieved so as to prevent death, transmission and the emergence of drug resistance. Treatment is long-term and the use of a combination of medicines is required for success [3]. The treatment of active TB with a single compound should not be attempted and the addition of a single compound to a failing regimen should be avoided so as to prevent the development of MDR-TB [4]. The WHO recommends that TB therapy should involve multi-drug therapy [5] comprising of an initial intensive phase of rifampicin (RIF), isoniazid (INH), pyrazinamide (PZA), and ethambutol (ETB) administered daily for 2 months followed by a continuation phase with RIF and INH administered either daily or 3 times weekly, for a further 4 months The recommended regimens are summarised in Table 1.1.

Table 1. 1 Treatment regimens for new smear positive adult patients [6].

Intensive Phase – 2 months	**< 50 kg**	**> 50 kg**
RIF/INH/PZA/ETB Combination tablet 120/60/300/200 mg daily, 5 days per week	4 tablets	5 tablets
Continuation phase – 4 months	**< 50 kg**	**> 50 kg**
RIF/INH Combination tablet 150/100 mg Combination tablet 300/150 mg	3 tablets	2 tablets

Most rapidly replicating bacilli are eradicated by INH within the first two weeks of treatment initiation in combination with streptomycin and ETB. RIF and PZA play an important role in the sterilisation of lesions by eradicating organisms and are crucial for ensuring the success of 6-month treatment regimens. RIF is responsible for killing low- or non-replicating organisms and the high sterilising effect of PZA acts on semi-dormant bacilli not affected by other anti-TB agents, in sites hostile to the penetration and action of other medicines [7, 8]. INH and RIF are two potent anti-TB compounds and are responsible for killing > 99 % of tubercular bacilli within the first two months of initiating therapy [9, 10]. The use of these medicines in combination reduces the duration of treatment from 18 to 6 months.

1.2 TREATMENT OF MULTIDRUG (MDR-TB) AND EXTENSIVELY DRUG RESISTANT TB (XDR-TB)

TB strains classified as MDR-TB are those resistant to two of the most potent first-line anti-TB compounds viz., INH and RIF [11-14]. XDR-TB strains are resistant to either INH or RIF, any fluoroquinolone analogue and at least one of three second-line anti-TB injectable compounds viz., capreomycin, kanamycin and amikacin [11-14]. The treatment of TB becomes more complicated as the antibiotic resistance profile of *Mycobacterium tuberculosis* broadens, especially in the case of MDR and XDR-TB [14]. There are several basic rules for the management of patients with MDR or XDR-TB. The recommended regimen is a combination of at least four compounds to which the *Mycobacterium tuberculosis* isolate is likely to be susceptible, although in some cases more than four agents may be required. The medicines are selected in a stepwise approach from five groups of anti-TB drugs (Table 1.2) on the basis of safety, efficacy and cost. The duration of the intensive phase of treatment when an injectable

medicine is administered should be at least 6 months, or 4 months after culture conversion. The continuation phase without injectable medicines should last until 18 months after culture conversion. Surgery may be considered under specific conditions such as when less than four second-line medicines are suitable for use, when a patient has localized lesions or when the patient has enough respiratory reserve, to tolerate surgery [11, 15, 16]. These principles are the same for the treatment of MDR-TB and XDR-TB, but the treatment of patients with XDR-TB is much more challenging since more patients require dosing with group five compounds in addition to surgery for successful outcomes [16].

Table 1. 2 Categories of anti-TB drugs and dosing [15].

	Daily Dose
Group 1 - first-line oral drugs (use all possible compounds)	
Rifampicin	5 mg/kg
Isoniazid	10 mg/kg
Ethambutol	15-25 mg/kg
Pyrazinamide	30 mg/kg
Group 2 - fluoroquinolones (use only one due to shared genetic targets)	
Ofloxacin	15 mg/kg
Levofloxacin	15 mg/kg
Moxifloxacin	7.5 – 10 mg/kg
Group 3 - injectable drugs (use only one due to shared and similar genetic targets)	
Streptomycin	15 mg/kg
Kanamycin	15 mg/kg
Amikacin	15 mg/kg
Capreomycin	15 mg/kg
Group 4 - less-effective second-line drugs (use all possible drugs if necessary)	
Ethionamide/ prothionamide	15 mg/kg
Cycloserine/terizidone	15 mg/kg
P-aminosalicylic acid	150 mg/kg
Group 5 - (use all necessary drugs if regimen has < four from other groups)	
Clofazimine	100 mg
Amoxicillin with clavulanate	875/125 mg/ 12hourly
Linezolid	600 mg
Imipenem	500 - 1000 mg/6 hourly
Clarithromycin	500mg/12 hourly
High-dose isoniazid	10 – 15 mg/kg
Thioacetazone	150 mg

1.3 CHALLENGES WITH CURRENT THERAPY

The use of a multi-drug regimen suggests that there is likely to be a high incidence of side effects and patient adherence is expected to be compromised with associated slow clinical improvement of patients [17]. Although highly effective treatments for TB are available, cure rates remain low since anti-TB medicines are inconvenient to administer and patients do not adhere to prescribed regimens for sufficient lengths of time to achieve a cure [18]. The non-adherence of patients to short course regimens results in deterioration of therapeutic potential, increased mortality in addition to an increased risk of acquiring drug resistance [18-20]. The development of MDR-TB is a global problem in immune-competent and HIV-infected populations [22, 23].

1.4 PHYSICOCHEMICAL PROPERTIES OF INH AND RIF

1.4.1 Description, Chemical Structure and Biopharmaceutics Classification System (BCS)

The physicochemical properties of INH and RIF are summarised in Table 3.

Table 1. 3 Physicochemical properties of INH and RIF.

Properties	Isoniazid	Rifampicin
Molecular weight	137.1[24]	823 [25]
Chemical formula	$C_6H_7N_3O$ [24]	$C_{43}H_{58}N_4O_{12}$ [25]
Description	A white or almost white, crystalline powder or colourless crystals [24]	Practically odourless, brick-red to reddish-brown, crystalline powder [25]
pH (in water)	The BP specifies that a 5 % solution in water has a pH of 6.0 to 8.0, the USP specifies that a 10 % solution has a pH of 6.0 to 7.5, a 1 % solution has been reported to have a pH of 5.5 to 6.5 [25]	A 1 % w/v suspension has a pH of 4.5 to 6.5 [25]
Dissociation constant, pKa	1.8 (hydrazine nitrogen), 3.5 (pyridine nitrogen), 10.8 (acidic group) [25]	1.7 (naphthalene hydroxyl groups), 7.9 (piperazine nitrogen) [25]
Partition coefficient, Log P	-1.1 [25]	1.2 [25], 1.086 [26]
Melting point	170 - 174 °C [24]	185 °C [25]
Solubility in water (m/v)	Soluble 1 in 8 parts of water [245]	Slightly soluble [25]
Solubility in organic solvents (m/v)	1 in 45 parts of ethanol, and 1 in 1000 parts of chloroform, very slightly soluble in ether and in benzene [25]	Slightly soluble in ethanol, in acetone, in carbon tetrachloride, and in ether. It is practically insoluble butanol, in cyclohexane, in glycerol, and in propylene glycol. It is soluble in ethyl acetate, in methanol, and in tetrahydrofuran. It is freely soluble in chloroform and in dimethyl sulphoxide [25] Effect of pH: Rifampicin solubility is greater at low pH values. At 37°C, it is soluble 1 in approximately 100 parts of phosphate buffer, pH 7.4, and 1 in 5 parts of 0.1 M hydrochloric acid [27]. At 25 °C, rifampicin is soluble 1 in approximately 10, 250, and 360 parts of water at pH 2.0, 5.3, and 7.5, respectively [28].
BCS classification [29]	I	II
Chemical structure [25, 30]	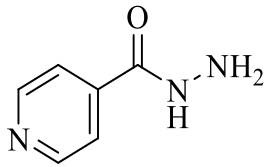	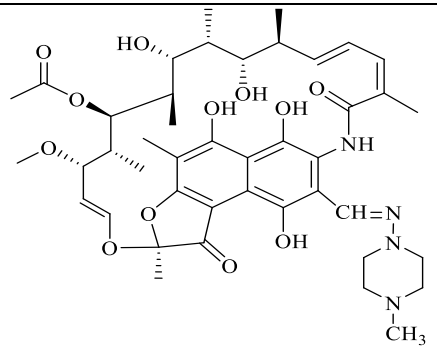

1.4.2 Polymorphism

1.4.2.1 Isoniazid (INH)

INH does not exhibit polymorphism or form defined hydrate analogues. Synthesis of INH results in orthorhombic crystals [31].

1.4.2.2 Rifampicin (RIF)

The structural complexity of RIF results in polymorphism and it exists in two polymorphic forms, viz. a stable or form I and a metastable or form II polymorph [31]. RIF also exists as different solvates that eventually convert to an amorphous form at temperatures between 22 °C – 25 °C or following desolvation [33]. However, little solubility advantage has been associated with the different polymorphic forms and is inconsequential from a clinical and regulatory point of view [34].

1.5 SYNTHETIC PATHWAYS

1.5.1 Isoniazid (INH)

The methods used to synthesise INH are either a (i) reaction of hydrazine and isonicotinic acid or a (ii) reaction of the ester of isonicotinic acid and hydrazine [35]. The synthesis of INH using the option (i) involves placing the ethyl ester of isonicotinic acid, ethanol and hydrazine hydrate into a flask and heating at 70 °C for 2 hours. The mixture is then cooled and INH precipitates, is filtered and washed with water. The product is then purified by recrystallisation from water. The synthesis using option (ii) involves directly reacting isonicotinic acid with hydrazine in a flask and heating the mixture at 70 °C for 2-3 hours. INH crystallises on cooling, is filtered under vacuum, purified by recrystallisation and dried. The two reaction schemes are summarised in Figures 1.1 and 1.2. The reaction of the ester and hydrazine is shown in Figure 1.1 and that of hydrazine and isonicotinic acid in Figure 1.2.

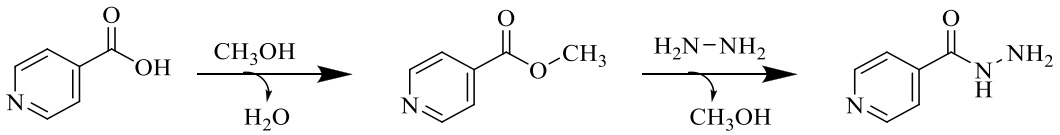

Figure 1. 1 Reaction scheme option (i) for synthesising INH from hydrazine and isonicotinic acid.

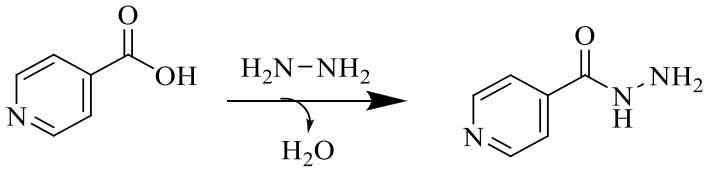

Figure 1. 2 Option (ii) for the synthesis of INH.

1.5.2 Rifampicin (RIF)

RIF is one of a group of rifamycin antibiotics that are fermentation products of *Streptomyces mediterranei* [36]. The rifamycins are ansa compounds consisting of a chromophoric naphthoquinone or naphthohydroquinone ring which is spanned by a long aliphatic bridge. One of the substances originally produced by *Streptomyces mediterranei* is rifamycin B. Rifamycin B can be oxidized and hydrolysed to form rifamycin S, a naphthoquinone derivative that following reduction, yields the naphthohydroquinone derivative rifamycin SV (Figure 1.3) [37-39]. Rifamycin SV is modified by introduction of substituents at position 3, which contains the only aromatic hydrogen to produce potent therapeutic anti-TB compounds [40, 41]. RIF is a 3-(4-methyl-piperazanyl)-iminomethyl derivative of rifamycin SV [40, 41].

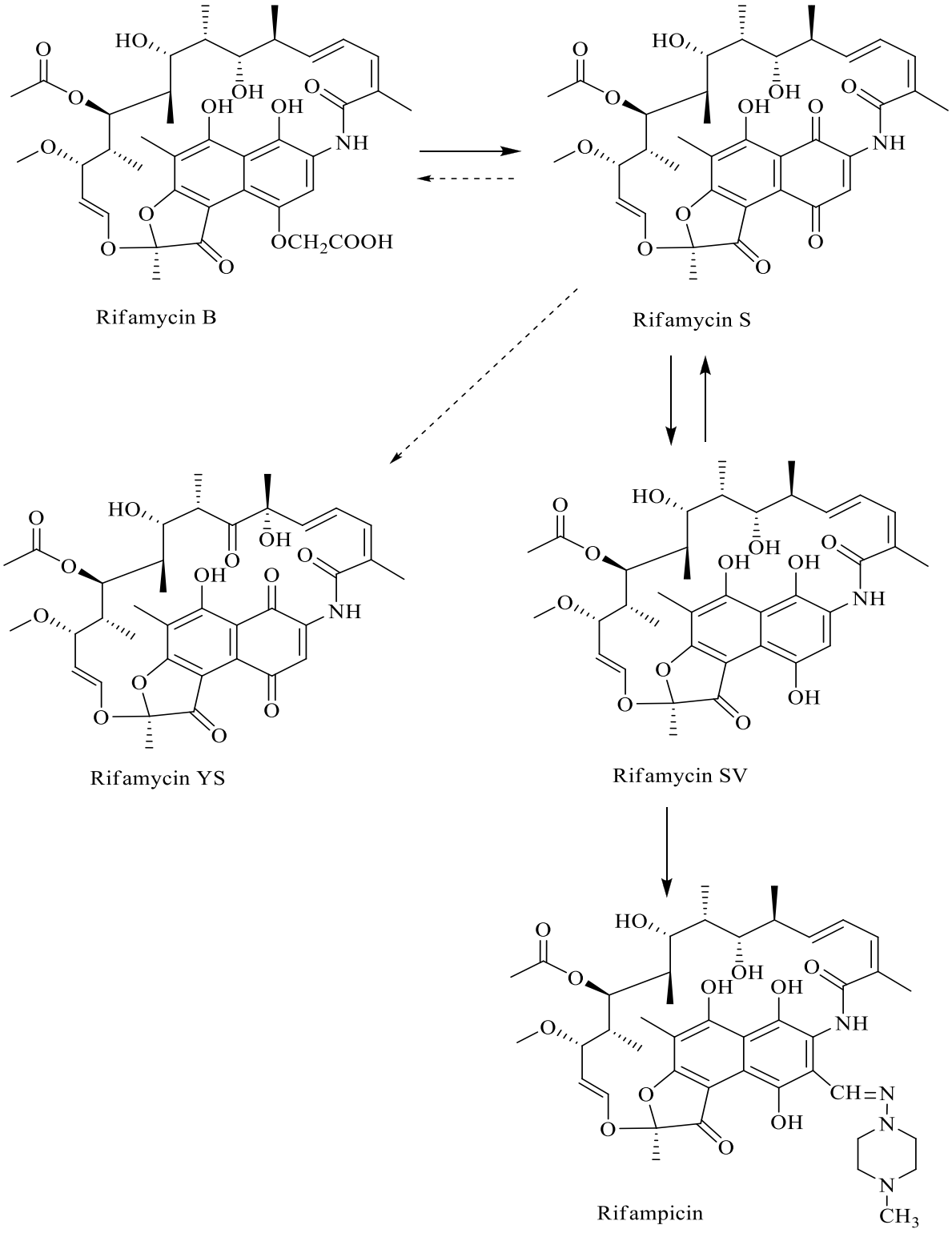

Figure 1. 3 Structural formulae of rifamycin derivatives produced via chemical (→) or biosynthetic pathways (- - - - ▸) [42-44].

1.6 STRUCTURE ACTIVITY RELATIONSHIPS (SAR)

1.6.1 Isoniazid (INH)

Highlights of the SAR of INH analogues are shown in Figure 1.4. There are two independent tracks of SAR for this series, one governing the activation of a prodrug and the other the interaction of the active species with 2-trans-enoyl-acyl carrier protein reductase, called InhA. Many functional groups located at position 4 can be activated inside the cell of *Mycobacterium tuberculosis* bacterium and are possible prodrug options [45]. Following activation, the structural requirements for InhA binding appear to be stringent and of the many aryl and heteroaryl groups explored, only the isonicotinoyl core structure was found to be active [46].

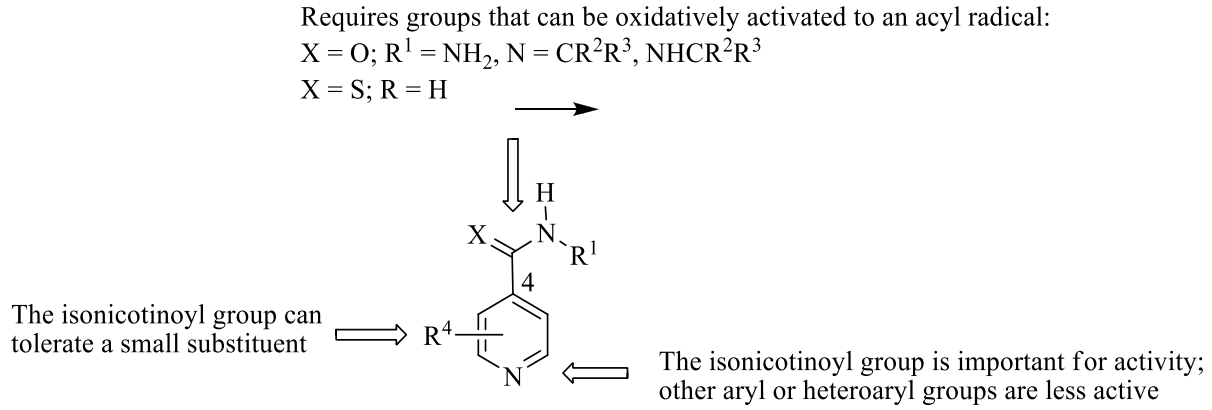

Figure 1. 4 SAR of INH series of antitubercular drugs.

In comparison to other compounds within this class, INH is the most commonly used as it exhibits a relatively good safety and efficacy and is therefore a key component of current TB treatment regimens. Ethionamide and prothionamide are used as second line agents to treat MDR-TB and patients that are not responsive to first line agents. Both ethionamide and prothionamide are not as well tolerated as INH [47].

1.6.2 Rifampicin (RIF)

Chemical modifications of natural products have yielded several clinically important semi-synthetic rifamycin derivatives exhibiting improved pharmacological activity in comparison to the parent compound. The SAR is summarised in Figure 1.5 [48]. The four hydroxyl functional

groups located at positions C-1, C-8, C-21 and C-23 of the rifamycin scaffold are essential for antibacterial activity. Any modification of the hydroxyl groups, with the exception of the C-1-OH to C=O conversion, lead to the formation of compounds with reduced activity. Other modifications that change the conformation of the hydroxyl groups produce inactive compounds. Based on the co-crystal structure of rifampicin-RNA-polymerase (RNAP), the hydroxyl groups directly interact with RNAP through hydrogen bonding and modifications that interfere with hydrogen bonding results in compounds with a reduced binding capacity and low activity.

Saturation of one or more of the double bonds located at positions C-16/C-17, C-18/C-19, and C-28/C-29 generally leads to the formation of compounds with equivalent or slightly reduced activity compared to that of the parent compound. These modifications are not significant and do not have a major impact on potency, or exhibit advantages over the activity of the parent compound. The C-25 deacetylation product is observed as metabolites of the rifamycin analogues. The C-25 hydroxy metabolites are generally as potent as the parent compound. Other modifications of the acetyl group also lead to the formation of potent compounds with different physicochemical properties. However any modification at this position is temporary, since the ester functional groups attached at this position are readily cleaved *in vivo*. The labile nature of the C-25 ester linkage has been exploited to develop rifamycin-based „Trojan Horse" compounds that permit impermeable drug molecules to translocate into cells [49]. Siderophore scaffolds attached to this position permit successful transport of rifamycins into Gram-negative bacterial cells [50].

The most important rifamycin derivatives are those with modifications at positions C-3 and C-4. Synthetically, these positions are accessible and easy to modify and structurally these positions orient towards the open space of the RNAP-binding pocket permitting significant modifications to be made. Modification of the functional groups at positions C-3 and C-4 yields compounds with significantly improved physicochemical properties and pharmacokinetic profiles [50]. Structural modification of 3-formyl rifamycin SV (3-FRSV) leads to the formation of RIF, a potent orally active compound that has become the cornerstone of current TB therapy. Further modification of the RIF analogue series produces rifapentine, a cyclopentyl analogue of RIF. Rifapentine has a longer half-life than RIF and can therefore be used for intermittent therapy. Rifabutin was produced by bridging C-3 and C-4 to form a spiro structure having the advantage

of improved tissue penetration and reduced cytochrome P-450 enzyme induction, relative to RIF. Rifalazil is a new member of the rifamycin series of compounds that has a benzoxazino functional group fused to positions C-3 and C-4 and has a half-life of 61 hours, exhibits little or no substantial cytochrome P-450 induction, and is active against certain RIF-resistant bacteria [52].

The co-crystal structure of RIF-RNAP provides some insight into potential locations of functional groups for future modification. The carbonyl functional group at position C-11 orients towards the open space of the RIF-binding pocket that is a potential site for the modulation of the physicochemical and pharmacokinetics properties of this class of drug [53].

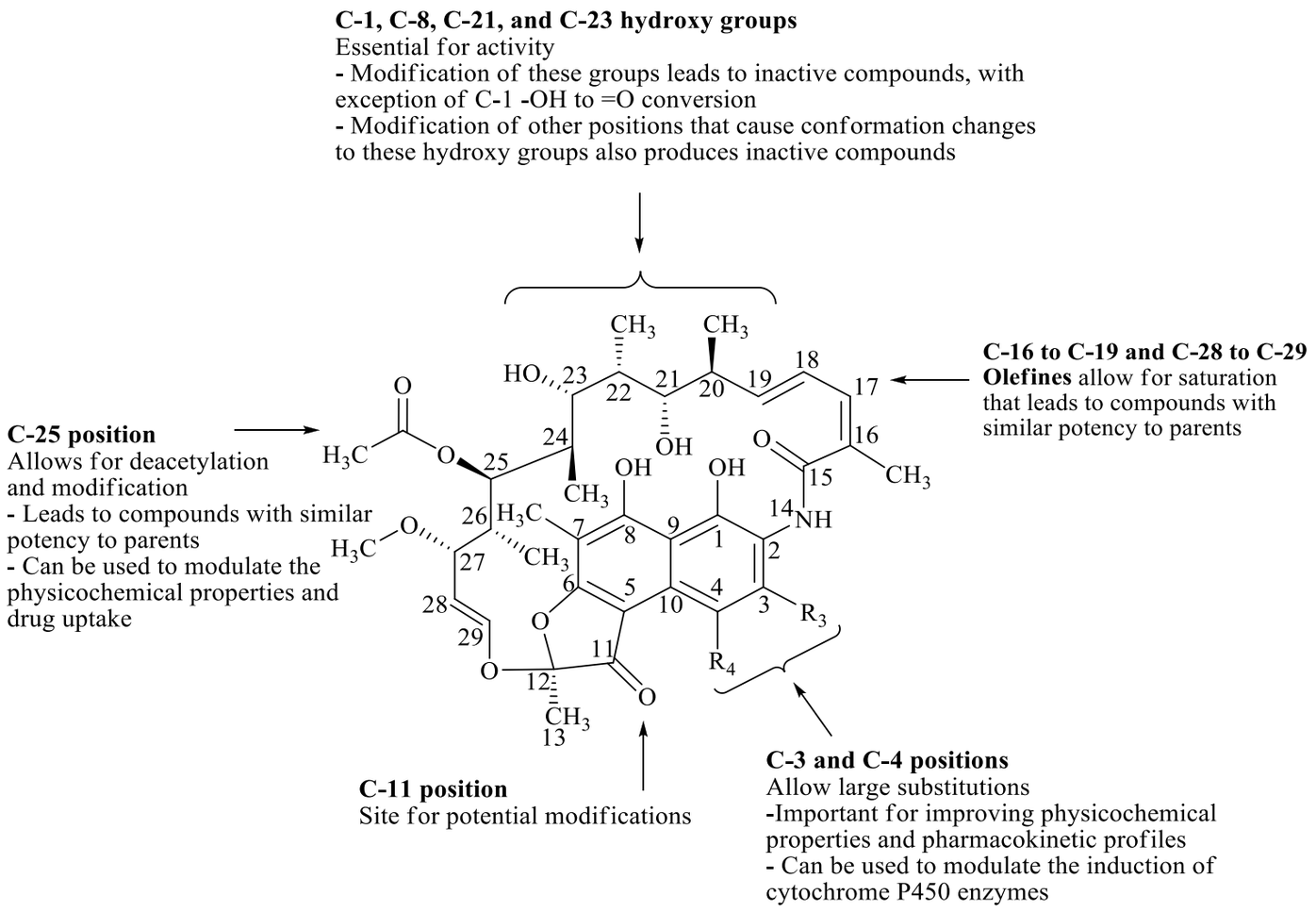

Figure 1. 5 Important structural requirements for SAR of rifamycin analogues.

1.7 STABILITY

1.7.1 Isoniazid (INH)

INH is incompatible with aldehydes and ketones as it reacts with reducing sugars to produce isonicotinyl hydrazone. Reducing sugars such as lactose and maltose should therefore not be used as excipients in INH formulations [54]. INH undergoes hydrolysis and oxidation under stress conditions and the route of degradation and resultant products depend on the conditions under which the reaction is conducted [54]. INH was found to be stable in 0.1M HCl and simulated gastric fluid for 50 minutes [55]. In degradation studies performed in 0.1M HCl at 37 °C and a comparative study in simulated gastric fluid [54] INH degraded to an extent of 3.2 – 4.7 % in 50 minutes. A mono-suspension of INH prepared for the treatment of tuberculosis in children remained stable for 28 days when stored at temperatures of 4 °C, 24 °C and 40 °C [56, 57]. An oral liquid dosage form of INH stored in amber-coloured containers for at least 42 days remained stable with a pH decrease from 5.9 to 5.6 and a colour change from an almost colourless to light brown solution over that period [58]. Exposure of solid INH to a temperature of 50 °C for 60 days and 60 °C for 15 days did not result in significant decomposition, indicating that INH is stable to dry heat [59].

Forced degradation studies conducted by Bhutani *et al.* [59] revealed that INH degraded slowly over time when heated to 80 °C in 0.05 M HCl, resulting in the formation of a single major peak that was resolved at a retention time (RT) of 4.89 minutes by liquid chromatography-mass spectroscopy (LC-MS). Similar behaviour was observed in 0.5 M HCl with a more rapid rate of decomposition observed and > 50 % INH degraded in 4 days. Overall, the rate of hydrolysis in acid was greater than in water or alkali. On heating INH in water for 2 days at 80 °C, approximately 16 % reduction in INH content was observed and after 6 days > 40 % INH had degraded. The major peak in this case also had a RT of 4.89 minutes. Another small peak appeared at a RT of 8.91 minutes. The reaction in 0.1M NaOH at 80 °C was mild and approximately 9 % INH degraded in 4 days. Similar studies at 80 °C in 0.5 M NaOH resulted in 22 % degradation of INH in 4 days. The degradation of INH was associated with the appearance of peaks at a RT 4.89 (major) and 8.91 (minor) minutes. INH was stable in 3 % v/v hydrogen peroxide at a temperature of 25 °C and no significant degradation was observed. However 19 % decomposition occurred in 30 % v/v hydrogen peroxide, resulting in the formation of degradation products that resolved at a RT 4.89 and 8.91 minutes. The liquid chromatographic profiles of INH exposed to light in acid, water and

alkali were similar to those stored away from light, suggesting that light has no effect on the stability of INH in solution. The photolytic studies were outperformed in solid state by spreading a thin layer of drug in a petri-dish and exposing it directly to a combination of UV and florescent light in a photostability chamber set at accelerated conditions of temperature of 40 °C and humidity of 75 % for 60 days. The resultant chromatogram revealed a small peak at a RT of 4.89 minutes and a new peak at a RT of 28.82 minutes which had not been observed in previous studies. The structures of known degradation products of INH are shown in Figure 1.6.

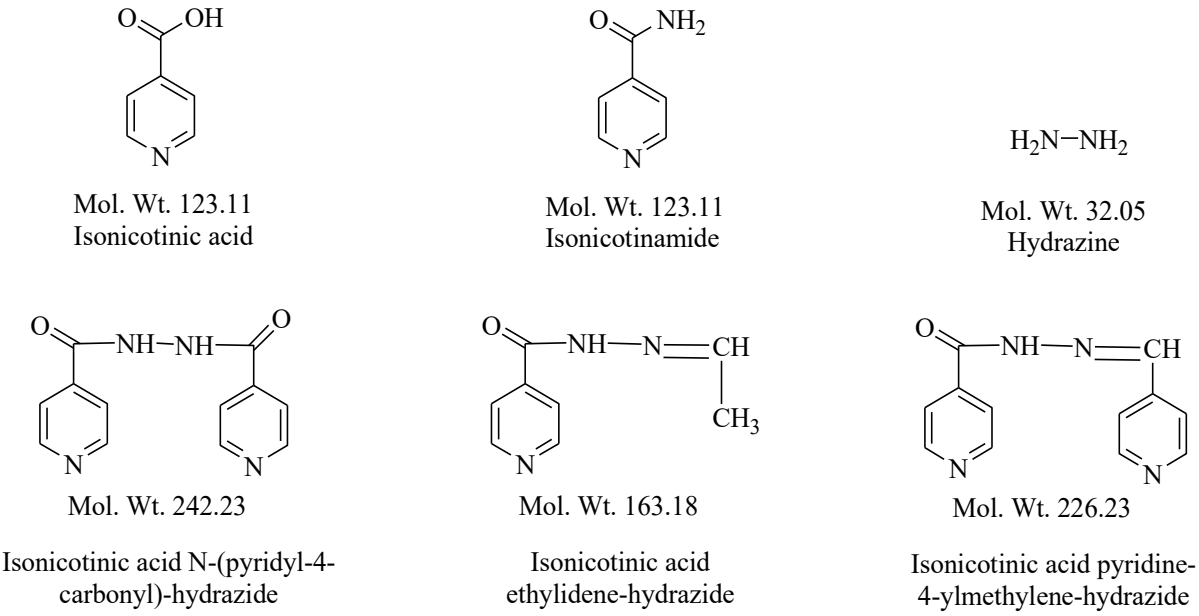

Figure 1. 6 Chemical structures of known degradation products of INH [59, 60].

The mechanism of formation of isonicotinic acid *N*-(pyridine-4-carbonyl)-hydrazide from INH on exposure of solid API to light is shown in Figure 1.7. The first step entails transfer of an electron to isoniazid (I) in the presence of light, leading to formation of a radical anion (Ia). The latter is assumed to disintegrate through a uni-molecular process to form a 4-pyridoyl radical (II) and hydrazine anion (III). In the second step the anion III abstracts a proton from the NH_2 group of I to form an anion of isoniazid (Ib) and hydrazine. The nucleophilic attack by Ib on II in the third step leads to formation of the radical anion IV that finally transfers an electron to I to produce the end product. In the process, radical anion Ia is released and continues to propagate the reaction.

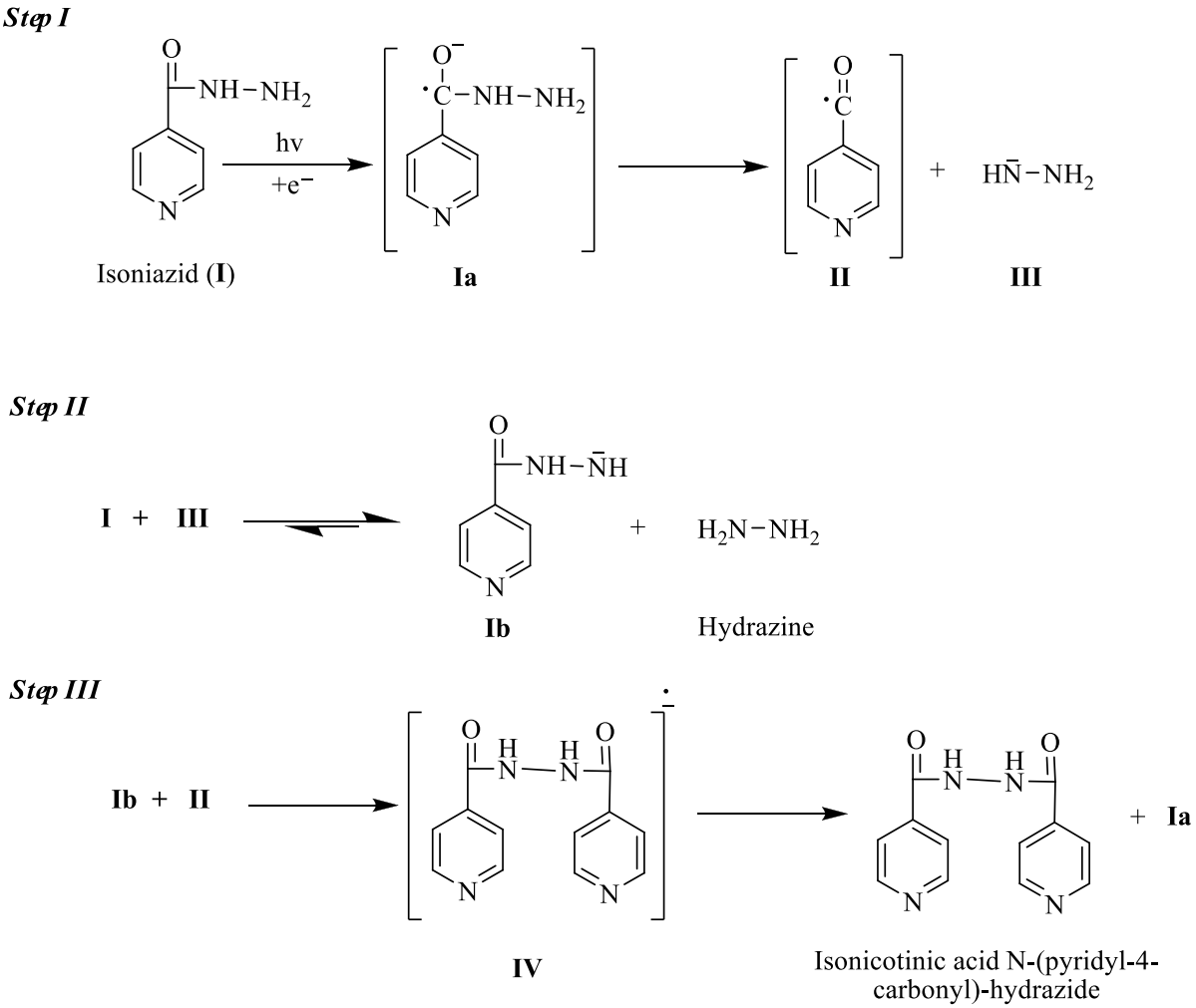

Figure 1. 7 Mechanism of formation of isonicotinic acid *N*-(pyridine-4-carbonyl)-hydrazide following exposure of INH to light [61].

1.7.2 Rifampicin (RIF)

In acidic solution, RIF undergoes hydrolysis to yield 3-formyl-rifamycin and 1-amino 4-methylpiperazine. Under alkaline conditions, viz. pH of 7.5 to 9.0, RIF oxidizes to form RIF-quinone [62, 63]. Maximum stability of RIF is achieved in near-neutral solutions and the addition of ascorbic acid to solutions increases the solubility of RIF with a decrease in oxidation [62]. RIF decomposed by 6.5 % when reacted in 0.1 M HCl at 37°C for 50 minutes [55]. In another study [64] it was established that RIF degraded by approximately 12.4 % to form 3-FRSV in a dissolution medium of 0.05 M HCl over 60 minutes. In a comparative degradation study [55] performed at 37 °C for 50 min in 0.1 M HCl and simulated gastric fluid, RIF decomposed by 17. 8 – 24.4 % under both conditions.

1.7.3 Stability of RIF in the presence of INH

The hydrolysis of RIF in acidic conditions has been reported to be accelerated in the presence of INH [55, 64, 65]. A study to determine the extent of RIF decomposition at 37 °C in the presence of INH over the pH range 1 – 3 for 50 minutes [65] revealed that as the pH increased from 1 to 2 the rate of degradation increased, and a further increase in pH resulted in a decrease in degradation, producing a bell-shaped pH decomposition profile. This suggested that RIF degradation in the presence of INH was greater at pH 2, the maximum pH observed in fasted conditions under which TB FDC products are usually administered. At this pH, RIF decomposed by 34% in 50 minutes, while INH degraded by only 10 %. The extent of decomposition with stomach residence times of 15 min and 3 h were 11.94 % and 62.57 %, respectively for RIF, and 4.78 % and 11.12 %, respectively, for INH. Shishoo *et al.* [64] observed that RIF degraded by 12.4 % in 0.05 M HCl to form 3-FRSV and in presence of INH degradation increased to 21.5 %.

It was reported that whereas the decomposition of RIF in acidic media in the absence of INH ceases with the formation of 3-formylrifamycin, the reaction proceeds to form a hydrazone between 3-formylrifamycin and INH when the latter is present [55]. It was postulated that once 3-formylrifamycin is formed, the compound interacts with INH to form a hydrazone through a reversible reaction mechanism involving a fast second-order forward reaction and a slower first-order backward reaction. In this complex reaction process, RIF degrades further while INH is regenerated. It was suggested that direct interaction can be best explained through transhydrazone formation that occurs *via* nucleophilic attack on the imine group of RIF by the amino group of INH and follows a tetrahedral mechanism [66] as shown in the reaction scheme in Figure 1.8. It was also postulated that this reaction is catalysed by PZA and ETB, involving intra-molecular proton transfer during the reaction between RIF and INH, as shown in the reaction schemes in Figures 1.9 and 1.10 respectively.

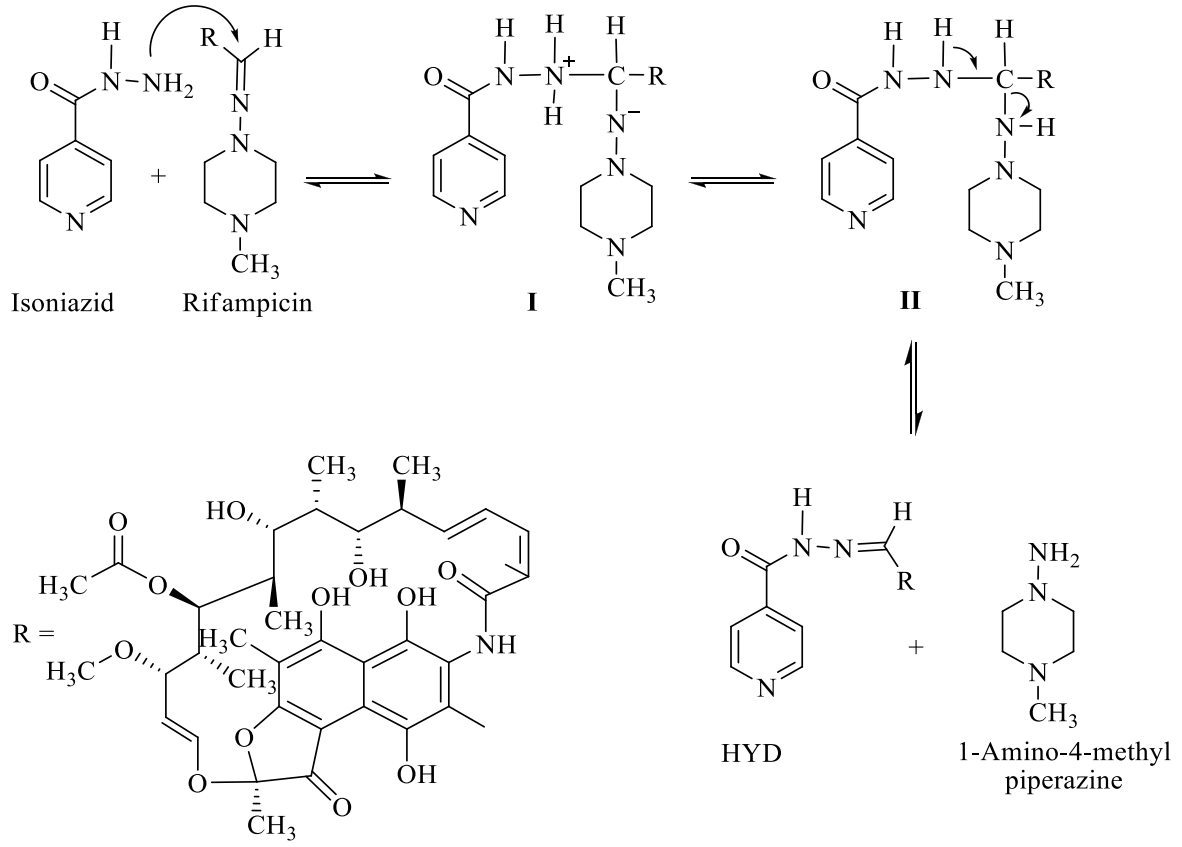

Figure 1. 8 Postulated mechanism of formation of HYD for the direct interaction between RIF and INH [66].

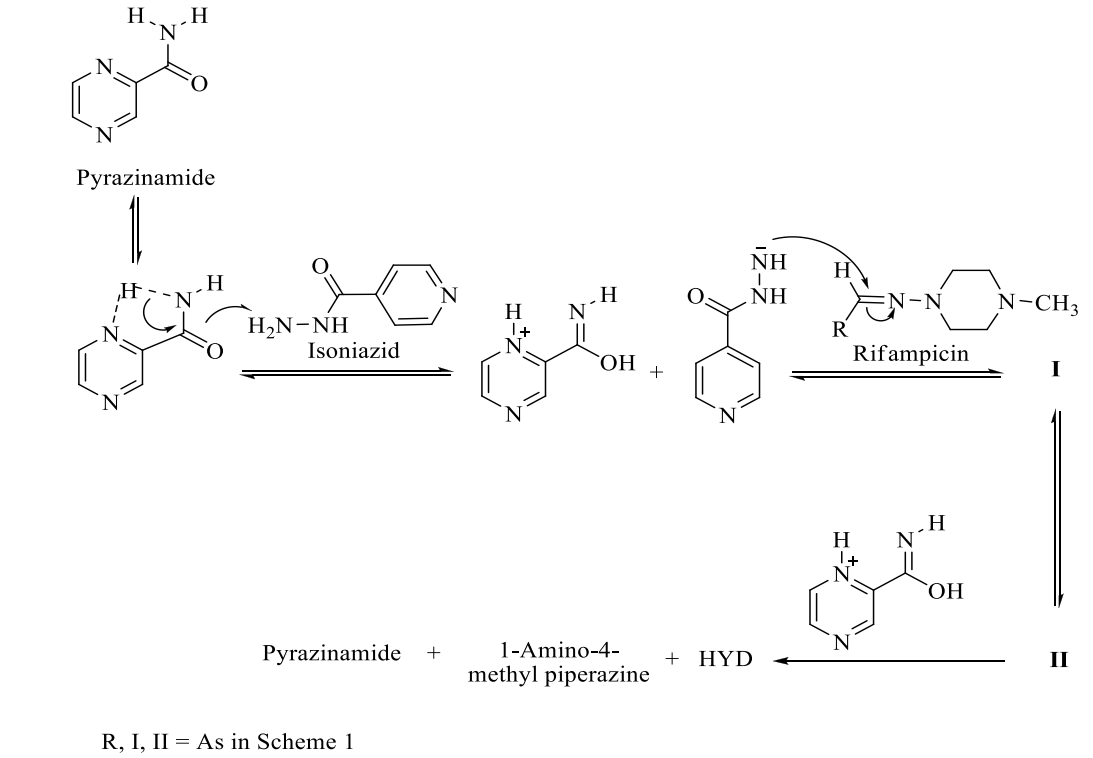

Figure 1. 9 Mechanistic explanation for the catalytic effect of PZA on the interaction between RIF and INH [66].

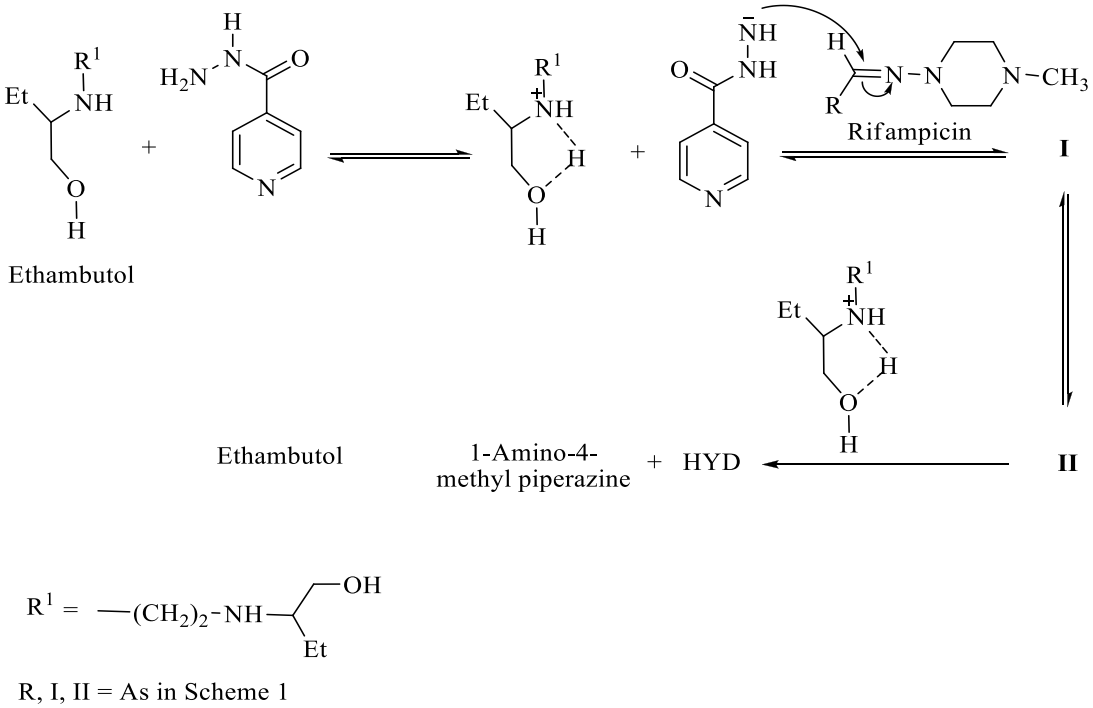

Figure 1. 10 Mechanistic explanation for the catalytic effect of ETB on the interaction between RIF and INH [66].

A mechanism for the degradation of RIF in which 3-FRSV and INH possibly undergo a Schiff's reaction to form a complex as shown in Figure 1.11, has been proposed [67, 68]. The carbonyl and amine functional groups rearrange to yield an iminium ion. The hydroxyl group located at position C-4 enhances complex formation by possible formation of a hydrogen bond with the hydrogen atom attached to the nitrogen at that location. This is a fundamental requirement of a Schiff's base reaction. In addition, carboxylic acids and alcohols can undergo carbonyl condensation reactions [68]. INH may react with RIF in this manner, which may account for the instability of RIF when co-administered with INH (Figure 1.12). This interaction may also occur between RIF and PZA, however it has been observed that INH further enhances the degradation of RIF compared to PZA due to the fact that carboxylic acids and alcohol further undergo Fischer's esterification [69]. The hydroxyl functional groups of RIF are readily able to react with aqueous carboxylic acid degradation products yielded by INH and PZA to form an ester, as shown in Figure 1.13. However as PZA lacks an electron-withdrawing group, such as the secondary nitrogen located in the hydrazide group of INH, there is a smaller tendency for the reaction to be observed between PZA and RIF.

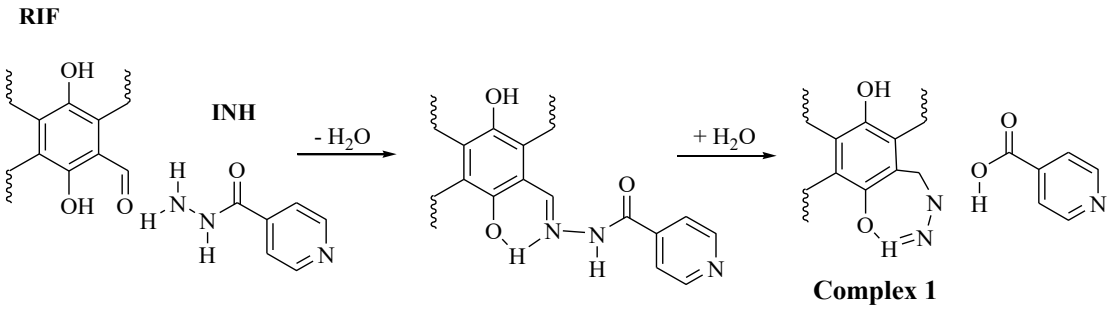

Figure 1. 11 Schiff's base reaction mechanism for the interaction of RIF and INH [68].

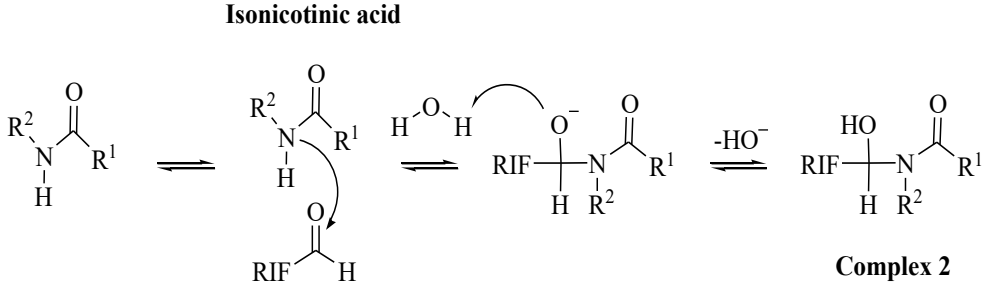

Figure 1. 12 Carbonyl condensation reaction mechanism for the interaction of RIF and INH [68].

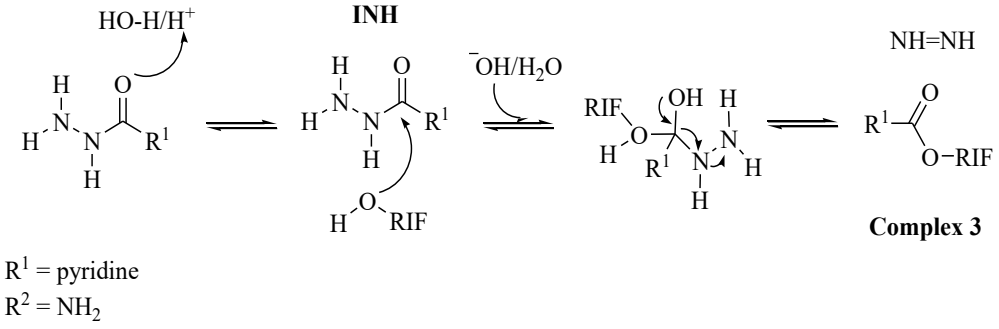

Figure 1. 13 Fischer"s esterification reaction mechanism for the interaction of RIF and INH [68].

The production of 3-FRSV, which is a poorly soluble compound exhibiting antimicrobial activity *in vitro* but is inactive *in vivo*, is one of the factors associated with the poor bioavailability of RIF [41, 69]. The accelerated degradation of RIF to form 3-formylrifamycin via reversible binding of the isonicotinyl hydrazone of 3-FRSV to INH in acidic conditions has been postulated to further contribute to the poor bioavailability of RIF from FDC medicines [63, 65, 70, 71].

1.8 CLINICAL PHARMACOLOGY

1.8.1 Mechanism of action

1.8.1.1 Isoniazid (INH)

INH is the most active compound for the treatment of TB caused by susceptible organisms. INH is a prodrug activated by mycobacterial catalase peroxidase, *kat*G, to form an isonicotinic acyl anion. The isonicotinic acyl anion exerts lethal activity through inhibition of synthesis of mycolic acids, an essential component of mycobacterial cell walls. It acts by formation of a covalent complex with the acyl carrier protein (AcpM) and KasA, a beta-ketoacyl carrier protein synthetase [72, 73]. INH inhibits tubercular bacilli at a concentration of 0.2 µg/mL [74] and is the only bactericidal compound active against viable dividing *Mycobacterium tuberculosis* cells but bacteriostatic to semi-dormant micro-organisms of that species [75].

1.8.1.2 Rifampicin (RIF)

RIF binds to the beta subunit of bacterial DNA-dependent RNA-polymerase, thereby inhibiting the initiation of chain formation during RNA synthesis. RIF is one of the most effective anti-TB agents available and is bactericidal to intra- and extra-cellular bacteria [25, 72]. RIF inhibits susceptible bacteria at concentrations < 1 µg/mL [72]. RIF has the unique ability to kill bacilli when semi-dormant tubercular bacilli undergo sporadic bursts of metabolism and growth [76].

1.8.2 Adverse Effects

1.8.2.1 Isoniazid (INH)

The incidence of adverse effects when using INH is fairly low and except for hypersensitivity reactions are associated with the dose and duration of therapy. INH, when used alone for TB prophylaxis, rarely causes side effects at doses of 10 mg/kg/day up to 300 mg [77]. Peripheral neuritis is the most common adverse effect and appears to be due to pyridoxine deficiency that has been attributed to the competition of INH and pyridoxal phosphate for the enzyme apotryptophanase. Supplementation of pyridoxine can correct most side effect reactions. INH is secreted in breast milk and may result in pyridoxine deficiency in infants, unless the mother takes supplements of the vitamin [78].

Potentially fatal hepatitis is the most severe adverse effect associated with INH use and is assumed to be a consequence of formation of the toxic metabolite monoacetylhydrazine, formed by metabolism of INH. The incidence of hepatitis increases in patients with increasing age, those taking RIF, or patients using alcohol on a daily basis [78].

Other adverse effects include mental abnormality, convulsions in patients prone to seizure, optic neuritis and hypersensitivity reactions including rash and fever [78].

1.8.2.2 Rifampicin (RIF)

Adverse effects are considered a minor problem with RIF use and include nausea, vomiting, rash and fever. RIF should be used with caution in patients with hepatic failure, as jaundice occurs in patients with chronic liver disease, alcoholics or in the elderly [79]. Transitory and asymptomatic increases in serum levels of bilirubin and hepatic enzymes occur in 5 % of patients treated with RIF. The levels subsequently normalize, without the need to discontinue

treatment. Cholestatic hepatitis occurs in about 2.7 % of patients treated with RIF and in up to 1.1 % of those receiving RIF in combination with other anti-TB medicines [80]. RIF causes discoloration of body fluids and patients may present with orange-coloured tears, sweat and/or urine and this has the potential to reduce adherence to the medication. The orange tears may stain contact lenses [80]. Thrombocytopenia, leukopenia, eosinophilia, haemolytic anaemia, agranulocytosis, vasculitis, acute interstitial nephritis and septic shock can occur following administration of RIF and although rare occurs in < 0.1 % of patients, a change of therapeutic regimen is required [80].

1.8.3 Drug Interactions

1.8.3.1 Isoniazid (INH)

INH inhibits cytochrome P-450 (CYP-450) enzymes, specifically the CYP2C9, CYPC19, CYP2E1 isozymes and the CYP3A isozyme to a lesser extent. Some of the interactions include the inhibitory effect of INH on these systems and may result in an increase in the plasma concentrations of some compounds to toxic levels [77, 81]. Other reported interactions include INH causing an increase in the plasma concentration of anticonvulsants such as phenytoin and carbamazepine [82]. INH inhibits the metabolism of phenytoin and thus potentiates side effects of phenytoin such as nystagmus and ataxia, with slow acetylator patients at particularly high risk [78]. INH increases the plasma concentration of benzodiazepines such as diazepam and triazolam that are metabolized by oxidation, in addition to theophylline, valproic acid, disulfiram, acetaminophen and oral anticoagulant. The combination of INH and levodopa may result in hypertension, palpitation and flushing of the face [19, 77, 82, 83].

1.8.3.2 Rifampicin (RIF)

RIF is known to induce CYP-450 enzymes and thus increase metabolism of many compounds such as oral contraceptives, warfarin, prednisolone, digoxin, ketoconazole, beta-adrenergic blocking agents, corticosteroids, cyclosporine, dapsone, haloperidol, barbiturates, enalapril, antidepressants such as nortyriptyline and sertraline, valproic acid, macrolide antibiotics, simvastatin, theophylline and verapamil amongst many others. The subsequent reduction of plasma concentration and half-life of the drugs may require dose adjustment to achieve desired therapeutic outcomes [77, 78, 84, 85]. The concomitant use of RIF with ketoconazole or para-aminosalicylic acid reduces the concentration of RIF requiring the

medicines to be administered separately at least 12 hours apart [84, 86, 87]. RIF also induces the uridine diphosphate-glucuronosyltransferase enzyme that has been implicated in the metabolism of many compounds resulting in a reduction in plasma levels of the co-administered compound(s) [88, 89]. RIF reduces the plasma concentration of oral hypoglycaemic agents, often necessitating replacement with insulin [90]. RIF decreases the plasma concentration of protease inhibitors (PI) and nucleoside reverse transcriptase inhibitors (NRTI), although efavirenz and a combination of saquinavir and ritonavir can be used without need for discontinuing RIF treatment [91].

1.8.4 Precautions and use in special patient groups

1.8.4.1 Isoniazid (INH)

The use of INH in pregnancy is considered safe, however there is a risk of developing hepatitis in the postpartum period and therefore the WHO recommends that all pregnant women treated with INH also take 25 – 50 mg pyridoxine daily. Neonates born to mothers treated with INH are at risk of developing convulsive seizures [19, 77, 92]. Breastfeeding infants should be monitored for jaundice even though INH is considered suitable for use during lactation [93]. The half-life of INH is longer and serum levels of the drug higher in patients with liver disease, in alcoholics and individuals > 50 years of age. Therefore such patients should undergo clinical examinations and laboratory testing more frequently when treated with INH [77, 94]. There is no requirement for dose adjustment in patients with kidney failure or those requiring haemodialysis [77, 95, 96].

1.8.4.2 Rifampicin (RIF)

RIF has not been implicated in teratogenicity when used to treat pregnant women [19, 77]. Mothers treated with RIF should be administered vitamin K in order to avoid postpartum haemorrhage [97] and breastfeeding infants should be monitored for jaundice [19, 93]. RIF clearance may be impaired in liver failure and patients must be frequently monitored clinically and augmented with appropriate laboratory testing [77]. RIF can be used at full dose levels in patients in renal kidney failure as RIF is metabolised by liver enzymes [19, 77, 96].

1.9 PHARMACOKINETICS

The pharmacokinetic characteristics of INH and RIF are summarised in Table 1.4.

Table 1. 4 Pharmacokinetic and biopharmaceutic characteristics of INH and RIF [75].

Drug	Absorption	Distribution	Metabolism	Excretion
Isoniazid	Rapidly and well absorbed from an empty stomach [98]. Peak plasma concentration (C_{max}) =1.4 µg/mL, with t_{max} in 1-2 h [101, 102]. Food impedes absorption and reduces bioavailability [103-106].	Not protein bound and is extensively distributed [98]. Cerebrospinal fluid concentration approximately 90 to 100 % of plasma levels within 3 to 6 h [102]. Concentration in pulmonary tissue is similar to that in serum [104].	Metabolised in the liver through acetylation by N-acetyltransferase to produce acetylisoniazid and isonicotinic acid [98, 99]. Acetylation rate is a genetic characteristic. Humans may be slow or fast acetylators [100-105].	Excreted in the urine to extent of 70-90 %) [98-101]. Forms inactive metabolites In rapid acetylators, 7 % INH excreted in urine can appear as free INH 37 % appears as conjugated INH in slow acetylators [104]. $t_{½}$ of INH in fast acetylators is approximately 1 h $t_{½}$of INH in slow acetylators is approximately 2-5h 75-95 % excreted in urine unchanged [104].
Rifampicin	Rapidly absorbed with a bioavailability of 90-95 % prior to enzyme induction [100-102]. Plasma levels peak at 5-10 µg/mL within 2-4 h after an oral dose of 600 mg [100-102]. Rapid absorption from an empty stomach [100-102]. Food and antacids decrease oral absorption [111-113].	Extensively distributed with body fluid discoloration [100-102]. Good cerebrospinal fluid (CSF) penetration in the presence of inflamed meninges [104-106]. 80 % protein bound to albumin and α-l-acid glycoprotein [104-106].	Undergoes enterohepatic circulation, deacetylation, active metabolite, hepatic enzyme inducer [100-102]. Approximately 85 % RIF is metabolised in the liver by CYP450 microsomal enzymes [104-106].	60 – 65 % excreted via the biliary tract [105]. 6 – 15 % is excreted unmetabolised form and is reabsorbed from the intestine resulting in an increase in serum level [104-106]. $t_{½}$ is 3 – 5 h [104, 111-113]. After approximately 14 days, enzymes that increase metabolism of RIF cause auto-induction of metabolism and $t_{½}$ decreases to 2 – 3 h [111-113]. A small proportion of the dose is excreted in the urine [104].

1.9.1 Bioavailability of rifampicin

The greatest concern relating to the use of FDC for the treatment of TB is the issue of low bioavailability of RIF observed from a number of FDC formulations [26, 110]. The decomposition of RIF in the acidic environment of the gastric compartment has been estimated to vary between 8.5 and 50 % over the time corresponding to the gastric residence of most dosage units in humans, viz. between 15 minutes and 150 minutes [70, 111]. An increase in gastric emptying time for some single dosage units, as long as 6 hours, may also contribute to poor bioavailability [112]. The use of FDC that do not meet compendial requirements can ultimately result in the development of drug resistant TB and treatment failure [110]. The variability in bioavailability of RIF from different FDC formulations has been attributed to differences in particle size and the crystalline form of RIF, manufacturing process reproducibility and the excipients used [113, 114]. The hydrolysis of RIF, in acidic media, to insoluble 3-FRSV further contributes to the poor bioavailability of RIF. The accelerated degradation of RIF to form this poorly absorbed compound in the presence of INH via reversible formation of isonicotinyl hydrazone has been suggested as a further compounding factor for the poor bioavailability of RIF. Shishoo *et al.* [70] indicated that RIF in the presence of INH in a FDC, may undergo greater decomposition in the acidic conditions of the stomach, compared to RIF administered alone [15]. Consequently less RIF is available for absorption from some FDC products than when RIF is administered as a separate formulation, and is often reflected by poor bioavailability from the former FDC formulations [70, 111, 115-117].

There is thus an urgent need to develop a formulation from which RIF and INH are not released simultaneously in the acidic environment of the stomach to ensure optimum availability of RIF.

1.9.2 Novel drug delivery systems to prevent interaction between RIF and INH

In an attempt to prevent contact between RIF and INH, a gastroretentive dosage form of RIF was combined with an enteric coated INH capsule [118]. RIF (150 mg) floating tablets were manufactured by wet granulation using hydroxypropyl methylcellulose (HPMC), calcium carbonate and polyethethylene glycol (PEG) 4000. Enteric coated capsules of INH were manufactured by pan coating hard gelatin capsules containing a compacted mass of 150 mg INH, with 20 % w/w Eudragit® L100-55. RIF was gradually released from the novel dosage form with

90 % released between 3.5 and 4 hours in 0.05 M HCl. The RIF floating tablets revealed a lag time of < 3 minutes and a floating duration > 5 hours in 0.05 M HCl. No release of INH from the enteric coated INH capsule occurred, however > 90 % INH was released in an alkaline medium in 30 minutes. A comparison of the amount of RIF that degraded when administered from an immediate release capsule containing RIF and INH and from the floating dosage form revealed that 25 % RIF degraded after 75 minutes of testing in 0.05 M HCl at pH 1.5, compared to 8 % observed when testing the novel dosage form. The greater degradation of RIF observed with the immediate release dosage form was attributed to accumulation of the API in the dissolution vessel in the presence of INH. The degradation of RIF to form 3-FRSV was arrested when the novel technology was tested and only 3.6 % - 4.8 % degradation of RIF occurred at 4 hours, which was attributed to minimisation of the interaction between RIF and INH.

In another study gastroretentive floating RIF tablets and enteric coated INH tablets were manufactured separately and then filled into a single size 00 hard gelatin capsule [119]. The floating tablets (average weight 200 mg) were manufactured by direct compression and contained 75 % w/w RIF, 15 % w/w polyethylene oxide, 1.5 % w/w ascorbic acid, 8 % w/w calcium carbonate and 0.5% w/w magnesium stearate. The tablets had a floating lag time of 2.5 minutes and a duration of floating of 5.1 hours. The core INH tablets were manufactured by direct compression and contained 65.2 % w/w INH, 32.6 % w/w dibasic calcium phosphate (DCP) and 2.17 % w/w magnesium stearate. The INH tablets were coated with a dispersion of hypromellose phthalate HP-55S, using conventional pan coating. The coating dispersion contained 3.5 % w/w HP-55S, 10 % w/w dibutyl phthalate, 1 % w/w magnesium stearate and 1 % w/w titanium dioxide dispersed in a 1:1 blend of acetone and isopropyl alcohol. Two RIF and INH tablets were filled into a size 00 hard gelatin capsule and the *in vitro* release and degradation profiles characterized. Approximately 90 % RIF was released from the novel dosage form in 224 minutes and < 8 % INH was released in acidic pH from this novel dosage form. Approximately 90% INH was released from the novel dosage form in alkali media in 180 minutes. Greater than 29 % RIF degraded in 120 minutes when a capsule containing a powder blend of RIF and INH was subjected to *in vitro* conditions to assess RIF degradation. The amount of RIF degraded in the presence of INH from the novel dosage form was < 0.21 % in 120 minutes. The greater degradation of RIF observed for the powder blend of RIF and INH was attributed to the catalytic effect of INH on RIF degradation [64, 116], which had been reported

to be as much as 12 % to form 3-FRSV in acidic media in 45 minutes and 17 % to 24 % degradation in the presence of INH.

A floating bi-layered FDC tablet containing RIF, INH and PZA was manufactured by direct compression with a sustained release layer containing 120 mg RIF and 300 mg PZA and an immediate release layer with 50 mg INH [120]. INH was formulated into a separate layer as it catalyses the degradation of RIF in acidic media and the immediate release component was designed to release INH in the small intestine by preparing a solid dispersion of INH using Eudragit® L100 as the enteric polymer. The sustained release portion with RIF and PZA was manufactured using HPMC K100M, sodium bicarbonate, polyvinyl pyrrolidone, PVP-K30, magnesium stearate and microcrystalline cellulose (MCC). RIF and PZA were released over a period of 16 hours in the stomach, due to the floating mechanism used, with 97.56 % RIF and 98.97 % PZA released over 16 and 12 hours, respectively. Buoyancy studies performed using a 0.05M HCl solution of pH 1.2 revealed a floating lag time between 35 and 310 seconds, depending on the amount of sodium bicarbonate used in the formulation, and floating duration of > 12 hours. The immediate release solid dispersion of INH contained sodium starch glycolate, PVP K30, MCC and lactose, and did not release INH in the 0.05 M HCl for 4 hours but released 99.56 % INH in 60 minutes in alkali media. This study did not investigate the degradation of RIF either alone or in combination with INH in the acidic medium.

Two formulations were manufactured in which RIF and INH were included as uncoated immediate release tablets (formulation 1), and RIF in an uncoated and INH in an enteric coated form (formulation 2) [121]. All tablets were manufactured by direct compression and contained magnesium stearate, SuperTab® 11SD lactose and talc. Eudragit® L100 was used as the enteric coat for the INH tablets. Dissolution studies were performed for formulations 1 and 2 separately in 0.05M HCl. The cumulative percent RIF released after 2 hours in 0.05 M HCl was approximately 80 % and 91 % for formulations 1 and 2, respectively, revealing an 11% decrease in degradation of RIF when co-administered with enteric coated INH tablets.

A novel drug delivery system for modulating the release kinetics of anti-TB drugs was developed and evaluated [122]. The solid dosage form was comprised of an immediate release RIF tablet, an effervescent gastroretentive RIF tablet and an enteric coated INH capsule. The technology released RIF in a controlled manner in the stomach and INH in the small intestine. The total dose

of RIF was subdivided into two components, viz. an immediate release tablet containing a loading dose of RIF and a gastroretentive floating tablet containing a maintenance dose of RIF. The floating hydrophilic matrix tablets were prepared by direct compression and were comprised of different amounts of HPMC K4M, HPMC K100M and sodium bicarbonate. Enteric coated hard gelatin capsules (size 4) were filled with 100 mg compressed INH, 50 mg dicalcium phosphate dihydrate and then coated with Eudragit® L-100 using a dip coating process. The novel solid dosage form was manufactured by placing an immediate release RIF tablet, a gastric floating RIF tablet and a filled enteric coated size 4 INH capsule into a size 00 hard gelatin capsule. The release and degradation of the payload was compared to that from a commercially available dosage form, R-Cinex® tablets (Lupin Ltd, India). It was observed that approximately 42 % degradation of RIF occurred within 60 minutes when the R-Cinex dosage form was tested, whereas only 10 % degradation of RIF occurred when the novel dosage form was tested.

Gastric resistant INH pellets were manufactured to prevent direct physical contact between RIF and INH and to investigate the effectiveness of the formulation to reduce the degradation of rifampicin in acid media [123]. The pellets were manufactured by extrusion-spheronization and were comprised of INH and microcrystalline cellulose PH 101 in a 85:15 weight ratio, and a 1 % w/w solution of Methocel® E6 was used to bind the powders. The pellets were coated using methacrylic acid copolymer, Acrycoat L100 dissolved in a 1:1 v/v mixture of isopropanol and ethanol. To evaluate the influence of the presence of INH on the dissolution of RIF in acidic media an accurately weighed aliquot of coated and uncoated pellets containing the equivalent of 200 mg INH were mixed with 300 mg RIF and filled into a size 00 hard gelatin capsule. The evaluation was conducted in 0.05 M HCl for 60 minutes and the release of RIF from the capsules containing uncoated INH pellets was 80 % at 15 minutes, after which the concentration of RIF decreased. In the presence of enteric coated pellets, INH was not released into the dissolution medium and RIF concentrations were higher, indicating that when the contact of RIF and INH is minimized in solution, *in vitro* degradation of RIF decreased by 11.5 %. These results are in agreement with the findings of Shishoo *et al.* [64], who reported that 12 % RIF degraded in acidic fluids within 45 minutes and only 11 % degraded in the presence of INH in 0.05 M HCl after 2 hours [121].

In a separate study a formulation for a once daily dosed oral FDC pellet of RIF and INH was developed to facilitate the delivery of these compounds enhanced RIF stability [124]. Two formulations were manufactured and included capsules of RIF and INH containing immediate release uncoated pellets (formulation I) and capsules containing enteric coated pellets of RIF and INH (formulation II). The pellets were manufactured by extrusion and spheronization and were comprised of talc, magnesium stearate and SuperTab® 11SD lactose. Eudragit® L-100 was used as the enteric polymer and pellets were coated using pan coating. The cumulative percent RIF released from formulation I in 0.05 M HCl after 2 hours was 81 %, whereas no RIF was released from formulation II and an increased amount of 89 % was released in phosphate buffer of pH 6.8. The study proved that RIF degradation is catalysed in the presence of INH in acidic media. It was suggested that the stability of RIF can be enhanced by formulating INH and RIF as enteric coated pellets to avoid contact between the two compounds in acidic media, thus to ensure l release could be achieved in fluids at intestinal pH. This study did not take into account the pH dependent solubility of RIF, which is generally higher in acidic media and subsequently absorption would be greater from the stomach compared to the small intestine, where the pH is alkaline [27, 28].

Controlled release porous RIF microspheres were developed with the aim of preventing acid-catalysed decomposition and promoting controlled release of RIF over a prolonged period [125]. The porous microspheres were manufactured using emulsion solvent diffusion at 40 °C to facilitate evaporation of dichloromethane. The amount of Eudragit® used was important, and determined the stability of microspheres during manufacture. RIF-to-polymer ratio ranges between 1:1 and 1:4 ensured the formation of stable porous microspheres. Simulated gastric fluid (SGF) without pepsin was used as the test medium for assessing the relative decomposition of RIF over 3 hours. The degradation of RIF in the microspheres was lower than that of pure API, and 18.5 % degradation was observed with low RIF and high polymer ratio microspheres, viz. 1:4. Low levels of RIF with high levels of polymer exhibited maximum stability of RIF in SGF. A maximum of 34.3 % degradation was observed from microspheres with RIF to Eudragit® ratios of 1:1 and 4:3. Stability studies for RIF revealed that the use of microspheres reduced the degradation of RIF and may possibly enhance the stability of RIF in the stomach. The study did not however assess the stability of RIF in microspheres in the presence of INH. This would be necessary to explore the clinical applicability of using such RIF microspheres.

Pellets designed for site-specific release of INH in the small intestine have been developed [126]. The pellets were manufactured by extrusion-spheronization and coated to a 35 % weight gain using a 10 % w/w aqueous suspension of Sureteric® with a fluid-bed drier. The complete release profile of the site-specific INH pellets revealed that only 10 % of the INH was released in 120 minutes in 0.05 M HCl, indicating the gastric acid resistance of the coated pellets. The INH released when the pellets were tested in buffer of intestinal pH 6.8 was > 85 % of the payload. The study did not combine the pellets with RIF, and it would be interesting to evaluate the impact of 10 % INH powder on the degradation of RIF in acidic media. In a separate study a sustained release gastroretentive mucoadhesive delivery system for RIF was developed with a view to improving the bioavailability of RIF from the stomach, where the compound exhibits high solubility and permeability [127]. The RIF delivery system was comprised of a loading and maintenance dose component, with the loading dose formulated as pellets for immediate release and the maintenance dose as a mucoadhesive tablet. The immediate release pellets were manufactured by extrusion and spheronization. They were comprised of 85 % w/w RIF, 5 % w/w MCC, 5 % w/w povidone pyrrolidone and 5% w/w lactose. The mucoadhesive tablets were manufactured by dry granulation and were comprised of 150 mg RIF per tablet, 4-19 % w/w Carbopol® 71G , 2.5-5 % w/w MCC and 8 mg HPMC per tablet. Gamma scintigraphic imaging revealed that the formulation was retained in the stomach for > 6 hours. Furthermore, mean gastric emptying or the time required for 50 % of the formulations to be emptied from the stomach was approximately 5.3 hours. Although this study did not assess the stability of RIF in the presence of INH in acidic media the sustained release of RIF from this novel gastroretentive delivery system has the potential to minimise concentration dependent decomposition of RIF in the stomach. It would be interesting to evaluate the performance of the delivery technology as a combination pellet dosage form [126] and mucoadhesive system [127], particularly in respect of the impact on stability and bioavailability of RIF.

A swellable sustained release floating bioadhesive gastrointestinal delivery bilayer tablet containing RIF and INH has been developed [128]. The tablets were manufactured from a combination of Psyllium husk, Carbopol® 934, sodium carboxy methylcellulose, chitosan, sodium alginate, polymethacrylic acid ethyl acrylate and basil seed in different amounts. Radiographic images revealed that the tablet remained intact with respect to structural integrity and shape when evaluated in the stomach of rabbits. Changes in the position of the tablet in the

stomach at 30 minutes and 1 hour post administration, provided evidence of the floating nature of the tablets. The unchanged position of the tablets, in the stomach, between 12 and 24 hours proved the bioadhesive properties of the formulation that were attributed to the presence of the Psyllium husk which contains two major polysaccharide fractions with equivalent molecular weight of about 700 and 4000 that result in mucilage formation. Psyllium husk in contact with aqueous media swells and may facilitate bioadhesion through simple hydrogen bonding of the mucilage with components of gastric mucous secretions. Although this study did not evaluate INH-catalysed degradation of RIF in an acidic medium it is possible that concentration-dependent degradation of RIF may be reduced despite the release of INH and RIF in the stomach. The study highlighted the potential of combining floating and bioadhesion technologies for the design of gastroretentive dosage forms which would be ideal for an API exhibiting high solubility and permeability in and from the stomach. Psyllium husk has potential for use in the design of effective muco-bioadhesive sustained release formulations.

pH sensitive hydrogels manufactured from blends of polyvinyl alcohol (PVA) with acrylic acid-graft-guar gum for delivery of INH have been developed [129]. Microspheres of approximately 10 μm diameter were produced using a water-in-oil (w/o) emulsification approach to investigate controlled release of INH. A novel graft copolymer was synthesized by grafting polyacrylic acid to guar gum and then blended with PVA to produce a pH sensitive PVA-(AA-g-GG) hydrogel matrix. *In vitro* INH release studies conducted in buffers of pH 1.2 and 7.4 revealed that the cumulative % INH released was 25 % in pH 1.2 and 65 % in pH 7.4 buffer from microspheres cross-linked with 7.5 mL GG which induced greater polymer cross-linking. Although this study was aimed at sustaining the delivery of INH, this strategy may be useful for the formulation of pH-sensitive INH microspheres which reduce the release of INH in the stomach when INH is dosed with RIF.

An alternate strategy used to prevent acid catalysed INH-induced degradation of RIF was the use of solid lipid nanoparticles (SLN) to encapsulate API [130]. RIF and INH were loaded into solid lipid nanoparticles to limit degradation and interaction of RIF with INH in acidic conditions. The lipid phase of 13 % v/v lipid and polysorbate 80 were heated to approximately 10 °C above the melting temperature for the lipid, of 70 °C. The API was added to the lipid phase with magnetic stirring at 600 rpm. An aqueous phase was added to the lipid-surfactant mixture whilst stirring at

1500 rpm. Stirring was continued for between 2-10 minutes, after which the hot micro-emulsion was transferred into an equivalent amount of cold water at 2 °C with continuous mechanical stirring at 5000 rpm for 1.5 hours. The SLN were formed by crystallization of the molten lipid droplets present in the micro-emulsion. In the case of INH SLN, the lipid and aqueous phase of polysorbate 80, water and soy lecithin were heated to approximately 10 °C above the melting temperature of the lipid (70 °C) and INH then added to the aqueous phase. The degradation of RIF was studied alone and in the presence of INH at pH 1.2. Studies in which RIF SLN were in combination with INH and INH SLN in acidic pH were also performed to determine the stability enhancing effects of using SLN. It was observed that the degradation of RIF powder was enhanced in the presence of free INH, with degradation increasing from 26.5 % to 48.8 % in the presence of INH. Only 13 % INH degraded when present in combination with RIF. However with RIF SLN only 19.5 % degradation was observed in the presence of INH and only 12 % in the presence of INH SLN. The INH entrapped in SLN degraded by only 3 % in the presence of RIF. RIF SLN exhibited 70 % release in phosphate buffer pH 6.8 after 9 days, whereas INH SLN exhibited 62 % release in phosphate buffer pH 6.8 after 24 hours. Although this study did not report the *in vitro* release behaviour of the API from the SLN in pH 1.2 solutions, it demonstrated that SLN may be used to prevent the interaction of RIF and INH. In addition sustained delivery of API could be achieved and may be important for the prevention of concentration dependent degradation of RIF and improvement of bioavailability.

1.10 CONCLUSIONS

The treatment of TB often requires the use of multi-drug regimens, which are often presented as FDC dosage forms. The recommended first line treatment of TB includes RIF, INH, PZA and ETH. INH, PZA and ETH are BCS class I compounds whereas RIF is a class II compound that exhibits high permeability and low solubility [29]. RIF has a solubility of 2.5 mg/mL, a log P of 1.086 and a pKa of 4.96 ± 0.7 and has been reported to exhibit poor bioavailability from fixed and single dose technologies [26]. The poor bioavailability of RIF has been attributed to changes in crystal structure, interaction with excipients and other API, degradation in gastrointestinal tract contents, pH dependent solubility, variable absorption and metabolism. The poor bioavailability of RIF has been cited as a potential cause of poor therapeutic outcomes, including treatment failure and development of resistance [125]. Chemotherapeutic treatment of TB is complicated by the need for multi-drug regimens dosed over extended periods, non-adherence and the development of MDR-TB strains [26], although patient non-adherence is the single most common cause for TB treatment failure [70].

The rapid degradation of RIF in acidic media in the presence of INH [63, 65, 116, 117] is a major concern in respect of treatment outcomes. The mechanism of the interaction involves a reaction between 3-FRSV, a degradation product of RIF, and INH, leading to the formation of isonicotinyl hydrazone of 3-FRSV [116, 117], resulting in a decrease of almost 33 % in the mean stomach residence time of RIF [65]. A similar decrease in the bioavailability of RIF has been reported in an *in vivo* human study in which the bioavailability of a combination formulation of RIF and INH was compared to that of a reference formulation containing RIF only [70]. The results suggest that a solution to prevent the in situ loss and decrease in bioavailability of RIF from FDC lies in the redesign of current FDC products that include RIF and INH, to release the API in different segments of the GIT. This approach requires that one of the two API should be included in an enteric coated technology to ensure that one API is released in the stomach and the other in the proximal region of the small intestine [131].

As INH has a pKa of 2, it is prominently protonated in acidic solution, and exhibits low permeability in the stomach and is primarily absorbed from the small intestine [131]. Therefore it is preferred that INH be formulated for site-specific release in the small intestine. Since RIF is

primarily absorbed from the stomach and duodenum and exhibits greater solubility in acidic pH [131] it is best delivered from a technology developed for site-specific release in the stomach.

The main objective of these studies was to design, develop, formulate, manufacture and assess a novel delivery technology system for gastroretentive delivery of RIF and enteric delivery of INH in order to overcome the challenge related to the stability of RIF in the acidic contents of the stomach when dosed simultaneously with INH in FDC dosage forms for the treatment of TB.

CHAPTER TWO

PHYSICAL CHARACTERISATION OF ISONIAZID AND RIFAMPICIN

2.0 INTRODUCTION

The properties of active pharmaceutical ingredients (API) and drug delivery technologies are critical for ensuring that an API is delivered at a rate and extent suitable for absorption [132]. The API and raw materials used for the manufacture of medicines often exhibit differences in physical characteristics such as polymorphism, particle size distribution and crystal habits, amongst others, which are often supplier dependent [132]. These characteristics have the potential to affect the stability and/or availability of an API and should be monitored and controlled as far as possible [132]. It is for these reasons that physical characterisation of API has become extremely important during pharmaceutical dosage form development. Variability in the solid state properties of an API can imply differences in the physical and chemical properties of that API which may interfere with the therapeutic properties and manufacturing processes of the compounds [133]. The characterisation of the physical properties of API using appropriate techniques is therefore an essential prerequisite for the development of quality pharmaceutical dosage forms [134]. Regulatory agencies such as the Food and Drug Administration (FDA) have outlined specific requirements for examining the characteristics of an API in the solid state [135]. Numerous analytical techniques have been used for the characterisation of API in the solid state including X-ray diffraction (XRD), thermal analysis, spectroscopic and microscopic techniques [136]. In these studies, ultraviolet-visible spectroscopy (UV-VIS), powder X-ray diffraction (PXRD), Fourier-transform infrared spectroscopy (FTIR), Raman spectroscopy, Nuclear Magnetic Resonance (NMR) spectroscopy, Differential Scanning Calorimetry (DSC) and Scanning Electron Microscopy (SEM) were used to characterise the RIF and INH purchased.

2.1 EXPERIMENTAL

2.1.1 Materials, Apparatus and Methods

2.1.1.1 UV-VIS Spectroscopy

Solutions of RIF and INH (20 µg/mL) were scanned using a Lambda 25 UV/VIS spectrometer (Perkin Elmer®, Ayer Rajah, Singapore) over the wavelength range 200 nm - 700 nm to

determine the wavelength of maximum absorption (λ_{max}) for each molecule, with methanol and water used as solvent references for the RIF and INH, respectively.

2.1.1.2 FTIR Spectroscopy

A Spectrum 100 FT-IR ATR Spectrophotometer (Perkin Elmer® Ltd, Beaconsfield, England) was used to generate infra-red absorption spectra for RIF and INH. A small amount of each powder was placed on a diamond crystal and a force of approximately 100 N applied to the powder prior to analysis over the wavelength number range 4000 - 650 cm^{-1} using a resolution of 4 cm^{-1}.

2.1.1.3 FT Raman Spectroscopy

A Bruker Ram II (Billerica, Massachusetts, USA) fitted with a liquid nitrogen germanium detector and CaF_2 beam splitter was used to record the FT Raman spectra for each compound. Powder samples were packed into a small stainless steel cup and irradiated with a YAG laser beam at 1064 nm and 20 mW power to generate Raman scattered light. The FT Raman spectra were recorded over the wavenumber range 4000 cm^{-1} to 50 cm^{-1}.

2.1.1.4 Powder X-Ray Diffraction

The powder XRD diffractograms for INH and RIF were developed with the aid of a Bruker D8 Discover diffractometer (Billerica, Massachusetts, USA) equipped with a proportional counter, using Cu-Ka radiation of 1.5405 Å, a nickel filter at 30 KV and a general current of 40 mA. Diffractograms were collected in the 2θ range 10° to 60° at a scanning rate of 1.5° min^{-1} and a filter time constant of 0.38 sec per step with a slit width of 6.0 mm. Samples were placed on a silicon wafer slide and diffraction data evaluated using evaluation curve fitting (Eva) software (Billerica, Massachusetts, USA). Baseline correction was performed for each diffraction pattern by subtracting a spline function fitted to a curved background.

2.1.1.5 Nuclear Magnetic Resonance Spectroscopy

NMR spectra were generated in dimethyl sulfoxide (DMSO) using a Bruker 400 MHz NMR spectrometer (Bruker, Rheinstetten, Germany) in the ^2H lock mode. Chemical shifts were reported in parts per million (ppm) relative to tetra-methylsilane (TMS) which was used as a

standard for all proton (^{1}H) and carbon-13 (^{13}C) NMR measurements. Each sample was transferred to a 178 mm ultra-precision glass ASTM Type 1 Class A borosilicate thin-walled NMR tube (Norell, Inc. Mays Landing, NJ). The tubes are specifically designed for use in high resolution NMR studies and are recommended for chemical structure determination, low and high temperature applications and low temperature sample storage. The ^{1}H (400 MHz) and ^{13}C (100 MHz) NMR spectra were generated using standard pulse sequences. Experimental data were generated at 298 K and a frequency of 400.13MHz with a 5mm probe and *p*w (90◦) = 12.6 s. All chemical shifts were recorded and analysed using MestRe-C and MestRe Nova software (Bruker, Rheinstetten, Germany).

2.1.1.6 Differential Scanning Calorimetry

DSC thermograms were generated using a Model DSC 7 (Perkin Elmer®, Norwalk, USA) with the aid of a TAC 7 PC control unit (Perkin Elmer®, Norwalk, USA) at 10 °C/min heating rate and a nitrogen flow rate of 20 mL/min. Approximately 3.0 – 5.0 mg of each sample to be tested was weighed directly into an aluminium DSC pan and hermetically sealed prior to analysis, after which they were heated at a constant rate using an empty pan as a reference. The samples were placed directly onto a micro hot stage DSC and thermograms were generated at temperatures between 30 and 450 °C. The temperature of the DSC microscopy cell was monitored using a central processor and each thermogram generated during the heating process was collected using 10 scans with a resolution of 4 cm^{-1}. The DSC cell was calibrated for temperature and enthalpy with Indium (m.p. 156.6 °C; ΔH_{fus} = 28.4 j/g) and the resultant data were analysed using Pyris™ Manager Software (Perkin Elmer®, Norwalk, USA).

2.1.1.7 Scanning Electron Microscopy

Particle size and shape were evaluated using a Vega® Scanning Electron Microscope (Tescan, Vega LMU, Czechoslovakia Republic). Separate samples of RIF and INH powder were dusted onto a graphite plate and then sputter coated with gold for 10 minutes under vacuum. The samples were visualised using SEM at an accelerated voltage of 20 KV.

2.2 RESULTS AND DISCUSSION

2.2.1 UV-VIS Spectroscopy

INH exhibited maximum UV absorption at a wavelength of 262 nm, whereas RIF exhibited maximum absorption at 239 nm. A lambda maximum of 254 nm [137] and 334 nm [138] for RIF and 261 nm [137] for INH have been reported [137]. The UV-Vis spectra for RIF and INH are shown in Figure 2.1.

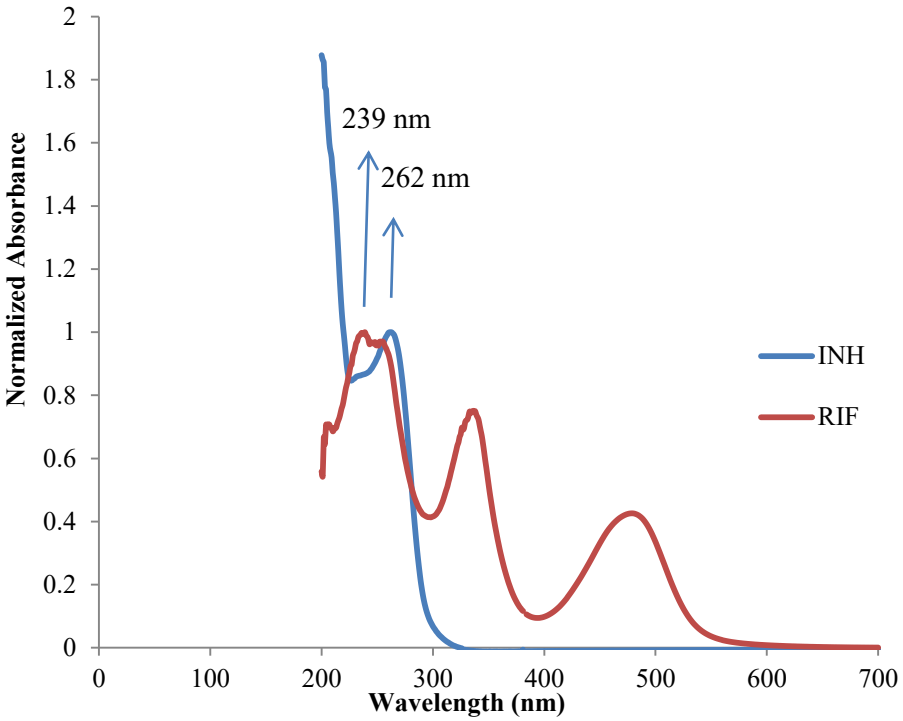

Figure 2. 1 UV-VIS absorption spectra for RIF in methanol and INH in water.

2.2.2 FTIR Spectroscopy

2.2.2.1 Isoniazid (INH)

The FTIR absorption spectrum for INH is shown in Figure 2.2. The spectrum exhibits frequency vibrations at 1410.91 cm^{-1}, 1549.20 cm^{-1}, 1661.68 cm^{-1} and 1331.18 cm^{-1}, corresponding to –C=C symmetrical, C=N symmetrical, C=O and –C-N stretching respectively. Other recorded

frequency vibrations and their respective functional group assignments in comparison to those reported in the literature [139] are summarised in Table 2.1. The FTIR results confirm the presence of key functional groups of INH and therefore confirm the identity of the API purchased as INH.

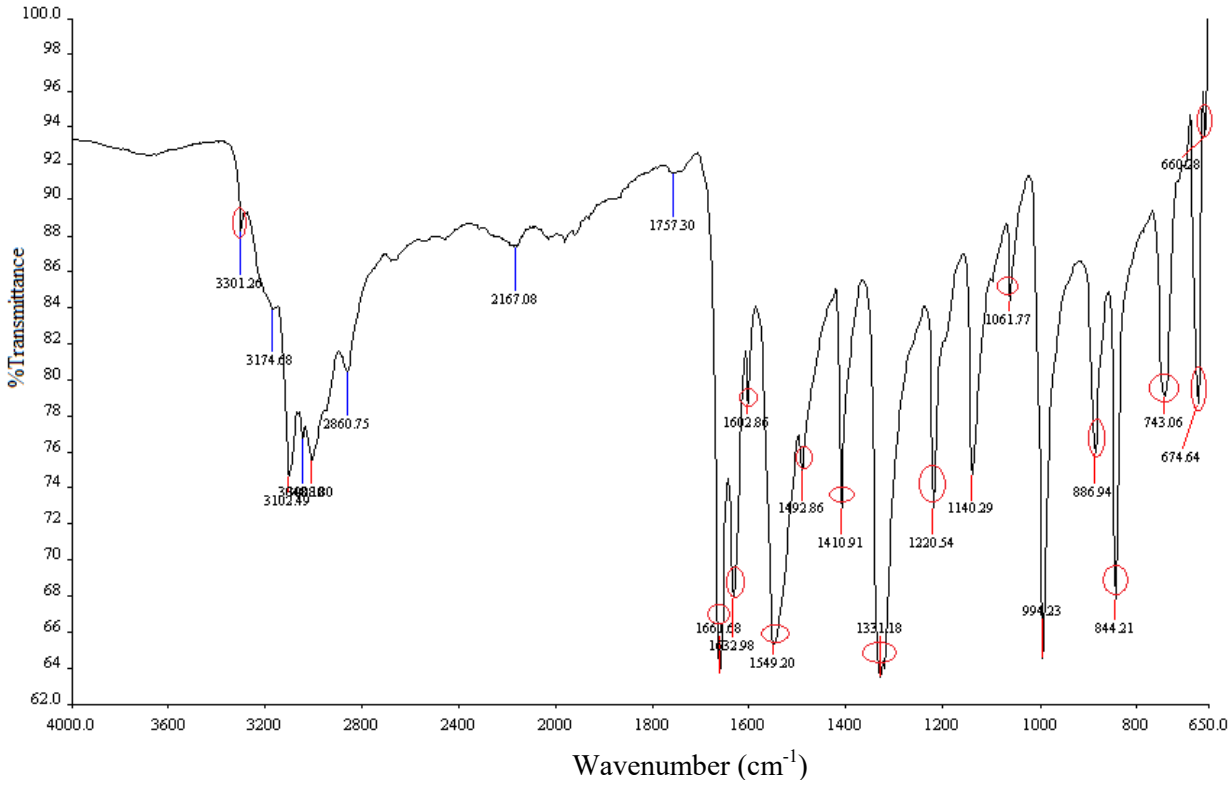

Figure 2. 2 FTIR absorption spectrum of INH.

Table 2. 1 FTIR frequency assignments for INH.

Experimental wavenumber cm^{-1}	Literature wavenumber cm^{-1} [139]	Functional Group Assignment
1410.91	1412	C=C symmetrical stretching
1549.20	1556	C=N symmetrical stretching
2855.69	2863	C-H symmetrical stretching
1061.77	1061	C-C stretching
1661.68	1667	C=O stretching
1331.18	1334	C-N stretching
3296.20	3303	N-H stretching
844.21	845	Ring C-C-H symmetrical bending
660.28	660	-C-C-C bending
674.64	674	-C-C=O bending
1492.86	1492	-C-N-H bending
1602.86	1602	Ring C=C asymmetrical stretching
1632.98	1635	Ring C=N asymmetric stretching
743.06	745	Ring C-C-C asymmetrical bending
1061.77	1020	Ring C-C-N asymmetrical bending
1220.54	1220	Ring C-C-H asymmetrical bending
886.94	888	Ring C-N-C bending

2.2.2.2 Rifampicin (RIF)

The FTIR absorption spectrum for RIF is shown in Figure 2.3. The spectrum exhibited frequency vibrations at 29.36.66 cm^{-1}, 1733.38 cm^{-1}, 1676.40 cm^{-1} and 1428.17 cm^{-1}, corresponding to $-CH_3$, -C=O acetyl , -C=C and -C-N stretching respectively. Other recorded frequency vibrations and functional group assignments in comparison to what has been reported in the literature [140] are listed in Table 2.2.

Table 2. 2 FTIR frequency assignments for RIF.

Experimental wavenumber cm^{-1}	**Literature wavenumber cm^{-1} [140]**	**Functional Group Assignment**
2936.66	2930	$-CH_3$ stretching
2875.94	2820	$-CH_3O$ asymmetric stretching
1710.55, 1733.38	1715, 1730	-C=O acetyl stretching
1676.40	1670	-C=N asymmetric bending
1562.96	1570	-C=C- stretching
1428.17	1400	-C-N- stretching
3582.8 – 3444.8 broad peak	3500-300	-OH stretching
1237.57 – 1019.91	1255-1020	-C-O-C- acetyl group

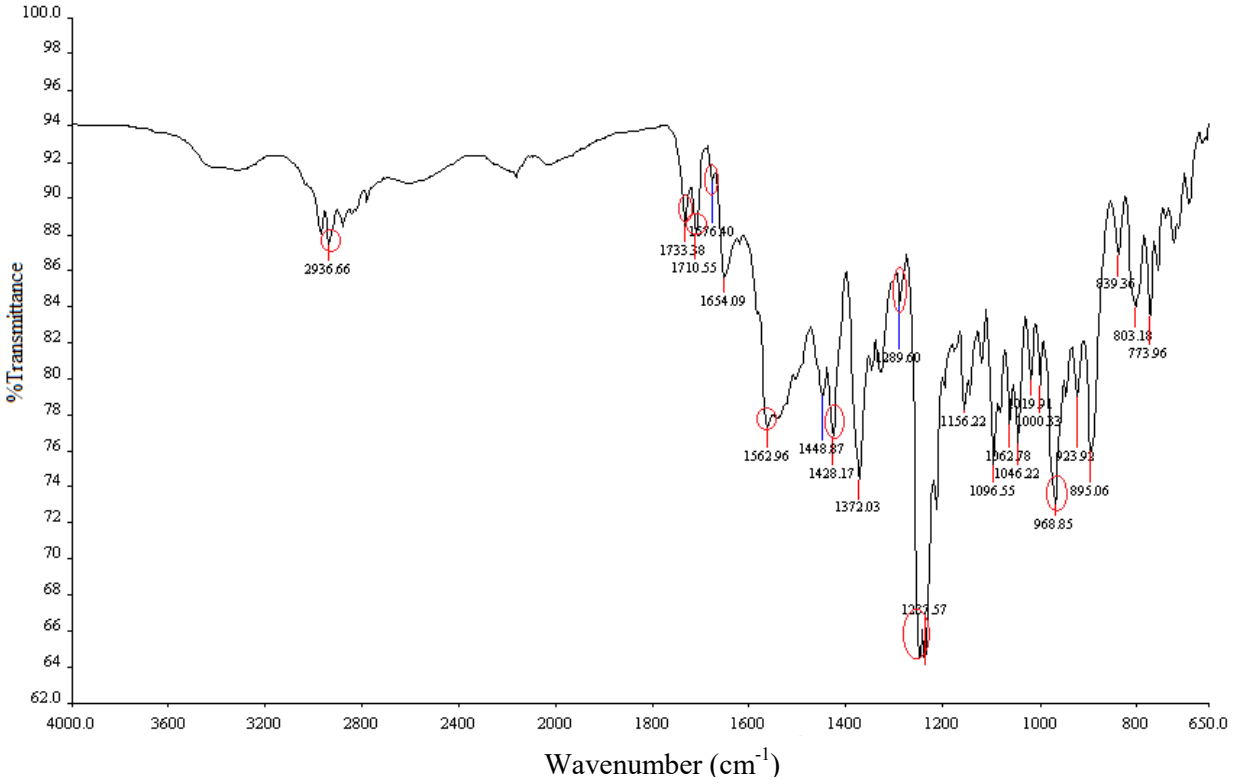

Figure 2. 3 FTIR absorption spectrum for RIF.

Infrared absorption spectra data for the amorphous, polymorph forms I and II of RIF have been reported [141] and are summarised in Table 2.3.

Table 2. 3 FTIR wavenumber assignments for three forms of RIF [141].

	Wavenumber cm^{-1}				
Sample	**Ansa -OH**	**Furanone C=O**	**Acetyl C=O**	**Amide C=O**	**N-CH_3**
Form I	3480	1644	1725	1567	2878
Form II	3565-3150	1734	1712	1566	2883
Amorphous	3565-3150	1644	1723	1567	2877

A double peak assigned to a furanone and acetyl C=O functionality at a wavenumber of 1734 and 1712 cm^{-1} is characteristic of form II of RIF and is appropriate for qualitative assessment.

Based on this criterion it was confirmed that the sample analysed was form II RIF due to presence of a double peak at wavenumbers 1733.38 and 1710.55 cm^{-1}. The presence of this significant functional group in the FTIR absorption spectrum of this material confirms the presence of RIF.

2.2.3 FT Raman spectroscopy

2.2.3.1 Isoniazid (INH)

The FT Raman absorption spectrum of INH is shown in Figure 2.4. A Raman spectrum of INH with active vibrations at wavenumbers of 1334 cm^{-1}, 1604 cm^{-1} and 670 cm^{-1} has been reported [142] and correspond to C-N stretching, ring C=C asymmetric stretching and C-C-C bending respectively. Vibrations recorded at 1330.99 cm^{-1}, 1602.90 cm^{-1} and 665.67 cm^{-1} are closely similar to reported data and confirm the identity of INH. Other frequency vibrations of different functional groups compared to what has been reported in the literature [139] are summarised in Table 2.4.

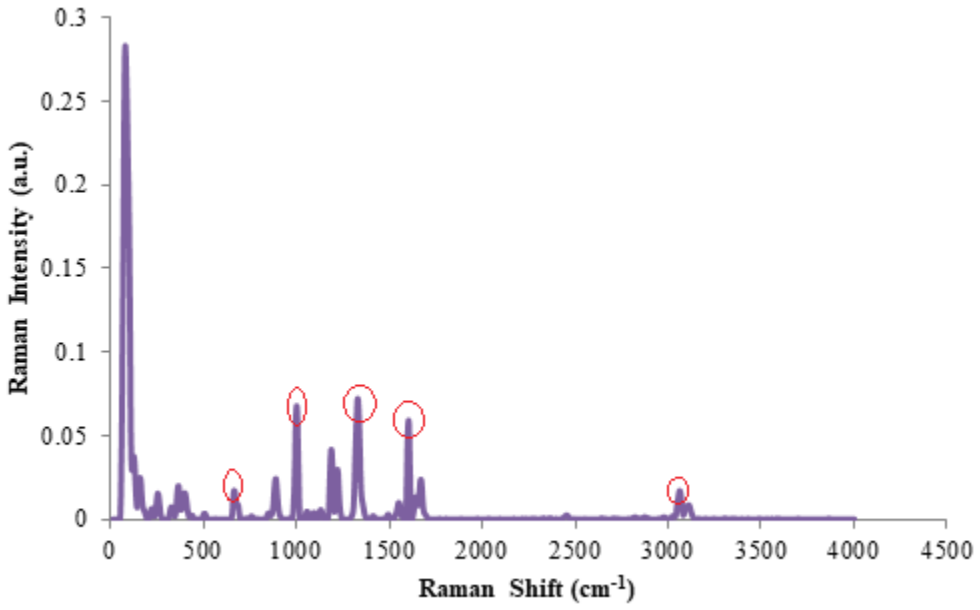

Figure 2. 4 FT Raman absorption spectrum of INH.

Table 2. 4 FT Raman shift signals and assignments for INH.

Experimental FT Raman Shifts cm^{-1}	Reported FT Raman Shifts cm^{-1} [139]	Functional Group Assignment
1410.054	1410	Ring C=C symmetrical stretching
1550.832	1551	Ring C=N symmetrical stretching
1057.146	1057	C-C stretching
1668.467	1669	C=O stretching
1330.987	1331	C-N stretching
3300.132	3300	N-H stretching
1130.428	1131	N-NH_2 stretching
503.6787	504	Ring C-C-C symmetrical bending
848.8727	849	Ring C-C-H symmetric bending
665.6692	666	-C-C-C bending
681.0968	682	-C-C=O bending
1552.76	1551	H-N-N bending
1494.906	1495	C-N-H bending
1602.9	1602	Ring C=C asymmetrical stretching
1641.469	1642	Ring C=N Asymmetric stretching
2979.919	2980	C-H asymmetrical stretching
3064.671	3065	C-H asymmetrical stretching
750.5213	750	Ring C-C-C asymmetric bending
1001.221	1002	Ring C-C-N asymmetric bending
1186.353	1187	Ring C-C-H asymmetric bending
1219.137	1219	Ring C-C-H asymmetric bending
887.7419	887	Ring C-N-C bending

2.2.3.2 Rifampicin (RIF)

The FT Raman absorption spectrum of RIF is shown in Figure 2.5 and the shifts of different functional groups assigned on the basis of FTIR frequency reported in literature [140] are summarized in Table 2.5. Raman spectroscopy of RIF exhibits intense bands around wavenumbers of 1300 cm^{-1} to 1400 cm^{-1} and at 1570 cm^{-1} [143, 144], which are attributed to an acetyl group, –C-N , and –C=C stretching, respectively. FT Raman spectroscopy also confirmed the presence of other significant functional groups and the identity of RIF.

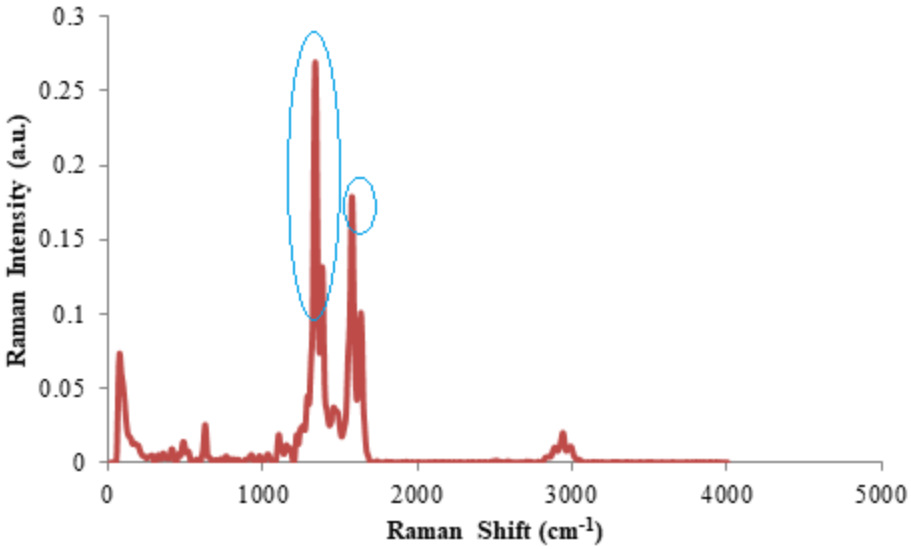

Figure 2. 5 Raman absorption spectrum of RIF.

Table 2. 5 FT Raman shifts and signal assignments for RIF.

Experimental FT Raman Shifts cm^{-1}	Reported FT Raman Shifts cm^{-1} [139]	Functional Group Assignment
3024.17304	3500 - 3000	-OH stretching
1570.116	1570	-C=C- stretching
2929.679	2930	$-CH_3$ stretching
2819.757	2820	$-CH_3O$ asymmetric stretching
2800.472	2800	$-CH_3N$ stretching
1714.75, 1730.178	1715, 1730	-C=O acetyl stretching
1670.396	1670	-C=N asymmetric bending
1570.116	1570	-C=C stretching
1400.412	1400	-C-N stretching
1255.777 – 1020.505	1055 - 1020	-C-O-C acetyl group

2.2.4 Power X-Ray Diffraction

2.2.4.1 Isoniazid (INH)

The X-ray diffractogram generated for INH is shown in Figure 2.6 and reveals the presence of sharp high intensity peaks at 12.485°, 14.854°, 17.253°, 20.198°, 24.697°, 25.964° and 29.494° over the 2θ range, 10° to 60° confirming the highly crystalline nature of INH. The angles of

some peaks compared to literature data [145] are summarised in Table 2.6, and the close similarity observed further confirms the identity of the INH purchased. These data will be used as a reference to track changes, if any to, the crystalline structure that might occur during formulation development activities.

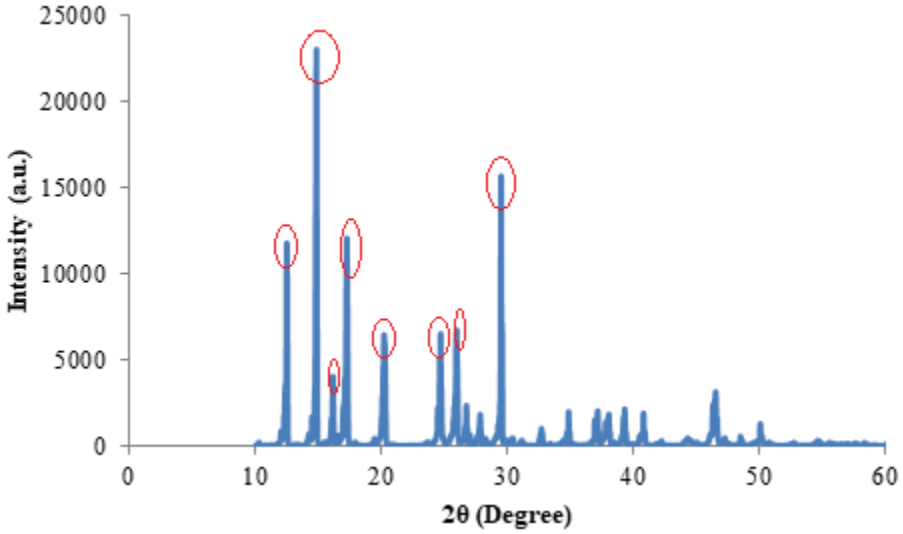

Figure 2. 6 Powder X-Ray diffractogram for INH.

Table 2. 6 Powder XRD data over the 2θ range, 10° - 60° for INH.

Experimental XRD data °	**Reported XRD data [145]** °
20.208	20.20
29.648	29.64
32.756	32.75
36.776	36.77
44.662	44.66
59.839	59.84

2.2.4.2 Rifampicin (RIF)

The X-ray diffractogram for RIF is shown in Figure 2.7 and reveals the presence of high intensity peaks at angles of 11.439°, 13.012°, 16.025°, 17.368°, 18.404°, 20.246°, 22.155° and 25.964° over the 2θ range, 10° to 60°, confirming the crystalline nature of RIF. Characteristic

peaks for the form II polymorph of RIF at 9.93° and 11.10° have been reported [141] and the presence of peaks at 10.125° and 11.439° indicate that the RIF purchased was the form II polymorph.

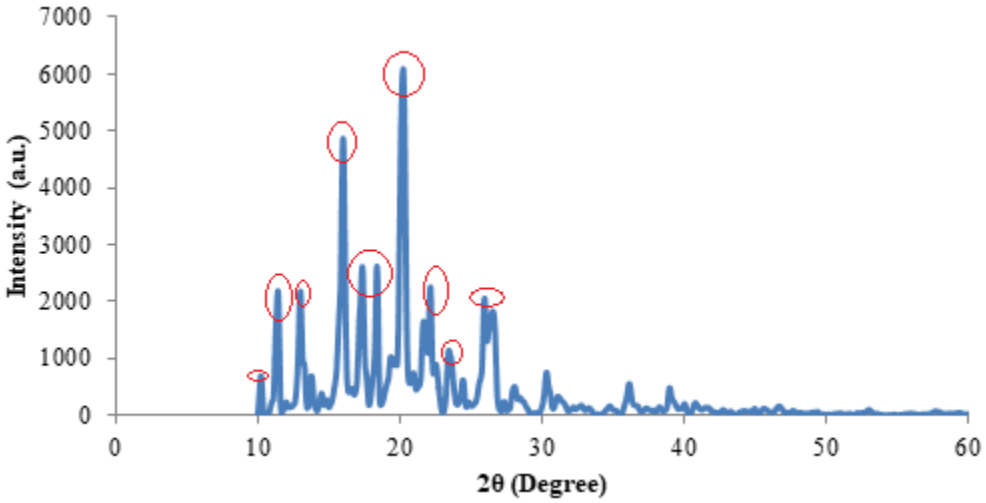

Figure 2. 7 Powder X-Ray diffractogram for RIF.

2.2.5 Differential Scanning Calorimetry

2.2.5.1 Isoniazid (INH)

The DSC thermogram generated for INH is shown in Figure 2.8 and revealed a single sharp endothermic peak between 172.08 °C and 177.19 °C with a ΔH = -360.0894 J/g and an additional peak at 175.35 °C corresponding to the melting point and range of melting for INH [146]. The sharp peak further confirms the crystalline nature of INH, and similar results have been reported elsewhere [147].

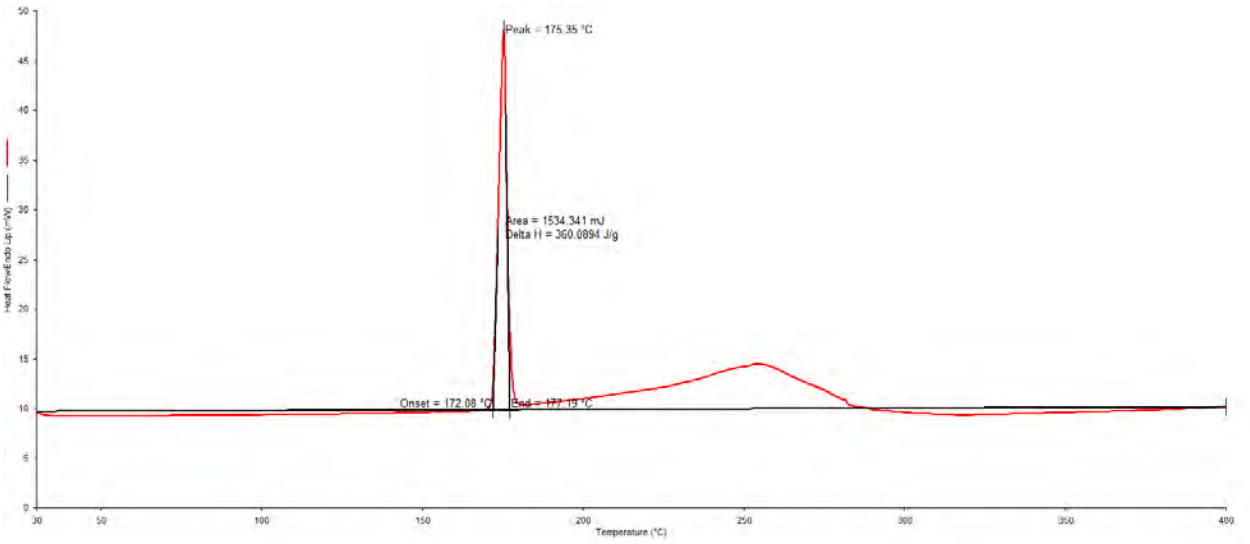

Figure 2. 8 DSC thermogram for INH over the temperature range 30 - 400 °C generated at a heating rate of 10 °C/min.

2.2.5.2 Rifampicin (RIF)

The DSC thermogram generated for RIF is shown in Figure 2.9 and was characterized by the presence of a melting endotherm between 180.27 °C – 208.97 °C, immediately followed by an exothermic recrystallisation event at between 208.97°C – 228.31°C, which is a characteristic of a solid-liquid-solid transition, and finally a decomposition event at between 248.63 °C – 298.61 °C. These results are similar to those previously reported [141] in which polymorph form II of RIF exhibited a melting endotherm at between 180°C - 197°C, immediately followed by recrystallisation to polymorph form I with an exothermic peak occurring at between 197 °C – 223 °C and ultimately decomposition between 247 °C – 266 °C. These data confirm that the RIF purchased was the form II polymorph.

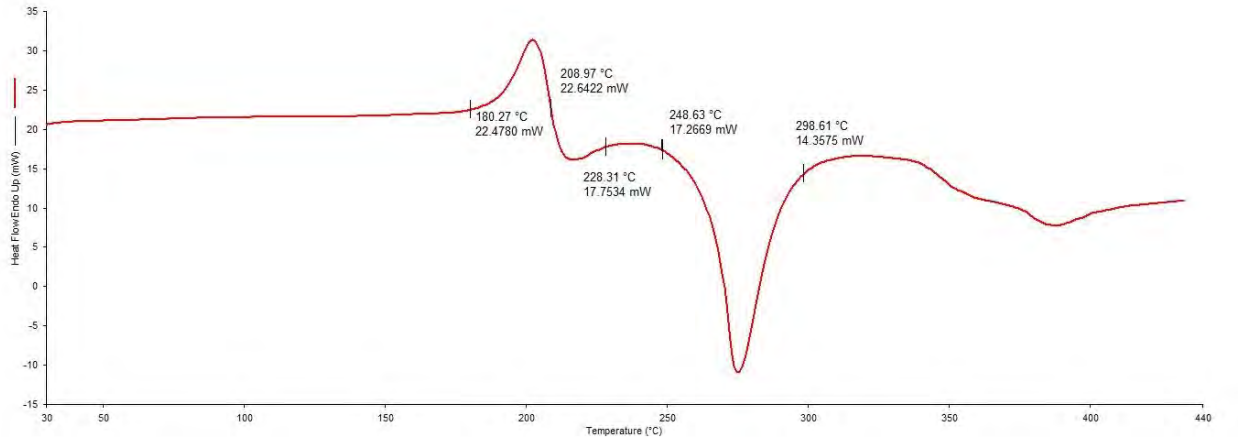

Figure 2. 9 DSC thermogram for RIF generated between 30 - 400°C at a heating rate of 10°C/min.

2.2.6 Nuclear Magnetic Resonance Spectroscopy

2.2.6.1 Isoniazid (INH)

The ^{1}H NMR and ^{13}C NMR spectra for INH are shown in Figures 2.10 and 2.11 respectively. The ^{1}H NMR spectrum shows proton shifts at 4.63 ppm, 7.73 and 8.70 ppm, and 10.10 ppm, corresponding to hydrazino H-(NH_2), aromatic protons and CO-NH_2 functionalities, respectively. The ^{13}C NMR shows carbon shifts at 163.81 ppm, 121.08 ppm, 140.14, and 150.29 corresponding to the carbon attached to the hydrazino group, C_4, C_3 and C_5, C_2 and C_6 respectively. The proton and carbon chemical shifts and group assignments generated experimentally compared to reported data [148-150] are listed in Table 2.7. The NMR spectra clearly identify the sample as INH.

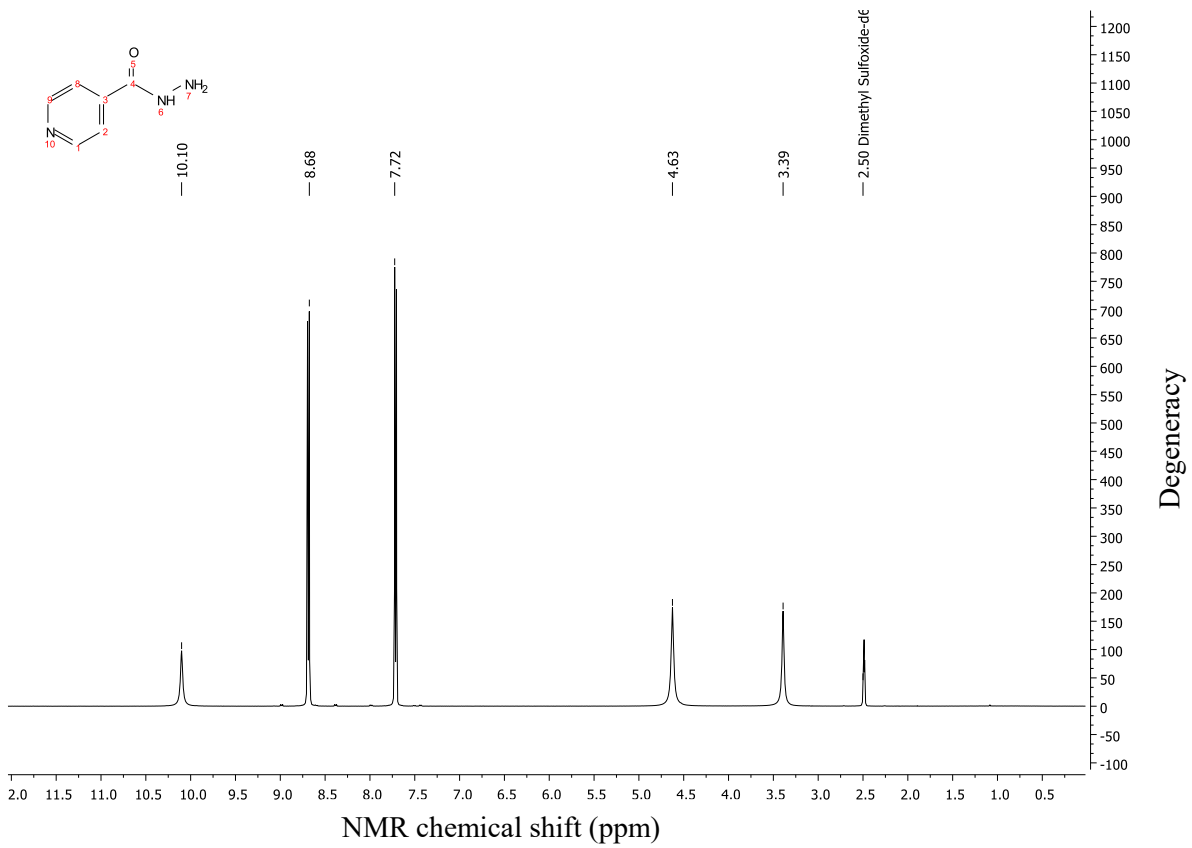

Figure 2. 10 ^{1}H NMR spectrum for INH

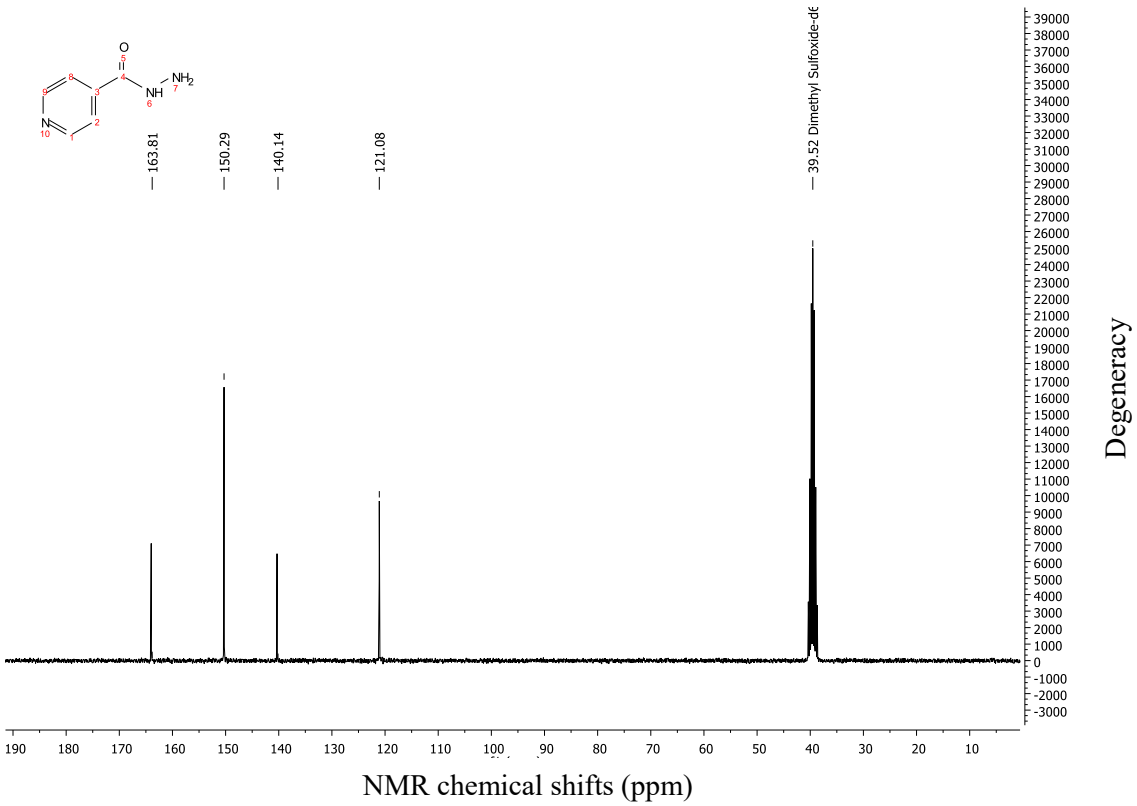

Figure 2. 11 ^{13}C NMR spectrum for INH.

Table 2. 7^{1}H NMR and ^{13}C NMR chemical shifts for INH.

^{1}H NMR data for INH		
Proton signal	**Literature data [148-150] ppm**	**Experimental data ppm**
Hydrazino H-(NH_2)	4.60 or 4.65	4.63
Aromatic H	7.72, 8.68	7.73, 8.70
CO-NH	10.15	10.10
^{13}C NMR data for INH		
Carbon signal	**Literature data [148-150] ppm**	**Experimental data ppm**
Hydrazino	164.4	163.81
Heteroaromatic C_4, C_3 and C_5, C_2 and C_6	121.6, 140.0, 150.0	121.08, 140.14, 150.29

2.2.6.2 Rifampicin (RIF)

The ^{1}H NMR and ^{13}C NMR spectra for RIF are shown in Figures 2.12 and 2.13 respectively. The ^{1}H NMR and ^{13}C chemical shifts and group assignments generated experimentally and compared to reported data [140, 151, 152] are listed in Tables 2.8 and 2.9.

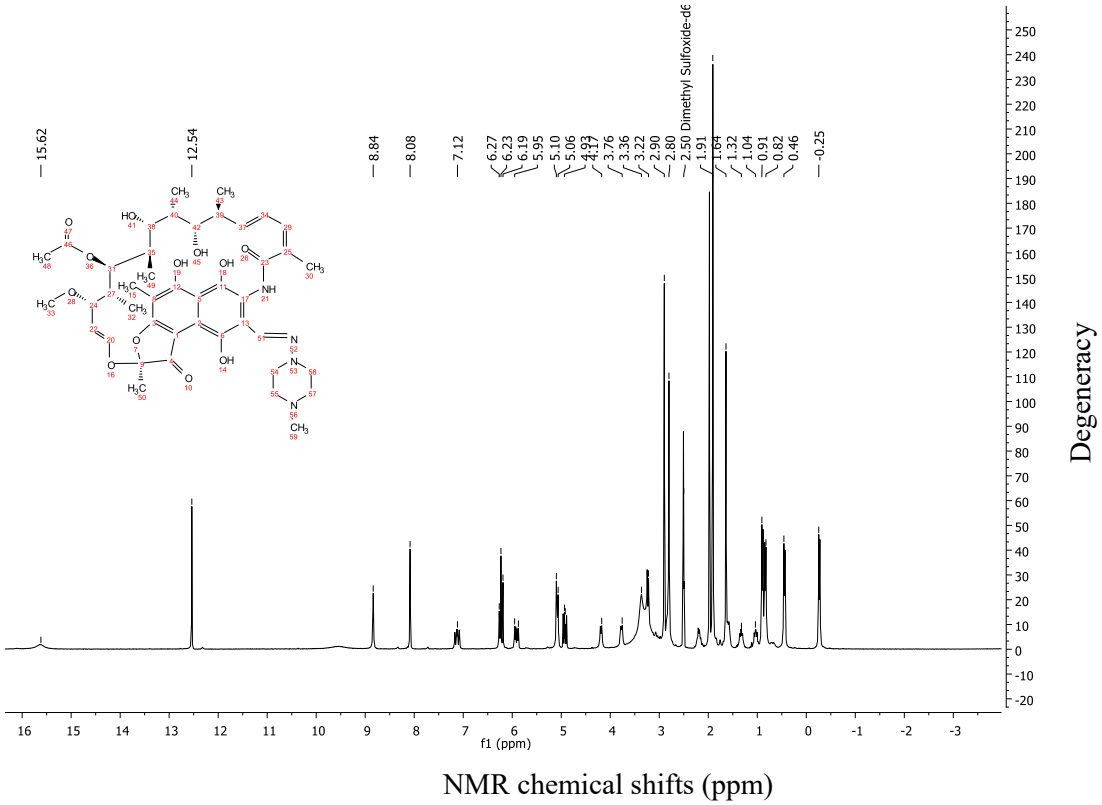

Figure 2. 12 ^{1}H NMR spectrum for RIF.

Table 2. 8[1]H NMR shifts and assignments for RIF.

^{1}H NMR data for RIF		
Proton signal	**Literature data [140, 151, 152] Ppm**	**Experimental data Ppm**
NH	13.17	13.17
CH=N	8.22	8.24
CH_2 (2‟ and 6‟)	2.9 – 3.3	2.9 – 3.22
N-CH_3	2.34	2.32
OH (1)	13.17	13.17
OH (4 and 8)	11.99	11.97
CH_3 (13)	1.81	1.79
CH_3 (14)	2.21	2.20
H (17)	6.39	6.39
H (18)	6.58	6.52
H (19)	5.93	5.95
H (20)	2.3 – 2.5	2.32 – 2.55
H (21)	3.77	3.77
OH (21 and 23)	3.0 – 3.1	3.03 – 3.15
H (22)	1.70	1.68
H (23)	3.04	3.03
H (24)	1.52	1.52
H (25)	4.95	4.95
H (26)	1.34	1.33
H (27)	3.47	3.47
H (28)	5.10	5.10
H (29)	6.20	6.21
CH_3 (30)	2.09	2.07
CH_3 (31)	0.88	0.88
CH_3 (32)	1.01	1.01
CH_3 (33)	0.59	0.59
CH_3 (34)	-0.32	-0.31
CH_3 (36)	2.06	2.07
CH_3 (37)	3.04	3.03

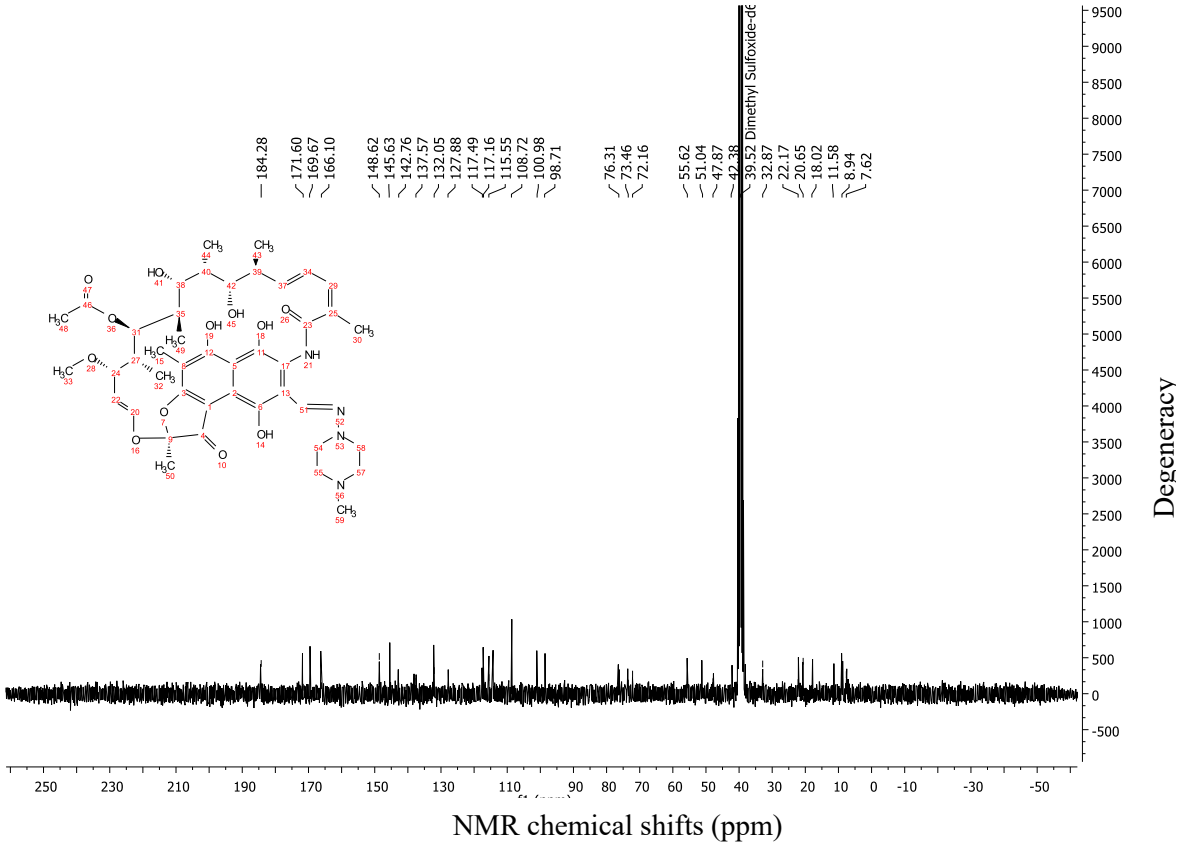

Figure 2. 13 ^{13}C NMR spectrum for RIF.

Table 2. 9 ^{13}C NMR chemical shifts and assignments for RIF.

^{13}C NMR data for RIF		
Carbon represented	**Literature Data (ppm) [140, 151, 152]**	**Experimental Data (ppm)**
1	138.5	138.72
2	120.3	120.58
3	110.7	111.01
4	147.9	148.09
5	117.8	118.04
6	174.4	174.62
7	106.0	106.21
8	169.2	169.36
9	112.8	112.97
10	104.5	104.69
11	195.3	195.56
12	108.7	108.9
13	21.4	21.58
14	7.5	7.66
15	169.6	169.8
16	129.3	129.49
17	135.1	135.25
18	123.1	123.33
19	142.7	142.81
20	38.5	38.69
21	70.6	70.74
22	32.3	33.50
24	37.4	37.62
25	74.3	74.55
26	39.4	39.62
28	118.5	118.76
29	142.6	142.81
30	20.7	20.87
31	17.8	17.97
32	10.8	11.0
33	8.4	8.57
34	8.9	9.02
35	172.0	172.19
36	20.7	20.87
37	57.0	57.21
1‟	134.6	134.55
4‟	50.0	50.40
5‟	53.8	54.08
7‟	53.8	54.08
8‟	50.0	50.4

Some differences in the ^{13}C NMR peak shifts for the two polymorphs of RIF, viz. forms I and II have been observed [141]. The IR absorbance spectrum for form I indicate the C_{23} hydroxyl functionality is not hydrogen bonded to an acetyl carbonyl group and hence the C_{36} methyl (acetyl) resonance singlet is displayed [141]. For form II the C_{36} methyl functionality displays a doublet that may be due to long range dipolar coupling to nitrogen, as in form II the C_{23} hydroxyl is bonded to an acetyl group and that acetyl group is in a suitable conformation that permits coupling with the nitrogen atom of the NH functionality. Other differences observed in the ^{13}C NMR spectra of the two polymorphs included the amide carbonyl at C_{15} that exhibits a doublet for form I and a singlet for form II, the C_{23} carbon atom showing a singlet for form I and doublet for form II, the C_{37} methyl functionality showing a singlet for form I and multiplet for form II and the C_{24} carbon exhibiting a singlet for form I and a doublet for form II. These differences in splitting patterns for the two polymorphs are attributed to long-range coupling or crystallographic splitting. The aromatic carbons C_1–C_{10} reveal a similar pattern, indicating that the naphthalene ring has a similar conformation in both forms. The peaks observed for forms I and II are summarised in Table 2.10.

Table 2. 10 Observed differences in ^{13}C NMR peaks between RIF form I and form II.

	^{13}C NMR data for RIF	
Carbon represented	**Form I (ppm)**	**Form II (ppm)**
C_1 and C_8	150	153
C_4	147	150
C_6	171	-
C_{11}	198	196, 187, 191
C_{15}	174	
C_6 and C_{15}	-	172
C_{35}	178	176

The upfield shift for the peak due to the C_{11} atom and the downfield shift due to the C_4 atom for form II indicate a hydrogen bond interaction between the furanone and hydroxyl functional groups located at position C_4. Similarly, this effect was also observed at position C_{15} with a C_1 and C_8 interaction. The experimental results 195.56 ppm (C_{11}) and 172.19 ppm (C_6 and C_{15}) were used to identify RIF as the form II polymorph [141], although the value of 147.9 ppm (C_4) may indicate the presence of trace amounts of the form I polymorph.

2.2.7 Scanning Electron Microscopy

SEM images revealing the particle shape of INH and RIF are shown in Figure 2.14, and it is clear that INH is a predominantly cylindrical-tabular crystal (I) and RIF predominantly an almost cuboidal-rectangular crystal (II).

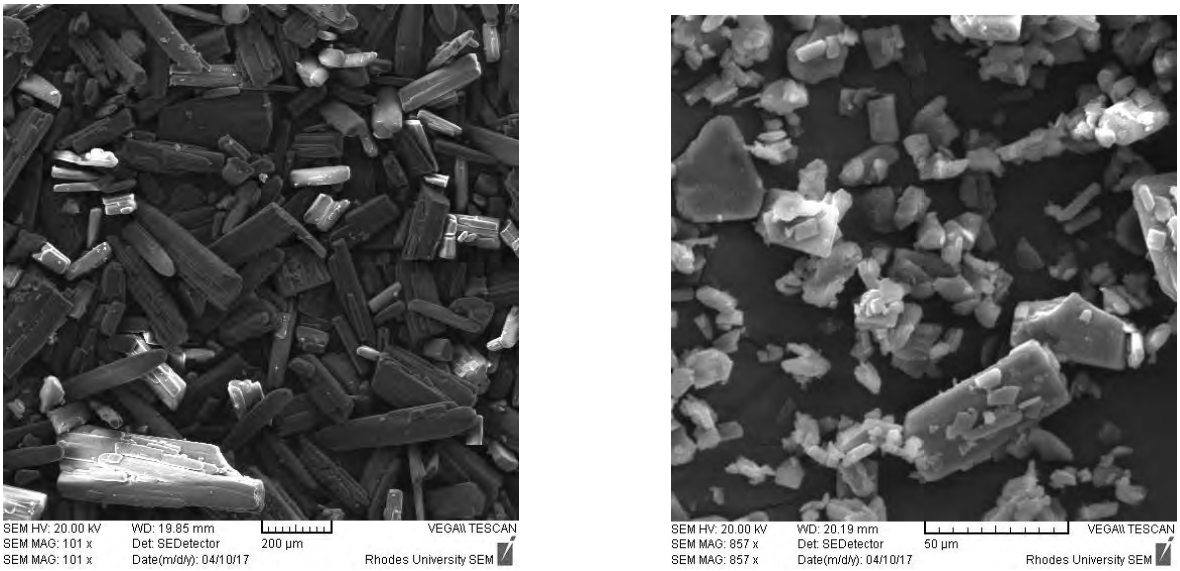

I II

Figure 2. 14 SEM images of INH (I) and RIF (II) generated at magnification of 101x and 857x respectively.

2.3 CONCLUSIONS

INH and RIF raw materials have been successfully identified and characterised using spectroscopic, thermal and microscopic analysis. The studies revealed that the two compounds are crystalline and exhibit distinct characteristic sharp peaks in XRD diffractograms and DSC thermograms. The DSC thermogram, ^{13}C NMR and FTIR results identified RIF as the form II polymorph, but there are no significant biopharmaceutical differences between the RIF polymorphs, and this information was used for identification purposes only. The results generated are baseline data that will be used to monitor changes that may occur when RIF and INH are subjected to formulation development, dosage form manufacture and characterisation studies of a FDC technology designed to deliver both compounds.

CHAPTER THREE

APPLICATION OF A BOX BEHNKEN DESIGN FOR THE DEVELOPMENT OF A RP-HPLC METHOD FOR THE SIMULTANEOUS ANALYSIS OF RIFAMPICIN, ISONIAZID AND PYRAZINAMIDE

3.0 INTRODUCTION

The traditional approach of changing one variable at a time involves performing a large number of experiments and does not permit identification of multiple interacting parameters when attempting to optimize a system [153]. Experimental design methodologies have the advantage of enabling simultaneous screening of multiple factors that affect a response, in addition to estimating the magnitude of possible interactions [153-155].

Response Surface Methodology (RSM) has been successfully used to develop and optimize HPLC methods [153-163] and generally involves the performance of experiments in the region of a best known solution, fitting the experimental data to a response model and then optimization of the estimated response model to establish the best possible conditions for ensuring the required response(s) [154, 155, 159, 162]. RSM refers to statistical and mathematical techniques used for the development of an adequate and functional relationship between a response of interest, Y, and a number of associated control or input variables viz., X_1, X_2,….X_k. In general the relationship is unknown but can be approximated using a low-degree polynomial model such as that reported as Equation 3.1.

$$Y = f'(X)\,\beta + \epsilon \qquad \text{Equation 3.1}$$

Where,

$X = X_1, X_2, \ldots..X_k$,
$f'(X)$ = vector function of elements that consist of powers and cross-products of powers for $X_1, X_2, \ldots..X_k$ up to a degree denoted $d \geq 1$,
β = vector of unknown constant coefficients referred to as parameters, and
ϵ = random experimental error assumed to have a mean of zero.

This assumption is conditioned on the basis that Equation 3.1 is an adequate representation of the response under investigation. The value of the product f'(X) β represents the mean response and is the expected value for Y, denoted μ(X) [162, 163].

Two important models common in RSM are special cases represented by Equation 3.2 for a first degree model (d = 1) and Equation 3.3 for a second degree model (d=2).

$$Y = \beta_0 + \sum_{i=1}^{k} \beta i \, Xi + \epsilon \qquad \text{Equation 3.2}$$

$$Y = \beta_0 + \sum_{i=1}^{k} \beta i \, Xi + \sum_{i<j} \sum \beta ij \, XiXj + \sum_{i=1}^{k} \beta ii \, Xi^2 + \epsilon \qquad \text{Equation 3.3}$$

Where,

β_0, β_i, β_{ii} and β_{ij} = coefficients of constants,
X_i and X_j = coded independent factors, and
ϵ = random experimental error assumed to have a mean of zero.

There are three reasons for considering the model represented by Equation 3.2. The first one is to establish an approximate relationship between Y and X_1, X_2, ..., X_k that can be used to predict values for a response for any given set of input variables. The second one is to determine through hypothesis testing the significance of the factors denoted X_1, X_2, …, X_k, and the third one is to determine the optimum settings for X_1, X_2, …, Xk that result in a maximum or minimum response over the range of interest investigated. In order to achieve the objectives, a series of experiments, n, should be performed initially, and for each experiment a response Y is identified for the specific input variable and associated value thereof. The totality of these settings constitutes a response surface design [164].

The selection of an appropriate design is crucial for any response surface approach since the quality of a prediction as measured by the extent of variance is dependent on the design of the experimental matrix used. Furthermore, the determination of an optimum response requires identification of an optimum value in a defined region of the experimental matrix [162-165].

The first and second degree models are most frequently used when approximating polynomial simulations for classic RSM approaches. The most commonly used first order designs include 2^k factorial, where k is the number of input variables, Plackett-Burman (PBD) and simplex designs. For a 2^k factorial design each variable is measured at two levels that are coded as 1 and -1

corresponding to high and low levels for each variable investigated. In this case, the number of experimental runs, n, is 2^k provided no single design point is replicated [162-164]. Plackett-Burman designs permit evaluation of two levels for each of the variables investigated, k, but requires fewer experimental runs, particularly if k is large, and therefore this design is economical to implement. A PBD design is possible only if n is a multiple of 4 and therefore can only be used when the number of variables investigated is 3, 7, 11, 15, … etc. [164].

A simplex design is less frequently used since the actual settings in the design are, in general, difficult to achieve in experimental situations [163, 164].

The most commonly used second degree order design are 3^k factorial, Central Composite (CCD) and Box-Behnken (BBD) designs. A 3^k factorial design evaluates all combinations of all levels of variable(s), k viz., three levels for each. For equally spaced levels, -1, 0, and 1 are the coded values used. The number of experiments to be undertaken is 3^k, and can be very large when many variables are to be investigated [163, 164].

The Central Composite Design (CCD) is the most popular of all second-order designs and evaluates three levels, viz. a complete or fraction of a 2^k factorial design with factor levels coded as -1 and 1 and defined as factorial points, an axial component of 2k points in order to select two points located on the axis of each variable at a distance α from the centre of the design (the point at the origin of coordinates) and n_0 centre points [162-165].

A CCD is generated by augmentation of a first order or 2^k factorial model with additional experimental runs including 2^k axial points in addition to n_0 centre point replicates. A CCD is developed in a manner consistent with the sequential nature of a response surface investigation, commencing with a first-order design, fitting to a first degree model followed by addition of design points to ensure a fit to a second order model.

A first order design is useful in the preliminary phases of an investigation to generate initial information about the response of a system and to assess the importance of factors for a specific experiment. Additional experimental runs are then used to generate information that can be used to identify and achieve the optimum operating conditions for input variables using a second degree model [164].

The Box-Behnken Design (BBD) permits evaluation of three levels for each factor under investigation and is comprised of a particular subset of factorial combinations from a 3^k factorial design. A BBD is popular for industrial research since it is economical and requires only three levels viz., -1, 0 and 1 to be investigated for each input factor [163-165]. A five-factor, three-level BBD experimental design was used in this study since it is suitable for exploring quadratic response surfaces and produces a second order polynomial model to facilitate achievement of an optimum locale using fewer experiments than normally required [166]. This design requires the use of four centre points and a set of inputs that lie at the midpoint of each edge of a multi-dimensional cube that defines the region under investigation. The ultimate model constructed can be mathematically represented using Equation 3.4.

$$-Y = a_0 + a_1x_1 + a_2x_2 + a_3x_3 + a_4x_1x_2 + a_5x_2x_3 + a_6x_1x_3 + a_7x_1^2 + a_8x_2^2 + a_9x_3^2 + E$$

Equation 3.4

Where,

a_0 - a_9 = regression coefficients,
X_1, x_2 and x_3 = input factors studied,
Y = a response associated with each factor and level combination, and
E = an error term.

Several analytical methods for the identification and quantitation of rifampicin (RIF), isoniazid (INH) and pyrazinamide (PZA), either alone or in combination, have been reported. They are listed in Table 3.1. Most of the methods make use of gradient elution or complex mobile phase compositions and exhibit long analysis times. The use of Artificial Neural Networks (ANN) for the optimization of a reversed-phase HPLC method for the simultaneous analysis of the three API has been reported [167]. To date no method for the separation of all three API has made use of gradient elution and been optimized with the aid of RSM.

Table 3. 1 Published analytical methods for the analysis of rifampicin, isoniazid and pyrazinamide.

Sample Matrix	Technique	Mobile Phase	Column	Internal standard	Wavelength nm	Flow rate and method ml/min	Reference
PZA tablets/bulk	RP-HPLC	10 mM Phosphate buffer (pH4.4): Acetonitrile 80:20 % v/v	Hypersil® C_8 250 x 4.6 mm, 3.5 µm	-	269	Isocratic, 1.0	[168]
3FDC tablets/ DM/SGF	RP-HPLC	10mM Phosphate buffer containing 0.05%w/v tetramethyammonium chloride (pH 3.5): methanol	Supelcosil® LC-18 DB C_{18} 250 x 4.6 mm, 5 µm	-	254	Gradient, 1.0	[169]
4FDC tablets	RP-HPLC	Acetonitrile and 8mM phosphate buffer (pH 6.8)	Phenomenex® Luna C_{18} 250 x 4.6 mm, 5 µm	-	210	Gradient, 1.0	[170]
3FDC tablets	RP-HPLC	Acetonitrile and tetrabutyl ammonium hydroxide (pH = 3.10) 42.5: 57.5 v/v	Waters® µbondapak C_{18} 250 x 4.6 mm, 10 µm	-	260	Isocratic, 1.0	[167]
3FDC tablets	HPTLC	Ethyl acetate: ammonia: ethyl alcohol: cyclohexane 20:9:4.5:5 v/v/v	Glass baked silica gel 60 F 254 plates	-	440, 275	-	[171]
3FDC tablets	RP-HPLC	Methanol and tetrabutyl ammonium hydroxide (pH 3.0) 80:20 v/v	ODS-CN bonded phase column	Clofazimine	265	Isocratic, 1.5	[172]
Human plasma	RP-HPLC	Acetonitrile and trifluoroacetic acid 80:10 v/v	RP- C_8 250 x 4.6 mm, 10 µm	-	-	Isocratic, 1.0	[173]
2FDC capsule	RP-HPLC	Methanol: 10 mM disodium hydrogen phosphate (pH = 4.6) 70:30 v/v.	Waters® µbondapak C_{18} 300 x 390 mm	-	254	Isocratic, 1.2	[174]
Human plasma	GC-MS	Nitrogen gas	15 m **x** 0.32 mm i.d.. glass capillary column	benzaldehyde isonicotinoyl hydrazone	-	-	[175]
Human plasma/CSF	HPLC/MS/ MS	Acetonitrile containing 0.01 % v/v formic acid: 15 mM ammonium formate buffer (pH 5)	Hypersil®-Hypurity C_{18} 150 x 2.1 mm, 5 µm	Rifapentine	_	-	[176]
2FDC	RP-HPLC	Methanol: 20 mM disodium hydrogen	RP-C_{18} 250 x 4.6 mm, 5µm	-	254	Isocratic, 1.0	[177]

suspension		orthophosphate 75:25 v/v					
Plasma/CSF	RP-HPLC	Acetonitrile: water: triethylamine (70:30:0.4 v/v) containing 5mM heptanesulphonic acid	Waters® µbondapak 300 x 3.9 mm, 10 µm linked to a pre-column	Phenelzine	320	Isocratic, 1.0	[178]
Human plasma	RP-HPLC	Acetonitrile: 5 mM Phosphate buffer (pH 3.5)	Waters® C_8 30 x 4. 6 mm, 30 µm Spherisorb®, 250 x 4.6 mmi.d., S5 ODS2 linked to a C_8 pre-column 50 x 4.6 mm i.d., 30 µm	-	248, 280	Gradient, 2.0	[179]
Human serum	RP-HPLC	Acetonitrile: 10 mM potassium dihydrogen phosphate buffer (pH 3.5)	RP- Hibar, LiChrosorb C_8 250 x 4.6 mm, 5 pm linked to a Cs pre-column 30 pm, 50 **x** 4.6 mm	p-acetamidobenzoic acid	215	Gradient, 1.5	[180]
Human plasma	RP-HPLC	0.2 M Phosphate buffer (pH 7.4): methanol (96.8: 3.2 v/v)	Supelcosil® LC DB C_{18} 150 x 4.6 mm, 5µm.	Nicotinamide	268	Isocratic, 1.5	[181]

3.1 EXPERIMENTAL

3.1.1 Materials and Methods

3.1.1.1 HPLC Instrumentation

The HPLC system consisted of a Model 2695 Waters® Alliance separation module equipped with a solvent delivery module, auto-sampler, online degasser and a Model 2998 PDA Detector (Milford, MA, USA) set at 254, 265 and 268 nm for RIF, INH and PZA, respectively. Data acquisition, processing and reporting were achieved using Waters® Empower 3 software (Milford, MA, USA). Separation was achieved using a Phenomenex® C_{18} (2) 5 µm, 250 x 4.6 mm i.d. stationary phase (Separations, Johannesburg, South Africa).

3.1.1.2 Chemicals and Reagents

All chemicals used were at least of analytical reagent grade. RIF, INH and PZA analytical standards were purchased from Sigma Aldrich® (St Louis, MI, USA). Chromatographic grade methanol 215 far UV Romil-SPS™ Super Purity Solvent was purchased from Romil® (Waterbeach, Cambridge, UK) and was used for all analyses. Zidovudine (AZT), the internal standard, and ascorbic acid were purchased from Sigma Aldrich® (St Louis, MI, USA). HPLC grade water for the preparation of mobile phase and analyte solutions was purified with a Milli-RO® water purification system (Millipore®, MA, USA) fitted with two ion-exchange cartridges, an Organex-Q® and a Super-C carbon cartridge prior to filtration through a 0.22µm Millipak® stack filter (Millipore®, MA, USA).

3.1.1.3 Preparation of stock solutions

Standard stock solutions of RIF, INH and PZA (1 mg/mL) and the internal standard AZT (300 µg/mL) were prepared by accurately weighing 100 mg of each compound and 30 mg AZT, using a top-loading analytical balance (Mettler® Model AE163, Zurich, Switzerland) and transferring into separate 100 mL A grade volumetric flasks. Approximately 50 mL methanol was added to RIF and AZT and approximately 50 mL HPLC grade water was added to INH and PZA. The solutions were sonicated for 10 minutes using a Branson® B12 sonicator (Shelton, CN, USA). The RIF solution was made to volume with a 40µg/mL ascorbic acid solution and 30 mL

methanol. The AZT solution was made to volume with methanol and the INH and PZA solutions were made to volume with HPLC grade water. The standard stock solutions were diluted serially to produce solutions of concentration of 5, 10, 20, 60, 100, 150 and 200 µg/mL for RIF, 1, 5, 10, 40, 60, 80 and 100 µg/mL for INH and 1, 5, 20, 50, 100, 350 and 500 µg/mL for PZA. A 0.4 mL aliquot of each of the RIF and INH solutions and 0.2 mL of the PZA solution were transferred into an amber HPLC vial in addition to 0.2 mL of the AZT solution and the mixture vortexed in the vial prior to HPLC analysis.

3.1.1.4 Preparation of mobile phase

The mobile phase was comprised of methanol and 10 mM potassium dihydrogen orthophosphate buffer. The pH was monitored using a Model GLP 21 Crison pH meter (Crison Instruments, Johannesburg, South Africa) and adjusted to pH 3.0 using a 0.1M solution of NaOH. The buffer was filtered through a 0.45 µm Millipore® HVLP membrane filter (Millipore®, Bedford, MA, USA) and degassed under vacuum using an Eyela® Aspirator A-2S vacuum pump (Rikakikai® Co. Ltd, Tokyo, Japan) prior to use. The buffer and methanol were transferred to separate 1000 mL Scott® Duran bottles (Scott® Duran GmbH, Wertheim, Germany) for use.

3.1.1.5 Experimental Design for Optimisation of the Separation

Forty-six experiments were conducted using the conditions described in Table 3.2.

Table 3. 2 Experimental factors and levels used for the Box-Behnken Design.

Factor	Level		
Independent/Input variables	[-1]	[0]	[+1]
10 mM phosphate buffer pH = A	3	5	7
Start % Methanol (%MeOH) = B	3	4	5
End % Methanol (%MeOH) = C	75	80	85
Curve profile = D	8	6	4
Gradient duration (min) = E	3	4	5
Output responses			
Retention time (RT) of INH (min) = Y_1			
Retention time (RT) of PZA (min) = Y_2			
Retention time (RT) of AZT = Y_3			
Retention time (RT) of RIF = Y_4			
Capacity factor (CF) for INH = Y_5			
Resolution factor (RF) for AZT and RIF = Y_6			
Tailing factor (TF) for INH = Y_7			
Tailing factor (TF) for PZA = Y_8			
Tailing factor (TF) for RIF = Y_9			

The levels for the input variables, viz. buffer pH, % methanol content at the start, % methanol content at the end, gradient curve profile and gradient duration were based on results of preliminary studies. The use of different buffer molarities of 10 mM, 20 mM and 30 mM did not result in significant changes in chromatographic responses, viz. retention time, capacity factor and peak symmetry, and indicated that any of these buffer molarities could be used. The curve profile relates to the rate of change of percent content of an eluent as a function of time. Some HPLC systems permit different curve profiles, however the most common type is linear: the change in percent content of an eluent as a function of time follows a linear relationship. Convex- type curves are generated when changes of the eluting strength are more rapid at the beginning and slower at the end of a separation, whilst the opposite effect can be achieved when a concave curve profile is desired [182]. The different gradient curve profiles possible are shown in Figure 3.1. The effects of the three types of curve profiles, viz. linear, convex and concave, on retention times of APIs, capacity factor of INH, tailing factors of peaks of APIs and the resolution factor between AZT and RIF, were investigated in these studies.

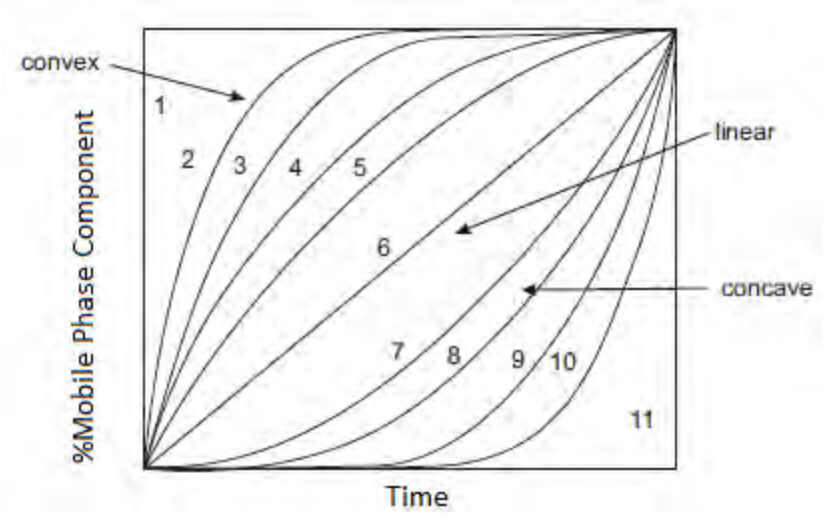

Figure 3. 1 Gradient curve profiles available on the Alliance HPLC system [182].

The retention time of RIF, INH, AZT and PZA, capacity factor for INH and resolution factor for AZT and RIF were the responses monitored using predefined constraints. Design® Expert Version 7.0.1, (Stat-Ease Inc., Minneapolis, MN, USA) statistical software was used to analyse the data. Fisher‟s statistical test for analysis of variance (ANOVA) for the response surface quadratic model was used to determine the significance of each factor. The effectiveness of the model was evaluated by computing the F-ratio, coefficient of variation (% C.V), adequate precision, adjusted R^2 and predicted R^2 and predicted residual error sum of squares (PRESS). The experiments were conducted in a randomized manner and in replicate (n=3) to minimise bias.

3.1.2 Chromatographic system suitability

3.1.2.1 Theoretical number of plates (N)

The theoretical number of plates of a column is an important characteristic, as the parameter defines the ability of a stationary phase to produce sharp, narrow peaks in addition to the achievement of good resolution between band pairs with associated low values for selectivity [183].

The theoretical number of plates can be calculated using any of Equations 3.6, 3.7 or 3.8.

$$N = 5.54 \frac{RT}{W1/2}$$ Equation 3.6

$$N = 16(\frac{RT}{W})^{1/2}$$ Equation 3.7

$$N = \frac{3500L\ (cm)}{Dp(\mu m)}$$ Equation 3.8

Where,

N = the number of theoretical plates,
RT = the retention time of the test peak,
$W_{1/2}$ = the peak width at half peak height of the test peak,
W = the peak width at the baseline of the test peak,
L = the length of the column (cm), and
Dp = the particle diameter µm.

Columns of 15 cm or 25 cm length with particles 5 µm in diameter are preferred as a starting point for an analysis, as they generally have sufficiently large values of N and close overlapping peaks can be readily recognized. Although short columns packed with particles 3 µm in diameter are advantageous and ensure rapid separations, they are susceptible to sampling problems such as variation in amounts sampled, are operator dependent and are affected by instrumental band broadening effects [183].

3.1.2.2 Peak Asymmetry factor (Peak Tailing Factor)

Peak shape was determined by calculating the peak symmetry factor, A_s, using Equation 3.9.

$$As = \frac{B}{A}$$ Equation 3.9

Where,

B = the width of the peak to the tailing edge at 10% peak height, and

A = the width of the peak to the leading edge of the peak at 10% peak height.

Poor peak asymmetry may result in inaccurate plate number and resolution factor calculation, imprecise quantitation, poor resolution and no detection of minor bands located at or near the tail of the peak(s) of interest and/or poor retention time reproducibility. As a result peak shape is an important parameter to monitor during HPLC method development. Peak asymmetry factor values between 0.95 and 1.1 are considered good, however, column manufacturers specify A_s values of between 0.95 and 1.3 for new columns. Values of < 1.5 for samples of interest are generally considered acceptable. Exactly symmetrical peaks will produce an $A_s = 1.0$. The peak tailing factor (PTF) is another parameter that can be used to determine peak shape and can be calculated using Equation 3.10 [183].

$$\text{PTF} = \frac{\text{A+B}}{\text{2A}} \qquad \text{Equation 3.10}$$

Where,

A = the width of the peak at the leading edge at 5% peak height, and
B = the width of the peak at the tailing edge at 10% peak height.

3.1.2.3 Resolution factor

The resolution factor (RF) is an indication of the extent and quality of a separation between peaks of interest and is a function of the performance of a column, instrumental effects and/or variability in the conditions of a separation. A value for RF > 2.0 indicates adequate separation has been achieved, and a value < 1.5 is indicative of a poor separation [183]. The RF can be calculated using Equation 3.11.

$$\text{RF} = \frac{\text{RT2}-\text{RT1}}{0.5(\text{Tw1}-\text{Tw2})} \qquad \text{Equation 3.11}$$

Where,

RT1 = retention time of first peak,

RT2 = retention time of second peak,
Tw1 = width of the first peak at baseline, and
Tw2 = width of the second peak at baseline.

3.1.2.4 Capacity Factor

The capacity factor (K′) is an indicator of the length of retention of a sample on a column relative to peaks eluting in the void volume. The value of K′ indicates the rate at which an analyte migrates through a column [183]. Variables influencing K′ include mobile phase composition, age of column and the temperature at which the operating system is used [183, 184]. The capacity factor can be calculated using Equation 3.12.

$$K' = \frac{V1-V0}{V0} \qquad \text{Equation 3.12}$$

Where,

V0 = Void volume of column
V1 = Retention volume of analyte (retention time x flow rate)

The void volume is calculated using the retention time of a molecule such as uracil that is not retained on a column. A capacity factor ≥ 2.0 is desirable and conditions resulting in K′ < 2.0 are considered unacceptable [183, 184].

3.1.3 Method Validation

The method was validated for linearity, precision, accuracy and specificity using the ICH Q2A Guideline [185].

3.1.3.1 Linearity

Linearity was determined by calculating the least squares linear regression line for a series of calibration standards. The least squares linear regression correlation coefficient (R^2) is a measure of the linearity of a set of data and the closer the value is to unity, the more linear the relationship between independent and dependent variables [183, 186, 187].

3.1.3.2 Precision

The ICH guideline recommends that precision studies be performed at three different levels, viz. repeatability or intra-assay precision, intermediate or inter-day precision and reproducibility or the precision observed in different laboratories [185]. Precision was determined at two levels: repeatability and intermediate precision. Precision was established following analysis of calibration curve samples and the tolerance for percent relative standard deviation (% RSD) was set at ± 5% for these studies. FDA recommends that precision at selected concentration levels should not exceed 15 % RSD or 20 % RSD in the case of the LOQ for analysis of biological samples such as urine or plasma [187].

3.1.3.2.1 Repeatability

Repeatability is an indication of the performance of an analytical method when used for the analysis of samples within a single laboratory undertaken over a short period of time by the same analyst using the same equipment [183, 187]. Repeatability was evaluated by determining the % RSD for the peak height ratio of API to IS for calibration curve samples (n = 5) analysed on a single day.

3.1.3.2.2 Intermediate precision

Intermediate precision is the precision of a method when it is applied to the analysis of samples within a laboratory on different days, or by different analysts using the same or different equipment [183, 186, 187]. Intermediate precision was evaluated following analysis by establishing the % RSD for peak height ratio of API to IS for calibration curve samples on three consecutive days.

3.1.3.2.3 Reproducibility

Reproducibility is the precision of the analytical method when it is intended to be applied to the analysis of samples in a different laboratory and is important for inter-laboratory crossover studies [188, 189]. If intermediate precision is evaluated the determination of reproducibility is normally not required [188]. Reproducibility studies where not performed as intermediate precision was established and the analytical method was intended to be used by one analyst in the same laboratory using the same instruments for the entire duration of the study.

3.1.3.3 Accuracy

Accuracy of the analytical method was established following analysis of samples to which a known amount of API was added. The ICH guidelines recommend that accuracy be established using a minimum of nine determinations and a minimum of three concentrations covering the specific calibration range to be used when applying the analytical method [185]. Three samples representing low, medium and high concentrations within the concentration range were analysed in replicate (n=5).

Accuracy results were reported as % recovery, % RSD and % Bias. The % Bias was calculated using Equation 3.5 and is the difference between a calculated mean value and the true value. The parameter is used to assess the influence of an analyst on the performance of an analytical method and is designed to measure the effectiveness of sample preparation prior to analysis [190].

$$\% \text{ Bias} = \frac{\text{True value} - \text{measured value}}{\text{True value}} \text{ x } 100 \qquad \text{Equation 3.5}$$

3.1.3.4 Limits of Quantitation (LOQ) and Detection (LOD)

The LOD is the lowest level of an analyte that produces a measurable response that is detectable but cannot be quantitated as an exact value with the necessary precision and accuracy [190, 191]. Four techniques have been described to establish the LOQ and LOD of analytical methods. These include establishing the lowest concentration at which the % RSD is ≤ 5 %, plotting standard deviation versus concentration, calculating a confidence interval for a best-fit line and using the signal to noise ratio of the responses [191].

The LOQ was established using a specification for precision of ≤ 5 % and by convention the LOD was then established as 30 % of the LOQ concentration [191]. Five concentrations were evaluated initially as the potential LOQ.

3.1.3.5 Specificity

The specificity of an analytical method can be established by forced degradation studies [192, 193]. To ensure that the method developed is stability-indicating, and to monitor the appearance of degradation products during formulation and product development activities, stress studies in acidic, basic and oxidative conditions were undertaken.

3.1.3.5.1 Oxidative degradation

Approximately 100 mg RIF, INH and PZA was transferred into separate 100 mL A-grade volumetric flasks. RIF was dissolved in 40 mL methanol and INH and PZA in HPLC grade water. The solutions were sonicated for 10 minutes after which they were made to volume with 30 % v/v H_2O_2 (Allied Drug Company Ltd, Durban, KwaZulu-Natal, South Africa). The samples were stored at room temperature (22 °C) for 72 hours. Aliquots (0.4 mL for RIF and INH and 0.2 mL for PZA) were harvested and 0.2 mL internal standard solution added, after which the solution was agitated using a Vortex-2 Genie mixer (Scientific Industries Inc., New York, USA) for 60 seconds at a frequency of 350 Hz, prior to HPLC analysis.

3.1.3.5.2 Acid degradation

Approximately 100 mg RIF, INH and PZA was transferred into separate 100 ml A-grade volumetric flasks. RIF was dissolved in 40 mL methanol and INH and PZA in HPLC grade water and the solution sonicated for 10 minutes, after which it was made to volume with 0.1 M HCl (Allied Drug Company Ltd, Durban, KwaZulu-Natal, South Africa). Samples were stored at 22 °C for 72 hours. Aliquots (0.4 mL for RIF and INH and 0.2 mL for PZA) were harvested and 0.2 mL internal standard solution added, after which the solution was agitated using a Vortex-2 Genie mixer (Scientific Industries Inc., New York, USA) for 60 seconds at a frequency of 350 Hz, prior to HPLC analysis.

3.1.3.5.3 Alkali degradation

Approximately 100 mg RIF, INH and PZA was transferred into separate 100 ml A-grade volumetric flasks. RIF was dissolved in 40 mL methanol and INH and PZA in HPLC grade water and the solution sonicated for 10 minutes, after which it was made to volume with 0.1 M NaOH (Allied Drug Company Ltd, Durban, KwaZulu-Natal, South Africa). Samples were stored

at 22 °C for 72 hours. Aliquots (0.4 mL for RIF and INH and 0.2 mL for PZA) were harvested and 0.2 mL internal standard solution added, after which the solution was agitated using a Vortex-2 Genie mixer (Scientific Industries Inc., New York, USA) for 60 seconds at a frequency of 350 Hz, prior to HPLC analysis.

3.1.3.6 Assay

The applicability of the HPLC method for the analysis of RIF, INH and PZA in dosage forms was established by testing commercially available dosage forms summarised in Table 3.3.

Table 3. 3 Tested commercially available dosage forms

Product	API	Source
Winthrop® isoniazid 100 mg tablets	INH	Sanofi-Aventis®, Midrand, South Africa
BE-TABS® isoniazid 100 mg tablets	INH	Ranbaxy® Laboratories, Roodepoort, South Africa
Sandoz® pyrazinamide 500 mg tablets	PZA	Sandoz Ltd, Johannesburg, South Africa
Pyrazide® 500 mg tablets	PZA	Sanofi-Aventis, Midrand, South Africa
Rimactane® 150 mg capsules	RIF	Sandoz Ltd, Johannesburg, South Africa
Rifafour® tablets	INH, PZA, RIF	Sanofi-Aventis, Midrand, South Africa

For tablets containing INH and PZA, twenty tablets were weighed and then ground using a mortar and pestle, and an amount equivalent to 200 mg each of INH and PZA transferred into separate 100 mL volumetric flasks. Approximately 20 mL HPLC grade water was added and the mixtures sonicated using a Branson B2 ultrasonicator (Cole-Parmer Instrument Company, Illinois, USA) for 5 minutes prior to making to the 100 mL volume with HPLC grade water. For capsules containing RIF, ten capsules were put in a 100 mL volumetric flask and 20 mL of 0.1 M HCl pH 1.2 added to ensure dissolution of the capsule shells. After dissolution of the capsule shells, 20 mL of methanol was added and the mixture sonicated for 5 minutes prior to making to the 100 mL volume with methanol. For tablets containing INH, PZA and RIF, twenty tablets were weighed and then ground using a mortar and pestle and an amount equivalent to 75 mg INH, 150 mg RIF and 400 mg PZA transferred into a 100 mL volumetric flask. Approximately 20 mL dimethyl sulfoxide (DMSO) was added and the mixture sonicated for 5 minutes prior to making to volume with DMSO. Solutions were filtered and 1 mL of each of the solutions

containing INH and PZA was separately transferred to a 20 mL volumetric flask and diluted to 20 mL with HPLC grade water. A 1 mL aliquot of the solution containing RIF was transferred to a 100 mL volumetric flask and diluted to 100 mL volume with methanol. A 1 mL aliquot of the solution containing INH, PZA and RIF was transferred to a 20 mL volumetric flask and diluted to 20 mL with DMSO. The diluted samples were agitated with a Vortex-2 Genie mixer for 60 seconds prior to injecting onto the HPLC system.

3.2 RESULTS AND DISCUSSION

3.2.1 Box Behnken Design

The responses monitored for the BBD are listed in Table 3.4 and represent the data generated from forty-six experiments. The data were evaluated using Design Expert® software by fitting to a number of quadratic models. The adequacy of each model for describing the relationship between independent input variables and outputs or responses was determined and ANOVA was used to identify significant parameters. By way of example the evaluation of model adequacy and ANOVA for retention time and capacity factor for INH will be discussed in detail while the rest of the data for all output analyses are summarised in Appendix 1A. Relationships that had been established were subsequently used to derive and predict a set of input parameters that would, if implemented, yield the responses required for this analytical system.

Table 3. 4 Measured responses for experiments conducted following the Box Behnken Design.

Run	Buffer pH	Start % MeOH	End% MeOH	Curve Profile	Gradient Duration	RT INH Y_1 min	RT PZA Y_2 min	RT AZT Y_3 min	RT RIF Y_4 min	CF INH Y_5	RF AZT/RIF Y_6	TF INH Y_7	TF PZA Y_8	TF RIF Y_9
1	5	3	85	6	4	6.07	8.591	11.408	12.198	3.157	4.849	1.046	1.063	1.450
2	5	4	80	6	4	5.426	7.467	11.467	12.465	2.716	5.512	1.073	1.08	1.256
3	3	4	80	6	5	2.982	7.545	11.466	12.338	1.042	7.606	0.927	1.078	1.726
4	5	4	80	4	5	5.321	7.447	11.161	12.369	2.645	5.392	1.056	1.066	1.265
5	7	4	80	6	3	5.64	7.793	11.467	12.85	2.863	11.489	1.063	1.091	1.903
6	5	5	80	6	5	4.75	6.599	11.46	12.541	2.253	5.869	1.08	1.091	1.347
7	5	5	80	6	3	5.077	7.008	11.477	12.528	2.477	5.803	1.106	1.113	1.891
8	7	4	80	6	5	5.438	7.717	11.455	12.693	2.725	11.126	1.058	1.085	1.891
9	5	4	80	6	4	5.509	7.717	11.463	12.49	2.773	6.273	1.083	1.086	1.246
10	7	5	80	6	4	5.049	6.928	11.457	12.679	2.458	10.917	1.083	1.088	1.810
11	5	3	75	6	4	6.149	8.69	11.549	13.169	3.211	6.831	1.062	1.071	1.263
12	7	4	80	4	4	5.565	7.697	11.146	12.371	2.812	10.925	1.064	1.071	1.725
13	5	4	80	8	5	5.218	7.38	11.65	12.646	2.573	6.15	1.079	1.093	1.433
14	3	4	80	8	4	3.068	7.596	11.641	12.504	1.102	7.453	0.945	1.091	1.848
15	5	5	80	8	4	4.936	6.802	11.625	12.741	2.381	5.801	1.098	1.098	1.396
16	5	4	80	6	4	5.628	7.866	11.462	12.539	2.855	6.363	1.069	1.067	1.568
17	5	4	75	6	5	5.451	7.661	11.543	13.382	2.734	8.408	1.074	1.084	1.171
18	5	3	80	6	5	6.015	8.546	11.477	12.619	3.12	6.372	1.049	1.058	1.549
19	5	4	80	4	3	5.65	7.897	11.163	12.255	2.87	6.086	1.076	1.077	1.600
20	5	3	80	6	3	6.328	8.95	11.474	12.593	3.334	5.873	1.059	1.071	1.469
21	3	4	75	6	4	3.096	7.794	11.553	12.835	1.121	1.034	0.951	1.084	1.753
22	3	3	80	6	4	3.28	8.826	11.465	12.349	1.246	7.749	0.934	1.072	1.793
23	5	3	80	8	4	6.218	8.793	11.657	12.858	3.259	5.594	1.053	1.065	1.283
24	3	5	80	6	4	2.905	6.912	11.452	12.337	0.99	7.753	0.95	1.104	1.853
25	7	4	75	6	4	5.627	7.796	11.541	13.815	2.815	15.961	1.079	1.093	1.429

26	3	4	85	6	4	3.063	7.693	11.407	12.039	1.098	5.751	0.942	1.094	1.821
27	5	3	80	4	4	6.23	8.796	11.181	12.359	3.267	5.843	1.065	1.08	1.311
28	5	4	75	4	4	5.563	7.737	11.247	12.871	2.81	5.497	1.137	1.121	1.213
29	3	4	80	4	4	3.092	7.735	11.184	12.017	1.117	6.956	1.057	1.11	1.965
30	3	4	80	6	3	3.109	7.773	11.499	12.335	1.1295	6.832	1.056	1.124	1.969
31	5	5	80	4	4	5.07	6.963	11.176	12.282	2.473	5.037	1.156	1.139	1.408
32	5	4	85	6	5	5.401	7.569	11.426	12.226	2.699	4.215	1.121	1.105	1.546
33	5	4	75	6	3	5.672	7.869	11.562	13.302	2.885	5.27	1.145	1.129	1.438
34	5	4	85	8	4	5.548	7.719	11.606	12.37	2.8	3.851	1.121	1.101	1.524
35	5	4	80	8	3	5.644	7.834	11.675	12.747	2.866	4.756	1.133	1.12	1.433
36	7	4	85	6	4	5.63	7.785	11.424	12.174	2.856	6.153	1.112	1.102	2.211
37	5	4	85	4	4	5.593	7.779	11.11	11.818	2.831	4.454	1.131	1.111	1.791
38	5	5	75	6	4	5.064	6.964	11.552	13.167	2.469	5.741	1.177	1.154	1.312
39	5	4	80	6	4	5.577	7.759	11.503	12.535	2.82	5.303	1.137	1.119	1.485
40	5	5	85	6	4	5.038	6.927	11.409	12.156	2.45	4.357	1.151	1.126	1.689
41	7	3	80	6	4	6.34	8.854	11.498	12.684	3.342	9.442	1.087	1.085	1.761
42	7	4	80	8	4	5.626	7.784	11.661	12.79	2.853	8.964	1.126	1.111	1.789
43	5	4	85	6	3	5.642	7.832	11.431	12.141	2.865	4.435	1.139	1.121	1.877
44	5	4	75	8	4	5.586	7.776	11.757	13.293	2.826	6.043	1.118	1.103	1.106
45	5	4	80	6	4	5.574	7.777	11.497	12.502	2.818	5.568	1.123	1.103	1.495
46	5	4	80	6	4	5.569	7.769	11.495	12.509	2.815	5.533	1.118	1.1	1.465

*Table 3.2 for definitions of parameters used in this table.

3.2.1.1 Evaluation of Model Adequacy for Retention Time of INH

The values of factors assessed to determine model adequacy are summarised in Table 3.5. The most important parameters for the evaluation of model adequacy are the model F-value, % C.V, adequate precision, PRESS and R^2 values. The importance of these parameters and their respective values are discussed in detail *vide infra*.

Table 3. 5 Summary of model adequacy parameters and associated values.

Parameter	Value	Parameter	Value
Std. Deviation	0.088	R-Squared	0.9959
Mean	5.13	Adjusted R-Squared	0.9926
% C.V	1.71	Predicted R-Squared	0.9849
PRESS	0.70	Adequate precision	61.399
F-Value	302.27		

3.2.1.1.1 Model F-Value

The model F-value is used to ascertain the utility of a model to which the data have been fitted, to and establish whether the model is the best fit for a set of data. The F-value is a ratio of explained and unexplained variability and the larger the value for F, the more useful a model [194, 195]. A model F-value of 302.27 was observed and represents a 0.01% chance that a model F-value this large may occur due to noise. This implies that the model is able to describe the fitted data accurately and permit navigation of the design space with only 0.01% chance of model inaccuracy.

3.2.1.1.2 Coefficient of Variation

The % C.V is a ratio of the standard deviation and mean and is indicative of the normalised measure of dispersion of a probability distribution [196, 197]. The % C.V is a measure of the reproducibility of a model; a value < 10% is desirable [198]. The observed value of 1.71 falls within this limit, and implying that the model is reproducible over time, which is important for any laboratory analytical procedure.

3.2.1.1.3 Adequate Precision

Adequate precision compares predicted values located at the design points of the BBD to the average prediction error. A ratio > 4 indicates that adequate model discrimination exists [194, 199]. A value of 61.399 was calculated, which is much greater than the limit and implies that the model can be used to predict experimental outcomes with acceptable accuracy.

3.2.1.1.4 R^2, Predicted R^2 and Adjusted R^2 Values

It is important to establish whether a model is able adequately to describe all experimental data under consideration [194, 199]. The process of evaluation includes determination of different coefficients of correlation. The R^2 coefficient has a value between 0 and 1 and the closer the value to 1, the more reliable the model. All values generated were > 0.9, signifying that the model is reliable and that predicted experimental outcomes will be reasonably close to actual values.

3.2.1.1.5 Residual Analysis

The adequacy of a model may be investigated by examining residuals that are differences between observed and predicted responses [199]. Residuals are examined using normal probability plots of residuals, and a plot of residuals versus predicted responses. If a model is adequate, the points of the normal probability plot of residuals should fall on a straight line and the location of points on a plot of residuals versus predicted responses should be structureless, i.e. should not follow a specific pattern [194, 195, 199]. The data shown in Figures 3.2 and 3.3 clearly indicate that these criteria were met and the model can therefore be deemed adequate.

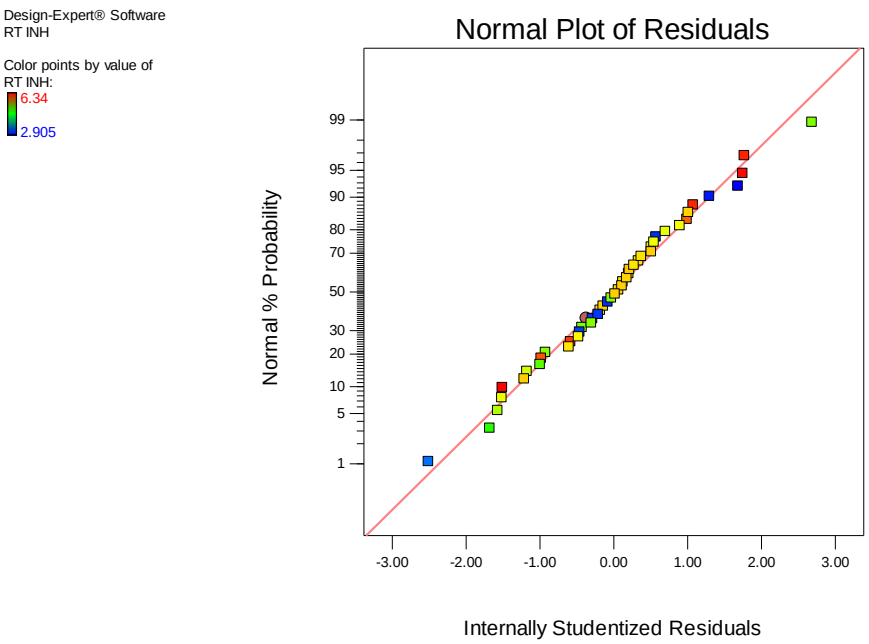

Figure 3. 2 Normal probability plots of residuals for retention time of INH.

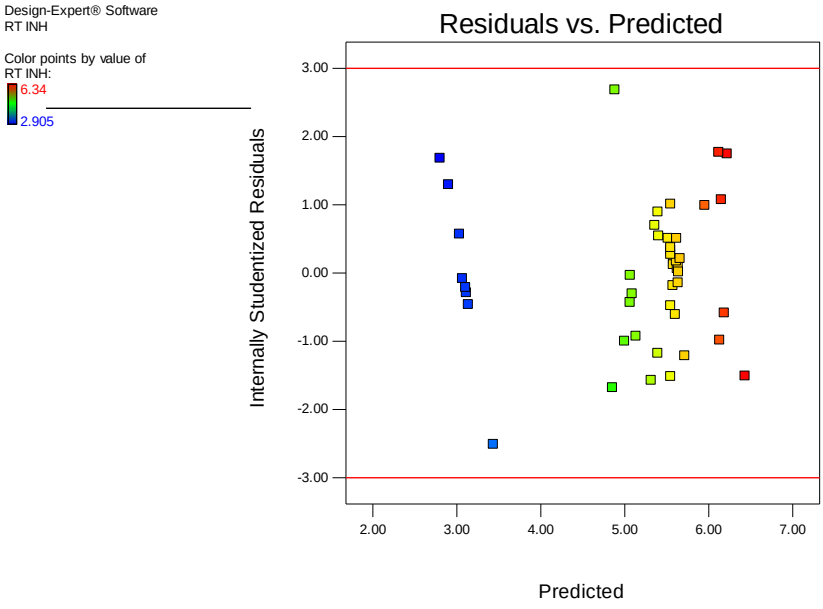

Figure 3. 3 Plot of residuals versus predicted response for retention time of INH.

3.2.1.1.6 PRESS

PRESS is the sum of squares of residuals and is a measure of the discrepancy between experimental data and those estimated by a model. A low value for PRESS indicates a good fit to the model selected [194]. The calculated value of 0.70 suggests that the data were well fitted to the model, indicating that the model was accurate and can be used to describe the data and navigate the design space adequately.

3.2.1.1.7 Box-Cox Plot for Power Transformation

Most statistical tests and confidence intervals are based on an assumption of normality of distribution of data as this approach permits simple, mathematically tractable and powerful testing compared to those that do not make an assumption of normality [194, 195]. However, many data sets do not follow normality and transformation of resultant data may be necessary to yield results that follow a normal distribution, albeit approximately in some cases. Box-Cox plots of normality are used when transformation is required to increase the applicability and usefulness of an applied statistical test [200]. In this case, inspection of the Box-Cox plot suggests that an inverse transformation, $\lambda = -1$, if undertaken, may improve the applicability and usefulness of the model (Figure 3.4). The ratio of maximum to minimum response was 2.8368, and transformation is required only if the ratio > 10. However the ratio < 3 indicates that a power transformation is likely to have little or no effect on the experimental responses, therefore transformation was not performed for these data.

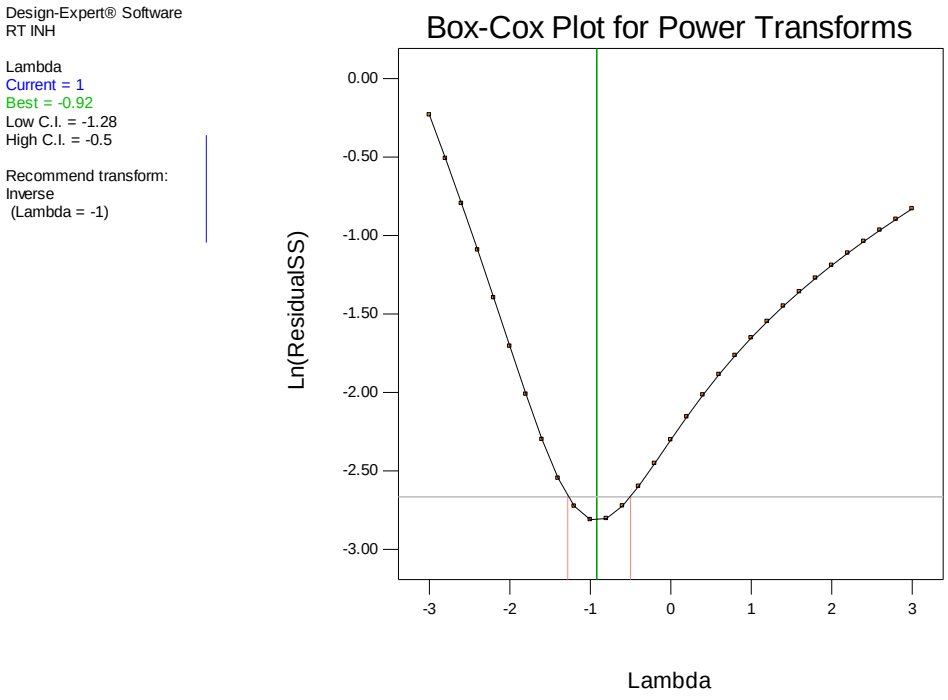

Figure 3. 4 Box-Cox plot for power transformation for retention time of INH.

3.2.1.1.8 Lack of fit

The Lack of Fit F-value of 1.69 and a p-value of 0.2947 implies that Lack of Fit is not significant relative to the pure error for the analysis. There is therefore a 29.47% chance that a "Lack of Fit F-value" this large could occur due to noise, and a non-significant lack of fit is desirable and shows the model can be used to navigate the design space.

3.2.1.2 ANOVA for Retention Time of INH

3.2.1.2.1 Significant Factors Affecting the Retention Time of INH

The results of ANOVA following the completion of the BBD and the significant factors affecting the retention time of INH are summarised in Table 3.6. Values of $p > F$ that are < 0.0500 indicate that the model terms investigated are significant.

Table 3. 6 ANOVA data for response surface quadratic model [partial sum of squares-type III] for retention time of INH.

Source	Sum of Squares	Df	Mean Square	F-Value	P-value	Prob > F
Model	46.35	20	2.32	302.27	< 0.0001	Significant
A = Buffer pH	25.81	1	25.81	3365.67	< 0.0001	Significant
B = Start % MeOH	4.78	1	4.78	622.8	< 0.0001	Significant
C = End % MeOH	$3.11E^{-03}$	1	$3.11E^{-03}$	0.41	0.5301	
D = Curve profile	$3.60E^{-03}$	1	$3.60E^{-03}$	0.47	0.4995	
E = Gradient duration	0.3	1	0.3	38.95	< 0.0001	Significant
AB	0.21	1	0.21	27.36	< 0.0001	Significant
AC	$3.24E^{-04}$	1	$3.24E^{-04}$	0.042	0.8388	
AD	$1.81E^{-03}$	1	$1.81E^{-03}$	0.24	0.6316	
AE	$1.41E^{-03}$	1	$1.41E^{-03}$	0.18	0.6721	
BC	$7.02E^{-04}$	1	$7.02E^{-04}$	0.092	0.7647	
BD	$3.72E^{-03}$	1	$3.72E^{-03}$	0.49	0.4925	
BE	$4.90E^{-05}$	1	$4.90E^{-05}$	$6.39E^{-03}$	0.9369	
CD	$1.16E^{-03}$	1	$1.16E^{-03}$	0.15	0.7011	
CE	$1.00E^{-04}$	1	$1.00E^{-04}$	0.013	0.91	
DE	$2.35E^{-03}$	1	$2.35E^{-03}$	0.31	0.5846	
A^2	12.67	1	12.67	1652.48	< 0.0001	Significant
B^2	0.018	1	0.018	2.39	0.1346	
C^2	$3.04E^{-03}$	1	$3.04E^{-03}$	0.4	0.5346	
D^2	$1.02E^{-04}$	1	$1.02E^{-04}$	0.013	0.9092	
E^2	0.024	1	0.024	3.15	0.0882	
Residual	0.19	25	$7.67E^{-03}$			
Lack of Fit	0.17	20	$8.35E^{-03}$	1.69	0.2947	not significant
Pure Error	0.025	5	$4.952E^{-003}$			
Cor Total	46.54	45				

The relationship between independent variables and the retention time of INH as a mathematical function including interaction of parameters is described by Equation 3.13.

$$Y_1 = 5.55 + 1.27A - 0.55B - 0.014C - 0.015D - 0.14E - 0.23AB + 9.000E^{-003}AC + 0.021AD - 0.019AE + 0.013BC - 0.030BD - 3.500^{-003}BE - 0.017CD - 5.000^{-003}CE - 0.024DE - 1.20A^2 + 0.046B^2 + 0.019C^2 - 3.417E - 003D^2 - 0.053E^2 \quad \text{Equation 3.13}$$

The data generated reveal that buffer pH, start % MeOH and gradient duration had a significant effect on the retention time of INH. Buffer pH was significant and increasing the buffer from pH

3 to 7 resulted in an increase in the retention time of INH: an observation that is similar to reported data [201]. The acidic silanol groups (pKa = 7.1) act as cation-exchangers at pH between 2 and 6. At a pH < 2 (isoelectric state) the functional groups are anion exchangers and at pH > 9 they are largely deprotonated [202]. The first protonation of INH (pKa 2.0) occurs at the pyridine nitrogen and the second (pKa 3.6) at the hydrazine functional group [54]. The retention time of INH at pH 3 is short due to high polarity and therefore limited interaction with the hydrophobic stationary phase. The retention time is constant between pH 4 and pH 6 at which the molecule is neutral, after which a slight decrease in retention time is observed at pH 7 due to the decreased potential for cation exchange [201]. The amount of organic solvent at the start of the separation and the duration of the gradient had a significant effect on the retention time of INH. Increasing the amount of organic solvent at the start of the separation resulted in a shorter retention time of INH, which can be attributed to a decrease in hydrophobic interactions between INH and the stationary phase [185, 203]. Increasing the gradient duration resulted in a reduction in the retention time of INH, which can be attributed to the presence of a high concentration of organic solvent on the column and a reduced time for conditioning with the buffer. The response surface and contour plots, showing the impact of input variables on the retention time of INH, are given in Figure 3.5.

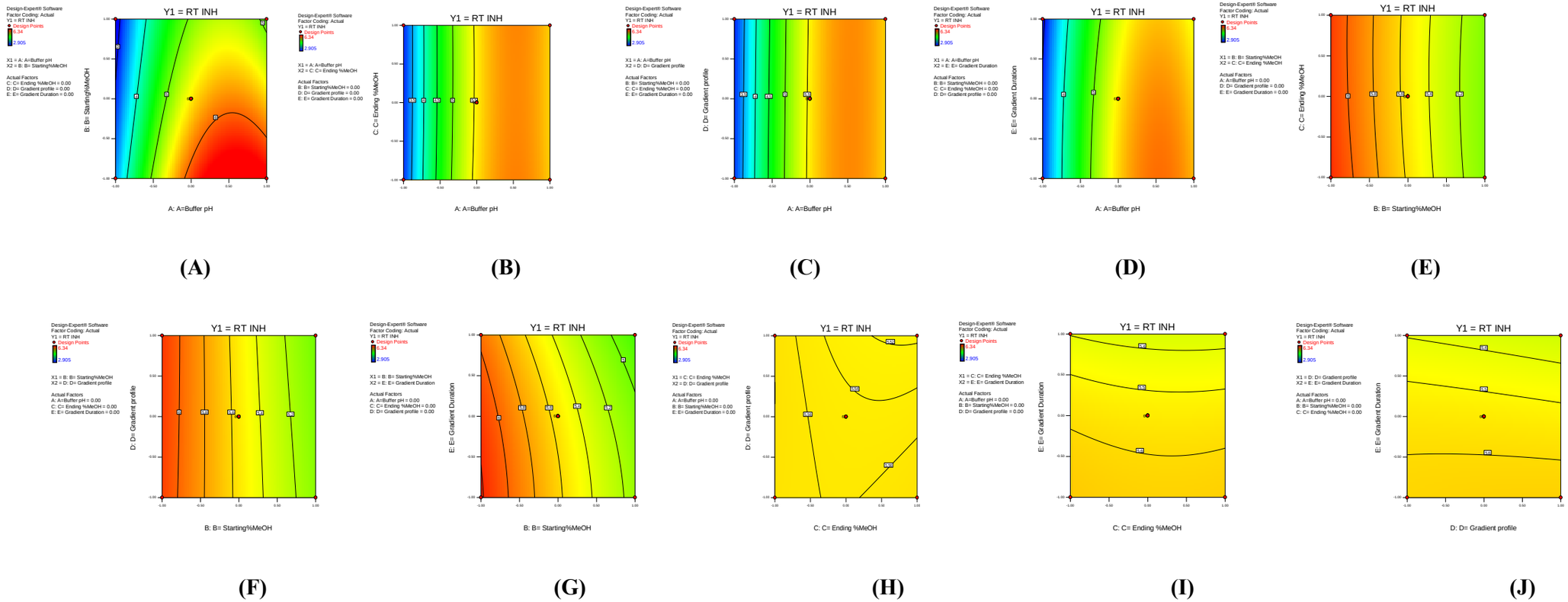

Figure 3. 5 Contour plots showing the impact of (A) start % MeOH and buffer pH, (B) end % MeOH and buffer pH, (C) gradient profile and buffer pH, (D) gradient duration and buffer pH, (E) end % MeOH and start % MeOH, (F) gradient profile and start% MeOH, (G) gradient duration and start % MeOH, (H) gradient profile and end % MeOH, (I) gradient duration and End % MeOH and (H) gradient duration and gradient profile on the retention time of INH obtained using the chromatographic conditions reported in Tables 3.2 and 3.10.

3.2.1.3 Evaluation of Model Adequacy for Capacity Factor for INH

The values of the factors assessed to determine model adequacy are summarised in Table 3.7. The most important parameters for the evaluation of model adequacy, viz. model F-value, coefficient of variation, adequate precision, PRESS and R^2 values revealed that the quadratic model selected was appropriate to establish relationships between input variables and outputs. The normal probability plots of residuals, plot of residuals versus predicted response and Box-Cox plot for power transformation listed in Appendix 1A revealed that the model was adequate.

Table 3. 7 Summary of model parameters and values used to evaluate adequacy of the model for capacity factor of INH.

Parameter	Value	Parameter	Value
Std. Deviation	0.061	R-Squared	0.9958
Mean	2.51	Adjusted R-Squared	0.9924
% C.V	2.41	Predicted R-Squared	0.9846
PRESS	0.34	Adequate precision	60.677
F-Value	392.23		

3.2.1.4 ANOVA for Capacity Factor for INH

3.2.1.4.1 Significant Factors Affecting Capacity Factor for INH

The results of ANOVA following completion of the BBD and significant factors affecting the capacity factor of INH are summarised in Table 3.8.

Table 3. 8 ANOVA for response surface quadratic model [partial sum of squares-type III] for the capacity factor of INH.

Source	Sum of Squares	df	Mean Square	F-Value	p-Value	Prob > F
Model	21.72	20	1.09	296.05	< 0.0001	Significant
A = Buffer pH	12.04	1	12.04	3281.99	< 0.0001	Significant
B = Start % MeOH	2.24	1	2.24	610.35	< 0.0001	Significant
C = End % MeOH	$8.27E^{-04}$	1	$8.27E^{-04}$	0.23	0.6391	
D = Gradient profile	$1.70E^{-03}$	1	$1.70E^{-03}$	0.46	0.5021	
E = Gradient duration	0.14	1	0.14	38.26	< 0.0001	Significant
AB	0.099	1	0.099	26.88	< 0.0001	Significant
AC	$1.02E^{-03}$	1	$1.02E^{-03}$	0.28	0.6019	
AD	$7.84E^{-04}$	1	$7.84E^{-04}$	0.21	0.6478	
AE	$6.38E^{-04}$	1	$6.38E^{-04}$	0.17	0.6803	
BC	$3.06E^{-04}$	1	$3.06E^{-04}$	0.083	0.775	
BD	$1.76E^{-03}$	1	$1.76E^{-03}$	0.48	0.4944	
BE	$2.50E^{-05}$	1	$2.50E^{-05}$	$6.82E^{-03}$	0.9349	
CD	$5.52E^{-04}$	1	$5.52E^{-04}$	0.15	0.7013	
CE	$5.63E^{-05}$	1	$5.63E^{-05}$	0.015	0.9024	
DE	$1.16E^{-03}$	1	$1.16E^{-03}$	0.32	0.5795	
A^2	5.98	1	5.98	1630.44	< 0.0001	Significant
B^2	$8.93E^{-03}$	1	$8.93E^{-03}$	2.43	0.1312	
C^2	$9.30E^{-04}$	1	$9.30E^{-04}$	0.25	0.619	
D^2	$1.99E^{-05}$	1	$1.99E_{-05}$	$5.43E^{-03}$	0.9419	
E^2	0.011	1	0.011	2.95	0.0982	
Residual	0.092	25	$3.67E^{-03}$			
Lack of Fit	0.08	20	$4.00E^{-03}$	1.7	0.2911	not significant
Pure Error	0.012	5	$2.35E^{-03}$			
Cor Total	21.81	45				

The relationship between independent variables and the capacity factor of INH as a mathematical function including interaction of parameters is described by Equation 3.14.

$$Y_5 = 2.80 + 0.87A - 0.37B - 7.187^{-003}C - 0.010D - 0.094E - 0.16AB + 0.016AC + 0.014AD - 0.013AE + 8.750^{-003}BC - 0.021BD - 2.500^{-003}BE - 0.012CD - 3.750^{-003}CE - 0.017DE - 0.83A^2 + 0.032B^2 + 0.010C^2 - 1.510^{-003}D^2 - 0.35E^2 \quad \text{Equation 3.14}$$

The data generated revealed that buffer pH, start % MeOH and gradient duration had a significant effect on the capacity factor of INH. Increasing the pH of the buffer resulted in an

increase of the capacity factor of INH that was attributed to an increase in retention time associated with the increase in buffer pH. Increasing the start % MeOH resulted in rapid elution of INH and thus a reduced capacity factor. Increasing the end % MeOH also resulted in a reduction in the capacity factor as a high end % MeOH content resulted in a shorter retention time for INH and was attributed to a high organic solvent content in the column and reduced time for conditioning with buffer. Figure 3.6 shows the response surface plots in which the impacts of different input variables on the capacity factor of INH are given.

A summary of the models describing all observed responses, in addition to the significant factors and mathematical equations describing the responses in relation to the independent variables, is presented in Table 3.9.

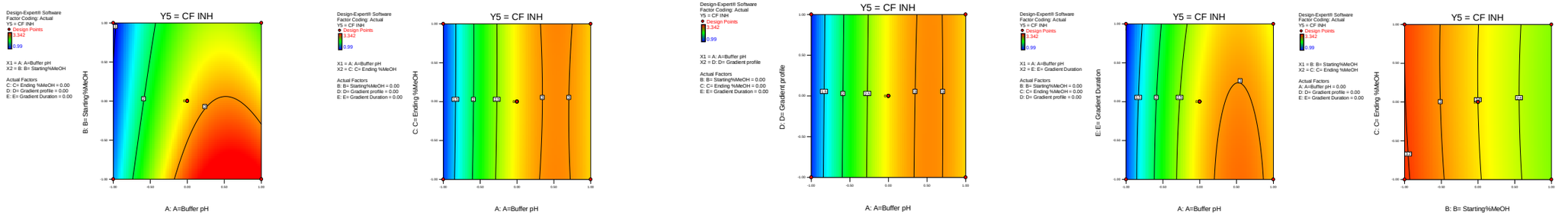

(A) **(B)** **(C)** **(D)** **(E)**

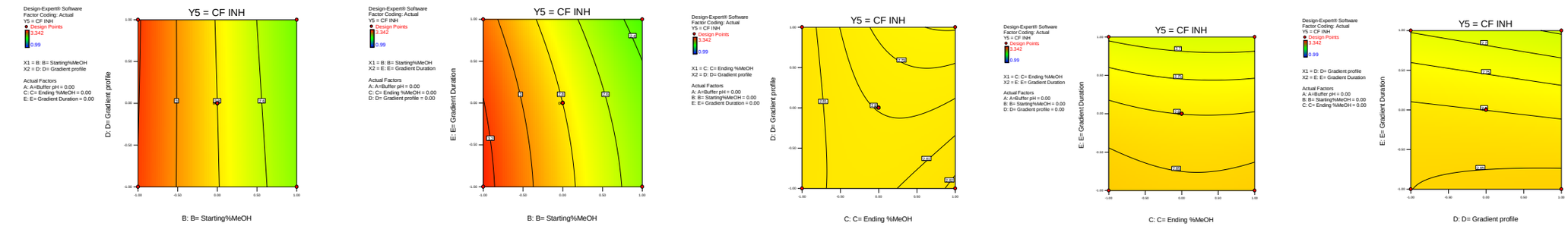

(F) **(G)** **(H)** **(I)** **(J)**

Figure 3. 6 Contour plots depicting the impact of (A) start % MeOH and buffer pH, (B) end % MeOH and buffer pH, (C) gradient profile and buffer pH, (D) gradient duration and buffer pH, (E) end % MeOH and start % MeOH, (F) gradient profile and start% MeOH, (G) gradient duration and start % MeOH, (H) gradient profile and end % MeOH, (I) gradient duration and End % MeOH and (H) gradient duration and gradient profile on the CF for INH obtained using the chromatographic conditions reported in Tables 3.2 and 3.10.

Table 3. 9 Summary of best fit models, significant factors and equations describing the relationship between input variables and response

Response	Fitting model	Significant factors	Equation
RT INH	Quadratic	Buffer pH, start % MeOH and gradient duration	$Y_1 = 5.55 + 1.27A - 0.55B - 0.014C - 0.015D - 0.14E - 0.23AB + 9.000E^{-003}AC + 0.021AD - 0.019AE + 0.013BC - 0.030BD - 3.500^{-003}BE - 0.017CD - 5.000^{-003}CE - 0.024DE - 1.20A^2 + 0.046B^2 + 0.019C^2 - 3.417E - 003D2 - 0.053E^2$
RT PZA	Quadratic	Start % MeOH and gradient duration	$Y_2 = 7.73 + 0.030A - 0.93B - 0.025C - 0.023D - 0.16E - 3.000^{-003}AB + 0.022AC + 0.056AD + 0.038\ AE + 0.015BC - 0.040BD - 1.250^{-003}BE - 0.025CD - 0.014CE - 1.000^{-003}DE + 0.024A^2 + 0.10B^2 + 0.020C^2 - 0.017D^2 - 0.044E^2$
RT AZT	Quadratic	End % MeOH and gradient profile	$Y_3 = 11.48 - 1.125^{-003}A - 6.313E - 003B - 0.068C + 0.24D - 6.875^{-003}E - 7.000^{-003}AB + 7.250^{-003}AC + 0.014AD + 5.250^{-003}AE - 5.000^{-004}BC - 6.750^{-003}BD - 5.000^{-003}BE - 3.500^{-003}CD + 3.500^{-003}CE - 5.750^{-003}DE - 7.833^{-003}A^2 - 7.750^{-003}B^2 + 9.583^{-003}C^2 - 0.064D^2 - 2.000^{-003}E^2$
RT RIF	Quadratic	Buffer pH, end % MeOH and gradient profile	$Y4 = 12.51 + 0.21A - 0.025B - 0.54C + 0.23D + 3.937^{-003}E + 1.750^{-003}AB - 0.21AC - 0.017AD - 0.040AE - 1.000^{-002}BC - 0.010\ BD - 3.250^{-003}BE + 0.033CD + 1.250^{-003}CE - 0.054DE - 7.521^{-003}A^2 + 0.030B^2 + 0.17C^2 - 0.051D^2 + 0.055E^2$
CF INH	Quadratic	Buffer pH, start % MeOH and gradient duration	$Y_5 = 2.80 + 0.87A - 0.37B - 7.187^{-003}C - 0.010D - 0.094E - 0.16AB + 0.016AC + 0.014AD - 0.013AE + 8.750^{-003}BC - 0.021BD - 2.500^{-003}BE - 0.012CD - 3.750^{-003}CE - 0.017DE - 0.83A^2 + 0.032B^2 + 0.010C^2 - 1.510^{-003}D^2 - 0.035E^2$
RF AZT/ INH	Quadratic	Buffer pH and end % MeOH	$Y_6 = 5.76 + 2.12A - 0.080B - 1.04C - 0.099D + 0.29E + 0.37AB - 3.63AC - 0.61AD - 0.28\ AE + 0.15BC + 0.25BD - 0.11BE - 0.29CD - 0.84CE + 0.52DE + 2.87A^2 + 0.18B^2 - 0.74C^2 - 0.24D^2 + 0.33E^2$
TF INH	Quadratic	Buffer pH, start % MeOH and gradient duration	$Y_7 = 1.10 - 0.057A - 0.028B + 1.250E^{-003}C - 4.313E^{-003}D - 0.021E - 5.000^{-003}AB + 0.011AC + 0.043AD + 0.031AE - 2.500^{-003}BC - 0.011BD - 4.000^{-003}BE + 2.250^{-003}CD + 0.013CE - 8.500^{-003}DE - 0.074A2 - 0.014B^2 + 0.016C^2 + 7.958^{-003}D^2 - 8.208^{-003}E^2$
TF PZA	Linear	Start% MeOH and gradient duration	$Y_8 = 1.10 - 1.938E^{-003}A + 0.022B - 1.000E^{-003}C + 4.375E^{-004}D - 0.012E$
TF RIF	Quadratic	Starting %MeOH, ending %MeOH and gradient duration	$Y_9 = 1.42 - 0.013A + 0.052B + 0.20C - 0.029D - 0.10E - 2.750^{-003}AB + 0.18AC + 0.045AD + 0.058AE + 0.048BC + 4.000^{-003}\ BD - 0.16BE - 0.040CD - 0.016CE + 0.084DE + 0.39A^2 + 5.602^{-003}B^2 + 6.327E - 003C^2 - 0.036D^2 + 0.083E^2$

3.2.1.5 Factors affecting responses Y_2-Y_4 and Y_6-Y_9

The retention time of PZA, Y_2, was affected by the start % MeOH and gradient duration with an increase in both variables, resulting in a significant reduction in retention time of the API. The retention time of the internal standard AZT, Y_3, was affected by the end % MeOH and gradient profile with an increase end % MeOH and change of profile from concave to convex profile resulting in a reduction in retention time for of the compound. Changing the gradient profile from concave to convex profile resulted in an increase in the rate of change of % MeOH in the mobile phase, resulting in higher % MeOH within a short period of time, and hence reduced retention time. The retention time of RIF, Y_4, was significantly affected by buffer pH, end % MeOH and gradient profile. Increasing buffer pH resulted in an increase in retention time of RIF, possibly due to increase in polarity as a result of ionisation of the phenolate group [201], whilst an increase in end % MeOH content and a change of gradient profile from concave to convex profile resulted in a decrease in retention time of RIF. The resolution factor between AZT and RIF, response Y_6, was significantly affected by buffer pH and end % MeOH, with an increase in buffer pH resulting in an increase in resolution factor, whilst an increase in ending % MeOH content had a negative impact on resolution. The tailing factor of INH, Y_7, was significantly affected by buffer pH and start % MeOH with an increase in buffer pH resulting in a decrease of the tailing factor. Due to reduced interaction of INH with silanol groups of the column at higher pH values [201], an increase in start % MeOH resulted in a decrease for the tailing factor. The tailing factor of PZA,Y_8, was significantly affected by the start % MeOH and gradient duration, with an increase in these parameters resulting in a decrease in the tailing factor. The tailing factor for RIF, Y_9, was significantly affected by the start % MeOH, end % MeOH and gradient duration, with an increase in all these factors resulting in a decrease in tailing factor. The response surface plots showing the impact of input variables on responses are presented in Appendix 1A.

The use of BBD enabled simultaneous analysis of the impact of the various input variables on the responses monitored, making it possible to select suitable chromatographic conditions, which would otherwise be time consuming if the traditional method of changing one variable at a time was to be used.

3.2.1.6 Optimisation of chromatographic conditions

The Design® Expert software was fed with desired chromatographic conditions to generate a set of input variables that would result in such desirable parameters based on the experiments which were conducted. The final chromatographic conditions identified were based on achieving a short analysis time with acceptable peak tailing, resolution and capacity factors. A summary of the optimised chromatographic conditions and system suitability parameters is listed in Table 3.10. The system suitability parameters were deemed satisfactory for this chromatographic separation and the system and separation was then validated.

Table 3. 10 Summary of optimised chromatographic and system suitability parameters.

Parameter	Setting		
Chromatographic parameters			
Flow rate (mL/min)	1.0		
Start % MeOH	3.0		
End % MeOH	75		
Curve profile	6		
Gradient duration (min)	4		
Injection volume (µL)	10		
Column temperature (°C)	22		
Wavelength (nm)	254 (RIF), 265 (INH), 268 (PZA)		
Mobile phase composition	Methanol:10 mM phosphate buffer pH 3.0		
System suitability parameters	**INH**	**PZA**	**RIF**
Theoretical number of plates (N)	8262.616	10993.81	83450.80
Capacity factor	1.065600	4.316160	7.772620
Resolution factor	-	21.54936	8.090810
Tailing factor	1.087560	1.099920	1.657200

A typical chromatogram of the separation of INH, PZA, AZT and RIF using the optimised chromatographic conditions is shown in Figure 3.7.

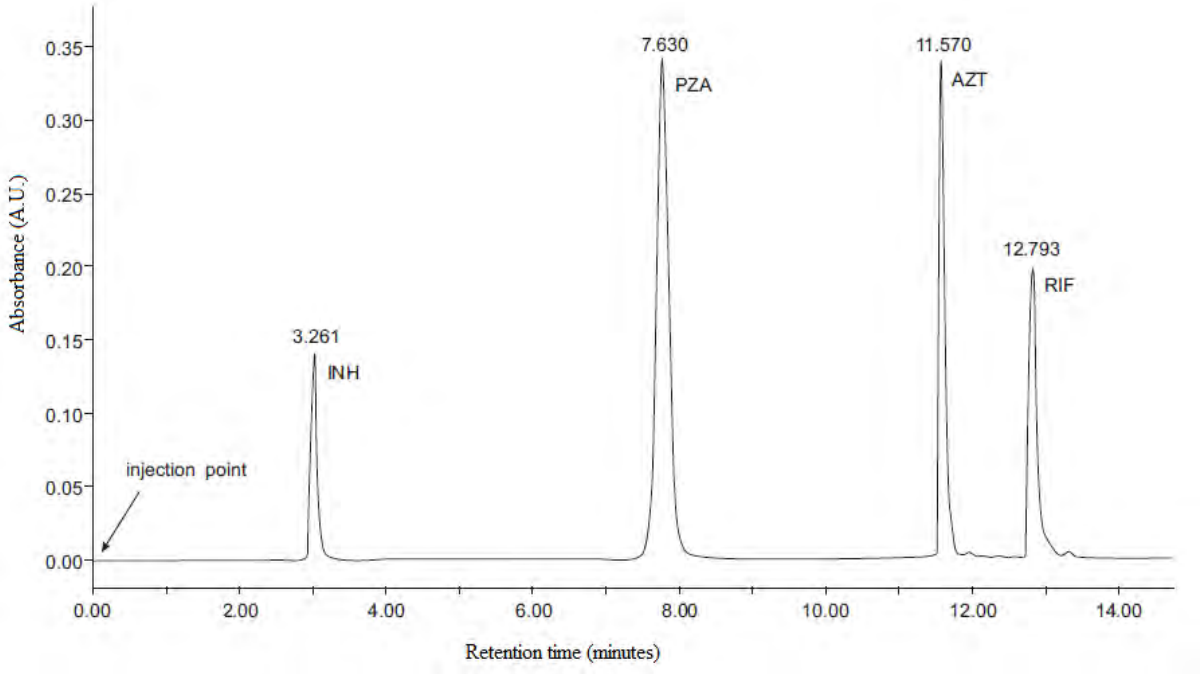

Figure 3. 7 Typical chromatogram for the separation of INH (100 µg/mL), PZA (400 µg/mL), AZT (300 µg/mL) and RIF (200 µg/mL).

3.2.1.7 Method Validation

A summary of the validation results for establishing linearity and range, precision, accuracy and the limits of quantitation (LOQ) and detection (LOD) are listed in Table 3.11. The results reveal that the method is linear, precise and accurate over the concentration ranges studied.

Table 3. 11 Summary of validation results for HPLC method of analysis for INH, PZA and RIF.

Parameter	API		
	INH	**PZA**	**RIF**
Linearity			
R^2	0.9991	0.9995	0.9990
Equation	Y = 0.004x + 0.0095	Y = 0.005x + 0.0226	Y = 0.0022x + 0.0002
Intra-day precision % RSD range	0.1927-1.9338	0.0263-2.5812	0.0031-3.6493
Inter-day precision % RSD range			
Day 1	0.0843-1.1234	0.0714-2.1452	0.0559-2.7759
Day 2	0.0457-0.4854	0.0535-1.5889	0.2877-0.7069
Day 3	0.0268-3.0489	0.0086-1.7885	0.1468-2.8514
Accuracy (n=5)			
Theoretical concentration µg/mL	100	100	100
% Recovery ± % RSD	99.70±0.36	101.12±0.43	98.63±2.03
% Bias	0.30	1.12	1.37
LOQ µg/mL (n=5)	1.0±0.17	1.0±1.87	5.0±0.75
LOD µg/mL	0.30	0.30	1.50

3.2.1.7.1 Assay

The average content of INH, PZA and RIF in comparison to the label claim for the products tested is summarised in Table 3.12 and the % recovery and corresponding % RSD values were < 5 % in all cases, suggesting the method is suitable for the analysis of INH, PZA and RIF in dosage forms.

Table 3. 12 Assay results following analysis of commercially available dosage forms.

Product		Theoretical concentration µg/mL	Actual concentration µg/mL	Recovery %	RSD %
Winthrop Sanofi® Isoniazid 100 tablets		100	96.67 ± 0.773	97.67	0.7914
BE-TABS® Isoniazid 100 tablets		100	97.55 ± 0.934	97.55	0.9575
Sandoz® Pyrazinamide 500 tablets		100	95.97 ± 0.668	95.97	0.6961
Pyrazide® Sanofi 500 tablets		100	96.93 ± 0.827	96.93	0.8532
Rimactane® 150 capsules		150	146.45 ± 0.433	97.63	0.4435
Rifafour® tablets	INH	37.5	53.77 ± 0.322	95.39	0.9099
	RIF	75	71.89 ± 0.116	95.85	0.1210
	PZA	200	192.49 ± 0.573	96.25	0.5950

3.2.1.7.2 Specificity

The method was found to be specific and stability-indicating as the peaks of degradation products were well separated from the peaks of interest and would therefore not interfere with the analysis of each compound. Typical chromatograms of a separation of INH, PZA and RIF and degradation peaks following exposure to acidic, oxidative and alkaline conditions for 72 hours are shown in Figures 3.8 – 3.10, respectively.

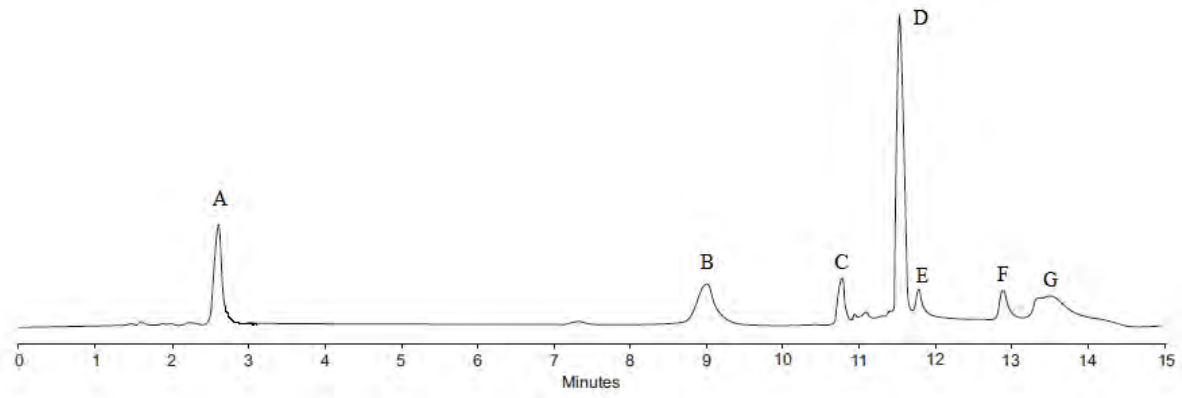

Figure 3. 8 Typical chromatogram of the separation of (A) INH, (B) PZA, (D) AZT and (F) RIF and unidentified peaks C, E and G following exposure to 0.1M HCl for 72 h.

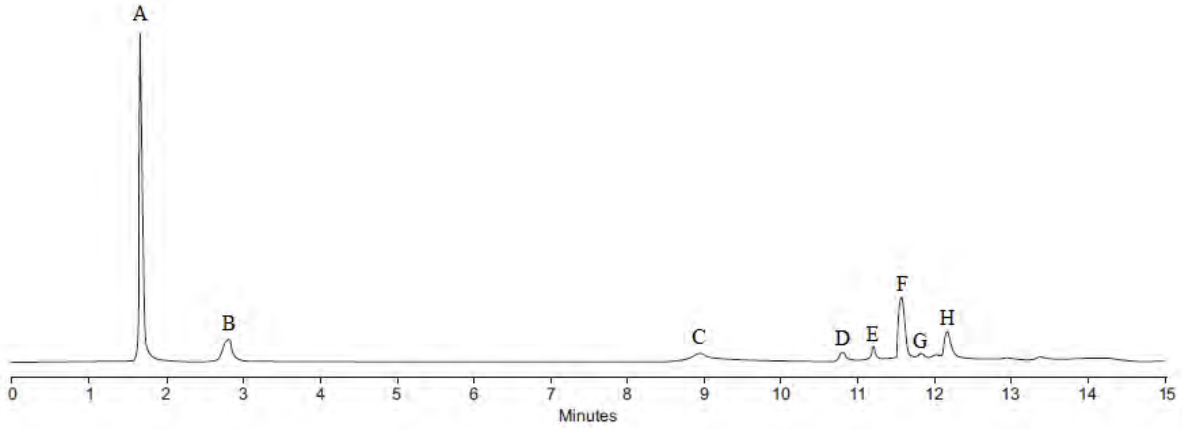

Figure 3. 9 Typical chromatogram of the separation of (A) H_2O_2 solvent peak, (B) INH, (C) PZA, (F) AZT, (H) RIF (H) and unidentified peaks D, E and G following exposure to 30% v/v H_2O_2 for 72 h.

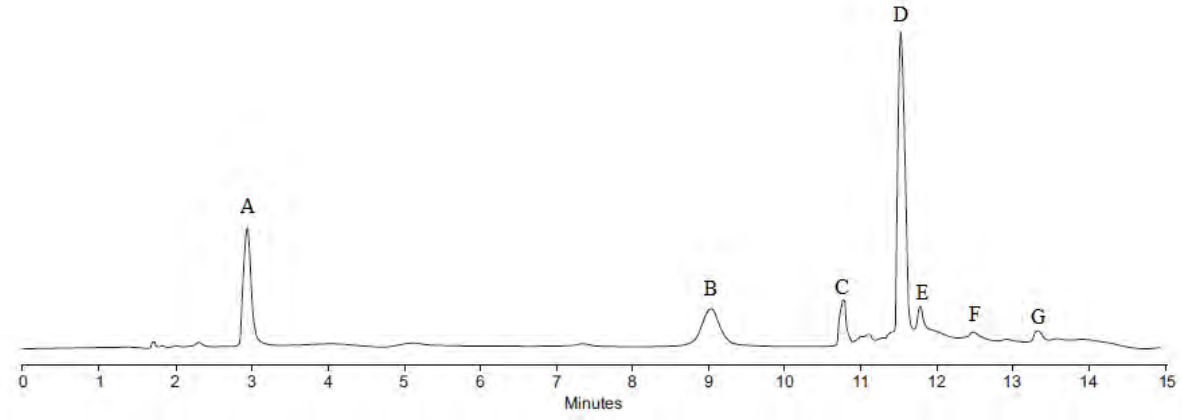

Figure 3. 10 Typical chromatogram of the separation of (A) INH, (B) PZA, (D) AZT, (F) RIF and unidentified peaks C, E and G following exposure to 0.1 M NaOH for 72 h.

3.3 CONCLUSIONS

A Box Behnken design has been successfully used for the optimization of a rapid, accurate stability-indicating gradient elution RP-HPLC method for the simultaneous analysis of isoniazid, pyrazinamide and rifampicin. Response surface methodology was used to establish the impact of input variables on outputs and it is the first time such an approach has been applied to the optimization of a gradient RP-HPLC method for the simultaneous analysis of INH, PZA and RIF. Considering the various factors that can influence chromatographic separation of these API when analysed simultaneously, this work was important in helping understand the significant input variables in order to select suitable chromatographic conditions. The relationships between input variables and outputs were then used to define the optimum chromatographic conditions to achieve a good separation within a reasonable period of time, viz. 15 minutes. The lack of interference with the main API peaks from the many peaks of degradation products and the shorter analysis time makes this method better than most published methods which are not stability-indicating and have longer analysis time. The method was validated using ICH guidelines and the results reveal that it can be applied to the analysis of commercially available TB FDC formulations containing the three API, and exhibits a short analysis time. The method is precise, sensitive and has the necessary selectivity for use during formulation development and optimisation studies for a combination of RIF, INH and PZA.

CHAPTER FOUR

FORMULATION AND MANUFACTURE OF SUSTAINED RELEASE GASTRIC RESISTANT ISONIAZID MICROSPHERES

4.0 INTRODUCTION

Microparticle formulations, in a pharmaceutical context, refer to particles of diameter in the range 1-1000 μm containing an API, without consideration of the precise internal or external structure of the particles [204]. Broadly defined, microparticles include microspheres that are spherical or are comprised of a core surrounded by a material that is significantly different to the core [205] that may be a solid, liquid or gaseous material [206, 207]. A microsphere is assumed to comprise a homogenous mixture of polymer and API, whereas microcapsules have at least a single discrete domain and sometimes more into which the API is sequestered [208-210]. The different categories of microparticles are depicted in Figure 4.1.

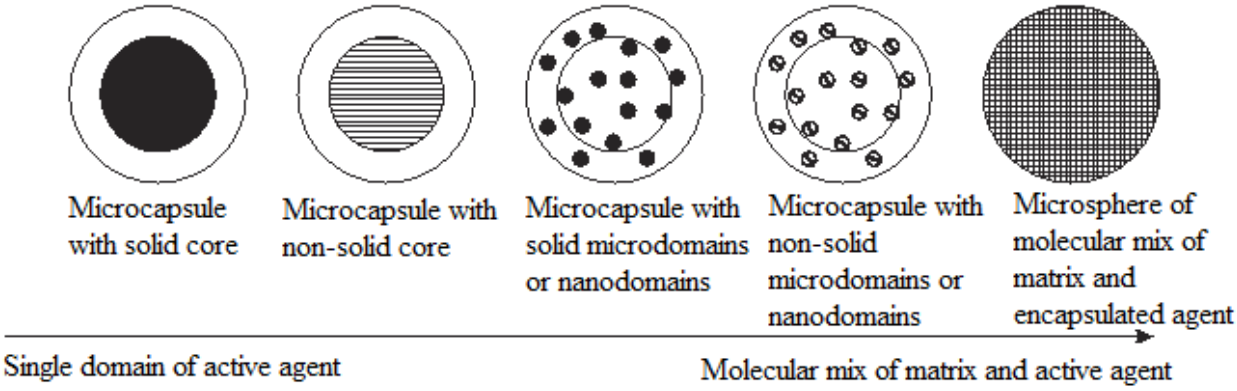

Figure 4. 1 Schematic representation of different microcapsules and microspheres [204].

4.1 METHODS OF MANUFACTURE

There are a number of techniques that have been used for the manufacture of microparticles for pharmaceutical applications and some of these are discussed, *vide infra*.

4.1.1 Solvent evaporation and extraction

This technique for particle manufacture makes use of single or multiple emulsion approaches that exhibit some advantages for specific applications.

4.1.1.1 Single emulsion

The single emulsion approach makes use of oil-in-water (o/w) emulsification that initially involves dissolving a polymer in a water miscible, volatile organic solvent and then adding an API to the polymer solution, to form a solution or dispersion of the API particles [211]. The resultant solution/dispersion is then emulsified, in a large volume of an aqueous vehicle, in the presence of an emulsifier to produce an o/w emulsion. Emulsification is achieved using appropriate stirring and temperature conditions, as these parameters can, and often do, influence the process of particle formation. The solvent is removed from the emulsion by evaporation or extraction in order to harden core droplets [212]. In the case of evaporation, the emulsion is maintained at atmospheric or a reduced pressure whilst stirring to facilitate evaporation of the volatile solvent. In the case of extraction, the emulsion is transferred to a large volume of water, with or without surfactant or other quenching medium into which the solvent associated with the oil droplets diffuses from [211, 212]. The microspheres are washed and then collected by filtration, sieving or centrifugation [212], after which they are dried or lyophilized using predetermined conditions, to produce free-flowing microspheres. The manufacture of microparticles by a single emulsion solvent evaporation process is illustrated in Figure 4.2.

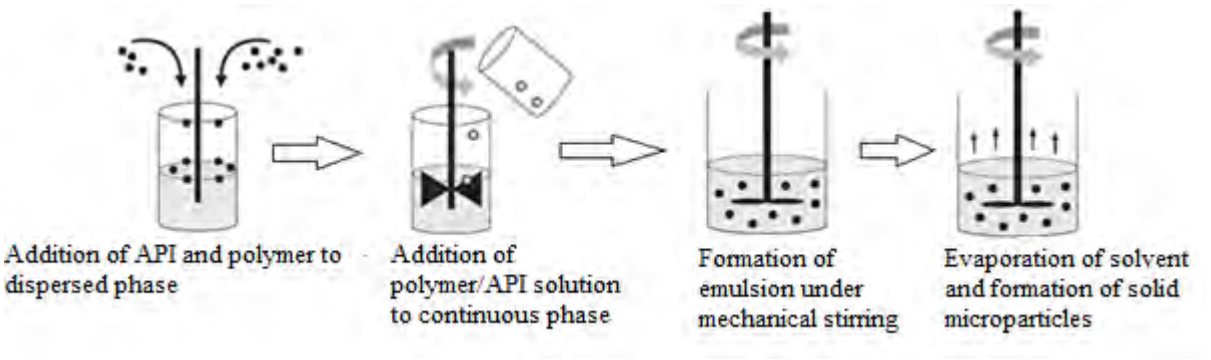

Figure 4. 2 Manufacture of microspheres using a single emulsion solvent evaporation process.

The rate at which solvent is removed by extraction or evaporation is dependent on the temperature and volume of the quench medium in addition to the solubility of the polymer, solvent and dispersion medium used [212]. Rapid evaporation of the solvent may result in the formation of porous surfaces on microspheres [212]. One drawback associated with an o/w emulsification approach is poor encapsulation efficiency for water soluble API [211-213], as these tend to diffuse or partition into the continuous aqueous phase and microcrystalline

fragments of hydrophilic API deposit on the surfaces of microspheres and/or are dispersed in the polymer matrix [214, 215]. The encapsulation of water soluble API can be better achieved using an oil-in-oil (o/o) emulsification approach [211, 213, 216] which uses a water miscible organic solvent, in which the coating polymer is soluble, to solubilize the API. The resultant solution is dispersed into an oil in the presence of an oil-soluble surfactant such as Span to yield an o/o emulsion. The microspheres are eventually produced by evaporation or extraction of the organic solvent from the dispersed oil droplets using an additional solvent such as n-hexane.

The main factors affecting the microencapsulation process and the final characteristics of the microspheres produced include the chemical nature and solubility of the API to be encapsulated in addition to the composition, content and molecular weight of the polymer used. The API to polymer ratio, organic solvent, concentration and nature of emulsifier, temperature and stirring speed used for the emulsification process and the viscosity and volume ratio of the continuous and dispersed phases are also implicated in the manufacture of a high quality product [211, 213, 217].

4.1.1.2 Double or multiple emulsion

This process makes use of a water-in-oil-in-water (w/o/w) emulsion and is particularly useful for the encapsulation of water soluble API such as peptides, proteins and vaccines [211, 213, 217]. A buffered or an unbuffered aqueous solution of API that may also contain a viscosity building and/or stabilizing protein, such as gelatin, is added to an organic solvent with vigorous stirring to form a micro-fine w/o emulsion. This emulsion is then added with gentle stirring to a large volume of water containing an emulsifying agent to form the w/o/w emulsion, after which the solvent is removed by either evaporation or extraction. The solid microspheres are then washed and harvested by sieving, filtration or centrifugation. A number of formulation and process variables have a significant impact on the quality of the final microsphere produced and the kinetics of API release from the microspheres. The manufacture of microparticles using a double emulsion solvent evaporation process is schematically illustrated in Figure 4.3.

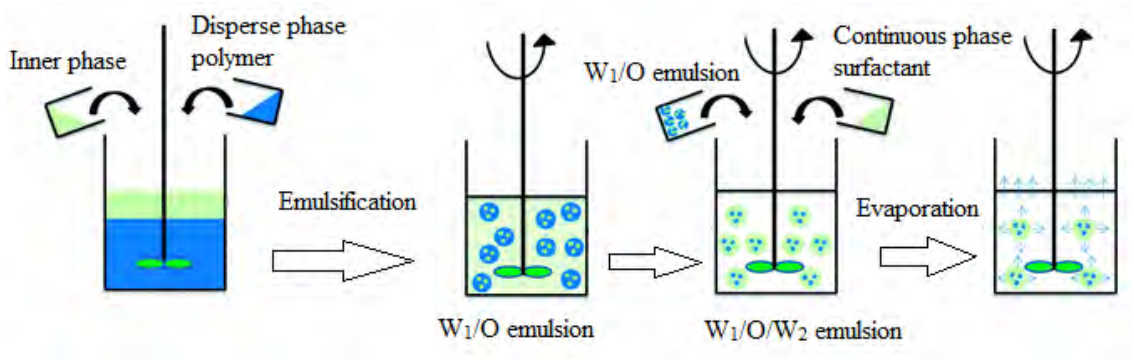

Figure 4. 3 Schematic representation of a typical $W_1/O/W_2$ double emulsion process for the manufacture of microparticles [210].

4.1.2 Phase separation or coacervation

Coacervation involves the reduction of solubility of an encapsulating polymer in solution, by the addition of a non-solvent for the polymer to that solution [211, 213, 217]. This results in the formation of two phases viz., a polymer-rich coacervate phase and a supernatant phase depleted of polymer. The coacervate material forms a coat around any API dispersed/dissolved in the polymer solution. The coacervation approach can be summarised into three stages viz., (i) manufacture of a coating solution, (ii) adsorption of the coacervate around API particles/droplets, and (iii) solidification of coated microspheres [218]. A schematic representation of the manufacture of microparticles using complex coacervation is depicted in Figure 4.4.

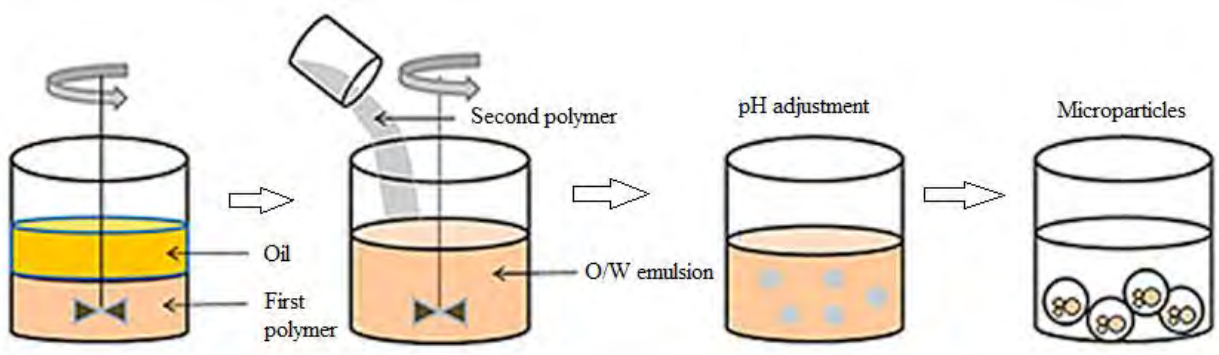

Figure 4. 4 Schematic representation of the manufacture of microparticles using complex coacervation [219].

Initially the polymers to be used are dissolved in an organic solvent and hydrophilic API is dissolved in water, after which the API solution is dispersed in the polymer solution to form a w/o emulsion. In the case of insoluble API, these may be solubilized or dispersed in the

polymer solution. The addition of an organic non-solvent for the polymer, to the polymer-API-solvent system, with stirring, results in gradual extraction of the solvent for the polymer. Consequently, the polymer undergoes phase separation and forms soft coacervate droplets that encapsulate and coalesce around the dispersed API particle or droplet, the size of which can be controlled by the stirring rate. The resultant system is then transferred to a large volume of an alternate organic non-solvent to harden the micro-droplets, ultimately forming microspheres. The microspheres are washed and collected by sieving, filtration or centrifugation and are then dried [211, 218]. This approach is suitable for the encapsulation of hydrophobic and hydrophilic API. The addition of a non-solvent should occur at a rate such that the solvent is extracted slowly to permit sufficient time for the polymer to deposit around and evenly coat the API particles during the coacervation stage of manufacture [211].

The use of high polymer concentrations may result in rapid phase separation and non-uniform coating of dispersed API particles with the polymer. The most common challenge encountered during coacervation is agglomeration due to absence of an emulsion stabilizer [211]. Another common challenge is adhesion of coacervate droplets, prior to completion of the phase separation or hardening stage of manufacture, that can be rectified by adjusting the stirring rate, temperature of production and/or addition of an additive such as polyvinyl alcohol [211].

The requirements for the solvent for dissolution of the polymer(s) to be used are not as stringent as those for solvent evaporation/extraction, as in this case the solvent need not be immiscible with the continuous phase and the boiling point may be higher than that of water [211]. Examples of organic solvents that have been used for coacervation include dichloromethane (DCM), acetonitrile, ethyl acetate and toluene [218, 220-226]. Non-solvents affect the phase separation and hardening stages of microsphere production and therefore should not dissolve the polymer or API used, nor should they be miscible with the solvent for the polymer [218, 220-223]. The second non-solvent should be relatively volatile and easily dissolve and remove the first viscous non-solvent during the washing stage of production. Examples of oils used as non-solvents include silicone; vegetable oil, such as arachis oil; light liquid paraffin; low molecular weight liquid poly-butadiene; and low molecular weight methacrylic acid block copolymers. Examples of second non-solvents include aliphatic hydrocarbons such as hexane, heptane and petroleum ether [211, 218, 220-226]. Equilibrium is never reached during the phase separation process, hence the system is constantly out of equilibrium [211]. Consequently formulation and process variables can and do have a

significant impact on the kinetics of the process and ultimately on the final characteristics and performance of the microspheres produced.

4.1.3 Spray drying

A schematic representation of the production of microparticles using spray drying is depicted in Figure 4.5.

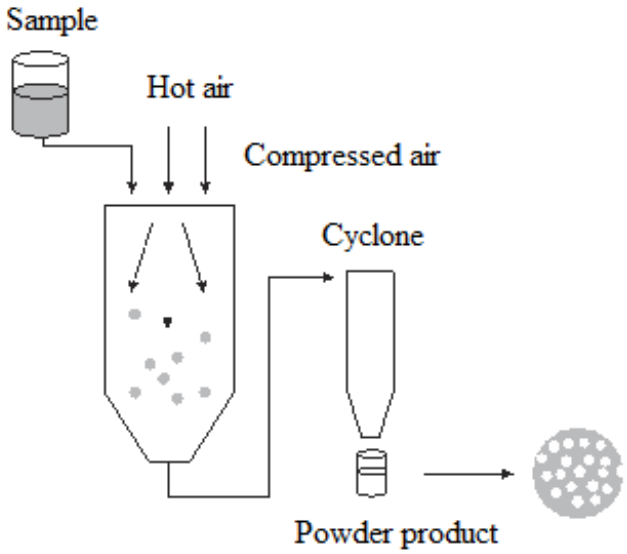

Figure 4. 5 Schematic representation of the manufacture of microparticles by spray drying [219].

The initial phase of the spray drying process involves the preparation of a dispersion, emulsion or solution of the solid polymer matrix, to which the API to be encapsulated is added. The type of polymer used is dependent on the intended application for the microcapsules. The polymer is dissolved in a solvent in which the API core is usually insoluble (solid) or immiscible (liquid). The API is added to the polymer solution with vigorous stirring to produce a dispersion (solids) or an emulsion (liquids). The emulsion produced must have small diameter droplets to improve stability and avoid droplet coalescence during the drying stage of the process [227]. The emulsion or dispersion is then transferred to a spray dryer, in which it is subjected to drying via the typical stages of a drying process using fluidized bed driers [228]. Initially, the dispersion or emulsion is transformed into droplets with the aid of an atomiser. Hot air that flows either in a current or counter-current direction, comes into contact with the atomised droplets and evaporates the aqueous component of the droplets. The physical composition of the drops is fixed, due to the rapid drying process, and the structure of the resulting powder particles is uniform. The dry

particles, in which the core material is sequestered as a micro-dispersion in a polymer, descends through the gaseous medium, to the base of the dryer and are then collected [227].

Successful microencapsulation by spray drying is dependent on attaining high retention of core materials during processing, in addition to prolonged storage. The core material may escape during the drying of droplets, prior to the formation of a crust on the surface of the droplets and volatile cores may be lost, by diffusion, from within the liquid phase during drying. Once a crust has been formed, further loss of the payload may occur if the core material diffuses through the crust via the solid material or through pores or channels that form in the coat. Non-volatile core materials may also be lost during the drying of droplets when present on the surface of the droplets, as they evaporate during atomisation. Alternatively, they may be lost through migration to the surface of the particles, prior to the formation of the crust around the drying materials, and consequently are swept from the surface of the particles by the fluidised air [227].

4.2 APPLICATIONS OF MICROCAPSULES AND MICROSPHERES

Microencapsulation can used to achieve a number of drug delivery objectives viz., manufacture of sustained release technologies, particularly tablets, capsules and/or parenteral dosage forms [229], enteric coated dosage forms to promote absorption from the small intestine and not the stomach [230], taste masking of bitter drugs [231, 232], the addition of oily medicines to tableted dosage forms to overcome the inherent challenges of producing tablets from tacky granulations and/or direct compression manufacture [233, 234], enhancement of stability of API by protection from environmental conditions such as humidity, light, oxygen and heat [212, 235], separation of incompatible substances in eutectic mixtures in which direct contact of materials results in liquid formation and stability enhancement of incompatible aspirin and chlorpheniramine maleate by microencapsulation of the compounds prior to mixing [231], minimisation of volatility for prolonged storage [231], the reduction of toxicity when handling toxic or noxious materials such as fumigants, herbicides, insecticides and pesticides [235], the reduction of hygroscopic properties of core materials [236], reduction of gastric irritation of some API [236], manufacture of intrauterine contraceptive devices [237], and for the fabrication of multi-layered tablet formulations for controlled release of API from middle layers of tableted particles [205, 208, 238].

Consequently, microencapsulation was used to manufacture sustained release gastric resistant INH microspheres to prevent release in the stomach, thereby preventing an interaction with

rifampicin. Since INH is hydrophilic, a solvent evaporation approach using an o/o emulsion was selected for the manufacture of microspheres. This approach would also potentially improve the possibility of achieving high encapsulation efficiency of the highly water soluble INH.

4.3 EXPERIMENTAL

4.3.1 Excipient Selection

The ICH guidelines recommend that excipients should be selected with caution, as the quality and source of material varies by supplier and batch [239]. The specifications for excipients must meet guidelines put in place to aid the selection process as they should be safe, physiologically inert, non-toxic and must be listed as GRAS (Generally Regarded as Safe) materials [240]. The excipients should also exhibit stability with no evidence of drug-excipient incompatibility, either physical or chemical, between the API or packaging materials and/or other excipients used in a formulation [241, 242]. It is also important that excipients do not interfere with validation processes for the manufacture and analytical testing of dosage forms [243]. The ease of accessibility, distribution, cost, satisfactory compliance with regulatory requirements including environmental issues in countries where the product is marketed, are other factors to be considered when identifying and selecting pharmaceutical excipients [244].

There are numerous other factors to be considered when selecting excipients for use in a formulation. For example, the type of excipient selected is highly dependent on the API to be delivered and the intended form and route for delivery. As a result, appropriate formulation composition and process parameters are critical and must be identified and evaluated as an integral part of the product development process [245].

4.3.1.1 Eudragit® L100

Eudragit® L100 is an anionic block co-polymer of methacrylic acid and methyl methacrylate. The ratio of free carboxyl functional groups to the ester is approximately 1:1 in Eudragit® L100 that has a mean relative molecular mass of approximately 135,000 Da and is available as a 12.5 % v/v solution in propan-2-ol without plasticiser and as a 12.5 % w/v ready-to-use solution in propan-2-ol with 1.25 % v/v dibutyl phthalate as a plasticiser. Eudragit® L100 solutions are colourless, with the characteristic odour of the solvent used and have an apparent viscosity of 50 – 200 mPas [246]. Eudragit® L100 is also available as a white free-

flowing powder with at least 95 % dry polymer. Eudragit® L100 is a pH-dependent polymer that is soluble in intestinal fluids of pH 6 and is widely used in the manufacture of coated and matrix tablets, microspheres and nanoparticles [247-252].

4.3.1.2 Hydroxypropyl Methylcellulose Acetate Succinate (HPMC-AS)

HPMC-AS is a cellulosic polymer that has four different, semi-randomly distributed substituents located at the hydroxyl and methoxy functional groups with a mass content of 12-28 wt %, hydroxypropyl functionalities with a mass content of 4-23 wt %, acetate functionalities with a mass content of 2-16 wt % and succinate functionalities with a mass content of 4-28 wt % [253]. The succinate functional groups have a p*K*a of approximately 5, consequently the molecule is < 10% ionised at pH < 4 and at least 50% ionised at pH > 5. Different weight % content of acetyl and succinoyl functional groups are used to produce different grades of HPMC-AS that dissolve in solutions of different pH. Type L HPMC-AS has a high ratio of succinoyl to acetyl substitution (S/A ratio), whereas type H has a low S/A ratio and type M a medium S/A ratio. A high S/A ratio, such as for, type L HPMC-AS dissolves at pH ≥ 5.5, type M at pH ≥ 6.0 and type H at pH ≥ 6.8 [254]. HPMC-AS grade MF was used in these studies, due to the presence of relatively hydrophobic methoxy and acetate substituents that impart water-insoluble properties to the polymer when un-ionized and that remains in a predominantly colloidal state at intestinal pH viz., pH 6.0 -7.5 [255]. In the un-ionised state, amorphous HPMC-AS has a high glass transition temperature (*T*g) and in the dry state the *T*g is 120 °C and when exposed to humid air, HPMC-AS adsorbs moisture that plasticises the polymer, increasing mobility of the polymeric chains. This is reflected as a decrease in the *T*g however, the relative hydrophobicity of HPMC-AS results in much less adsorption of moisture than observed with water-soluble polymers. Consequently, the *T*g of HPMC-AS is > 70 °C, even when equilibrated to 75% RH and the low mobility of API molecules dispersed in high *T*g glassy polymers leads to excellent physical stability of dispersions [255].

4.3.1.3 Microcrystalline cellulose (MCC)

MCC is a purified, partially depolymerised, form of cellulose that occurs as a white, odourless, tasteless, crystalline powder and exists as porous particles. MCC is available in different grades, in respect of particle size and moisture content, that exhibit different properties and applications. Avicel® PH101 has a true density of 1.420-1.460 g/cm^3, a

nominal mean particle size of 50 μm and a specific surface area of 1.21-1.30 m^2/g with a moisture content ≤ 5.0%. MCC is a stable hygroscopic bulk material that should be stored in well closed containers in a cool dry place [256]. Avicel® PH101 was used as a diluent in these studies.

4.3.2 Materials

INH powder was purchased from China Skyrun Industrial (Tsim Sha Tsui, Hongkong, China). HPMC-AS grade AS-MF was donated by Shin-Etsu Chemicals Co. Ltd (Tokyo, Japan). Microcrystalline cellulose (MCC) Avicel® PH101 was donated by FMC (Philadelphia, USA). Eudragit® L100 was donated by Rohm Pharma (GmbH, Darmstadt, Germany). Span 80 was purchased from Sigma Aldrich (Darmstadt, Germany). Liquid paraffin was supplied by ADC Laboratories (Durban, KwaZulu-Natal, South Africa). Acetone was purchased from Associated Chemical Enterprises (Southdale, Gauteng, South Africa) and n-hexane was purchased from VWR Chemicals (Fontenay-sous-Bois, France). All chemicals were at least of analytical grade and were used without any further purification.

4.3.2 Methods

4.3.3.1 Preformulation Studies - INH-excipient compatibility

4.3.3.1.1 Differential Scanning Calorimetry (DSC)

DSC thermograms were generated using a Model DSC 7 (Perkin Elmer®, Norwalk, USA), with a: PC control unit TAC 7 (Perkin Elmer®, Norwalk, USA), at a heating rate of 10 °C/min and a nitrogen flow rate of 20 mL/min. Approximately 5.0 mg of individual samples and 1:1 mixtures of INH and excipient to be assessed for compatibility, were weighed directly into aluminium DSC pans and hermetically sealed prior to analysis. The samples were heated at a constant rate using an empty pan as a reference. Samples were placed directly onto a micro hot stage DSC and thermograms were generated at temperatures between 30 and 440 °C. The DSC cell was calibrated for temperature and enthalpy with Indium (mp. 156.6 °C, ΔH_{fus} = 28.4 j/g) and the resultant data were analysed using Pyris™ Manager Software (Perkin Elmer®, Norwalk, USA).

4.3.3.1.2 Fourier Transform (FT) Raman Spectroscopy

A Bruker Ram II spectroscope (Billerica, Massachusetts, USA) fitted with a liquid nitrogen germanium detector and CaF_2 beam splitter was used to record FT Raman spectra. Powder samples of INH and microcapsules manufactured using a formulation composed of 0.75 g INH, 3.41 g Eudragit® L100, 2.1 g HPMC-AS and 1.0 g MCC PH101, were packed separately into small stainless steel cups and subjected to irradiation with a 1064 nm YAG laser beam of 20 mW power to generate Raman scattered light. The FT Raman spectra were recorded over the wavenumber range 40000 cm^{-1} to 50 cm^{-1}.

4.3.3.2 Design of Experiments

A hybrid statistical experimental design was used to assess the influence of amount of (A) HPMC-AS, (B) Eudragit® L100 and (C) homogenisation speed on (Y_1) % yield of microspheres, (Y_2) % INH released in acidic and (Y_3 and Y_5) basic media and (Y_4) encapsulation efficiency. The hybrid design is generated using a Central Composite Design (CCD) for all factors except the last. The levels of the last factor are generated using a D-optimal design. The designs are limited by marginal design properties, have little co-linearity, are rotatable or nearly rotatable, are extremely sensitive to outliers and missing data but are still considered better than using a small CCD only. Each factor is tested at three or five levels and the region of operability must be greater than the region of interest, to accommodate axial assessment or experimental runs. The design has no replication and therefore lack of fitness data is not available for data evaluation. The design is duplicated for every combination of categoric factor level and is used when information must be gathered with a minimum number of experiments [257]. The input variables and concentration range(s) studied were selected based on preliminary investigations and are summarised with the output responses analysed, in Table 4.1.

Table 4. 1 Input variables (coded) and responses monitored for the Hybrid experimental design.

Factor	Code	Coded level				
Independent						
Level		-1.41	-1	0	+1	+1.41
HPMC-AS (g)	A	0.585	1.00	2.00	3.00	3.41
Eudragit® L100 (g)	B	0.585	1.00	2.00	3.00	3.41
Homogenization Speed (rpm, x1000)	C	0.50	1.00	2.00	3.00	3.40
Dependent				**Constraints**		
Y_1 = percent yield				Maximise		
Y_2 = % INH released in 0.1 M HCl at 4 h				Minimise		
Y_3 = % INH released in 0.1 M buffer 6.8 at 12 h				Maximise		
Y_4 = Encapsulation efficiency				Maximise		
Y_5 = % INH released in 0.1 M buffer pH 6.8 at 24 h				Maximise		

A total of 11 experiments, generated using Design Expert Version 7.01 (Stat-Ease Inc., Minneapolis, USA) statistical software, were conducted in a random manner to avoid bias and are summarised in Table 4.2.

.

Table 4. 2 Actual experimental inputs as defined by DOE for the manufacture of microspheres.

Run	HPMC-AS g	Eudragit® L100 g	Homogenisation speed rpm
1	3.414	2.000	1500
2	2.000	2.000	2000
3	2.000	2.000	500
4	3.000	3.000	2500
5	0.585	2.000	1500
6	3.000	1.000	2500
7	1.000	3.000	2500
8	2.000	0.585	1500
9	2.000	2.000	3500
10	1.000	1.000	2500
11	2.000	3.414	1500

Statistical analysis and Response Surface Methodology (RSM) was applied to the responses using Design® Expert software and significant factors ($p < 0.05$) were selected for further investigation and to derive mathematical relationships between input variables and the responses monitored. The best fit models were selected following analysis of several statistical parameters including model p-value, % C.V, correlation coefficient (R^2), adequate precision, and PRESS values in addition to using diagnostic plots such as normal plots of residuals, plots of residuals vs. predicted responses and Box-Cox plots. The results of statistical analysis were used for the optimisation process to identify and select input variables that would categorically yield the desired outcome or responses required in respect of microsphere characteristics and performance.

4.3.3.3 Manufacture of microspheres

Microspheres were manufactured using a modified emulsification solvent evaporation process [258]. A schematic representation of the manufacturing process used is depicted in Figure 4.6.

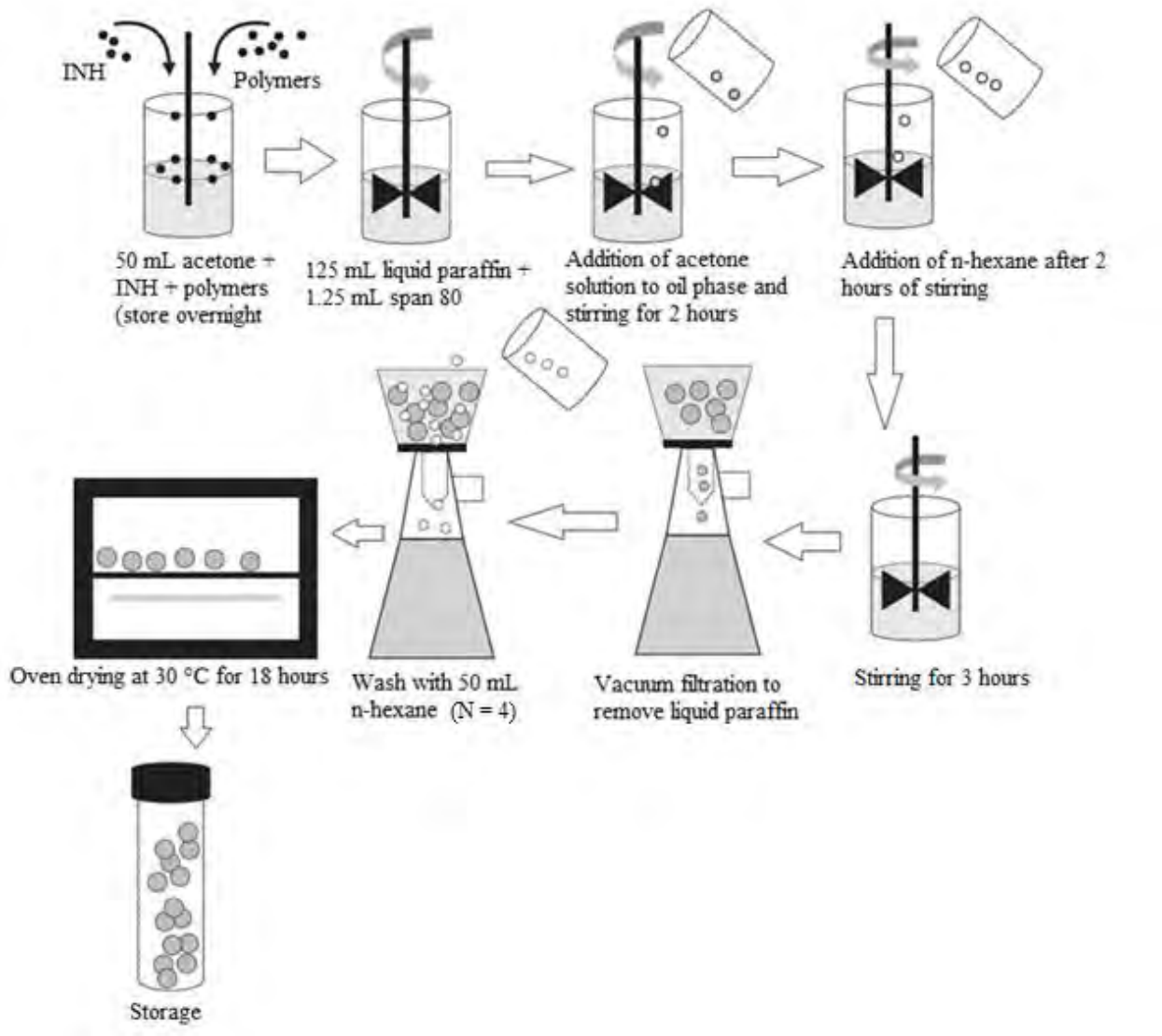

Figure 4. 6 Schematic representation of the manufacturing process used for the production of INH microspheres by solvent evaporation.

HPMC-AS was dispersed in 50 mL acetone in a 400 mL beaker and the mixture left to stand overnight at 22 °C to ensure that the polymer was completely dissolved. Eudragit® L100, MCC PH101 and 0.75g INH were then dispersed in the polymer solution. Light liquid paraffin (125 mL) containing 1 % v/v Span 80 was transferred into a 250 mL beaker and agitated with a homogeniser fitted with a four-blade „„butterfly"" propeller of 50 mm diameter (Virtis Company, New York, USA) to produce an homogeneous oily phase. The entire volume of the acetone solution was poured into the oil solution and dispersed with continuous stirring at 22 °C to facilitate evaporation of the acetone. The volume of liquid paraffin and the acetone solution, amount of MCC PH101 and INH were constant for all batches produced.

After two hours homogenisation, 20 mL n-hexane, the non-solvent, was added to harden the microspheres and stirring continued for a further 3 hours. The hardened microspheres were collected using a Buchner funnel and washed four (4) times with 50 mL n-hexane to remove residual liquid paraffin. The microspheres were dried for 18 hours in an oven maintained at 30°C and then sieved to remove any residual powder prior to storage in 50 mL well-sealed amber bottles. The yield of microspheres was calculated using Equation 4.1.

$$\% \text{ Yield} = \frac{\text{mass of microspheres obtained (g)}}{\text{Theoretical mass of microspheres (g)}} \text{ X } 100 \qquad \text{Equation 4.1}$$

4.3.3.4 Mean particle size and size distribution

The size distribution of the microspheres was determined using a shaking sieve stack (Labortechnik, Ludwigshafen, Germany). The nest of sieves was vibrated at 100 rpm for five minutes, using a mechanical shaker (Kraemer Elektronik GmbH, Darmstadt, Germany) and was constructed with standard sieves of 315, 800, 1250 and 2000 µm mesh/aperture size. The weight of microspheres retained on each sieve was determined and the percent mass retained on each sieve, relative to the cumulative mass used, was calculated. The mean particle size distribution of the microspheres was determined by measuring the diameters of microspheres (n = 20) using Olympus® AnalySIS Soft Imaging System (Olympus®, Munster, Germany)

4.3.3.5 Bulk and tapped density

The tapped density of the microspheres was determined using a model SVM 203 Erweka Tapped Density tester (Heuseastamm, Germany) at a rate of 220 taps per minute for two minutes. The microspheres were poured into a graduated 25 mL A-grade measuring cylinder and the bulk volume before and after tapping (tapped volume) was determined. Carr‟s index (CI) [259] and the Hausner ratio (HR) [260] were calculated using Equations 4.2 and 4.3.

$$\text{CI} = \frac{\text{Tapped density} - \text{bulk density}}{\text{Tapped density}} \text{ X } 100 \qquad \text{Equation 4.2}$$

$$\text{HR} = \frac{\text{Tapped density}}{\text{Bulk density}} \qquad \text{Equation 4.3}$$

4.3.3.6 Encapsulation efficiency

A sample of microspheres containing approximately 50 mg INH was weighed and crushed in a mortar and pestle before dissolving in 50 mL HPLC grade water. The solution was left to stand at 22 °C for 12 hours to ensure complete dissolution of INH. The solution was then vortexed using a Vortex-2 Genie (Scientific Industries Inc., New York, USA) at a frequency of 350 Hz for 5 minutes and filtered through a 0.45 µm HVLP membrane filter (Millipore Millex-HV, Bedford, USA) prior to analysis. A 1.0 mL aliquot was withdrawn from the solution and diluted to 10 mL with HPLC grade water in an A-grade volumetric flask. A 0.6 mL aliquot of the dilute solution was then mixed with 0.3 mL of a 300 µg/mL zidovudine solution in an amber HPLC sample vial and analysed using the validated reversed-phase HPLC method, described in Chapter 3 of this thesis. The encapsulation efficiency as a percent (% EE), was calculated using Equation 4.4 [261].

$$\% \text{ EE} = \frac{\text{Real loaded drug}}{\text{Theoretical loaded drug}} \text{X } 100 \qquad \text{Equation 4.4}$$

4.3.3.7 Scanning electron microscopy (SEM)

The shape and surface morphology of the microspheres was investigated using SEM with a Tescan electron microscope (Vega LMU, Czechoslovakia Republic). The microspheres were mounted onto a double-sized carbon stub that was placed onto a sample disc carrier of 3 mm height and 10mm diameter, prior to sputter coating with gold under a vacuum of 0.25 Torr with a sputter coater (Balzers Union Ltd, Balzers, Lichtenstein). The sample images were generated using a 20 KV electron beam.

4.3.3.8 INH release studies

INH release studies were performed using a Hanson SR8 USP Apparatus 1 (Hanson Research, Chatsworth, USA) instrument modified for this study coupled with an autosampler. A glass basket dialysis method (Figure 4.7) [262] was adapted for use with 900 mL enzyme free pH 6.8 0.1 M phosphate buffer that was continuously stirred at 100 rpm whilst the temperature was maintained at 37 ± 0.5 °C.

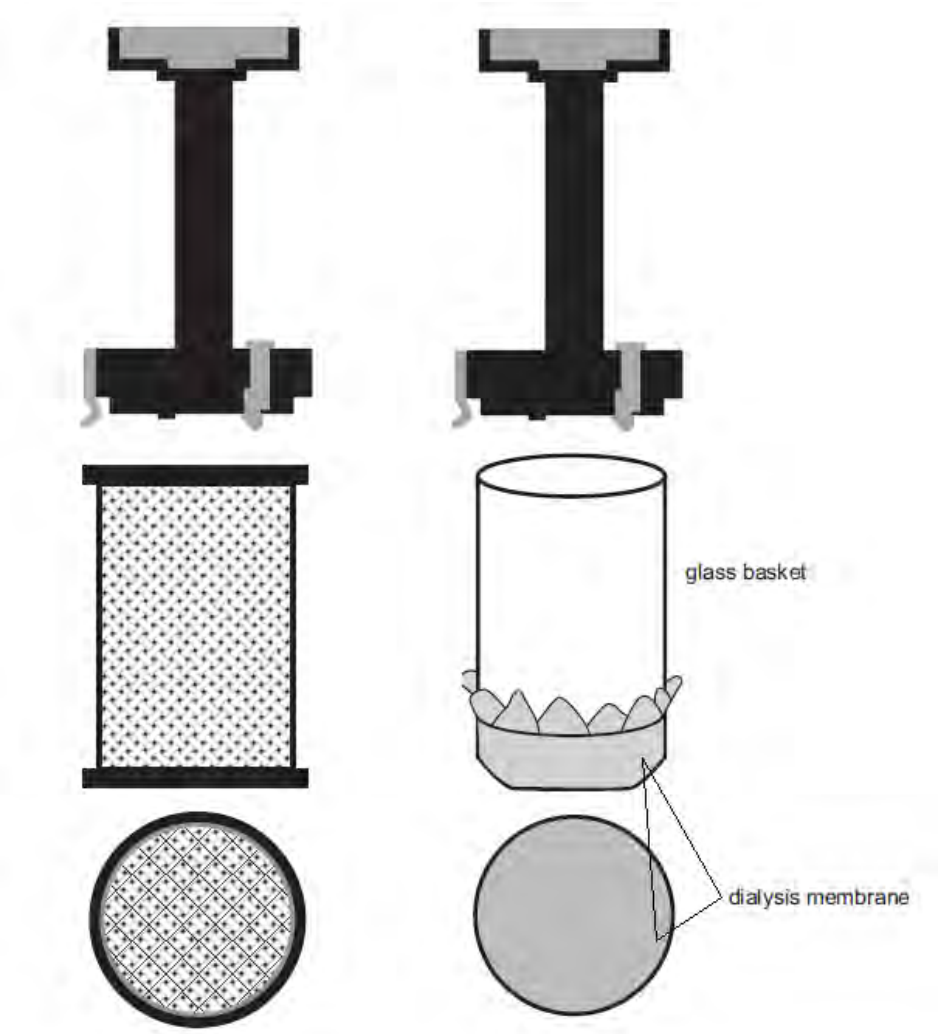

Figure 4. 7 Design of glass basket (right) used in these studies and conventional basket (left) apparatus [262].

0.1 M phosphate buffer was prepared by dissolving 1.36 g potassium dibasic orthophosphate in 500 mL HPLC grade water and then poured into a 1000 mL A grade beaker before making up to volume with HPLC grade water. The pH was monitored using a Model GLP 21 Crison pH meter (Johannesburg, South Africa) and the solution adjusted to the required pH using a 0.1 M NaOH solution or 85 % v/v orthophosphoric acid. A 900 mL aliquot, measured using an A grade measuring cylinder, of the medium was transferred to a 1000 mL dissolution vessel prior to commencing release studies and sink condition was assured as the saturation solubility of INH in a phosphate buffer determined experimentally at 37°C is 18.09 g/L. A sample of microspheres containing approximately 100 mg INH was accurately weighed and placed into glass tube sealed with a dialysis membrane that had been soaked overnight in the dissolution medium. A regenerated cellulose dialysis membrane of MWCO 12-14 KDa

(Sigma Aldrich, Johannesburg, South Africa) was attached to the lower end of a glass tube of 22 mm internal diameter and 35 mm length thereby replacing the dissolution basket (Figure 4.7). The total surface area available for INH release was 380 mm^2. Approximately 2 mL of the dissolution medium was added to the microcapsules to maintain hydration of the membranes and ensure they did not tear when mounting on the glass tube. The dialysis membranes were attached to the tube with an elastic band to prevent leakage and the glass unit was then attached to the shaft of the dissolution apparatus. The tubes were then immersed in the dissolution medium. Dissolution test samples (n = 6) were analysed following withdrawal of 5 mL aliquots of dissolution fluid at 0.5, 4, 6, 12, 18 and 24 hour intervals. The withdrawn dissolution fluid was replaced with fresh one. Aliquots of 0.6 mL were then taken from the withdrawn dissolution fluid and mixed with 0.3 mL of the internal standard solution prior to analysis using the validated reversed-phase HPLC method described in Chapter 3 of this thesis.

4.3.3.9 Kinetics of INH release

The dissolution data for INH microspheres were fitted to zero order [263], first order [264, 265], Higuchi [266], Korsmeyer and Peppas [267, 268], Hixson-Crowell Cube Root Law [269], Baker and Lonsdale [270], Weibull [270] and Hopfenberg [271, 272] models. The data was analysed using DDSolver, a menu-driven add-in program for Microsoft Excel written in Visual Basic for Applications [273]. The model that produced the highest R^2 value was selected as the model that best described the kinetics of INH release from each of the test formulations.

4.4 RESULTS AND DISCUSSION

4.4.1 Preformulation Studies - INH-excipient compatibility

4.4.1.1 Differential Scanning Calorimetry

The DSC thermograms for INH, 1:1 mixtures of INH with HPMC-AS or Eudragit® L100 are depicted in Figures 4.8, 4.9 and 4.10.

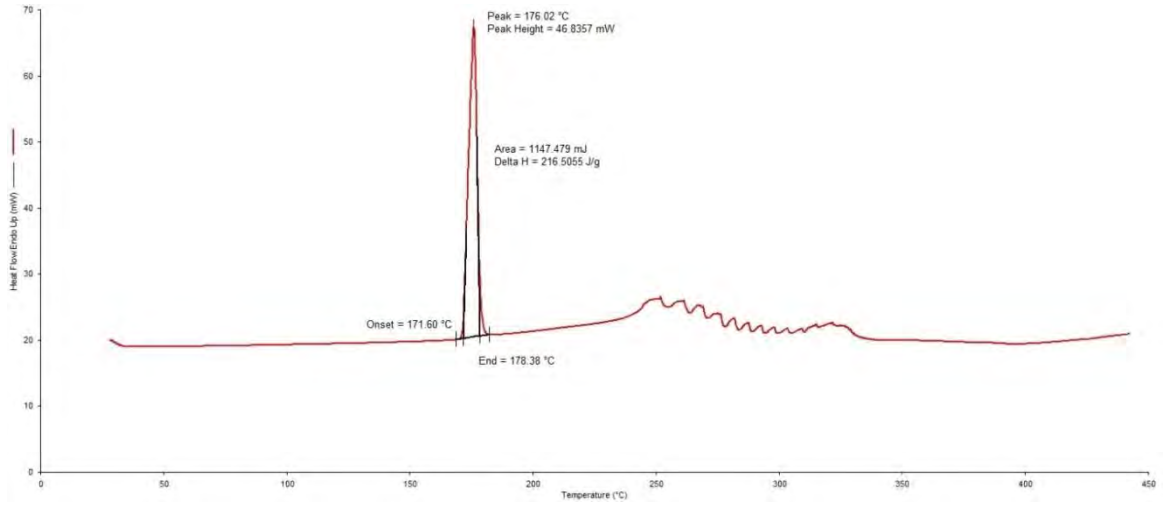

Figure 4. 8 Typical DSC thermogram for INH generated at a heating rate of 10 °C/min over the temperature range 30 – 400 °C.

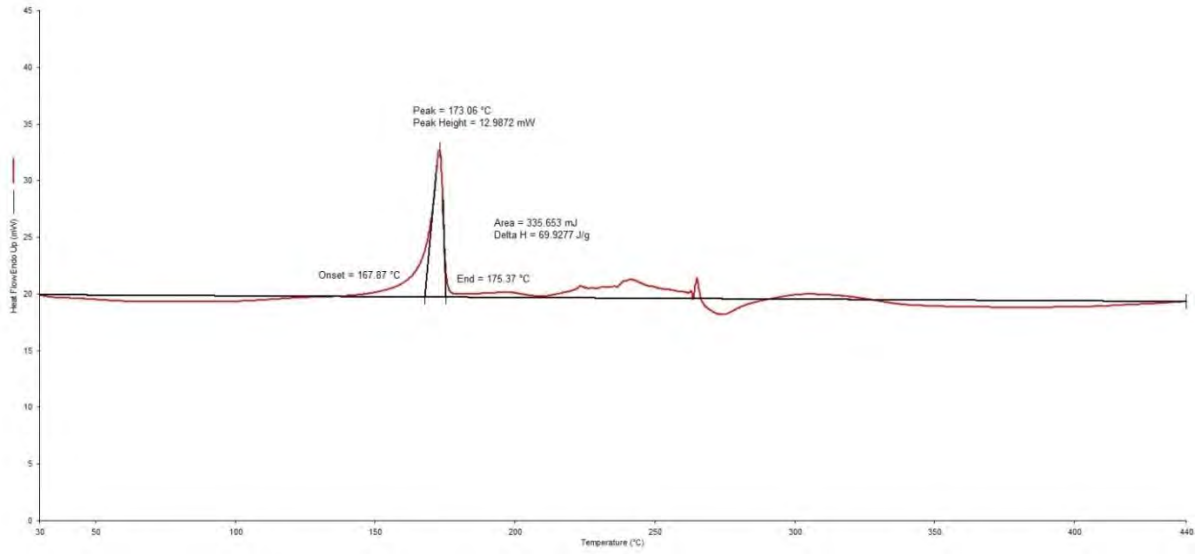

Figure 4. 9 Typical DSC thermogram for a 1:1 mixture of INH and HPMC-AS generated at a heating rate of 10 °C/min over the temperature range 30 – 400 °C.

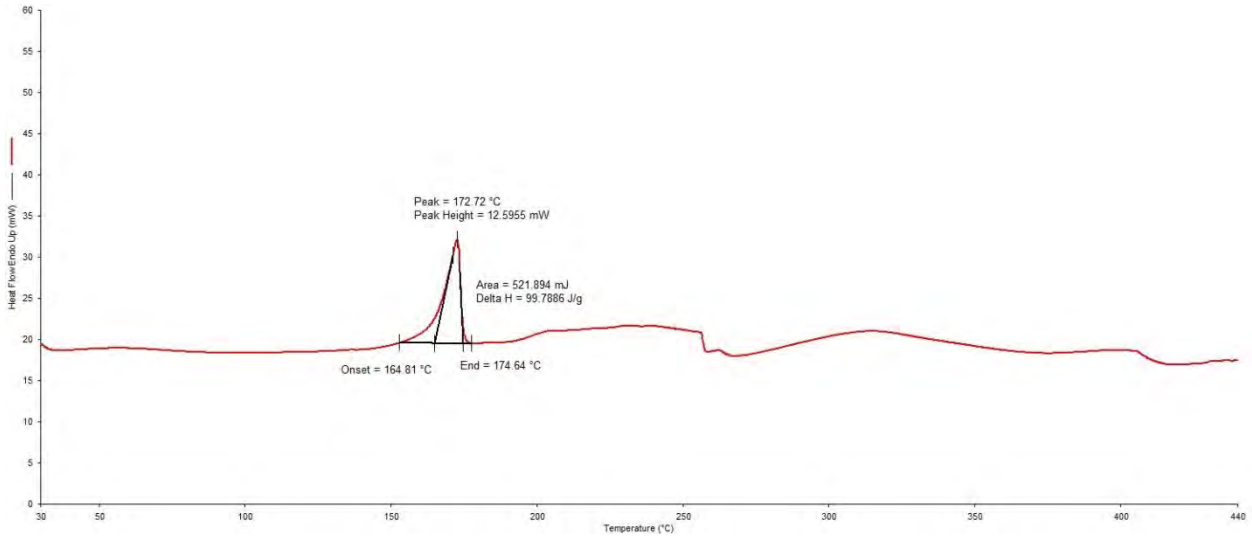

Figure 4. 10 Typical DSC thermogram for a 1:1 mixture of INH and Eudragit® L100 generated at a heating rate of 10 °C/min. over the temperature range 30 – 400 °C.

The DSC thermogram for INH revealed a single sharp endothermic peak ranging at 171.60 °C - 178.38 °C with the apex of the peak at 176.02 °C corresponding to the reported melting range of INH [24] and the sharp peak confirms the crystalline nature of INH with background noise at 250 °C corresponding to degradation of INH. These results are similar to previously reported data [274]. The thermogram of a 1:1 mixture of INH and HPMC-AS revealed the presence of an endothermic peak for INH between 167.87 °C and 175.37 °C with an apex at 173.06 °C and the thermogram for the 1:1 mixture of INH and Eudragit® L100 revealed the presence of an endothermic peak for INH between 164.81 °C and 174.64 °C with the apex at 172.72 °C. The thermograms of the mixtures of INH and polymers revealed a minimal decrease in the melting point of INH with slight broadening at the base of the peak, indicating a slight reduction in the crystallinity of INH. The background presented in Figures 4.8 and 4.9 at 250°C is that of decomposition products of INH and HPMC-AS. These results do not however, suggest a potential or significant incompatibility between INH and the excipient tested, However real time long term stability studies would be required to ensure that this is indeed the case.

4.4.1.2 FT Raman spectroscopy

The FT Raman spectra for INH alone and in microspheres in the presence of all excipients are depicted in Figure 4.11. The comparative frequencies for important functional groups of INH and the microspheres, in relation to what has been reported in literature [275, 276] are summarised in Table 4.3.

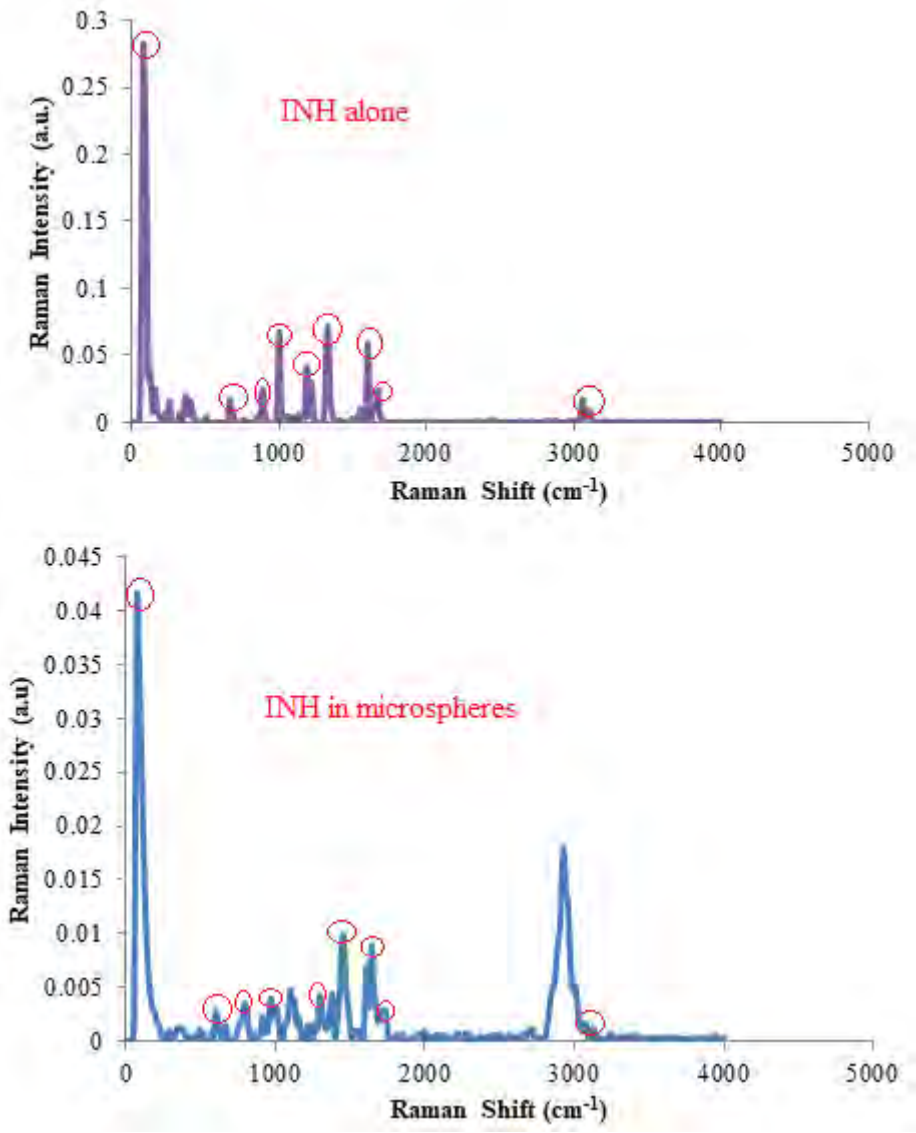

Figure 4. 11 FT Raman spectral data for INH alone and in microspheres.

Table 4. 3 FT Raman shifts and assignments for INH powder and microspheres

Experimental wavenumber cm^{-1}		Literature wavenumber [275] cm^{-1}	Functional Group Assignment
INH	**Microspheres**		
1410.054	1410.054	1410	Ring C=C symmetrical stretching
1550.832	1550.832	1551	Ring C=N symmetrical stretching
1057.146	1057.146	1057	C-C stretching
1668.467	1668.467	1669	C=O stretching
1330.987	1330.987	1331	C-N stretching
3300.132	3301.872	3300	N-H stretching
1130.428	1130.428	1131	$N-NH_2$ stretching
503.6787	503.6787	504	Ring C-C-C symmetrical bending
848.8727	848.8727	849	Ring C-C-H symmetric bending
665.6692	665.6692	666	-C-C-C bending
681.0968	681.0968	682	-C-C=O bending
1552.76	1552.76	1551	H-N-N bending
1494.906	1494.906	1495	C-N-H bending
1602.9	1602.9	1602	Ring C=C asymmetrical stretching
1641.469	1641.469	1642	Ring C=N Asymmetric stretching
2979.919	2979.819	2980	C-H asymmetrical stretching
3064.671	3064.671	3065	C-H asymmetrical stretching
750.5213	750.5213	750	Ring C-C-C asymmetric bending
1001.221	1001.221	1002	Ring C-C-N asymmetric bending
1186.353	1186.353	1187	Ring C-C-H asymmetric bending
1219.137	1219.137	1219	Ring C-C-H asymmetric bending
887.7419	887.4419	887	Ring C-N-C bending

The FT Raman spectroscopic study of the microspheres confirmed the presence of all relevant functional groups for INH and the absence of potential detrimental interactions between INH when incorporated into a microsphere formulation in combination with HPMC-AS and Eudragit® L100. However, real time long term stability studies would be required to ensure that this is indeed the case.

4.4.2 Manufacture of microspheres

4.4.2.1 Microencapsulation

Manufacture using solvent evaporation is based on the evaporation of an internal phase of an emulsion with the aid of agitation. The organic phase is emulsified with agitation in a continuous or bulk phase containing an appropriate surfactant or emulsification agent. When an emulsion is stabilised, in this case with Span 80, maintaining agitation facilitates organic solvent evaporation after diffusion through the continuous phase, resulting in the formation of solid microspheres as depicted in Figure 4.12 [277].

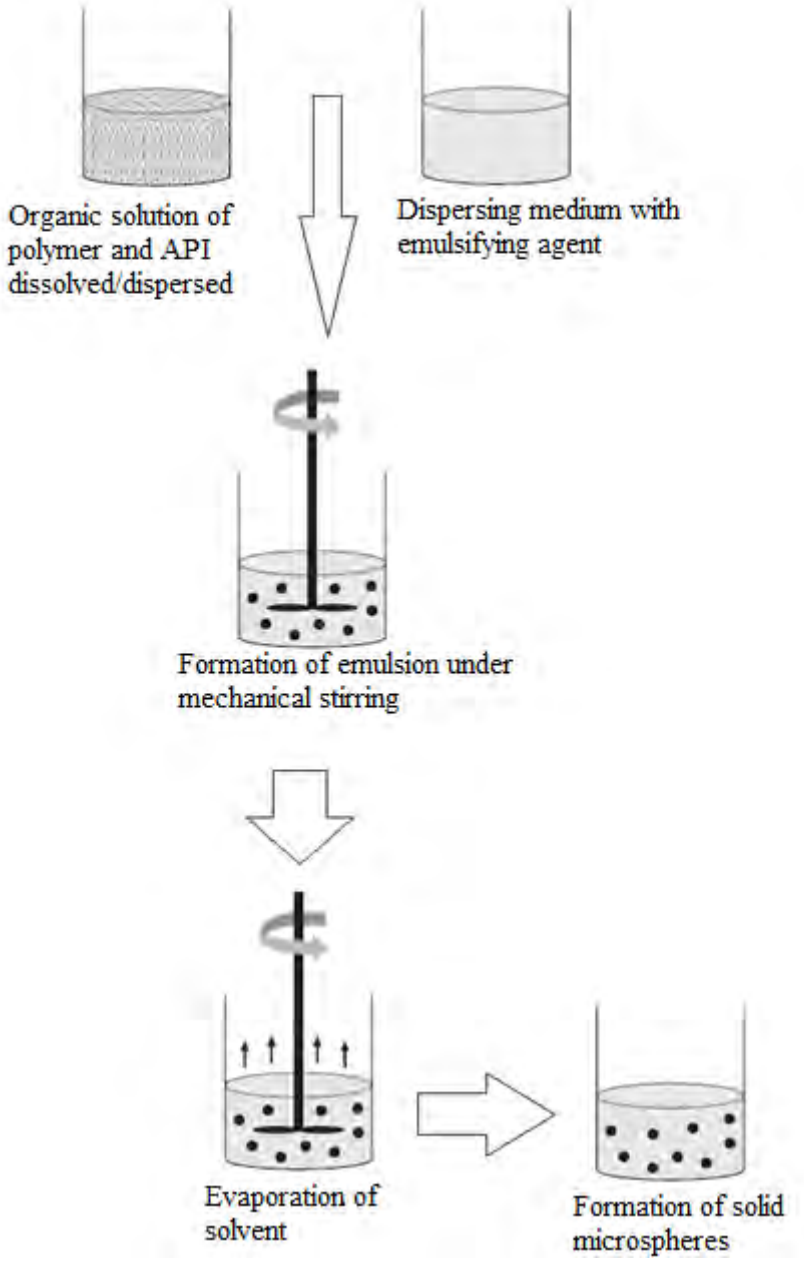

Figure 4. 12 Schematic representation of the formation of microspheres by solvent evaporation [278].

In this study, non-aqueous emulsions of acetone (dispersed phase) and liquid paraffin (continuous phase or dispersion medium) were used as they prevent partitioning of the highly water soluble INH from microspheres that are formed [258, 278, 279]. Acetone was selected for use as the dispersed phase as it is immiscible with liquid paraffin that was used as the continuous phase for this process [258, 280].

4.4.2.2 Response Surface Methodology – Application of a Hybrid Experimental Design

The actual experiments conducted and the responses observed using the Hybrid experimental design are summarised in Table 4.4. ANOVA was applied to the responses to identify input variables that had a significant effect on the responses monitored. The evaluation of model adequacy and ANOVA for % yield, % INH released at 4 h in pH 1.2 0.1 M HCl, % INH released at 24 h in pH 6.8 buffer and encapsulation efficiency are discussed in detail vide infra. The diagnostic plots, ANOVA summary and contour plots depicting the impact of input variables on % INH released at 12 h in pH 6.8 buffer are presented in Appendix 1B.

Table 4. 4 Actual experiments conducted and responses observed using the hybrid DOE.

Run	HPMC-AS	Eudragit®L 100	Homogenisation speed rpm	Yield	INH released at 4 h	INH released at 12 h	Encapsulation Efficiency	INH released at 24 h
	g	g		%	%	%	%	%
1	3.41	2.00	1500	51.32	17.45	45.35	89.67	80.26
2	2.00	2.00	2000	43.30	29.74	64.44	72.57	89.56
3	2.00	2.00	500	56.52	23.30	55.35	77.42	87.45
4	3.00	3.00	2500	48.32	19.05	36.25	65.16	71.28
5	0.485	2.00	1500	21.91	38.42	65.41	50.51	93.16
6	3.00	1.00	2500	45.83	39.33	53.99	70.99	88.67
7	1.00	3.00	2500	40.00	13.02	59.45	68.65	95.20
8	2.00	0.485	1500	21.14	71.04	55.78	55.48	89.81
9	2.00	2.00	3500	31.83	36.66	68.89	60.84	93.58
10	1.00	1.00	2500	22.27	45.86	67.51	66.72	90.96
11	2.00	3.41	1500	47.17	8.82	47.75	89.41	87.87

4.4.2.2.1 Percent Yield (Y_1)

The ANOVA results for % yield are summarised in Table 4.5.

Table 4. 5 ANOVA data for the response surface linear model [Partial sum of squares - Type III] for % yield.

Source	Sum of squares	Df	Mean square	F-value	p-value	Prob > F
Panel A						
Model	1155.74	3	385.25	5.80	0.0260	Significant
A- HPMC-AS	674.77	1	674.77	10.16	0.0153	Significant
B- Eudragit® L100	406.58	1	406.58	6.12	0.0426	Significant
C- Homogenisation speed	74.39	1	74.39	1.12	0.3251	
Residual	465.06	7	66.44			
Cor total	1620.80	10				
Panel B						
Std. deviation	8.15					
Mean	39.06					
% C.V	20.87					
Press	1185.72					
R^2	0.7131					
Adjusted R^2	0.5901					
Predicted R^2	0.2684					
Adeq precision	6.839					

A linear model was selected for data analysis as all diagnostic parameters viz., p-value < 0.05 , PRESS, R^2, adequate precision and normal plot of residuals (Figure 4.13) and the other diagnostic plots (Appendix 1B) were within the limits described in subsections 3.2.1.1.1 – 3.2.1.1.8, implying that the model was adequate for use.

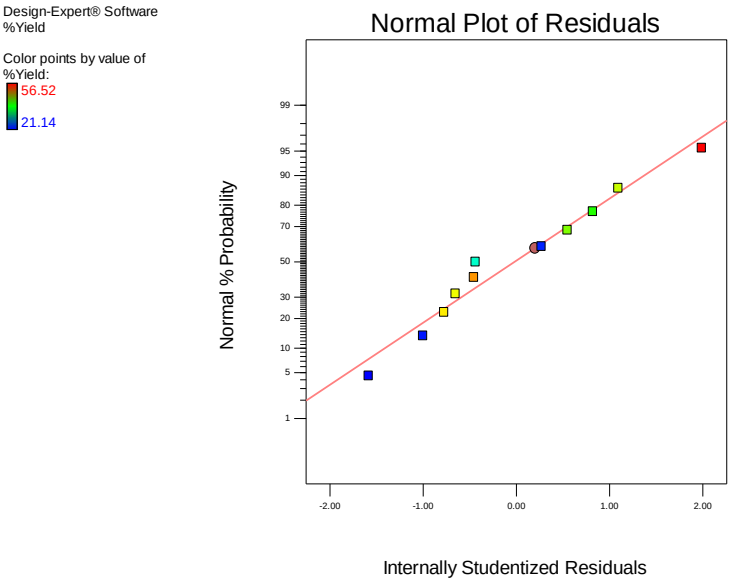

Figure 4. 13 Normal plots of residuals for % yield.

Model terms with values of Prob > F < 0.0500 indicate that the model terms are significant. In this case % yield was significantly affected by HPMC-AS and Eudragit® L100. A contour plot used to visualise the impact of HPMC-AS and Eudragit® L100 is shown in Figure 4.14.

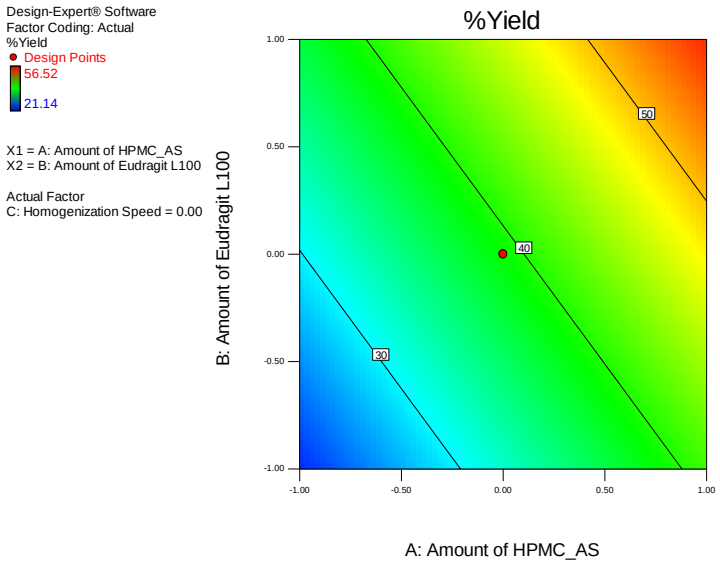

Figure 4. 14 Contour plot depicting the impact of HPMC-AS and Eudragit®L100 content content on % yield.

The results show that increasing HPMC-AS and Eudragit® L100 content resulted in an increase in the % yield, which was attributed to the availability of the polymer to encapsulate formed emulsion droplets. The influence of polymer concentration on % yield of microspheres is discussed in detail in subsection 5.6.3.10. The contour plot used to visualise the impact of homogenisation speed and Eudragit® L100 is shown in Figure 4.15.

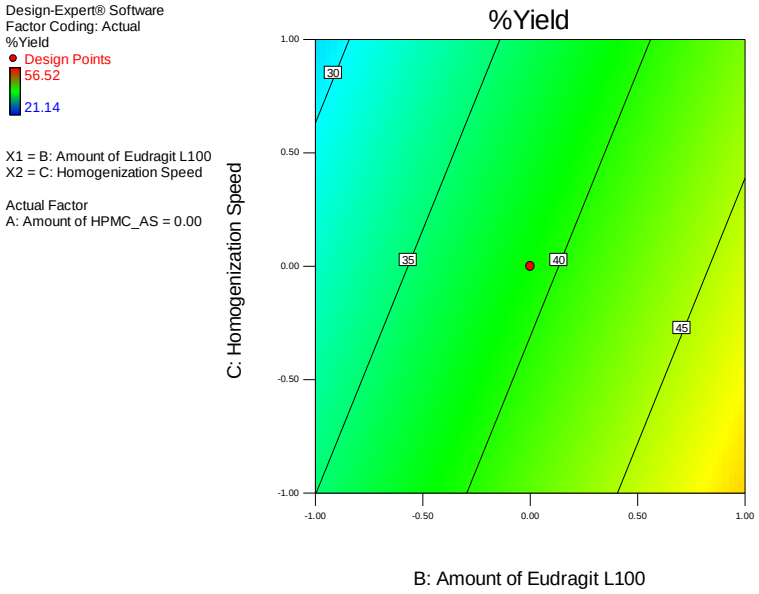

Figure 4. 15 Contour plots depicting the impact of homogenisation speed and Eudragit® L100 content on % yield.

The results show that an increase homogenisation speed resulted in a reduction in the yield and increasing the Eudragit® L100 content increased the yield. Although not significant, increasing the homogenisation speed to speeds > 2000 rpm resulted in a reduction in the yield, a fact corroborated when evaluating Equation 4.5 that describes the relationship between input variables and % yield.

$$Y_1 = 39.06 + 9.18A + 7.13B - 3.05C \qquad \text{Equation 4.5}$$

A similar observation was made when a contour plot (Figure 4.16) used to visualise the impact of homogenisation speed and HPMC-AS content showed that increasing the homogenisation speed resulted in a decrease in the yield and increasing the HPMC-AS content caused an increase in the yield.

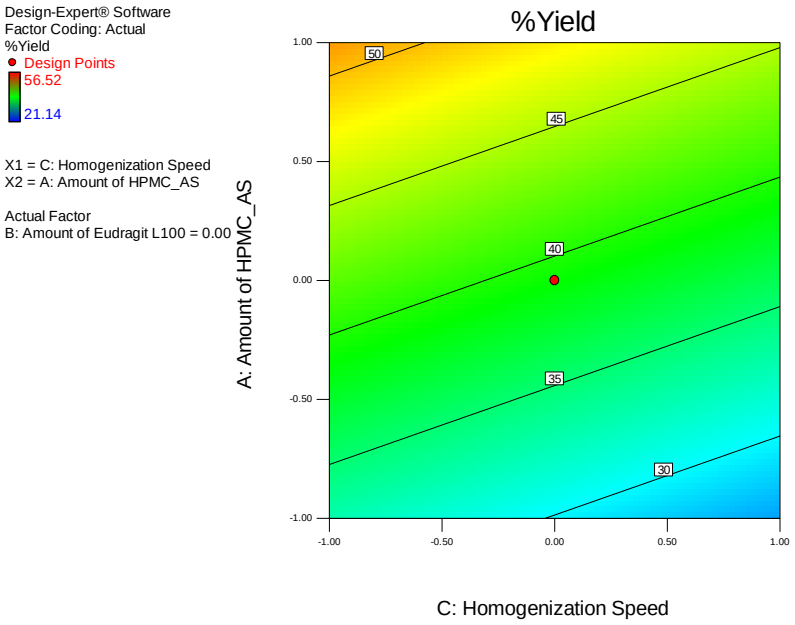

Figure 4. 16 Contour plots depicting the impact of homogenisation speed and HPMC-AS content on % yield.

The decrease in % yield associated with an increase in homogenisation speed may be attributed to the disruption of small o/o emulsion droplets to form a finer dispersion, thereby preventing aggregation of small microspheres [281]. In general, the % yield of microspheres was low and this was attributed to possible small number of emulsion droplets formed when the acetone solution was added to the liquid paraffin. These results suggested a potential challenge with the manufacturing process and issues that may arise when scale up of manufacturing process is required. Although use of low stirring speeds improved the % yield, speeds < 500 rpm could not be used as they did not effectively homogenise the highly viscous polymer solutions and resulted in formation of clumps in the mixing vessel.

4.4.2.2.2 Gastric-resistance and % INH Released at 4h in pH 1.2 0.1 M HCl (Y_2)

A linear model was selected for data analysis as all diagnostic parameters viz., p-value < 0.05, PRESS, R^2, adequate precision and normal plot of residuals (Figure 4.17) and other diagnostics plots (Appendix 1B) were within the defined specifications listed in subsections 3.2.1.1.1 – 3.2.1.1.8 implying that the model is adequate for use.

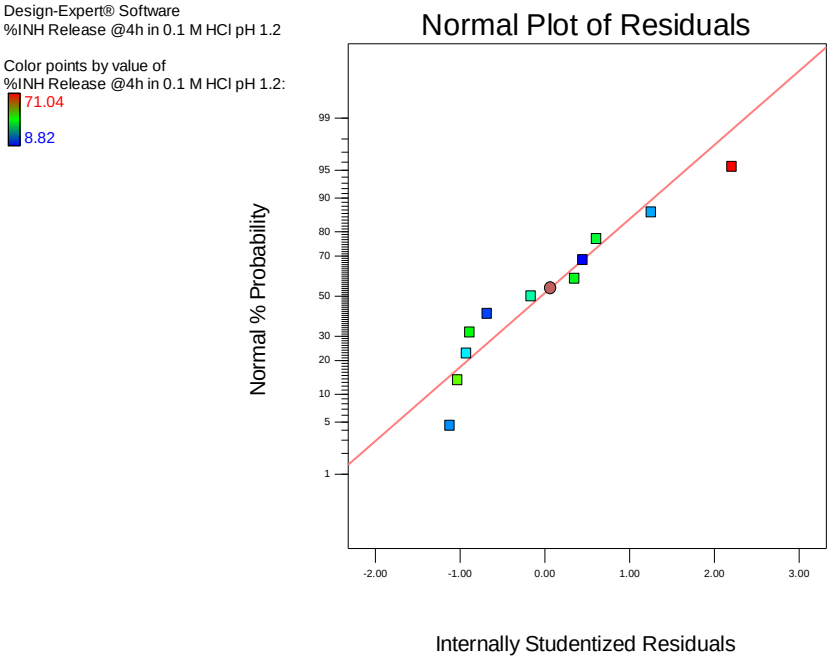

Figure 4. 17 Normal plot of residuals for % INH released at 4 h in pH 1.2 0.1 M HCl.

The ANOVA data for the % INH released at 4 h in pH 1.2 0.1 M HCl are summarised in Table 4.6.

Table 4. 6 ANOVA data for the response surface linear model [Partial sum of squares - Type III] for % INH released at 4h in pH 1.2 0.1 M HCl.

Source	Sum of squares	Df	Mean square	F-value	p-value	Prob > F
Panel A						
Model	2607.01	3	869.00	10.57	0.0054	Significant
A-HPMC-AS	113.67	1	113.67	1.38	0.2782	
B-Eudragit® L100	2489.08	1	2489.08	30.26	0.0009	Significant
C-Homogenisation speed	4.25	1	4.25	0.052	0.8266	
Residual	575.75	7	82.25			
Cor total	3182.76	10				
Panel B						
Std. deviation	9.07					
Mean	31.15					
% C.V	29.11					
Press	1580.64					
R^2	0.8191					
Adjusted R^2	0.7416					
Predicted R^2	0.5034					
Adeq precision	9.123					

Model terms with values of Prob > F < 0.0500 indicate that the model terms are significant. In this case Eudragit® L100 content had a significant impact on gastric-resistance. The contour plot used to visualise the impact of Eudragit® L100 and HPMC-AS content on gastric resistance is shown in Figure 4.18.

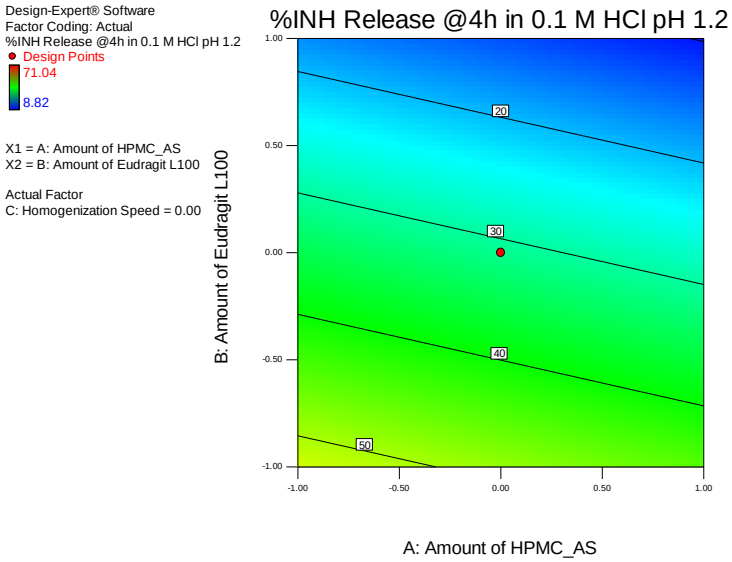

Figure 4. 18 Contour plots depicting the impact of HPMC-AS and Eudragit® L100 content content on gastric-resistance.

The results show that increasing Eudragit® L100 content resulted in a reduction in the extent of INH released in acidic solution that was attributed to the insoluble nature of Eudragit® L100 in pH 1.2 dissolution fluid [246] preventing entry of the medium into the microspheres to dissolve INH. In addition the increase in the diffusional path length for INH to be released from the core of the microspheres results in delay in release. The HPMC-AS content did not have a significant impact on gastric-resistance, although an increase in polymer content resulted in a reduction in the % INH released in the acidic medium confirmed by the negative sign for this parameter in Equation 4.6 that is a mathematical representation of the impact of input variables on gastric-resistance.

$$Y_2 = 31.15 - 3.77A - 17.64B + 0.73C \qquad \text{Equation 4.6}$$

The reduction in % INH released was attributed to the low solubility of HPMC-AS in acidic media in addition to the low flexibility of the polymer as it has a high glass transition temperature in the unionised state in acidic media resulting in a decrease in API mobility [255]. HMPC-AS is reported to be approximately 10 % ionised at pH < 4 and it is therefore

expected to interact with the dissolution medium resulting in release of any INH located on the surface of the microspheres.

The contour plot used to visualise the impact of homogenisation speed and Eudragit® L100 is depicted in Figure 4.19.

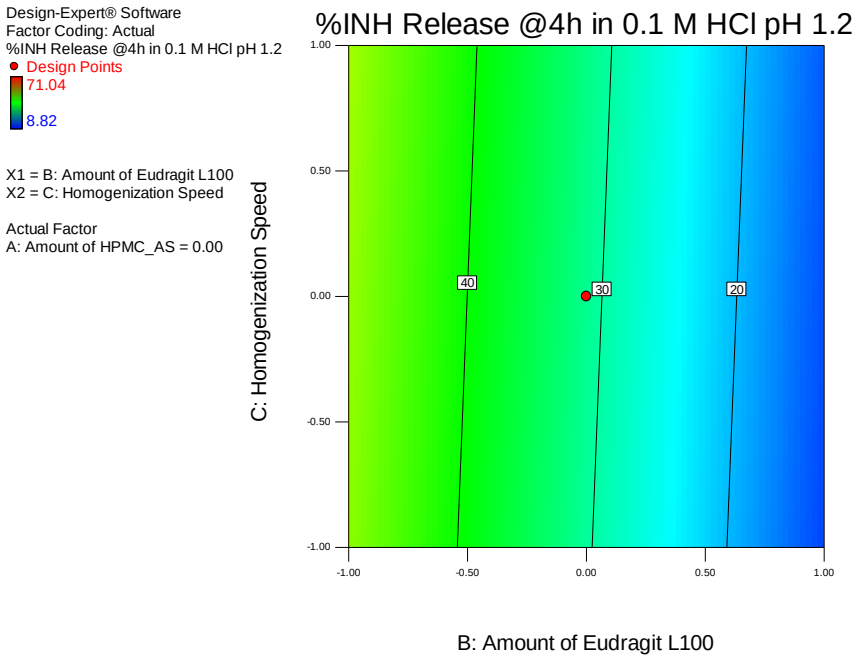

Figure 4. 19 Contour plots depicting the impact of homogenisation speed and Eudragit® L100 content on gastric-resistance.

The results show that increasing the homogenisation speed resulted in a slight reduction in gastric-resistance that is attributed to the formation of small microspheres, at high agitation speeds, that increases the surface area available for INH release, and increasing Eudragit® L100 content resulted in an increase in gastric-resistance. A contour plot (Figure 4.20) used to visualise the impact of homogenisation speed and HPMC-AS content on gastric-resistance also showed that increasing the homogenisation speed reduced gastric-resistance and increasing HPMC-AS content resulted in slightly increased gastric-resistance.

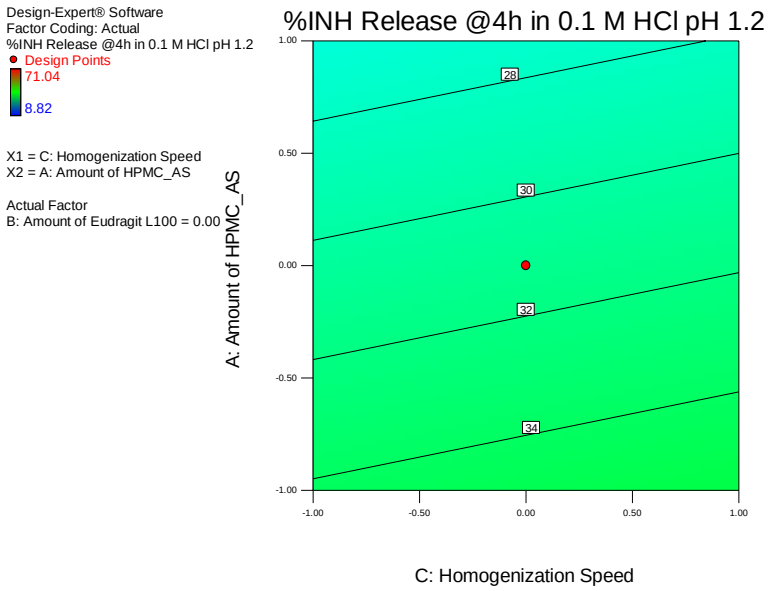

Figure 4. 20 Contour plots depicting the impact of homogenisation speed and HPMC-AS content on gastric-resistance.

Eudragit® L100 has been successfully used as an enteric coating polymer for the manufacture of pH sensitive formulations [282-284], solid dispersions and floating beads [285], microspheres [286, 287], nanoliposomes and nanoparticles [288, 289]. HPMC-AS has also been used as a matrix for the manufacture of pH sensitive formulations [290], solid dispersions [291], enteric coated dosage forms [292] and microspheres [293]. Since INH is highly water soluble, difficulty in controlling release from microspheres in an aqueous medium was anticipated and it was expected that a formulation in which a combination of Eudragit® L100 and HPMC-AS was used, would exhibit excellent gastric-resistance. Analysis of SEM images (Figure 4.21) of microspheres in which the HPMC-AS content was greater than the Eudragit® L100 content revealed formulations with rough surfaces as opposed to smooth surfaced microspheres where the Eudragit® L100 content was greater than HPMC-AS content. The rough surfaces were attributed to deposition of INH particles on the surface of the microspheres that is readily removed on exposure to dissolution medium resulting in an apparent reduction in gastric-resistance of the microspheres in which greater amounts of HPMC-AS than Eudragit® L100 was used. For instance, microspheres from batch INH-006 which contained 3.00 g HPMC-AS and 1.00 g Eudragit® L100 released 39.33 % INH at 4 h in pH 1.2 0.1 M HCl whereas microspheres from batch INH-007 which contained 1.00 g HPMC-AS and 3.00 g Eudragit® L100 released 13.02 % INH at 4 h in pH 1.2 0.1 M HCl. In general, the results suggest significant promise for use in preventing the release of

INH from microspheres in an acidic medium and that high gastric resistance may be achieved when Eudragit® L100 content is high.

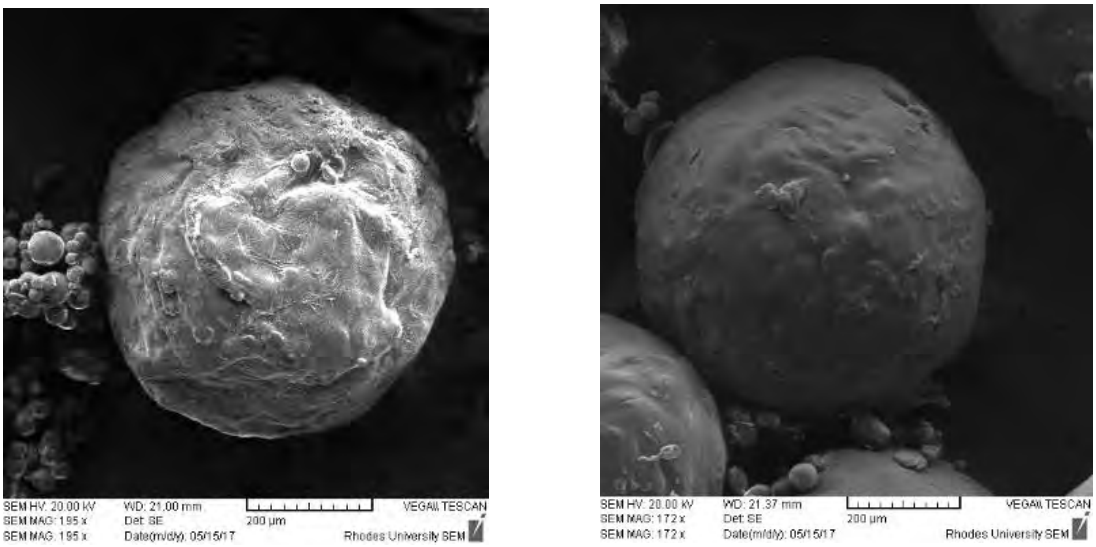

(A) (B)

Figure 4. 21 SEM images of INH microcapsules (A) batch INH-006 (3.00 g HPMC-AS and 1.00 g Eudragit® L100) and (B) batch INH-007 (1.00 g HPMC-AS and 3.00 g Eudragit® L100).

4.4.2.2.3 Percent INH Released in pH 6.8 0.1M phosphate buffer at 24 h (Y_5)

The ANOVA results for % INH released in pH 6.8 0.1 M phosphate buffer at 24 h are summarised in Table 4.7.

Table 4. 7 ANOVA data for a 2FI model [Partial sum of squares - Type III] for % INH released in pH 6.8 0.1 M phosphate buffer at 24 hours.

Source	Sum of squares	Df	Mean square	F-value	p-value	Prob > F
Panel A						
Model	420.28	6	70.05	6.37	0.0472	Significant
A-HPMC-AS	246.99	1	246.99	22.48	0.009	Significant
B-Eudragit® L100	31.57	1	31.57	2.87	0.1654	
C-Homogenisation speed	3.29	1	3.29	0.30	0.6134	
AB	116.98	1	116.98	10.65	0.0310	Significant
AC	7.93	1	7.93	0.72	0.4434	
BC	13.53	1	13.53	1.23	0.3294	
Residual	43.96	4	10.99			
Cor total	464.24	10				
Panel B						
Std. deviation	3.31					
Mean	87.98					
% C.V	3.77					
Press	1655.17					
R^2	0.9053					
Adjusted R^2	0.7633					
Predicted R^2	-2.5653					
Adeq precision	9.045					

A 2-factor interaction (2FI) model was selected for the analysis as all diagnostic statistical parameters viz., a p-value < 0.05, PRESS, % C.V, R^2, adequate precision and normal plot of residuals (Figure 4.22) and other diagnostic plots (Appendix 1B) met all specifications as described in subsections 3.2.1.1.1 – 3.2.1.1.8, implying that the model is adequate for use.

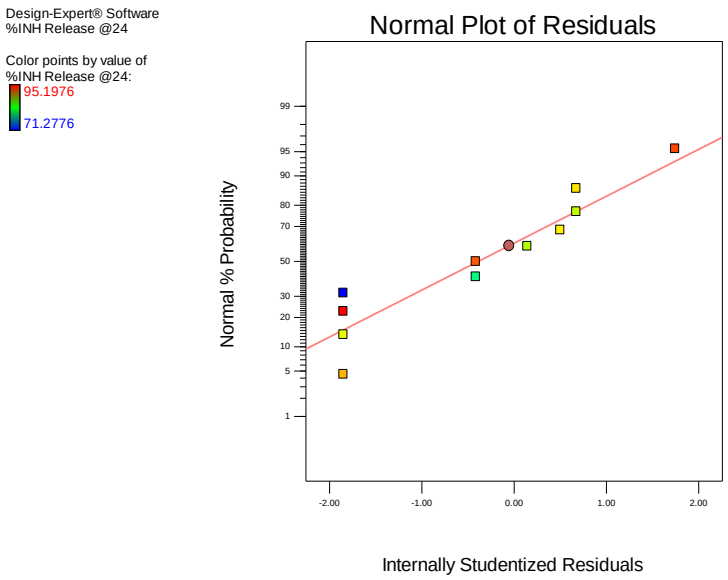

Figure 4. 22 Normal plot of residuals for % INH released in pH 6.8 0.1 M phosphate buffer at 24 h.

Model terms with values of Prob > F < 0.0500 indicate that the model terms are significant. In this case HPMC-AS and ratio of HPMC-AS to Eudragit® L100 had a significant impact on the release of INH in pH 6.8 0.1 M phosphate buffer. The contour plot used to visualise the impact of HPMC-AS and Eudragit® L100 is shown in Figure 4.23.

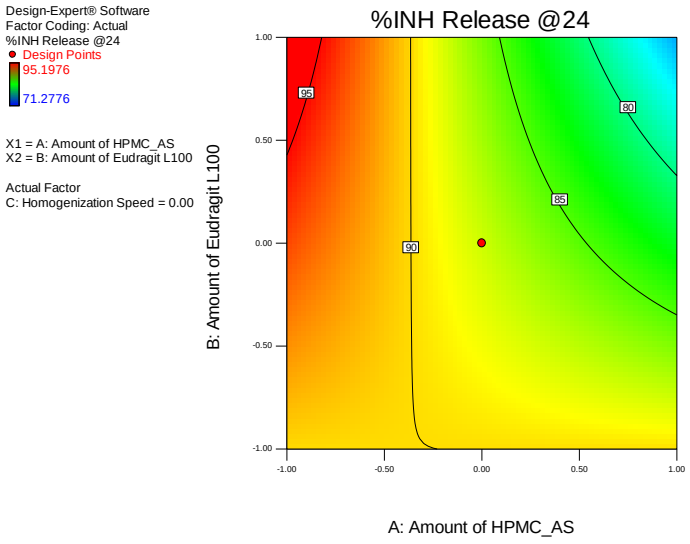

Figure 4. 23 Contour plots depicting the impact of (A) HPMC-AS and Eudragit®L100 content on % INH released in pH 6.8 0.1 M phosphate buffer at 24 h.

The results show that the release of INH was affected by HPMC-AS content with increasing polymer content resulting in decrease in the % INH released which was attributed to increase in the thickness of the diffusional barrier for INH. Increasing the Eudragit® L100 content did not reveal a significant reduction in % INH released, however the interactive effects of HPMC-AS and Eudragit® L100 content had a significant impact on INH release that was confirmed by a p-value of 0.0310 for the model term AB, suggesting that the ratio of HPMC-AS to Eudragit® L100 was an important factor impacting the release of INH.

The contour plot used to visualise the impact of homogenisation speed and Eudragit® L100 is depicted in Figure 4.24.

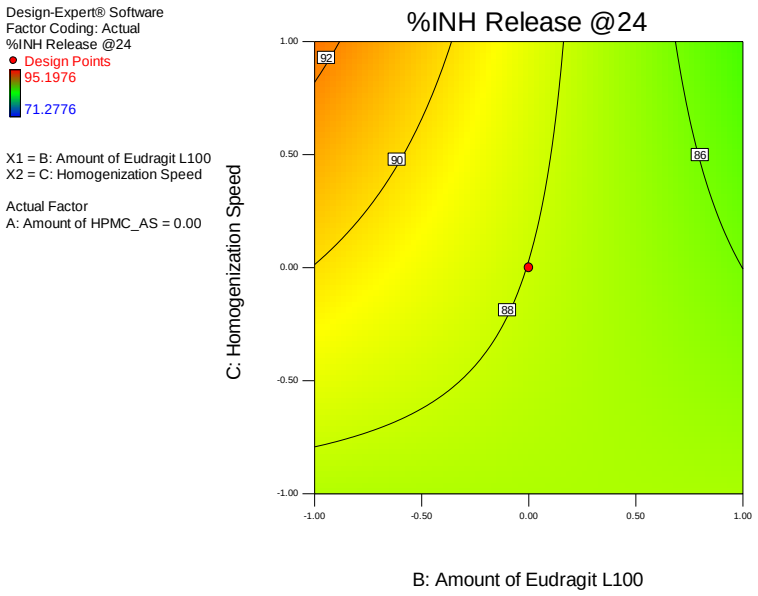

Figure 4. 24 Contour plots depicting the impact of Eudragit® L100 content and homogenisation speed on % INH released in pH 6.8 0.1 M phosphate buffer at 24 h.

The results show that increasing the homogenisation speed resulted in an increase in INH release that could be attributed to the production of small microcapsules with a narrow size distribution, resulting in a large surface area and a reduced barrier for INH diffusion. Increase in the Eudragit® L100 reduced INH release, possibly due an increase in thickness of the diffusion pathway. The contour plot (Figure 4.25) used to visualize the impact of homogenisation speed and HPMC-AS content also showed that increasing the homogenisation speed resulted in an increase in INH release and increase in HPMC-AS content resulted in a reduction in INH release.

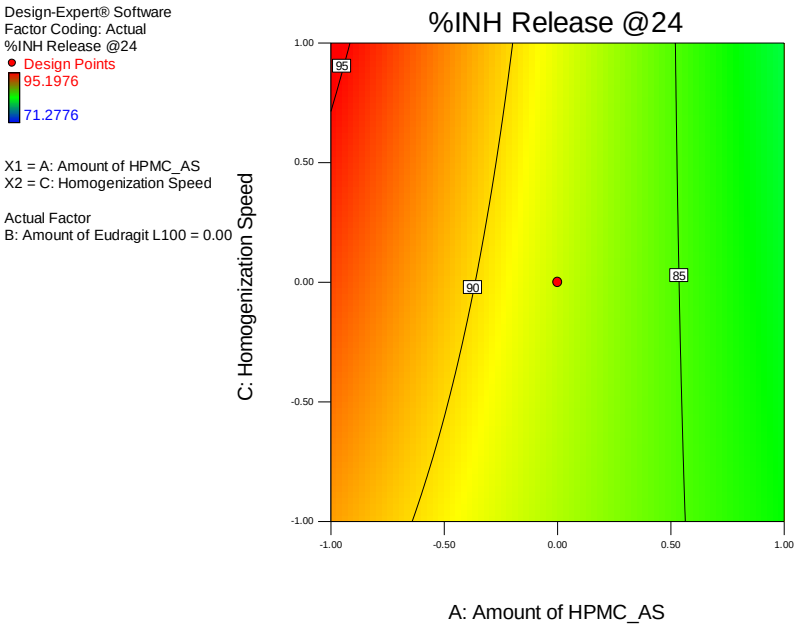

Figure 4. 25 Contour plots depicting the impact of homogenisation speed and HPMC-AS content on % INH released in pH 6.8 0.1 M phosphate buffer at 24 h.

The relationship between the input variables and INH released at 24 h is described in Equation 4.7

$$Y_5 = 87.98 - 5.56A - 1.99B + 0.64C - 5.41AB - 1.41AC - 1.84BC \qquad \text{Equation 4.7}$$

In general, the results suggest that INH release was retarded and sustained despite the use of polymers which were expected to dissolve in pH 6.8 0.1 M phosphate buffer and this was attributed to the presence of HPMC-AS in the formulation. The significant impact of HPMC-AS content on INH release can be attributed to the physicochemical characteristics of this polymer. The succinate functional groups of HPMC-AS have a p*K*a of approximately 5, therefore the polymer is < 10 % ionised at pH values < 4 and is at least 50 % ionised at pH values ≤ 5 [255]. Due to the presence of relatively hydrophobic methoxy and acetate substituents, HPMC-AS is water-insoluble when unionised and remains predominantly colloidal at intestinal pH viz., pH 6.0-7.5. HPMC-AS has many substituents that are relatively hydrophobic and as a result, even when HPMC-AS is ionized at intestinal pH, the polymer remains only sparingly soluble and exists as colloidal polymer aggregates in aqueous solution [255] thereby possibly preventing the entry of dissolution medium into the microspheres and inhibiting rapid dissolution of Eudragit® L100 and INH resulting in a reduction in erosion of

microspheres. The results reveal that > 80 % INH would be released within 24 h, except from microspheres of batch INH004 that were manufcatured with the highest total polymer content.

4.4.2.2.4 Encapsulation efficiency (Y_4)

A 2-factor interaction (2FI) model was selected for data analysis as all diagnostic parameters viz., p-value < 0.05, PRESS, % C.V, R^2, adequate precision and normal plot of residual (Figure 4.26) and other diagnostic plots (Appendix 1B) met all specifications as described in subsections 3.2.1.1.1 – 3.2.1.1.8, implying that the model is adequate for use.

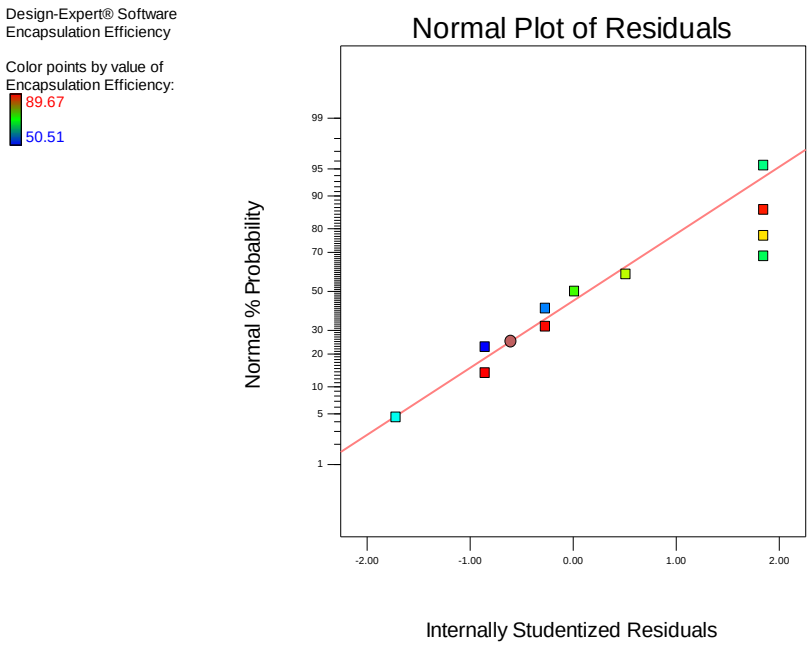

Figure 4. 26 Normal plot of residuals for encapsulation efficiency.

The ANOVA results for % EE are summarised in Table 4.8.

Table 4. 8 ANOVA data for a 2FI model [Partial sum of squares - Type III] for microencapsulation efficiency.

Source	Sum of squares	Df	Mean square	F-value	p-value	Prob > F
Panel A						
Model	1746.84	6	291.14	6.21	0.0494	Significant
A-HPMC-AS	266.35	1	266.35	5.68	0.0757	
B-Eudragit® L100	365.64	1	365.64	7.80	0.0492	Significant
C-Homogenisation speed	17.45	1	17.45	0.37	0.5747	
AB	356.45	1	356.45	7.60	0.0510	Significant
AC	521.66	1	521.66	11.13	0.0289	Significant
BC	219.29	1	219.29	4.68	0.0969	
Residual	187.51	4	46.88			
Cor total	1934.35	10				
Panel B						
Std. deviation	6.85					
Mean	72.49					
% C.V	9.44					
Press	7074.11					
R^2	0.9031					
Adjusted R^2	0.7577					
Predicted R^2	-2.6571					
Adeq precision	7.170					

Model terms with values of Prob > F < 0.0500 indicate that the model terms are significant. The Eudragit® L100 content, interactive effects of HMPC-AS and Eudragit® L100 content and the interactive effects of Eudragit® L100 content and homogenisation speed, had a significant impact on the % EE for INH. The contour plot used to visualise the impact of Eudragit® L100 and HPMC-AS content on % EE of INH is shown in Figure 4.27.

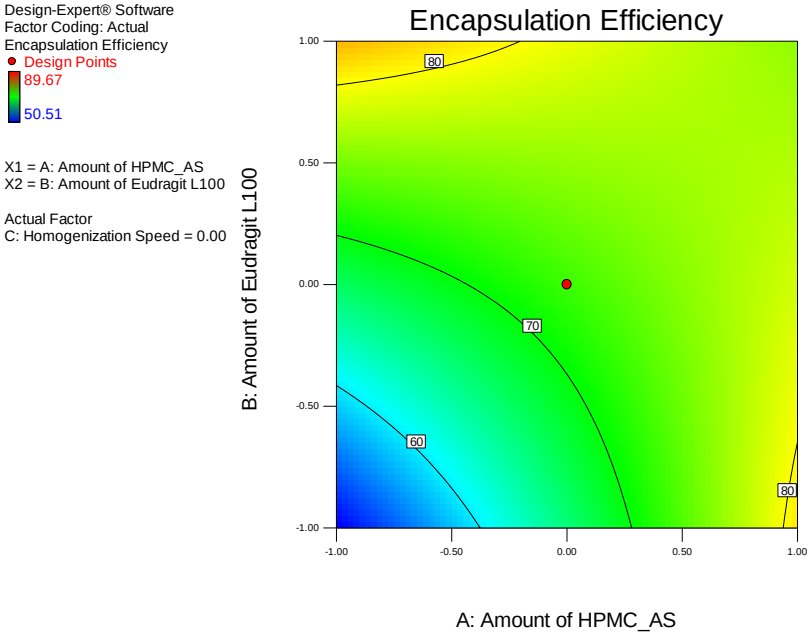

Figure 4. 27 Contour plots depicting the impact of HPMC-AS and Eudragit®L100 content on % EE of INH.

The results show that increasing the content of HPMC-AS and Eudragit® L100 resulted in an increase in % EE that was attributed to an increase in the amount of polymer available to encapsulate INH. The effects of polymer concentration on the % EE in microencapsulation is discussed in detail in subsection 5.6.3.7. The contour plot used to visualise the impact of homogenisation speed and Eudragit® L100 on % EE of INH is depicted in Figure 4.28.

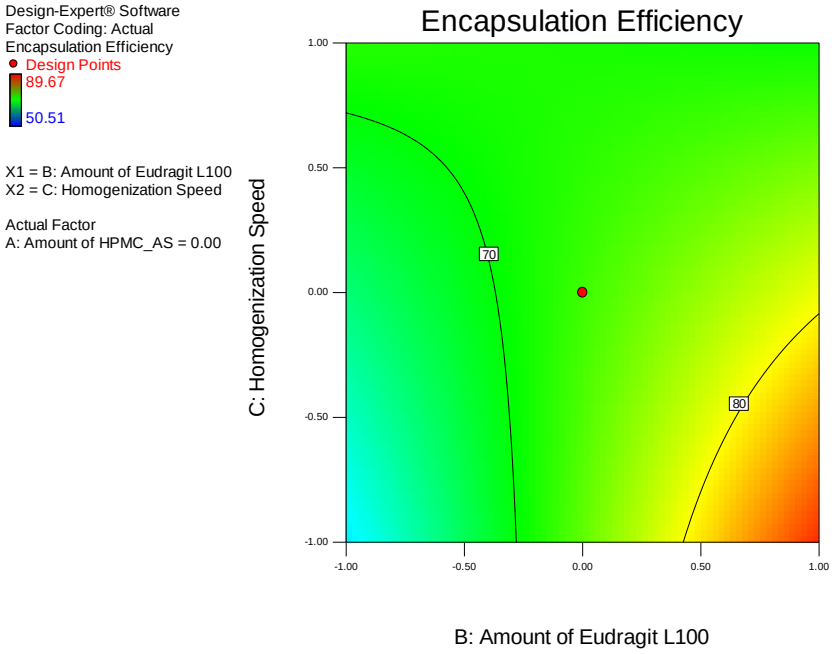

Figure 4. 28 Contour plots depicting the impact of homogenisation speed and Eudragit® L100 content on the % EE of INH.

The results show that an increase in homogenisation speed resulted in a reduction in % EE of INH and an increase in Eudragit® L100 resulted in an increase in the % EE of INH. Similar observation was made on the contour plot (Figure 4.29) used to visualise the impact of homogenisation speed and HPMC-AS content.

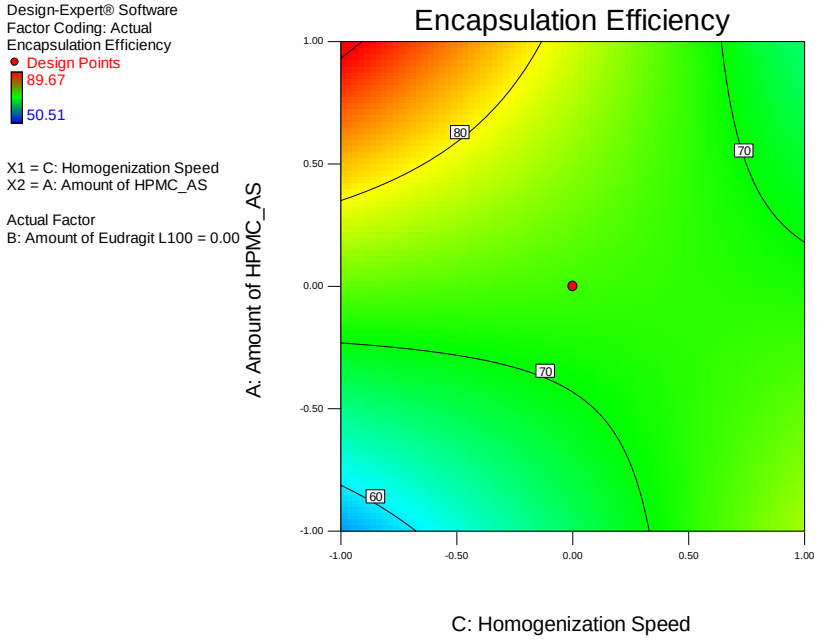

Figure 4. 29 Contour plots depicting the impact of HPMC-AS content and homogenisation speed on encapsulation efficiency of INH.

Although an increase in the amount of polymers resulted in an increase in the % EE, this observation was only applicable when homogenisation speeds < 2000 rpm were used. Increasing the homogenisation speed reduced the % EE regardless of the total polymer content used. The decrease in % EE associated with an increase in homogenisation speed may be attributed to the break up and disruption of small o/o emulsion droplets thereby preventing encapsulation of INH, as aggregation of smaller microspheres during the formation stage could not be achieved [283]. The % EE ranged between 55.48% and 89.67%, with the highest % EE achieved when the total polymer content was 5.41 g and a homogenisation speed of 1500 rpm was used. The lowest % EE were observed for formulations in which the total polymer content was < 3.0 g and homogenisation speeds > 2000 rpm were used. In general, the % EE for INH from all formulations were relatively high, justifying the selection of the o/o emulsification method of manufacture of microspheres with the water soluble INH as the payload. The relationship between input variables and % EE is mathematically represented in Equation 4.8.

$$Y_4 = 72.49 + 5.77A + 6.76B - 1.48C - 9.44AB - 11.42AC - 7.40BC \qquad \text{Equation 4.8}$$

4.4.2.2.5 Particle size distribution

The data generated following sieve analysis is listed in Table 4.9. It is evident that the microspheres had ranged in diameter from 800 to 2000 µm, except for batch INH009 in which particles ranged between 315 µm and 1250 µm. The particle size distribution was influenced by homogenisation speed and total polymer content. Larger microspheres were produced when the total polymer content was high and slow homogenisation speeds were used. The production of larger particles at higher total polymer content may be attributed to the production of a more viscous polymer solution that when poured into the aqueous phase results in the formation of large droplets leading to formation of large microspheres [294]. The decrease in particle size associated with an increase in homogenisation speed may be attributed to the formation of small particle droplets and thus the formation of small microspheres [281].

Table 4. 9 Particle size distribution following sieve analysis

Run	**HPMC-AS**	**Eudragit®**	**Homogenisation speed**	**% mass retained on each sieve**			
	g	**g**	**rpm**				
				315 µm	**800** µm	**1250** µm	**2000** µm
1	3.41	2.00	1500	-	44.7	55.3	-
2	2.00	2.00	2000	-	52.4	47.6	-
3	2.00	2.00	500	-	0	56.1	43.9
4	3.00	3.00	2500	-	58.9	41.1	-
5	0.485	2.00	1500	-	79.6	19.4	-
6	3.00	1.00	2500	-	59.5	40.5	-
7	1.00	3.00	2500	-	58.8	41.2	-
8	2.00	0.485	1500	-	78.7	21.3	
9	2.00	2.00	3500	44.3	47.2	8.5	-
10	1.00	1.00	2500	-	100	-	-
11	2.00	3.41	1500	-	45.3	54.7	-

The intra-batch mean particle size distribution of microspheres from the hybrid design batches and that of the optimised batch formulation is summarised in Table 4.10 and ranged between 415.76 ± 76.93 µm to 903.35 ± 197.10 µm.

Table 4. 10 Mean particle size distribution of INH microspheres

Formulation	Mean particle size µm	Standard Deviation	% RSD
INH-001	745.99	104.26	13.98
INH-002	680.60	367.07	53.93
INH-003	891.28	161.02	18.07
INH-004	615.85	84.20	13.67
INH-005	494.15	113.84	23.04
INH-006	496.82	105.24	21.18
INH-007	515.07	103.39	20.07
INH-008	903.35	197.10	21.82
INH-009	659.30	206.35	31.30
INH-010	415.76	76.93	18.50
INH-011	693.43	154.20	22.24
INH-012	695.22	124.90	17.97

Analysis of the intra-batch mean particle size distribution reveals that the size of microspheres was wide with a % RSD ranging between 13.67 – 53.93 %. The implications of the microsphere size distribution are discussed in detail in Section 5.6.5.

4.4.2.2.6 Carr's Index and Hausner Ratio

Carr"s Index (CI) and the Hausner ratio (HR) were used to assess the flowability of the microspheres. All batches exhibited excellent flow characteristics that were attributed to the spherical nature of the microspheres. The mean CI for the microspheres was 4.934 ± 0.775% and HR was 1.148±0.033 and indicated good packability of the microspheres and would ensure good weight and content uniformity of the dosage units. The microspheres were also hard and bouncy and the hard nature of the microspheres was attributed to the high glass transition temperature of HPMC-AS [255] and the addition of n-hexane as hardening agent contributed to the formation of hard free flowing microspheres.

4.4.2.2.7 Scanning electron microscopy

The SEM images of microspheres from the batches manufactured are depicted in Figure 4.30 (A – I). In general the microspheres were spherical and uniform in shape, thereby explaining their free flowing characteristics. The microspheres were characterised by rough and corrugated surfaces, particularly formulations for which the content of HPMC-AS was high and for which high homogenisation speeds were used. Microspheres in which the Eudragit®

L100 content was > HPMC-AS content appeared, in general, to have smooth surfaces, for example batch INH-005 (Figure 4.30E) and batch INH-012 (Figure 4.30J). In general the microsphere surfaces were devoid of pores, which may also have contributed to the gastric-resistance and sustained release characteristics of the formulations, except for batches in which the total polymer content was < 3.0 g, as for batch INH-008 (Figure 4.30F) and batch INH-010 (Figure 4.30H).

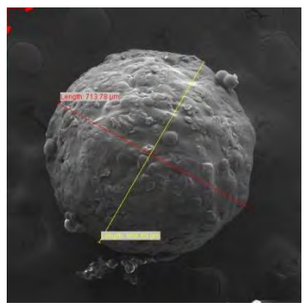

(A)

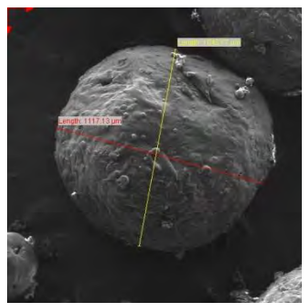

(B)

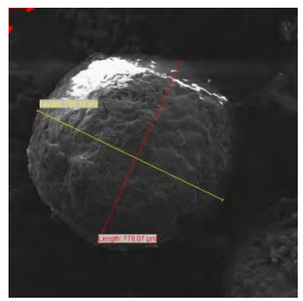

(C)

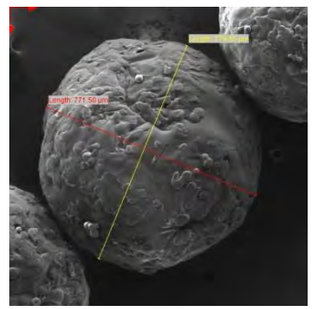

(D)

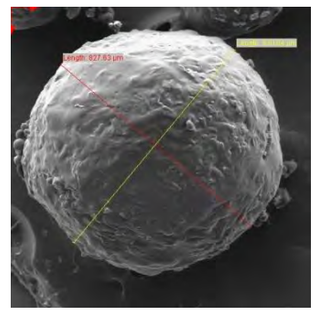

(E)

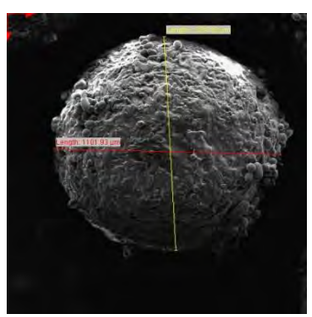

(F)

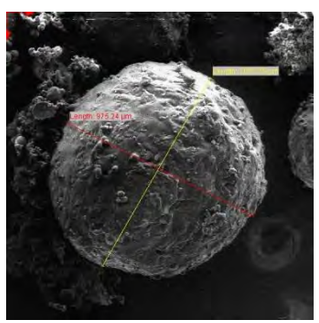

(G)

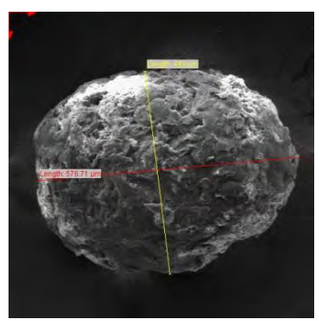

(H)

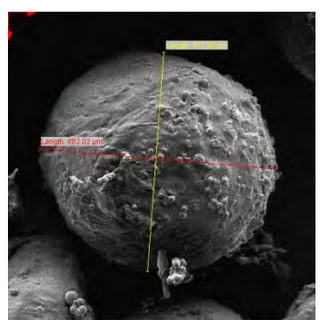

(I)

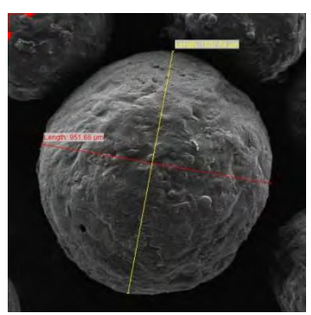

(J)

Figure 4. 30 SEM micrographs of INH loaded microspheres (A) batch INH-001, (B) batch INH-002, (C) batch INH-003, (D) batch INH-004, (E) batch INH-005, (F) batch INH-008, (G) batch INH-009, (H) batch INH-010, (I) batch INH-011 and (J) batch INH-012.

4.4.2.3 Optimisation of formulation and process variables

The polynomial equations in which the dependent and independent variables are related were used in combination with observations made during the manufacturing process to identify and optimise formulation variables that would produce microspheres that met the target responses defined vide infra. The desired target constraints of the highest % yield, minimal % INH released at 4 h in pH 1.2 0.1 M HCl, > 80 % INH released at 24 h in pH 6.8 buffer and the high encapsulation efficiency possible were entered into Design® Expert software and possible options of combinations of input variables that would yield these outputs were identified. The input variables selected were then used to manufacture three batches viz., INH-012, INH-013 and INH-014 and were considered the optimised option. The experimentally generated outputs following evaluation of the three optimised batches were then compared to the predicted responses generated by Design Expert software (Table 4.11) to assess the prediction accuracy of the optimisation process.

Table 4. 11 Comparison of predicted and experimentally derived responses.

Batch	Response	Predicted value	Observed value	Residual	%P.E.
INH-012	% Yield	51.35	50.41	0.940	1.830
	% INH released at 4 h in pH1.2 0.1 M HCl	5.745	8.510	5.989	48.13
	% INH released at 12 h in pH 6.8 0.1M	47.88	67.13	19.25	40.21
	phosphate buffer	90.81	87.37	3.440	3.788
	Encapsulation efficiency (%)	86.62	90.96	4.340	5.010
	% INH released at 24 h in pH 6.8 0.1M				
	phosphate buffer				
INH-013	% Yield	51.35	52.89	1.540	2.999
	% INH released at 4 h in pH 1.2 0.1 M HCl	5.745	8.810	3.219	53.35
	% INH released at 12 h in pH 6.8 0.1 M	47.88	68.22	20.34	42.48
	phosphate buffer	90.81	80.79	10.02	11.03
	Encapsulation efficiency (%)	86.62	99.20	12.58	14.52
	% INH released at 24 h in pH 6.8 0.1M				
	phosphate buffer				
INH-014	% Yield	51.35	53.92	2.570	5.004
	% INH released at 4 h in pH 1.2 0.1 M HCl	5.745	8.720	2.975	51.78
	% INH released at 12 h in pH 6.8 0.1M	47.88	67.75	19.87	41.50
	phosphate buffer	90.81	80.77	10.04	11.06
	Encapsulation efficiency (%)	86.62	87.87	1.250	1.443
	% INH released at 24 h in pH 6.8 0.1M				
	phosphate buffer				

The prediction accuracy of the process was established by calculating the residuals, (R), and percent prediction error (% P.E.) for the three optimised batches. The residuals and % P.E. for the responses were considered acceptable for % yield, encapsulation efficiency and % INH released at 24 h in pH 6.8 buffer where the % P.E. was < 12 %. The % P.E. values for % INH released at 4 h in pH 1.2 0.1 M HCl and % INH released at 12 h in pH 6.8 buffer were very high, indicating the models used were poor predictors for these two responses and that the use of a hybrid experimental design may not be accurate and perhaps the absence of replication points and lack of fit data for model evaluation is a disadvantage suggesting other experimental designs and selection of models which exhibit a good fit for parameters under investigation should be considered in future studies. The optimised formulation was comprised of 2.1 g HPMC-AS, 3.41 g Eudragit® L100, 1.0 g MCC PH101 and 0.75 g INH, using 125 mL liquid paraffin containing 1.0 % v/v Span 80, 50 mL acetone and a homogenisation speed of 1500 rpm. The use of the identified input variables produced an average yield of 52.41 ± 1.80 % with significant gastric-resistant microspheres as only 0.523 ± 0.13 % INH was released after 2 h and 8.68 ± 0.16% released after 4 h in pH 1.2 0.1 M HCl. The optimised formulation exhibited an average encapsulation efficiency of 82.92 ± 3.80 % and 92.68 ± 5.86 % INH was released after 24 h of dissolution testing. The dissolution profile for % INH released from the optimised formulation in pH 6.8 0.1M phosphate buffer is depicted in Figure 4.31 and the dissolution profiles for % INH released for all other batches manufactured are reported in Appendix 2A.

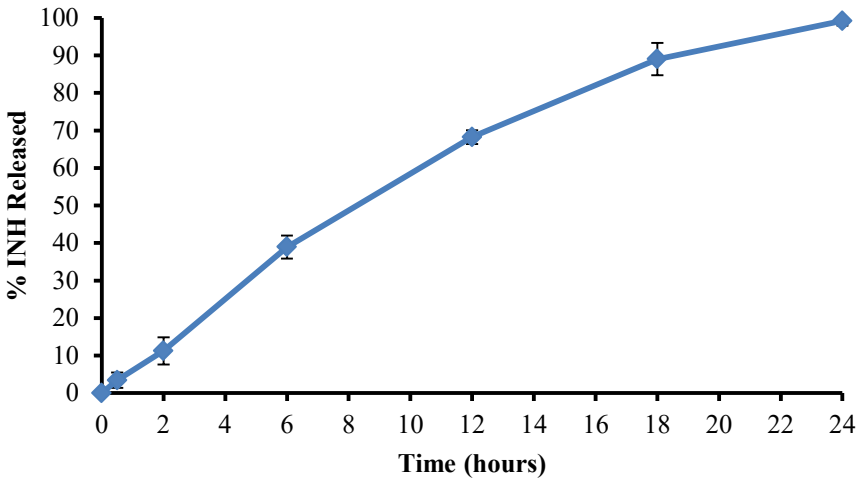

Figure 4. 31 Mean dissolution profile (n=6) of % INH released from the optimised formulation in pH 6.8 0.1 M phosphate buffer.

4.4.2.4 INH Release Kinetics

A summary of the results following fitting of dissolution data for INH from microspheres to different mathematical models is summarised in Table 4.12. The results reveal that INH release from batches INH001, INH002, INH006 and INH007 followed the Hopfenberg model (R^2 = 0.9832) indicating that erosion of the spherical matrix of the microspheres is the rate limiting step for INH release [271, 272, 295]. This observation was further supported by a high R^2 value of 0.9827 from the Hixson-Crowell model that also suggests a change in the surface area of the microspheres is implicated in release as erosion of the polymers occurs [269, 295]. The high R^2 value for the Weibull model further confirms that INH release occurred by the transport of INH molecules through the matrix of this technology [210, 295]. The release of INH from batch INH003 fitted the Weibull model with a R^2 value of 0.9945. The microspheres from this batch were manufactured at the lowest homogenisation speed and were therefore the largest in size indicating that factors affecting transport of INH through the matrix would play an important role in INH release. This observation was supported by high R^2 values following fitting of data to the Hopfenberg and Korsmeyer-Peppas models with R^2 values of 0.9791 and 0.9717 respectively, indicating that INH release is dependent on erosion of microspheres as well as diffusion of INH through the matrix of the technology [271, 272, 295-298]. INH release from microspheres of batches INH004 and INH005 was best fitted to the Korsmeyer-Peppas model indicating that erosion of the matrix and diffusion of INH through the matrix was critical for release [267, 268, 295].

The high R^2 values observed for the Weibull, Hopfenberg and Zero-order models indicate that INH release occurred through a spherical matrix and the rate of release was dependent on the amount of API dispersed in the matrix [210, 264, 271, 272]. The release of INH from microspheres of batches INH008, INH009, INH010, INH011 and INH012 were best fitted to the Weibull model indicating that INH release occurred predominantly through the matrix. The high R^2 values associated with the Higuchi, Korsmeyer-Peppas, Hixson-Crowell and Hopfenberg models suggests that a number of factors are responsible for INH release from the microspheres. The value of the release exponent, n, following fitting of data to the Korsmeyer-Peppas model ranged between 0.416 to 1.066 for most batches, confirming that INH release is controlled by multiple mechanisms [267, 268]. The value of n for most batches was $0.43 < n < 0.85$ and was >

1 for batch INH-004 only, indicating that INH release from the spherical dosage form followed an anomalous mechanism and occurred via a thin film or encapsulation layer comprised of HPMC-AS and Eudragit® L100. INH release therefore occurs via a combination of diffusion, polymer relaxation and dissolution and/or erosion from these microspheres and selection of polymers and other excipients that would promote these characteristics should be considered [295-298].

Table 4. 12 Summary of results of mathematical modelling of dissolution data for INH from batches of microsphere.

MODEL	BATCH NUMBER											
	INH001	**INH002**	**INH003**	**INH004**	**INH005**	**INH006**	**INH007**	**INH008**	**INH009**	**INH010**	**INH011**	**INH012**
Zero-Order												
R^2	0.9576	0.8991	0.9696	0.9929	0.9004	0.8609	0.9736	0.6580	0.8079	0.8051	0.9667	0.9500
K_0	3.745	4.385	4.026	3.401	4.326	4.480	4.411	4.756	4.691	4.573	4.115	4.645
First-Order												
R^2	0.9755	0.9973	0.9428	0.9466	0.9811	0.9899	0.9571	0.9522	0.9929	0.9913	0.9694	0.9446
K_1	0.063	0.091	0.068	0.051	0.088	0.099	0.082	0.134	0.115	0.109	0.074	0.091
Higuchi												
R^2	0.9250	0.9777	0.8712	0.8564	0.9713	0.9694	0.9133	0.9534	0.9874	0.9839	0.9162	0.9040
K_H	15.333	18.337	16.211	13.562	18.065	18.842	17.945	20.517	19.922	19.428	16.780	18.957
Korsmeyer-Peppas												
R^2	0.9789	0.9901	0.9717	0.9942	0.9844	0.9759	0.9850	0.9649	0.9875	0.9841	0.9816	0.9670
K_{KP}	7.153	13.560	5.017	2.803	13.169	15.267	7.169	25.720	19.505	18.966	7.098	8.255
n	0.778	0.611	0.925	1.066	0.616	0.578	0.834	0.416	0.508	0.509	0.813	0.803
Hixson-Crowell												
R^2	0.9827	0.9958	0.9652	0.9669	0.9796	0.9840	0.9804	0.9161	0.9793	0.9739	0.9860	0.9688
K_{HC}	0.018	0.025	0.020	0.015	0.024	0.027	0.023	0.036	0.031	0.029	0.021	0.026
Hopfenberg												
R^2	0.9832	0.9984	0.9791	0.9935	0.9819	0.9899	0.9972	0.9521	0.9929	0.9913	0.9910	0.9832
K_{HB}	0.022	0.012	0.036	0.035	0.011	0.003	0.049	0.000	0.000	0.000	0.032	0.048
n	2.354	7.150	1.339	0.918	7.566	32.474	0.998	1141.203	2197.787	3491.386	1.701	1.218
Baker-Lonsdale												
R^2	0.8861	0.9449	0.8192	0.8119	0.9376	0.9433	0.8561	0.9701	0.9721	0.9710	0.8673	0.8449
K_{BL}	0.005	0.009	0.006	0.004	0.008	0.009	0.008	0.013	0.011	0.010	0.007	0.009
Weibull												
R^2	0.9827	0.9981	0.9945	0.9908	0.9811	0.9899	0.9956	0.9754	0.9948	0.9946	0.9962	0.9898
K_α	25.330	12.685	74.693	88.523	11.622	10.491	47.193	4.284	7.170	7.159	38.308	47.738
K_β	1.184	1.062	1.644	1.557	1.008	1.015	1.552	0.733	0.912	0.889	1.415	1.630

4.5 CONCLUSIONS

HPMC-AS and Eudragit® L100 have been successfully used for manufacture of INH loaded gastric-resistant sustained release microspheres. A Hybrid experimental design was used to investigate the influence of input variables such as homogenisation speed and amount of HPMC-AS and Eudragit® L100 on gastric-resistance, INH release and % EE. The manufacturing process resulted in the production of hard spherical particles and particle size analysis revealed that the microspheres ranged between 415.76 ± 76.93 µm to 903.35 ± 197.10 µm in diameter. The microspheres exhibited excellent flow properties that were attributed to the spherical nature of particles. The CI was 4.934 ± 0.775 % and the HR was 1.148 ± 0.033 indicating good packability of the microspheres that would help in achieving weight and content uniformity of dosage units. The manufacturing process however produced a low % yield which suggests potential scale up difficulties, although the recorded high % EE may counter the challenges associated with a low yield. The microspheres also exhibited sustained release characteristics and exhibited no burst release in pH 6.8 buffer as < 5 % INH was released at 0.5 h and only 11 % INH was released at 2 h. The release of INH was sustained over the entire period of dissolution testing with > 85 % INH released at 24 h implying that the majority of encapsulated INH would be available for absorption. The approach of using coating polymers viz., HPMC-AS and Eudragit® L100, to manufacture gastric resistant sustained release microspheres of INH is unique and is efficient at preventing the release of INH in an acidic environment. As only 0.523 % INH was released from the optimised formulation after 2 h exposure to pH 1.2 0.1 M HCl there is also the potential to minimise the accelerated degradation of RIF that occurs in the presence of INH. The prevention of degradation also enhances the possibility of improving the bioavailability of RIF from a FDC containing INH and RIF. The formulation has the potential to be used in combination TB dosage forms that include RIF as there is a potential to prevent an interaction between INH and RIF in the acidic environment of the stomach, since little or no INH is likely to be released in the stomach. The potential application of these microspheres in reducing degradation of RIF in the presence of INH in acidic media is discussed further in Chapter 6 of this thesis.

CHAPTER FIVE

MANUFACTURE OF MICROPOROUS FLOATING RIFAMPICIN MICROSPHERES

5.0 INTRODUCTION

Floating drug delivery systems (FDDS) are a group of gastric retentive dosage forms (GRDF) that are designed to remain in the stomach for a prolonged and predicted period of time [299]. Prolongation of gastric retention may improve bioavailability, reduce waste and improve the solubility of API that are less soluble in high pH environments thereby enhancing local delivery in the stomach and/or the proximal small intestine [299, 300]. Prolonging gastric residence times permit dosing interval adjustment possibly enhancing patient adherence behaviour [301].

5.1 BASIC GASTROINTESTINAL ANATOMY AND PHYSIOLOGY

Anatomically the stomach is divided into three regions viz., fundus, body, and antrum or pylorus. The proximal part or fundus and body are a reservoir for retention of undigested materials whereas the antrum is the primary location for mixing, and is the pump site for gastric emptying [302]. Gastric emptying occurs in the fed and fasted state, however the pattern of motility is distinct for each state. In the fasted state an inter-digestive series of electrical events take place that cycle through the stomach and intestine every two to three hours [303]. This activity is known as the inter-digestive myoelectric cycle or migrating myoelectric cycle (MMC), which is further divided into four phases [304] viz., Phase I (basal phase) which is between forty and sixty minutes in duration and is characterized by rare contractions; Phase II (pre-burst phase) that also has a duration of forty to sixty minutes and is characterised by intermittent action potential and contractions; Phase III (burst phase) that lasts for four to six minutes and includes intense and regular contractions of short duration in which all undigested material is swept from the stomach into the small intestine and is also known as the “housekeeper” wave. Phase IV is a refractory phase that is approximately of five minutes duration and occurs between Phases III and I of two consecutive cycles.

Following ingestion of a meal, the pattern of contractions changes from the fasted state to that of the fed state and is known as the digestive motility pattern that is comprised of continuous contractions as for Phase II, of the fasted state [305]. The contractions ensure a reduction in the

size of food particles to < 1 mm that are then propelled toward the pylorus in suspension form. In the fed state, the onset of MMC is delayed, resulting in a reduction of the gastric emptying rate [305].

5.2 FACTORS AFFECTING GASTRIC RETENTION

The gastric residence time of an oral dosage form is affected by several factors. In order to pass through the pyloric valve into the small intestine, the particle size of the gastric contents should be in the range of 1 - 2 mm [304]. The pH of the stomach may affect gastric emptying and in the fasted state ranges between 1.5 and 2.0 whereas in the fed state between 2.0 and 6.0. In general a large volume of water is administered with an oral dosage form that results in an increase in the pH of the stomach contents to between 6.0 and 9.0. Sufficient acid is not produced when liquid enters the stomach and therefore API that exhibit better solubility in high pH environments are dissolved better in the fed than the fasted state [304].

The rate of gastric emptying is dependent on the viscosity, volume and caloric content of meals or the contents of the stomach [306]. An increase in the acidity and caloric value of a meal results in an increase in gastric emptying time [306]. Biological factors such as age, body mass index (BMI), gender, posture and diseases, such as diabetes and Crohns disease, can influence gastric emptying [306] and in general, elderly patients exhibit slowing of gastric emptying time [306]. In general females have slower gastric emptying rates than males [306] and stress increases the gastric emptying rate whereas depression slows it down [306].

The resting volume of the stomach is approximately 25 to 50 mL and the volume of liquids administered can affect gastric emptying time [299]. If the volume of fluid administered is large, gastric emptying is rapid. Fluids administered at body temperature are emptied more rapidly from the stomach than cold or warm liquids [299]. Studies have revealed that gastric emptying of a dosage form in the fed state may also be influenced by the dimensions of the delivery technology [299]. Small tablets may pass through the stomach during the digestive phase whereas large tablets are only emptied when the housekeeper wave empties the contents of the stomach.

A number of formulation parameters may also affect gastric residence time [307]. Reliable gastric emptying patterns have been observed for multi-particulate dosage forms when compared

to single unit technologies that are delivered using an „all or none concept". Since the individual units of multi-particulate systems are freely distributed throughout the gastrointestinal tract, transport of the small particles is affected to a lesser extent by food transit times when compared to single unit technologies [307].

As mentioned, the dimensions (size and shape) of a dose unit may also affect the gastric emptying time of stomach contents [299]. The diameter of the dose unit is an equally important formulation consideration [308]. The density of a dosage form may also affect gastric emptying rates [299] and buoyant dosage forms with a density less than that of the gastric fluids float. Since a floating dosage form will be located at a distance from the pyloric sphincter, they are retained in the stomach for a prolonged period of time [299].

In a study to assess the effect of buoyancy, posture and content of meals on gastric emptying *in vivo*, gamma scintigraphy of floating and non-floating capsules of different size viz., 4.8 mm (small), 7.5 mm (medium) and 9.9 mm (large) were manufactured [308]. A comparison of floating and non-floating dosage units revealed that, regardless of size, the floating dosage units remained buoyant in the gastric compartment throughout the time of residence in the stomach, whereas non-floating units sank and remained in the lower part of the stomach. Floating units, distal to the gastro-duodenal junction were protected from peristaltic waves during the digestive phase of activity, whereas non-floating forms were located proximally to the pylorus and were subjected to propelling and retro-pelling waves of the digestive phase of motility.

It was observed that the floating units of small and medium dimension had a longer gastric residence time when compared to non-floating units and no significant difference was observed for all large unit dosage forms. When subjects were in the supine position, floating dosage forms were retained in the stomach due to their size, as buoyancy was no longer adequate for gastric retention. A comparison between dosing in the fed and fasted states, on gastric emptying was also undertaken. All subjects remained in an upright position and one group fed a light breakfast and the other a succession of meals at predefined time intervals. It was established that as meals were taken at a time when the previous digestive phase had not yet been completed, the floating dosage forms were retained in the stomach for another digestive phase period as it was transported with peristaltic waves in the upper part of the stomach. These nuances, in respect of

gastric emptying, must form an integral part of design process for dosage forms, particularly if there is a need to target specific delivery sites and profiles for an API.

5.3 CONSIDERATIONS WHEN DESIGNING FLOATINING DOSAGE FORMS

Various approaches have been used for the design of floating delivery systems for single- and multiple-unit dosage forms and these are discussed *vide infra.*

5.3.1 Single-Unit Dosage Forms

A number of approaches can be used to ensure that single dose units float. The low-density approach makes use of a body or shell of lower density than gastric fluid and can also be used as a controlled release carrier for an API [309]. Coated shells, popcorn, pop rice and polystyrol have been exploited for buoyant technologies [310]. Sugar-based polymeric materials, such as methacrylic acid and cellulose acetate phthalate, have been used as an undercoat for shells that are further coated with an API-polymer mixture. The coating polymer may be ethyl or hydroxypropyl cellulose and is selected on the basis of the target release characteristics desired. Such products float on the surface of gastric fluids whilst releasing their payload slowly over a prolonged period [310].

Buoyant dosage forms can also be developed using fluid-filled systems that float in the stomach [309] and therefore an alternate strategy makes use of fluid-filled floating chambers that include gas-filled floatation chambers, merged into a micro-porous compartment that houses a reservoir [311]. An aperture or opening is located along the top and bottom walls of the device through which gastrointestinal tract fluids can enter and dissolve the API in the reservoir. The other walls, in contact with the fluid, are sealed so that undissolved API is sequestered within the chamber. The fluid used may be air, under partial vacuum or any other suitable gas, liquid or solid with an appropriate specific gravity and should be inert. The device must be suitable to swallow, remain afloat in the stomach for a prolonged period of time and be designed to ensure that the shell disintegrates or transits from the intestine and is eliminated once the payload has been released [311].

Hydrodynamic balanced systems (HBS) are single unit systems designed to prolong residence in the gastrointestinal tract and enhance API absorption [299]. HBS are suited for API that are

soluble in acidic environments and those that exhibit site specific absorption in the upper part of the small intestine. In order to remain in the stomach for prolonged periods, the dosage form must have a bulk density < 1 g/cm^3 [301], retain structural integrity and release API constantly. Some of the polymers used in the design of HBS include hydroxypropyl cellulose, hydroxypropyl methylcellulose, crosspovidone, sodium carboxymethyl cellulose and ethyl cellulose [299]. Single-unit formulations are associated with challenges such as adhesion to other units and obstruction possibly resulting in irritation of the GIT mucosae [299].

5.3.2 Multiple-Unit Dosage Forms

The purpose of designing multiple-unit dosage forms is to develop reliable formulations that exhibit similar advantages to single-unit systems without the obvious disadvantages of single-unit formulations. In pursuit of this endeavour, many multiple-unit floatable dosage forms have been designed and include microspheres with a high loading capacity manufactured using polymers such as albumin, gelatin, starch, polymethacrylate, polyacrylamine and polyalkylcyanoacrylate [312]. Spherical polymeric micro-sponges, also referred to as "micro-balloons", have been developed such that the microspheres include a hollow internal structure and exhibit excellent *in vitro* floating ability [312]. Carbon dioxide generating multiple-unit oral formulations are devices with features that extend, unfold or are inflated by carbon dioxide generated, in the device, following administration and have been described in the recent patent literature [313]. These dosage forms, if in the expanded state, are excluded from passage through the pyloric sphincter as the diameter exceeds approximately 12 to 18 mm.

5.4 CLASSIFICATION OF FLOATING DRUG DELVERY SYSTEMS

Floating delivery technologies are classified into one of two groups viz., effervescent and non-effervescent dosage forms.

5.4.1 Effervescent Dosage Forms

Effervescent floating systems are generally matrices, manufactured using swellable polymers such as methylcellulose and chitosan, in combination with sodium bicarbonate, tartaric acid and/or citric acid as the effervescent components and are manufactured in a manner that when exposed to gastric fluids, CO_2 is liberated and trapped in the swollen hydrocolloid matrix providing buoyancy to the dosage form(s) [299, 313].

5.4.2 Non-Effervescent Dosage Forms

Non-effervescent floating dosage forms make use of a gel forming or swellable cellulose based hydrocolloids, polysaccharides or other matrix-forming polymeric materials such as polycarbonate, polyacrylate, polymethacrylate and/or polystyrene [299]. The manufacturing process is simple and includes thorough mixing of the API and gel-forming hydrocolloid, such that following oral administration, the dosage form swells and has a bulk density of < 1 g/cm^3. The air trapped by the swollen matrix imparts buoyancy to the dosage form and the swollen gel-like structure acts as a reservoir that ensures sustained release of an API through the swollen colloidal mass [299].

RIF is primarily absorbed from the stomach and duodenum [131] and therefore there is a possibility that RIF can be incorporated into a technology to promote site-specific release in the stomach and/or proximal part of the small intestine.

The objective of this study was to develop, manufacture and evaluate a microporous floating sustained release microsphere technology for the delivery of RIF to the stomach and proximal small intestine. Initial studies focused on *in vitro* evaluation and future studies will be required to assess the performance of this technology *in vivo*.

5.5 EXPERIMENTAL

5.5.1 Polymers

5.5.1.1 Ethylcellulose

Ethylcellulose (EC), an ethyl ether substituted derivative of cellulose, is a long-chain polymer comprised of β-anhydro-glucose units joined by acetal linkages [314]. EC is a tasteless, free-flowing white to light tan-coloured powder that is generally regarded as a non-toxic, non-allergenic, non-irritating excipient. In oral formulations EC is used as a water insoluble coating material for coating tablets and granules [315 - 317] and as a matrix forming excipient [318]. High-viscosity grades of EC are used for microencapsulation [319] and since EC adsorbs very little water from humid air or when immersed the polymer dries readily when a small amount of water evaporates and it is therefore considered an excellent barrier to water [320]. EC has been used for the manufacture of floating dosage forms [321, 322].

5.5.1.2 Eudragit® RLPO

Eudragit® RLPO is a block copolymer comprised of ethyl acrylate, methyl methacrylate and a limited amount of methacrylic acid ester with 10 % quaternary ammonium functional group substitution. The ammonium groups are present as salts that increase the permeability of the polymer. It is a white powder with a slight amine odour that is a pH independent material and has been used for the manufacture of controlled release dosage forms [323, 324].

5.5.1.3 Anhydrous citric acid

Anhydrous citric acid is 2-hydroxy-ß-1, 2, 3-propanetricarboxylic acid and exists as an odourless or almost odourless colourless crystalline or white crystalline powder. It is widely used in pharmaceutical formulations and food products, primarily to adjust the pH of solutions. It has also been used experimentally to adjust the pH of tablet matrices in enteric-coated dosage forms designed for colon-targeted drug delivery. Anhydrous citric acid is widely used for the manufacture of effervescent tablets [325]. At a relative humidity of between 25 and 50 % and temperature of 25 °C, anhydrous citric acid adsorbs insignificant amounts of water. However, at a relative humidity of between 50 % and 75 % it adsorbs significant amounts of moisture to form a monohydrate at a relative humidity approaching 75 %. At a relative humidity > 75 % substantial amounts of water are adsorbed by the monohydrate form [325]. Citric acid was included so that it could maintain the microenvironment an acidic medium once the microspheres reached the stomach.

5.5.1.4 Sodium bicarbonate

Sodium bicarbonate is generally used in effervescent tablet and granule formulations in combination with organic acids. The tablets and granules are usually formulated with sodium bicarbonate, citric and/or tartaric acid. When the tablets or granules come into contact with water carbon dioxide is evolved and the product disintegrates [326], consequently sodium bicarbonate was used as a source of carbon dioxide, to facilitate floating of microspheres for these studies.

5.5.2 Materials

RIF powder was purchased from China Skyrun Industrial (Tsim Sha Tsui, Hong Kong, China). Ethylcellulose (EC) grade N50 was donated by Hercules Incorporated (Aqualon Division, North Carolina, USA). Avicel® PH101 (MCC) was donated by FMC (FMC, Philadelphia, USA). Eudragit® RL PO was donated by Rohm Pharma (GmbH, Darmstadt, Germany). Span 80 was purchased from Sigma Aldrich (Johannesburg, Gauteng, South Africa). Liquid paraffin was supplied by ADC Laboratories (Durban, Kwazulu-Natal South Africa). Acetone was purchased from Associated Chemical Enterprises (Southdale, Gauteng, South Africa) and n-hexane was purchased from VWR Chemicals (Fontenay-sous-Bois, France). Dichloromethane was purchased from Merck Ltd (Wadeville, Gauteng, South Africa). Anhydrous d-glucose was used as a pore forming agent and was purchased from SAARCHEM Ltd (Muldersdrift, Gauteng, South Africa). Sodium bicarbonate and anhydrous citric acid were donated by Aspen® Pharmacare (Port Elizabeth, Eastern Cape, South Africa). All chemicals used were at least of analytical grade and were used without any further purification.

5.5.3 Methods

5.5.3.1 RIF-Excipient Compatibility studies

5.5.3.1.1 Differential Scanning Calorimetry

DSC studies used to evaluate the compatibility of RIF and the excipients were conducted as described in Section 4.3.3.1.1 of this thesis.

5.5.3.1.2 FTIR Spectroscopy

A Spectrum Model 100 FT-IR ATR Spectrophotometer (Perkin Elmer®, Beaconsfield, England) was used to generate infrared spectra for RIF and mixtures of RIF and the excipients to be used. A small amount of RIF and a 1:1 blend of RIF and each excipient was placed on a diamond crystal and a force of approximately 100 N applied to the powder mass prior to analysis over the wavenumber range 4000-650 cm^{-1} at resolution of 4 cm^{-1}.

5.5.3.2 Experimental Design

A Box-Behnken design was used to generate seventeen experiments and the input variable levels used were derived from preliminary studies. The experiments were generated using Design® Expert Version 7.01 (Stat-Ease Inc., Minneapolis, USA) software. The input factors studied were Eudragit® RLPO, EC and anhydrous d-glucose content. The input levels and responses monitored are summarised in Table 5.1.

Table 5. 1 Input variables (coded) and responses monitored for the Box-Behnken Design.

Factor	**Code**	**Coded Level**		
Independent				
Level		[-1]	[0]	[+1]
Eudragit® RLPO content (g)	A	1	2	3
Ethylcellulose content (g)	B	1	1.5	2
Anhydrous d-glucose content (g)	C	0.25	0.5	0.75
Dependent		**Constraints**		
% RIF released at 0.5h = R_1		$R_1 \leq$ 15% [327]		
% RIF released at 2h = R_2		R_2 = maximise		
% RIF released at 4h = R_3		R_3 = maximise		
% RIF released at 6h = R_4		R_4 = maximise		
% RIF released at 8h = R_5		R_5 = maximise		
Encapsulation efficiency (%) = R_6		R_6 = maximise		
Buoyancy = R_7		R_7 = maximise		
Lag time (seconds) = R_8		R_8 = minimise		
% RIF released at 12h = R_9		R_9 = maximise [328]		
% Yield = R_{10}		R_{10} = maximise		

5.5.3.3 Manufacture of microspheres

Microspheres were manufactured using an emulsification approach and solvent diffusion/evaporation as described in Section 4.3.3.3 of this thesis. The manufacturing process used is illustrated in Figure 5.1.

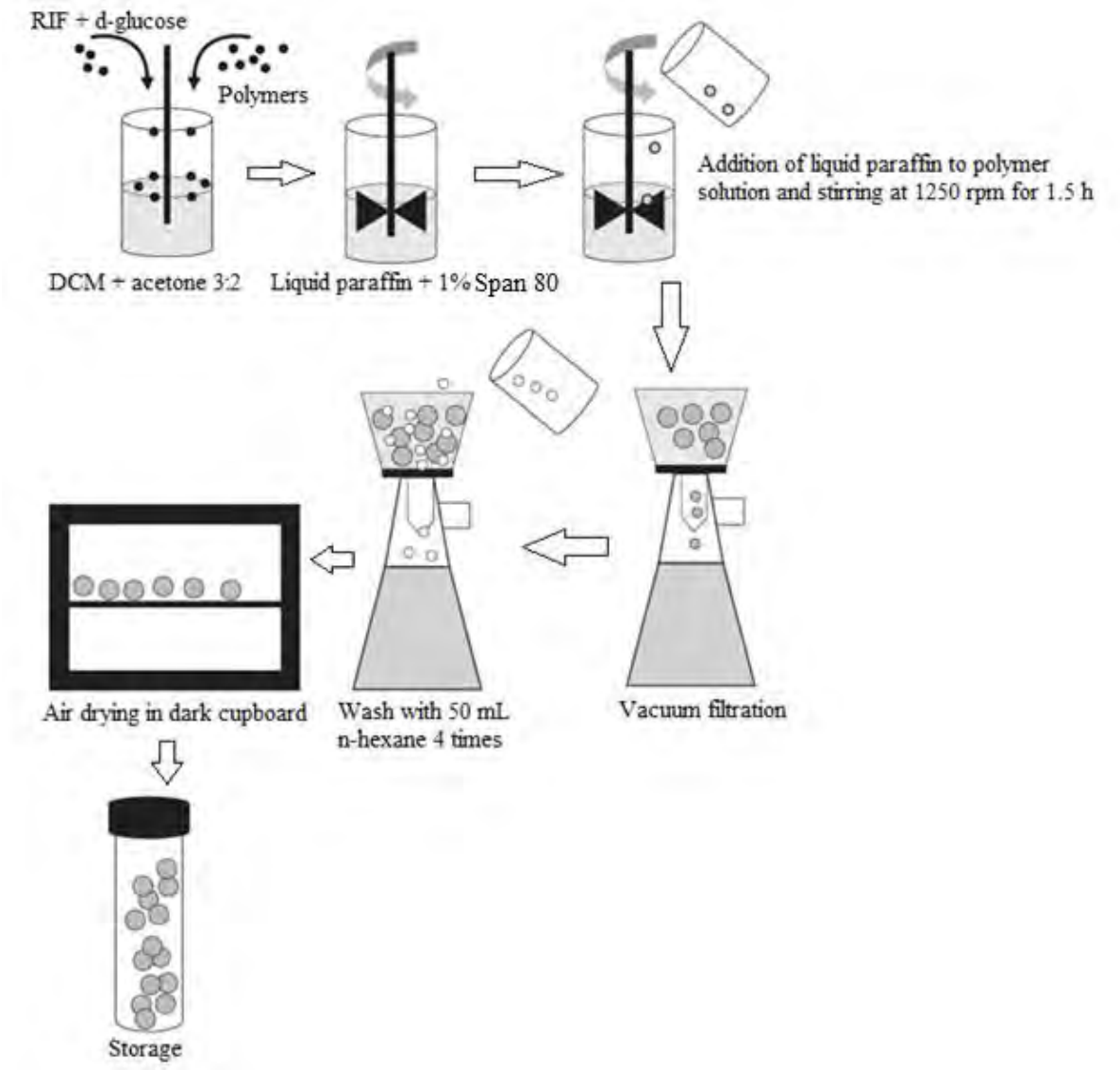

Figure 5. 1 Schematic representation of the manufacturing process for RIF microspheres using a solvent diffusion/evaporation process.

Eudragit® RLPO, EC and MCC pH101 were dissolved or dispersed in 50 mL of an organic solvent system comprised of dichloromethane (DCM) and acetone in a 3:2 ratio in a 400 mL teflon beaker (Lasec®, Cape Town, South Africa). RIF and anhydrous d-glucose were mixed in a mortar and approximately 10 mL 95 % v/v absolute ethanol was added and the powder mixture then levigated to ensure a homogenous paste was produced, prior to air drying at 22 °C for 24 h. A predetermined amount of the RIF and d-glucose mixture containing 1.0 g RIF and desired

amount of d-glucose was then added to the polymer solution and left to stand at 22 °C for 1 h, to ensure complete dissolution of the RIF. Light liquid paraffin (125 mL) containing 1 % v/v Span 80 was placed into a 250 mL beaker and agitated at 1000 rpm with a Model SS10 overhead stirrer (Stuart®-Equipment, Staffordshire, UK) fitted with a four-blade butterfly propeller of 50 mm diameter, for 10 minutes. The total volume of liquid paraffin was then poured into the teflon beaker containing the polymer and RIF solution and stirred continuously at 1250 rpm for 1.5 h. Hardened microcapsules were collected using a Buchner funnel and washed four (4) times with 50 mL n-hexane to remove any residual liquid paraffin. The microspheres were air dried in a dark cupboard at 22 °C for 24 hours after which the product was sieved to remove residual powder, prior to storage in well-sealed 50 mL amber bottles. The yield of microspheres was calculated using Equation 4.1 on page 120 of this thesis.

5.5.3.4 Determination of Mean Particle Size

The size distribution and particle size of the microspheres was determined as described in Section 4.3.3.4 on page 120 of this thesis.

5.5.3.5 Bulk and Tapped Density

The bulk and tapped density of the microspheres was determined as described in Section 4.3.3.5 on page 121 of this thesis.

5.5.3.6 Encapsulation Efficiency

A sample of microspheres containing approximately 100 mg RIF was weighed and crushed in a mortar and pestle before dissolving in 100 mL methanol and then sonicated using a Branson B2 ultrasonic bath (Cole-Parmer Instrument Company, Illinois, USA) for 1 h to ensure complete dissolution of RIF. The solution was then vortexed using a Vortex-2 Genie (Scientific Industries Inc., New York, USA) at a frequency of 350 Hz for 60 seconds and then filtered through a 0.45 µm HVLP membrane filter (Millipore Millex-HV, Bedford, USA) prior to analysis. A 1.0 mL aliquot was withdrawn from the solution and diluted to 10 mL with methanol in an A-grade volumetric flask. A 0.6 mL aliquot of the dilute solution was then mixed in an amber HPLC sample vial with 0.3 mL of a 300 µg/mL zidovudine solution, prior to analysis using the

validated reversed-phase HPLC method, described in Chapter 3 of this thesis. The encapsulation efficiency as a percent (% EE), was calculated using Equation 4.4 on page 121 of this thesis.

5.5.3.7 Scanning Electron Microscopy

The shape and surface morphology of the microspheres was investigated as described in Section 4.3.3.7 on page 121 of this thesis.

5.5.3.8 RIF Release Studies

Dissolution testing was conducted using a USP Apparatus 3 Vankel Bio-Dis dissolution tester fitted with a Model VK 750 (Vankel Industries, NJ, USA) digitally controlled water circulation heater set at 37 ± 0.5 °C. The dissolution medium was 250 mL pH 1.2 0.1 M HCl. The test samples were placed in inner cylinders (n = 6) with a 177 µm mesh placed at the top and a 74 µm mesh at the bottom of the cylinder, to prevent leakage of the dosage form and/or API powder and facilitate drainage of the dissolution medium during testing [329]. The samples were agitated at 10 dips per minute (dpm) and samples were withdrawn at 0.5, 2, 4, 6, 8 and 12 h and analysed using the RP-HPLC method reported in Chapter 3 of this thesis.

5.5.3.9 Stability of RIF in dissolution medium

The stability of RIF in the dissolution medium was established by exposing a known quantity of RIF powder to pH 1.2 0.1 M HCl maintained at 37.0 ± 0.5 °C for 24 hours. The % recovery of RIF was established at 0, 0.5, 2, 4, 6, 8, 12 and 24 hours (n = 3).The samples were analysed using the validated RP-HPLC method reported in Chapter 3 of this thesis.

5.5.3.10 *In Vitro* Buoyancy Studies

A 250 mg sample of microspheres was placed into 900 mL pH 1.2 0.1 M HCl in USP Apparatus 2 dissolution vessels maintained at 37.0 ± 0.5 °C. The time taken for the microspheres to move from the bottom of the flask to the surface of the dissolution fluid was monitored and recorded, in seconds, as the floating lag time for the microspheres [330]. The medium was agitated with a paddle at 100 rpm for 12 hours after which the microspheres that remained afloat were recovered, separately from those that had settled, and air dried at 22 °C for 24 h after

which the fractions were weighed (n = 3). The buoyancy was calculated using Equation 5.1 [331].

$$\% \text{ Buoyancy} = \frac{Qf}{Qf+Qs} \text{ X } 100 \qquad \text{Equation 5.1}$$

Where,

Qf = weight of floating microspheres, and
Qs = weight of settled microspheres.

5.5.3.11 Kinetics of RIF Release

The kinetics of RIF release were evaluated and studied as described in section 4.3.3.9, of this thesis.

5.6 RESULTS AND DISCUSSION

5.6.1 RIF-Excipient Compatibility Studies

5.6.1.1 Differential Scanning Calorimetry

The DSC thermograms for RIF is depicted in Figure 5.2.

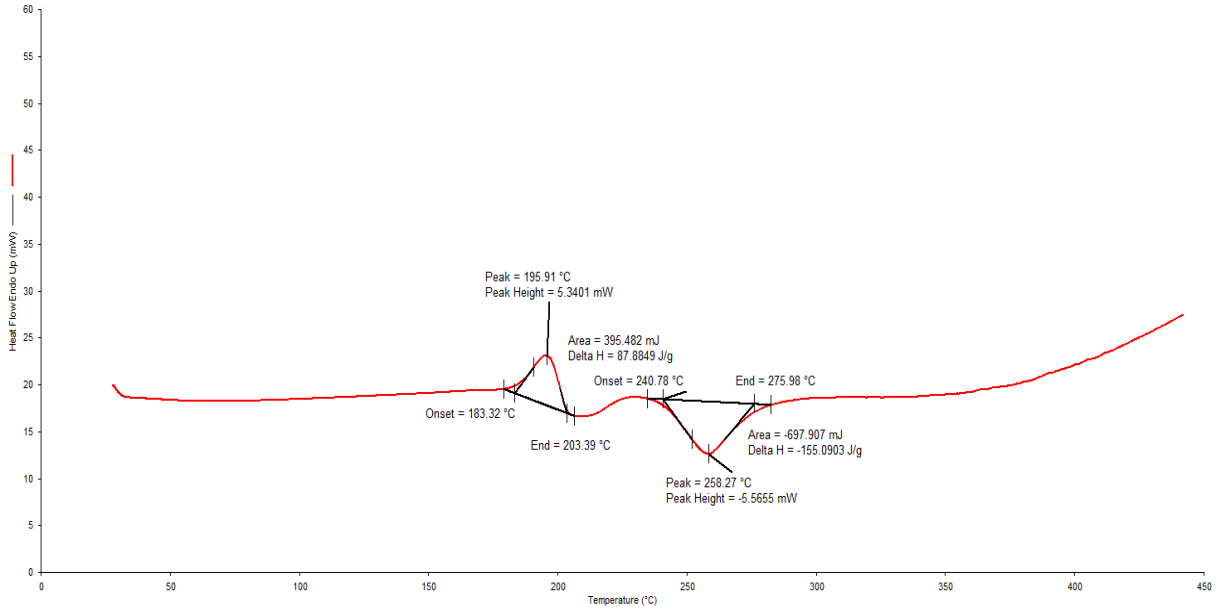

Figure 5. 2 Typical DSC thermogram for RIF generated at a heating rate of 10 °C/min over the temperature range 30 – 400 °C.

The DSC thermogram for RIF was characterized by a melting endotherm between 183.32 °C – 203.39 °C, immediately followed by an exothermic recrystallisation event that is a characteristic of a solid-liquid-solid transition, and finally a decomposition event at 240.78 °C – 275.58 °C. These results were similar to those in which the form II polymorph of RIF exhibited a melting endotherm at between 180 °C - 197 °C that was immediately followed by recrystallisation to the form I polymorph with an exothermic peak at between 197 °C - 223 °C and a final decomposition event that was observed between 247 °C – 266 °C [141].

The DSC thermogram for a 1:1 mixture of RIF and d-glucose is depicted in Figure 5.3.

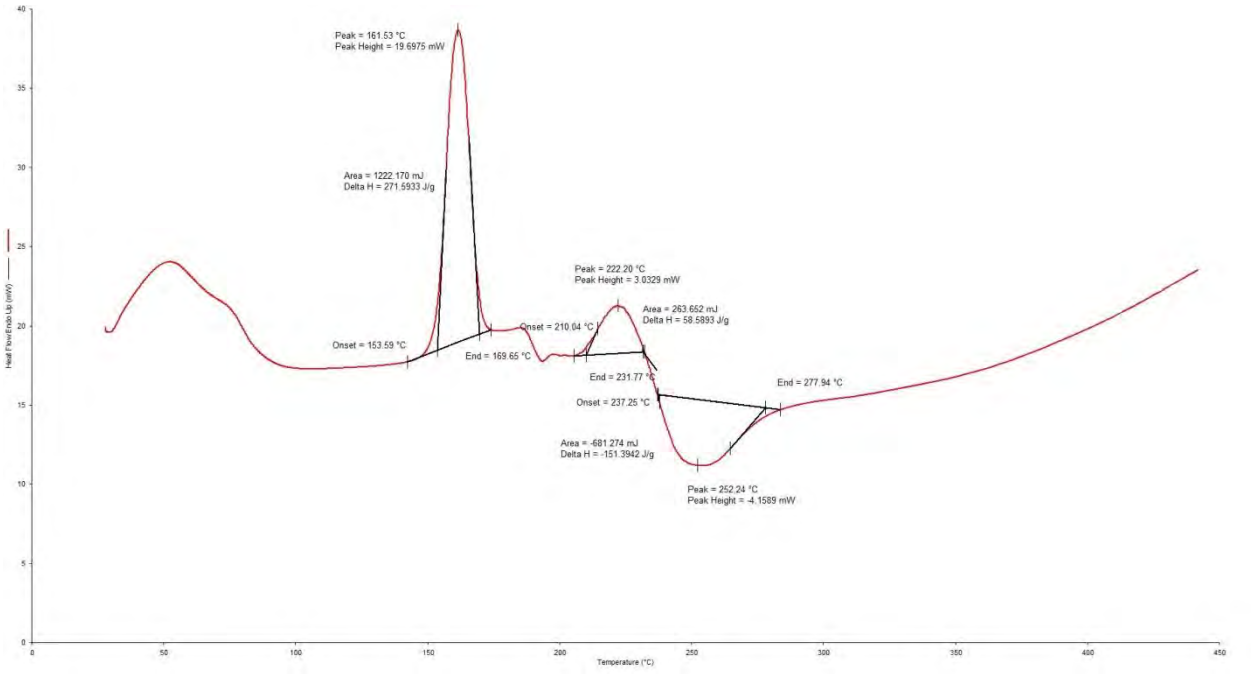

Figure 5. 3 Typical DSC thermogram for a 1:1 mixture of RIF and d-glucose generated at a heating rate of 10 °C/min over the temperature range 30 – 400 °C.

The thermogram for the 1:1 mixture of RIF and d-glucose revealed a melting endotherm for RIF between 210.04 °C – 231.77 °C, no recrystallisation exothermic event and decomposition between 231.77°C – 279.94°C. This behaviour suggests a more rapid transition from polymorphic form II to form I, in the presence of d-glucose and manifests as a decrease in the melting point of RIF in the presence of d-glucose. This phenomenon however, has no biopharmaceutic significance.

The thermogram for the 1:1 mixture of RIF and EC revealed a melting endotherm for RIF between 184.02 °C – 202.66 °C, immediately followed by a recrystallisation event at 202.66 °C - 239.69 °C and decomposition between 239.69 °C – 271.92 °C and is depicted in Figure 5.4.

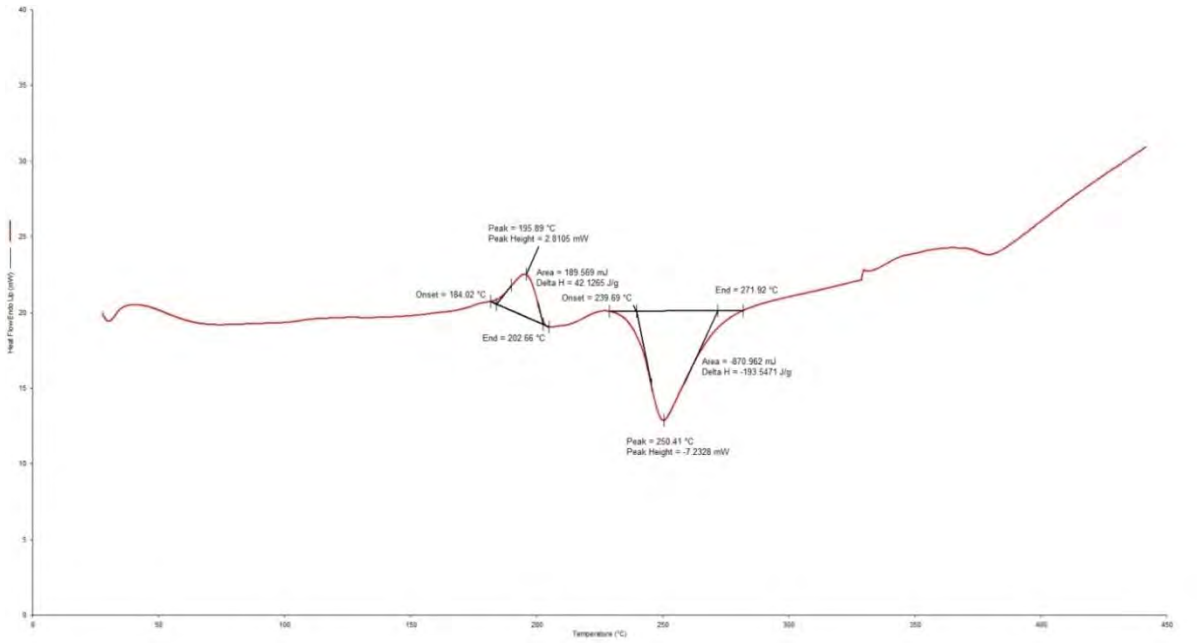

Figure 5. 4 Typical DSC thermogram for a 1:1 mixture of RIF and EC generated at a heating rate of 10 °C/min over the temperature range 30 – 400 °C.

The thermogram for the 1:1 mixture of RIF and Eudragit® RLPO revealed a melting endotherm for RIF between 182.19 °C – 204.04 °C, a recrystallisation event at 204.04 °C - 232.18 °C and decomposition between 232.18 °C – 276.15 °C and is depicted in Figure 5.5.

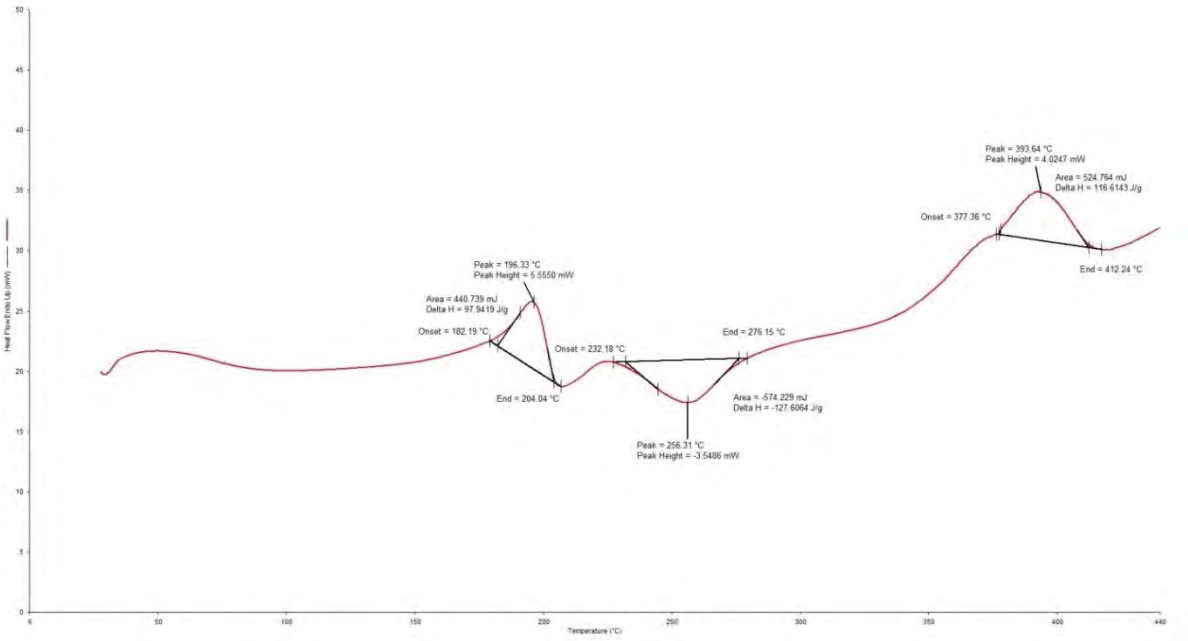

Figure 5. 5 Typical DSC thermogram for a 1:1 mixture of RIF and Eudragit® RLPO generated at a heating rate of 10 °C/min over the temperature range 30 – 400 °C.

The thermogram for the 1:1 mixture of RIF and sodium bicarbonate is depicted in Figure 5.6 and revealed overlapping endothermic peaks at 137.82 °C – 194.66 °C which were identified as melting endotherms for sodium bicarbonate and polymorph form II of RIF. The overlapping endothermic peaks were immediately followed by a period of recrystallisation at between 194.66 °C – 240.59 °C and decomposition at 240.59 °C – 273.46 °C. The thermogram for sodium bicarbonate alone has been reported to depict two endothermic events, one at 96 °C and one at 150 °C that is evidence of thermal decomposition of $NaHCO_3$ generating H_2O and CO_2 and sodium carbonate and commences at approximately 50 °C and ends at 170 °C [332].

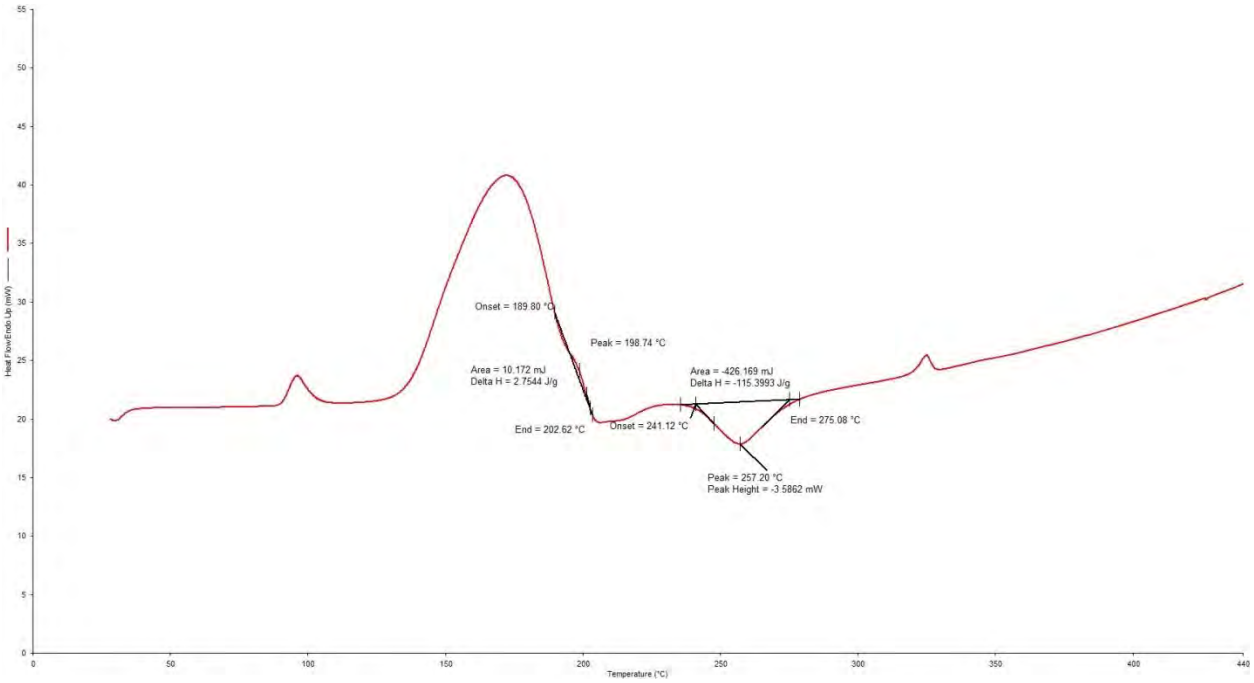

Figure 5. 6 Typical DSC thermogram for a 1:1 mixture of RIF and sodium bicarbonate generated at a heating rate of 10 °C/min over the temperature range 30-400°C.

The thermogram for the 1:1 mixture of RIF and anhydrous citric acid is depicted in Figure 5.7 and revealed a melting endotherm for RIF at 175.81 °C – 200.49 °C, a recrystallisation event at 200.49 °C and decomposition between 238.41 – 279.18 °C.

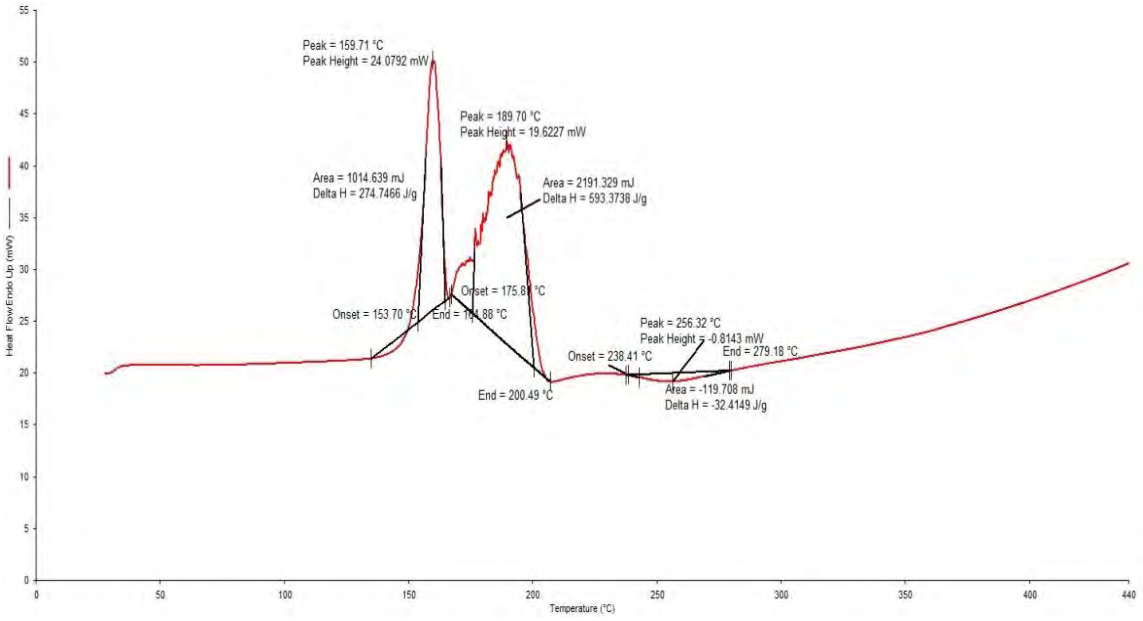

Figure 5. 7 Typical DSC thermogram for a 1:1 mixture of RIF and sodium bicarbonate generated at a heating rate of 10 °C/min over the temperature range 30 – 400 °C.

The overlapping peaks in the thermogram for the 1:1 mixture of RIF and sodium bicarbonate, in addition to the interference with the melting endotherm for RIF from possible degradation products of anhydrous citric acid in the thermogram of the 1:1 mixture of RIF and citric acid makes the analysis cumbersome and suggests that other analytical techniques would be more useful in determining compatibility of RIF with these excipients and that long term stability of the manufactured product containing RIF, sodium bicarbonate and citric acid should be assessed. These results suggest that the intended excipients were compatible with RIF and may be used in the same formulation composition, however, real time long term stability studies would be required to confirm this is indeed, the case.

5.6.1.2 FTIR Spectroscopy

The FTIR spectra of 1:1 mixtures of RIF and EC, d-glucose, Eudragit® RLPO, sodium bicarbonate and citric acid are depicted in Figures 5.8 - 5.12.

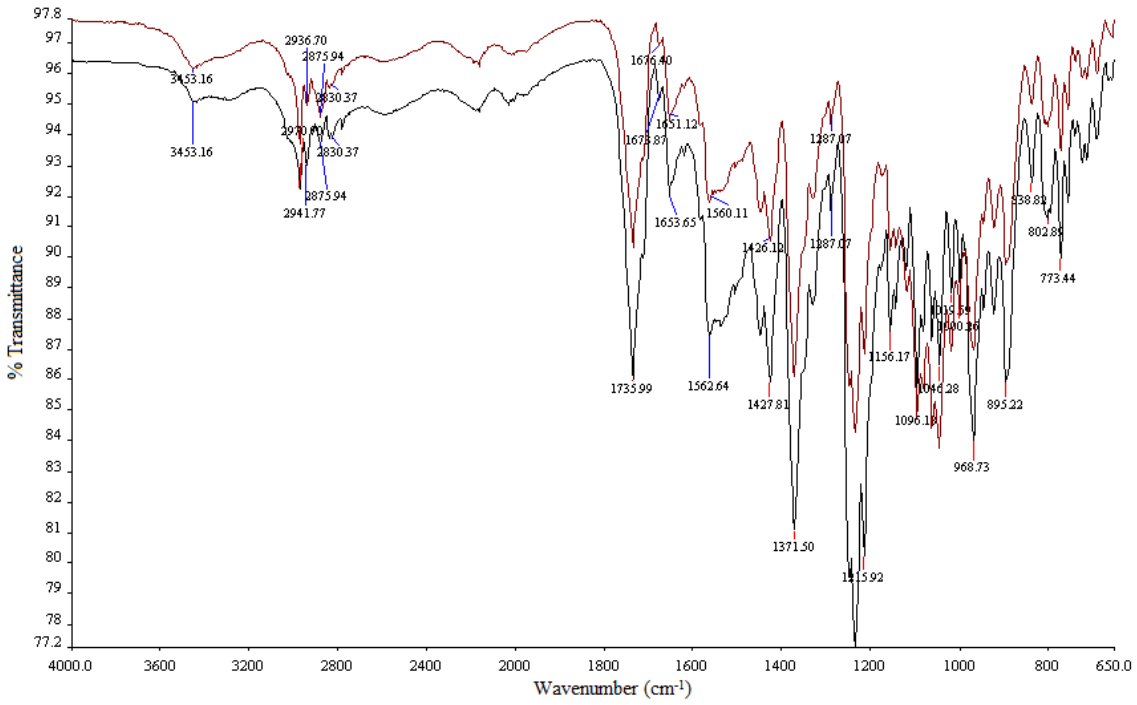

Figure 5. 8 FTIR absorption spectrum of RIF (black) and a 1:1 mixture of RIF and EC (red).

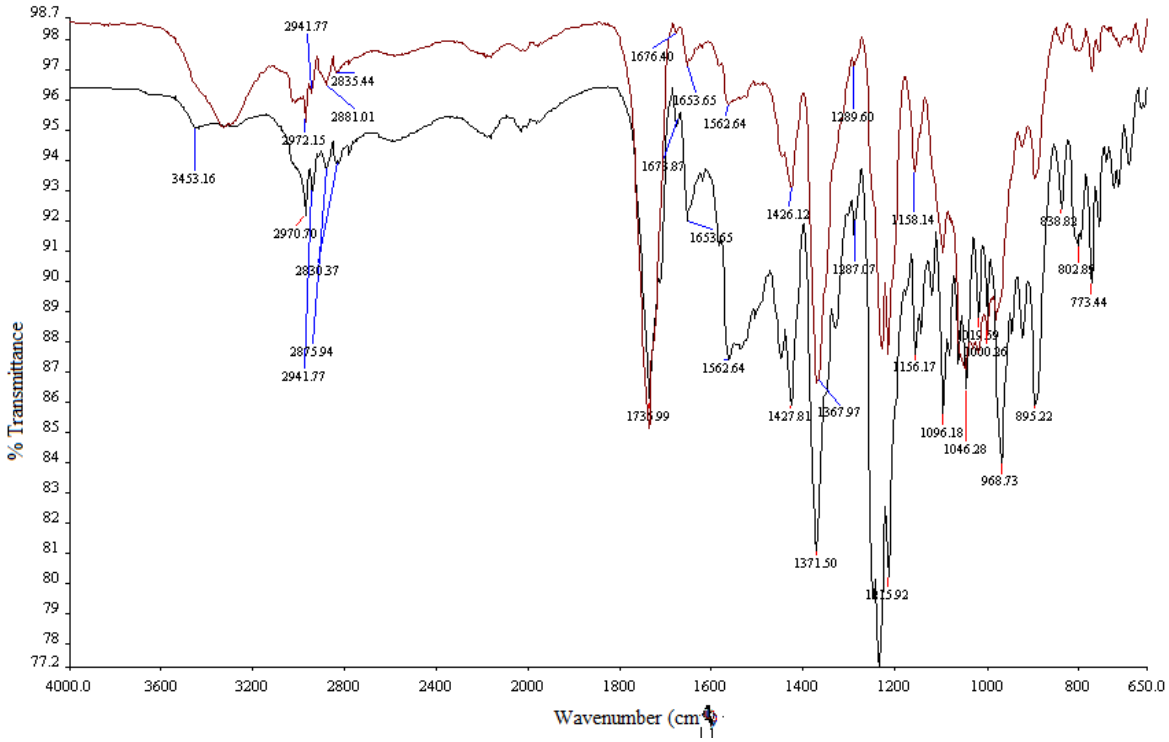

Figure 5. 9 FTIR absorption spectrum of RIF (black) and a 1:1 mixture of RIF and d-glucose (red).

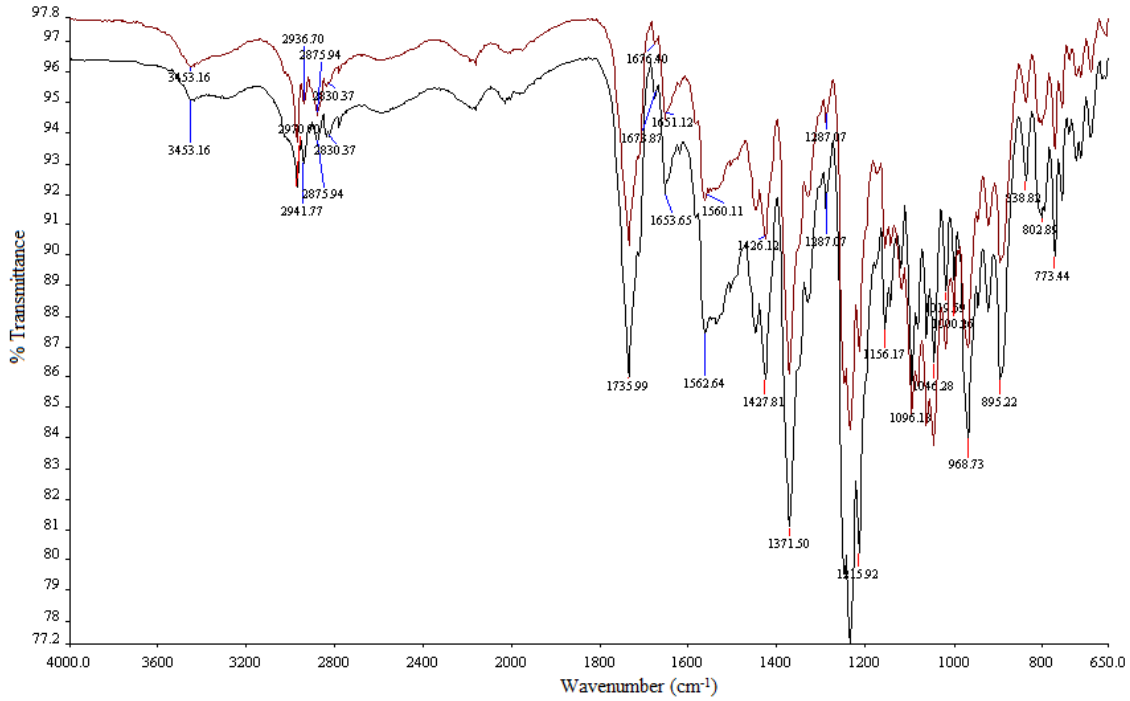

Figure 5. 10 FTIR absorption spectrum of RIF (black) and a 1:1 mixture of RIF and Eudragit® RLPO (red).

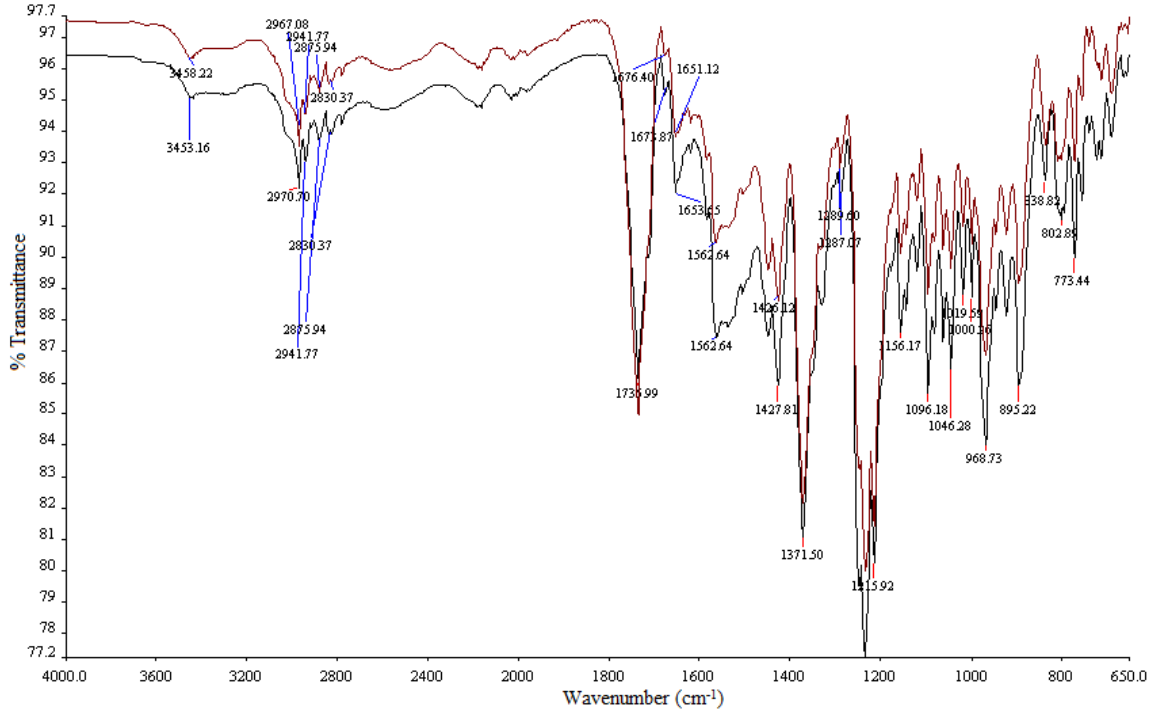

Figure 5. 11 FTIR absorption spectrum of RIF (black) and a 1:1 mixture of RIF and sodium bicarbonate (red).

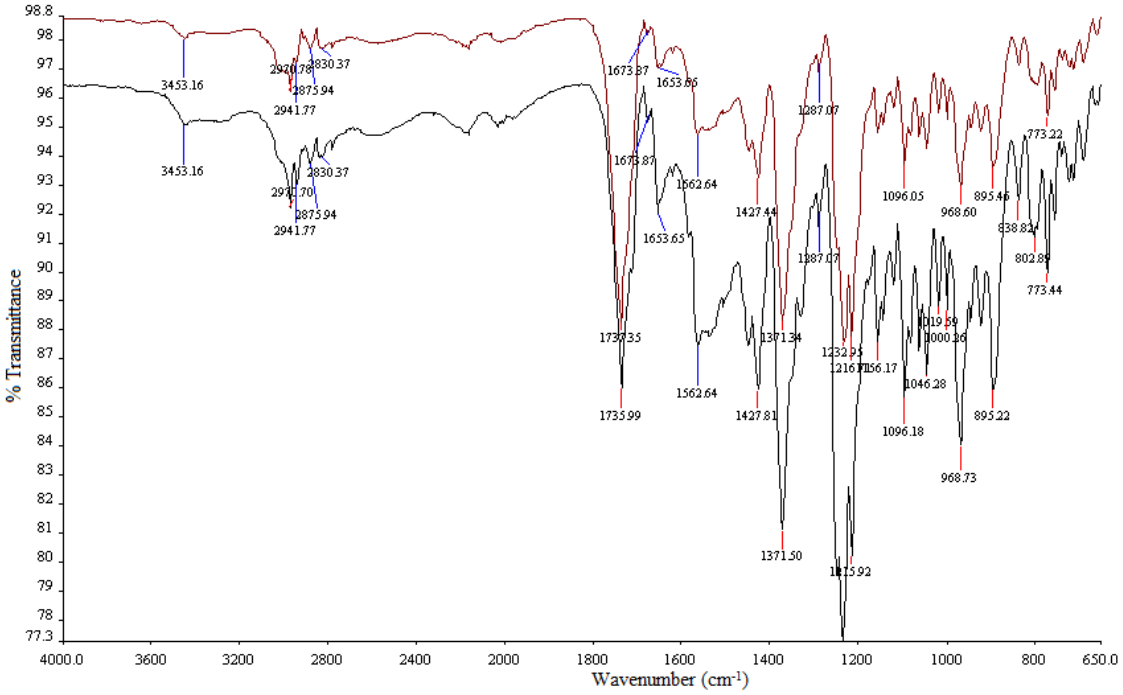

Figure 5. 12 FTIR absorption spectrum of RIF (black) and a 1:1 mixture of RIF and citric acid (red).

The infrared absorption spectra for the 1:1 mixtures do not reveal any significant shifts in the frequency of resonation for RIF and the minor shifts in the FTIR frequencies of resonance observed for the functional groups of RIF (Table 5.2) were attributed to potential weak hydrogen bonding, further confirming the absence of potential interactions between RIF and the excipients to be used for the manufacture of the floating microspheres. However, real time long term stability studies would be necessary to ensure this is, indeed the case.

Table 5. 2 FTIR wavenumber number assignments for RIF and 1:1 mixtures.

Functional group	**RIF**	**1:1 mixture of RIF and**				
		Ethylcellulose	Eudragit® RLPO	d-glucose	Sodium bicarbonate	Citric acid
-CH_3 stretching	2941.77	2936.70	2936.70	2941.77	2941.77	2941.78
-CH_3O asymmetric stretching	2875.94	2875.94	2875.94	2881.01	2875.94	2875.94
-C=O acetyl stretching	1735.99	1735.99	1735.99	1735.99	1735.35	1735.99
-C=N asymmetric bending	1673.87	1676.40	1676.40	1676.40	1676.40	1673.87
-C=C stretching	1562.64	1560.11	1560.11	1560.11	1562.40	1562.64
-C-N- stretching	1427.81	1426.10	1426.12	1426.12	1426.12	1427.44

5.6.2 Manufacture of microspheres

An o/o emulsion with a mixed organic solvent system of DCM and acetone as the dispersed and liquid paraffin as the continuous phase was used to manufacture the RIF microspheres. The use of a single phase of acetone resulted in the production of non-spherical microparticles with a poor yield that was attributed to the failure to form stable emulsion droplets of the polymer solution in liquid paraffin [333, 334]. The use of a mixture of organic solvents, such as acetonitrile and DCM [335] or acetone and methanol [336], was reported to improve the formation of stable emulsion droplets and ultimately the formation of microspheres.

DCM is nonpolar, is miscible in oil and was included to decrease the polarity of acetone to enhance the formation of a stable emulsion [333, 335]. The use of DCM alone resulted in the formation of large droplets that aggregated and the use of a solvent mixture of DCM and acetone was considered suitable for this process. Acetone and DCM are miscible [337] and the use of DCM and acetone in a 1:1 ratio resulted in the production of microspheres with a smooth surface

however, the microspheres adhered to each other and to the walls of the beaker reducing the yield of discrete units that were difficult to harvest. A solvent mixture of DCM and acetone in a 2:3 ratio resulted in an improved product with smooth surfaces that did not appear to aggregate however, the solubility of RIF in this mixture was low and resulted in the suspension of some large API particles resulting in large microparticles following microencapsulation.

A mixture of DCM and acetone in a 1:4 ratio resulted in the formation of a highly viscous solution in which large particles of undissolved API formed lumps, following homogenization, although some small microspheres were observed on the surface(s) of the lumps that had formed. A mixture of DCM and acetone in a 4:1 ratio resulted in the formation of a single large lump within seconds of adding the RIF /polymer solution. The use of a solvent mixture of DCM and acetone in a 3:2 ratio produced smooth spherical particles that did not adhere to other particles and the walls of the beaker. Consequently, this ratio of solvents was selected for the manufacture of floating RIF particles. RIF was sufficiently soluble in the solvent mixture and following addition of the RIF solution to liquid paraffin small discrete oil droplets stabilized with Span 80, were formed. The deposition of polymer onto the surface of the droplets and eventual diffusion and evaporation of the organic solvents, with continued stirring, resulted in the formation of hard, discrete, smooth and spherical microspheres with a limited number of pores and/or cracks on the surface(s) when imaged using SEM as shown in Appendix 2B.

5.6.3 Box-Behnken Design

The actual experiments conducted and responses observed following use of a BBD experimental design are summarised in Table 5.3. Analysis of variance (ANOVA) was used to establish the impact of EC, Eudragit® RLPO and d-glucose content on the % RIF released in pH 1.2 0.1 M HCl, encapsulation efficiency, *in vitro* buoyancy characteristics and % yield.

Table 5. 3 Actual experiments conducted and responses observed.

Run	Eudragit® RLPO g	Ethyl-cellulose g	d-glucose g	RIF released at 0.5h %	RIF released at 2h %	RIF released at 4h %	RIF released at 6h %	RIF released at 8h %	EE %	Buoyancy %±SD	Lag time Seconds ±SD	RIF released at 12h %	Yield %
				R_1	R_2	R_3	R_4	R_5	R_6	R_7	R_8	R_9	R_{10}
1	3	1.5	0.75	3.85	16.94	41.01	68.34	79.86	88.36	56.44±0.22	180±3.6	88.84	81.86
2	3	1	0.5	14.21	19.65	46.10	73.66	81.94	88.23	52.56±0.34	220±2.8	92.18	76.23
3	2	1.5	0.5	7.41	34.40	47.49	69.17	84.39	77.07	59.72±0.08	150±4.9	90.51	70.00
4	1	2	0.5	4.08	11.63	35.24	56.13	72.99	74.80	69.44±0.11	62±6.7	81.43	68.00
5	2	1.5	0.5	7.03	34.06	47.12	69.99	83.37	77.20	58.00±0.72	152±5.4	90.61	71.30
6	3	1.5	0.25	2.61	13.70	39.56	58.29	71.01	90.80	51.76±0.93	170±3.9	79.03	84.22
7	2	1.5	0.5	7.27	34.57	47.44	69.98	84.39	77.26	58.40±0.87	152±4.6	90.02	71.67
8	3	2	0.5	1.53	12.64	30.72	50.64	63.24	91.63	68.52±0.75	80±4.4	75.29	85.33
9	2	1.5	0.5	7.92	34.21	47.38	69.94	83.65	76.78	57.02±1.02	151±4.8	90.42	71.50
10	2	2	0.25	2.61	14.16	26.66	59.08	67.54	88.35	64.60±0.98	65±3.2	78.51	76.56
11	2	1.5	0.5	7.65	34.95	47.06	69.52	83.92	78.98	56.92±2.77	150±4.5	90.28	71.33
12	1	1.5	0.75	8.79	36.70	48.92	70.98	84.78	69.72	65.00±1.87	70±6.8	87.79	67.71
13	1	1.5	0.25	7.00	28.92	35.35	66.54	80.40	77.65	60.44±1.39	50±6.5	84.12	67.47
14	2	1	0.25	15.17	26.08	48.46	70.57	85.54	80.22	58.48±0.79	110±7.3	95.71	68.00
15	2	1	0.75	16.98	27.15	49.95	74.21	87.97	79.74	62.96±2.88	120±28	97.91	63.39
16	1	1	0.5	19.82	38.37	52.23	74.46	88.65	61.37	55.20±1,67	45±4.9	98.99	55.70
17	2	2	0.75	6.21	21.42	36.36	67.52	70.11	89.13	67.40±0.58	130±3.7	87.16	76.11

5.6.3.1 % RIF Released at 0.5 h, R_1

A summary of ANOVA results for the % RIF released at 0.5 h is listed in Table 5.4.

Table 5. 4 ANOVA data for response surface quadratic model [Partial sum of squares - Type III] for % RIF released at 0.5 h.

Source	Sum of squares	Df	Mean square	F-value	p-value	Prob > F
Panel A						
Model	444.24	9	49.36	75.19	< 0.0001	Significant
A-Eudragit® RLPO	38.36	1	38.36	58.43	0.0001	Significant
B-Ethylcellulose	334.76	1	334.76	509.90	< 0.0001	Significant
C-d-glucose	8.88	1	8.88	13.52	0.0079	Significant
AB	2.34	1	2.34	3.56	0.1011	
AC	0.078	1	0.078	0.12	0.7399	
BC	0.80	1	0.80	1.22	0.3053	
A^2	5.24	1	5.24	7.98	0.0256	Significant
B^2	53.64	1	53.64	81.70	< 0.0001	Significant
C^2	2.57	1	2.57	3.92	0.0881	
Residual	4.60	7	0.66			
Lack of fit	1.79	1	1.79	0.89	0.7200	
Pure error	0.46	4	0.12			
Cor total	448.84	16				
Panel B						
Std. deviation	0.81					
Mean	8.24					
% C.V	9.83					
Press	66.87					
R^2	0.9898					
Adjusted R^2	0.9766					
Predicted R^2	0.8510					
Adeq precision	27.866					

A quadratic model was selected for this analysis as all diagnostic parameters viz., p-value, PRESS, R^2, adequate precision and diagnostic plots including a normal plot of residuals, plot of residuals versus predicted responses and Box-Cox plot for power transformation (Appendix 1C) were satisfactory and met the specifications described in subsections 3.2.1.1.1 - 3.2.1.1.8, thereby implying that the model was adequate for use. Model terms with values of Prob > F < 0.0500 indicate that the model terms are significant. In this case Eudragit® RLPO, EC and d-glucose content had a significant impact on the % RIF released at 0.5 h. A three dimensional

(3D) response surface plot used to visualise the effects of Eudragit® RLPO and EC content on % RIF released at 0.5 h is depicted in Figure 5.13.

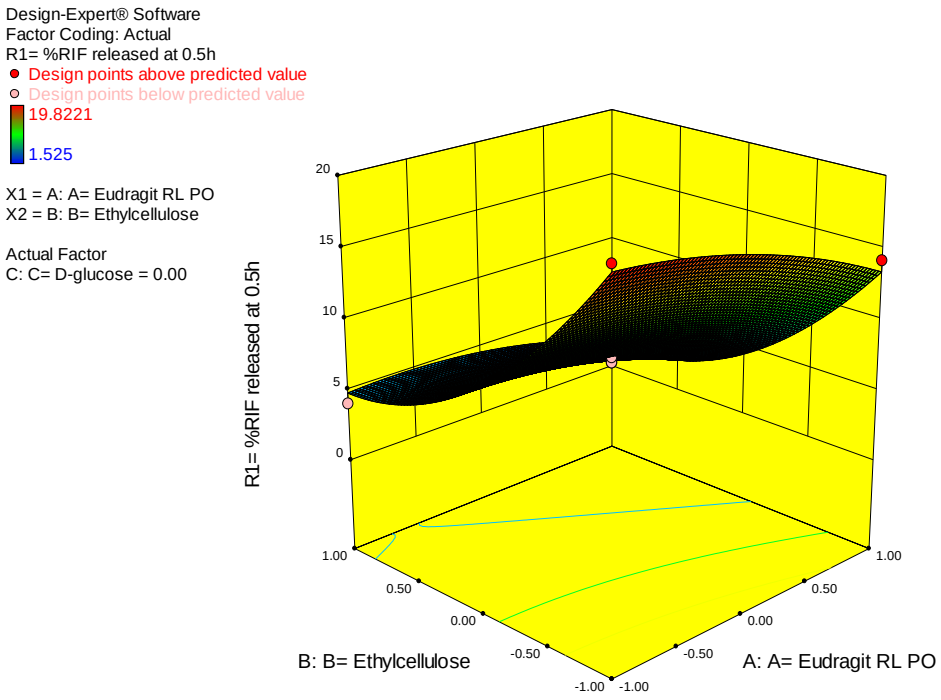

Figure 5. 13 3D response surface depicting the impact of EC and Eudragit® RLPO content on the % RIF released at 0.5h.

The results reveal that an increase in the Eudragit® RLPO and EC content resulted in a decrease in the % RIF released at 0.5 h with the highest % RIF released at 0.5 h when these two polymers were used at the lowest levels. This effect was attributed to an increase in the thickness of the barrier coat, thereby increasing the diffusional path length through which RIF must diffuse to be released [338, 339]. An increase in the amount of EC used resulted in less dissolution medium entering the microspheres and reducing release of RIF through a reduction in dissolution of d-glucose forming fewer channels through which RIF diffusion could occur and erosion of the microsphere matrix [315, 316]. The results also reveal that maintaining EC at low levels and increasing the Eudragit® RLPO content resulted in an increase in the % RIF released and these results were similar to previously reported data [340] in which this was attributed to the rapid ingress of dissolution medium into the microspheres due to the presence of quaternary

ammonium ions in Eudragit® RLPO that facilitate dissolution of RIF present on the surface of microspheres, as well as promoting outward diffusion of RIF from the core.

The 3D response surface plot used to visualise the effect of d-glucose and Eudragit® RLPO content on the % RIF released at 0.5 h is depicted in Figure 5.14.

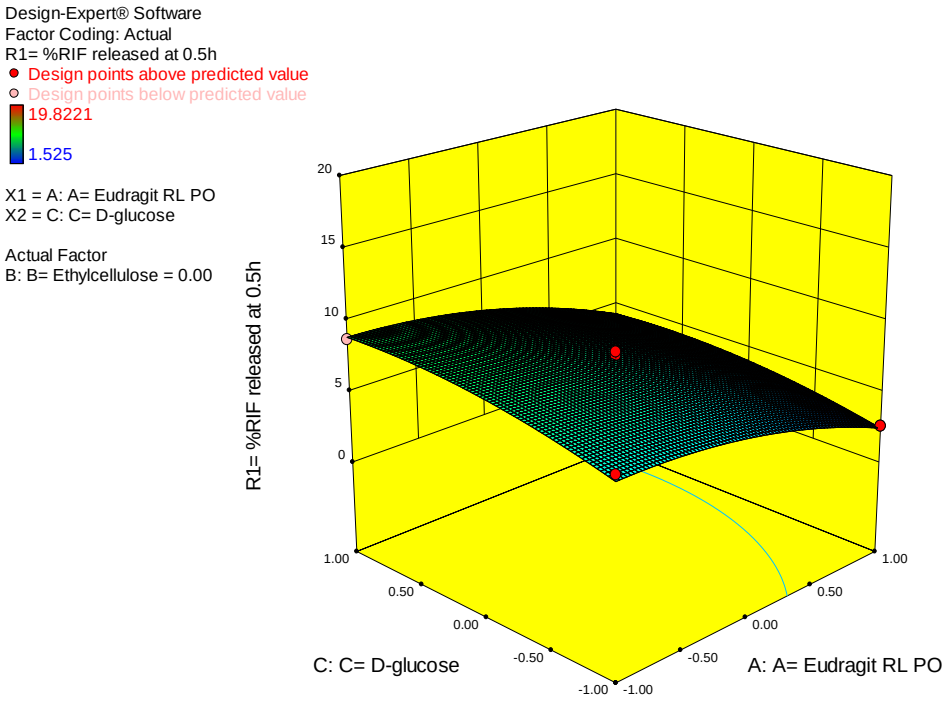

Figure 5. 14 3D response surface plot depicting the impact of d-glucose and Eudragit® RLPO content on the % RIF released at 0.5h.

The results reveal that increasing d-glucose content resulted in an increase in the % RIF released, while increasing the amount of Eudragit® RLPO decreased the % RIF released with the highest % RIF released when d-glucose content was at the highest and Eudragit® RLPO content at the lowest levels. As RIF is hydrophobic, release from the microspheres would be dependent on the availability of pores and/or erosion or dissolution of the dosage form [340]. The dissolution of d-glucose is expected to create pores in the surface(s) of the microsphere coating, facilitating entry of dissolution medium into the microspheres and outward diffusion of RIF from the core of the particle and similar results have been reported [341, 342]. It was expected that increasing the amount of d-glucose would result in a greater number of pores forming on the surface(s) of the

microspheres with a subsequent increase in the % RIF released due to channel formation, through which diffusion could occur, as has been reported [343, 344]. However, at 0.5 h, most of RIF released would be from the surface(s) of the microspheres as opposed to the innermost core of the microspheres. The d-glucose was also expected to improve wetting of the microsphere matrix and improve dissolution of RIF. The 3D response surface plot to visualise the impact of d-glucose and EC content (Figure 5.15) revealed similar results with an increase in d-glucose content resulting in an increase in the % RIF released at 0.5 h and an increase EC content resulting in a decrease in % RIF released at 0.5 h.

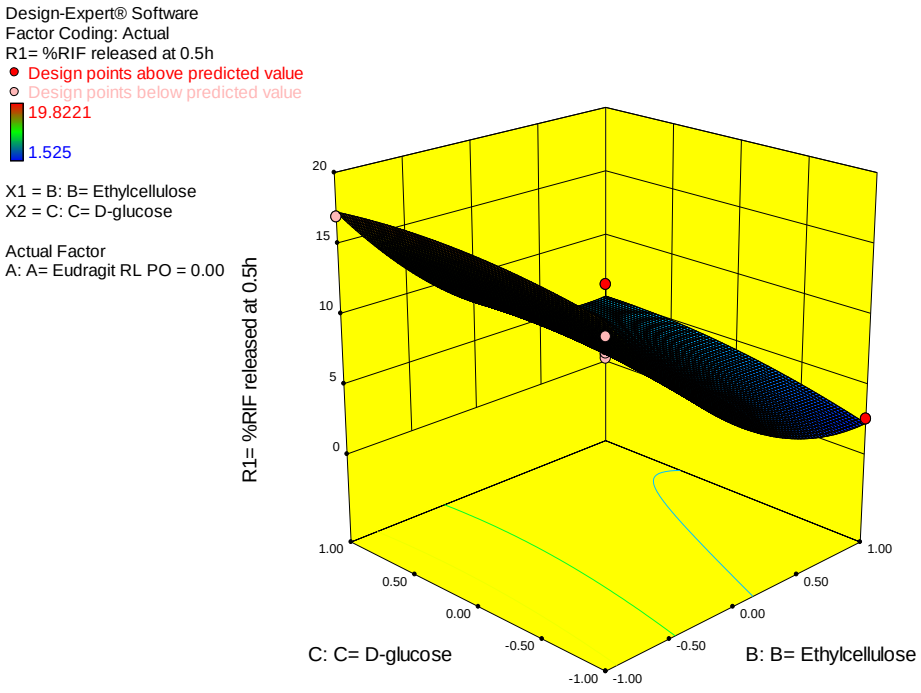

Figure 5. 15 3D response surface plot depicting the impact of d-glucose and EC content on the % RIF released at 0.5h.

The results revealed that the % RIF released from microspheres for all BBD formulation except batches RIF015 and RIF016 did not exhibit a burst release or dose dumping, a phenomenon that is desirable for sustained release dosage form performance [327]. Since EC acts as a barrier to water [314] it was postulated that the amount of the RIF released at 0.5 h was a consequence of dissolution of RIF located at the surface of the microspheres and outward diffusion of RIF

through pores created by the permeability imparted on the surface of the microspheres by quaternary ammonium ions present in Eudragit® RLPO that facilitate diffusion of the entrapped RIF from the surface of the microspheres in the initial phase of the dissolution process. In addition, the dissolution of d-glucose may result in dissolution of RIF particularly on the surface(s) of the microspheres due to improved wettability of the microspheres. The relationship between the input variables and % RIF released at 0.5 hours is mathematically described as Equation 5.2.

$$R_1 = 7.46-2.19-6.47B+1.05C+0.76AB-0.14AC+0.45BC-1.12A^2+3.57B^2-0.78C^2 \quad \text{Equation 5.2}$$

6.6.3.2 % RIF Released at 2 h, R_2

A summary of ANOVA results for the % RIF released at 2 h is listed in Table 5.5.

Table 5. 5 ANOVA data for response surface quadratic model [Partial sum of squares - Type III] for % RIF released at 2 h.

Source	Sum of squares	Df	Mean square	F-value	p-value	Prob > F
Panel A						
Model	1382.25	9	153.58	15.12	0.0008	Significant
A-Eudragit® RLPO	347.03	1	347.03	34.17	0.0006	Significant
B-Ethylcellulose	330.09	1	330.09	32.50	0.0007	Significant
C-d-glucose	46.81	1	46.81	4.61	0.0689	
AB	97.39	1	97.39	9.59	0.0174	Significant
AC	5.17	1	5.17	0.51	0.4987	
BC	9.58	1	9.58	0.94	0.3638	
A^2	151.71	1	151.71	14.94	0.0062	Significant
B^2	260.37	1	260.37	25.64	0.0015	Significant
C^2	80.46	1	80.46	7.92	0.0260	Significant
Residual	71.10	7	10.16			
Lack of fit	9.51	3	6.50	1.79	0.2180	
Pure error	0.48	4	0.12			
Cor total	1453.35	16				
Panel B						
Std. deviation	3.19					
Mean	25.85					
% C.V	12.33					
Press	1130.67					
R^2	0.9511					
Adjusted R^2	0.8882					
Predicted R^2	0.2220					
Adeq precision	10.925					

A quadratic model was selected for this analysis as all diagnostic parameters viz., p-value, PRESS, R^2, adequate precision and diagnostic plots viz., normal plot of residuals, plot of residuals versus predicted responses and a Box-Cox plot of power transformations (Appendix 1C) were satisfactory and met the specifications described in Subsections 3.2.1.1.1-3.2.1.1.8, thereby implying that the model was adequate for use. Model terms with values of Prob > F < 0.0500 indicate that the model terms are significant. In this case the amount of Eudragit® RLPO, EC and d-glucose had a significant impact on the % RIF released at 2 h. A 3D response surface plot was used to visualise the impact of Eudragit® RLPO and EC on % RIF released at 2 h and is depicted in Figure 5.16.

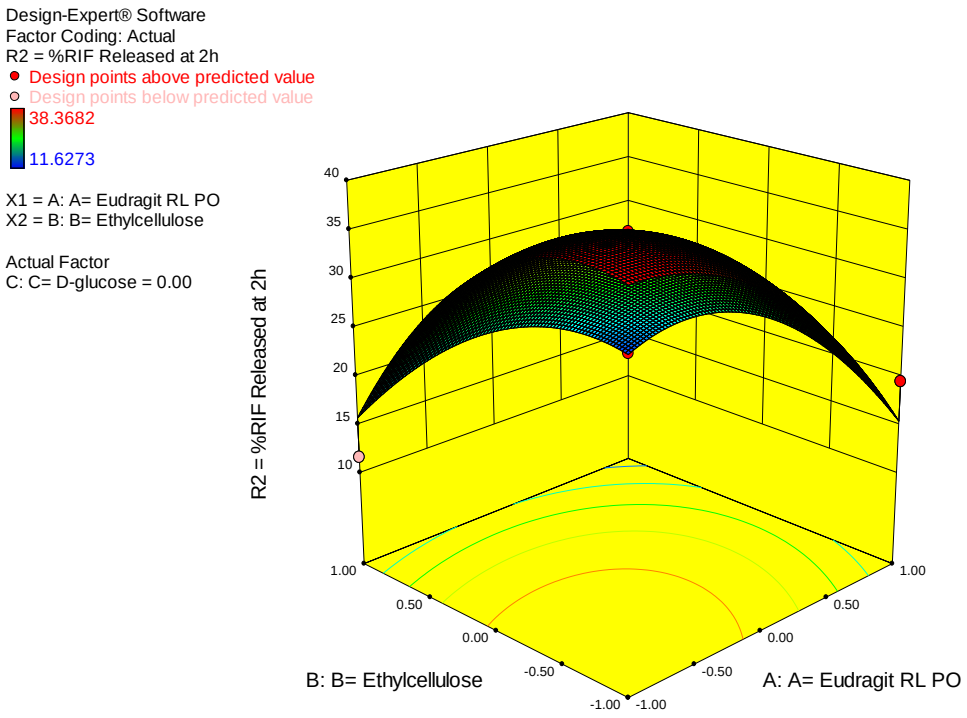

Figure 5. 16 3D response surface plot depicting the impact of EC and Eudragit® RLPO content on % RIF released at 2h.

The results reveal that an increase in the amount of Eudragit® RLPO and EC resulted in a decrease in the amount of RIF released at 2 h. The highest % RIF released was observed when the polymers were used at the lowest level. The decrease in % RIF released with an increase in Eudragit® RLPO and EC content was attributed to the increased thickness of the microsphere

coating and longer diffusional path length for RIF to be released from the microspheres. A decrease in API release with an increase in the content of Eudragit® RLPO has been reported [345] and has been attributed to the ability of this polymer to swell in aqueous media that may result in increase in the diffusional pathlength for the API [346, 347]. A decrease in API release with increase in EC has also been reported [345, 348] and has been attributed to the ability of EC to reduce penetration of solvent molecules into matrix systems.

The 3D response surface plot used to visualise the impact of d-glucose and Eudragit® RLPO content on % RIF released is depicted in Figure 5.17.

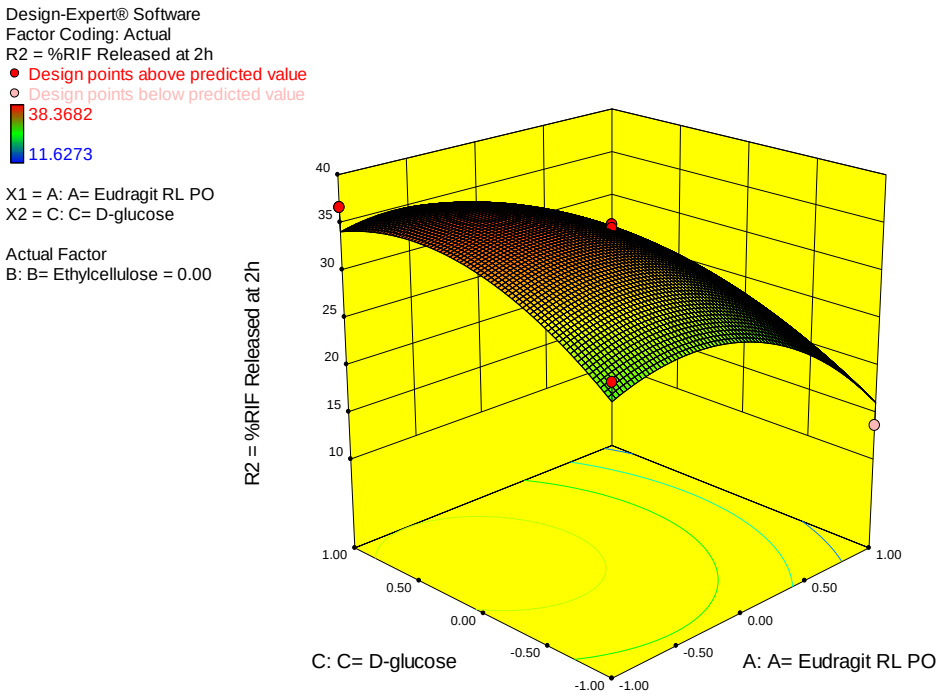

Figure 5. 17 3D response surface plot depicting the impact of d-glucose and Eudragit® RLPO content on % RIF released at 2h.

The results revealed that an increase in the amount of d-glucose used resulted in an increase in the % RIF released at 2 h, possibly due to increase in the porosity of the microspheres which resulted in increased number of channels for the entry of dissolution medium into the microspheres facilitating outward diffusion of RIF [341-344]. Visual observation of the

microspheres revealed that there was negligent erosion at 2 h and it was therefore postulated that most of the RIF released occurred by diffusion through the microsphere matrix. A similar observation was made when evaluating the 3D response surface plot (Figure 5.18) depicting the impact of d-glucose and EC on % RIF released at 2 h.

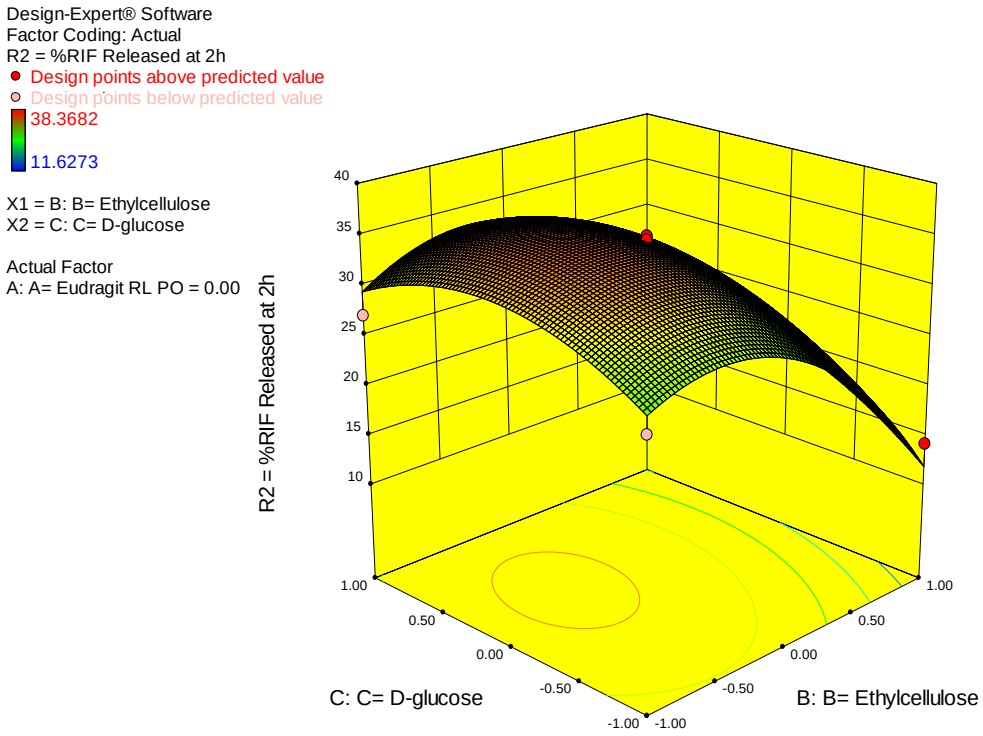

Figure 5. 18 3D response surface plot depicting the impact of d-glucose and EC content on % RIF released at 2h.

The relationship between input variables and % RIF released at 2 h is represented mathematically by Equation 5.3.

$$R_2 = 34.44 - 6.59A - 6.42B + 2.42C + 4.93AB - 1.14\,AC + 1.55BC - 6.00A^2 - 7.86B^2 - 4.37C^2$$

Equation 5.3

5.6.3.3 % RIF Released at 4 h, R_3

A summary of ANOVA results for the % RIF released at 4 h is listed in Table 5.6.

Table 5. 6 ANOVA data for response surface quadratic model [Partial sum of squares - Type III] for % RIF released at 4 h.

Source	Sum of squares	Df	Mean square	F-value	p-value	Prob > F
Panel A						
Model	824.80	9	91.64	15.29	0.0008	Significant
A-Eudragit® RLPO	2.37	1	2.37	0.39	0.5496	
B-Ethylcellulose	573.55	1	573.55	95.70	< 0.0001	Significant
C-d-glucose	32.90	1	32.90	5.49	0.0516	Significant
AB	0.66	1	0.66	0.11	0.7502	
AC	1.12	1	1.12	0.19	0.6789	
BC	16.90	1	16.90	2.82	0.1370	
A^2	65.37	1	65.37	10.91	0.0131	Significant
B^2	22.03	1	22.03	3.68	0.0967	
C^2	91.01	1	91.01	15.18	0.0059	
Residual	41.95	7	5.99			
Lack of fit	108.50	6	18.08	1.37	0.3958	
Pure error	0.15	4	0.038			
Cor total	866.76	16				
Panel B						
Std. deviation	2.45					
Mean	42.18					
% C.V	5.80					
Press	669.06					
R^2	0.9516					
Adjusted R^2	0.8894					
Predicted R^2	0.2281					
Adeq precision	12.077					

A quadratic model was selected for the analysis as all diagnostic parameters viz., p-value, PRESS, R^2, adequate precision and diagnostic plots viz., normal plot of residuals, plot of residuals versus predicted responses and Box-Cox plot of power transformations (Appendix 1C) were satisfactory and met the specifications described in Subsections 3.2.1.1.1-3.2.1.1.8, implying that the model was adequate for use. The model terms with values of Prob > F < 0.0500 indicates that the model terms are significant. In this case, the amount of EC, Eudragit® RLPO and d-glucose used had a significant impact on the % RIF released at 4 h. The 3D response surface plot used to visualise the impact of EC and Eudragit® RLPO content on RIF release is depicted in Figure 5.19.

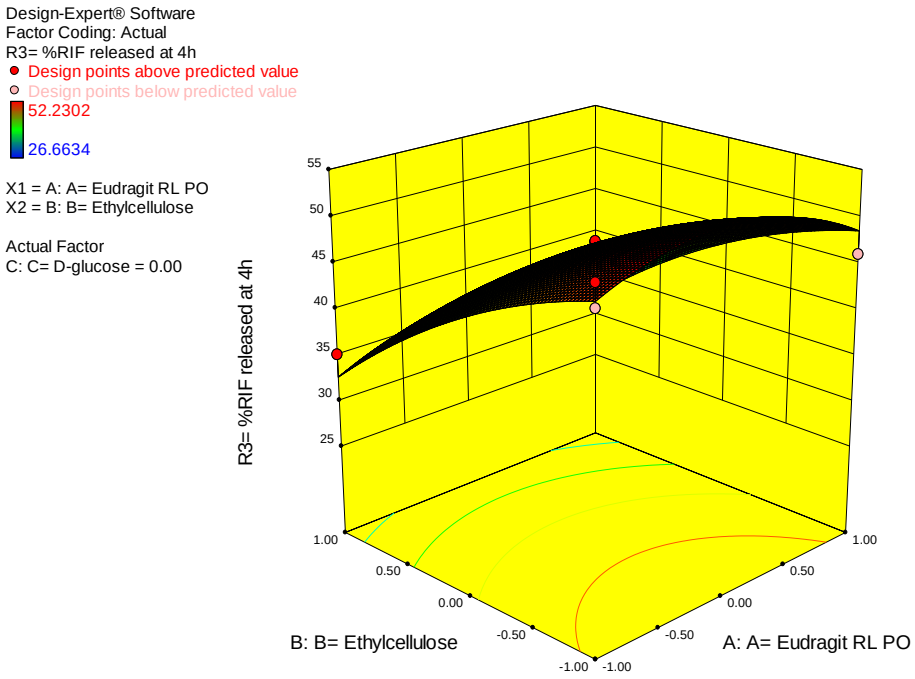

Figure 5. 19 3D response surface plot depicting the impact of EC and Eudragit® RLPO content on % RIF released at 4h.

The results revealed that increasing the amount of EC used resulted in a decrease in % RIF released at 4 h that was attributed to the insoluble characteristics of EC. As EC does not dissolve, RIF release would be a consequence of diffusion through the membrane after dissolution media had diffused into the microspheres. Erosion of the microspheres would be minimal therefore RIF release would be reduced and delayed as has been reported in other studies [344, 348, 349]. An increase in the Eudragit® RLPO content resulted in an increase in the % RIF released at 4 h that was attributed to its permeability to dissolution fluid as a result of a high number of quaternary ammonium ions [340, 344, 349] that would facilitate the diffusion of RIF from the microspheres and these data are similar to those reported elsewhere [344, 349].

The 3D response surface plot used to visualise the impact of d-glucose and Eudragit® RLPO content on the % RIF released at 4 h is depicted in Figure 5.20.

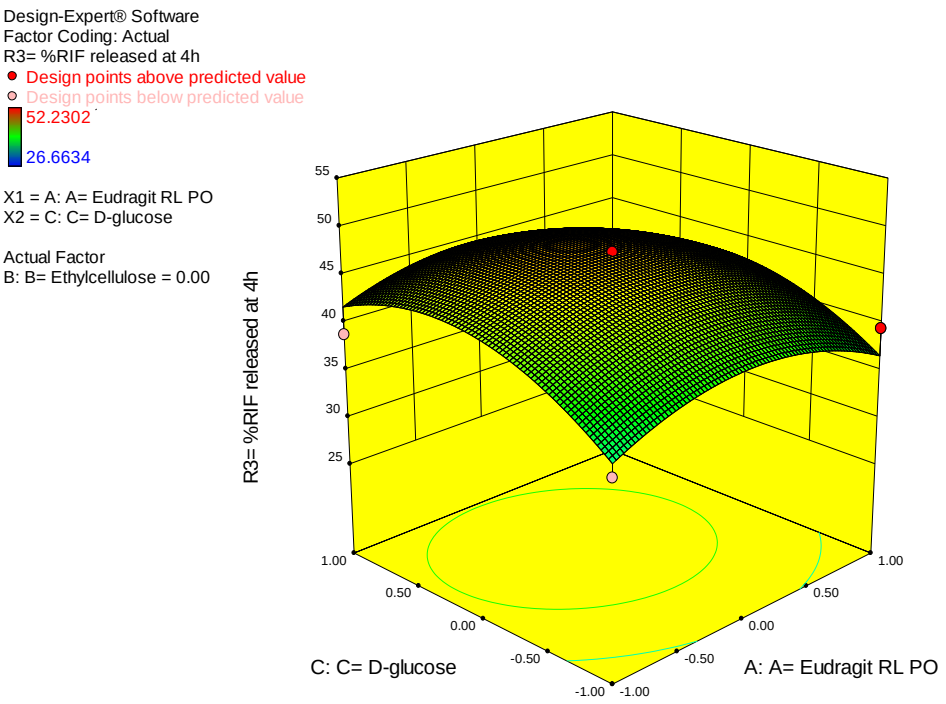

Figure 5. 20 3D response surface plot depicting the impact of d-glucose and Eudragit® RLPO content on % RIF released at 4h.

The results reveal that an increase in the amount of d-glucose used resulted in an increase in the % RIF released at 4 h that was attributed to an increase in the number of pores formed in the surface(s) of the microspheres and a possible increase in the rate of erosion of microspheres resulting in faster and more complete release of RIF as reported in other studies [341, 342]. Increasing the amount of Eudragit® RLPO in the formulation resulted in a decrease in the % RIF released at 4 h that was attributed to an increase in the thickness of the barrier for RIF diffusion as a result of swelling characteristics of Eudragit® RLPO and similar results have been reported [345].

The 3D response surface plot used to visualise the impact of d-glucose and EC (Figure 5.21) content on % RIF released also revealed that an increase in d-glucose content resulted in an increase in the % RIF released, whilst increasing the EC content resulted in a decrease in the % RIF released at 4 h.

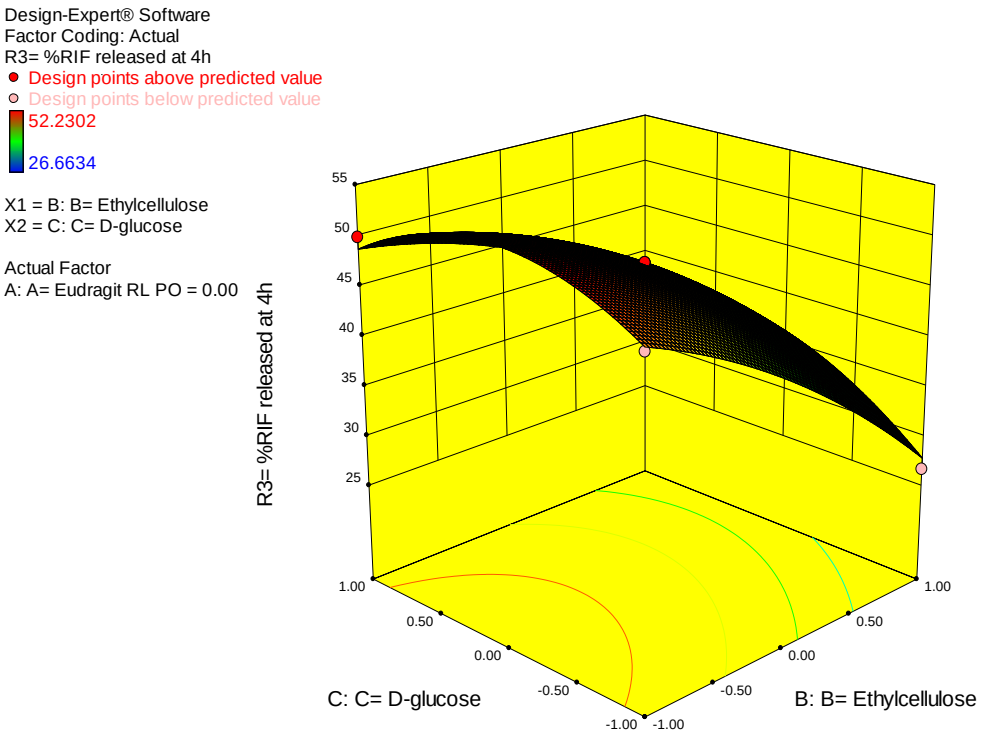

Figure 5. 21 3D response surface plot depicting the impact of d-glucose and EC content on the % RIF released at 4h.

The relationship between input variables and % RIF released at 4 h is mathematically represented by Equation 5.4.

$$R_3 = 47.3 - 0.54A - 8.47B + 2.03C + 0.41AB - 0.53AC + 2.06BC - 3.94A^2 - 2.29B^2 - 4.65C^2$$

Equation 5.4

5.6.3.4 % RIF Released at 6 h, R_4

A summary of ANOVA results for modelling the % RIF released at 6 h is listed in Table 5.7.

Table 5. 7 ANOVA data for response surface linear model [Partial sum of squares - Type III] for % RIF released at 6 h.

Source	Sum of squares	Df	Mean square	F-value	p-value	Prob > F
Panel A						
Model	568.10	3	189.37	13.94	0.0002	Significant
A-Eudragit® RLPO	36.93	1	36.93	2.72	0.1232	
B-Ethylcellulose	443.07	1	443.07	32.61	< 0.0001	Significant
C-d-glucose	88.11	1	88.11	6.49	0.0243	Significant
Residual	176.60	13	13.58			
Lack of fit	908.50	3	302.83	3.13	0.0732	
Pure error	0.53	4	0.13			
Cor total	744.71	16				
Panel B						
Std. deviation	3.69					
Mean	67.00					
% C.V	5.50					
Press	333.54					
R^2	0.7629					
Adjusted R^2	0.7081					
Predicted R^2	0.5521					
Adeq precision	12.037					

A linear model was selected for this analysis as all diagnostic parameters viz., p-value, PRESS, R^2, adequate precision and diagnostic plots viz., normal plot of residuals, plot of residuals versus predicted responses and Box-Cox plot for power transformation (Appendix 1C) were satisfactory and met the specifications described in Subsections 3.2.1.1.1-3.2.1.1.8, implying that the model was adequate for use. The model terms with values of Prob > F < 0.0500 indicates that the model terms are significant. In this case the amount of EC and d-glucose used in the technology had a significant impact on the % RIF released at 6 h. The 3D response surface plot used to visualise the impact of EC and Eudragit® RLPO content on % RIF released at 6 h is depicted in Figure 5.22.

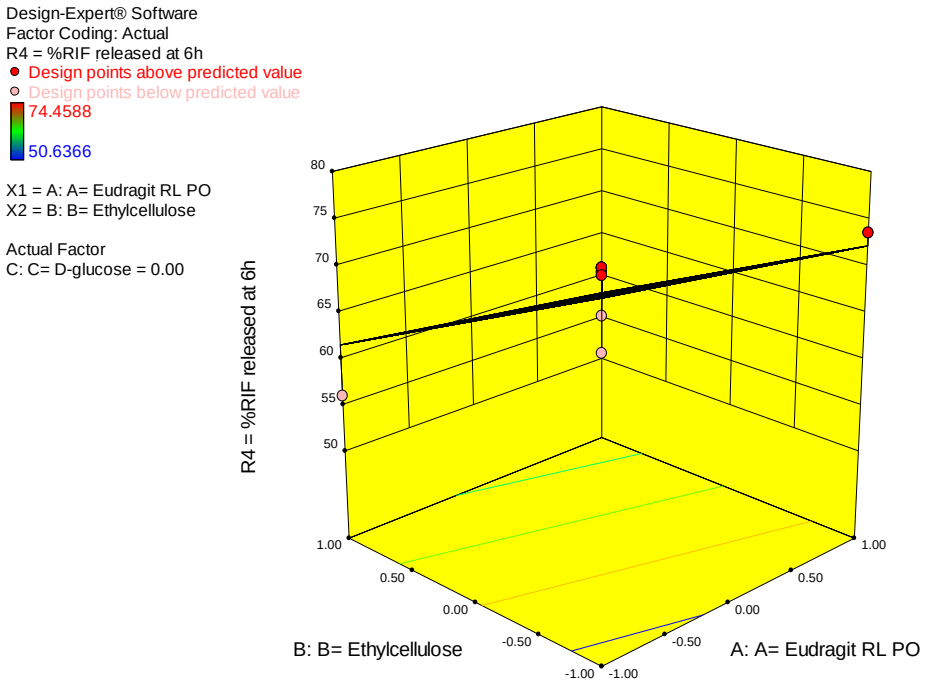

Figure 5. 22 3D response surface plot depicting the impact of EC and Eudragit® RLPO content on % RIF released at 6h.

The results reveal that increasing the amount of EC resulted in a decrease in the % RIF released at 6 h that could be attributed to a reduction in dissolution medium entering the microspheres [340, 347, 348]. API release from EC based matrices has been reported to be released by diffusion and erosion [350, 351] and therefore factors that can affect these two processes are likely to affect RIF release. Increasing the amount of d-glucose used resulted in an increase in the % RIF released at 6 h and was attributed to the generation of more pores and increased wetting of the microspheres as suggested earlier vide infra. The results of the % RIF released at 6 h revealed that RIF would be released in a sustained manner from the microspheres and the relationship between input variables and % RIF released at 6 h is mathematically represented as Equation 5.5.

$$R_4 = 67.00 - 2.15A - 7.44B + 3.32C \qquad \text{Equation 5.5}$$

5.6.3.5 % RIF Released at 8 h, R_5

A summary of ANOVA results for the modelling of % RIF released at 8 h is listed in Table 5.8.

Table 5. 8 ANOVA data for response surface quadratic model [Partial sum of squares - Type III] for % RIF released at 8 h.

Source	Sum of squares	Df	Mean square	F-value	p-value	Prob > F
Panel A						
Model	926.22	9	102.91	71.08	< 0.0001	Significant
A-Eudragit® RLPO	118.37	1	118.37	81.75	< 0.0001	Significant
B-Ethylcellulose	616.55	1	616.55	425.82	< 0.0001	Significant
C-d-glucose	41.50	1	41.50	28.66	0.0011	Significant
AB	2.32	1	2.32	1.60	0.2463	
AC	5.02	1	5.02	3.47	0.1049	
BC	5.766E-003	1	5.766E-003	3.982E-003	0.9514	
A^2	38.12	1	38.12	26.33	0.0014	Significant
B^2	75.42	1	75.42	52.09	0.0002	Significant
C^2	15.59	1	15.59	10.77	0.0135	Significant
Residual	10.14	7	1.45			
Lack of fit	1081.23	3	360.41	3.03	0.0790	
Pure error	0.82	4	0.20			
Cor total	936.35	16				
Panel B						
Std. deviation	1.20					
Mean	79.63					
% C.V	1.51					
Press	150.40					
R^2	0.9892					
Adjusted R^2	0.9753					
Predicted R^2	0.8394					
Adeq precision	27.620					

A quadratic model was selected for this analysis as all diagnostic parameters viz., p-value, PRESS, R^2, adequate precision and diagnostic plots viz., normal plot of residuals, plot of residuals versus predicted responses and Box-Cox plot for power transformation (Appendix 1C) were satisfactory and met the specifications described in Subsections 3.2.1.1.1-3.2.1.1.8, implying that the model was adequate for use. The model terms with values of Prob > F < 0.0500 indicate that the terms are significant. In this case the % RIF released at 8 h was impacted by all input variables viz., amount of Eudragit® RLPO, EC and d-glucose used. The 3D response

surface plot used to visualise the impact of EC and Eudragit® RLPO content on the % RIF released at 8 h is depicted in Figure 5.23.

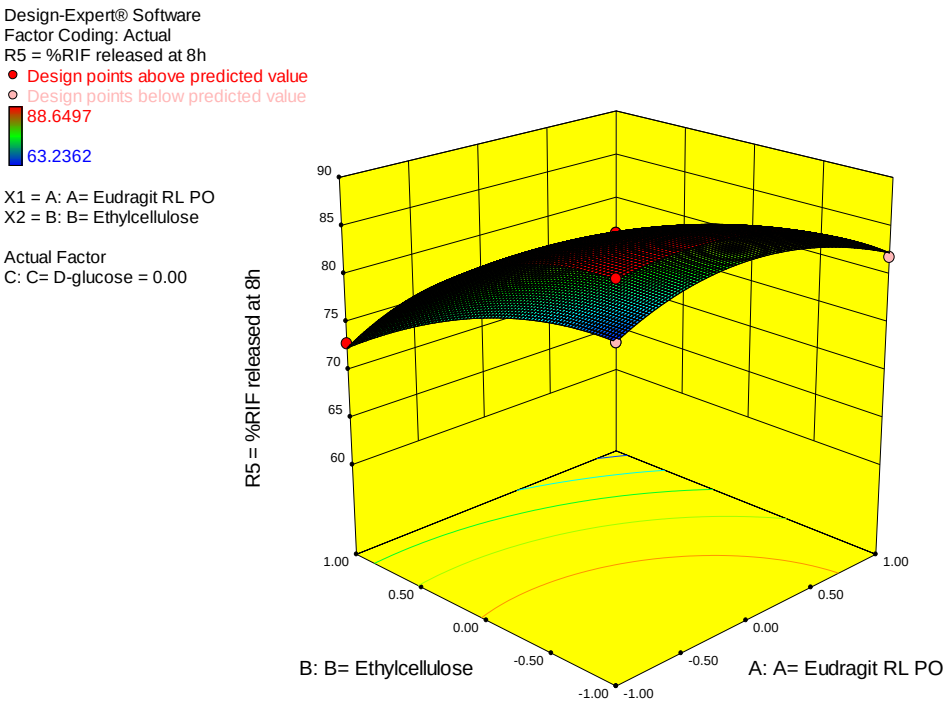

Figure 5. 23 3D Response surface plot depicting the impact of EC and Eudragit® RLPO content on the % RIF released at 8 h.

The results reveal that an increase in the amount of Eudragit® RLPO and EC resulted in a decrease in the % RIF released at 8 h that was attributed to the use of an intermediate molecular weight EC N50 for formulation with a sparingly soluble RIF. API release rates are reported to be drastically reduced with the increase in the molecular weight of EC used which results in the formation of a stronger film with a high tensile strength and elasticity that may resist hydrostatic pressure, ensuring less structural damage to the film due to stress fractures or channel formation [352]. These results were similar to those reported where formulations coated with lower molecular weight EC exhibited faster release rates and extent of API release when compared to formulations coated with higher molecular weight EC [353].

The 3D response surface plot used to visualise the impact of d-glucose and Eudragit® RLPO content on the % RIF released at 8 h is depicted in Figure 5.24.

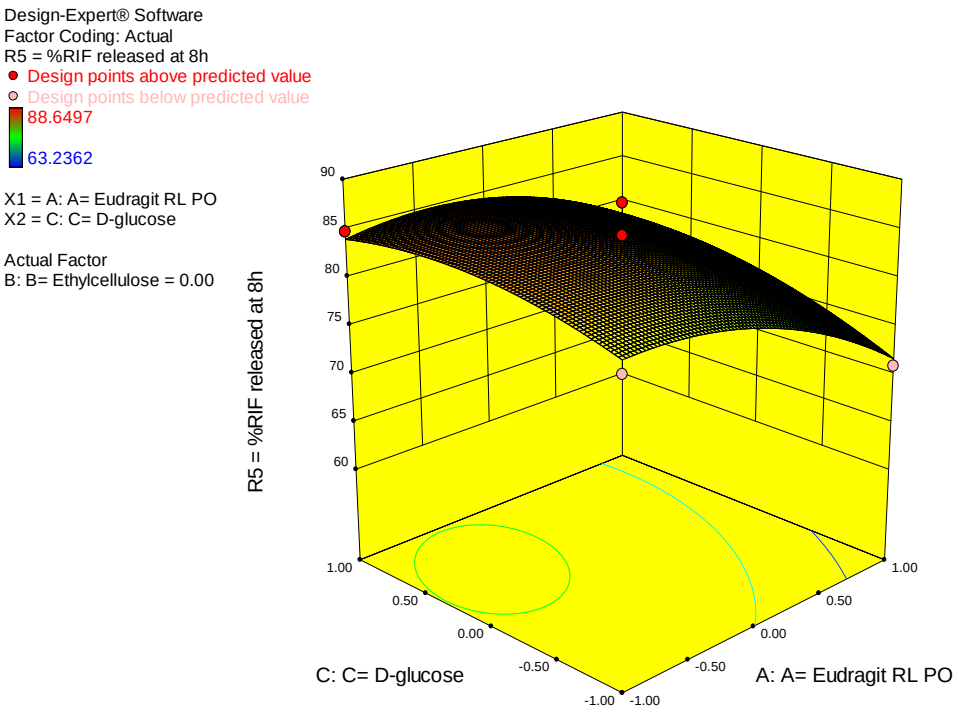

Figure 5. 24 3D response surface plot depicting the impact of d-glucose and Eudragit® RLPO content on % RIF released at 8 h.

The results reveal that an increase in the amount of d-glucose used resulted in an increase in the % RIF released whilst an increase in Eudragit® RLPO content resulted in a decrease in the % RIF released at 8 h. As stated earlier, the use of EC N50 may have resulted in the formation of stronger films that are less likely to undergo structural damage [352] even after 8 h of exposure to dissolution fluid. The expected mode of RIF release would be diffusion control and the channels for diffusion would have been created by dissolution of d-glucose and the number of the channels were expected to increase with an increase in the amount of d-glucose included [341, 342]. Eudragit RLPO was expected to undergo time dependent erosion [314] at 8 h and its effect on RIF release may have been a result of restricted entry of dissolution medium by EC, into the microspheres [314] or initial swelling in aqueous media [345] that may impede RIF diffusion. Similar reasons were advanced for the observation in the 3D response surface plot (Figure 5.25) used to visualise the impact of d-glucose and EC content on the % RIF released at

8 h that revealed that an increase in the amount of d-glucose used resulted in an increase in the % RIF released at 8 h and increasing the EC content resulted in a decrease in the % RIF released at 8 h.

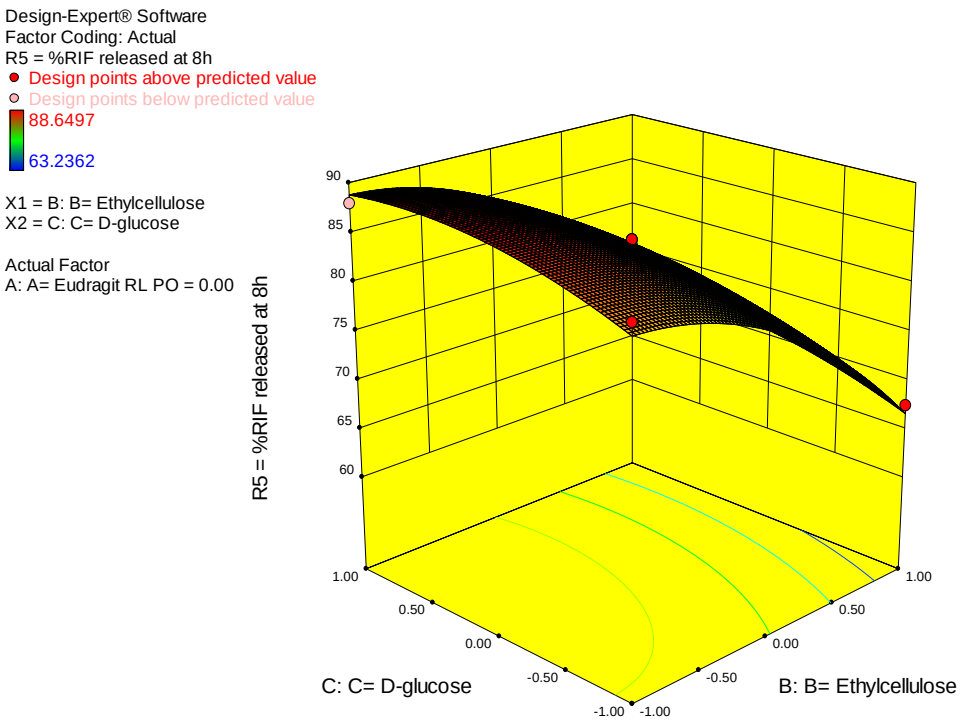

Figure 5. 25 3D response surface plot depicting the impact of d-glucose and EC content on the % RIF released at 8 h.

The data for % RIF released at 8 h indicate that the release of RIF would be sustained over 8 hours as approximately 80 % RIF was released from the microspheres for most batches except batches RIF004 (72.99 %), RIF006 (71.01 %), RIF008 (63.24 %), RIF010 (67.54 %) and RIF017 (70.11) in which either a high amount of Eudragit® RLPO and EC and/or low amounts of d-glucose had been used. The relationship between input variables and the % RIF released at 8 h is represented mathematically by Equation 5.6.

$$R_5 = 83.95-3.85A-8.78B+2.28C-0.76AB+1.12AC+0.038BC-3.01A^2-4.23B^2-1.92C^2$$

Equation 5.6

5.6.3.6 %RIF Released at 12 h, R_9

A summary of the ANOVA results for modelling the % RIF released at 12 h is listed in Table 5.9.

Table 5. 9 ANOVA data for response surface quadratic model [Partial sum of squares - Type III] for % RIF released at 12 h.

Source	Sum of squares	Df	Mean square	F-value	p-value	Prob > F
Panel A						
Model	699.25	9	77.69	33.33	< 0.0001	Significant
A-Eudragit® RLPO	36.09	1	36.09	15.48	0.0056	Significant
B-Ethylcellulose	486.75	1	486.75	208.84	< 0.0001	Significant
C-d-glucose	74.03	1	74.03	31.76	0.0008	Significant
AB	0.11	1	0.11	0.049	0.8308	
AC	9.43	1	9.43	4.04	0.0842	
BC	10.42	1	10.42	4.47	0.0723	
A^2	72.04	1	72.04	30.91	0.0009	Significant
B^2	2.29	1	2.29	0.98	0.3545	
C^2	6.98	1	6.98	3.00	0.1271	
Residual	16.32	1	2.33			
Lack of fit	981.48	3	327.16	2.91	0.0866	
Pure error	0.21	4	0.052			
Cor total	715.56	16				
Panel B						
Std. deviation	1.53					
Mean	88.16					
% C.V	1.73					
Press	258.03					
R^2	0.9772					
Adjusted R^2	0.9479					
Predicted R^2	0.6394					
Adeq precision	18.645					

A quadratic model was selected for the analysis of these data, as all diagnostic parameters viz., p-value, PRESS, R^2, adequate precision and diagnostic plots viz., normal plot of residuals, plot of residuals versus predicted responses and Box-Cox plot for power transformation (Appendix 1C) were satisfactory and met the specifications described in subsections 3.2.1.1.1-3.2.1.1.8, implying that the model was adequate for use. The model terms with values of Prob > F < 0.0500 indicate that model terms are significant. In this case the % RIF released at 12 h was significantly

affected by the amount of Eudragit® RLPO, EC and d-glucose used. The 3D response surface plot used to visualise the impact of EC and Eudragit® RLPO on % RIF released at 12 h is depicted in Figure 5.26.

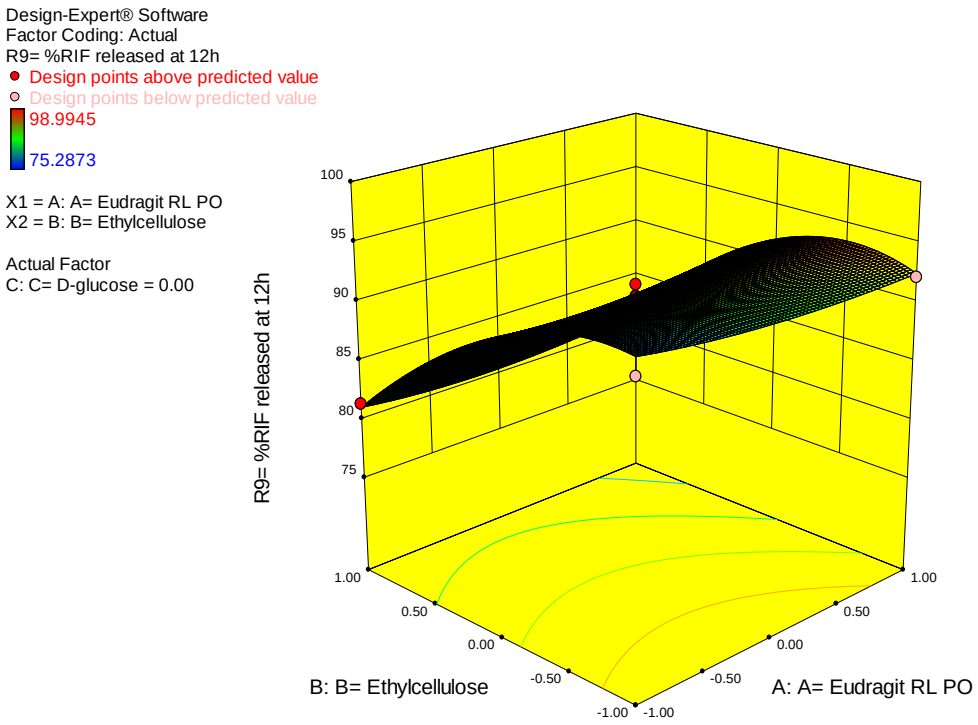

Figure 5. 26 3D response surface plot depicting the impact of EC and Eudragit® RLPO content on % RIF released at 12h.

The results revealed that an increase in amount of Eudragit® RLPO and EC used resulted in a decrease in the % RIF released. The effect of EC was attributed to lower permeability of EC to dissolution fluid observed in other studies [340, 347, 348] in addition its ability to form strong films that are resistant to structural damage [354]. An increase in thickness due to swelling of Eudragit® RLPO [349] was cited as a potential reason for the delay of RIF release.

The 3D response surface plot used to visualise the impact of d-glucose and Eudragit® RLPO content on % RIF released at 12 hours is depicted in Figure 5.27.

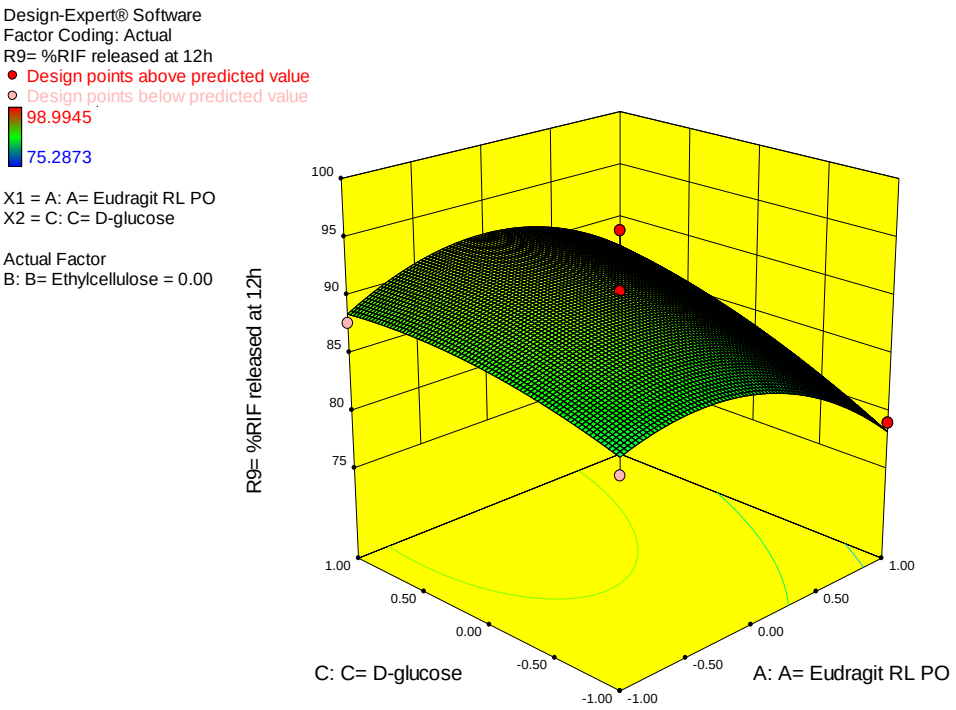

Figure 5. 27 3D response surface plot depicting the impact of d-glucose and Eudragit® RLPO content on % RIF released at 12 h.

The results reveal that increasing the amount of d-glucose used resulted in an increase in the extent of % RIF released at 12 h due to an increase in wetting of the microsphere and formation of a greater number of channels in the technology [341, 342] through which diffusion of RIF occurs. Increasing the amount of Eudragit® RLPO used resulted in a decrease in the % RIF released at 12 h due to increase in thickness of the barrier coat [349].

The 3D response surface plot used to visualise the impact of d-glucose and EC content on % RIF released at 12 hours (Figure 5.28) also revealed that an increase in the amount of d-glucose used resulted in an increase in the % RIF released at 12 h due to an increase in porosity [341, 342], whereas an increase in EC content resulted in a decrease in the extent of RIF released at 12 h as previously [340, 347, 348].

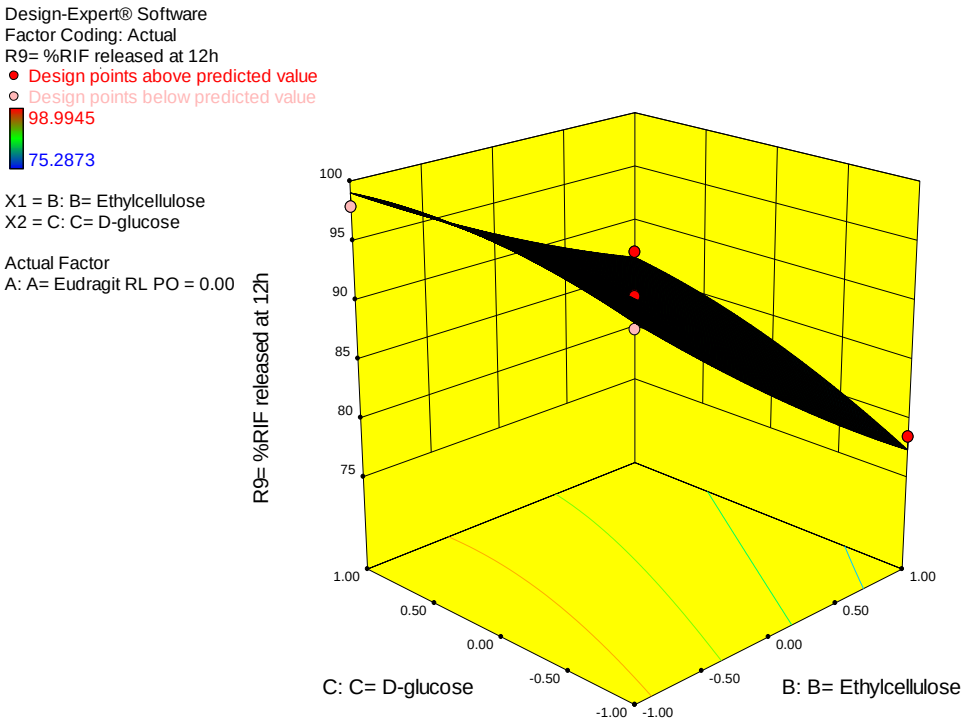

Figure 5. 28 3D response surface plot depicting the impact of D-glucose and EC content on % RIF released at 12 h.

The data for % RIF released at 12 h indicates that the microspheres released > 90 % RIF in 12 hours. Therefore almost all the RIF would be available for absorption from the stomach over a 12 hour period for most batches except for batches RIF004 (81.43 %), RIF006 (79.03 %), RIF008 (75.29 %), RIF010 (78.51 %) and RIF013 (84.12 %) in which a high amount of each polymer and a low amount of d-glucose was used, resulting in incomplete release of RIF. The relationship between input variables and % RIF released at 12 h is mathematically represented by Equation 5.7.

$$R_9 = 90.37-2.12A-7.80B+3.04C+0.17AB+1.54\ AC+1.61BC-4.14A^2+0.74B^2-1.29C^2$$

Equation 5.7

5.6.3.7 Encapsulation Efficiency, R_6

A summary of ANOVA results for % EE of RIF are listed in Table 5.10.

Table 5. 10 ANOVA data for response surface quadratic model [Partial sum of squares - Type III] for encapsulation efficiency of RIF.

Source	Sum of squares	Df	Mean square	F-value	p-value	Prob > F
Panel A						
Model	1025.16	9	113.91	22.80	0.0002	Significant
A-Eudragit® RLPO	712.22	1	712.22	142.57	< 0.0001	Significant
B-Ethylcellulose	147.35	1	147.35	29.50	0.0010	Significant
C-d-glucose	12.65	1	12.65	2.53	0.1555	Significant
AB	25.12	1	25.12	5.03	0.0599	
AC	7.54	1	7.54	1.51	0.2591	
BC	0.40	1	0.40	0.080	0.7857	
A^2	1.46	1	1.46	0.29	0.6058	
B^2	19.25	1	19.25	3.85	0.0904	
C^2	95.61	1	95.61	19.14	0.0033	Significant
Residual	34.97	7	5.00			
Lack of fit	31.94	3	10.65	4.07	0.0631	
Pure error	3.03	4	0.76			
Cor total	1060.13	16				
Panel B						
Std. deviation	2.24					
Mean	80.43					
% C.V	2.78					
Press	515.78					
R^2	0.9670					
Adjusted R^2	0.9246					
Predicted R^2	0.5135					
Adeq precision	16.574					

A quadratic model was selected for the analysis of these data as all diagnostic parameters viz., p-value, PRESS, R^2, adequate precision and diagnostic plots viz., normal plot of residuals, plot of residuals versus predicted responses and Box-Cox plot for power transformation (Appendix 1C) were satisfactory and met the specifications described in Subsections 3.2.1.1.1-3.2.1.1.8, implying that the model was adequate for use. The model terms with values of Prob > F < 0.0500 indicates the terms are significant. In this case the amounts of Eudragit® RLPO, EC and d-

glucose had a significant impact on the EE of RIF. The 3D response surface plot used to visualise the impact of EC and Eudragit® RLPO content on % EE is depicted in Figure 5.29.

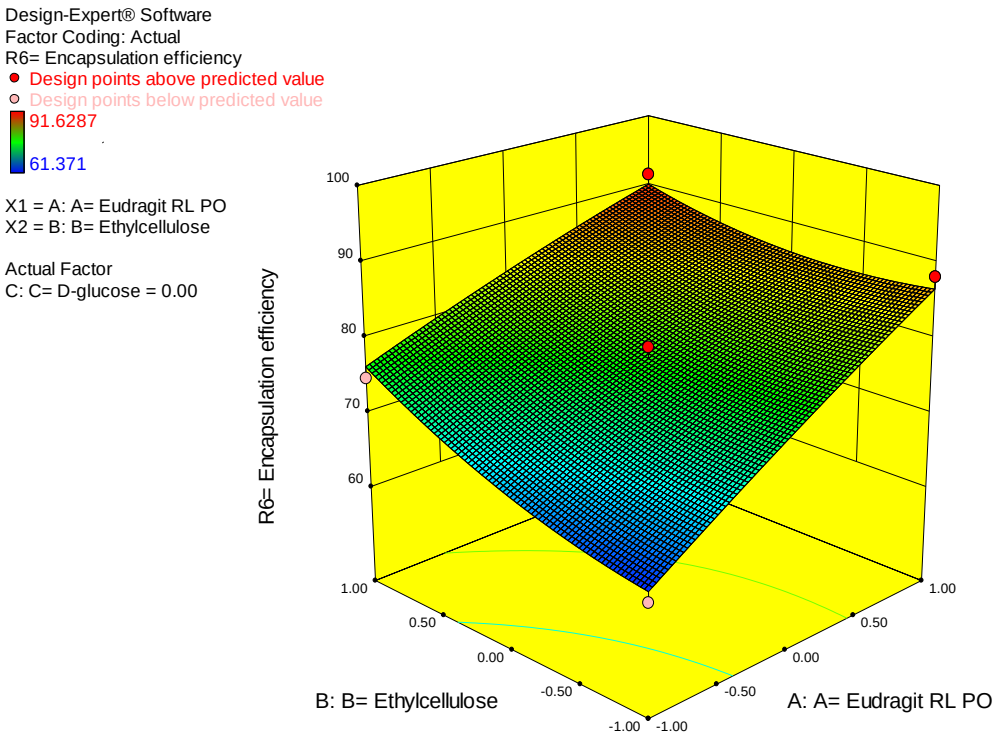

Figure 5. 29 3D response surface plot depicting the impact of EC and Eudragit® RLPO content on % EE of RIF.

The results revealed that increasing the amount of polymer used resulted in an increase in the % EE due to an increase in the amount of polymer available for encapsulation of RIF and similar data has been reported [354 - 357]. The contribution of a high polymer content to the % EE can be interpreted in two ways viz., (i) in highly concentrated solutions, the polymer precipitates more rapidly onto the surfaces of the dispersed phase and prevents API diffusion across the phase boundary [358] or (ii), the use of a high concentration of polymer results in an increase in the viscosity of the solution and delays API diffusion within the polymer droplets [359].

The rapid formation of microspheres was evident from the short manufacturing times observed, suggesting rapid diffusion of DCM into the continuous phase occurred as it is miscible with liquid paraffin [356]. The diffusion of DCM from the droplets into the continuous phase results

in precipitation and solidification of polymers and entrapment of RIF. The rapid entrapment of RIF prevented the diffusion of RIF into the continuous phase and generally resulted in high % EE which is dependent on of the availability of polymers to entrap RIF. The results were similar to those reported in which an increase in EE was associated with use of a co-solvent, miscible with the continuous phase [350]. The 3D response surface plot used to visualise the impact of d-glucose and Eudragit® RLPO content on % EE is depicted in Figure 5.30.

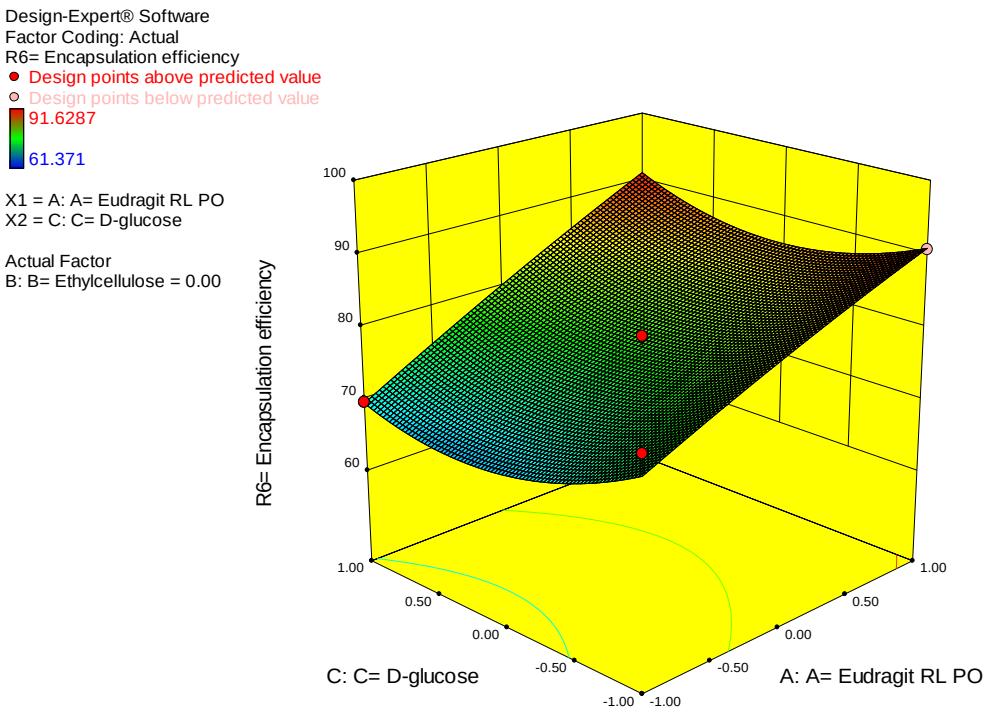

Figure 5. 30 3D response surface plot depicting the impact of d-glucose and Eudragit® RLPO content on % EE of RIF.

The results indicate that an increase in the amount of d-glucose used, resulted in a reduction in the % EE of RIF that was attributed to possible disruption of the structure of the microsphere wall and leaving spaces through which diffusion of RIF into the continuous medium could have occurred. Similar results, in which use of additives insoluble in the dispersed phase was associated with reduced % EE, have been reported [360].

The 3D response surface plot used to visualise the impact of d-glucose and EC content on % EE (Figure 5.31) also revealed that an increase in d-glucose content resulted in a decrease in % EE, whereas an increase in EC content resulted in an increase in % EC which was attributed to the ability of EC to form strong membrane films with no significant channels for RIF to diffuse through, as stated earlier [340, 347, 348].

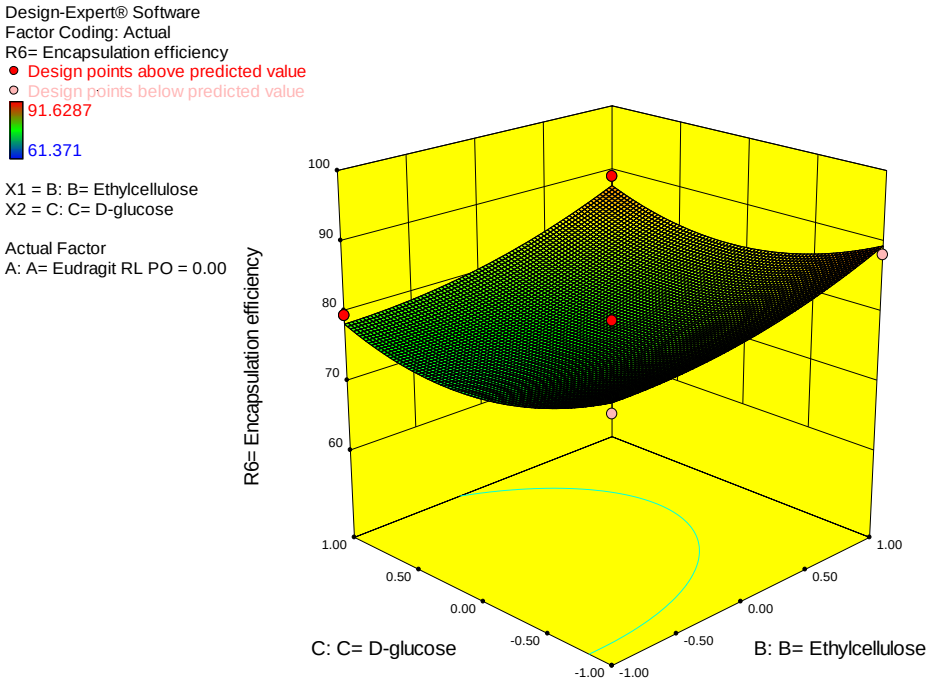

Figure 5. 31 3D response surface plot depicting the impact of d-glucose and EC content on % EE of RIF.

The relationship between input variables and % EE for RIF is mathematically represented by Equation 5.8.

$$R_6=77.46 + 9.44A + 4.29B - 1.26C - 2.51AB + 1.37AC + 0.32BC - 0.59A^2 + 2.14B^2 + 4.77C^2$$

Equation 5.8

5.6.3.8 Buoyancy, R_7

A summary of the ANOVA results for *in vitro* buoyancy of microspheres is listed in Table 5.11.

Table 5. 11 ANOVA data for the response surface linear model [Partial sum of squares - Type III] for *in vitro* buoyancy.

Source	Sum of squares	Df	Mean square	F-value	p-value	Prob > F
Panel A						
Model	295.87	3	98.62	7.94	0.0029	Significant
A-Eudragit® RLPO	54.08	1	54.08	6.35	0.0472	Significant
B-Ethylcellulose	207.67	1	207.67	16.72	0.0013	Significant
C-d-glucose	34.11	1	34.11	2.75	0.1214	
Residual	161.51	13	12.42			
Lack of fit	156.27	9	17.36	3.24	0.121	
Pure error	5.24	4	1.31			
Cor total	457.38	16				
Panel B						
Std. deviation	3.52					
Mean	60.17					
% C.V	5.86					
Press	310.61					
R^2	0.6469					
Adjusted R^2	0.5654					
Predicted R^2	0.3209					
Adeq precision	9.001					

A linear model was selected for data analysis as all diagnostic parameters viz., p-value, PRESS, R^2, adequate precision and diagnostic plots viz., normal plot of residuals, plot of residuals versus predicted responses and Box-Cox plot for power transformation (Appendix 1C) were satisfactory and met the specifications described in Subsections 3.2.1.1.1-3.2.1.1.8, implying that the model was adequate for use. The model terms with values of Prob > F < 0.0500 indicates that the terms are significant. In this case the amount of Eudragit® RLPO and EC had a significant impact on the floating properties of the microspheres produced. The 3D response surface plot used to visualise the impact of EC and Eudragit® RLPO content on % buoyancy of microspheres is depicted in Figure 5.32.

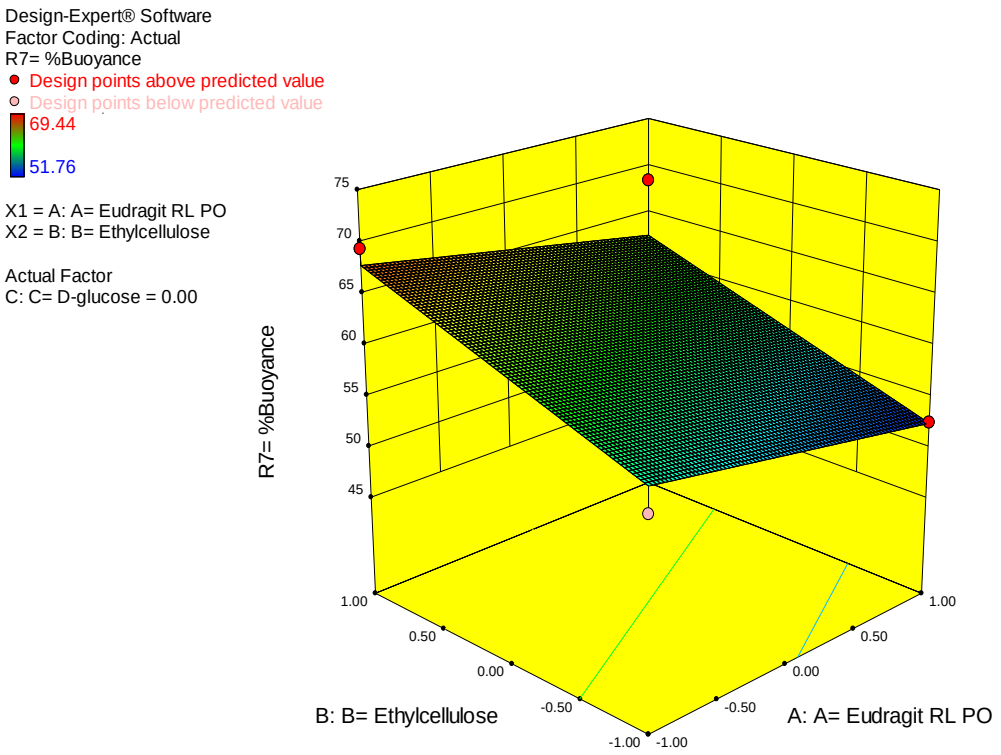

Figure 5. 32 3D surface plot depicting the impact of EC and Eudragit® RLPO content on the *in vitro* buoyancy of microspheres.

The results revealed that increasing the amount of Eudragit® RLPO used, resulted in a reduction in the floating capacity of the microspheres, which was attributed to the permeability of Eudragit® RLPO, due to the quaternary ammonium ion content, to water thereby increasing the density of the microspheres that has also been reported elsewhere [349]. It has been reported that microspheres manufactured using Eudragit® EPO exhibit low buoyancy that was attributed to the solubility of the polymer in gastric fluids [349]. Increasing the amount of EC used, resulted in an increase in the % buoyancy, *in vitro*, that was attributed to excellent barrier characteristics to water thereby preventing entry of dissolution fluid into the microspheres, a consequence of which is that an increase in density of the microspheres is avoided and have been reported [320, 361].

Inspection of Equation 5.9 that describes the relationship between input variables and % buoyancy revealed that an increase in d-glucose content resulted in an increase in buoyancy. An increase in the buoyancy of microspheres with an increase in the content of a pore forming agent has been reported [362] and was attributed to an increase in the number of pores in the microsphere. The pores created, allow entry of dissolution medium that erodes the inner surface of the matrix resulting in reduced density of microspheres thereby making them float. At 12 h, significant erosion caused by entry of dissolution fluid through pores created initially, is expected to have taken place.

$$R_7 = 60.17 - 2.60A + 5.10B + 2.07C \qquad \text{Equation 5.13.}$$

It was anticipated that the creation of pores in the microspheres would result in high buoyancy due to increased erosion resulting in a reduction of the density of the microspheres [362, 363] however this was not realised as the pronounced effects of Eudragit® on permeability and EC on escape of imbibed dissolution fluid prevail. This observation points to a possibility of the microspheres maintaining their integral architecture, albeit with a change in size and morphology during testing. In general, the buoyancy of microspheres of all batches was low with the highest buoyancy recorded of 68 % suggesting that a significant number of microspheres did not float in acidic solution. Consequently many of the microspheres would be emptied into the small intestine fairly rapidly *in vivo*, which has bioavailability implications as the solubility and absorption of RIF are low from this part of the GIT. Therefore the inclusion of sodium bicarbonate to the formulation was considered, as CO_2 is generated when the compound is exposed to acid, would therefore improve the floating and buoyancy of the microspheres [364].

5.6.3.9 Floating Lag time, R_8

A summary of the ANOVA results for floating lag time of microspheres is listed in Table 5.12.

Table 5. 12 ANOVA data for response surface quadratic model [Partial sum of squares - Type III] for floating lag time.

Source	Sum of squares	Df	Mean square	F-value	p-value	Prob > F
Panel A						
Model	40709.75	9	4523.31	22.68	0.0002	Significant
A-Eudragit® RLPO	22366.12	1	22366.12	112.13	< 0.0001	Significant
B-Ethylcellulose	3120.50	1	3120.50	15.64	0.0055	Significant
C-d-glucose	1378.13	1	1378.13	6.91	0.0340	Significant
AB	6162.25	1	6162.25	30.89	0.0009	Significant
AC	25.00	1	25.00	0.13	0.7337	
BC	756.25	1	756.25	3.79	0.0926	
A^2	1520.00	1	1520.00	7.62	0.0281	Significant
B^2	3852.89	1	3852.89	19.32	0.0032	Significant
C^2	885.26	1	885.26	4.44	0.0731	
Residual	1396.25	7	199.46			
Lack of fit	392.25	3	64.08	44.08	0.1210	
Pure error	4.00	4	1.00			
Cor total	42106.00	16				
Panel B						
Std. deviation	14.12					
Mean	121.00					
% C.V	11.67					
Press	22282.25					
R^2	0.9668					
Adjusted R^2	0.9242					
Predicted R^2	0.4708					
Adeq precision	17.010					

A quadratic model was selected for data analysis as all diagnostic parameters viz., p-value, PRESS, R^2, adequate precision and diagnostic plots viz., normal plot of residuals, plot of residuals versus predicted responses and Box-Cox plot for power transformation (Appendix 1C) were satisfactory and met the specifications described in Subsections 3.2.1.1.1-3.2.1.1.8, implying that the model was adequate for use. Model terms with values of Prob > F < 0.0500 indicate that terms are significant. In this case the amount of Eudragit® RLPO, EC and d-glucose used had a significant impact on the floating lag time of the microspheres. The 3D response surface plot used to visualise the impact of EC and Eudragit® RLPO content on floating lag time is depicted in Figure 5.33.

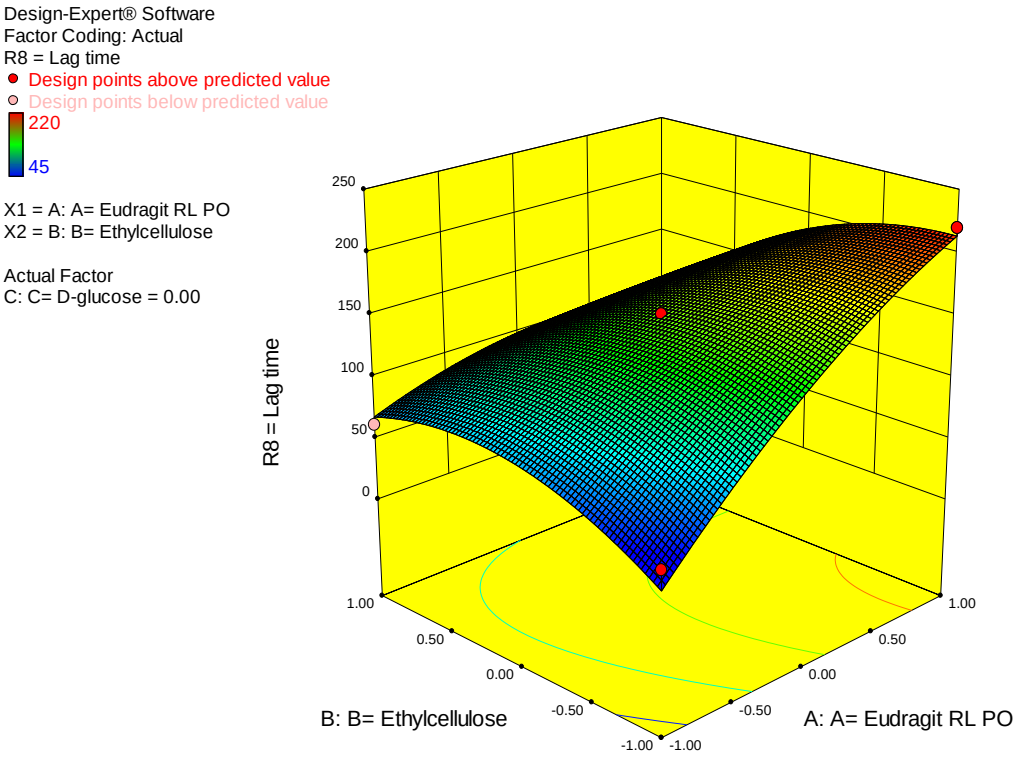

Figure 5. 33 3D response surface plot depicting the impact of EC and Eudragit® RLPO content on floating lag time of the microspheres.

The results reveal that increasing the Eudragit® RLPO content resulted in an increase in floating lag time, with the highest floating lag time recorded when Eudragit® RLPO content was at the highest and EC content at the lowest levels, posibily due to an increase in the density of microspheres following rapid uptake of dissolution fluid by the quaternary ammonium ions present in Eudragit® RLPO [349]. Increasing the amount of EC used, resulted in a decrease in floating lag time, possibly due to the barrier properties of EC which resulted in minimal uptake of dissolution fluid [340].

The 3D response surface plot used to visualise the impact of d-glucose and Eudragit® RLPO content on floating lag time is depicted in Figure 5.34.

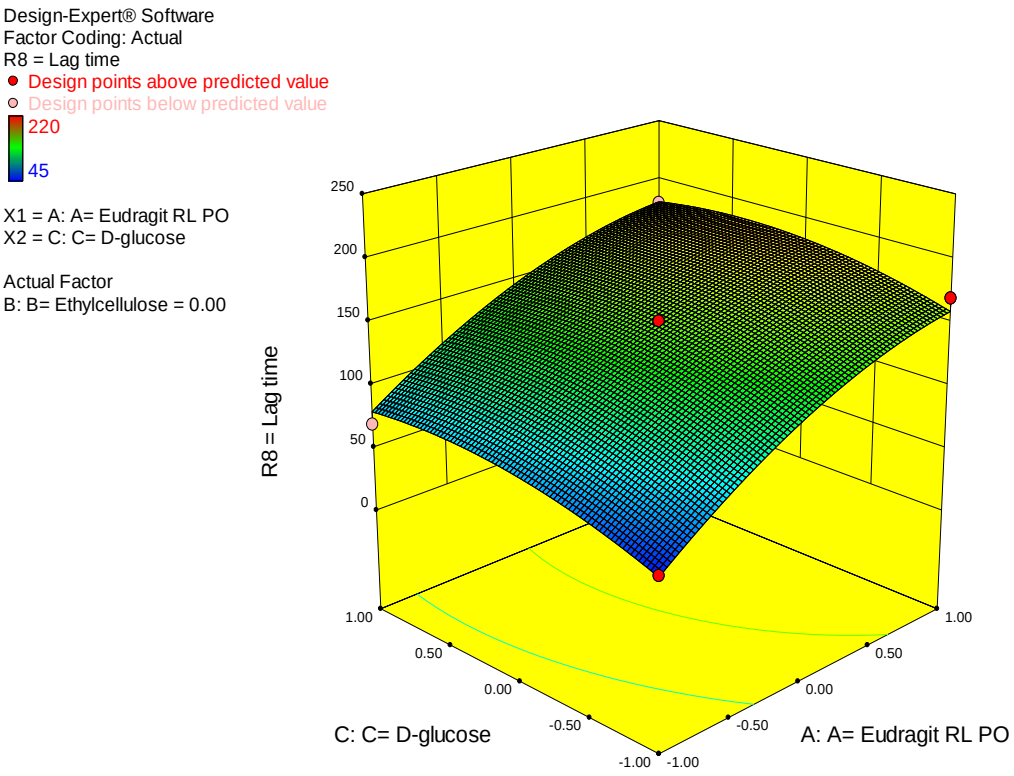

Figure 5. 34 3D response surface plot depicting the impact of d-glucose and Eudragit® RLPO content on floating lag time of the microspheres.

The results reveal that an increase in d-glucose content resulted in an increase in floating lag time that was attributed to the ability of d-glucose to adsorb dissolution fluid resulting in an increase in the density of the microspheres, during the initial stages of testing. In addition, an increase in the amount of Eudragit® RLPO used also resulted in an increase in the floating lag time due to ingress of dissolution medium as a result of quaternary ammonium ions as stated earlier [349].

The 3D response surface plot used to visualise the impact of d-glucose and EC content (Figure 5.35) revealed that an increase in d-glucose content resulted in an increase in floating lag time whereas increasing the EC content decreased floating lag time.

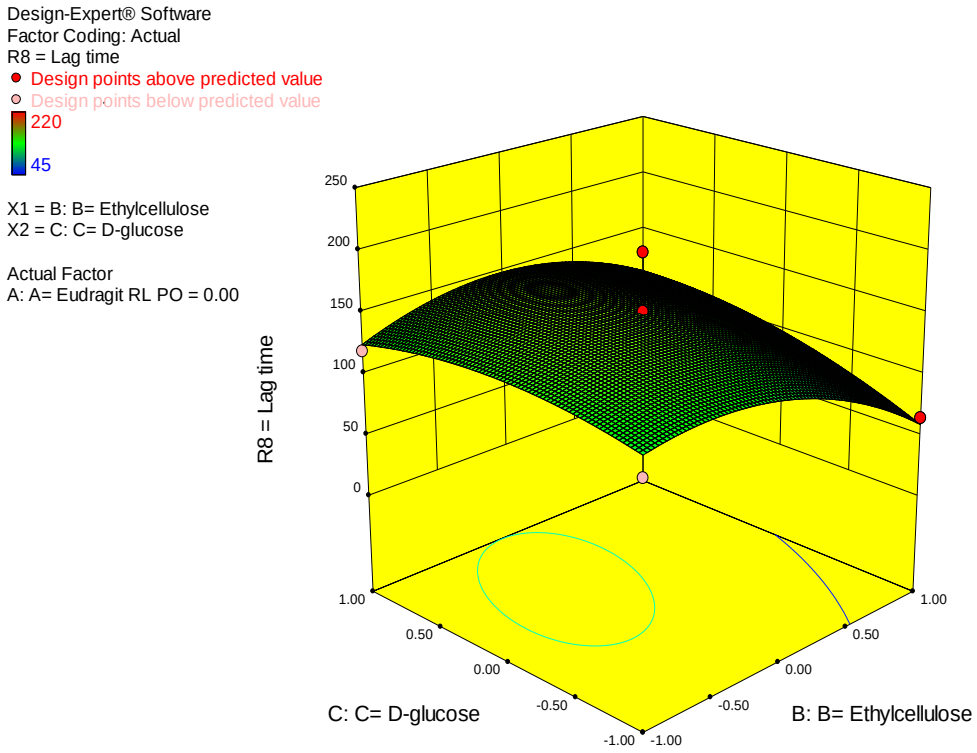

Figure 5. 35 3D response surface plot depicting the impact of d-glucose and EC content on floating lag time of the microspheres.

These results revealed that floating lag time of the microspheres for BBD batches was long and ranged between 110 – 220 seconds for most formulations. Although some microspheres would float from the bottom of the dissolution vessel to the surface of the dissolution fluid, some sank to the bottom after a short period of time, suggesting these microspheres would be emptied from the stomach rapidly, due to their proximity to the gastric-duodenal junction and that the RIF would not be available for absorption from the stomach. This observation further supports the decision to add a CO_2 generating component to the formulation. The relationship between input variables and floating lag time is mathematically represented by Equation 5.10.

$$R_8 = 151.00 + 52.88A - 19.75B + 13.13C - 39.25AB - 2.50AC + 13.75BC - 19.00A^2 - 30.25B^2 - 14.50C^2$$ Equation 5.14

5.6.3.10 %Yield, R_{10}

A summary of the ANOVA results for % yield of microspheres is listed in Table 5.13.

Table 5. 13 ANOVA data for response surface quadratic model [Partial sum of squares - Type III] for % yield.

Source	Sum of squares	Df	Mean square	F-value	p-value	Prob > F
Panel A						
Model	886.62	9	98.51	77.42	< 0.0001	Significant
A-Eudragit® RLPO	590.99	1	590.99	464.45	< 0.0001	Significant
B-Ethylcellulose	227.70	1	227.70	178.94	< 0.0001	Significant
C-d-glucose	6.44	1	6.44	5.06	0.0592	
AB	2.56	1	2.56	2.01	0.1990	
AC	1.69	1	1.69	1.33	0.2870	
BC	4.33	1	4.33	3.40	0.1077	
A^2	20.89	1	20.89	16.42	0.0049	Significant
B^2	18.09	1	18.09	14.21	0.0070	Significant
C^2	15.64	1	15.64	12.29	0.0099	Significant
Residual	8.91	7	1.27			
Lack of fit	7.14	3	2.38	5.38	0.0689	
Pure error	1.77	4	0.44			
Cor total	895.53	16				
Panel B						
Std. deviation	1.13					
Mean	72.14					
% C.V	1.56					
Press	116.96					
R^2	0.9901					
Adjusted R^2	0.9773					
Predicted R^2	0.8694					
Adeq precision	33.372					

A quadratic model was selected for this analysis as all diagnostic parameters viz., p-value, PRESS, R^2, adequate precision and diagnostic plots viz., normal plot of residuals, plot of residuals versus predicted responses and Box-Cox plot for power transformation (Appendix 1C) were satisfactory and met the specifications described in Subsections 3.2.1.1.1-3.2.1.1.8, implying that the model was adequate for use. The model terms with values of Prob > F < 0.0500 indicate that the terms are significant. In this case the amount of Eudragit® RLPO, EC and d-glucose had a significant impact on the % yield. The 3D response surface plot used to visualise the impact of Eudragit® RLPO and EC content on % yield is depicted in Figure 5.36.

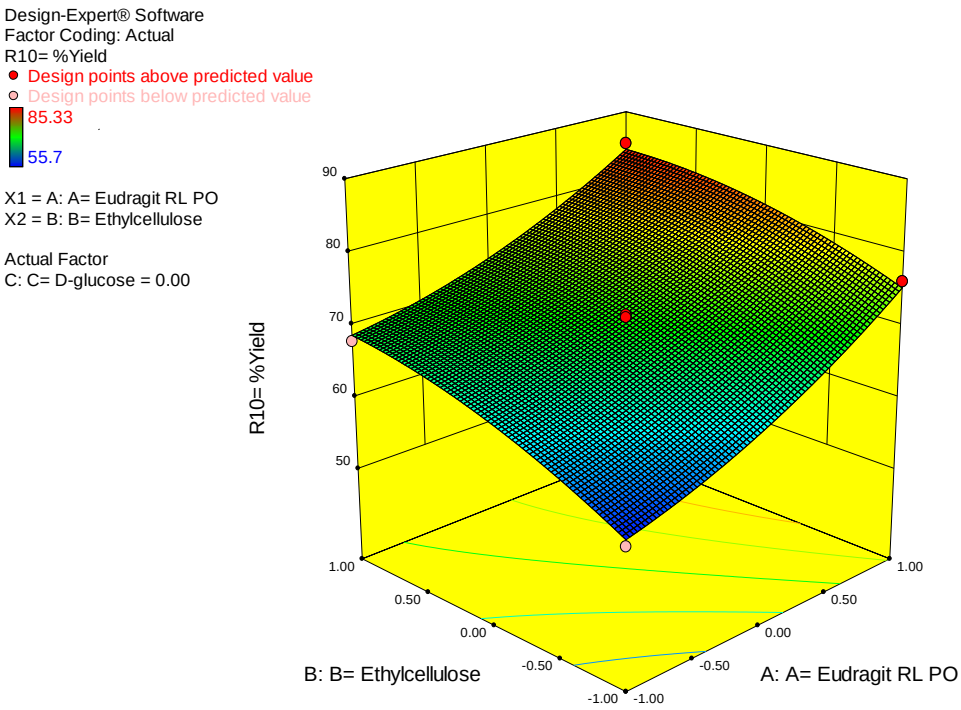

Figure 5. 36 3D response surface plot depicting the impact of EC and Eudragit® RLPO content on % yield.

The results reveal that increasing the amount of Eudragit® RLPO and EC used resulted in an increase in the % yield and was attributed to the increase in total polymer available for microencapsulation. These results were in contrast to those reported elsewhere [365] in which yield was unchanged despite changes in API-polymer ratio. In these studies, particularly when Eudragit® RLPO and EC were used at the lowest level, the microspheres were not sufficiently robust and may have reverted to powder during filtration, drying and sieving resulting in a low yield. This observation suggests that a total polymer content of ≤ 2.0 g would not be sufficient for effective microencapsulation of RIF using the described manufacturing approach.

The 3D response surface plot used to visualise the impact of d-glucose and Eudragit® RLPO content on % yield is depcited in Figure 5.37.

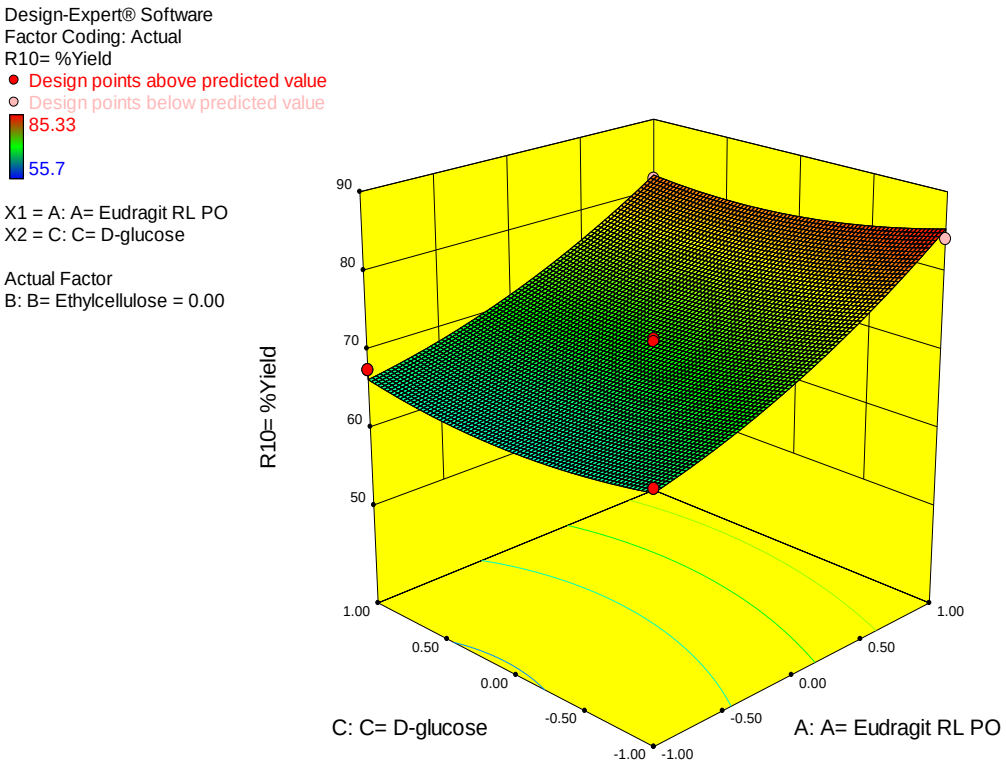

Figure 5. 37 3D response surface plot depicting the impact of d-glucose and Eudragit® RLPO content on % yield.

The results reveal that an increase in d-glucose content resulted in a decrease in % yield. It was observed that an increase in d-glucose, whilst keeping Eudragit® RLPO at the lowest content, resulted in the formation of microspheres that may break, and the reduction in yield could be as a result of damage of microspheres during filtration, drying and sieving. Similar results, in which high levels of pore forming agent were used, resulted in low yields of microspheres [366]. An increase in the Eudragit® RLPO content whilst keeping d-glucose content low resulted in an increase in % yield and was attributed to the formation of microspheres with a resilient microsphere wall.

The 3D response surface plot used to visualize the impact of d-glucose and EC content (Figure 5.38) also revealed that an increase in d-glucose content resulted in a decrease in % yield and increasing EC content results in an increase of the % yield.

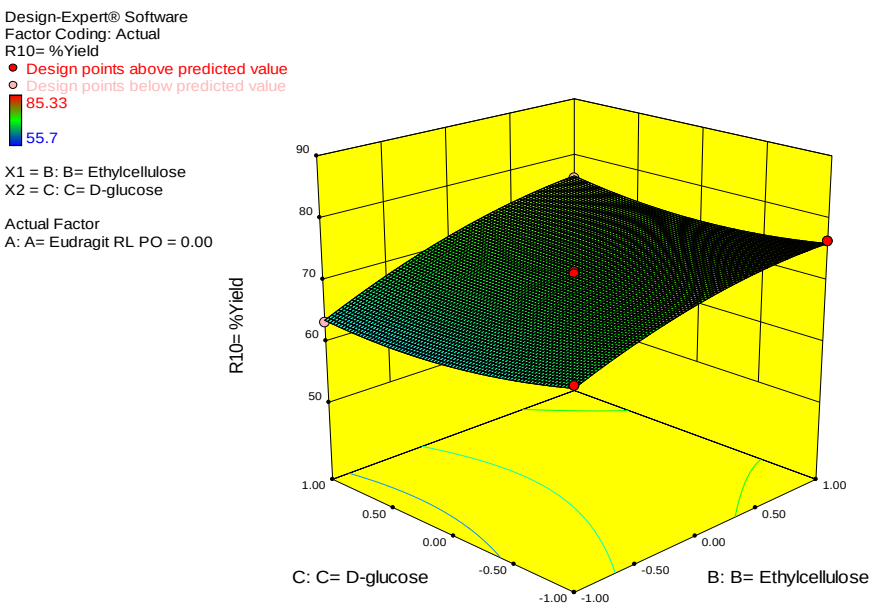

Figure 5. 38 3D response surface plot depicting the impact of d-glucose and EC content on % yield.

In general, the % yield was high and was, in part, due to stable emulsion and droplet formation on addition of the dispersed phase to continuous phase and therefore the availability of polymers to encapsulate dispersed droplets to form microspheres. As a constant homogenization speed was used for product manufacture, only formulation variables had an impact on the % yield. The relationship between formulation variables and % yield is represented mathematically by Equation 5.11.

$$R_{10}=71.16 + 8.60A + 5.34B - 0.90C - 0.80AB - 0.65AC + 1.04BC + 2.23A^2 - 2.07B^2 + 1.93C^2$$

Equation 5.11

5.6.4 Formulation and Process Optimisation

The polynomial equations relating input variables to responses, in conjunction with observations made during manufacturing and testing were used to identify and predict formulation and process variables that would result in the production of an optimised product. The responses based on defined quality product attributes are listed in Table 5.1 and were entered into Design® Expert software that established the amount of each excipient to use. The optimised formulation

was comprised of 2.0 g Eudragit® RLPO, 1.5 g EC, 1.0 g RIF, 0.65 g d-glucose and 1.0 g MCC Avicel® PH101. The optimised product (n= 3) was manufactured using 125 mL liquid paraffin containing 1.0 % v/v Span 80, 30 mL dichloromethane, 20 mL acetone and agitated at a homogenisation speed of 125000 rpm. The prediction accuracy of the process was determined by calculating residuals, (R) and percent prediction error (% P.E.) for the three batches that were manufactured using the optimised input variables. The residuals and % P.E. for the responses summarised in Table 5.14 were in general < 10 % with only buoyancy exceeding this limit for two batches. These data suggests that the models used are useful and were successful for the development and manufacture of RIF microspheres.

Table 5. 14 Prediction accuracy for the Box Behnken Design optimisation process.

BATCH	RESPONSE	PREDICTION ACCURACY			
		Predicted	**Actual**	**Residual**	**%PE**
A	% RIF released at 0.5 h (R^1)	15.39	15.65	0.26	1.66
	% RIF released at 2 h (R_2)	36.99	38.04	1.05	2.76
	% RIF released at 4 h (R_3)	48.58	49.18	0.6	1.22
	% RIF released at 6 h (R_4)	68.71	65.70	3.01	4.58
	% RIF released at 8 h (R_5)	76.55	78.55	2	2.55
	Encapsulation efficiency (%) (R_6)	94.71	94.80	0.09	0.095
	% Buoyancy (R_7)	62.23	58.62	3.61	6.16
	Floating lag time (seconds) (R_8)	149.63	144	5.63	3.91
	% RIF released at 12 h (R_9)	92.12	87.89	4.23	4.81
	% Yield (R_{10})	82.19	81.95	0.24	0.29
B	% RIF released at 0.5 h (R_1)	15.39	15.81	0.42	2.66
	% RIF released at 2 h (R_2)	36.99	38.58	1.59	4.12
	% RIF released at 4 h (R_3)	48.58	49.11	0.53	1.08
	% RIF released at 6 h (R_4)	68.71	64.57	4.14	6.41
	% RIF released at 8 h (R_5)	76.55	77.08	0.53	0.688
	Encapsulation efficiency (%) (R_6)	94.71	99.19	4.48	4.52
	% Buoyancy (R_7)	62.23	56.22	6.01	10.69
	Floating lag time (seconds) (R_8)	149.63	140	9.63	6.88
	% RIF released at 12 h (R_9)	92.12	86.44	5.68	6.57
	% Yield (R_{10})	82.19	87.97	5.78	6.57
C	% RIF released at 0.5 h (R_1)	15.39	16.03	0.64	3.99
	% RIF released at 2 h (R_2)	36.99	39.32	2.33	5.93
	% RIF released at 4 h (R_3)	48.58	47.22	1.36	2.88
	% RIF released at 6 h (R_4)	68.71	66.73	1.98	2.97
	% RIF released at 8 h (R_5)	76.55	78.44	1.89	2.41
	Encapsulation efficiency (%) (R_6)	94.71	96.99	2.28	2.35
	% Buoyancy (R_7)	62.23	55.81	6.42	11.50
	Floating lag time (seconds) (R_8)	149.63	142	7.63	5.37
	% RIF released at 12 h (R_9)	92.12	94.71	2.59	2.74
	% Yield (R_{10})	82.19	85.88	3.69	4.20

Use of the variables recommended by the optimisation process resulted in the production of batches with an average yield of 85.27 ± 3.06%. The release of RIF was sustained over 12 hours with 88.82 ± 2.95% RIF released at 12 h. The average % EE was 96.99 ± 2.19%. The buoyancy for the optimised formulation was low with all exhibiting long floating lag times. In order to improve the buoyancy and reduce the floating lag time sodium bicarbonate (1.0 g) was added to the formulation. Sodium bicarbonate would react with acid in the stomach to produce $C0_2$, that may improve the buoyancy characteristic of the microspheres. Since the RIF microspheres were to be used in combination with the INH gastric resistant microspheres reported in Chapter 4, the impact of possible changes in the microenvironment as a result of the reaction between $NaHCO_3$ and HCl was mitigated by inclusion of 0.5 g anhydrous citric acid to the formulation. The dissolution profile of RIF release from the optimised formulation in pH 1.2 0.1 M HCl over12 h is depicted in Figure 5.39. The dissolution profiles for % RIF released from all manufactured batches are depicted in Appendix 2B.

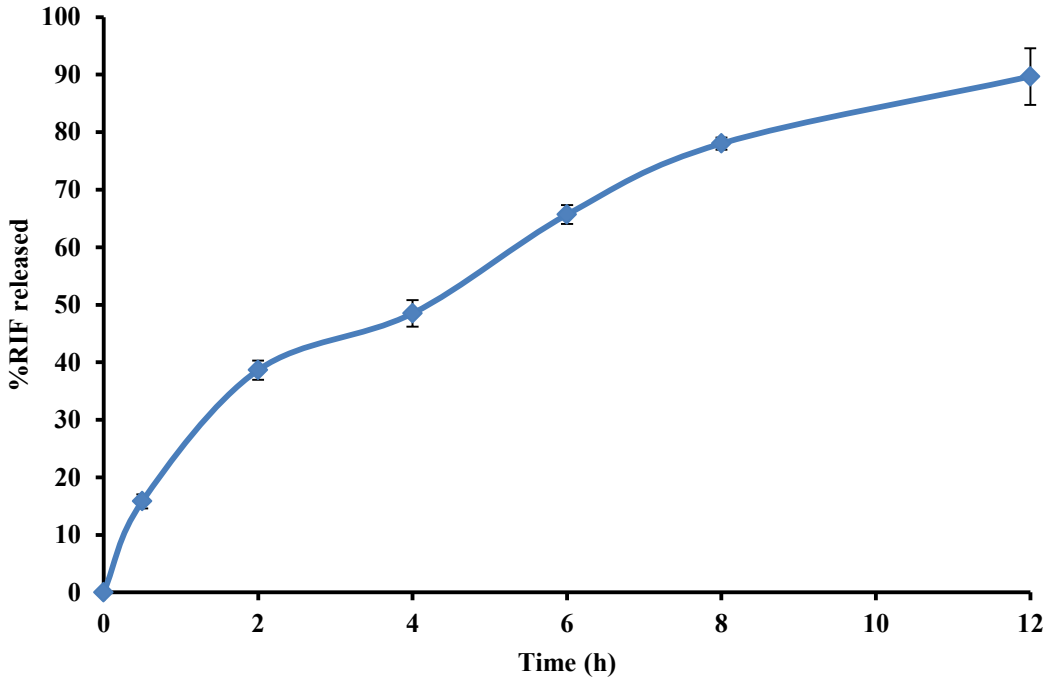

Figure 5. 39 Dissolution profile depicting % RIF released from the optimised formulation (RIF018) in pH 1.2 0.1 M HCl for 12 h (n = 6).

5.6.5 Manufacture and Assessment of Modified Optimised Batch

As the optimised process and formulation exhibited low buoyancy and long floating lag times, sodium bicarbonate and anhydrous citric acid were added to the composition in a bid to improve the floating characteristics of the microspheres. The modified optimised batches were manufactured and tested viz., batches RIF021, RIF022 and RIF023.

5.6.5.1 Manufacturing Process

The manufacturing process was slightly modified by accurately weighing sodium bicarbonate (1.0 g) and citric acid (0.5 g) and adding the materials to the polymer and RIF solution/dispersion prepared as described in Section 5.5.3.3. All other processes were unaltered and the microspheres were characterised as described in Sections 5.5.3.4 – 5.5.3.10. The manufacturing process produced discrete spherical microspheres with a % yield of 97.56 %.

5.6.5.2 *In vitro* buoyancy and floating lag time

The modified microspheres exhibited a % buoyancy of 87.66 ± 1.28 % (n = 6) and floating lag time of 15 ± 3.2 (n = 6) seconds. Furthermore, the microspheres remained buoyant for up to 12 h. The improvement in floating behaviour of the microspheres was attributed to the generation of CO_2 on contact with the dissolution fluid resulting in the microspheres floating and these observations are similar to what has been reported [346]. The dissolution of sodium bicarbonate and production of CO_2 may have created spaces within the microspheres into which dissolution medium diffused leading to erosion and reduced density of core [364].

5.6.5.3 Encapsulation efficiency

The % EE of RIF for the modified formulation was 88.26 ± 1.25 % that was reduced when compared to that of the optimised formulation which was 96.99 ± 2.19 %. This reduction was attributed to possible disruption of the film structure as a result of incorporation of sodium bicarbonate and citric acid, which could have left voids through the microsphere core through which RIF may have diffused to reach the continuous medium and these data are similar to what has been reported elsewhere [360].

5.6.5.4 *In vitro* RIF release

RIF release from the modified microspheres occurred at a faster rate than from the optimized batch, with 39.71 %, 68.97 %, 83.61 % and 87.10 % as compared to 15.83 %, 38.65 %, 65.67 % and 89.68 % RIF released at 0.5 h, 2 h, 6 h and 12 h respectively. The dissolution profile for % RIF released from modified batch formulation in pH 1.2 0.1 M HCl is depicted in Figure 5.40.

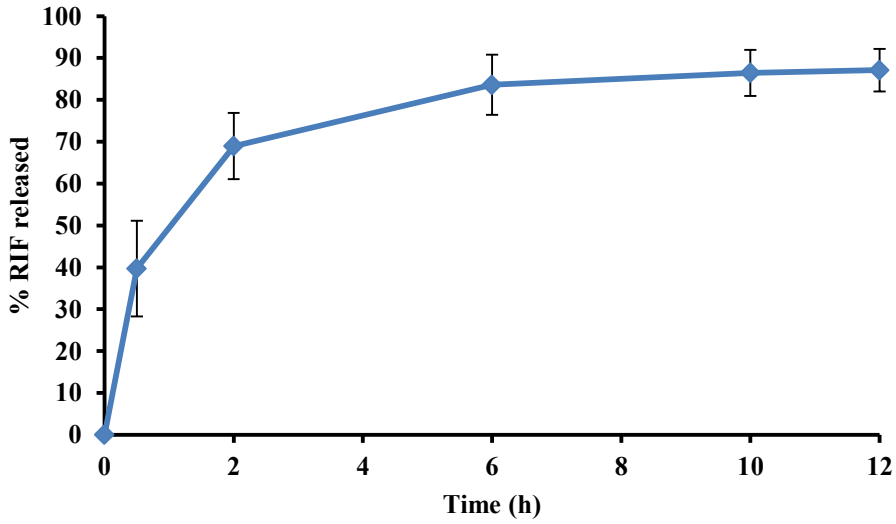

Figure 5. 40 Dissolution profile depicting % RIF released from the modified formulation in pH 1.2 0.1 M HCl after 12 h (n = 6).

The increase in the rate and extent of RIF release was attributed to the creation of pores in the matrix on contact with the dissolution medium which allowed better penetration of the dissolution medium into the matrix, subsequent dissolution and release from the microsphere matrix. The more rapid entry of dissolution medium into the microspheres resulted in more rapid dissolution of d-glucose further increasing the channels for diffusion of RIF, as well as increased erosion of the matrix and these results are similar to those reported elsewhere [366]. Other studies reported a more sustained release of API from floating drug delivery system [313, 349] and attributed that to the rapid swelling of polymers and creation of a more torturous path for the API to traverse in addition to reduced exposure to dissolution medium. The discrepancy observed was attributed to the inclusion of a pore forming agent resulting in the formation of a highly porous structure and increased erosion as can be seen on microsphere surfaces (Figure 5.41) observed using SEM following dissolution testing.

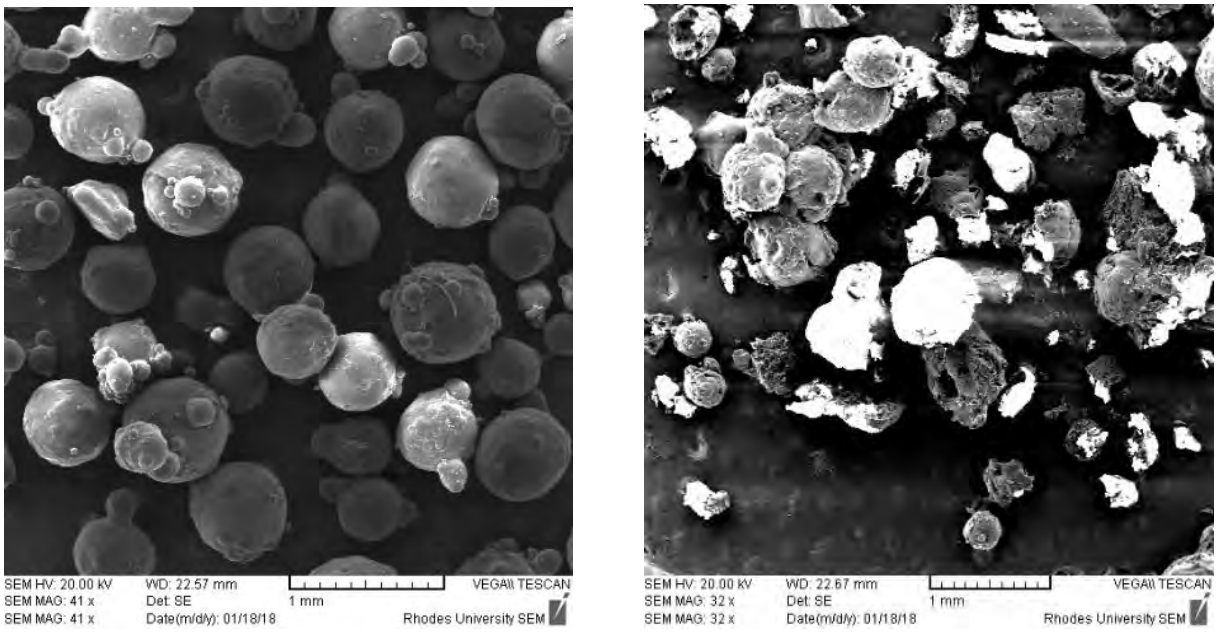

(A) (B)

Figure 5. 41 SEM image of microspheres of the modified batch (A) prior to and (B) following 12 h dissolution testing in pH 1.2 0.1 M HCl.

5.6.5 Mean Particles Size Distribution

The results generated following sieve analysis of the microspheres are summarised in Table 5.15 and reveal that the microspheres produced ranged in diameter between 800 µm to 1250µm. Most of the microspheres, > 90% of the experimental design products in addition to the optimized batch (RIF018) had diameters < 800 µm and suggested a fairly uniform particle size distribution. The inter-batch uniform size distribution can be attributed to the use of a constant homogenization speed for all batches as homogenization is reported to be a key determinant of microsphere size [367]. It has been reported that microsphere size increases with an increase in polymer content and was attributed to an increase in viscosity of polymer solution and that swell significantly as polymer content is increased [368]. However, this may not have been the case in this study, as the Eudragit® RLPO and EC do not swell significantly in the solvents used.

Table 5. 15 Size distribution of microspheres for BBD, optimised and modified batches.

Batch	Eudragit® RLPO	Ethylcellulose	d-glucose	% mass of microspheres retained per sieve size	
	g	g	g	µm	
				800	1250
RIF001	3	1.5	0.75	95.50	4.50
RIF002	3	1	0.5	97.27	2.73
RIF003	2	1.5	0.5	92.54	7.46
RIF004	1	2	0.5	94.91	5.09
RIF005	2	1.5	0.5	97.33	2.67
RIF006	3	1.5	0.25	98.42	1.58
RIF007	2	1.5	0.5	96.71	3.29
RIF008	3	2	0.5	97.88	2.12
RIF009	2	1.5	0.5	96.33	3.67
RIF010	2	2	0.25	100	0.00
RIF011	2	1.5	0.5	98.11	1.89
RIF012	1	1.5	0.75	81.83	18.17
RIF013	1	1.5	0.25	72.78	27.22
RIF014	2	1	0.25	92.64	7.36
RIF015	2	1	0.75	93.12	6.88
RIF016	1	1	0.5	54.18	45.82
RIF017	2	2	0.75	96.67	3.33
RIF018	2	1.5	0.65	94.45	5.55
RIF021	2	1.5	0.65	96.77	3.23

The intra-batch mean particle size distribution of microspheres from the BBD batches and that of the modified batch formulation is summarised in Table 5.16 and ranged between 423.19 ± 121.86 µm to 620.07 ± 102.67 µm in diameter.

Table 5. 16 Mean particle size distribution of microspheres

Formulation	Mean particle size µm	Standard Deviation	%RSD
RIF001	515.08	209.79	40.72
RIF002	489.77	115.63	23.61
RIF003	476.59	188.78	39.61
RIF004	459.02	145.89	31.78
RIF005	540.00	125.39	23.22
RIF006	481.42	92.81	19.28
RIF007	541.87	108.41	20.01
RIF008	423.19	121.86	28.80
RIF009	545.96	185.57	33.99
RIF010	452.69	88.34	19.51
RIF011	499.55	177.19	35.47
RIF012	601.71	167.94	27.91
RIF013	620.07	102.67	16.56
RIF014	537.71	128.39	23.88
RIF015	576.73	95.39	16.54
RIF016	485.38	170.33	35.09
RIF017	477.58	102.58	21.48
RIF018	547.22	108.63	19.85
RIF021	526.49	91.88	17.45

Analysis of the intra-batch mean particle size distribution reveals that the size of microspheres was wide with a % RSD ranging between 16.56 – 40.72 %. Since the size of microspheres influences the rate of drug release [369], the data suggest that the rate of RIF release from the different batches would be different which, in turn, may result in variable plasma concentration. This observation was correlated with the high % RSD values and error bars on dissolution profiles for % RIF released from microspheres of the BBD formulations (Appendix 2B) which were, in some cases, as high as 15 %. However a mean particle size distribution with % RSD values as high as 50 % for microspheres is uncommon and these are similar to that observed in a previous report [369]. The % RSD for RIF release at different time points for the modified optimised microspheres ranged between 5.52 % to 11.41 % which was within the acceptable range of not > 20 % for early time points and not > 10 % at the later time points [370].

5.6.6 Flow Characteristics

The microspheres from all batches exhibited excellent flow properties with a CI of 1.998 ± 0.043 % and HR of 1.020 ± 0.001 for all formulations manufactured according to the Box Behnken design. The optimised and modified formulations also exhibited similar flow characteristics with a CI of 1.422 ± 0.074 % and 1.521 ± 0.002 %, and HR of 1.034 ± 0.002 and 1.04 ± 0.001 for microspheres of batches RIF018 and RIF021, respectively. The excellent flow characteristics were attributed to the spherical nature of the microspheres and indicate that filling of microspheres into hard gelatin capsules was unlikely to pose a challenge in respect of producing a product of uniform content.

5.6.7 Scanning Electron Microscopy

The micrographic images of microspheres manufactured using the BBD and those of the optimized (RIF018) and modified formulations (RIF021) are depicted in Figure 5.42. The microspheres for most batches were spherical had smooth surfaces with some cracks and pores. The surfaces of the microspheres from batches RIF012, RIF013, RIF014, and RIF015 were however, rough. Batches RIF012 and RIF013 were manufactured using a 1:1.5 Eudragit® RLPO to EC ratio and batches RIF014 and RIF015 a 2:1 ratio of the polymers. It is clear that the ratio of Eudragit® RLPO to EC is important when producing microspheres with a smooth surface. Microspheres from batch RIF016 also had a rough surface and appeared to be highly porous without complete formation of spheres. This batch was manufactured with the lowest polymer content suggesting that insufficient material was available for efficient microencapsulation to occur. Batch RIF016 also showed the lowest % EE suggesting the incomplete microsphere barrier could have allowed diffusion of RIF into the continuous medium that was correlated with the highest rate of release with almost 20 % RIF released at 0.5 h.

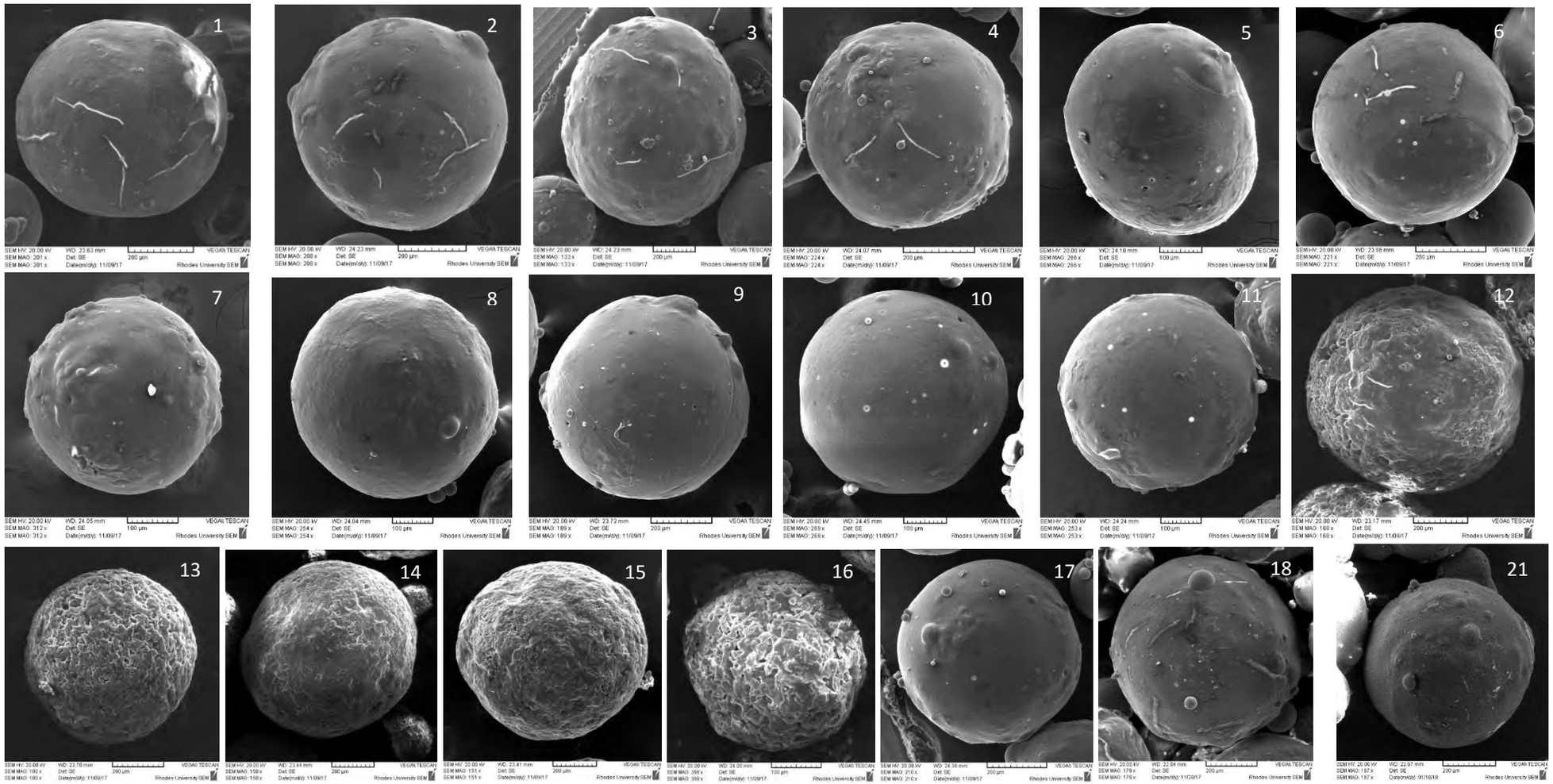

Figure 5. 42 SEM images of microspheres of batches RIF001- RIF017, the optimised batch RIF018 and modified batch RIF021.

In order to monitor pore formation, microspheres that had been exposed to dissolution fluid for 4 h were also examined using SEM and the micrographs are depicted in Figure 5.43. The images reveal that pores were successfully formed in the microspheres following dissolution of d-glucose and that the number of pores formed was dependent on the amount of Eudragit® RLPO, EC and d-glucose used. Batches in which the ratio of Eudragit® RLPO to EC was 3:2, 2:1, 2.1.5 and 1:1 exhibited greater porosity than batches in which the EC content used was greater than Eudragit® RLPO content. This phenomenon was attributed to the permeability of Eudragit® RLPO that facilitated dissolution fluid uptake by the microspheres resulting in dissolution of d-glucose and the generation of pores. EC is insoluble and may slow the uptake of dissolution fluid by the microspheres resulting in slower dissolution d-glucose and eventual erosion of the microspheres. This behaviour may have resulted in the reduction in RIF release observed when EC content of the microspheres was high.

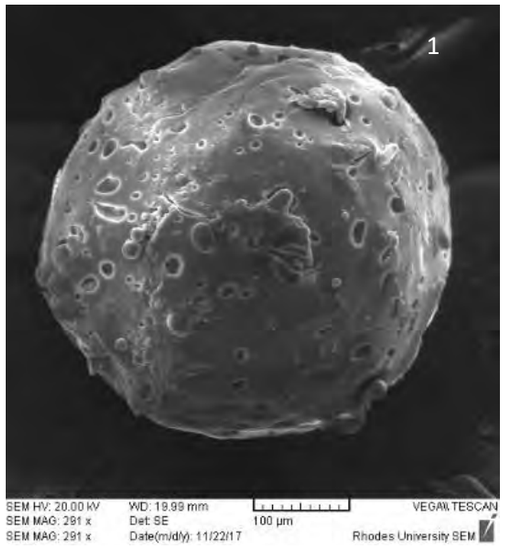
1
SEM HV: 20.00 kV
SEM MAG: 291 x
SEM MAG: 291 x
WD: 19.99 mm
Det: SE
Date(m/d/y): 11/22/17
100 µm
VEGA\\ TESCAN
Rhodes University SEM

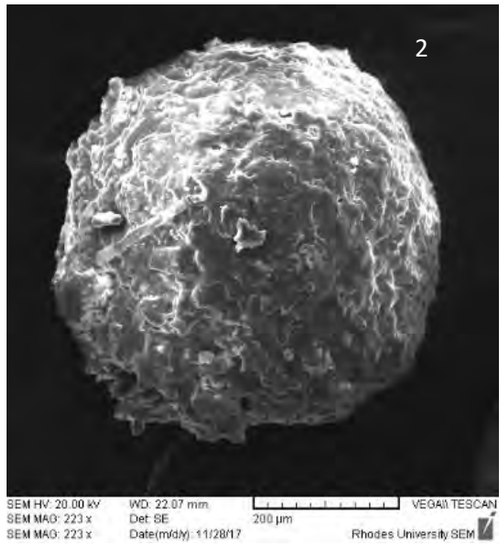
2
SEM HV: 20.00 kV
SEM MAG: 223 x
SEM MAG: 223 x
WD: 22.07 mm
Det: SE
Date(m/d/y): 11/28/17
200 µm
VEGA\\ TESCAN
Rhodes University SEM


3
SEM HV: 20.00 kV
SEM MAG: 141 x
SEM MAG: 141 x
WD: 19.94 mm
Det: SE
Date(m/d/y): 11/22/17
200 µm
VEGA\\ TESCAN
Rhodes University SEM

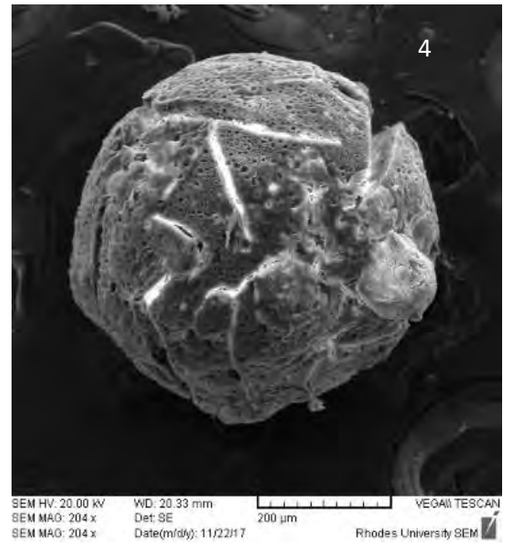
4
SEM HV: 20.00 kV
SEM MAG: 204 x
SEM MAG: 204 x
WD: 20.33 mm
Det: SE
Date(m/d/y): 11/22/17
200 µm
VEGA\\ TESCAN
Rhodes University SEM

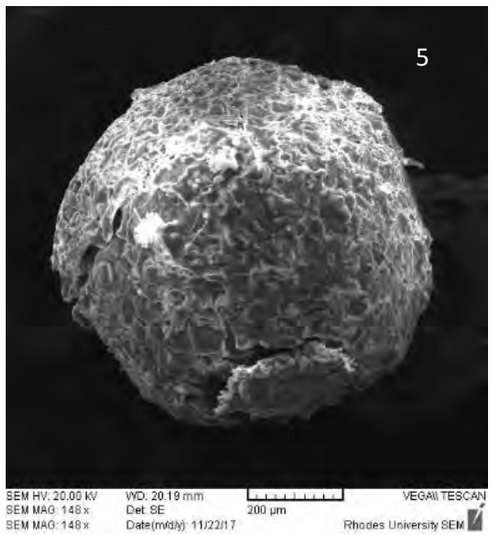
5
SEM HV: 20.00 kV
SEM MAG: 148 x
SEM MAG: 148 x
WD: 20.19 mm
Det: SE
Date(m/d/y): 11/22/17
200 µm
VEGA\\ TESCAN
Rhodes University SEM

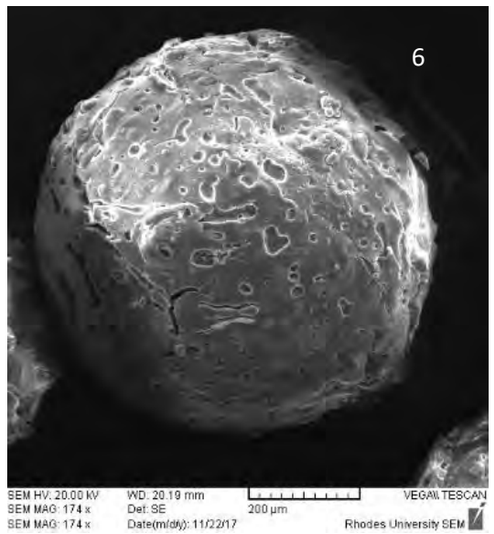
6
SEM HV: 20.00 kV
SEM MAG: 174 x
SEM MAG: 174 x
WD: 20.19 mm
Det: SE
Date(m/d/y): 11/22/17
200 µm
VEGA\\ TESCAN
Rhodes University SEM

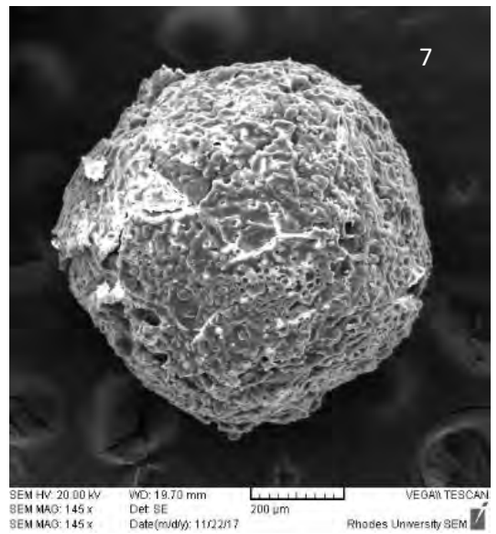
7
SEM HV: 20.00 kV
SEM MAG: 145 x
SEM MAG: 145 x
WD: 19.70 mm
Det: SE
Date(m/d/y): 11/22/17
200 µm
VEGA\\ TESCAN
Rhodes University SEM

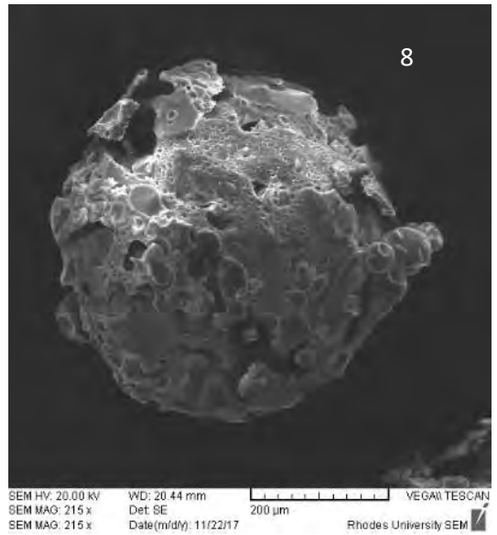
8
SEM HV: 20.00 kV
SEM MAG: 215 x
SEM MAG: 215 x
WD: 20.44 mm
Det: SE
Date(m/d/y): 11/22/17
200 µm
VEGA\\ TESCAN
Rhodes University SEM

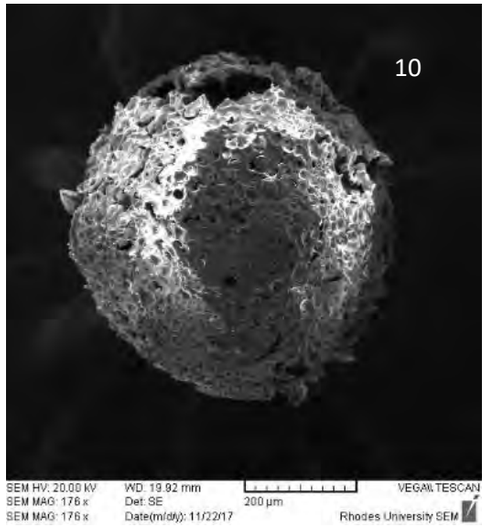
10
SEM HV: 20.00 kV
SEM MAG: 176 x
SEM MAG: 176 x
WD: 19.92 mm
Det: SE
Date(m/d/y): 11/22/17
200 µm
VEGA\\ TESCAN
Rhodes University SEM

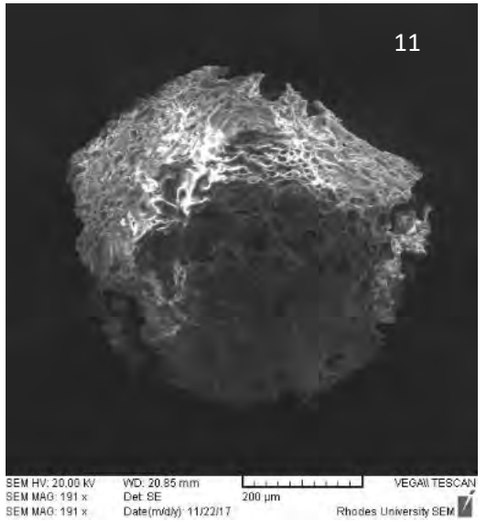
11
SEM HV: 20.00 kV
SEM MAG: 191 x
SEM MAG: 191 x
WD: 20.85 mm
Det: SE
Date(m/d/y): 11/22/17
200 µm
VEGA\\ TESCAN
Rhodes University SEM

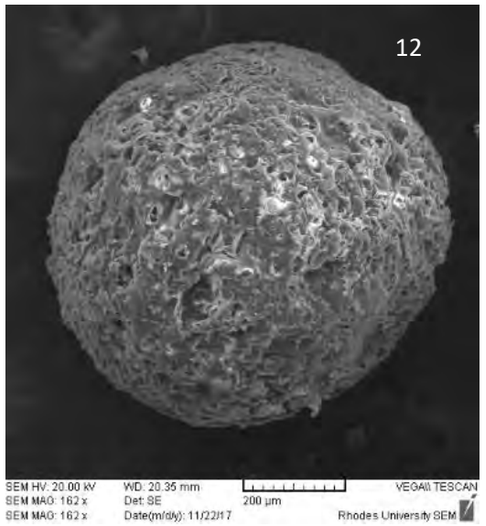
12
SEM HV: 20.00 kV
SEM MAG: 162 x
SEM MAG: 162 x
WD: 20.35 mm
Det: SE
Date(m/d/y): 11/22/17
200 µm
VEGA\\ TESCAN
Rhodes University SEM

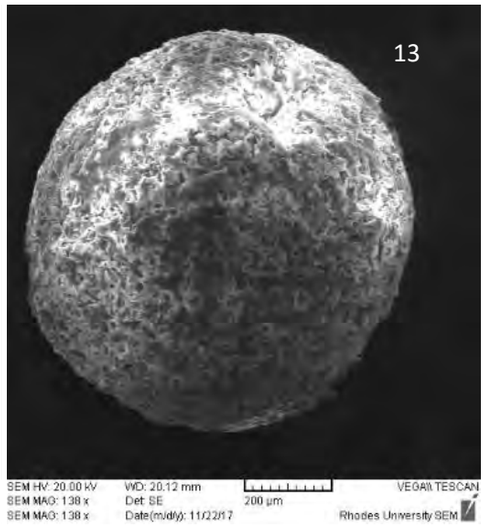
13
SEM HV: 20.00 kV
SEM MAG: 138 x
SEM MAG: 138 x
WD: 20.12 mm
Det: SE
Date(m/d/y): 11/22/17
200 µm
VEGA\\ TESCAN
Rhodes University SEM

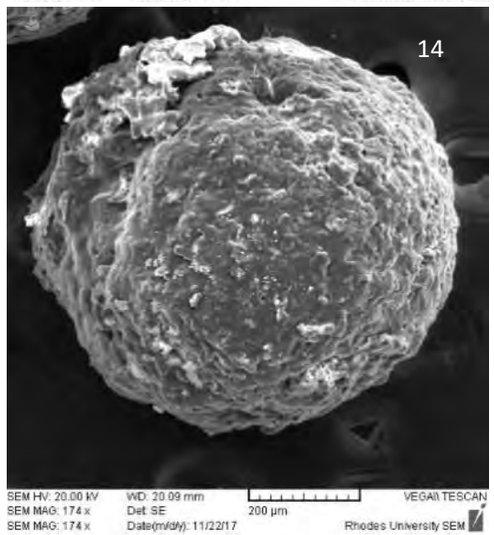
14
SEM HV: 20.00 kV
SEM MAG: 174 x
SEM MAG: 174 x
WD: 20.09 mm
Det: SE
Date(m/d/y): 11/22/17
200 µm
VEGA\\ TESCAN
Rhodes University SEM

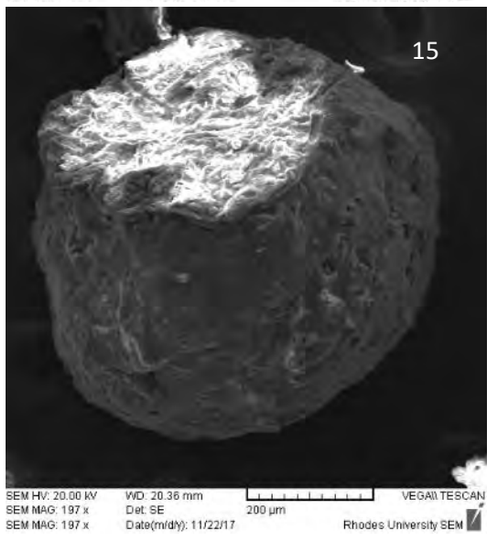
15
SEM HV: 20.00 kV
SEM MAG: 197 x
SEM MAG: 197 x
WD: 20.36 mm
Det: SE
Date(m/d/y): 11/22/17
200 µm
VEGA\\ TESCAN
Rhodes University SEM

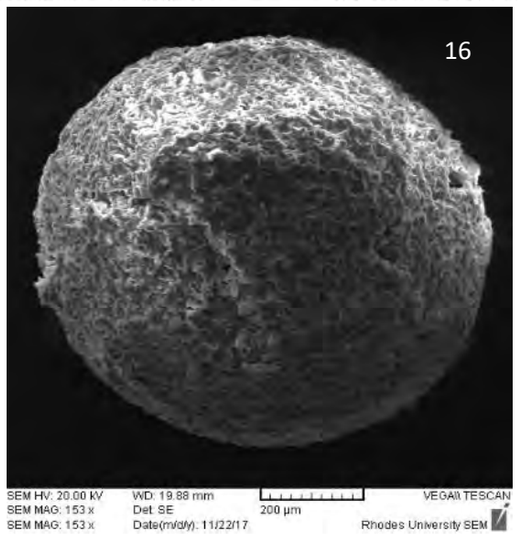
16
SEM HV: 20.00 kV
SEM MAG: 153 x
SEM MAG: 153 x
WD: 19.88 mm
Det: SE
Date(m/d/y): 11/22/17
200 µm
VEGA\\ TESCAN
Rhodes University SEM

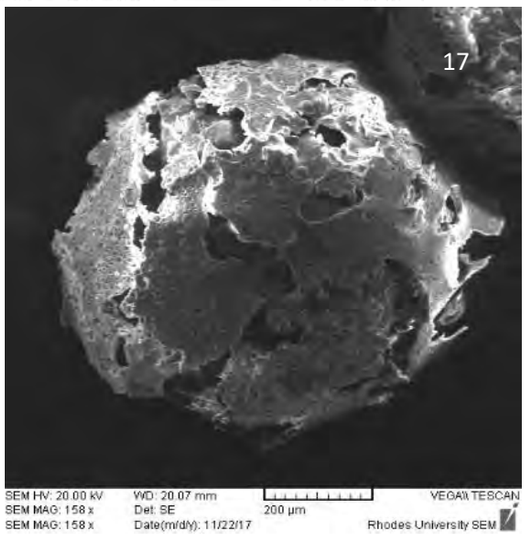
17
SEM HV: 20.00 kV
SEM MAG: 158 x
SEM MAG: 158 x
WD: 20.07 mm
Det: SE
Date(m/d/y): 11/22/17
200 µm
VEGA\\ TESCAN
Rhodes University SEM

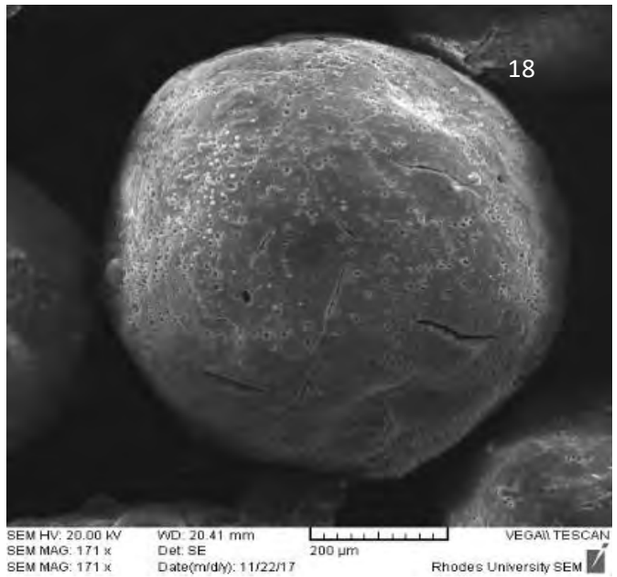

Figure 5. 43 SEM images of microspheres of batches RIF001-RIF017 and the optimised batch RIF018 after exposure to dissolution fluid for 4 h.

It was also observed that increasing the amount of d-glucose used when maintaining a constant ratio of EC and Eudragit® RLPO resulted in an increase in the number of pores formed resulting in increased erosion of microspheres as observed in SEM images of microspheres of batches RIF014 and RIF015 (Figure 5.44) after dissolution testing for 12 h. It was anticipated that the formation of pores would result in an increase in the percent RIF released and was confirmed as d-glucose was found to have had a significant impact on the extent of RIF release from the microspheres.

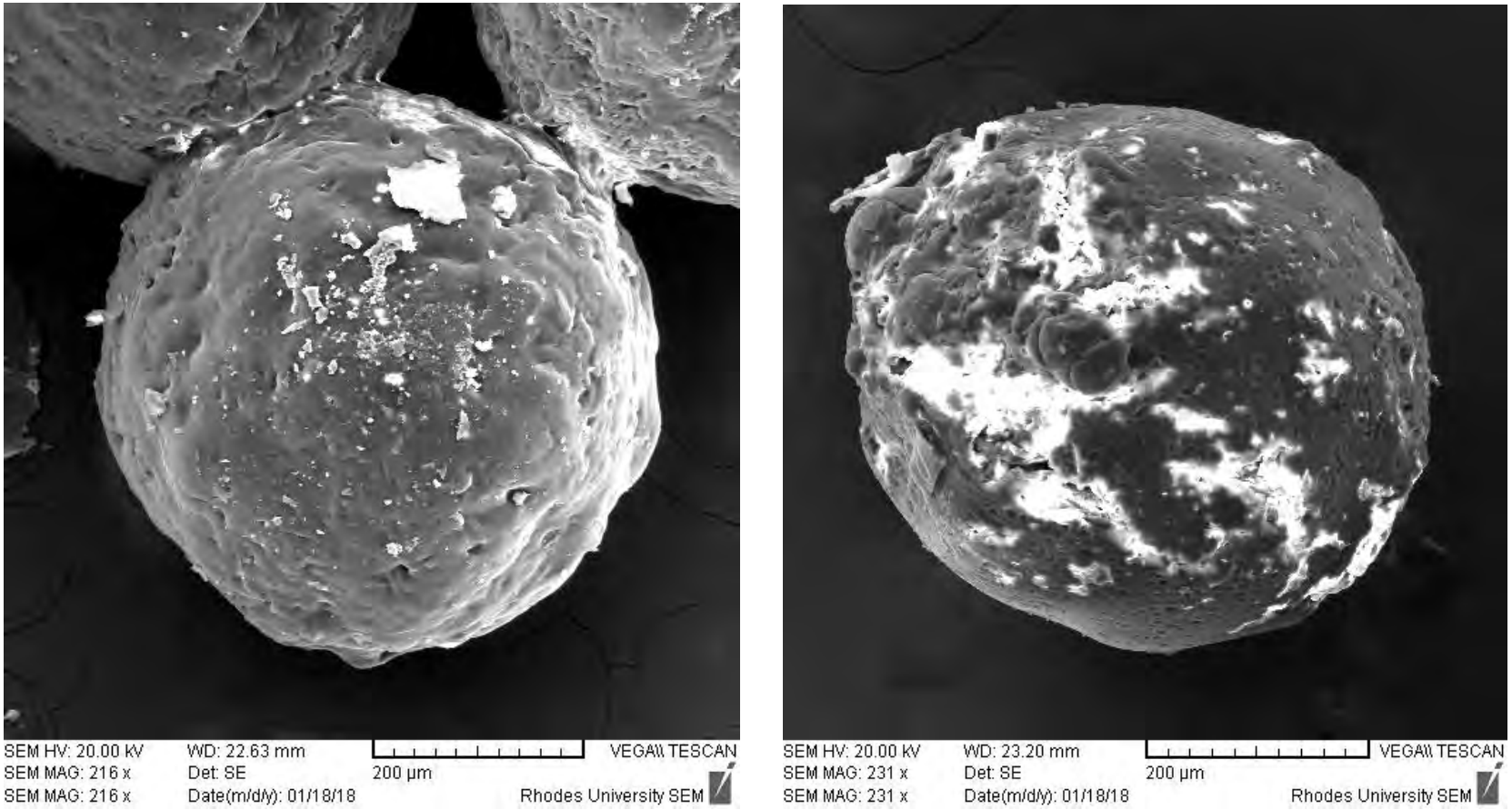

(A) (B)

Figure 5. 44 SEM images of microspheres from batches (A) RIF014 containing 2 g Eudragit RLPO, 1 g EC and 0.25 g d-glucose, and (B) RIF015 containing 2 g Eudragit® RLPO, 1 g EC and 0.75 g d-glucose following dissolution in pH 1.2 0.1 M HCl for 12 h.

5.6.8 Stability of Rifampicin in Dissolution Medium

The decrease in peak area of RIF with time when exposed to pH 1.2 0.1 M HCl is shown in Table 5.17. The extent of RIF degradation when exposed to pH 1.2 0.1M HCl at 37 °C for 24 h was 11.14 ± 0.16 % and was similar to previously reported data [64, 70, 117]. The degradation of RIF in the dissolution medium was considered in all *in vitro* release studies and the results revealed that complete release of RIF was observed for all batches of microspheres produced suggesting no or minimal degradation of RIF occurred.

Table 5. 17 Stability of RIF in pH 1.2 0.1M HCl

Time h	Peak Area µV/sec	% Decrease in peak area	% RSD
0	20126313	0.0	0.825
0.5	19582903	2.70	1.044
2	19403778	3.59	1.422
4	18856343	6.310	0.757
6	18562700	7.769	0.556
8	18376733	8.936	0.434
12	18181563	9.663	1.021
24	17883987	11.141	0.162

5.6.9 RIF Release Kinetics

A summary of results generated following fitting of dissolution data for RIF to different mathematical models is listed in Table 5.18. The results indicate that RIF release from microspheres was best fitted by the Hopfenberg and Weibull models, except for release from batches RIF016 and RIF018 in which RIF release was best fitted to the Korsemeyer and Higuchi models. RIF release from microspheres for which the Hopfenberg and Weibull models were best, was influenced by erosion and diffusion through the spherical matrices [270, 271, 295], whilst RIF release from batches RIF016 and RIF018 was controlled predominantly by diffusion [264-266] through the matrices and in fluid filled channels. Inspection of the data reveal that the R^2 values for first order, Higuchi, Korsmeyer-Peppas and Hixson-Crowell models were > 0.9, an indication that RIF release was influenced by a number of factors including RIF content in the microspheres, erosion and diffusion [263-267]. The value n ranged between 0.553-0.827 for all batches indicating that RIF release

occurred via an anomalous transport mechanism, implying RIF release occurred as a result of Fickian diffusion and polymer relaxation and these results were as expected based on previously reported data [295-298]. RIF release from microspheres for the modified batch RIF023 was best fitted to the Korsmeyer-Peppas model with an R^2 value of 0.9784 and the exponent value of 0.213, indicating anomalous transport through a spherical particle suggesting Fickian diffusion and polymer relaxation which could have resulted in eventual matrix erosion were key to RIF release from the microspheres [295]. The high R^2 values for the Hopfenberg (0.8835), Hixson-Crowell (0.7609) and Higuchi (0.7533) models also supported the conclusion that RIF release followed a number of different mechanisms and was controlled by a number of factors.

Table 5. 18 Summary of mathematical modelling of RIF dissolution data for batches RIF001 – RIF018

MODEL	FORMULATION																	
	RIF 001	**RIF 002**	**RIF 003**	**RIF 004**	**RIF 005**	**RIF 006**	**RIF 007**	**RIF 008**	**RIF 009**	**RIF 010**	**RIF 011**	**RIF 012**	**RIF 013**	**RIF 014**	**RIF 015**	**RIF 016**	**RIF 017**	**RIF 018**
Zero-Order																		
R^2	0.9209	0.8848	0.8593	0.9436	0.8624	0.9238	0.8533	0.9609	0.8576	0.9366	0.8555	0.8137	0.8771	0.8910	0.8773	0.8204	0.9255	0.8498
K_0	8.760	9.213	9.229	7.811	9.213	7.770	9.226	7.047	9.218	7.467	9.210	9.200	8.532	9.498	9.788	9.988	8.338	9.223
First-Order																		
R^2	0.9663	0.9663	0.9894	0.9645	0.9899	0.9764	0.9890	0.9782	0.9903	0.9538	0.9889	0.9882	0.9665	0.9778	0.9724	0.9757	0.9745	0.9833
K_1	0.164	0.185	0.195	0.131	0.194	0.134	0.195	0.111	0.194	0.122	0.194	0.200	0.162	0.198	0.212	0.233	0.151	0.195
Higuchi																		
R^2	0.9081	0.9361	0.9644	0.8907	0.9638	0.9081	0.9629	0.8962	0.9660	0.8757	0.9651	0.9649	0.9301	0.9633	0.9637	0.9878	0.9278	0.9925
K_H	24.914	26.509	26.785	22.025	26.724	22.084	26.796	19.818	26.765	21.011	26.749	26.883	24.565	27.412	28.309	29.194	23.787	26.870
Korsmeyer-Peppas																		
R^2	0.9575	0.9591	0.9747	0.9615	0.9748	0.9591	0.9724	0.9746	0.9756	0.9510	0.9745	0.9683	0.9525	0.9802	0.9771	0.9890	0.9692	0.9958
K_{KP}	15.313	19.458	22.143	11.803	21.932	13.462	22.350	10.175	22.279	10.895	22.327	24.239	18.135	21.181	22.596	27.421	15.308	24.189
n	0.744	0.656	0.596	0.811	0.600	0.748	0.592	0.832	0.593	0.827	0.591	0.553	0.653	0.630	0.614	0.532	0.721	0.553
Hixson-Crowell																		
R^2	0.9795	0.9774	0.9895	0.9759	0.9902	0.9802	0.9884	0.9855	0.9898	0.9639	0.9881	0.9811	0.9689	0.9889	0.9852	0.9777	0.9819	0.9775
K_{HC}	0.046	0.052	0.054	0.038	0.053	0.038	0.054	0.032	0.054	0.035	0.054	0.055	0.045	0.055	0.058	0.063	0.043	0.053
Hopfenberg																		
R^2	0.9811	0.9780	0.9911	0.9774	0.9917	0.9804	0.9904	0.9860	0.9918	0.9650	0.9902	0.9882	0.9695	0.9898	0.9874	0.9783	0.9819	0.9833
K_{HB}	0.061	0.062	0.031	0.051	0.032	0.033	0.028	0.040	0.029	0.047	0.027	0.002	0.034	0.068	0.090	0.046	0.046	0.003
n	2.124	2.386	5.658	2.091	5.543	3.624	6.313	2.336	6.142	2.127	6.497	119.251	4.230	2.252	1.681	4.413	2.737	62.148
Baker-Lonsdale																		
R^2	0.8623	0.8937	0.9327	0.8480	0.9316	0.8712	0.9324	0.8586	0.9349	0.8356	0.9343	0.9434	0.8959	0.9196	0.9194	0.9566	0.8865	0.9632
K_{BL}	0.015	0.018	0.018	0.011	0.018	0.011	0.019	0.009	0.018	0.010	0.018	0.019	0.015	0.019	0.021	0.024	0.013	0.019
Weibull																		
R^2	0.9934	0.9849	0.9907	0.9929	0.9915	0.9963	0.9902	0.9965	0.9914	0.9769	0.9898	0.9882	0.9708	0.9919	0.9896	0.9805	0.9846	0.9863
α	11.638	21.461	6.083	5.603	6.123	3.821	5.932	6.814	6.062	12.101	5.924	4.963	9.361	21.425	33.745	7.607	11.352	5.198
β	1.406	1.667	1.096	0.993	1.099	0.792	1.086	0.968	1.092	1.256	1.080	0.996	1.214	1.665	1.884	1.254	1.283	0.985

5.7 ASSESSMENT OF STABILITY OF RIFAMPICIN IN THE PRESENCE OF ISONIAZID

In order to assess the stability of RIF in pH 1.2 0.1 M HCl in the presence of INH, *in vitro* drug release studies were conducted using a Vankel Bio-Dis USP Apparatus 3 as described in Subsection 5.5.3.8. Sustained release microporous gastroretentive microspheres containing 150 mg RIF and sustained release gastric-resistant INH microspheres containing 75 mg INH were placed in inner cylinders (n = 6) and a mesh screen size 177 µm placed at the top and 74 µm at the bottom of the cylinder to prevent leakage of the dosage form and/or API powder but permitted drainage of dissolution medium. The percent RIF recovered from RIF microspheres alone, commercially available capsules (Rimactane® 150 mg, Norvatis) and RIF API separately, and in the presence of INH tablets (BE-TABS isoniazid 100, Ranbaxy), INH API and INH microspheres was established using the validated HPLC method reported in Chapter 3 of this thesis. The dissolution testing of commercially available RIF capsules, INH API and RIF API separately and in the presence of commercially available INH tablets and manufactured INH gastric resistant sustained release microspheres was undertaken for 2 h, whilst that of the dosage form comprised of manufactured RIF microporous microspheres and INH gastric resistant microspheres was conducted for 12 h.

The percent degradation of RIF after 2 h dissolution testing in pH 1.2 0.1 M HCl of Rimactane® 150 capsules, Rimactane® 150 capsules in presence BE-TABS isoniazid 100, RIF API, RIF API in presence of INH API, Rimactane® 150 capsules, RIF API in the presence of INH gastric resistant microspheres, and RIF microporous floating sustained release microspheres in the presence of INH gastric resistant microspheres are summarised in Table 5.18.

Table 5. 19 Dissolution of RIF in the presence of INH in pH 1.2 0.1 M HCl.

Product	Theoretical µg/mL	Actual µg/mL	% recovery, ±SD(n=6)	% degradation
Rimactane® 150	461.5	444.5	96.3±0.2	3.70
Rimactane® 150 in presence of BE-TABS Isoniazid 100	461.5	333.6	74.4±0.2	21.9
Rimactane® 150 in presence of INH API	461.5	335.8	72.8±0.2	24.4
RIF API	461.5	444.9	96.4±0.2	3.59
RIF API in presence of INH API	461.5	367.3	79.6±0.1	19.1
Rimactane® 150 in presence INH microspheres	461.5	426.6	92.4±0.3	4.05
RIF API in presence of INH microspheres	461.5	436.7	94.6±0.2	3.86
RIF microspheres in presence of INH microspheres	416.9	398.4	95.6.0±0.1	4.44

The results reveal that RIF in Rimactane® 150 capsules degraded with 24.1 % lost when tested in the presence of BE-TABS isoniazid 100 and in the presence of INH API where 24.4 % degradation was observed. However, the degradation of RIF from Rimactane® 150 and API, was significantly reduced in the presence of INH microspheres with only 4.05 % and 3.86 % degradation for Rimactane® 150 and RIF API, respectively. The degradation of RIF after 12 h dissolution in pH 1.2 0.1 M HCl from the microporous floating microspheres in the presence of INH gastric-resistant sustained release microspheres exhibited degradation of only 4.44 %. These results suggest that the degradation of RIF in the presence of INH in an acidic medium can be overcome by encapsulation of both API in a manner that permits product to release each compound in different segments of the GIT.

5.7 CONCLUSIONS

Microporous floating sustained release microspheres for the delivery of RIF in the stomach have been successfully manufactured using emulsification and a diffusion/evaporation process. A solvent system of acetone and dichloromethane, that has not been reported to date for the manufacture of RIF microspheres, was used and resulted in the formation of a stable emulsion that lead to the manufacture of uniform microspheres. In addition, the manufacturing process was shorter when compared to most other reported methods [259]. A Box-Behnken experimental design was successfully used to identify significant variables that affected the floating properties, % EE and % yield of the microspheres. The manufacturing process resulted in the production of microspheres with a high yield of > 80 % and high % EE. The results also revealed that RIF release from the microspheres from the optimised formulation did not exhibit a burst or dose dumping release characteristics an attribute that is desirable for sustained release dosage forms.

As the optimised formulation did not exhibit adequate buoyancy and short floating lag time, the composition was modified to include sodium bicarbonate and citric acid. The rate of RIF release from the modified formulation was higher than that of the optimised formulation and this was attributed to more rapid entry of the dissolution medium into the microspheres resulting in more rapid dissolution of RIF. The release of RIF from microspheres was influenced significantly by the amount of Eudragit® RLPO, EC and d-glucose used and occurred in a sustained manner with almost 90 % RIF released by 12 h. Buoyancy studies revealed that the microspheres manufactured using the modified composition and process would float in the stomach for 12 h, and since 90 % RIF would be released over that period, RIF would be primarily available for absorption from the stomach. The % RSD for the mean particle size distribution of microspheres ranged between 16.56 – 40.72 % which suggested that the rate of RIF release from different microspheres would be variable and was correlated with the high % RSD values indicated as error bars on dissolution profiles for % RIF released from microspheres (Appendix 2B) which were as high as 15 % in some cases. However, the % RSD for RIF release at different time points for the modified microspheres between 5.52 % - 11.41 % which was within the acceptable range of not > 20 % for early time points and not > 10 % for later time points. The microspheres ranged between 423.19 ± 121.86 µm to 620.07 ± 102.67 µm in diameter.

The microspheres exhibited excellent flow properties with a CI of 1.9981 ± 0.0428% and HR of 1.0204 ± 0.0005 for all formulations, implying suitable flow and packing properties that would permit ease of manufacture of a hard gelatin capsule product on a large scale. The spherical microspheres had smooth surfaces with some cracks and pores evident. The SEM images of microspheres exposed to dissolution fluid revealed additional pores generated following dissolution of d-glucose. In general, the number of pores formed was dependent on the amount of Eudragit® RLPO, EC and d-glucose used. RIF-excipient compatibility studies did not reveal any potential or significant interactions were likely suggesting that the excipients used for the manufacture of the microspheres were compatible, although long term stability studies would be required to ascertain this is indeed the case.

The micro-porous floating sustained release microspheres have the potential to increase the bioavailability of RIF as they can be retained in the stomach, where the solubility of RIF is high and from which absorption of RIF is best achieved. The use of sustained release microporous gastroretentive RIF microspheres in combination with sustained release gastric-resistant microspheres revealed that accelerated degradation of RIF in the presence of INH under acidic conditions can be minimised using this proposed approach. The floating and enteric microspheres containing RIF and INH have the potential to improve the bioavailability of RIF when co-administered as a FDC.

CHAPTER SIX

CONCLUSIONS

Despite the positive strides that have been made in the management and treatment of tuberculosis (TB), an infectious disease caused by *Mycobacterium tuberculosis* [1], it is ranked ninth as a leading cause of death with approximately 1.7 million patients dying in 2016 [2]. Treatment of TB is long-term and the use of a combination of medicines is required to prevent the development of MDR-TB [3, 4]. The WHO recommends that effective TB therapy can be achieved using multi-drug therapy [5], in which the initial intensive phase of treatment is accomplished using rifampicin (RIF), isoniazid (INH), pyrazinamide (PZA) and ethambutol (ETB) administered daily for two (2) months followed by a continuation phase in which treatment continues with RIF and INH for a further 4 months. The use of a multi-drug regimen suggests that there is a likelihood of a patient experiencing side effects and patient adherence would be compromised with slow clinical improvement of patients likely [17]. In order to overcome the pill burden, the API are formulated as fixed dose combination (FDC) products. RIF is one of the most effective anti-TB agents available and is bactericidal to intra and extra-cellular bacteria [25, 72]. However the greatest concern regarding the use of FDC when treating TB is the issue of low bioavailability of RIF that has been reported for a number of FDC anti-TB products [26, 110].

In acidic solution, RIF undergoes hydrolysis to form 3-formyl-rifamycin (3-FRSV) and 1-amino 4-methylpiperazine. The decomposition of RIF in acidic environments such as gastric fluid has been estimated to vary between 8.5 and 50 % over the period corresponding to the gastric residence time of most dosage units, in humans, of between 15 and 105 ± 45 minutes [70, 111]. In these studies, RIF degraded by 11.14 ± 0.16% when exposed to pH 1.2 0.1M HCl maintained at 37°C for 24 h and this was similar to the results reported by other authors [347-349]. The hydrolysis of RIF under acidic conditions is catalysed by the presence of INH [55, 64, 65]. It was reported that whereas the decomposition of RIF in acidic media in the absence of INH ceases at the formation of 3-formylrifamycin, the reaction in the presence of INH proceeds to form a hydrazone between 3-formylrifamycin and INH [55]. It has been postulated that once 3-formylrifamycin is formed interaction with INH occurs to form the hydrazone, through a reversible reaction mechanism, involving a fast second-order forward and a slower first-order backward reaction. In this complex reaction process, RIF degradation proceeds whereas INH is regenerated [55]. It was suggested that the direct interaction can be

best explained through transhydrazone formation, via nucleophilic attack at the imine functional group of RIF, by the amino functional group of INH following a tetrahedral mechanism [66]. It has also been postulated that this reaction is catalysed by PZA and ETB, involving intra-molecular proton transfer during the reaction between RIF and INH. The production of 3-FRSV, a poorly soluble degradation product of RIF that exhibits antimicrobial activity *in vitro* but is inactive *in vivo*, on hydrolysis of RIF in acidic media is one of the factors contributing to the poor bioavailability of the compound [41, 69]. The accelerated degradation of RIF to form 3-formylrifamycin via reversible binding to the isonicotinyl hydrazone functionality of 3-FRSV with INH in the presence of INH under acidic conditions has been postulated to further contribute to the poor bioavailability of RIF from FDC products [63, 65, 70, 71]. Furthermore, RIF may undergo decomposition more readily in the acidic conditions of the stomach in the presence of INH in a FDC, than RIF administered alone [70]. In these studies, the degradation of RIF in pH 1.2 0.1 M HCl in the presence of INH raw material was 19.1 ± 0.07 % and 43.02 ± 2.11 %, after 2 h and 24 h, respectively.

A potential solution to prevent the in situ loss and eventual low bioavailability of RIF from FDC products lies in redesigning current FDC technologies in such a way that RIF and INH are released in different segments of the GIT by enteric coating one compound for release in the intestinal lumen and retaining the other for a prolonged period of time in the stomach [131]. As INH (pKa = 2) exists in the protonated form at acidic pH, it is unable to permeate through the stomach mucosae and is therefore primarily absorbed from the small intestine [131]. Therefore, INH should be formulated for site-specific release in the intestine and as RIF is mainly absorbed from the stomach and duodenum and due to its high solubility in acidic solution [131] it should be formulated for site-specific release in the stomach. Therefore, the main objective of these studies was to design, formulate, manufacture and assess a novel delivery system for the gastroretentive delivery of RIF and enteric delivery of INH in order to minimise the instability of RIF in acidic media in the presence of INH.

Several strategies have been used to minimise the interaction between RIF and INH in order to improve the stability of RIF under acidic conditions and potentially enhance its bioavailability [118-130]. In these studies, a different approach in which INH was formulated into gastric-resistant sustained release microspheres with polymers traditionally used for enteric coating, viz., Eudragit® L100 and hydroxypropyl methylcellulose acetate succinate (HPMC-AS) and RIF was formulated into microporous floating sustained release

microspheres using ethylcellulose and Eudragit® RLPO has been used. A multiple-unit dosage form was considered suitable as these have been shown to exhibit advantages and are more reliable than single unit dosage forms that generally exhibit „all or none" delivery characteristics [305]. Furthermore there is a possibility of tailoring doses for patients through use of multi-particulate technologies.

A RP-HPLC method for the simultaneous analysis of INH, PZA and INH was developed and validated. Although reported methods [168-181] for the analysis of these compounds exist it was necessary to develop a method suitable for use in these studies. Most of the published methods involve gradient elution, use of complex mobile phases and exhibit long analysis times. Although PZA was not included in formulation development studies, it was important to include the compound during analytical method development as it could be considered for inclusion in the formulation with INH and RIF in future studies. No methods in which gradient elution and response surface methodology (RSM) was used to optimise the separation between RIF and INH has been reported, to date. A Box Behnken design was successfully used for the optimisation of a rapid, accurate and stability indicating RP-HPLC method for the simultaneous analysis of INH, PZA and RIF. RSM was used to determine the impact of input variables on the outputs or responses monitored. Increasing the buffer pH from 3 to 7 resulted in a significant increase in the retention time of INH. The retention time of INH at pH 3 was short due to the state of ionisation of the compound at this pH and limited interaction with the stationary reversed-phase used for the separation. The retention time was constant between pH 4 and pH 6 where the molecule is neutral and a slight decrease in retention time was observed at pH 7, due to cation exchange. The start methanol (% MeOH) content and duration of the gradient had a significant impact on the retention time of INH. Increasing the amount MeOH at the start of the gradient resulted in a shorter retention time for INH due to a decrease in interactions between INH and the hydrophobic stationary phase. Increasing gradient duration resulted in a shorter retention time for INH due to the use of a high proportion of organic solvent and a reduced conditioning time with buffer. Increasing the pH of the buffer used resulted in an increase in the capacity factor for INH, which was attributed to the increase in retention time associated with an increase in buffer pH. Increasing the start % MeOH resulted in more rapid elution of INH and thus a reduced capacity factor for INH. Increasing the end % MeOH also resulted in a reduced capacity factor as high levels of end % MeOH resulted in shorter retention times for INH due to the high proportion of organic solvent used and the reduced time for conditioning of the

stationary phase with buffer. RSM analysis revealed that the linear interaction of buffer pH and start % MeOH, in addition to the quadratic interaction of buffer pH had a negative impact on the capacity factor of INH, implying that an increase in start % MeOH and buffer pH resulted in a decrease in the capacity factor for INH. The retention time of RIF was significantly affected by buffer pH, end % MeOH and gradient profile. Increasing the pH of the buffer resulted in a longer retention time for RIF, whilst increasing the end % MeOH and changing the gradient profile from a concave to a convex profile resulted in a decrease in the retention time. The retention time of PZA was significantly affected by start % MeOH and gradient duration, with an increase in both factors resulting in a significant reduction in retention time. The retention time of the internal standard, AZT was significantly affected by the end % MeOH and gradient profile, with an increase in MeOH and change of gradient profile from a concave profile to a convex profile resulting in a shorter retention time. The resolution factor for AZT and RIF was significantly affected by buffer pH and end % MeOH, with an increase in buffer pH resulting in an increase in the resolution factor, whilst an increase in end % MeOH had a negative impact on the resolution factor. The tailing factor for INH was significantly affected by buffer pH and start % MeOH. Increasing buffer pH increased the tailing factor of the INH peak whilst increasing the start % MeOH decreased the tailing factor. The tailing factor of PZA was significantly affected by the start % MeOH and the gradient duration, with an increase in these parameters resulting in a decrease in the tailing factor. The tailing factor of RIF was significantly affected by the start % MeOH, end % MeOH and gradient duration, with an increase in all factors resulting in a decrease in tailing factor. The relationships between input variables and outputs were then used to establish the optimum chromatographic conditions to achieve a good separation within the shortest possible time. The method was validated using ICH guidelines and the results revealed that the method was suitable for the analysis of commercially available FDC formulations containing the three API and the analysis time was much shorter than previously reported methods. The method was subsequently used for the analysis of all dosage forms manufactured during development studies.

The API for the manufacture of medicines often exhibit differences in physical and chemical properties such as polymorphism, particle size distribution and crystal habit, amongst others, that is often supplier dependent [132]. These characteristics have the potential to affect the stability and/or availability of solid API and should be monitored and controlled as much as possible during processing [132]. For these reasons the physical characterisation of API is an

extremely important exercise to complete during pharmaceutical development. In these studies, Ultraviolet-Visible Spectroscopy, powder X-Ray Diffraction (PXRD), Fourier-transform Infrared Spectroscopy (FTIR), Raman spectroscopy, Nuclear Magnetic Resonance (NMR), Differential Scanning Calorimetry (DSC) and Scanning Electron Microscopy (SEM) were used to characterise RIF and INH. The API were identified and characterised using the spectroscopic, thermal and microscopic methods listed and revealed that INH is crystalline, showing distinct characteristic sharp peaks in XRD diffractograms and DSC thermogram. The ^{13}C NMR and FTIR results identified RIF samples as RIF polymorph form II, however, there are no significant biopharmaceutic differences between RIF polymorphs and this information was used for identification and as baseline data to monitor changes, if any, that might be observed during formulation development and dosage form manufacture with these two API.

HPMC-AS and Eudragit® L100 were successfully used for the design and manufacture of INH loaded gastric-resistant sustained release microspheres produced using a modified emulsification and solvent evaporation technique [259]. A Hybrid experimental design was used to study the impact of input variables viz., amounts of HPMC-AS and Eudragit® L100 and homogenisation speed on gastric-resistance, INH released and encapsulation efficiency. Gastric-resistance was significantly affected by the Eudragit® L100 content with an increase in polymer content resulting in a reduction in INH released in acidic media. The HPMC-AS content affected gastric-resistance with an increase in polymer content resulting in a reduction in the % INH released in acidic media. The reduction in % INH released was attributed to the low solubility of INH in acids and low flexibility of the polymer, due to the high glass transition temperature of the HPMC-AS polymer in its high unionised state in the acidic medium which decreased INH mobility in the microsphere matrix. INH release from microspheres was significantly affected by HPMC-AS content with increasing polymer content resulting in a decrease in the % INH released. Increasing the Eudragit® L100 content did not result in a reduction in the % INH released, however, the interactive impact HPMC-AS and Eudragit® L100 content, had a significant impact on INH release. Homogenisation speed did not have a significant impact on % INH released although increasing speeds resulted in an increase in the % INH released, that was attributed to the production smaller microspheres with a narrow particle size distribution and hence a large surface area for INH release. A study of the kinetics of INH release revealed that the value of the release exponent, n, following fitting of dissolution data to the Korsmeyer-Peppas model ranged between 0.416

- 1.066 for most batches, indicating that INH release was controlled by multiple mechanisms. The value of n for most batches was $0.43 < n < 0.85$ and was > 1 for batch INH-004 only, indicating that INH release occurred via a combination of diffusion, polymer relaxation and dissolution and/or erosion of microspheres and selection of polymers and other excipients that would promote these phenomena should be investigated.

The Eudragit® L100 content, interactive effects of HMPC-AS and Eudragit® L100 and interactive effects of Eudragit® L100 and homogenisation speed had a significant impact on encapsulation efficiency . Increasing the amount of HPMC-AS and Eudragit® L100 used resulted in an increase in EE and these results are similar to previously reported data [356-359]. However, this observation was only applicable when homogenisation speeds < 2000 rpm were used. Increasing the homogenisation speed to > 2000 rpm resulted in a reduction in EE, regardless of the total polymer content used. The decrease in EE associated with an increase in homogenisation speed was attributed to the possible break up and disruption of small o/o emulsion droplets into smaller drops thus preventing aggregation of small microspheres that may form during the microsphere formation stage of manufacture. The EE increased as the ratio of HPMC-AS to Eudragit® L100 increased, particularly when the total polymer content ranged between 4.0 g and 5.4 g and homogenisation speeds < 2000 rpm were used. The % yield was significantly affected by HPMC-AS and Eudragit® L100 content with an increase in polymer content resulting in an increase in % yield. Although not statistically significant, it was observed that increasing the homogenisation speed to > 2000 rpm resulted in reduction in the % yield, a fact that was also revealed in Equation 4.5 that describes the relationship between input variables and % yield. An increase in total polymer content resulted in an increase in the % yield with higher yields recorded as the ratio of HMPC-AS to Eudragit® L100 decreased due to formation of microspheres with resilient walls that could not revert to powders during filtration, drying and sieving . The prediction accuracy of the Hybrid design optimisation process determined by calculating residuals, (R) and percentage prediction error (% P.E.) for three formulations that were manufactured using the optimised level was considered acceptable for % yield, % EE and % INH released at 24 h where the % P.E. was < 12 % in all cases. The % P.E. for % INH released at 4 h and at 12 h were high, indicating the models used were poor predictors of these two responses and that the Hybrid experimental design might not be an appropriate experimental approach for defining optimum input variable levels for this response. The mean particle size distribution ranged between 415.76 ± 76.93 µm to 903.35 ± 197.10 µm in diameter. The microspheres

exhibited excellent flow properties due to their sphericity. Carr‟s Index was 4.888 ± 0.5659% and the HR was 1.058 ± 0.012 implying that the microspheres would not pose a challenge during filling into hard gelatin capsules and that dose uniformity would be assured. The microspheres exhibited gastric-resistance with only 0.523 % INH, released from the optimized formulation after 2 h exposure to pH 1.2 0.1 M HCl. The formulation also has the potential to improve the bioavailability of RIF as it prevents INH release and therefore the interaction between INH and RIF in the acidic environment of the stomach would be avoided since little or no INH is released in the initial 2 hours. Furthermore the microspheres exhibited sustained release characteristics with at least 85 % INH released in 24 h. The DSC thermograms of mixtures of INH and the polymers used in addition to the FT Raman spectra for INH powder and microspheres did not reveal any potential or significant INH-excipient incompatibility however, long terms stability studies would be require to establish if this is indeed the case.

Microporous floating sustained release microspheres for the delivery of RIF in the stomach have been successfully manufactured using solvent emulsification and diffusion/evaporation. In this study, an oil/oil emulsion system with a mixed organic solvent system of dichloromethane (DCM) and acetone, which has not as yet been reported, was used as a dispersed phase. The use of a mixture of organic solvents has been reported to improve the formation of stable emulsion droplets and ultimately microspheres with mixtures such as acetonitrile and DCM [341] or acetone and methanol [340]. DCM, a nonpolar solvent that is miscible in oil, was included to decrease the polarity of acetone and produced stable emulsions [335, 336]. The use of DCM alone resulted in the formation of large aggregates which clumped together whereas the use of a mixture of DCM and acetone did not and was selected for this process, as acetone and DCM are miscible [341]. The use of a mixture of DCM and acetone in a 3:2 ratio produced smooth spherical microspheres that did not stick together or to the walls of the beaker, therefore this ratio of solvents was selected for use for the manufacturing process. A Box-Behnken design was successfully used to identify significant factors that affected RIF release, floating properties, % EE and % yield of microspheres. The release of RIF from the microspheres was significantly affected by all input variables and an increase in the amount of Eudragit® RLPO and ethylcellulose (EC) used resulted in a decrease in the % RIF released due to an increase in thickness of the barrier, through which RIF had to diffuse to be released into the dissolution medium. An increase in EC, which is insoluble in aqueous media, content resulted in reduced wetting and

entry of the dissolution fluid into the microspheres and hence reduced RIF dissolution and % released. EC forms microsphere walls of high tensile strength and exhibits low structural damage when exposed to dissolution fluid and therefore the area for diffusion of RIF is reduced [354]. Eudragit® RLPO swells in aqueous fluids that may have contributed to the decrease in % RIF released. Increasing Eudragit® RLPO content whilst maintaining a low EC content was observed to improve RIF release due to the presence of quaternary ammonium ions that attract dissolution fluid and facilitated diffusion of RIF from the matrices. Increasing the amount of d-glucose used resulted in an increase in the amount of RIF released. The dissolution of d-glucose was expected to create pores in the microspheres for easy diffusion of RIF. The release of RIF from microspheres was expected to depend, in part, on the availability of pores in the microspheres in addition to erosion or dissolution of the dosage form.

The amount of Eudragit® RLPO, EC and d-glucose had a significant impact on the EE for RIF and an increase in polymer content resulted in an increase in EE due to an increase in the amount of polymer available to encapsulate RIF. The thickness of the microsphere wall and viscosity of polymeric material around the microspheres retards RIF release into the continuous phase during production of microspheres. Strong films formed by EC may also increase EE. The lowest polymer content resulted in formation of microspheres with weak walls and the poorest EE and an increase in d-glucose content resulted in a reduction in EE, possibly as a result of entrapment of the pore forming agent in the wall(s) of the microspheres, resulting in disruption of wall formation resulting in pores through which diffusion of RIF into the continuous phase during production, can occur.

The amount of Eudragit® RLPO and EC had a significant impact on the floating properties of the microspheres with an increase in the amount of Eudragit® RLPO resulting in a reduction in floating capacity due to the ability of this polymer to adsorb water, thereby increasing the density of the microspheres. Increasing the amount of EC used, resulted in an increase in the *in vitro* buoyancy of the microspheres due to the non-hygroscopic nature of the polymer that prevented adsorption of water and an increase in density of the microspheres. The Eudragit® RLPO, EC and d-glucose content all had a significant impact on floating lag time with increased amounts of Eudragit® RLPO resulting in an increase in floating lag time, due to an increase in the density of microspheres after initial adsorption of the dissolution medium. Increasing the amount of EC used resulted in a decrease in floating lag time, due to limited adsorption of the dissolution medium initially. An increase in the amount of d-glucose used,

resulted in an increase in floating lag time due to the ability of d-glucose to adsorb dissolution fluid, resulting in an increase in the density of the microspheres during the initial stages of testing.

Increasing the Eudragit® RLPO and EC content resulted in an increase in the % yield due to an increase in the total polymer available for microencapsulation and formation of microspheres with strong structural walls that did not rupture during filtration, drying and sieving.

The polynomial equations relating input variables to outputs, in conjunction with observations made during the manufacturing process, were used to predict and optimise formulation and process variables that would ensure the production of an optimized high quality product that exhibited sustained and complete release of RIF, a high EE, good floating characteristics and a high % yield. The parameters identified using Design® Expert software were used to manufacture three batches using the optimised conditions and the prediction accuracy of the process determined. The % P.E. for the three optimised batches were < 10 % and the conditions were therefore considered acceptable for most responses with the highest value of 11.50 % recorded for % buoyancy. The intra-batch mean particle size distribution of microspheres manufactured using the BBD and that of the modified batch ranged between 423.19 ± 121.86 µm to 620.07 ± 102.67 µm. Since particle size influences the rate of RIF release from the microspheres, the data suggest that the rate of RIF release from different microsphere batches would be different which might, in turn, result in variable plasma concentrations when used *in vivo*. This observation was correlated with the high % RSD values indicated as error bars on dissolution profiles for % RIF released from microspheres for the BBD formulations which were as high as 15 %. The % RSD values for RIF release at different time points for the modified microspheres ranged between 5.52 % to 11.41 % which was within the acceptable range of not > 20 % for early time points and not > 10 % at later time points, implying uniform RIF release from these dosage units would be assured. The microspheres exhibited excellent flow properties with the CI of 1.9981 ± 0.0428 % and HR of 1.0204 ± 0.0005 for all formulations, suggesting there would be no issues with filling into hard gelatin capsules and content uniformity within batches would be assured. The microspheres from most batches exhibited smooth surfaces with some cracks and were spherical with some pores evident. The SEM images of microspheres exposed to dissolution fluid revealed that pores were successfully generated in the microspheres following dissolution highlighting the potential of d-glucose, as a pore generating agent. The use of

optimised input variables produced an average % yield of 85.27 ± 3.06 % and exhibited sustained release characteristics with 88.82 ± 2.95 % RIF released after 12 h dissolution testing. The average % EE was 96.99 ± 2.19 %. The buoyancy of the optimised formulation was however low with an associated long floating lag time. In order to improve on the buoyancy and floating lag time sodium bicarbonate (1.0 g) that would react with HCl and generate carbon dioxide (CO_2) and result in improved floating of the microspheres was added to the formulation composition. The addition of $NaHCO_3$ resulted in microspheres that exhibited a % buoyancy of 87.66 ± 1.28% after 12 h and a floating lag time of 15 ± 3.2 seconds. RIF release from the modified microspheres occurred at a faster rate than from the original optimised batches, with 39.71 %, 68.97 %, 83.61 % and 87.10 % as compared to 15.83 %, 38.65 %, 65.67 % and 89.68 % RIF released at 0.5 h, 2 h, 6 h and 12 h respectively. The increase in rate of RIF release was attributed to the creation of pores in the matrix on contact with the dissolution medium which permitted penetration of the dissolution medium into the matrix resulting in rapid dissolution of RIF and subsequent diffusion from the microsphere matrix. The rapid entry of dissolution fluid into the microspheres resulted in dissolution of d-glucose, further increasing the number of channels through which diffusion of RIF could occur in addition to increasing erosion of the matrix. RIF release from microspheres for the modified batch RIF021 was best fitted to the Korsmeyer-Peppas model with a R^2 value of 0.9784 and a value for n of 0.213, indicating anomalous transport from the spherical particle occurred by Fickian diffusion and polymer relaxation which may result in eventual matrix erosion. This is critical for RIF release from microspheres. The DSC thermograms and FTIR spectra of the mixtures of RIF and the excipients used did not reveal any potential for significant RIF-excipient incompatibility. There is however a need to determine the residual content of DCM in each dosage form and should be considered in future product development studies. The microporous floating sustained release microspheres have the potential to increase the bioavailability of RIF as they may be retained in the stomach where RIF solubility is high and from which improved absorption can occur.

The INH loaded gastric-resistant sustained release microspheres and microporous floating sustained release microspheres of RIF were tested in combination using USP Apparatus 3. The degradation of RIF after 12 h dissolution testing in pH 1.2 0.1 M HCl in the presence gastric-resistant sustained release INH microspheres revealed only 4.44% degradation. These results are an improvement on the reported data in which degradation of RIF in the presence of INH was decreased by 11 % [121], 10 % [122], 11.5 % [123] and 12 % [130] when

technologies reported in chapter 1, of this thesis, were used. These results are similar to those reported in which 3.6 – 4.8 % reduction in RIF degradation when in the presence of INH, was observed [118].

The results indicate that the degradation of RIF in the presence of INH in acidic solution can be overcome by microencapsulation of the API in a manner that ensures the release of each API in different segments of the GIT. The drug delivery technology developed and reported in this study has the potential to ensure more RIF is available for absorption from the stomach where its solubility and absorption potential are high, and would thus improve the bioavailability of RIF thereby enhancing the clinical response and reduce the likelihood of resistance to RIF developing. Furthermore this approach permits dose titration based on weight for patients requiring different doses of each compound which also may be of use in reducing the side-effects associated with using existing products.

Future studies will require long term real time and accelerated stability studies, *in vivo* testing and attempts to include PZA into the technology to ensure a FDC that is suitable for use is produced. In the existing form, the approach to using two different microsphere formulations may be an improvement over existing delivery systems.

REFERENCES

[1] C. M. Porth. Alterations in respiratory function: respiratory tract infections, neoplasms, and childhood disorders. In Pathophysiology, Concepts of Altered Health States. Porth C. M and Kunert M. P (Editors). Lippincott Williams and Wilkins, Philadelphia, 2002, 615-619.

[2] World Health Organization. Global Tuberculosis Report 2017, http://www.who.int/tb/publications/global_report/en/. Accessed 11/12/2017.

[3] W. Fox, G. A. Ellard and D. A. Mitchison. Studies on the treatment of tuberculosis undertaken by the British Medical Research Council tuberculosis units, 1946–1986, with relevant subsequent publications. ***International Journal of Tuberculosis and Lung Diseases***, 3(Supplement 2) (1999) S231-S279.

[4] M. D. Iseman. Treatment of multidrug-resistant tuberculosis, ***New England Journal of Medicine***, 329(11) (1993) 784-791.

[5] World Health Organization. Fixed dose combination tablets for the treatment of tuberculosis, Geneva, 1999, http://www.who.int/tb/publications/fixed-dosecombination-report/en/ . Accessed 18/12/2017.

[6] MedicalAssociation of South Africa in co-operation with the PharmaceuticalSociety of South Africa. ***South African Medicines Formulary***, 11th Edition, (2014) 320-331.

[7] R. K. Garg. Classic diseases revisited, tuberculosis of the central nervous system (Review), ***Postgraduate Medical Journal*** 75(881) (1999) 133-140.

[8] L. B. Heifets and P. Lindholm-Levy. Comparison of bactericidal activities of streptomycin, amikacin, kanamycin, and capreomycin against Mycobacterium avium and Mycobacterium tuberculosis, ***Antimicrobial Agents and Chemotherapy***, 33(8) (1989) 1298-1301.

[9] M. D. Iseman and L. A. Madsen. Drug-resistant tuberculosis**,** ***Clinics in Chest Medicine***, 10(3) (1989) 341-353.

[10] D. A Mitchison. Mechanism of drug action in short-course chemotherapy. ***Bulletin International Union Against Tuberculosis***, 66(3) (1985) 219-225.

[11] J. A. Caminero. Treatment of multidrug-resistant tuberculosis: evidence and controversies [Review Article], ***The International Journal of Tuberculosis and Lung Disease***, 10(8) (2006) 829-837.

[12] E. D. Chan, V. Laurel, M. J. Strand, J. F. Chan, M. L. Huynh, M. Goble and M. D. Iseman. Treatment and outcome analysis of 205 patients with multidrug-resistant tuberculosis, ***American Journal of Respiratory and Critical Care Medicine***, 169(10) (2004) 1103-1109.

[13] C. D. Mitnick, S. S. Shin, K. J. Seung, M. L. Rich, S. S. Atwood, J. J. Furin, G. M. Fitzmaurice, V. F. A. Alcantara, S. C. Appleton, J. N. Bayona, C. A. Bonilla, K. Chalco, S. Choi, M. F. Franke, H. S. F. Fraser, D. Guerra, R. M. Hurtado, D. Jazayeri, K. Joseph, K. Llaro, L. Mestanza, J. S. Mukherjee, M. R. N. Munoz, E. Palacios, E. Sanchez, A. Sloutsky and M. C. Becerra. Comprehensive treatment of extensively drug-resistant tuberculosis, ***New England Journal of Medicine***, 359(6) (2008) 563-574.

[14] E. Barbara, O. Johannes, B. M. Giovanni, S. Giovanni, M. Ralf, C. Rosella, H. Harald, K. Detlef, S. Tom, R. Sabine and L. Christoph. Multidrug- and extensively drug-resistant tuberculosis, Germany, ***Emerging Infectious Diseases***,14(11) (2008) 1700-1706.

[15] J. A. Caminero, S. Giovanni, A. Zumla and G. B. Migliori. Best drug treatment for multidrug-resistant and extensively drug-resistant tuberculosis, ***The Lancet Infectious Diseases***, 10(9) (2010) 621-629.

[16] World Health Organization. Guidelines for the programmatic management of drug-resistant tuberculosis, 2011, http://apps.who.int/iris/bitstream/10665/44597/1/9789241501583_eng.pdf. Accessed 1/4/2017.

[17] D. Prabakaran, P. Singh, K. S. Jaganathan and S. P. Vyas. Osmotically regulated asymmetric capsular systems for simultaneous sustained delivery of anti-tubercular drugs, ***Journal of Controlled Release***, 95(2) (2004) 239-248.

[18] S. Murray. Challenges of tuberculosis control, ***Canadian Medical Association Journal***, 174(1) (2006) 33-34.

[19] World Health Organization.. Treatment of TB, guidelines for national programmes, Geneva, 2003, http://www.who.int/tb/publications/cds_tb_2003_313/en/. Accessed 18/12/2017.

[20] S. Agrawal, K. J. Kaur, I. Singh, S. R. Bhade, C. L. Kaul and R. Panchagnula. Assessment of bioequivalence of rifampicin, isoniazid and pyrazinamide in a four drug fixed dose combination with separate formulations at the same dose level, ***International Journal of Pharmaceutics***, 233(1-2) (2002) 169-177.

[21] A. Kochi, B. Vareldzis and K. Styblo. Multidrug-resistant tuberculosis and its control, ***Research in Microbiology***, 144(2) (1993) 104-110.

[22] B. R. Edlin , J. I. Tokars, M. H. Grico, J. T. Crawford, J. Williams, E. M. Sordillo, K. R. Ong, J. O. Kilburn, S. W. Dooley and K. G. Castro. An outbreak of MDR TB among hospitalized patients with the acquired immunodeficiency syndrome, ***New England Journal of Medicine***, 326(23) (1992) 1514-1521.

[23] M. A. Fischl, R. B. Uttamchandani, G. L. Daikos, R. B. Poblete, J. N. Moreno, R. R. Reyes, A. M. Boota, L. M. Thompson, T. J. Cleary and S. Lai. An outbreak of TB caused by multiple-drug-resistant tubercle bacilli among patients with HIV infection**,** ***Annals of Internal Medicine***, 117(3) (1992) 177-183.

[24] British Pharmacopoeial Commission. *British Pharmacopoeia,* Vol I&II, Pharmacopoeia Commission Office, London , 2009, 3259-3261.

[25] W. Lund. *The Pharmaceutical Codex*, Isoniazid, Rifapicin, 12th edition, The Pharmaceutical Press, London, 1994, 863-870.

[26] R. Panchagnula and S. Agrawal. Biopharmaceutic and pharmacokinetic aspects of variable bioavailability of rifampicin, ***International Journal of Pharmaceutics,*** 271(1-2) (2004) 1-4.

[27] J. K. Seydel. Physico-Chemical Studies on Rifampicin, ***Antibiotica Chemotherapia,*** 16 (1970) 380-391.

[28] M. T. Kenny and B. Strates. Metabolism and pharmacokinetics of the antibiotic rifampin, ***Drug Metabolism Reviews,*** 12(1) (1981) 159-218.

[29] N. A. Kasim, M. Whitehouse, C. Ramachandran and M. Bermejo. Molecular properties of WHO and provisional biopharmaceutical classification. ***Molecular Pharmaceutics,*** 1(1) (2004) 85-96.

[30] P. Grobelny, A. Mukherjee and G. R. Desiraju. Drug-drug co-crystals, temperature-dependent proton mobility in the molecular complex of isoniazid with 4-aminosalicylic acid, ***CrystEngComm,*** 13(13) (2011) 4358-4364.

[31] C. Becker, J. B. Dressman, G. L. Amidon, H. E. Junginger, S. Kopp, K. K. Midha, V. P. Shah, S. Stavchansky and D. M. Barends. Biowaiver monographs for immediate release solid oral dosage forms, isoniazid, ***Journal of Pharmaceutical Sciences,*** 96(3) (2008) 522-531.

[32] G. Pelliza, M. Nebuloni, P. Ferrari and G. G. Gallo. Polymorphism of rifampicin, ***Farmaco Science,*** 32(7) (1977) 471-481.

[33] Q. Stanley, W. Liebenberg, L. R. Tiedt, A. P. Lotter and M. M. de Villiers. Characterization of the solubility and dissolution properties of several new rifampicin polymorphs, solvates, and hydrates, ***Drug Development and Industrial Pharmacy,*** 27(10) (2001) 1017-1030.

[34] S. Agrawal, Y. Ashokraj, P. V. Bharatam, O. Pillai and R. Panchagnula. Solid-state characterization of rifampicin samples and its biopharmaceutic relevance, ***European Journal of Pharmaceutical Sciences,*** 22(2-3) (2004) 127-144.

[35] S. V. Stelluta and M. Dorina. Main Methods of Synthesizing isoniazid in the laboratory, ***Series of Chemistry,*** 22(2) (2013) 77-84.

[36] P. Sensi, A. M. Greco and R. Ballota. Rifomycins, isolation and properties of rifomycin B and rifomycin complex, ***Antibiotics Annual,*** 1959-60 (1960) 262-270.

[37] P. Sensi, G. Maffii and M. T. Timbal. Two new antibiotics of rifomycin family, rifomycin S and rifomycin SV, ***Experentia,*** 16(9) (1960) 412.

[38] P. Sensi. History of the development of rifampin, ***Reviews of Infectious Diseases***, 5(Supplement 3) (1983) S402-S406.

[39] V. Prelog. The Constitution of rifamycins, ***Pure and Applied Chemistry***, 3(2) (1964) 154-155.

[40] H. Bickel, F. Knusel, W. Kump and L. Neipp. New derivatives of rifamycin antibiotics. ***Antimicrobial Agents and Chemotherapy***, 6 (1966) 352-358.

[41] N. Maggi, C. R. Pasqualucci, R. Ballota and P. Sensi P. Rifampicin, a new orally active rifamycin, ***Chemotherapia***, 11(5) (1966) 285-292.

[42] M. Brufani, W. Fedeli, G. Giacomello and A. Vaciago. The X-ray analysis of the structure of rifamycin B, ***Experentia***, 20(6) (1964) 339-342.

[43] G. C. Lancini, J. E. Thiemann, G. Sartori and P. Sensi. Biogenesis of rifamycins. The conversion of rifamycin B into rifamycin Y, ***Experentia***, 23(11) (1967) 899-900.

[44] M. Liersch, J. Auden, J. Gruner and J. Nuesch. Biosynthesis of rifamycin, ***Pathology and Microbiology***, 34(3) (1969) 243.

[45] R. Maccari, R. Ottaná and M. G. Vigorita. *In vitro* advanced antimycobacterial screening of isoniazid-related hydrazones, hydrazides and cyanoboranes, Part 14, ***Bioorganic & Medicinal Chemistry Letters***, 15(10) (2005) 2509-2513.

[46] K. F. M. Pasqualoto, E. I. Ferreira, O. A. Santos-Filho and A. J. Hopfinger. Rational design of new antituberculosis agents, receptor-independent four-dimensional quantitative structure-activity relationship analysis of a aet of isoniazid derivatives, ***Journal of Medicinal Chemistry***, 47(15) (2004) 3755-3764.

[47] W. S. Schwartz. Comparison of ethionamide with isoniazid in original treatment cases of pulmonary tuberculosis, ***American Review of Respiratory Disease***, 93(5) (1966) 685-692.

[48] A. Bacchi, G. Pelizzi, M. Nebuloni and P. Ferrari. Comprehensive study on structure-activity relationships of rifamycins, discussion of molecular and crystal structure and spectroscopic and thermochemical properties of rifamycin O, ***Journal of Medicinal Chemistry***, 41(13) (1998) 2319-2332.

[49] A. F. Michaelis, H. V. Maulding, C. Sayada and C. Zha. Rifamycin derivatives for drug Targeting, [International Patent WO 2003045319], 2003, https://www.google.com/patents/WO2003045319A2?cl=fi. Accessed 19/12/2017.

[50] A. D. Ferguson, J. Kodding, G. Walker, C. Bos, J. W. Coulton, K. Diederichs, V. Braun and W. Welte. Active transport of an antibiotic rifamycin rerivative by the outer-membrane protein FhuA, ***Structure***, 9(8) (2001) 707-716.

[51] H. G. Floss and T. W. Yu. Rifamycin mode of action, resistance, and biosynthesis, ***Chemical Reviews***, 105(2) (2005) 621-632.

[52] D. M. Rothstein, A. D. Hartman, M. H. Cynamon, and B. I. Eisenstein. Development potential of rifalazil, ***Expert Opinion on Investigational Drugs***, 12(2) (2003) 255-271.

[53] E. A. Campbell, N. Korzheva, A. Mustaev, K. Murakami, S. Nair, A. Goldfarb and S. A. Darst. Structural mechanism for rifampicin inhibition of bacterial RNA polymerase, ***Cell***, 104(6) (2001) 901-912.

[54] W. Lund. *The pharmaceutical codex, principles and practice of pharmaceutics*, The Pharmaceutical Press, London, 1994, 1039-1041

[55] S. A. R. A. Singh, T. T. Mariappan, N. I. S. H. Sharda and B. A. L. J. Singh. Degradation of rifampicin, isoniazid and pyrazinamide from prepared mixtures and marketed single and combination products under acid conditions, ***Pharmacy and Pharmacology Communications***, 6(11) (2000) 491-494.

[56] H. I. Seifart, D. P. Parkin and P. R. Donald. Stability of isoniazid, rifampin and pyrazinamide in suspensions used for the treatment of tuberculosis in children, ***Paediatric Infectious Diseases***, 10(11) (1991) 827-831.

[57] B. Shadi, S. B. S. Nahid, N. Rocsanna and K. Farzad. Stability assessment of isoniazid and rifampin liquid dosage forms in a national referral center for tuberculosis, ***International Journal of Pharmaceutical Sciences and Research***, 6(4) (2015) 706-709.

[58] V. D. Gupta and A. Sood. Chemical stability of isoniazid in an oral liquid dosage form, ***International Journal of Pharmaceutical Compounding***, 9(2) (2005) 165-166.

[59] H. Bhutani, S. Singh, S. Vir, K. K. Bhutani, R. Kumar, A. K. Chakraborti and K. C. Jindal. LC and LC-MS study of stress decomposition behaviour of isoniazid and establishment of validated stability-indicating assay method, ***Journal of Pharmaceutical and Biomedical Analysis***, 43(4) (2007) 1213-1220.

[60] A. Carlin, N. Gregory and J. Simmons. Stability of isoniazid in isoniazid syrup, formation of hydrazine, ***Journal of Pharmaceutical and Biomedical Analysis***, 17(4-5) (1998) 885-890.

[61] F. A. Carry and J. Sundberg. Advanced Organic Chemistry, 4th Edition, 2000, , Springer Scince and Business Media Inc, New York, 2000, 727.

[62] G. G. Gallo and P. Radael. Rifampicin, ***Analytical Profiles of Drug Substances***, Florey K (Editor), Academic Press, New York, 1976, 467-575.

[63] S. Singh, T. T. Mariappan,, R. Shankar, N. Sarda and B. Singh. A critical review of the probable reasons for the poor variable bioavailability of rifampicin from anti-tubercular fixed-dose combination (FDC) products, and the likely solutions to the problem, ***International Journal of Pharmaceutics***, 228(1-2) (2001) 5-17.

[64] C. J. Shishoo, S. A. Shah, I. S. Rathod, S. S. Savale, J. S. Kotecha and P. B.. Stability of rifampicin in dissolution medium in presence of isoniazid, ***International Journal of Pharmaceutics***, 190(1) (1999) 109-123.

[65] R. Sankar, N. Sharda and S. Singh. Behavior of decomposition of rifampicin in the presence of isoniazid in the pH range 1-3, ***Drug Development and Industrial Pharmacy***, 29(7) (2003) 733-738.

[66] H. Bhutani, S. Singh, K. C. Jindal and A. K. Chakraborti. Mechanistic explanation to the catalysis by pyrazinamide and ethambutol of reaction between rifampicin and isoniazid in anti-TB FDCs, ***Journal of Pharmaceutical and Biomedical Analysis,*** 39(5) (2005) 892-899.

[67] Y. Chen. The solubility enhancement and the stability assessment of rifampicin, isoniazid and pyrazinamide in aqueous media, *Master of Science Thesis,* Rhodes University, South Africa, 2000, 216-218.

[68] L. C. du Toit, V. Pillay and M. P. Dankwerts. Tuberculosis chemotherapy, current drug delivery approaches, ***Respiratory Research***, 7(1) (2006) 118.

[69] P. Sensi, N. Maggi, S. Furesz and G. Maffi. Chemical modifications and biological properties of rifamycins, ***Antimicrobial Agents and Chemotherapy,*** 6 (1966) 699-714.

[70] C. J. Shishoo, S. A. Shah, I. S. Rathod, S. S. Savale and M. J. Vora. Impaired bioavailability of rifampicin in presence of isoniazid from fixed dose combination (FDC) formulation, ***International Journal of Pharmaceutics,*** 228(1-2) (2001) 53-67.

[71] S. Agrawal, I. Singh, K. J. Kaur, S. R. Bhade, C. L. Kaul and R. Panchagnula. Comparative bioavailability of rifampicin, isoniazid and pyrazinamide from a four drug fixed dose combination with separate formulations at the same dose levels, ***International Journal of Pharmaceutics,*** 276(1-2) (2004) 41-49.

[72] A. Rattan, A. Kalia and N. Ahmad. Multidrug-resistant *mycobacterium tuberculosis*, molecular perspectives, ***Emerging Infectious Diseases,*** 4(2) (1998) 194-205.

[73] L. M. Parsons, M. Salfinger, A. Clobridge, J. Dormandy, L. Mirabello, V. L. Polletta, A. Sanic, O. Sinyavskiy, S. C. Larsen, J. Driscoll, G. Zickas and H. W. Taber. Phenotypic and molecular characterization of mycobacterium tuberculosis isolates resistant to both isoniazid and ethambutol, ***Antimicrobial Agents and Chemotherapy,*** 49(6) (2005) 2218-2225.

[74] G. S. Timmins and V. Deretic. Mechanisms of action of isoniazid, ***Molecular Microbiology***, 62(5) (2006) 1220-1227.

[75] J. G. Douglas and M. J. McLeod. Pharmacokinetic factors in the modern drug treatment of tuberculosis, ***Clinical Pharmacokinetics,*** 37(2) (1999) 127-146.

[76] G. A. Ellard and P. B. Fourie. Rifampicin bioavailability, a review of its pharmacology and the chemotherapeutic necessity for ensuring optimal absorption, ***The international journal of tuberculosis and lung disease,*** 11(supplent 3) (1999) S301-S308.

[77] American Thoracic Society/Centers for Disease Control and Prevention/Infectious Diseases Society of America. Treatment of tuberculosis, ***American Journal of Respiratory and Critical Care Medicine,*** 167(4) (2003) 603-662.

[78] M. J. Mycek, R. A. Harvey, P. C. Chanpe and B. D. Fisher. Tuberculosis, *Lippincott's Illustrated Reviews, Pharmacology,* 2nd Edition, Lippincott-Raven, Washington, 1997, 333-334.

[79] T. H. Self, C. R. Chrisman, A. M. Baciewicz and M. S. Bronze. Isoniazid drug and food interactions, ***American Journal of the Medical Sciences,*** 317(5) (1999) 304-311.

[80] A. A. Marcos, L. V. M. de Castro, H. R. Ribeiro de Siqueira and F. A. F. de Mello. Antituberculosis drugs: drug interactions, adverse effects, and use in special situations, Part 1, first-line drugs, ***Brasileiro de Pneumologia,*** 36(5) (2010) 626-640.

[81] Z. Desta, N. V. Soukhova and D. A. Flockhart. Inhibition of cytochrome P450 (CYP450) isoforms by isoniazid, potent inhibition of CYP2C19 and CYP3A, ***Antimicrobial Agents and Chemotherapy,*** 45(2) (2001) 382-392.

[82] J. Campos-Franco, A. Gonzalez-Quintela and M. R. Alende-Sixto. Isoniazid induced hyperacute failure in a young patient receiving carbamazepine, ***European Journal of Internal Medicine,*** 15(6) (2004) 396-397.

[83] M. P. Pai, K. M. Momary, K. A. Rodvold. Antibiotic drug interactions, ***Medical Clinics of North America***, 90(6) (2006) 1223-1255.

[84] H. F. Chambers. Antimycobacterial Drugs, *Basic & clinical pharmacology,* 8th Edition, McGraw-Hill, San Francisco, 2001, 803-814.

[85] W. W. Yew. Clinically Significant interactions with drugs used in the treatment of tuberculosis, ***Drug Safety,*** 25(2) (2002) 111-133.

[86] D. Engelhard, H. R. Stutman and M. I. Marks. Interaction of ketoconazole with rifampin and isoniazid, ***New England Journal of Medicine,*** 311(26) (1984) 681-683.

[87] Joint Tuberculosis Committee of the British Thoracic Society. Chemotharapy and management of tuberculosis in the United Kingdom, recommendations, ***Thorax,*** 57(7) (1998), 536-548.

[88] A. M. Baciewicz, C. R. Chrisman, C. K. Finch and T. H. Self. Update on rifampin and rifabutin drug interactions, ***American Journal of the Medical Sciences,*** 335(2) (2008) 126-136.

[89] M. Niemi, J. T. Backman, M. F. Fromm, P. J. Neuvonen and K. T. Kivisto. Pharmacokinetic interactions with rifampicin, clinical relevance, ***Clinical Pharmacokinetics,*** 24(9) (2003) 819-850.

[90] K. E. Dooley and R. E. Chaisson. Tuberculosis and diabetes, convergence of two epidemics, ***Lancet Infectious Diseases,*** 9(12) (2009) 737-746.

[91] A. Kwara, G. Ramachandran and S. Swaminathan. Dose adjustment of the non-nucleoside reverse transcriptase inhibitors during concurrent rifampicin-containing

tuberculosis therapy, one size does not fit all, ***Expert Opinion on Drug Metabolism and Toxicology***, 6(1) (2010)55-68.

[92] S. Nardiello, T. Pizzella and R. Ariviello. Risks of antibacterial agents in pregnacy, ***Infez Med***, 10(1) (2002) 8-15.

[93] American Academy of Paediatrics Committee on Drugs. Transfer of drugs and other chemicals into Human Milk, ***Paediatrics***, 108(3) (2001) 776-789.

[94] H. Y. Sun, Y. J. Chen, C. S. Gau, S. C. Chang and K. T. Luh. A prospective study of hepatitis during antituberculous treatment in Taiwanese patients and a review of the literature, ***Journal of the Formasan Medical Association***, 108(2) (2009) 102-111.

[95] S. Vikrant, S. K. Agarwal, S. Gupta, D. Bhowmik, S. C. Tiwari and S. C. Dash. Prospective randomized control trial of isoniazid chemoprophylaxis during renal replacement therapy, ***Transplant Infectious Diseases***, 7(3-4) (2005) 99-108.

[96] World Health Organization. Guidelines for the programmatic management of drug-resistant tuberculosis, Emergence Update, Geneva, World Health Organization, Stop TB Department, 2008, http://www.who.int/tb/challenges/mdr/programmatic_guidelines_for_mdrtb/en/. Accessed 19/12/2017.

[97] J. P. Chouraqui, G. Bessard, M. Favier, L. Kolodie and P. Rambaud. Haemorrhage associated with vitamin K deficiency in pregnant women and newborns, Relationship with rifampicin therapy in two cases ***Therapie***, 37(4) (1982) 447-450.

[98] J. E. F. Reynolds (Editor). Isoniazid, In *Martindale*, Royal Pharmaceutical Society, London, 1996, 241-242.

[99] P. J. Brennan, D. B. Young and B. D. Robertson (Editors). Handbook of tuberculosis agents, ***Tuberculosis***, 88(2) (2008) 112-116.

[100] M. R. Holdiness. Clinical Pharmacokinetics of antituberculosis drugs, ***Clinical Pharmacokinetics***, 9(6) (1984) 511-544.

[101] G. L. Mandell and W. A. Petri. Drugs used in the chemotherapy of tuberculosis, mycobacetrium avium complex disease, and leprosy, *Goodman and Gilman's the pharmacological basis of therapeutics*, J. G. Hardman and L. E. Limbierd (Editors), McGraw-Hill, New York, 1996, 111-113.

[102] C. A. Peloquin. Pharmacology of antimycobacterial drugs, ***Medical Clinics of North America***, 77(6) (1993) 1253-1262.

[103] C. A. Peloquin, G. S. Jaresko and C. L. Yong. Population pharmacokinetic modeling of isoniazid, rifampicin and pyrazinamide, ***Antimicrobial Agents and Chemotherapy***, 41(12) (1997) 2670-2679.

[104] L. W. Riley. Isoniazid Chemistry, metabolism and mechanism of action, *Tuberculosis*, W. N. Rom and S. M. Garay (Editors), Lippincott-Raven, Philadelphia, 1997, 763-771.

[105] A. Srivastava, J. L. Maggs, D. J. Antoine, D. P. Williams, D. A. Smith and B. K. Park. Role of reactive metabolites in drug-induced hepatotoxicity, ***Handbook of Experimental Pharmacology***, 196 (2010) 165-194.

[106] W. W. Weber and D. W. Hein. Clinical pharmacokinetics of isoniazid, ***Clinical Pharmacokinetics***, 4(6) (1979) 401-422.

[107] R. C. Wallace Jr and D. E. Griffith. Antimycobacterial agents, *Mandell, Douglas, and Bennett's principles and practice of infectious diseases*, 7th Edition, G. L. Mandell, G. E. Bennett and R. Dolin (Editors), Churchill Livingstone/Elsevier, Philadelphia, 2009, 403-416

[108] S. A. H. Khalil L. K. El-Khordagui and Z. A. El-Gholmy. Effect of antacids on oral absorption of rifampicin, ***International Journal of Pharmaceutics***, 20(1-2) (1984) 99-106.

[109] R. Panchagnula, S. Rungta, P. Sancheti, S. Agrawal and C. Kaul. *In vitro* evaluation of food effect on the bioavailability of rifampicin from antituberculosis fixed dose combination formulations, ***Farmaco***, 58(11) (2003) 1099.

[110] G. Pillai, P. B. Fourie, N. Padayatchi, P. C. Onyebujoh, H. Mcllleron, P. J. Smith and G. R. Gabriels. Recent bioequivalence studies on fixed dose combination antituberculosis drug formulations available on the global market, ***International Journal of Tuberculosis and Lung Diseases***, 11(supplement 3) (1999) S309-S316.

[111] A. J. Coupe, S. S. Davis and I. R. Wilding. Variation in gastrointestinal transit of pharmaceutical dosage forms in healthy subjects, ***Pharmaceutical Research***, 8(3) (1991) 360-364.

[112] G. G. Digenis. The *in vivo* behavior of multiparticulate versus single unit dosage formulations, *Multiparticulate Oral Drug Delivery*, I. Ghebre-Sellassie (Editor), Marcel Dekker Inc, New York, 1994, 330-351.

[113] R. Laing, B. Fourie, G. Ellard, M. Sesay, S. Spinaci, B. Blomberg and D. Bryant. Fixed-dose combination tablets for the treatment of tuberculosis**,** *Report of an informal meeting held in Geneva Tuesday, 27 April 1999,* Geneva, World Health Organization, WHO/CDS/CPC/TB/99.267, 1999. http://www.who.int/tb/publications/fixed-dosecombination-report/en/. Accessed 19/12/2017.

[114] World Health Organization. Stop TB, Frequently asked questions about the 4-drug fixed-dose combination tablet recommended by the World Health Organization for treating tuberculosis, 2002. http://www.who.int/tb/publications/2002/en/index1.html. Accessed 19/12/2017.

[115] R. Sankar, N. Sharda and S. Singh. Behaviour of decomposition of rifampicin in the presence of isoniazid on the pH range 1-3, ***Drug Development and Industrial Pharmacy***, 29(7) (2003) 733-738.

[116] S. Singh, T. T. Mariappan, N. Sharda and A. K. Chakraborti. The reason for an increase in decomposition of rifampicin in the presence of isoniazid under acid conditions, ***Pharmacy and Pharmacology Communications***, 6(11) (2000) 405-410.

[117] S. Singh, T. T. Mariappan, N. Sharda and B. Singh. Degradation of rifampicin, isoniazid and pyrazinamide from prepared mixtures and marketed single and combination products under acid conditions, ***Pharmacy and Pharmacology Communications,*** 6(11) (2000) 491-494.

[118] C. M. Gohel and G. S. Krishnakant. A novel Solid dosage form of rifampicin and isoniazid with improved functionality, ***AAPS Pharmaceutical Science and Technology,*** 8(3) (2007) E133-E139.

[119] C. M. Gohel, K. G. Sarvaiya and S. A. Nagori. Design and evaluation of novel dosage form of rifampicin and isoniazid with improved functionality, ***Indian Journal of Pharmaceutical Education and Research,*** 44(1) (2010) 22-27.

[120] M. Hadassah, K. C. H. Swarna, D. Prasanthi, K. I. Sai and R. J. Vijaya. Formulation and evaluation of floating bilayered tablets of rifampicin, isoniazid and pyrazinamide, ***International Journal of Pharmacy and Technology,*** 4(4) (2012) 4931-4951.

[121] T. V. Krishna, K. G. Pai, D. Naveen and M. S. Reddy. Formulation and valuation of fixed dose combination product of rifampicin and isoniazid with improved rifampicin stability, ***International Journal of Pharmacy and Pharmaceutical Sciences,*** 5(Supplement 3) (2013) 431-433.

[122] B. Prasanthi, D. Prasanthi, B. Bhavani and J. V. Ratna. A novel drug delivery system designed for modulating the release kinetics of antitubercular drugs, ***International Journal of Pharmacy,*** 4(3) (2014) 189-196.

[123] D. F. Freire, M. B. Camara, M. G. Dantas, C. F. S. Aragao, T. F. A. Moura and F. N. Raffin. Gastric-resistant isoniazid pellets reduced degradation of rifampicin in acidic medium, ***Brazillian Journal of Pharmaceutical Sciences,*** 50(4) (2014) 749-755.

[124] T. V. Krishna and M. S. Reddy. Formulation and evaluation of enteric coated pellets of rifampicin and isoniazid with improved rifampicin stability, ***Asian Journal of Pharmaceutical and Clinical Research,*** 7(supplement 1) (2014) 154-156.

[125] S. B. Bhise, A. B. More and R. Malayandi. Formulation and *in vitro* evaluation of rifampicin loaded porous microspheres, ***Scientia Pharmaceutica,*** 78(2) (2010) 291-302.

[126] S. Pund, A. Joshi, K. Vasu, M. Nivsarkar and C. Shishoo. Multivariate optimization of formulation and process variables influencing physico-mechanical characteristics of site specific release isoniazid pellets, ***International Journal of Pharmaceutics,*** 388(1-2) (2010) 64-72.

[127] S. Pund, A. Joshi, K. Vasu, M. Nivsarkar and C. Shishoo. Gastroretentive delivery of rifampicin, *In vitro* mucoadhesion and *in vivo* gamma scintigraphy, ***International Journal of Pharmaceutics,*** 411(1-2) (2011) 106-112.

[128] T. Udayakumar and M. Vasudevan. Novel sustained selease swellable bioadhesive floating gastroretentive grug gelivery gystem of gilayer gablets containing

rifampicin and isoniazid, ***International Journal of Pharmaceutical Sciences Letters***, 1 (2012) 21-24.

[129] A. G. Sullad, L. S. Manjeshwar and T. M. Aminabhavi. Novel pH-sensitive hydrogels prepared from the blends of (poly(vinyl alcohol) with acrylic Acid-graft-guar gum matrixes for isoniazid delivery, ***Industrial and Engineering Chemistry Research***, 49(16) (2010) 7323-7329.

[130] H. Singh, R. Bhadari and I. P. Kaur. Encapsulation of rifampicin in solid Lipid nanoparticulate system to limit its degradation and interaction with isoniazid at acidic pH, ***International Journal of Pharmaceutics***, 446(1-2) (2013) 106-111.

[131] T. T. Mariappan and S. Singh. Regional gastrointestinal permeability of rifampicin and isoniazid (alone and their combination) in the rat, ***International Journal of Tuberculosis and Lung Diseases***, 7(8) (2003) 797-803.

[132] H. G. Brittain. Structural methods for the characterisation of polymorphs and solvates, ***Journal of Pharmaceutical Sciences***, 86(4) (1997) 405-412.

[133] B. S. Byrn, R. Pfeiffer, M. Garney, C. Hoiberg and G. Poochikian. Pharmaceutical Solids, a strategic approach to regulatory considerations, ***Pharmaceutical Research***, 12(7) (1995) 945-954.

[134] R. Gandhi, O. Pillai, R. Thilagavathi, B. Gopalakrishnan, C. L. Kaul and R. Panchagnula R. Characterisation of Azithromycin hydrates, ***European Journal of Pharmaceutical Sciences***, 16(3) (2002) 175-184.

[135] G. Chawla and A. K. Bansal. Challenges in polymorphism of pharmaceuticals, ***Current Research and Information on Pharmaceutical Sciences***, 5(1) (2004) 12-15.

[136] H. G. Brittain, S. J. Bogdanowich, D. E. Bugay, J. DeVicentis, G. Lewen, A. W. Newman. Physical Characterisation of Pharmaceutical Solids, ***Pharmaceutical Research***, 8(8) (1991) 963-973.

[137] E. Calleri, E. De Lorenzi, S. Furlanetto, G. Massolini and G. Cassialanza. Validation of a RP-LC method for the simultaneous determination of isoniazid, pyrazinamide and rifampicin in a pharmaceutical formulation, ***Journal of Pharmaceutical and Biomedical Analysis***, 29(6) (2002) 1089-1096.

[138] A. L. Allanson, M. M. Cotton, J. N. A. Tettey and A. C. Boyter. Determination of rifampicin in human plasma and blood spots by high performance liquid chromatography with UV detection, A potential method for therapeutic drug monitoring, ***Journal of Pharmaceutical and Biomedical Analysis***, 44(4) (2007) 963-969.

[139] S. Gunasekaran, E. Sailatha, S. Seshadri and S. Kumaresan. FTIR, FT Raman Spectra and molecular structural confirmation of isoniazid, ***Indian Journal of Pure and Applied Physics***, 47(1) (2009) 12-18.

[140] G. G. Gallo and P. Radaelli. Rifampicin: *Analytical Profiles of Drug Substances* Florey K (Editor), Academic Press, New York, 1976, 467-513.

[141] S. Agrawal, Y. Ashokraj, P. V. Bharatam, O. Pillai and R. Panchagnula. Solid-state characterisation of rifampicin samples and its biopharmaceutic relevance, ***European Journal of Pharmaceutical Sciences***, 22(2-3) (2004) 127-144.

[142] E. Akalin and S. Akyuz. Vibrational structure of free and hydrogen bonded complexes of isoniazid, FT-IR, FT-Raman and DFT study, ***Journal of Molecular Structure***, 834-836 (2007) 492-497.

[143] L. Angeloni, M. P. Marzocchi and G. Smulevic. Resonance Raman spectra and excitation profiles of some rifamycins, ***Journal of Raman Spectroscopy***, 15(2) (1984) 90-96.

[144] R. S. Johnson. A Resonance Raman Study on the interaction of rifampicin with Escherichia Coli RNA Polymerase, ***Biochimica et Biophysica Acta***, 839(1) (1985) 16-25.

[145] G. Radha, B. Anbarasan, V. A. Niranjana, N. S. Sriman and S. Ramaprabhu. Relative Study between Isoniazid Loaded Chitosan with the Gold Encapsulated with Isoniazid Loaded Chitosan Nanoparticles**,** ***Indo American Journal of Pharmaceutical Research***, 3(6) (2013) 4597-4604.

[146] British Pharmacopoeia Commission. *British Pharmacopoeia,* Vol. I&II, British Pharmacopoeia Commission Office, London, 2009, 3259-3261.

[147] D. F. Freire and S. C. F. Aragao. Thermal Studies of Isoniazid and Mixtures with Rifampicin, ***Journal of Thermal and Analytical Calorimetry***, 97 (2009) 333-336.

[148] J. V. de Assis, M. G. Teixeira, C. G. P. Soares, J. F. Lopes, G. S. Carvalho, M. C. S. Lourenco, M. V. de Almeida, W. B. de Almeida and S. A. Fernandes. Experimental and theoretical NMR determination of isoniazid and sodium p-sulfonatocalix[n]arenes inclusion complexes, ***European Journal of Pharmaceutical Sciences***, 47(3) (2012) 539-548.

[149] S. I. G. Cardoso, J. V. T. D. Assis, M. V. Almeida, M. C. Lourenco, F. R. C. Vicente and M. V. N. Souza. Synthesis and antitubercular activity of isoniazid condensed with carbohydrate derivatives, ***Quimica Nova***, 32(6) (2009) 1557-1560.

[150] S. Broussy, Y. Coppel, M. Nguyen, J. Bernadou and B. Meunier. ^{1}H and ^{13}C NMR Characterization of Hemiamidal Isoniazid-NAD(H) Adducts as Possible Inhibitors Of InhA Reductase of Mycobacterium tuberculosis, ***Chemistry, A European Journal***, 9(9) (2003) 2034-2038.

[151] A. A. Salem, H. A. Mossa and B. N. Barsoum. Quantitative determinations of levofloxacin and rifampicin in pharmaceutical and urine samples using nuclear magnetic resonance spectroscopy, ***Spectrochimica Acta Part A, Molecular and Biomolecular Spectroscopy***, 62(1-3) (2005) 466-472.

[152] L. Santos, M. A. Medeiros, S. Santos, M. C. Costa, R. Tavares and M. J. M. Curto. NMR studies of some rifamycins, ***Journal of Molecular Structure***, 563-564 (2001) 61-78.

[153] N. Torrealday, L. Gonzalez, R. M. Alonso, R. M. Jiminez and E. O. Lastra. Experimental design approach for the optimisation of a HPLC-fluorimetric method for the quantitation of angiotensin II receptor antagonist telmisartan in urine, ***Journal of Pharmaceutical and Biomedical Analysis***, 32(4-5) (2003) 847-857.

[154] S. M. Khamanga and R. B. Walker. The use of experimental design in the development of an HPLC-ECD method for analysis of captopril, ***Talanta***, 83(3) (2011) 1037-1049.

[155] V. Morris, J. Hughes and P. Marriott. Spherical coordinate representations of solvent composition for liquid chromatography method development using experimental design, ***Journal of Chromatography A***, 1008(1-2) (2003) 43-56.

[156] A. B. Eldin, A. A. Shalaby and M. El-Tohamy. Development and validation of a HPLC method for the determination of montelukast and its degradation products in pharmaceutical formulation using an experimental design, ***Acta Pharmaceutica Sciencia***, 53(53) (2010) 45-56.

[157] E. Cagigal, L. Gonzalez, R. Alonso and R. M. Jiminez. Experimental design methodologies to optimise the spectroflourimetic determination of losartan and valsartan in human urine, ***Talanta***, 54(6) (2001) 1121-1133.

[158] G. Iriarte, N. Ferreiros, I. Ibarrondo, R. M. Alonso, M. I. Maguregi, L. Gonzalez and R. M. Jimenez. Optimisation via experimental design of an SPE-HPLC-UV-flourescence method for the determination of valsartan and its metabolite in human plasma samples, ***Journal of separation science***. 29(15) (2006) 2265-2283.

[159] L. M. Osborne and T. W. Miyakawa. Use of Experimental design in the optimisation of HPLC methodology for the separation of stereoisomers, ***Journal of liquid chromatography and related technologies***, 20(4) (1997) 501-509.

[160] M. Kiendrebeogo, L. Choisnard, C. E. Lamien, A. Meda, D. Wouessidjewe and O. G. Nacoulma. Experimental design optimisation for screening relevant free phenolic acids from various preparations used in Burkina Faso folk medicine, ***The African Journal of Traditional, Complimentary and Alternative Medicine***, 3(1) (2006) 115-128.

[161] P. Barmpalexis, F. I. Kanaze and E. Georgarakis. Developing and optimizing a validated iscocratic reversed-phase high-performance liquid chromatography separation of nimodipine and impurities in tablets using experimental design methodology, ***Journal of Pharmaceutical and Biomedical Analysis***, 49(5) (2009) 1192-1202.

[162] Y. B. Wani and D. D. Patil. An experimental design approach for optimisation of spectrophotometric method for estimation of cefixime trihydrate using ninhydrin as derivatizing reagent in bulk and pharmaceutical formulation, ***Journal of Saudi Chemical Society***, 21(Supplement 1) (2017) S101-S111.

[163] D. B. Hibbert. Experimental design in chromatography, a tutorial review, ***Journal of Chromatography B***, 910(1) (2012) 2-13.

[164] A. I. Khuri and S. Mukhopadhyay. *WIREs Computation Statistics*, 2 edition, John Wiley and Sons, Indianapolis, 2010, 128-149.

[165] G. Iriarte, N. Ferreiros, I. Ibarrondo, R. M. Alonso, M. I. Maguregi, L. Gonzalez and R. M. Jimenez. Optimisation via experimental design of an SPE-HPLC-UV-flourescence method for the determination of valsartan and its metabolite in human plasma samples, ***Journal of separation science,*** 29(15) (2006) 2265-2283.

[166] S. L. C. Ferreira, R. E. Bruns, H. S. Ferreira, G. D. Matos, J. M. David, G. C. Brandao, E. G. P. da Silva, L. A. Portugal, P. S. dos Reis, A. S. Souza and W. N. L. dos Santos W. N. L. Box-Behnken design, An alternative for the optimisation of analytical methods, ***Analytica Chemica Acta,*** 597(2) (2007) 179-186.

[167] B. D. Glass, S. Agatonovic-Kustrin, Y. J. Chen and M. H. Wisch. Optimisation of a stability-indicating HPLC ethod for the simultaneous determination of rifampicin, isoniazid, and pyrazinamide in a fixed-dose combination using artificial neural networks. ***Journal of Chromatographic Science,*** 45(1) (2007) 38-44.

[168] G. C. Prasad, A. S. K. Shetty and J. B. Pai. Development and validation of RP-HPLC method for quantitative estimation of pyrazinamide in bulk and pharmaceutical dosage forms, ***International Journal of PharmTech Research,*** 3(3) (2011) 1275-1280.

[169] T. T. Mariappan, B. A. L. J. Singh and S. A. R. A. Singh. A validated reversed-Phase (C18) HPLC method for simultaneous determination of rifampicin, isoniazid and pyrazinamide in USP dissolution medium and simulated gastric fluid. ***Pharmacy and Pharmacology Communications,*** 6(8) (2000) 345-349.

[170] H. Wang, C. Cai, C. Chu, J. Liu, Y. Kong, M. Zhu and T. Zhang. A simple and rapid HPLC/UV method for simultaneous quantification of four constituents in anti-tuberculosis 4-FDC tablets by pre-column derivatization, *Asian* ***Journal of Pharmaceutical Sciences,*** 7(4) (2012) 303-309.

[171] A. P. Argekar, S. S. Kunjir and K. S. Purandare. Simultaneous determination of rifampicin, isoniazid and pyrazinamid by high performance thin layer chromatography, ***Journal of Pharmaceutical and Biomedical Analysis,*** 14(11) (1996) 1645-1650.

[172] C. D. Gaitonde and P. V. Pathak. Rapid and sensitive estimation of isoniazid, pyrazinamide and rifampicin in combined dosage form by reversed-phase liquid chromatography, ***Drug Development and Industrial Pharmacy,*** 17(9) (1991) 1201-1214.

[173] P. J. Smith, J. Van Dyk and A. Fredericks. Determination of rifampicin, isoniazid and pyrazinamide by high performance liquid chromatography after their simultaneous extraction from plasma, ***International Journal of Tuberculosis and Lung Diseases,*** 3(11 supplement 3) (1994) S325-S328.

[174] K. C. Jindal, R. S. Chaudhary, A. K. Singla, S. S. Gangwal and S. Khanna. Dissolution test method for rifampicin-isoniazid fixed dose formulations, ***Journal of Pharmaceutical and Biomedical Analysis,*** 12(4) (1994) 493-497.

[175] G. Karlaganis, E. Peretti and B. H. Lauterburg. Analysis of isoniazid, acetylhydrazine and [$^{15}N_2$]acetylhydrazine in serum by capillary gas chromatography-ammonia chemical ionisation mass spectrometry, *Journal of Chromatography B,* ***Biomedical Sciences and Applications****,* 420 (1987) 171-177.

[176] A. Srivastava, D. Waterhouse, A. Ardrey and S. A. Ward. Quantification of rifampicin in human plasma and cerebrospinal fluid by a highly sensitive and rapid liquid chromatographic-tandem mass spectrometric method, ***Journal of Pharmaceutical and Biomedical Analysis****,* 70(6) (2012) 523-528.

[177] Y. Shah, S. Khanna, K. C. Jindal and V. S. Dighe. Determination of rifampicin and isoniazid in pharmaceutical formulations by HPLC, *Drug* ***Development and Industrial Pharmacy****,* 18(14) (1992) 1589-1596.

[178] A. Walubo, K. Chan and C. L. Wong. Simultaneous assay for isoniazid and hydrazine metabolite in plasma and cerebrospinal fluid in the rabbit, ***Journal of Chromatography B, Biomedical Sciences and Applications****,* 567(1) (1991) 261-266.

[179] A. Walubo, P. Smith and P. I. Folb. Comprehensive assay for pyrazinamide, rifampicin and isoniazid with its hydrazine metabolites in human plasma by column liquid chromatography, ***Journal of Chromatography B, Biomedical Sciences and Applications****,* 658(2) (1994) 391-396.

[180] J. Woo, C. L. Wong, R. Teoh and K. Chan. Liquid chromatographic assay for the simultaneous determination of pyrazinamide and rifampicin in serum samples from patients with tuberculosis meningitis, ***Journal of Chromatography B, Biomedical Sciences and Applications****,* 420(1) (1987) 73-80.

[181] S. Revankar, N. Desai, A. Vaidya, A. Bhatt and B. Anjaneyulu. Determination of pyrazinamide in human by high performance liquid chromatography, ***Journal of Postgraduate Medicine****,* 40(1) (1994) 7-9.

[182] Waters. Gradient Elution: In Fundamentals of HPLC, Rev. TWLC02-A, 2015, 17.

[183] L. R. Snyder, J. J. Kirkland and J. L. Glajch. *Practical HPLC Method Development*, Second edition, John Wiley and Sons, New York, USA, 1997, 180-225.

[184] M. Ringo and C. Evans. Effect of mobile phase composition on pressure induced shifts in solute retention for LC separations using a- cyclodextrin stationary phase, ***Journal of microcolumn separations****,* 10(8) (1998) 647-652.

[185] International Conference on Harmonisation. ICH Harmonised Tripartite Guidelines, validation of analytical methods, definitions and terminology, ICH Topic Q2A, London, 1995.

[186] A. G. Causey, H. M. Hills and L. J. Phillips. Evaluation of criteria for the acceptance of bioanalytical data, ***Journal of Pharmaceutical and Biomedical Analysis****,* 8 (8-12) (1990) 625-628.

[187] US Department of Health and Human Services, Food and Drug Administration, Center for Drug Evaluation and Research, and Center for Veterinary medicine. Guidance for Industry: Bioanalytical methods validation. Rockville, 2001.

[188] G. A. Shabir. Validation of high performance liquid chromatography methods for pharmaceutical analysis: Understanding the differences and similarities between validation requirements of the US Food and Drug Administration, the US pharmacopoeia and the International Conference on Harmonization, ***Journal of Chromatography A***, 987(1-2) (2003) 57-66.

[189] M. Swartz and I. Krull. *Analytical Method Development and Validation*, Marcel Dekker Inc, USA, 1997, 11-92.

[190] G. C. Hokanson. A life cycle approach to the development of analytical methods during pharmaceutical product development Part I, the initial method validation process, ***Pharmaceutical Technology***, 18(9) (1994) 118-130.

[191] U. Sengul. Comparing determination methods of detection and quantification limits for aflatoxin analysis in hazelnut, ***Journal of Food and Drug Analysis***, 24(1) (2016) 56-62.

[192] European Medicines Agency. International Conference on Harmonisation of Technical Requirements for Registration of Pharmaceuticals for Human Use, Stability Testing of New Drug Substance and Product Q1A R2, London, 2006.

[193] M. Bakshi and S. Singh. Development of validated stability indicating assay methods critical review, ***Journal of Pharmaceutical and Biomedical Analysis***, 28(6) (2002) 1011-1040.

[194] M. Y. Noordin, V. C. Venkatesh, S. Sharif, S. Elting and A. Abdullah. Application of response surface methodology in describing the performance of coated carbide tools when turning AISI 1045 steel, ***Journal of Materials Processing Technology***, 145(1) (2004) 46-58.

[195] W. J. Hill and W. G. Hunter. A Review of response surface methodology, a literature survey, ***Technometrics***, 8(4) (1966) 571-590.

[196] T. B. L. Kirkwood. Geometric means and measures of dispersion, ***Biometrics***, 35 (1979) 908-909.

[197] W. A. Hendricks and K. W. Robey. The Sampling Distribution of the Coefficient of Variation, ***Annals of Mathematical Statistics***, 7(3) (1936) 129-132.

[198] P. Barmpalexis, F. I. Kanaze and E. Georgarakis. Developing and optimising a validated iscocratic reversed-phase high-performance liquid chromatography separation of nimodipine and impurities in tablets using experimental design methodology, ***Journal of Pharmaceutical and Biomedical Analysis***, 49(5) (2009) 1192-1202.

[199] M. Mourabet, A. El Rhilassi, H. El Boujaady, M. Bennani-Ziatni and A. Taitai. Use of response surface methodology for optimizstion of fluoride adsorption in an

aqueous solution by Brushite, ***Arabian Journal of Chemistry***, 10(supplement 2) (2017) S3292-S3302.

[200] G. E. P. Box and K. B. Wilson. On the Experimental Attainment of Optimum Multifactorial Conditions, ***Royal Statistics Society,*** 13 (1951) 1-12.

[201] G. N. Thoithi, I. O. Kibwage, O. King'ondu and J. Hoogmartens. Liquid chromatographic separation of isoniazid, pyrazinamide and rifampicin on a reversed-phase silica column, ***East and Central African Journal of Pharmaceutical Sciences,*** 5(1) (2002) 8-14.

[202] K. K. Unger, *Porous Silica*, First edition, Elsevier, Amsterdam, 1979, 130-138.

[203] J. F. Wheeler, T. L. Beck, S. J. Klatte, L. A. Cole and J. G. Dorsey. Phase transitions of reversed-phase stationary phases, Cause and effects in the mechanism of retention ***Journal of Chromatography A,*** 656(1-2) (1993) 317-333.

[204] M. N. Singh, K. S. Y. Hemant, M. Ram and H. G. Shivakumar. Microencapsulation, a promising technique for controlled drug delivery, ***Research in Pharmaceutical Sciences,*** 5(2) (2010) 65-77.

[205] C. Berkland, M. J. Kipper, B. Narasimhan, K. Kim and D. W. Pack. Microsphere size, precipitation kinetics and drug distribution control drug release from biodegradable polyanhydride microspheres, ***Journal of Controlled Release,*** 94(1) (2004) 129-141.

[206] C. S. Brazel and N. A. Peppas. Modeling of drug release from Swellable polymers, ***European Journal of Pharmaceutics and Biopharmaceutics***, 49(1) (2000) 47-58.

[207] D. T. Birnbaum and L. Brannon-Peppas. Microparticle drug delivery systems, *Drug delivery systems in cancer therapy,* Brown D.M Human (Editors), Press Inc,Totowa, 2003, 117-136.

[208] N. K Sachan, B. Singh and K. R. Rao. Controlled drug delivery through microencapsulation, ***Malaysian Journal of Pharmaceutical Sciences***, 4(1) (2006) 65-81.

[209] R. Arshady. Microspheres and microcapsules, a survey of manufacturing techniques, part III, solvent evaporation, ***Polymer Engineering Science***, 30(15) (1990) 915-924.

[210] F. Jung-Bing, H. Chao, J. Lei and W. Shutao. Nanoporous microspheres, from controllable synthesis to healthcare applications, ***Journal of Material Chemistry B***, 1 (2013) 2222-2235.

[211] X. S. Wu. Preparation, characterization, and drug delivery applications of microspheres based on biodegradable lactic/glycolic acid polymers, *Encyclopedic Handbook of biomaterials and bioengineering*, D. L. Wise, D. J. Trantolo, D. E. Altobeli, M. J. Yaszemski, J. D. Gresser and E. R. Schwartz (Editors), Marcel Dekker, New York, 1151-1200.

[212] R. Arshady. Preparation of biodegradable microspheres and microcapsules, 2, Polylactides and related polyesters, ***Journal of Controlled Release,*** 17(1) (1991) 1-22.

[213] R. Jalil and J. R. Nixon. Biodegradable poly(lactic acid) and poly(lactide-*co*-glycolide) microcapsules, problems associated with preparative techniques and release properties, ***Journal of Microencapsulation,*** 7(3) (1990) 297-325.

[214] R. Wada, S. K. Hyon, O. Ike, S. Watanabe, Y. Shimizu and Y. Ikada. Preparation of lactic acid oligomer microspheres containing anti-cancer drug by o/o type solvent evaporation process, ***Bulletin of the Institute for Chemical Research, ,*** 66(3) (1988) 241-250-806.

[215] M. Cavalier, J. P. Benoit and C. Thies. The formation and characterisation of hydrocortisone-loaded poly(+/-)-lactide) microspheres, ***Journal of Pharmacy and Pharmacology,*** 38(4) (1986) 249-253.

[216] D. C. Tsai, A. A. Howard, T. F. Hogan, C. J. Malanga, S. J. Kandzari and J. K. H. Ma. Preparation and *in vitro* evaluation of polylactic acidmitomycin C microcapsules, ***Journal of Microencapsulation,*** 3(3) (1986) 181-193.

[217] D. H. Lewis. Controlled release of bioactive agents from lactide/glycolide polymers, *Biodegradable polymers as drug delivery systems*, M. Chasin and R. Langer (Editors), Marcel Dekker, New York, 1990, 1-41.

[218] R. Edelman, R. G. Russell, G. Losonsky, B. D. Tall, C. O. Tacket, M. M. Levine and D. H. Lewis. Immunisation of rabbits with enterotoxigenic *E. coli* colonisation factor antigen (CFA/I) encapsulated in biodegradable microspheres of poly(lactide-*co*glycolide), ***Vaccine,*** 11(2) (1993) 155-158.

[219] T. A. Comunian and C. S. Favaro-Trindade. Microencapsulation using biopolymers as an alternative to produce food enhanced with phytosterols and omega-3 fatty acids, a review, ***Food Hydrocolloids,*** 61 (2016) 442-457.

[220] V. J. Csernus, B. E. L. A. Szende and A. V. Schally. Release of peptides from sustained delivery systems (microcapsules and microparticles) *in vivo*, ***International Journal of Peptide and Protein Research,*** 35(6) (1990) 557-565.

[221] N. Nihant, C. Grandfils, R. Jerome and P. Teyssie. Microencapsulation by coacervation of poly(lactide-co-glycolide) IV, Effect of the processing parameters on coacervation and encapsulation, ***Journal of Controlled Release,*** 35(2) (1995)117-125.

[222] A. V. Schally and T. W. Redding. Combination of long-acting microcapsules of the D-tryptophan-6 analog of luteinizing hormone-releasing hormone with chemotherapy, investigation in the rat prostate cancer model, ***Proceedings of the National Academy of Sciences of the United States of America,*** 82(8) (1985) 2498-2502.

[223] L. M. Sanders, J. S. Kent, G. I. McRae, B. H. Vickery, T. R. Tice and D. H. Lewis. Controlled release of a luteinizing hormone-releasing hormone analogue from

poly(d,l-lactide-co-glycolide) microspheres, ***Journal of Pharmaceutical Sciences***, 73(9) (1984) 1294-1297.

[224] N. Leelarasamee, S. A. Howard, C. J. Malanga, L. A. Luzzi, T. F. Hogan, S. J. Kandzari and J. K. H. Ma. Kinetics of drug release from polylactic acid-hydrocortisone microcapsules, ***Journal of Microencapsulation***, 3(3) (1986) 171-179.

[225] C. Thomasin, H. P. Merkle and B. A. Gander. Physico-chemical parameters governing protein microencapsulation into biodegradable polyesters by coacervation, ***International Journal of Pharmaceutics***, 147(2) (1997) 173-186.

[226] C. Thomasin, H. P. Merkle and B. Gander. Drug microencapsulation by PLA/PLGA coacervation in the light of thermodynamics 2, parameters determining microsphere formation. ***Journal of Pharmaceutical Sciences***, 87(3) (1998) 269-275.

[227] M. I Re. Microencapsulation by spray drying, ***Drying Technology***, 16(6) (1998) 1195-1236.

[228] K. C. Judson. Spray drying, retention of volatile compounds revisited, ***Drying Technology***, 13(5-7) (1995) 221-1240.

[229] S. Benita and M. Donbrow. Effect of polyisobutylene on ethylcellulose-walled microcapsules, wall Structure and thickness of salicylamide and theophylline microcapsules, ***Journal of Pharmaceutical Sciences***, 71(2) (1982) 205-210.

[230] O. Felt, P. Buri and R. Gurny. Chitosan, a unique polysaccharide for drug delivery, ***Drug Development and Industrial Pharmacy***, 24(11) (1998) 979-993.

[231] J. C. Chaumeil, C. Chemtob and M. Ndongo. Tablets of metronidazole microcapsules, release characterization, ***International Journal of Pharmaceutical Sciences***, 29 (1986) 83-92.

[232] S. Fukushima, S. Kishimoto, Y. Takeuchi and M. Fukushima. Preparation and evaluation of o/w type emulsions containing antitumor prostaglandin, ***Advanced Drug Delivery Reviews***, 45(1) (2000) 65-75.

[233] P. M. Hombreiro, C. Zinutti, A. Lamprecht, N. Ubrich, A. Astier, M. Hoffman, R. Bodmeier and P. Maincent. The preparation and evaluation of poly(epsilon-caprolactone) microparticles containing both a lipophilic and a hydrophilic drug, ***Journal of Controlled Release***, 65(3) (2000) 429-438.

[234] N. Passerini and D. Q. M Craig. Characterisation of ciclosporin loaded poly (D,L lactide-co-glycolide) microspheres using modulated temperature differential scanning calorimetry, ***Journal of Pharmacy and Pharmacology***, 54(7) (2002) 913-919.

[235] K. G. Carrasquillo, A. M. Stanley, J. C. Aponte-Carro, P. De Jesus, H. R. Costantino, C. J. Bosques and K. Griebenow. Non-aqueous encapsulation of excipient-stabilised spray-freeze dried BSA into poly(lactide-co-glycolide) microspheres results in release of native protein, ***Journal of Controlled Release***, 76(3) (2001) 199-208.

[236] W. Jiang and S. P. Schwendeman. Stabilisation of a model formalinizsd protein antigen encapsulated in poly(lactide-co-glycolide)-based microspheres, ***Journal of Pharmaceutical Sciences,*** 90(10) (2001) 1558-1569.

[237] J. Malakar, T. Das and S. Ghatak. Microencapsulation, an indespensable technology for drug delivery system, ***International Research Journal of Pharmacy,*** 3(4) (2012) 8-13.

[238] S. S. Davis, J. G. Hardy, M. J. Taylor, D. R. Whalley and C. G. Wilson. A comparative study of the gastrointestinal transit of a pallet and tablet formulation, ***International Journal of Pharmaceutics,*** 21 (1984) 167-177.

[239] International Conference on Harmonisation. ICH of technical requirements for registration of pharmaceuticals for human use, ICH harmonised tripartite guideline, pharmaceutical development Q8 (R2), 2009.

[240] U. S. Department of Health and Human Services, Food and Drug Administration, Center for Drug Evaluation and Research (CDER), Center for Biologics Evaluation and Research (CBER), Guidance for industry, nonclinical studies for the safety evaluation of pharmaceutical Excipients, 2005.

[241] A. Katdare and M. Chaubal (Editors). *Excipient Development for Pharmaceutical, Biotechnology and Drug Delivery Systems*, Informa Healthcare, New York, USA, 2006, 1-15.

[242] C. R. Moreton. Functionality and performance of excipients in a quality by-design world, Part VI, excipient composition, ***American Pharmaceutical Review***, 12(7) (2009) 48-51.

[243] G. S. Clarke. The Validation of analytical methods for drug substances and drug products in UK pharmaceutical laboratories, ***Journal of Pharmaceutical and Biomedical Analysis,*** 12(5) (1994) 643-652.

[244] B. J. Lee. Pharmaceutical Preformulation, physicochemical properties of excipients and powders and tablet characterisation in *Pharmaceutical Manufacturing Handbook- Production and Processes,* S. C. Gad (Editor), John Wiley and Sons, Cary, USA, 2008, pp. 881-1087.

[245] D. R. Karsa and R. A. Stephenson (Editors). *Excipients and Delivery Systems for Pharmaceutical Formulations*, The Royal Society of Chemistry, Cambridge, UK, 1995, 1-19.

[246] Rowe R.C, Sheskey P.J, and Owen S.C, *Handbook of pharmaceutical excipients*, 5th ed., Pharmaceutical Press and American Pharmacists Association, London, 2006, 525-533.

[247] M. Saffari, M. Shahbazi and M. S. Ardestani. Formulation and *in vitro* evaluation of Eudragit L100® microspheres of piroxicam, ***Nature Proceedings,*** 1544(1) (2008) 1-5.

[248] M. Cetin, A. Atila and Y. Kadioglu. Formulation and *in vitro* characterisation of Eudragit® - L100 and Eudragit® - L100-PLGA nanoparticles containing diclofenac sodium, ***AAPS PharmSciTech***, 11(3) (2010) 1250-1256.

[249] R. I. Moustafine, E. B. Margulis, L. F. Sibgatullina, V. A. Kemenova and G. V. D. Comparative evaluation of interpolyelectrolyte complexes of chitosan with Eudragit®-L100 and Eudragit® - L100-55 as potential carriers for oral controlled drug delivery, ***European Journal of Pharmaceutics and Biopharmaceutics***, 70(1) (2008) 215-225.

[250] G. P. Andrews, D. S. Jones, O. A. Diak, C. P. McCoy, A. B. Watts and J. W. McGinity. The manufacture and characterisation of hot-melt extruded enteric tablets, ***European Journal of Pharmaceutics and Biopharmaceutics***, 69(1) (2008) 264-273.

[251] L. F. A. Asghar and S. Chandran. Design and evaluation of pH modulated controlled release matrix systems for colon specific delivery of indomethacin, ***Die Pharmazie - An International Journal of Pharmaceutical Sciences***, 63(10) (2008) 736-742.

[252] P. V. Devarajan and G. S. Sonavane. Preparation and *in vitro/in vivo* evaluation of gliclazide loaded Eudragit® nanoparticles as a sustained release carriers, ***Drug Development and Industrial Pharmacy***, 33(2) (2007) 101-111.

[253] R. C. Rowe, P. J. Sheskey and M. E. Quinn (Editors). Hypromellose acetate succinate in the Handbook of Pharmaceutical Excipients, 6th Edition, Pharmaceutical Press, London, 2009, 330-332

[254] Shin-Etsu Chemical Co.Ltd. Hypromellose acetate succinate AQOAT product information brochure, 1992, 1-18.

[255] D. T. Friesen, R. Shanker, M. Crew, D. T. Smithey W. J. Curatolo and J. A. S. Nightingale. Hydroxypropyl methylcellulose acetate succinate-based spray-dried dispersions, an overview, ***Molecular Pharmaceutics***, 5(6) (2008) 1003-1019.

[256] R. C. Rowe, P. J. Sheskey and M. E. Quinn (Editors). *The Handbook of Pharmaceutical Excipients*, 6th Edition, Pharmaceutical Press, London, 2009, 129-133.

[257] Stat-Ease. *Handbook for Experiments*, 8th Edition, Stat-Ease, Inc, Minneapolis, 2005, 1-5.

[258] S. M. Khamanga, N. Parfitt, T. Nyamuhiwa, H. Haidula and R. B. Walker. The evaluation of Eudragit® microcapsules manufactured by solvent evaporation using USP Apparatus 1, ***Dissolution Technologies***, 16(2) (2009) 15-22.

[259] R. L. Carr. Classifying flow properties of solids, ***Chemical Engineering***, 72 (1965) 69-72.

[260] H. H. Hausner. Friction conditions in a mass of metal powders, ***International Journal of Powder Metallurgy***, 3(4) (1967) 7-13.

[261] Z. Zhang and S. Feng. The drug encapsulation efficiency, *in vitro* release, cellular uptake and cytotoxicity of paclitaxel-loaded poly(lactide)-tocopheryl polyethylene glycol succinate nanoparticles, ***Biomaterials,*** 27(21) (2006) 4025-4033.

[262] M. M. A. Abdel-Mottaleb and A. Lamprecht. Standardised *in vitro* drug release test for colloidal drug carriers using modified USP dissolution apparatus I, ***Drug Development and Industrial Pharmacy,*** 37(2) (2011) 178-184.

[263] C. G. Varelas, D. G. Dixon and C. A. Steiner. Zero-Order Release from biphasic polymer hydrogels, ***Journal of Controlled Release,*** 34(3) (1995) 185-192.

[264] A. Sood and R. Panchangnula. Drug Release Evaluation of Diltiazem CR Preparations, ***International Journal of Pharmaceutics,*** 175(1) (1998) 95-107.

[265] M. Gibalde and S. Feldman. Establishment of sink conditions in dissolution rate determinations- theoretical considerations and applications. ***Journal of Pharmaceutical Sciences,*** 56(10) (1967) 1238-1242.

[266] T. Higuchi. Rate of release of medicaments from ointment bases containing drugs in suspensions, ***Journal of Pharmaceutical Sciences,*** 50(874) (1961) 875.

[267] N. A. Peppas. Analysis of fickian and non-fickian drug release from polymers, ***Pharmaceutica Acta Helvetiae,*** 60(4) (1985) 110-111.

[268] N. Peppas and R. Korsmeyer. Dynamically swelling hydrogels in controlled release applications, In *Hydrogels in Medicine and Pharmacy*, N.Peppas (Editor), CRC PRESS, Boca Raton, 1986, 109

[269] P. J. Niebergall, G. Milosovich and J. E. Goyan. Dissolution rate studies, II, dissolution of particles under conditions of rapid agitation. ***Journal of Pharmaceutical Sciences,*** 52(3) (1963) 236-241.

[270] P. Costa and J. M. S. Lobo. Modeling and comparison of dissolution profiles, ***European Journal of Pharmaceutical Sciences,*** 13(2) (2001) 123-133.

[271] H. B. Hopfenberg. Controlled release polymeric formulations, D. R. Paul and F. W. Harris (Editors), ACS Symposium Series, American Chemical Society, Washington DC, 1976, 26-31.

[272] I. Katzhendler, A. Hoffman, A. Goldberger and M. Friedman. Modeling of drug release from erodible tablets, ***Journal of Pharmaceutical Sciences,*** 86(1) (1997) 110-115.

[273] Y. Zhang, M. Huo, J. Zhou, A. Zou, W. Li, C. Yao and S. Xie. DDSolver: an add-in program for modeling and comparison of drug dissolution profiles, ***The AAPS Journal,*** 12(3) (2010) 263-271.

[274] D. F. Freire and S. C. F. Aragao. Thermal studies of isoniazid and mixtures with rifampicin, ***Journal of Thermal and Analytical Calorimetry,*** 97 (2009) 333-336.

[275] S. Gunasekaran, E. Sailatha, S. Seshadri and S. Kumaresan. FTIR, FT Raman Spectra and molecular structural confirmation of isoniazid, ***Indian Journal of Pure and Applied Physics***, 47(1) (2009) 12-18.

[276] E. Akalin and S. Akyuz. Vibrational structure of free and hydrogen bonded complexes of isoniazid, FT-IR, FT-Raman and DFT study, ***Journal of Molecular Structure***, 834-836 (2007) 492-497.

[277] P. J. Watts, M. C. Davies and C. D. Melia. Microencapsulation using emulsification/solvent evaporation, an overview of techniques and applications, ***Critical Reviews in Therapeutic Drug Carriers***, 7(3) (1990) 235-259.

[278] N. T. Hwisa, P. Katakam, B. R. Chandu and S. K. Adiki. Solvent evaporation techniques as promising advancement in microencapsulation. ***Vedic Research International Biological Medicinal Chemistry***, 1(1) (2013) 8-22.

[279] K. Prakash, P. N. Raju, K. K. Shanta and M. N. Lakshmi. Preparation and characterization of lamivudine microcapsules using various cellulose polymers, ***Tropical Journal of Pharmaceutical Research***, 6(4) (2007) 841-847.

[280] T. Mateovic, B. Kriznar, M. Bogataj and A. Mrhar. The influence of stirring rate on biopharmaceutical properties of Eudragit® RS microspheres, ***Journal of Microencapsulation***, 19(1) (2002) 29-36.

[281] Z. Xiao, W. Liu, G. Zhu, R. Zhou and Y. Niu. Production and characterization of multinuclear microcapsules encapsulating lavender oil by complex coacervation, ***Flavour and Fragrance Journal***, 29(3) (2014) 166-172.

[282] P. Li, Z. Yang, Z. Peng, S. Lee, L. Kong and Q. Wang. Microencapsulation of coupled folate and chitosan nanoparticles for targeted delivery of combination drugs to colon, ***Journal of Microencapsulation***, 32(1) (2014) 40-45.

[283] B. Wilson, P. P. Babubhai, M. S. Sajeev, J. L. Jenita and S. R. Priyadarshini, Sustained release enteric coated tablets of pantoprazole, formulation, *in vitro* and *in vivo* evaluation, ***Acta Pharma***, 63(1) (2013) 131-140.

[284] N. A. ElKasabgy, I. Elsayed and A. H. Elshafeey. Design of lipotomes as a novel dual functioning nanocarrier for bioavailability enhancement of lacidipine, In-vitro and in-vivo characterisation, ***International Journal of Pharmaceutics***, 472(1) (2014) 369-379.

[285] H. Jiang, R. Tian, W. Hu, Y. Jia, P. Yuan, J. Wang and L. Zhang. Formulation and evaluation of gastroretentive floating drug delivery system of dipyridamole, ***Drug Development and Industrial Pharmacy***, 41(4) (2015) 674-680.

[286] A. M. Al-Ghananeem, M. Abbassi, S. Shrestha, G. Raman, H. Wulff, L. Pereira and A. Ansari. Formulation-based approach to support early drug discovery and development efforts, a case study with enteric microencapsulation dosage form development for a triarylmethane derivative TRAM-34, a novel potential immunosuppressant, ***Drug Development and Industrial Pharmacy***, 36(5) (2010) 563-569.

[287] R. Sareen, K. Nath, N. Jain and K. L. Dhar. Curcumin loaded microsponges for colon targeting in inflammatory bowel disease, fabrication, optimisation, and *in vitro* and pharmacodynamic evaluation, ***Biomedical Research International***, 2014 (2014) 1-7.

[288] Y. Zang, X. Du, Y. Zang, G. Li, C. Cai, J. Xu and X. Tang. Thiolated Eudragit®-based nanoparticles for oral insulin delivery, preparation, characterisation, and evaluation using intestinal epithelial cells *in vitro*, ***Macromolecular Bioscience***, 14(6) (2014) 842-852.

[289] K. M. Hosny, O. A. A. Ahmed and R. T. Al-Abdali. Enteric-coated alendronate sodium nanoliposomes, a novel formula to overcome barriers for the treatment of osteoporosis, ***Expert Opinion on Drug Delivery***, 10(6) (2013) 741-746.

[290] S. Fukui, H. Yano, S. Yada, T. Mikkaichi and H. Minami. Design and evaluation of an extended-release matrix tablet formulation, the combination of hypromellose acetate succinate and hydroxypropylcellulose, ***Asian Journal of Pharmaceutical Sciences***, 12(2) (2017) 149-156.

[291] Y. Zhao, T. Xin, T. Ye, X. Yang and W. Pan. Solid dispersion in the development of a nimodipine delayed-release tablet formulation, ***Asian Journal of Pharmaceutical Sciences***, 9(1) (2014) 35-41.

[292] Z. Dong and D. S. Choi. Hydroxypropyl Methylcellulose Acetate Succinate, Potential Drug-Excipient Incompatibility, ***AAPS PharmSciTech***, 9(3) (2008) 991-997.

[293] T. Uchida, N. Yasuda and K. Matsuyama. Preparation and characterisation of biodegradable or enteric-coated microspheres containing the protease inhibitor camostat, ***Journal of Pharmacy and Pharmacology***, 53(2) (2001) 255-261.

[294] C. Chemtob, J. C. Chaumeil and M. N'Dongo. Microencapsulation by ethylcellulose phase separation, microcapsule characteristics, ***International Journal of Pharmaceutics***, 29(1) (1986) 1-7.

[295] P. Costa and S. J. M. Lobo. Modeling and comparison of dissolution profiles, ***European Journal of Pharmaceutical Sciences***, 13(2) (2001) 123-133.

[296] P. L. Ritger and N. A. Peppas. A simple equation for description of solute release I, fickian and non-fickian release from non-swellable devices in the form of slabs, spheres, cylinders or discs, ***Journal of Controlled Release***, (51) (1987) 23-36.

[297] P. L. Ritger and N. A. Peppas. A simple equation for description of solute release II, fickian and anomalous release from swellable devices, ***Journal of Controlled Release***, 5(1) (1987) 37-42.

[398] J. Siepmann and N. A. Peppas. Modeling of drug release from delivery systems based on hydroxypropyl methylcellulose (HPMC), ***Advanced Drug Delivery Reviews***, 48(2) (2001) 139-157.

[299] S. Arora, J. Ali, A. Ahuja, R. K. Khar and S. Baboota. Floating drug delivery systems, a review, ***AAPS PharmSciTech***, 6(3) (2005) E372-E390.

[300] L. Kagan and A. Hoffman. Systems for region selective drug delivery in the gastrointestinal tract, biopharmaceutical considerations, ***Expert Opinion on Drug Delivery***, 5(6) (2008) 681-692.

[301] M. Neumann, F. Schneider, M. Koziolek, G. Garbacz and W. Weitschies. A novel mechanical antrum model for the prediction of the gastroretentive potential of dosage forms, ***International Journal of Pharmaceutics***, 530(1) (2017) 63-70.

[302] G. J. Tortora and B. Derrickson. Principles of Anatomy and Physiology, 11th Edition, John Wiley and Sons, New York, 2006, 866.

[303] G. R. Vantrappen, T. L. Eters and J. Janssens. The secretory component of interdigestive migratory motor complex in man, ***Scandinavian Journal of Gastroenterology***, 14(6) (1979) 663-667.

[304] C. G. Wilson and N. Washington. The stomach, its role in oral drug delivery In Physiological Pharmaceutics, Biological Barriers to Drug Absorption, M.H Ellis Horwood (Editor), Chichester, 1989, 47-70.

[305] S. Desai and S. Bolton. A floating controlled release drug delivery system, *in vitro- in vivo* evaluation, ***Pharmaceutical Research***, 10(9) (1993) 1321-1325.

[306] B. N. Singh and K. H. Kim. Floating drug delivery systems, an approach to oral controlled drug delivery via gastric retention, ***Journal of Controlled Release***, 63(3) (2000) 235-259.

[307] H. E. L. L. Bechgaard and K. A. R. I. Ladefoged. Distribution of pellets in the gastrointestinal tract, The influence on transit time exerted by the density or diameter of pellets, ***Journal of Pharmacy and Pharmacology***, 30(1) (1978) 690-692.

[308] J. Timmermans, V. B. Gansbeke and A. J. Moes. Assessing by gamma scintigraphy the *in vivo* buoyancy of dosage forms having known size and floating force profiles as a function of time, ***Proceedings of the 5th International Conference on Pharmacy Technology***, Paris, I (1989), 42-51.

[309] A. A. Deshpande, N. H. Shah, C. T. Rhodes and W. Malick. Development of a novel controlled-release system for gastric retention, ***Pharmaceutical Research***, 14(6) (1997) 815-819.

[310] S. J. Burns, D. Attwood and S. G. Barnwell. Assessment of a dissolution vessel designed for use with floating and erodible dosage forms, ***International Journal of Pharmaceutics***, 160(2) (1998) 213-218.

[311] N. J. Joseph, S. Lakshmi and A. Jayakrishnan. A floating-type oral dosage form for piroxicam based on hollow polycarbonate microspheres, *in vitro* and *in vivo* evaluation in rabbits, ***Journal of Controlled Release***, 79(1) (2002) 71-79.

[312] K. S. Soppimath, A. R. Kulkarni, W. E. Rudzinski and T. M. Aminabhavi. Microspheres as floating drug delivery system to increase gastric retention of drugs, ***Drug Metabolism Reviews,*** 33(2) (2001) 149-160.

[313] M. Ichikawa, S. Watanabe and Y. Miyake. A New multiple-unit oral floating dosage system I, preparation and *in vitro* evaluation of floating and sustained-release characteristics, ***Journal of Pharmaceutical Sciences,*** 80(11) (1991) 1062-1066.

[314] R. C. Rowe, P. J. Sheskey and M. E. Quinn (Editors). *The Handbook of Pharmaceutical Excipients*, 6th Edition,., Pharmaceutical Press, London, 2009, 262-265.

[315] A. G. Ozturk, S. S. Ozturk, B. O. Palsson, T. A. Wheatley and J. B. Dressman. Mechanism of release from pellets coated with an ethylcellulose-based film, ***Journal of Controlled Release,*** 14(3) (1990) 203-213.

[316] R. Bodmeier and O. Paeratakul. The effect of curing on drug release and morphological properties of ethylcellulose pseudolatex-coated beads, ***Drug Development and Industrial Pharmacy,*** 20(9) (1994) 1517-1533.

[317] S. C. Porter. Controlled-Release Film coatings based on ethylcellulose, ***Drug Development and Industrial Pharmacy,*** 15(10) (1989) 1495-1521.

[318] G. H. Klinger, E. S. Ghali, S. C. Porter and J. B. Schwartz. Formulation of controlled release matrices by granulation with a polymer dispersion, ***Drug Development and Industrial Pharmacy,*** 16(9) (1990) 1473-1490.

[319] M. G. Moldenhauer and J. G. Nairn. The control of ethylcellulose microencapsulation using solubility parameters, ***Journal of Controlled Release,*** 22(3) (1992) 205-218.

[320] G. V. de la Cruz, J. A. Torres and M. O. Martin-Polo. Temperature effect on the moisture sorption isotherms for methylcellulose and ethylcellulose films, ***Journal of Food Engineering,*** 48(1) (2001) 91-94.

[321] A. Streubel, J. Siepmann and R. Bodmeier. Floating microparticles based on low density foam powder, ***International Journal of Pharmaceutics,*** 241(2) (2002) 279-292.

[322] S. Mishra and K. Pathak. Formulation and evaluation of oil entrapped gastroretentive floating gel beads of loratadine, ***Acta Pharmaceutica,*** 58(2) (2008) 187-197.

[323] A. Gandhi, S. Jana and K. K. Sen. In-vitro release of acyclovir loaded Eudragit® RLPO-nanoparticles for sustained drug delivery, ***International Journal of Biological Macromolecules,*** 67 (2014) 478-482.

[324] P. R. P. Verma. Sustained release of theophylline from Eudragit® RLPO and RSPO tablets, ***Drug Development and Industrial Pharmacy,*** 22(12) (1996) 1243-1247

[325] R. C. Rowe, P. J. Sheskey and M. E. Quinn (Editors). *The Handbook of Pharmaceutical Excipients*, 6th Edition,., Pharmaceutical Press, London, 2009, 181-183.

[326] R. C. Rowe, P. J. Sheskey and M. E. Quinn (Editors). *The Handbook of Pharmaceutical Excipients*, 6th Edition,., Pharmaceutical Press, London, 2009, 629-633.

[327] S. Chandran, K. S. Sanjay and L. F. Ali Asghar. Microspheres with pH modulated release, design and characterisation of formulation variables for colonic delivery, ***Journal of Microencapsulation***, 26(5) (2009) 420-431.

[328] *United States Pharmacopoeia Incorporating The National Formulary*. United States Pharmacopoeial Convention, Washington, USA, 34th Edition, Vol. 1, 2011, 33-415.

[329] C. Mwila, S. M. M. Khamanga and R. B. Walker. Development and sssessment of a USP Apparatus 3 dissolution test method for sustained-release nevirapine matrix tablets**, *Dissolution Technologies***, 23(3) (2016) 22-30.

[330] N. Ozdemir, S, Ordu and Y. Ozkan. Studies of floating dosage forms of furosemide, *in vitro* and *in vivo* evaluations of bilayer tablet formulations, ***Drug Development and Industrial Pharmacy***, 26(8) (2000) 857-866.

[331] S. L. Harikumar and A. Sharma A. Development and evaluation of bromhexine hydrochloride floating microparticulates, ***Asian Journal of Pharmaceutics***, 6(1) (2012) 38-43.

[332] I. Pasquali, R. Bettini and F. Giordano. Thermal behaviour of diclofenac, diclofenac sodium and sodium bicarbonate compositions, ***Journal of Thermal Analysis and Calorimetry***, 90(3) (2007) 903-907.

[333] B. K. Kim, S. J. Hwang, J. B. Park and H. J. Park. Preparation and characterization of drug-loaded polymethacrylate microspheres by an emulsion solvent evaporation method, ***Journal of Microencapsulation***, 19(6) (2002) 811-822.

[334] N. B. Viswanathan, P. A. Thomas, J. K. Pandit, M. G. Kulkarni and R. A. Mashelkar. Preparation of non-porous microspheres with high entrapment efficiency of proteins by a (water-in-oil)-in-oil emulsion technique, ***Journal of Controlled Release***, 58(1) (1999) 9-20.

[335] M. Jelvehgari, S. Dastmalch and D. Nazila. Theophylline-ethylcellulose microparticles, screening of the process and formulation variables for preparation of sustained release particles, ***Iranian Journal of Basic Medical Sciences***, 15(1) (2012) 608-624.

[336] M. Jelvehgari, J. Barar, H. Valizadeh, S. Shadrou and A. Nokhodchi. Formulation, characterisation and *in vitro* evaluation of theophylline-loaded Eudragit® RS 100 microspheres prepared by an emulsion-solvent diffusion/evaporation technique, ***Pharmaceutical Development and Technology***, 16(6) (2011) 637-644.

[337] M. Jelvehgari and S. H. Montazam. Comparison of microencapsulation by emulsion-solvent extraction/evaporation technique using derivatives cellulose and acrylate-methacrylate copolymer as carriers, ***Journal of Natural Pharmaceutical Products***, 7(4) (2012) 144-152.

[338] M. Kilacarslan and T. Baykara. The effect of drug polymer ratio on the properties of the verapamil HCl loaded microspheres, ***International Journal of Pharmaceutics,*** 252(1) (2003) 99-109

[339] S. Chandran, L. F. A. Asghar and N. Mantha. Design and evaluation of ethyl cellulose based matrix tablets of ibuprofen with pH modulated release kinetics, ***Indian Journal of Pharmaceutical Sciences***, 70(5) (2008) 596-602.

[340] G. M. Khan and V. M. Meidan. Drug release kinetics from tablet matrices based upon ethylcellulose ether-derivatives, a comparison between different formulations, ***Drug Development and Industrial Pharmacy***, 33(6) (2007) 627-639.

[341] C. T. Sengel-Turk, C. Hascicek and N. Gonul. Ethylcellulose-based matrix-type microspheres, influence of plasticizer ratio as pore-forming agent, ***AAPS PharmSciTech,*** 12(4) (2011) 1127-1135

[342] J. Schnieders, U. Gbureck, E. Vorndran, M. Schossik and T. Kissel. The effect of porosity on drug release kinetics from vancomycin microsphere/calcium phosphate cement composites, ***Journal of Materials Research***, 99(2) (2011) 391-398.

[343] Y. Zhi-wei, R. Patrick, P. R. Jean and V. Chris. Correlation between permeability of metoprolol tartrate through plasticized isolated ethylcellulose/hydroxypropyl methylcellulose films and drug release from reservoir pellets, ***European Journal of Pharmaceutics and Biopharmaceutics,*** 67(2) (2007) 485-490.

[344] M. O. Emeje, O. O. Kunle and S. I. Ofoefule. Compaction characteristics of ethylcellulose in the presence of some chanelling agents, technical note, ***AAPS PharmSciTech***, 7(3) (2006) 58

[345] D. Katayoun and S. Marzieh. Formulation and *in vitro* evaluation of nifedipine controlled release tablet: Influence of combination of hydrophylic and hydrophobic matrix forms, ***Asian Journal of Pharmaceutics***, 4(4) (2010) 185-193,

[346] J. Akbuga. Preparation and evaluation of controlled release furosemide microspheres by spherical crystallisation, ***International Journal of Pharmaceutics***, 53(2) (1989) 99-105.

[347] C. N. Patra, A. B. Kumar, H. K. Pandit, S. P. Singh and M. V. Devi. Design and evaluation of sustained release bilayer tablets of propranolol hydrochloride, ***Acta Pharmaceutica***, 57(4) (2007) 479-489.

[348] M. Khandai, S. Chakraborty, A. Sharma, D. Panda, N. Khanam and S. K. Panda. Development of propranolol hydrochloride matrix tablets, an investigation on effects of combination of hydrophilic and hydrophobic matrix formers using multiple comparison analysis, ***International Journal of Pharmaceutical Sciences Review and Research,*** 1(2) (2010) 1-7.

[349] Y. M. Jagtap, R. K. Bhujbal, A. N. Ranade, N. s. Ranpise. Effect of various polymers concentrations on physicochemical properties of floating microspheres, ***Indian Journal of Pharmaceutical Sciences***, 74(6) (2012) 512-520.

[350] K. Prakash, P. N. Raju, K. K. Shanta and M. N. Lakshimi. Preparation and characterisation of lamivudine microcapsules using various cellulose polymers, ***Tropical Journal of Pharmaceutical Research***, 6(4) (2007) 841-847.

[351] P. K. Choudhury and M. Kar. Controlled release metformin hydrochloride microspheres of ethyl cellulose prepared by different methods and study on the polymer affected parameters, ***Journal of Microencapsulation***, 26(1) (2009) 46-53.

[352] G. Murtaza. Ethylcellulose microparticles, a review, ***Acta Poloniae Pharmaceutica-Drug Research***, 69(1) (2012) 11-22.

[353] R. C Rowe. The effect of the molecular weight of ethyl cellulose on the drug release properties of mixed films of ethyl cellulose and hydroxypropylmethylcellulose, ***International Journal of Pharmaceutics***, 29(1) (1986) 37-41..

[354] X. Fu, Q. Ping and Y. Gao. Effects of formulation factors on encapsulation efficiency and release behaviour *in vitro* of huperzine A-PLGA microspheres, ***Journal of Microencapsulation***, 22(7) (2005) 705-714.

[355] J. P. Raval, D. R. Naik, K. A. Amin and P. S. Patel. Controlled-release and antibacterial studies of doxycycline-loaded poly(ε-caprolactone) microspheres, ***Journal of Saudi Chemical Society***, 18(5) (2014) 566-573.

[356] R. C. Mehta, B. C. Thanoo and P. P. Deluca. Peptide containing microspheres from low molecular weight and hydrophilic poly(*d*,*l*-lactide-co-glycolide), ***Journal of Controlled Release***, 41(3) 1996 249-257.

[257] X. Li, X. Deng, M. Yuan, C. Xiong, Z. Huang, Y. Zhang and W. Jia. Investigation on process parameters involved in preparation of poly-DL-lactide-poly(ethylene glycol) microspheres containing Leptospira Interrogans antigens, ***International Journal of Pharmaceutics***, 178(2) 1999 245-255.

[358] H. Rafati, A. G. A. Combes, J. Adler and S. S. Davis. Protein-loaded poly(DL-lactide-co-glycolide) microparticles for oral administration, Formulation, structural and release characteristics, ***Journal of Controlled Release***, 43(1) (1997) 89-102.

[359] R. Bodmier, J. W. McGinity. Solvent selection in the preparation of PLA microspheres prepared by the solvent evaporation method, ***International Journal of Pharmaceutics***, 43(1-2) (1988) 179-186.

[360] F. Kang and J. Singh. Effect of additives on the release of a model protein from PLGA microspheres, ***AAPS PharmSciTech***, 2(4) (2001) Article 30.

[361] A. V. Pande, P. D. Vaidya, A. Arora, M. V. Dhoka. *In vitro* and *in vivo* evaluation of ethyl cellulose based floating microspheres of cefpodoxime proxetil, ***International Journal of Biomedical Research***, 1(4) (2010) 122-128.

[362] M. Saravanan and B. Anupama. Development and evaluation of ethylcellulose floating microspheres loaded with ranitidine hydrochloride by novel solvent evaporation-matrix erosion method, ***Carbohydrate Polymers***, 85(3) (2011) 592-598.

[363] N. Pandya, M. Pandya and V. H. Bhaskar. Preparation and *in vitro* characterisation of porous carrier–based glipizide floating microspheres for gastric delivery, ***Journal of Young Pharmacists***, 3(2) (2011) 97-104.

[364] Md. L. Amin, T. Ahmed and Md. A. Mannan. Development of floating-mucoadhesive microsphere for site specific release of metronidazole, ***Advanced Pharmaceutical Bulletin***, 6(2) (2016) 195-200.

[365] F. C. Kenechukwu and M. A. Momoh. Formulation, characterisation and evaluation of the effect of polymer concentration on the release behavior of insulin-loaded Eudragit®-entrapped mucoadhesive microspheres, ***International Journal of Pharmaceutical Investigation***, 6(2) (2016) 69-77.

[366] S. Jain, M. S. Srinath, C. Narendra, S. N. Reddy and A. Sindhu. Development of a floating dosage form of ranitidine hydrochloride by statistical optimisation technique, ***Journal of Young Pharmacists***, 2(4) (2010) 342-349.

[367] X. Huang, X. Cheng, Y. Luo, Z. Guo, C. Zhong and Y. Zhang. Effect of homogenisation speed on morphology and release of protein loaded PLGA microspheres made by W/O/W method, ***Acta Scientiarum Naturaliam Universitatis Sunyatseni***, 54(3) (2015) 119-124.

[368] S. Jakub, P. Adam, L. Raymond, J. Renata and K Pezhman. Empirical search for factors affecting mean particle size of PLGA microspheres containing macromolecular drugs, ***Computer Methods and Programs in Biomedicine***, 134 (2016) 137-147.

[369] K. K. Kim and D. W. Pack. Microspheres for Drug delivery In BioMEMS and Biomedical Nanotechnology, M. Ferrari, A. P. Lee and L. J. Lee (Editors) Springer International Publishing AG, Biological and Biomedical Nanotechnology, volume 1, 2006, 19-50

[370] R. E. Stevens, V. Gray, A. Dorantes, L. Gold and L. Pham. Scientific and Regulatory Standards for Assessing Product Performance Using the Similarity Factor, *f2,**The AAPS Journal***, 17(2) (2015) 301-306.

APPENDIX 1A

1.0 DIAGNOSTICS PLOTS, ANOVA DATA AND RESPONSE SURFACE PLOTS FOR RESPONSES Y_1-Y_9 OF BOX BEHNKEN DESIGN FOR RP-HPLC METHOD FOR SIMULTANEOUS ANALYSIS OF INH, PZA AND RIF.

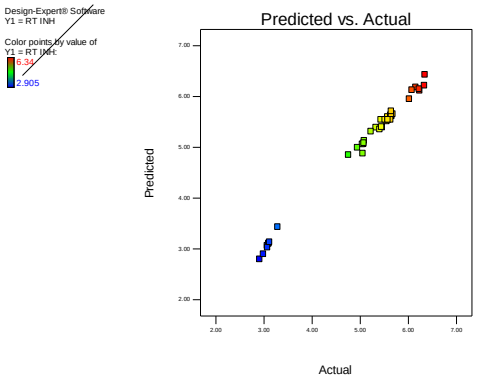

Figure 1.1A Plot of predicted versus actual responses for RT of INH.

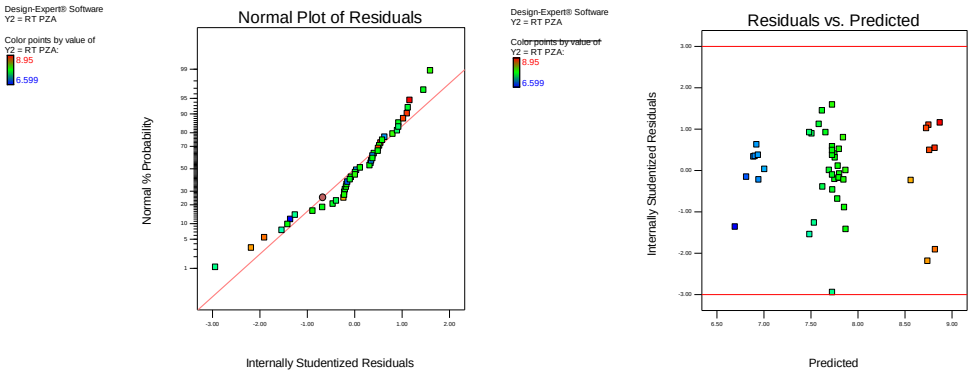

(A) (B)

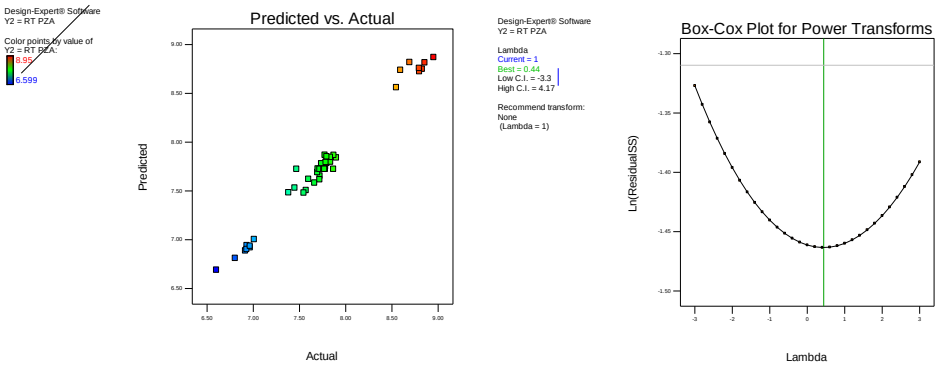

(C) (D)

Figure 1.2A Plot of (A) normal plot of residuals, (B) residuals versus predicted responses, (C) predicted versus actual responses and (D) Box-Cox plot of power transformation for PZA, (Y_2).

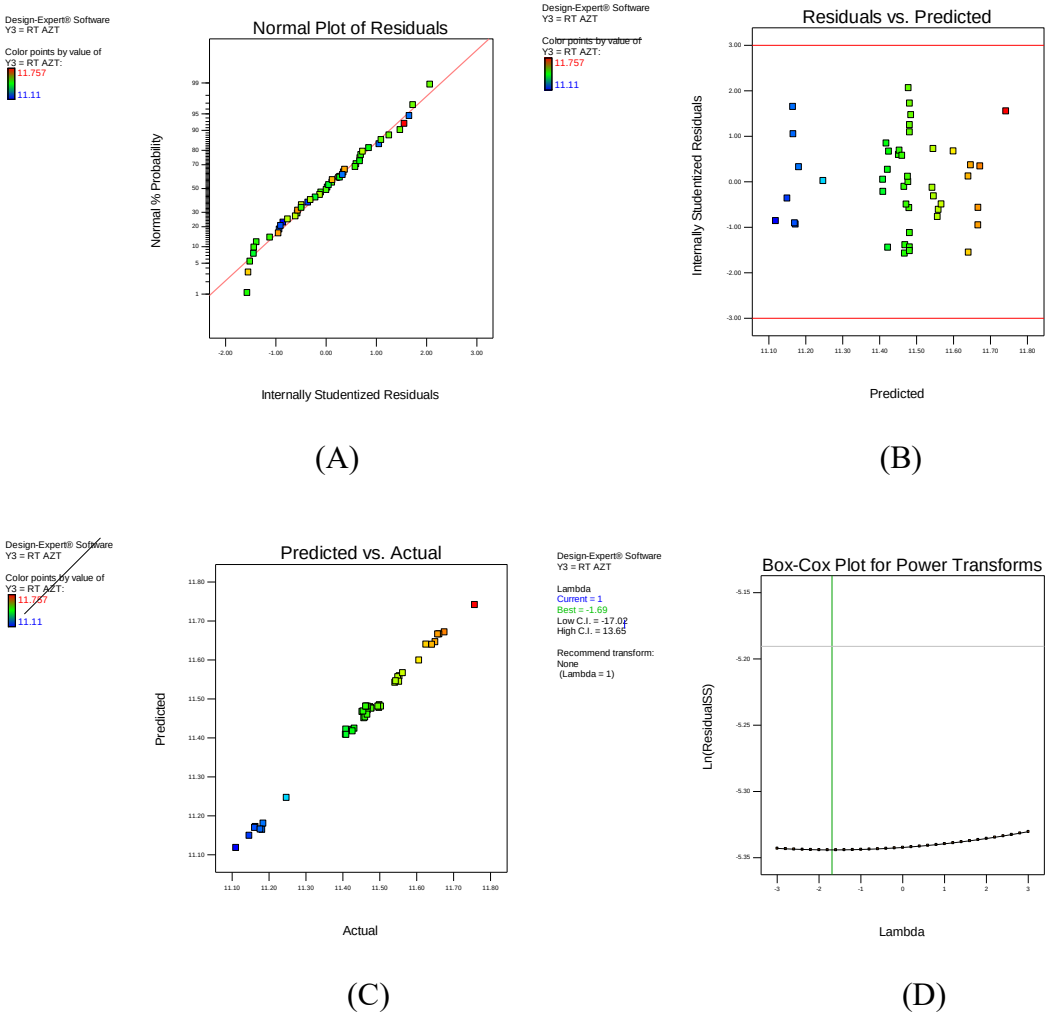

Figure 1.3A Plot of (A) normal plot of residuals, (B) residuals versus predicted responses, (C) predicted versus actual responses and (D) Box-Cox plot of power transformation of RT AZT (Y_3).

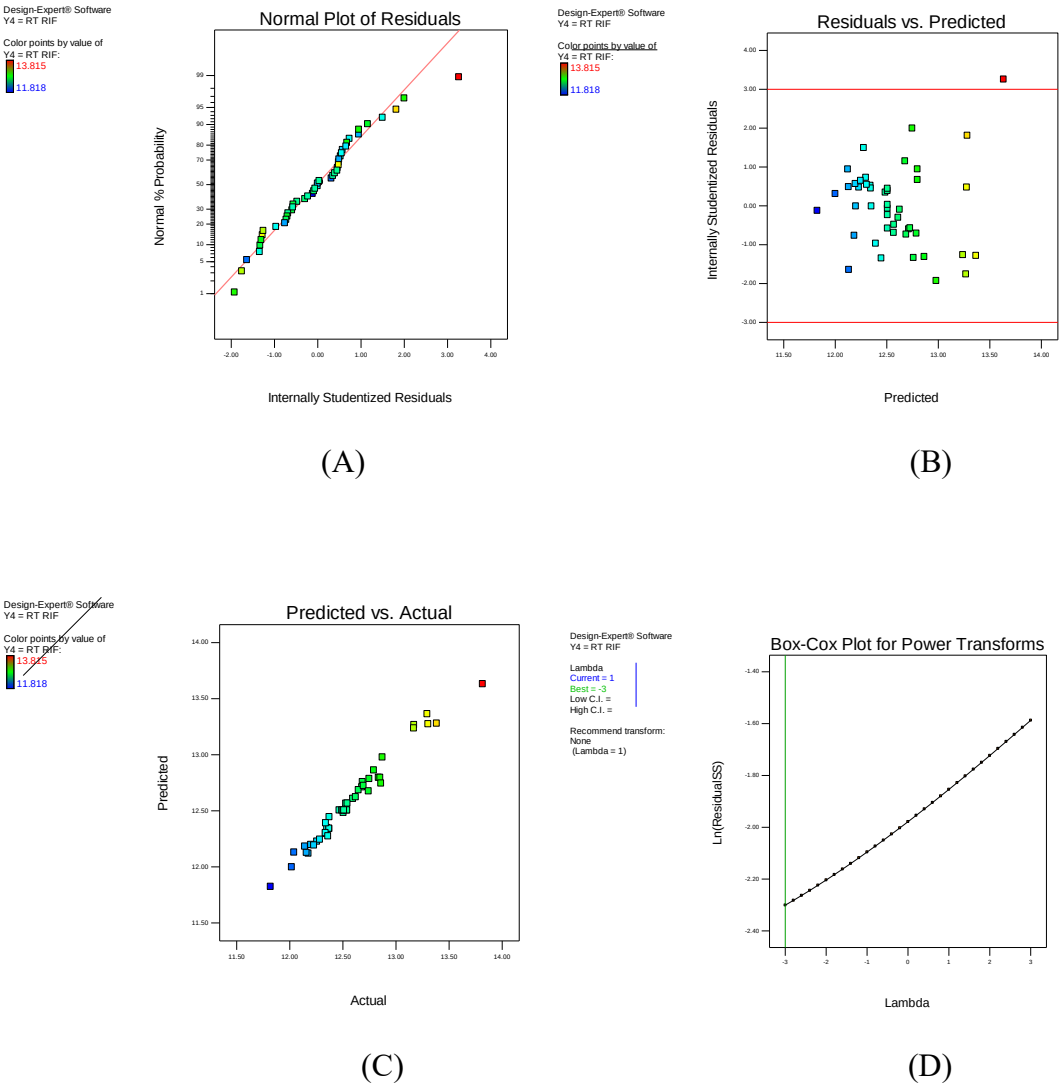

Figure 1.4A Plot of (A) normal plot of residuals, (B) residuals versus predicted responses, (C) predicted versus actual responses and (D) Box-Cox plot of power transformation of RT RIF (Y_4).

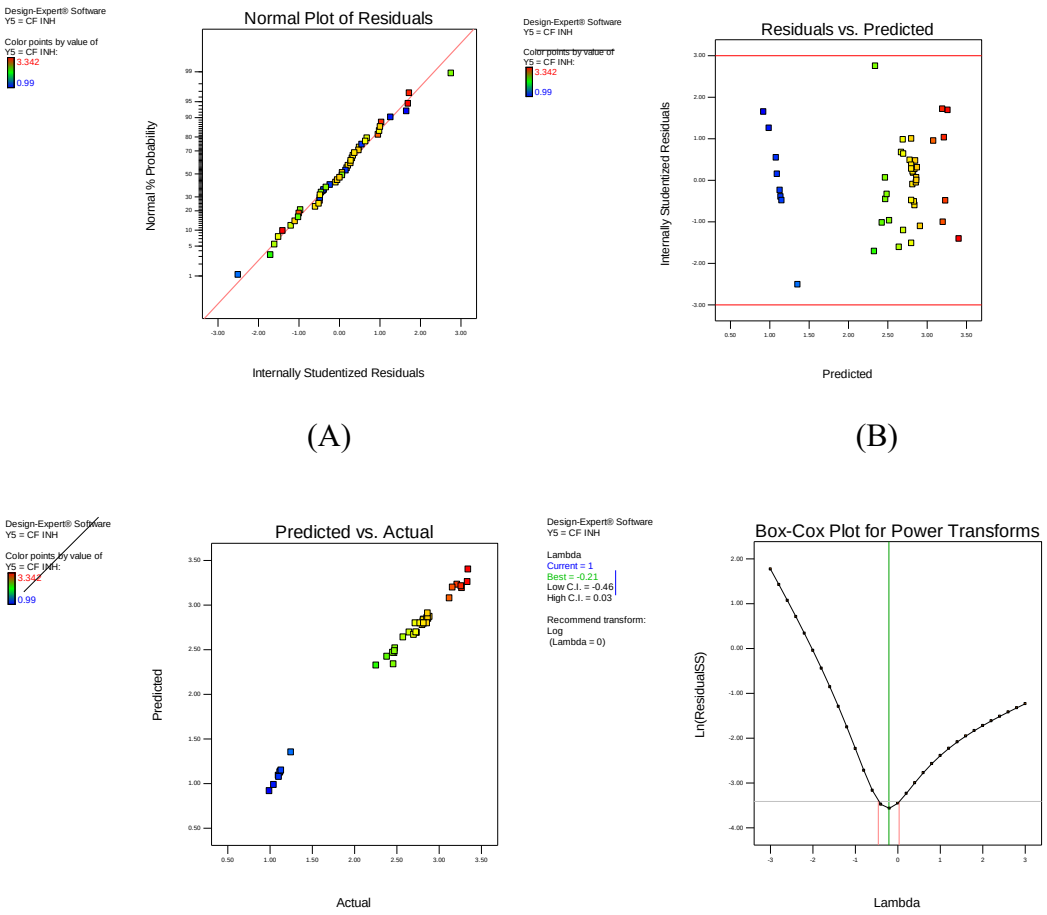

Figure 1.5A Plot of (A) normal plot of residuals, (B) residuals versus predicted responses, (C) predicted versus actual responses and (D) Box-Cox plot of power transformation of CF INH (Y_5).

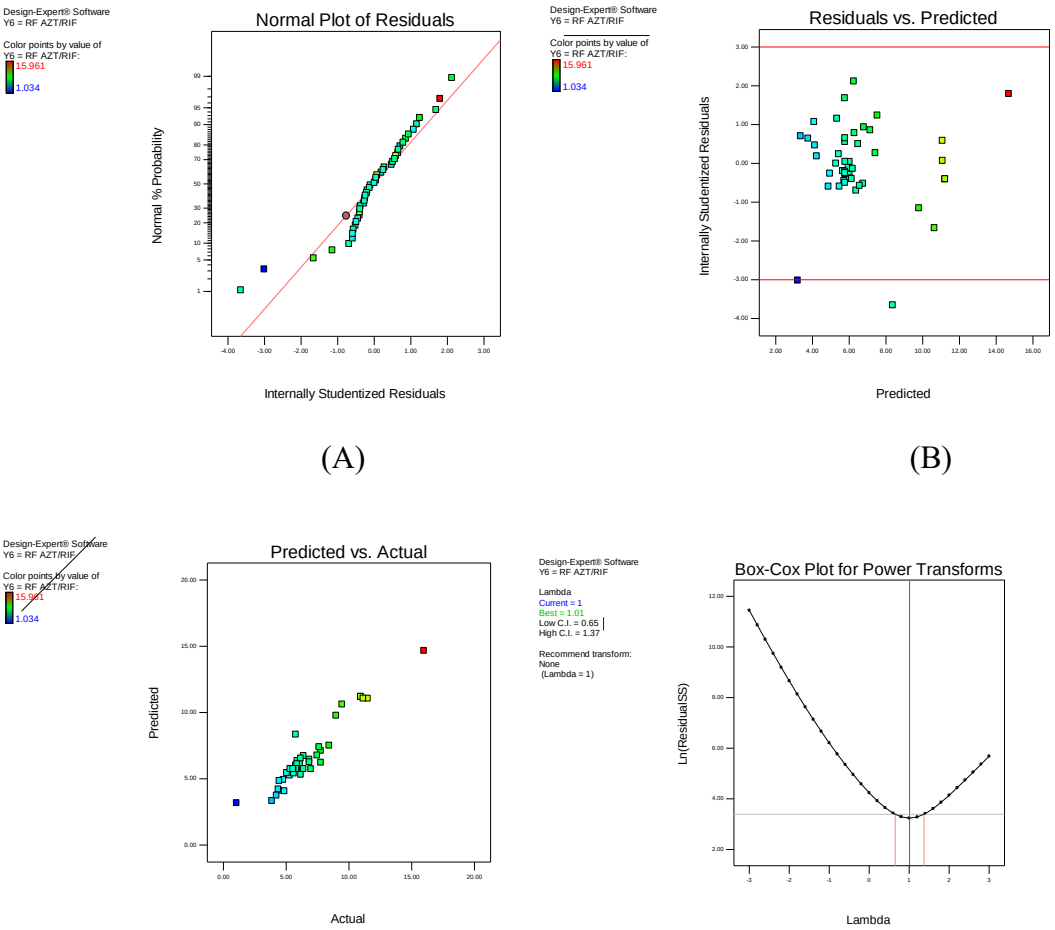

Figure 1.6A Plot of (A) normal plot of residuals, (B) residuals versus predicted responses, (C) predicted versus actual responses and (D) Box-Cox plot of power transformation of RF AZT/RIF (Y_6).

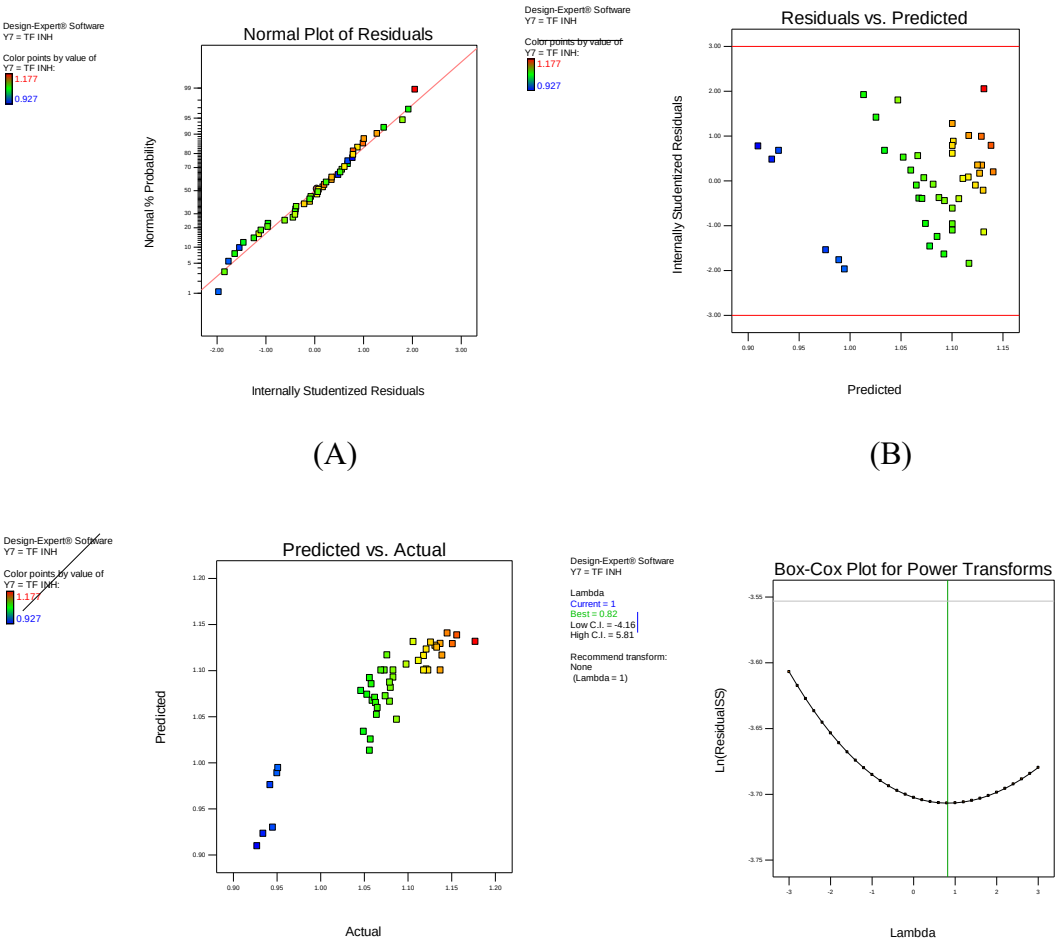

Figure 1.7A Plot of (A) normal plot of residuals, (B) residuals versus predicted responses, (C) predicted versus actual responses and (D) Box-Cox plot of power transformation of TF INH (Y_7).

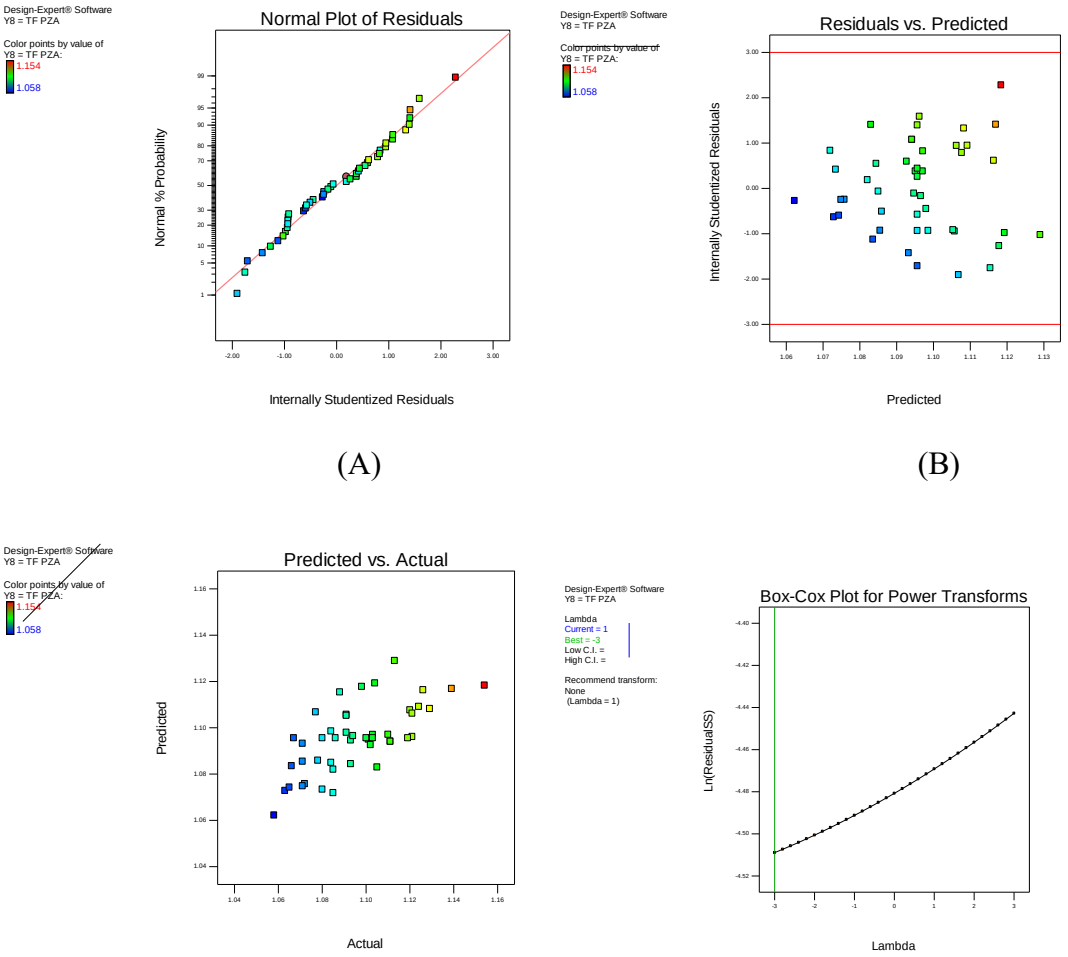

Figure 1.8A Plot of (A) normal plot of residuals, (B) residuals versus predicted responses, (C) predicted versus actual responses and (D) Box-Cox plot of power transformation of TF PZA (Y_8).

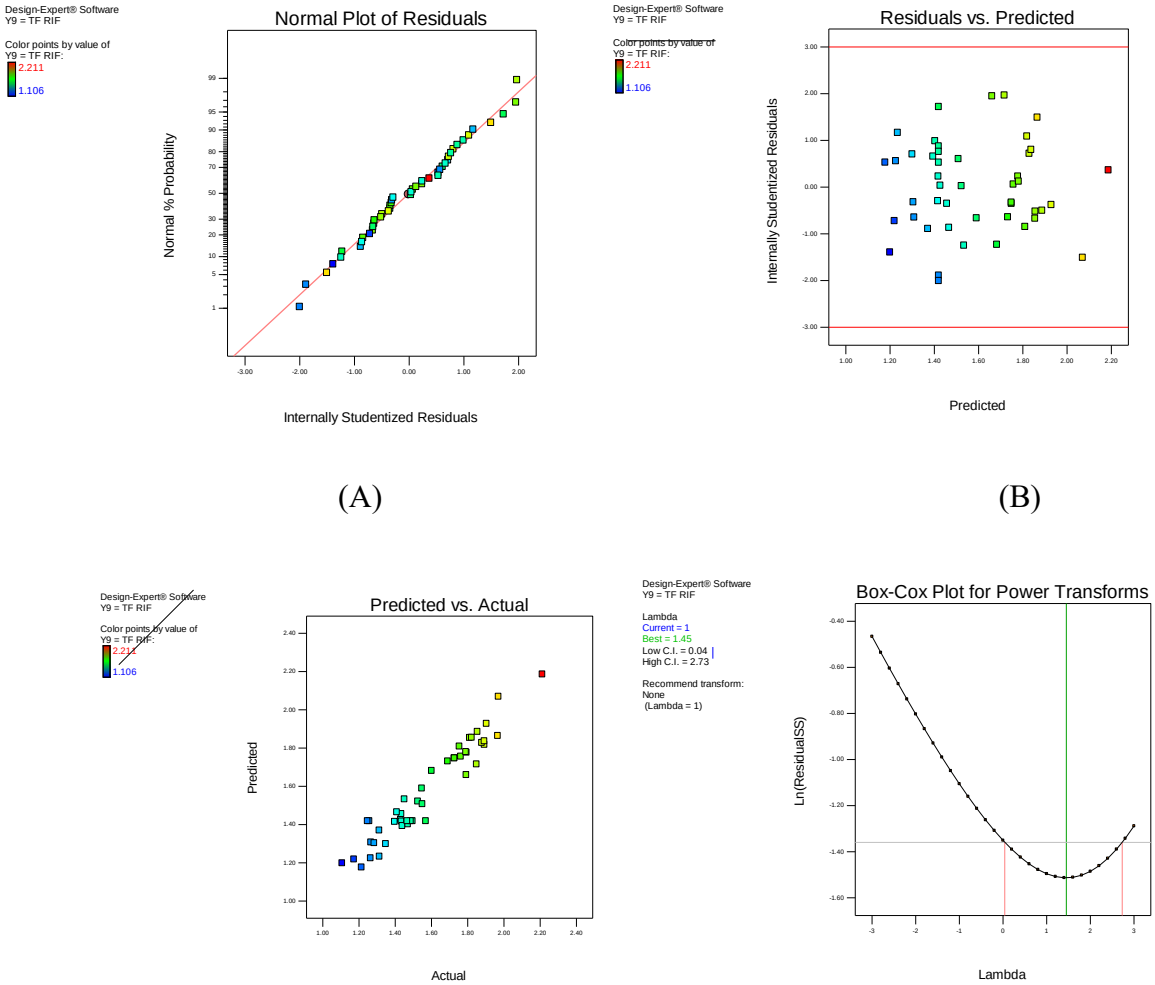

Figure 1.9A Plot of (A) normal plot of residuals, (B) residuals versus predicted responses, (C) predicted versus actual responses and (D) Box-Cox plot of power transformation of TF RIF (Y_9).

2.0 ANOVA DATA FOR RESPONSES Y_2-Y_4 and Y_6 – Y_9 OF BOX BEHNKEN DESIGN FOR RP-HPLC METHOD FOR SIMULTANEOUS ANALYSIS OF INH, PZA AND RIF.

Table 1.1A ANOVA data for response surface quadratic model [Partial sum of squares - Type III] for RT of PZA

Source	Sum of squares	Df	Mean square	F-value	p-value	Prob > F
Panel A						
Model	14.56	20	0.73	78.33	< 0.0001	Significant
A-Buffer pH	0.014	1	0.014	1.55	0.2247	
B-Start %MeOH	13.96	1	13.96	1502.11	< 0.0001	Significant
C-End %MeOH	9.604E-003	1	9.604E-003	1.03	0.3190	
D- Gradient profile	8.418E-003	1	8.418E-003	0.91	0.3503	
E- Gradient duration	0.39	1	0.39	41.78	< 0.0001	Significant
AB	3.600E-005	1	3.600E-005	3.875E-003	0.9509	
AC	2.025E-003	1	2.025E-003	0.22	0.6446	
AD	0.013	1	0.013	1.37	0.2521	
AE	5.776E-003	1	5.776E-003	0.62	0.4378	
BC	9.61E-04	1	9.61E-04	0.1	0.7504	
BD	6.24E-03	1	6.24E-03	0.67	0.4202	
BE	6.25E-06	1	6.25E-06	6.73E-04	0.9795	
CD	2.45E-03	1	2.45E-03	0.26	0.6121	
CE	7.56E-04	1	7.56E-04	0.081	0.7778	
DE	4.00E-06	1	4.00E-06	4.31E-04	0.9836	
A^2	4.88E-03	1	4.88E-03	0.53	0.4754	
B^2	0.088	1	0.088	9.47	0.005	
C^2	3.43E-03	1	3.43E-03	0.37	0.5492	
D^2	2.65E-03	1	2.65E-03	0.29	0.5978	
E^2	0.017	1	0.017	1.79	0.1926	
Residual	0.23	25	9.29E-03			
Lack of fit	0.14	20	7.00E-03	0.38	0.9453	
Pure error	0.092	5	0.018			
Cor total	14.79	45				
Panel B						
Std. deviation	0.096					
Mean	7.75					
%C.V	1.24					
Press	0.69					
R^2	0.9843					
Adjusted R^2	0.9717					
Predicted R^2	0.9532					
Adeq precision	33.464					

Table 1.2A ANOVA data for response surface quadratic model [Partial sum of squares - Type III] for RT AZT

Source	**Sum of squares**	**Df**	**Mean square**	**F-value**	**p-value**	**Prob > F**
Panel A						
Model	1.07	20	0.054	279.53	< 0.0001	Significant
A-Buffer pH	2.03E-05	1	2.03E-05	0.11	0.748	
B-Start %MeOH	6.38E-04	1	6.38E-04	3.32	0.0804	
C-End %MeOH	0.073	1	0.073	381.93	< 0.0001	Significant
D- Gradient profile	0.95	1	0.95	4963.01	< 0.0001	Significant
E- Gradient duration	7.56E-04	1	7.56E-04	3.94	0.0582	
AB	1.96E-04	1	1.96E-04	1.02	0.3219	
AC	2.10E-04	1	2.10E-04	1.1	0.3053	
AD	8.41E-04	1	8.41E-04	4.38	0.0466	
AE	1.10E-04	1	1.10E-04	0.57	0.4556	
BC	1.00E-06	1	1.00E-06	5.21E-03	0.943	
BD	1.82E-04	1	1.82E-04	0.95	0.3392	
BE	1.00E-04	1	1.00E-04	0.52	0.4771	
CD	4.90E-05	1	4.90E-05	0.26	0.6178	
CE	4.90E-05	1	4.90E-05	0.26	0.6178	
DE	1.32E-04	1	1.32E-04	0.69	0.4143	
A^2	5.36E-04	1	5.36E-04	2.79	0.1073	
B^2	5.24E-04	1	5.24E-04	2.73	0.1109	
C^2	8.02E-04	1	8.02E-04	4.18	0.0517	
D^2	0.036	1	0.036	187.22	< 0.0001	Significant
E^2	3.49E-05	1	3.49E-05	0.18	0.6734	
Residual	4.80E-03	25	1.92E-04			
Lack of fit	2.98E-03	20	1.49E-04	0.41	0.9298	
Pure error	1.82E-03	5	3.63E-04			
Cor total	1.08	45				
Panel B						
Std. deviation	0.014					
Mean	11.46					
%C.V	0.12					
Press	0.015					
R^2	0.9955					
Adjusted R^2	0.992					
Predicted R^2	0.9865					
Adeq precision	66.595					

Table 1.3A ANOVA data for response surface quadratic model [Partial sum of squares - Type III] for RT RIF

Source	Sum of squares	Df	Mean square	F-value	p-value	Prob > F
Panel A						
Model	6.82	20	0.34	54.44	< 0.0001	Significant
A-Buffer pH	0.68	1	0.68	108.78	< 0.0001	Significant
B-Start %MeOH	9.90E-03	1	9.90E-03	1.58	0.2203	
C-End %MeOH	4.74	1	4.74	757.24	< 0.0001	Significant
D- Gradient profile	0.81	1	0.81	129.8	< 0.0001	Significant
E- Gradient duration	2.48E-04	1	2.48E-04	0.04	0.8439	
AB	1.23E-05	1	1.23E-05	1.96E-03	0.9651	
AC	0.18	1	0.18	28.5	< 0.0001	Significant
AD	1.16E-03	1	1.16E-03	0.18	0.6712	
AE	6.40E-03	1	6.40E-03	1.02	0.3218	
BC	4.00E-04	1	4.00E-04	0.064	0.8026	
BD	4.00E-04	1	4.00E-04	0.064	0.8026	
BE	4.23E-05	1	4.23E-05	6.74E-03	0.9352	
CD	4.23E-03	1	4.23E-03	0.67	0.4193	
CE	6.25E-06	1	6.25E-06	9.98E-04	0.9751	
DE	0.012	1	0.012	1.84	0.1865	
A^2	4.94E-04	1	4.94E-04	0.079	0.7812	
B^2	7.84E-03	1	7.84E-03	1.25	0.2738	
C^2	0.26	1	0.26	40.89	< 0.0001	Significant
D^2	0.022	1	0.022	3.59	0.0697	
E^2	0.027	1	0.027	4.28	0.0492	Significant
Residual	0.16	25	6.26E-03			
Lack of fit	0.15	20	7.64E-03	9.82	0.0094	
Pure error	3.89E-03	5	7.78E-04			
Cor total	6.98	45				
Panel B						
Std. deviation	0.079					
Mean	12.58					
%C.V	0.63					
Press	0.62					
R^2	0.9776					
Adjusted R^2	0.9596					
Predicted R^2	0.9116					
Adeq precision	33.805					

Table 1.4A ANOVA data for response surface quadratic model [Partial sum of squares - Type III] for RF AZT/RIF

Source	Sum of squares	Df	Mean square	F-value	p-value	Prob > F
Panel A						
Model	248.97	20	12.45	12.21	< 0.0001	Significant
A-Buffer pH	71.58	1	71.58	70.21	< 0.0001	Significant
B-Start %MeOH	0.1	1	0.1	0.1	0.7549	
C-End %MeOH	17.47	1	17.47	17.14	0.0003	
D- Gradient profile	0.16	1	0.16	0.15	0.6993	
E- Gradient duration	1.32	1	1.32	1.29	0.2661	
AB	0.54	1	0.54	0.53	0.4731	
AC	52.74	1	52.74	51.73	< 0.0001	Significant
AD	1.51	1	1.51	1.48	0.2349	
AE	0.32	1	0.32	0.32	0.5784	
BC	0.089	1	0.089	0.088	0.7696	
BD	0.26	1	0.26	0.25	0.6203	
BE	0.047	1	0.047	0.046	0.832	
CD	0.33	1	0.33	0.32	0.5745	
CE	2.82	1	2.82	2.76	0.1088	
DE	1.09	1	1.09	1.07	0.3111	
A^2	71.72	1	71.72	70.34	< 0.0001	Significant
B^2	0.27	1	0.27	0.27	0.6099	
C^2	4.76	1	4.76	4.67	0.0405	Significant
D^2	0.51	1	0.51	0.5	0.4847	
E^2	0.96	1	0.96	0.94	0.3423	
Residual	25.49	25	1.02			
Lack of fit	24.5	20	1.23	6.22	0.026	Significant
Pure error	0.99	5	0.2			
Cor total	274.46	45				
Panel B						
Std. deviation	1.01					
Mean	6.59					
%C.V	15.32					
Press	99.44					
R^2	0.9071					
Adjusted R^2	0.8328					
Predicted R^2	0.6377					
Adeq precision	16.846					

Table 1.5A ANOVA data for response surface quadratic model [Partial sum of squares - Type III] for TF INH

Source	Sum of squares	Df	Mean square	F-value	p-value	Prob > F
Panel A						
Model	0.15	20	7.45E-03	7.58	< 0.0001	Significant
A-Buffer pH	0.052	1	0.052	52.68	< 0.0001	Significant
B-Start %MeOH	0.012	1	0.012	12.65	0.0015	Significant
C-End %MeOH	2.50E-05	1	2.50E-05	0.025	0.8745	
D- Gradient profile	2.98E-04	1	2.98E-04	0.3	0.587	
E- Gradient duration	6.93E-03	1	6.93E-03	7.05	0.0136	Significant
AB	1.00E-04	1	1.00E-04	0.1	0.7524	
AC	4.41E-04	1	4.41E-04	0.45	0.509	
AD	7.57E-03	1	7.57E-03	7.7	0.0103	Significant
AE	3.84E-03	1	3.84E-03	3.91	0.0591	
BC	2.50E-05	1	2.50E-05	0.025	0.8745	
BD	5.29E-04	1	5.29E-04	0.54	0.4699	
BE	6.40E-05	1	6.40E-05	0.065	0.8006	
CD	2.03E-05	1	2.03E-05	0.021	0.887	
CE	7.02E-04	1	7.02E-04	0.71	0.4059	
DE	2.89E-04	1	2.89E-04	0.29	0.5924	
A^2	0.048	1	0.048	48.37	< 0.0001	Significant
B^2	1.62E-03	1	1.62E-03	1.65	0.2109	
C^2	2.11E-03	1	2.11E-03	2.15	0.1555	
D^2	5.53E-04	1	5.53E-04	0.56	0.4602	
E^2	5.88E-04	1	5.88E-04	0.6	0.4464	
Residual	0.025	25	9.83E-04			
Lack of fit	0.02	20	1.02E-03	1.21	0.4533	
Pure error	4.20E-03	5	8.40E-04			
Cor total	0.17	45				
Panel B						
Std. deviation	0.031					
Mean	1.08					
%C.V	2.91					
Press	0.088					
R^2	0.8584					
Adjusted R^2	0.7451					
Predicted R^2	0.4956					
Adeq precision	10.899					

Table 1.6A ANOVA data for response surface linear model [Partial sum of squares - Type III] for TF PZA

Source	Sum of squares	Df	Mean square	F-value	p-value	Prob > F
Panel A						
Model	9.81E-03	5	1.96E-03	6.85	0.0001	Significant
A-Buffer pH	6.01E-05	1	6.01E-05	0.21	0.6495	
B-Start %MeOH	7.57E-03	1	7.57E-03	26.43	< 0.0001	Significant
C-End %MeOH	1.60E-05	1	1.60E-05	0.056	0.8144	
D- Gradient profile	3.06E-06	1	3.06E-06	0.011	0.9182	
E- Gradient duration	2.16E-03	1	2.16E-03	7.55	0.009	Significant
Residual	0.011	40	2.86E-04			
Lack of fit	9.74E-03	35	2.78E-04	0.81	0.686	
Pure error	1.72E-03	5	3.44E-04			
Cor total	0.021	45				
Panel B						
Std. deviation	0.017					
Mean	1.1					
%C.V	1.54					
Press	0.015					
R^2	0.4613					
Adjusted R^2	0.394					
Predicted R^2	0.2875					
Adeq precision	10.921					

Table 1.7A ANOVA data for response surface quadratic model [Partial sum of squares - Type III] for TF RIF

Source	Sum of squares	Df	Mean square	F-value	p-value	Prob > F
Panel A						
Model	2.81	20	0.14	15.68	< 0.0001	Significant
A-Buffer pH	2.73E-03	1	2.73E-03	0.3	0.5859	
B-Start %MeOH	0.043	1	0.043	4.77	0.0385	Significant
C-End %MeOH	0.65	1	0.65	72.47	< 0.0001	Significant
D- Gradient profile	0.014	1	0.014	1.51	0.23	
E- Gradient duration	0.17	1	0.17	19.04	0.0002	Significant
AB	3.03E-05	1	3.03E-05	3.38E-03	0.9541	
AC	0.13	1	0.13	14.22	0.0009	Significant
AD	8.19E-03	1	8.19E-03	0.91	0.3483	
AE	0.013	1	0.013	1.49	0.2339	
BC	9.03E-03	1	9.03E-03	1.01	0.3253	
BD	6.40E-05	1	6.40E-05	7.14E-03	0.9333	
BE	0.097	1	0.097	10.87	0.0029	
CD	6.40E-03	1	6.40E-03	0.71	0.4061	
CE	1.02E-03	1	1.02E-03	0.11	0.7382	
DE	0.028	1	0.028	3.13	0.0891	
A^2	1.36	1	1.36	151.2	< 0.0001	Significant
B^2	2.74E-04	1	2.74E-04	0.031	0.8626	
C^2	3.49E-04	1	3.49E-04	0.039	0.8451	
D^2	0.011	1	0.011	1.24	0.2763	
E^2	0.059	1	0.059	6.63	0.0163	Significant
Residual	0.22	25	8.96E-03			
Lack of fit	0.13	20	6.66E-03	0.37	0.9513	
Pure error	0.091	5	0.018			
Cor total	3.03	45				
Panel B						
Std. deviation	0.095					
Mean	1.58					
%C.V	6					
Press	0.66					
R^2	0.9262					
Adjusted R^2	0.8671					
Predicted R^2	0.7814					
Adeq precision	15.774					

3.0 RESPONSE SURFACE PLOTS FOR RT PZA, RT AZT, RT RIF, RF AZT/RIF, TF INH, TF PZA AND TF RIF FOR BOX BEHNKEN DESIGN FOR RP-HPLC METHOD FOR SIMULTANEOUS ANALYSIS OF INH, PZA AND RIF

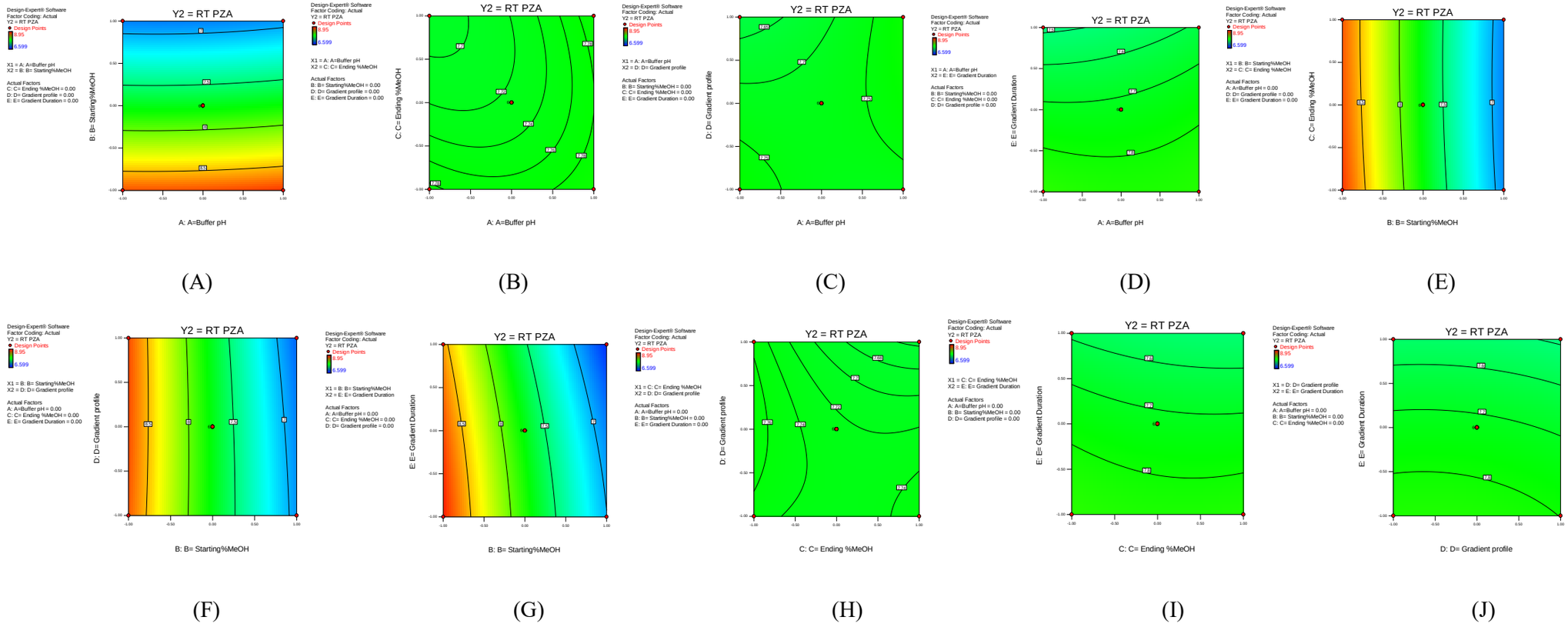

Figure 1.10A Contour plots depicting the impact of (A) start % MeOH and buffer pH, (B) end % MeOH and buffer pH, (C) gradient profile and buffer pH, (D) gradient duration and buffer pH, (E) end % MeOH and start % MeOH, (F) gradient profile and start% MeOH, (G) gradient duration and start % MeOH, (H) gradient profile and end % MeOH, (I) gradient duration and End % MeOH and (H) gradient duration and gradient profile on the RT for PZA.

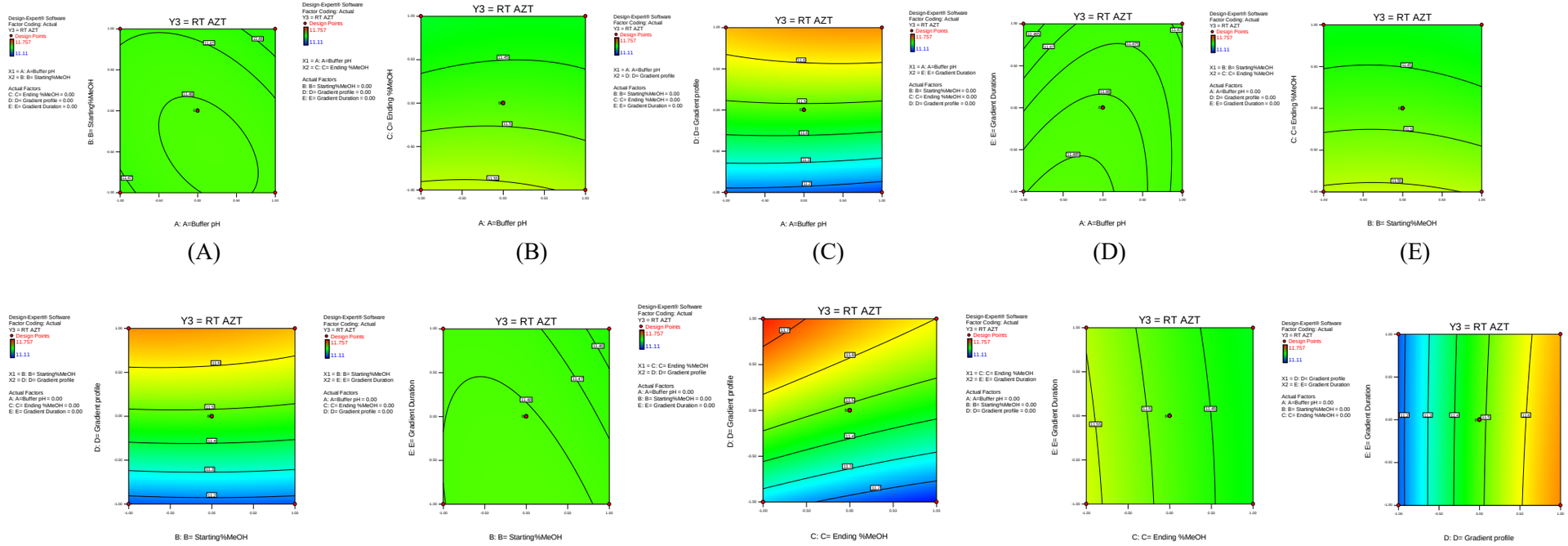

Figure 1.11A Contour plots depicting the impact of (A) start % MeOH and buffer pH, (B) end % MeOH and buffer pH, (C) gradient profile and buffer pH, (D) gradient duration and buffer pH, (E) end % MeOH and start % MeOH, (F) gradient profile and start% MeOH, (G) gradient duration and start % MeOH, (H) gradient profile and end % MeOH, (I) gradient duration and End % MeOH and (H) gradient duration and gradient profile on the RT for AZT.

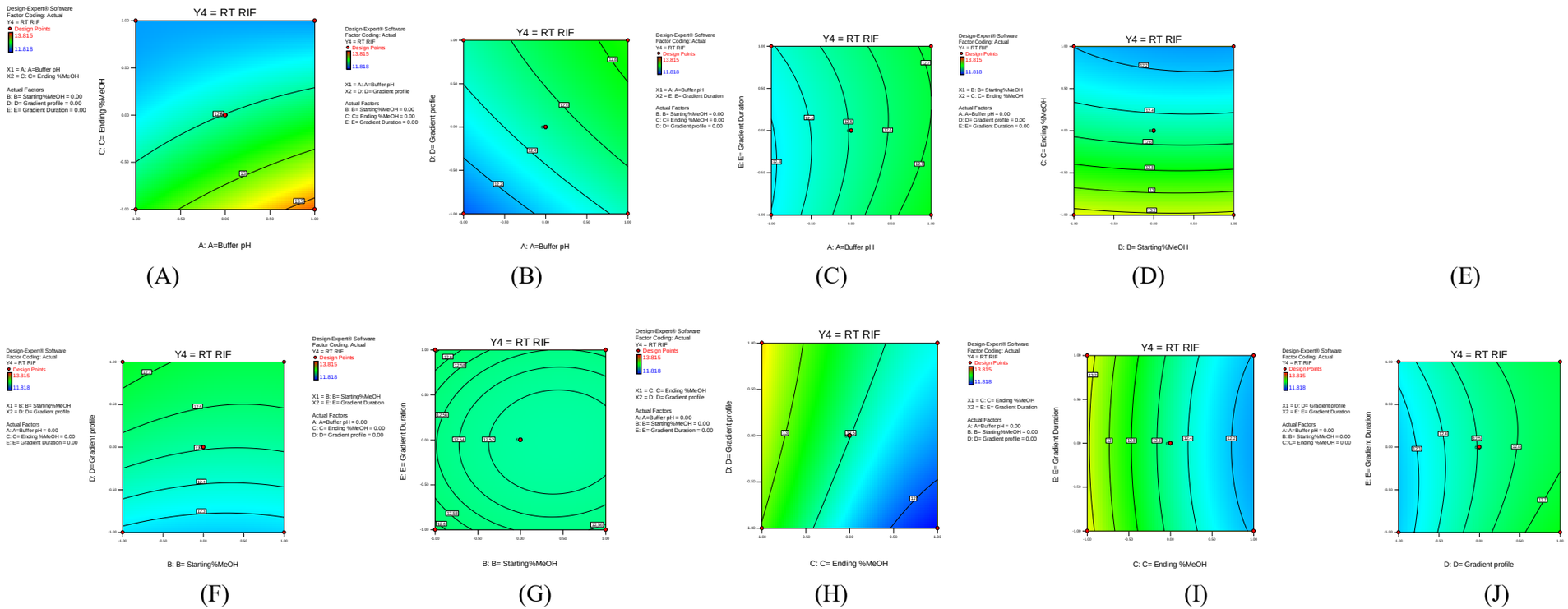

Figure 1.12A Contour plots depicting the impact of (A) start % MeOH and buffer pH, (B) end % MeOH and buffer pH, (C) gradient profile and buffer pH, (D) gradient duration and buffer pH, (E) end % MeOH and start % MeOH, (F) gradient profile and start% MeOH, (G) gradient duration and start % MeOH, (H) gradient profile and end % MeOH, (I) gradient duration and End % MeOH and (H) gradient duration and gradient profile on the RT for RIF.

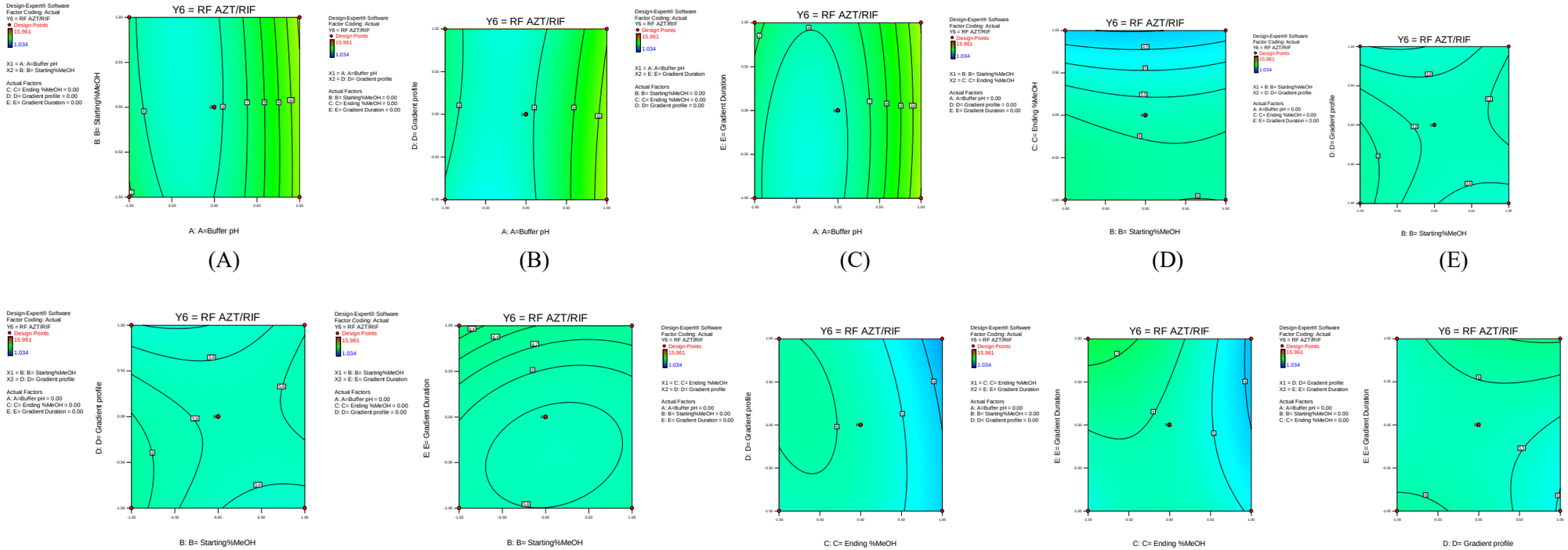

Figure 1.13A Contour plots depicting the impact of (A) start % MeOH and buffer pH, (B) end % MeOH and buffer pH, (C) gradient profile and buffer pH, (D) gradient duration and buffer pH, (E) end % MeOH and start % MeOH, (F) gradient profile and start% MeOH, (G) gradient duration and start % MeOH, (H) gradient profile and end % MeOH, (I) gradient duration and End % MeOH and (H) gradient duration and gradient profile on the RF for AZT/RIF.

.

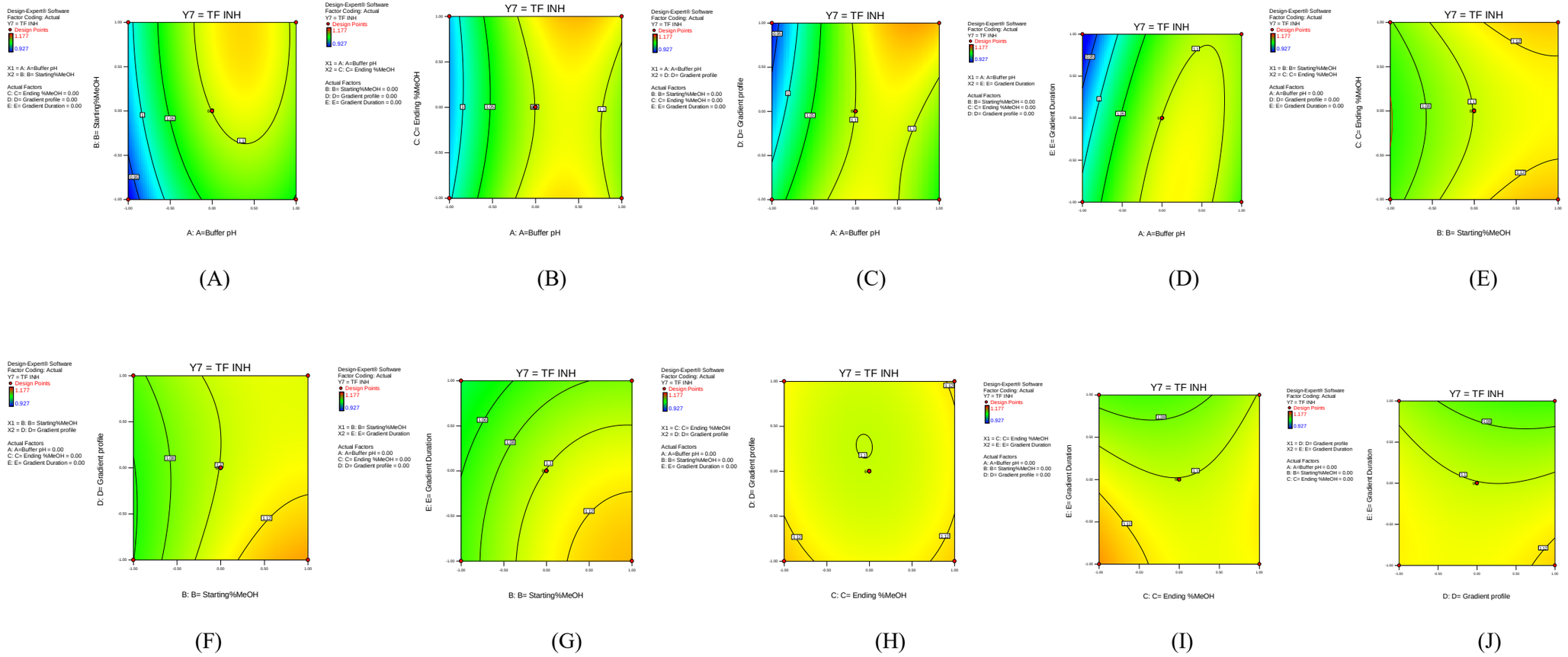

Figure 1.14A Contour plots depicting the impact of (A) start % MeOH and buffer pH, (B) end % MeOH and buffer pH, (C) gradient profile and buffer pH, (D) gradient duration and buffer pH, (E) end % MeOH and start % MeOH, (F) gradient profile and start% MeOH, (G) gradient duration and start % MeOH, (H) gradient profile and end % MeOH, (I) gradient duration and End % MeOH and (H) gradient duration and gradient profile on the TF for INH.

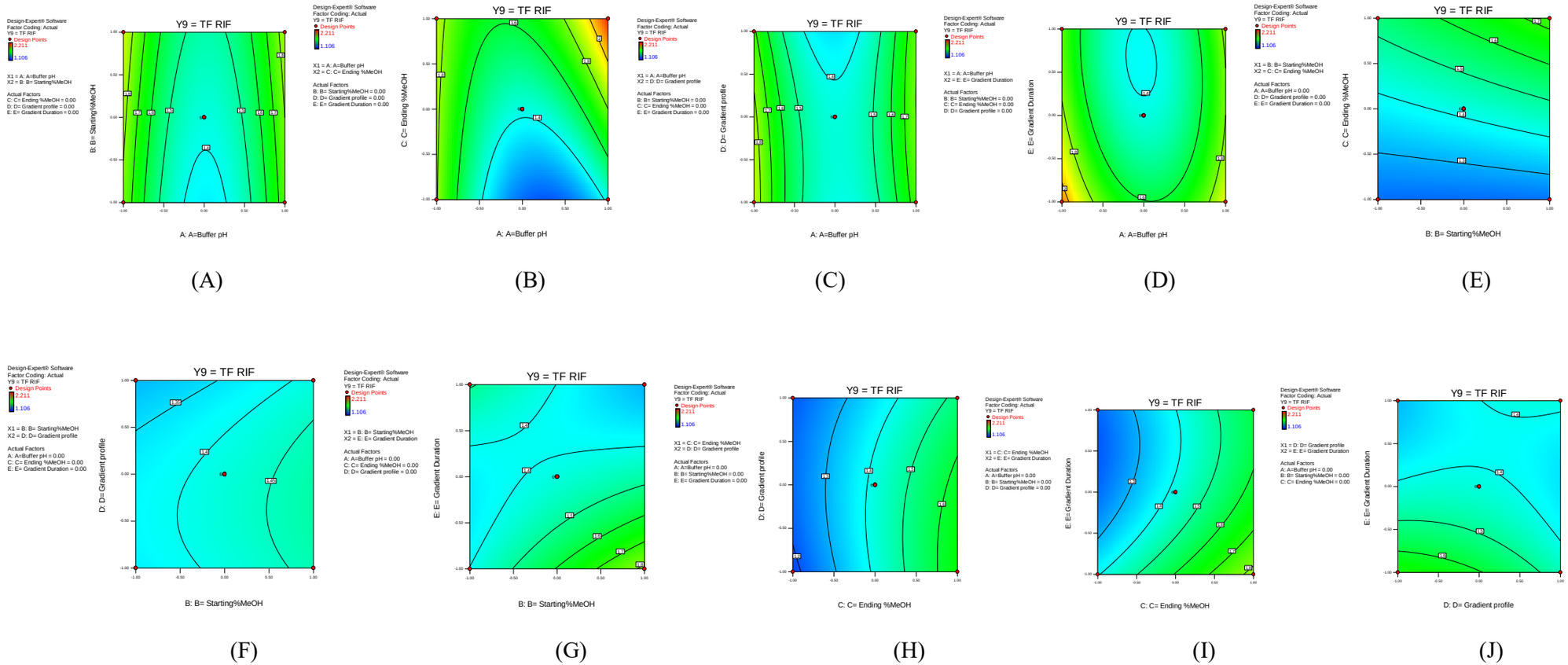

Figure 1.15A Contour plots depicting the impact of (A) start % MeOH and buffer pH, (B) end % MeOH and buffer pH, (C) gradient profile and buffer pH, (D) gradient duration and buffer pH, (E) end % MeOH and start % MeOH, (F) gradient profile and start% MeOH, (G) gradient duration and start % MeOH, (H) gradient profile and end % MeOH, (I) gradient duration and End % MeOH and (H) gradient duration and gradient profile on the TF for RIF.

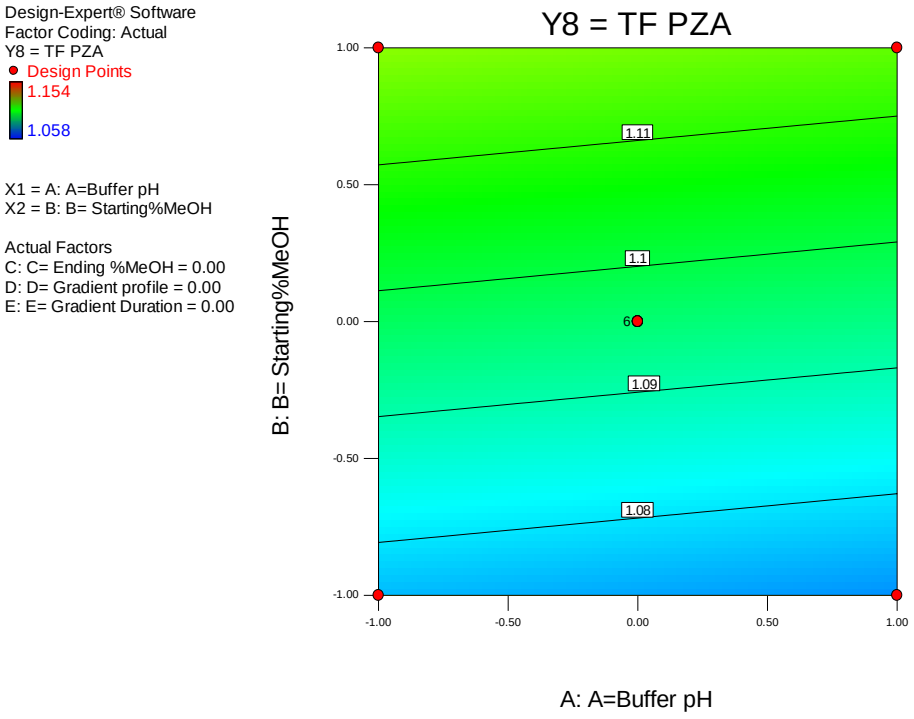

Figure 1.16A Contour plot depicting the impact of start % MeOH and buffer pH on the TF for PZA.

APPENDIX 1B

DIAGNOSTICS PLOTS, ANOVA DATA AND CONTOUR PLOTS FOR EVALUATION OF ENCAPSULAION EFFICIENCY, PERCENT YIELD AND PERCENT INH RELEASED FOR THE HYBRID DESIGN USED TO OPTIMIZE GASTRIC RESISTANT SUSTAINED RELEASE INH MICROSPHERES

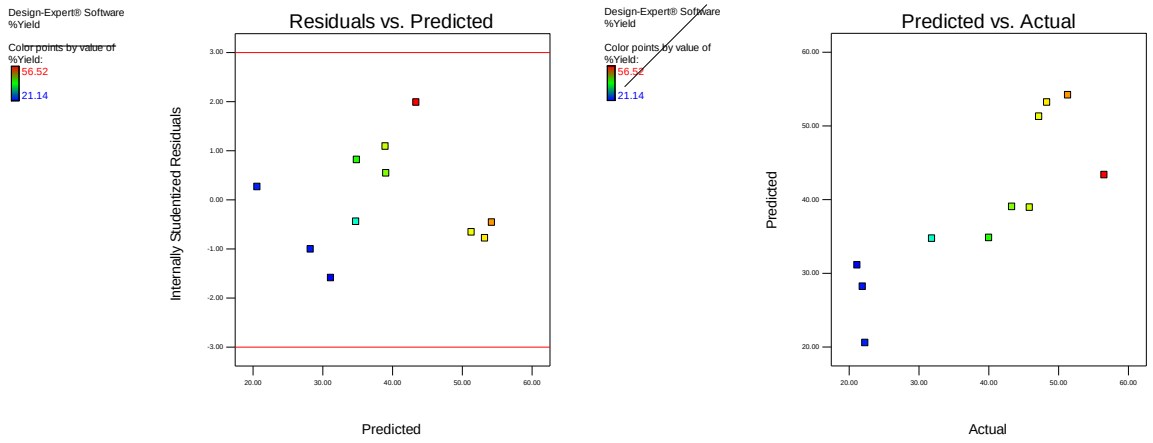

(A) (B)

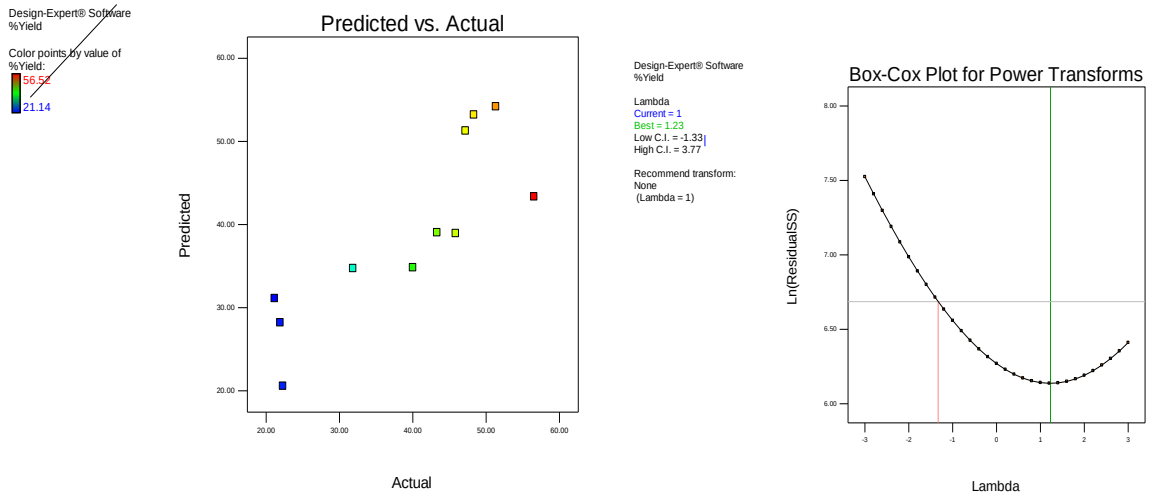

(C) (D)

Figure 1.1B Plot of (A) residuals versus predicted responses, (B) predicted versus actual responses, (C) predicted versus actual responses and (D) Box-Cox plot for power transformation for % yield.

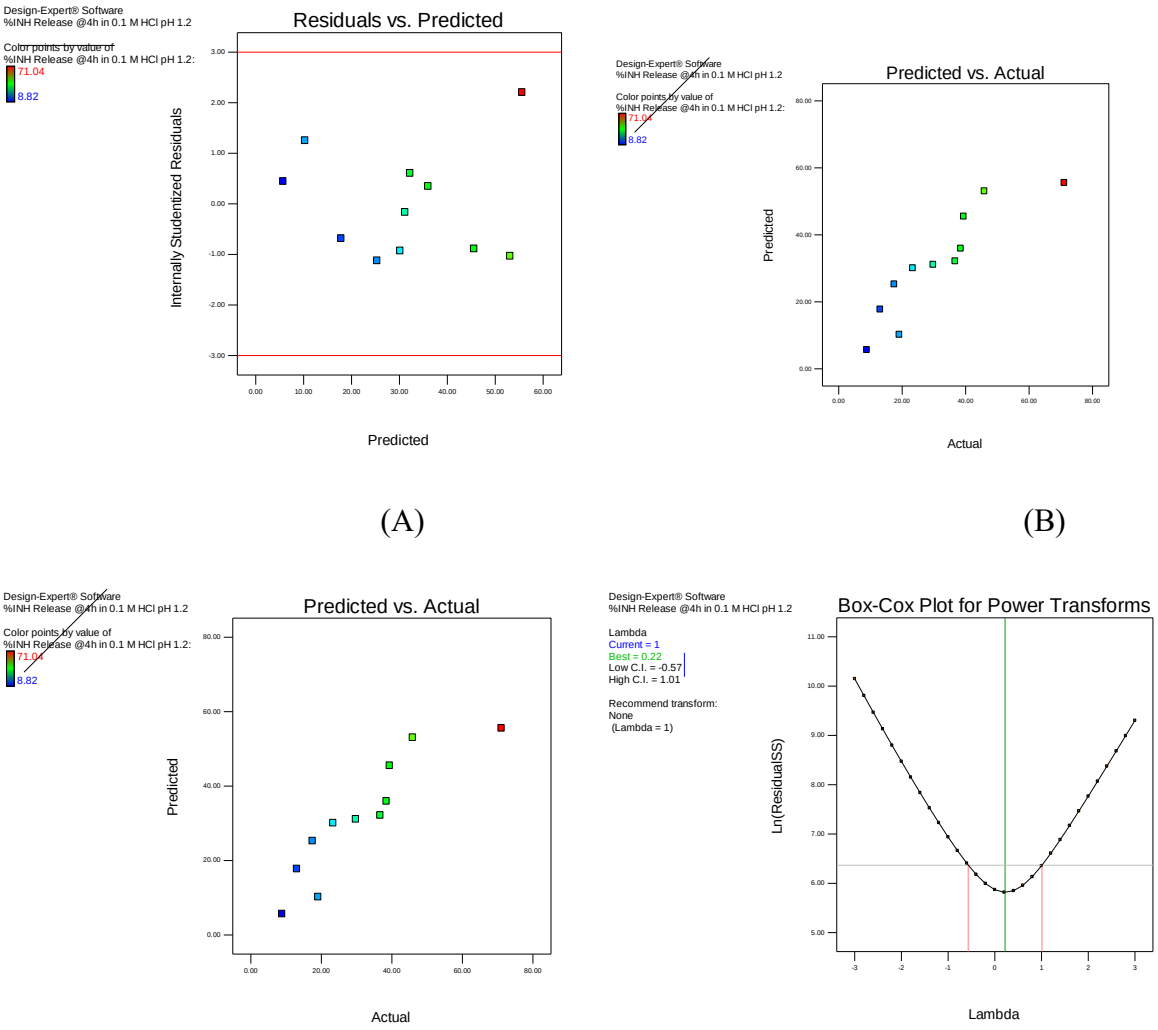

Figure 1.2B Plot of (A) residuals versus predicted responses, (B) predicted versus actual responses, (C) predicted versus actual responses and (D) Box-Cox plot for power transformation for % INH released at 4 h in pH 1.2 0.1 M HCl.

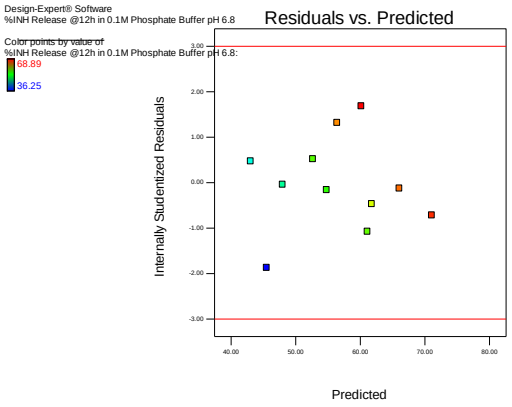

(A)

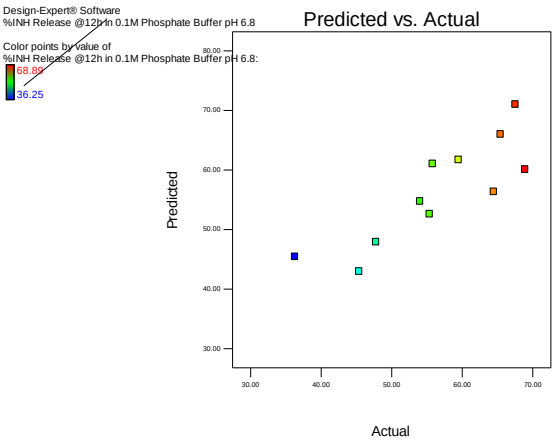

(B)

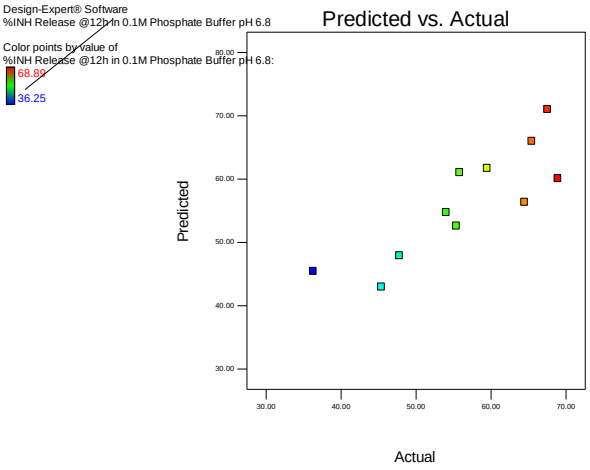

(C)

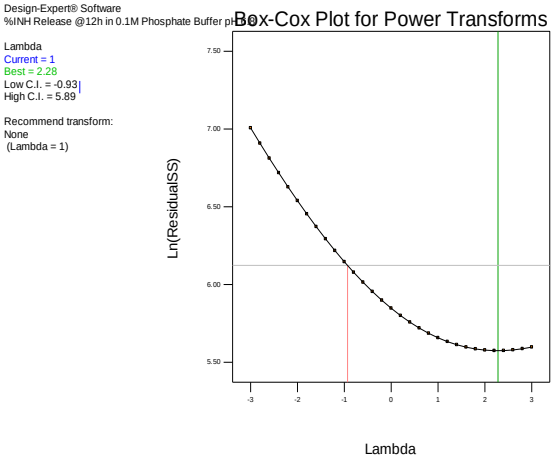

(D)

Figure 1.3B Plot of (A) residuals versus predicted responses, (B) predicted versus actual responses, (C) predicted versus actual responses and (D) Box-Cox plot for power transformation for % INH released at 12 h in pH 6.8 0.1 M phosphate buffer.

Table 1.1B ANOVA data for linear model [Partial sum of squares - Type III] for % INH released at 12 h in pH 6.8 0.1 M phosphate buffer.

Source	Sum of squares	Df	Mean square	F-value	p-value	Prob > F
Panel A						
Model	758.36	3	252.79	6.18	0.0223	Significant
A-HPMC-AS	529.57	1	529.57	12.94	0.0088	Significant
B-Eudragit® L100	172.57	1	172.57	4.22	0.0791	
C-Homogenization speed	56.21	1	56.21	1.37	0.2795	
Residual	286.43	7	40.92			
Cor total	1044.79	10				
Panel B						
Std. deviation	6.4					
Mean	56.38					
%C.V	11.35					
Press	658.1					
R^2	0.7258					
Adjusted R^2	0.6084					
Predicted R^2	0.3701					
Adeq precision	7.268					

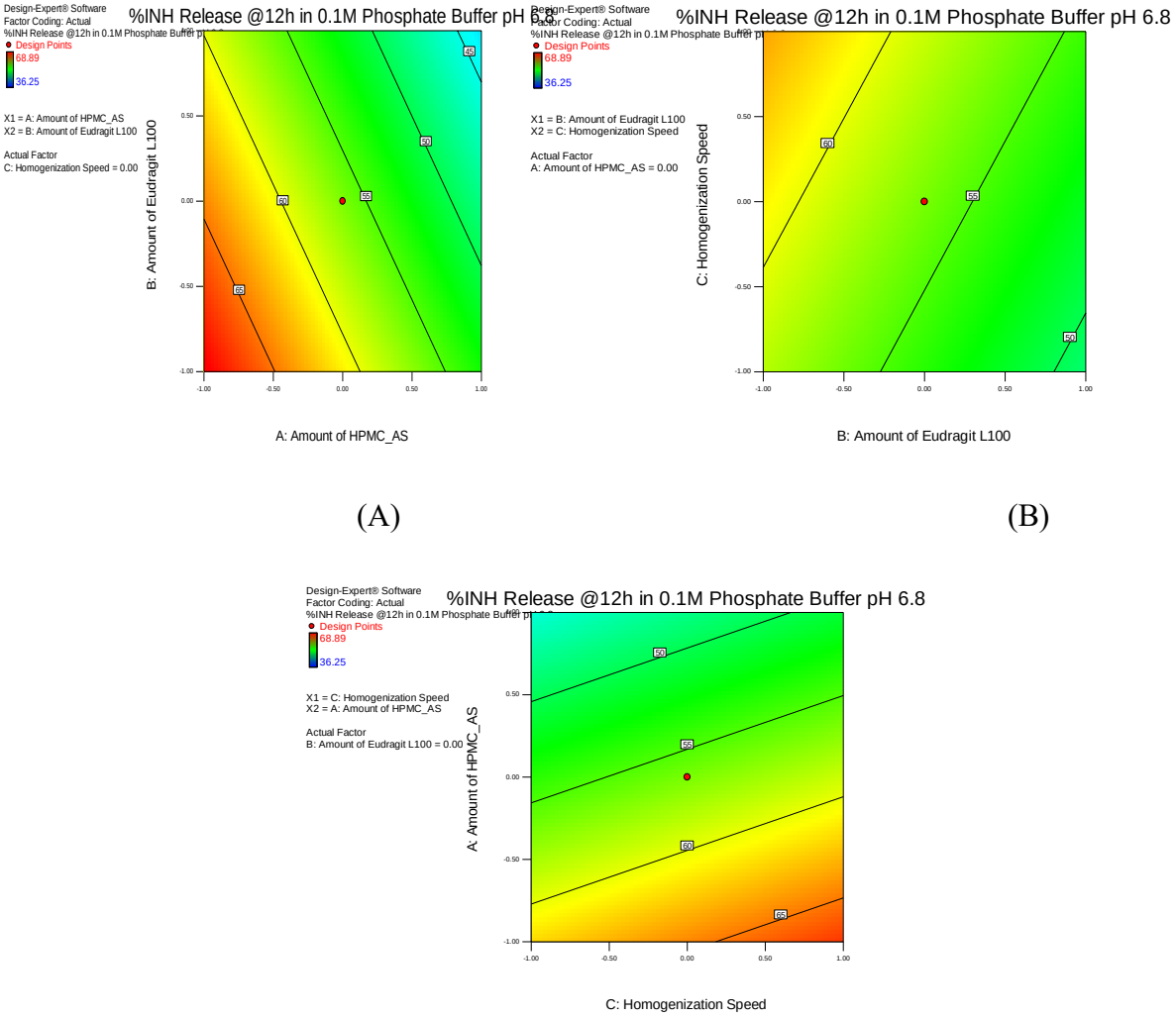

Figure 1.4B Contour plots depicting the impact of (A) HPMC-AS and Eudragit®L100 content, (B) homogenization speed and HPMC-AS content and (C) Eudragit® L100 content and homogenization speed on % INH released at 12 h in pH 6.8 0.1 M phosphate buffer.

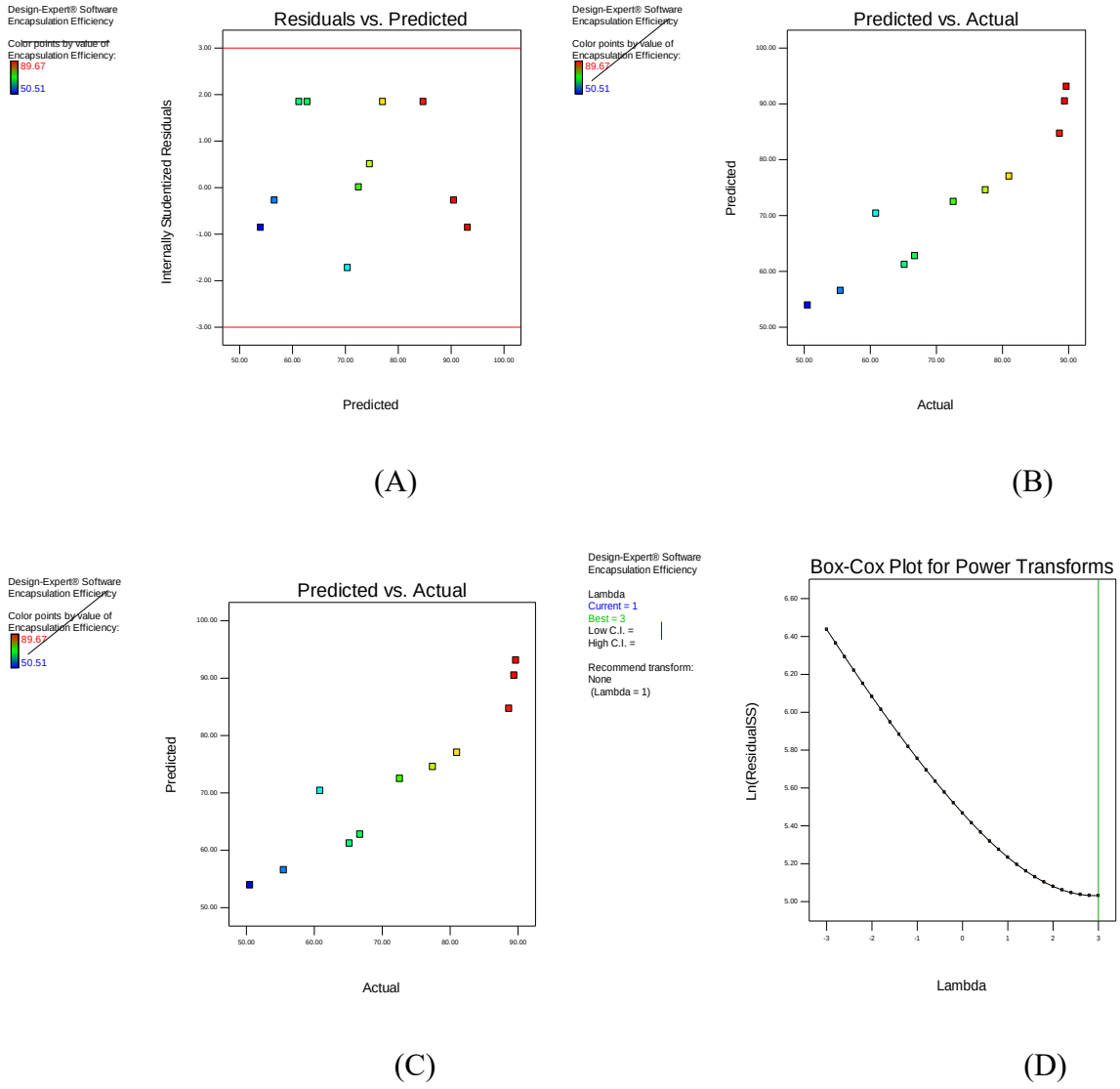

Figure 1.5B Plot of (A) residuals versus predicted responses, (B) predicted versus actual responses, (C) predicted versus actual responses and (D) Box-Cox plot for power transformation for encapsulation efficiency of INH.

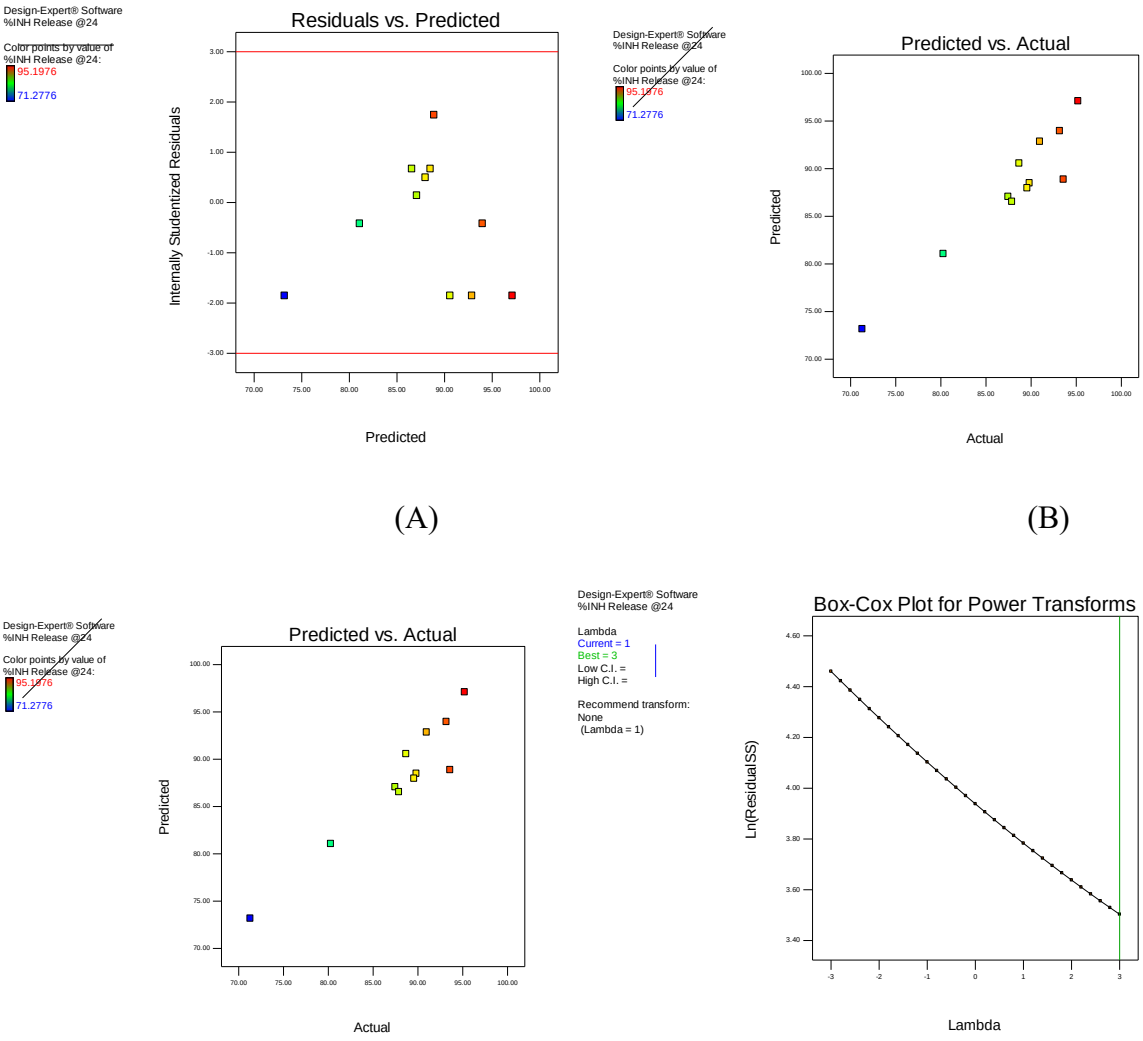

Figure 1.6B Plot of (A) residuals versus predicted responses, (B) predicted versus actual responses, (C) predicted versus actual responses and (D) Box-Cox plot for power transformation for % INH released at 24 h in pH 6.8 0.1 M phosphate buffer.

APPENDIX 1C

DIAGNOSTICS PLOTS FOR % RIF RELEASED, BUOANCY, YIELD, ENCAPSULATION EFFICIENCY AND FLOATING LAG TIME FOR THE OPTIMZATION OF MICROPOROUS FLOATING SUSTAINED RELEASE RIFAMPICIN MICROSPHERES

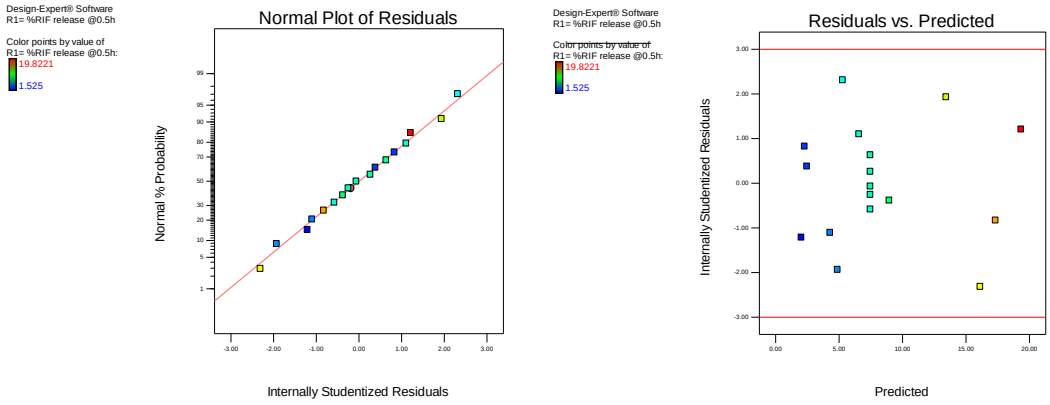

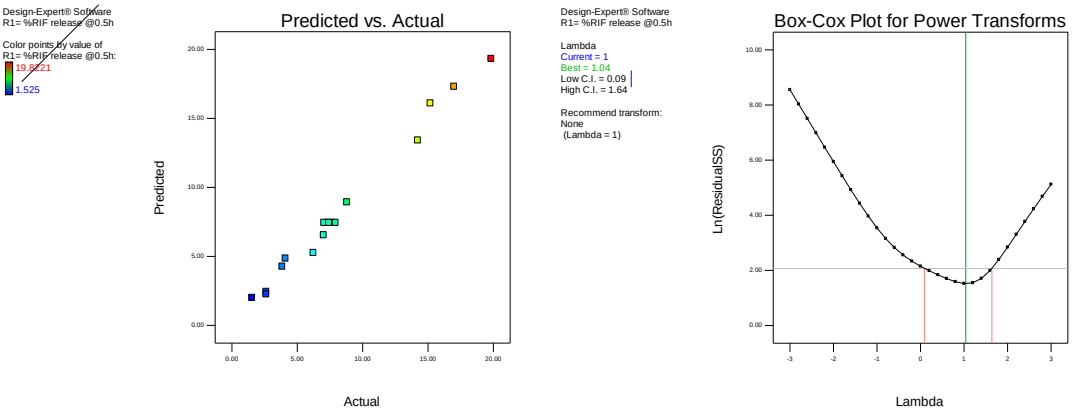

Figure 1.1C Plots of (A) normal plot of residuals, (B) residuals versus predicted responses, (C) predicted versus actual responses and (D) Box-Cox plot for power transformation for % RIF released at 0.5 h.

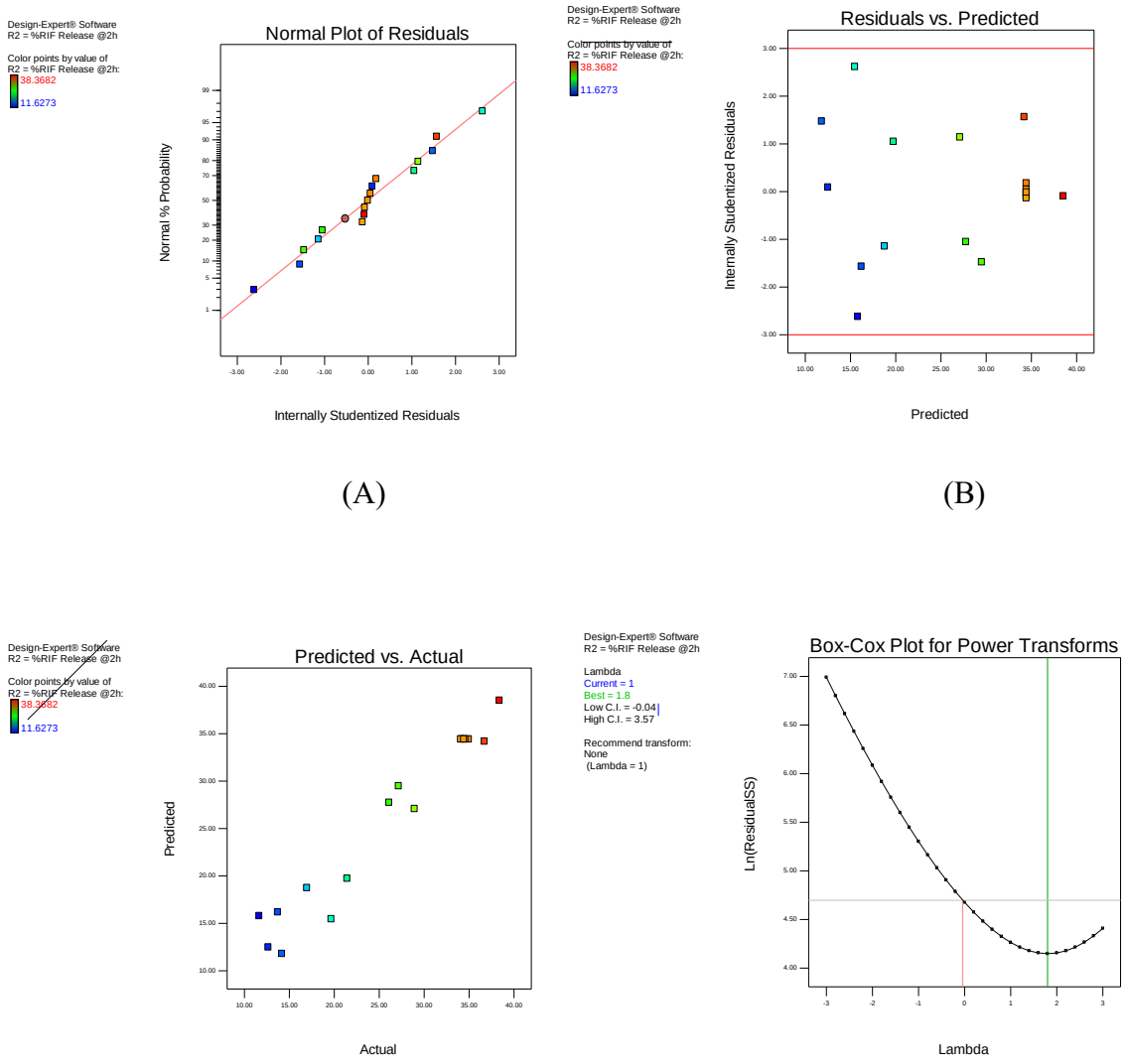

Figure 1.2C Plots of (A) normal plot of residuals, (B) residuals versus predicted responses, (C) predicted versus actual responses and (D) Box-Cox plot for power transformation for % RIF released at 2 h.

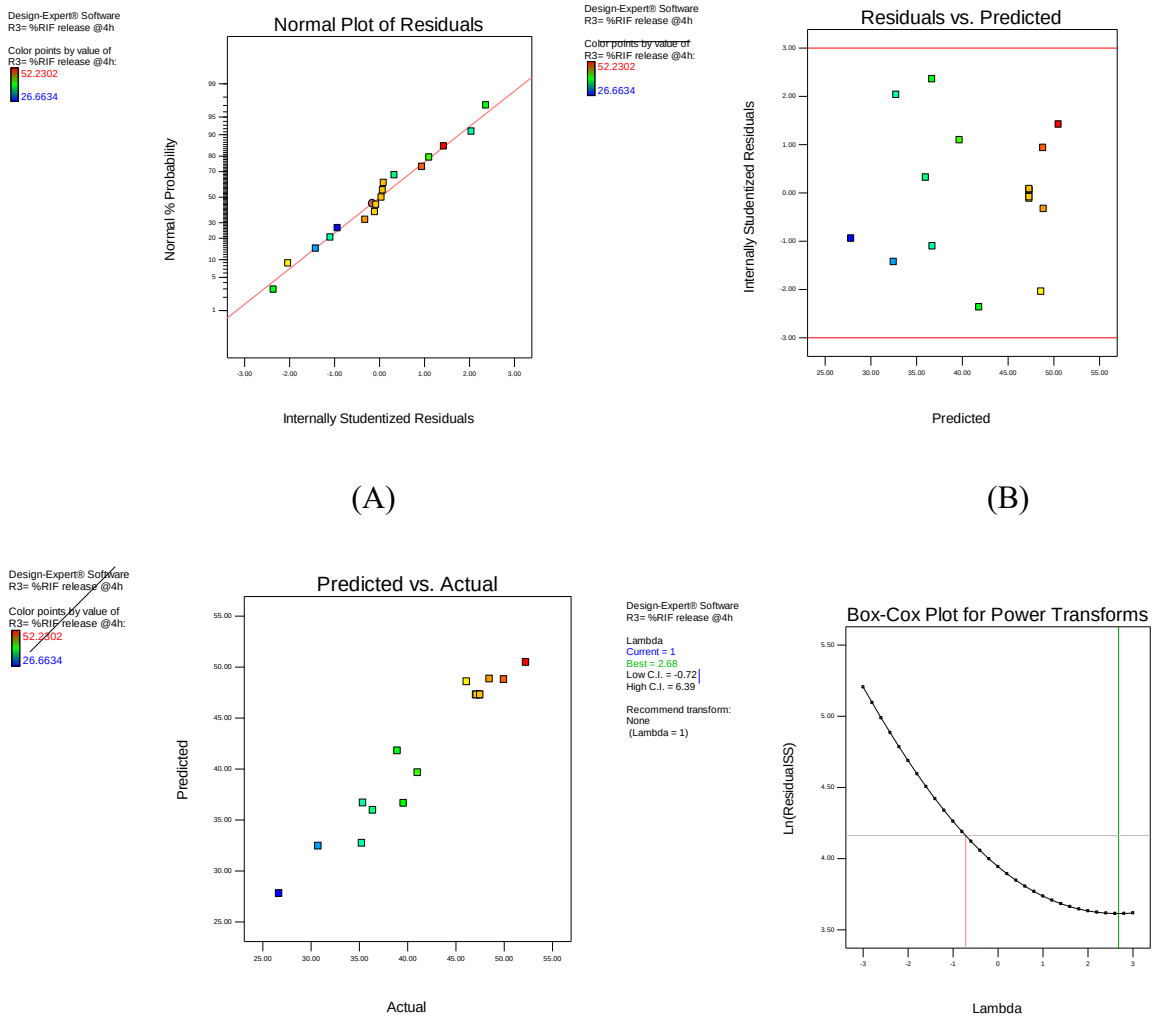

Figure 1.3C Plot of (A) normal plot of residuals, (B) residuals versus predicted responses, (C) predicted versus actual responses and (D) Box-Cox plot for power transformation for % RIF released at 4 h.

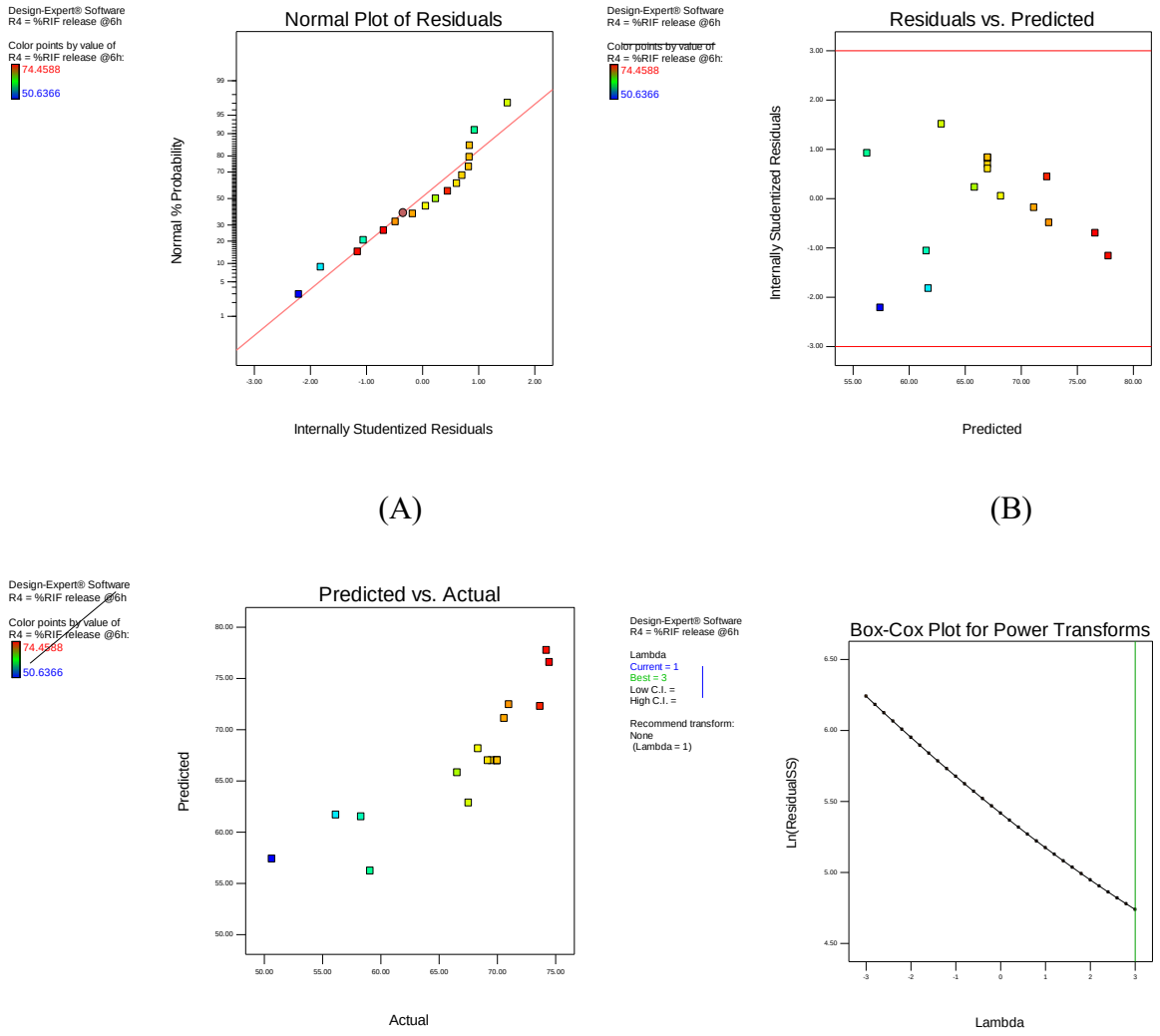

Figure 1.4C Plots of (A) normal plot of residuals, (B) residuals versus predicted responses, (C) predicted versus actual responses and (D) Box-Cox plot for power transformation for % RIF released at 6 h.

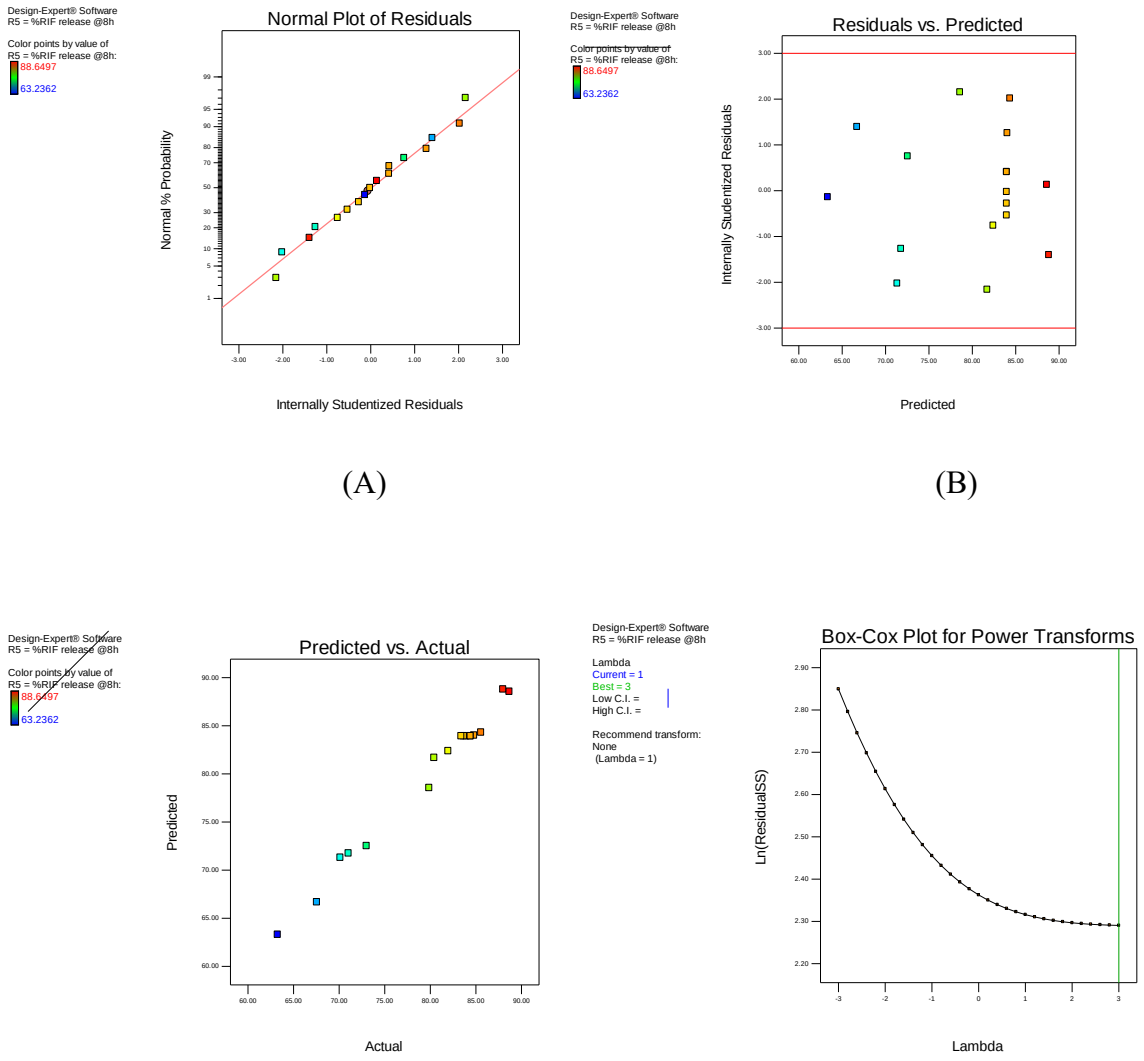

Figure 1.5C Plots of (A) normal plot of residuals, (B) residuals versus predicted responses, (C) predicted versus actual responses and (D) Box-Cox plot for power transformation for % RIF released at 8 h.

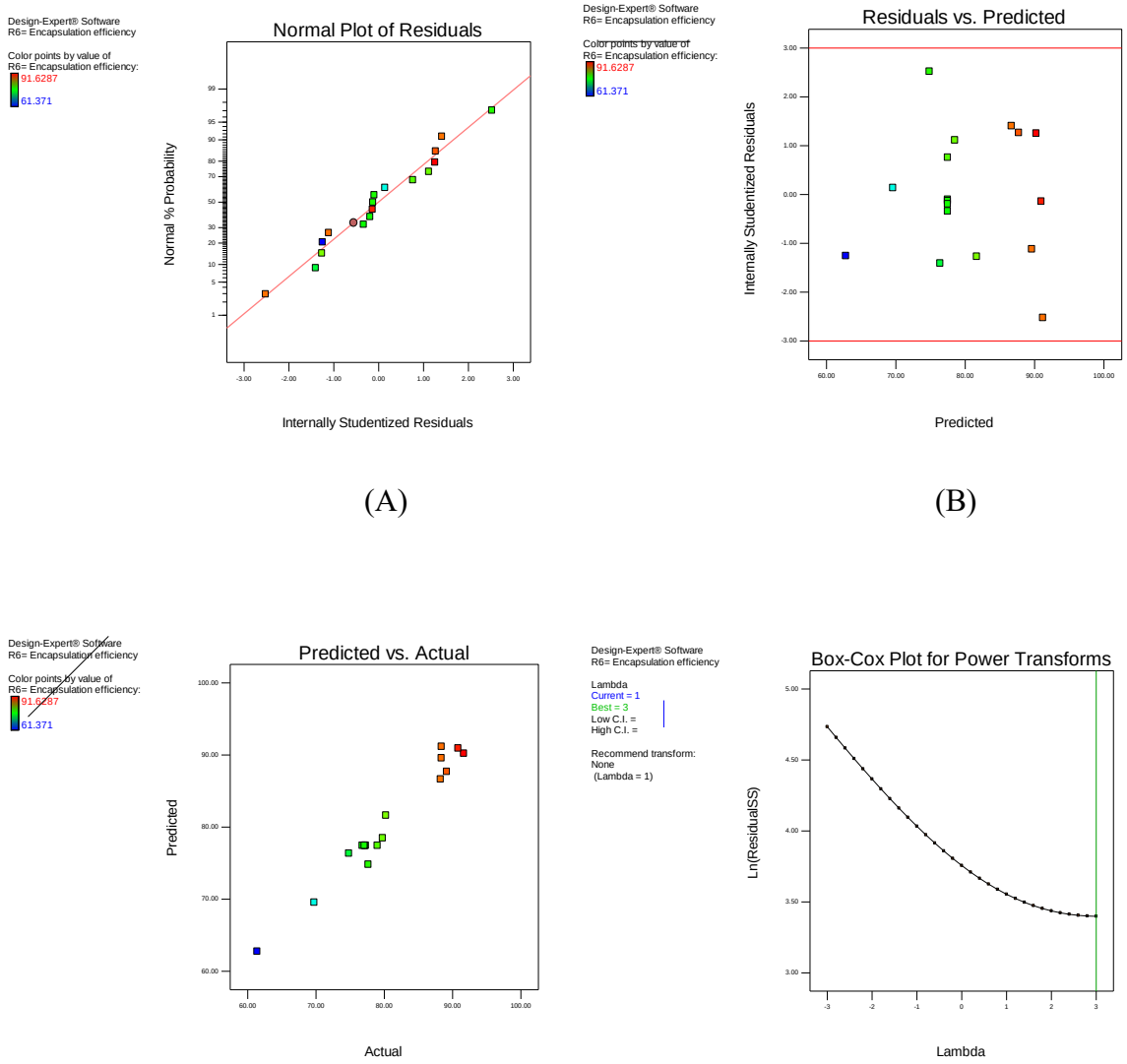

Figure 1.6C Plots of (A) normal plot of residuals, (B) residuals versus predicted responses, (C) predicted versus actual responses and (D) Box-Cox plot for power transformation for encapsulation efficiency of RIF.

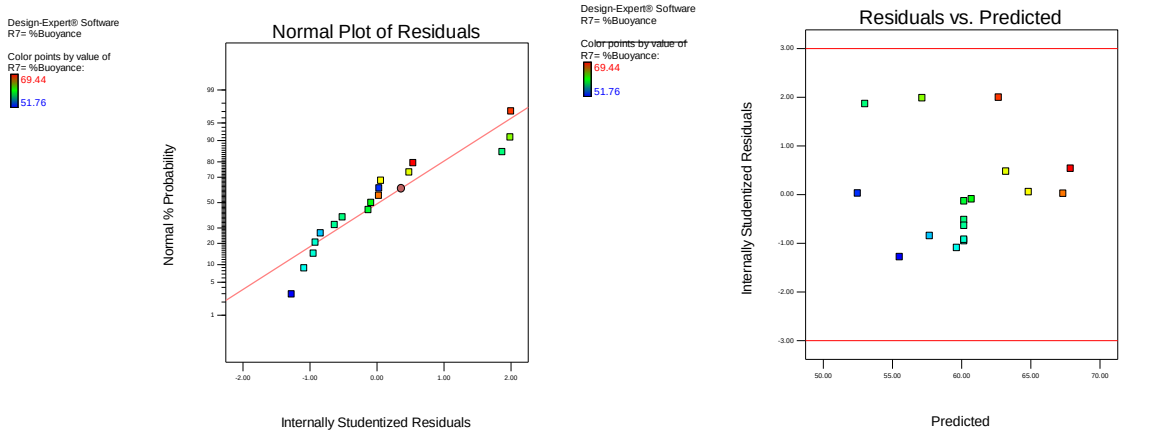

(A) (B)

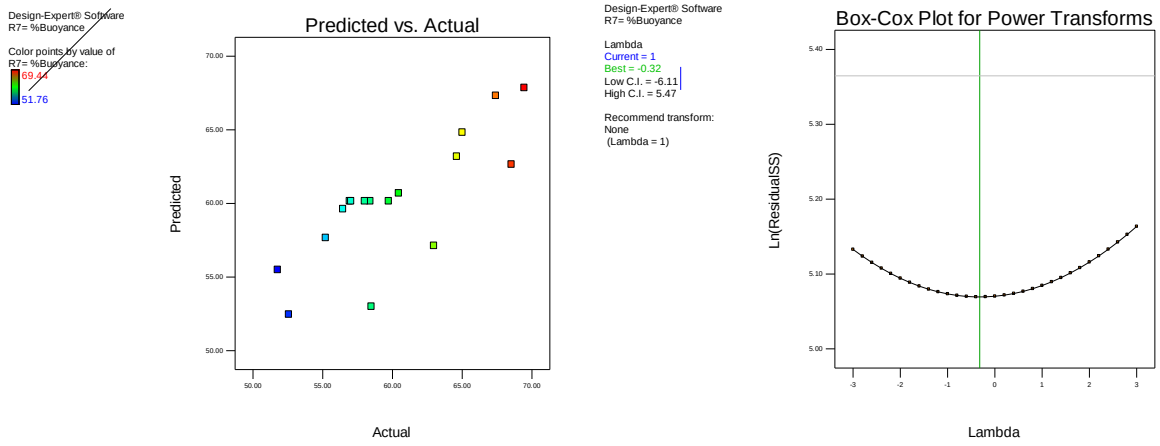

(C) (D)

Figure 1.7C Plots of (A) normal plot of residuals, (B) residuals versus predicted responses, (C) predicted versus actual responses and (D) Box-Cox plot for power transformation for % buoyancy of RIF microspheres.

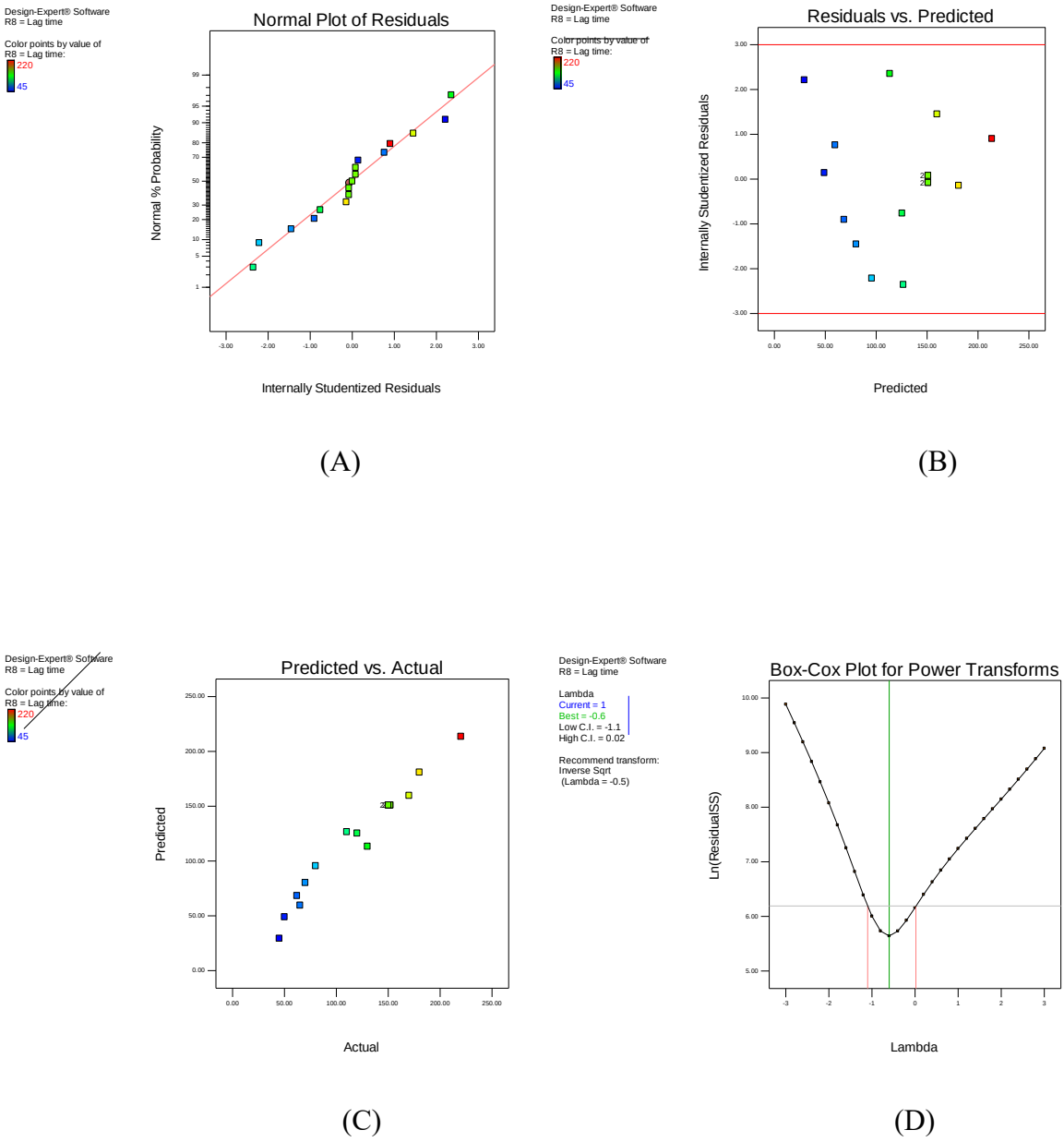

Figure 1.8C Plot of (A) normal plot of residuals, (B) residuals versus predicted responses, (C) predicted versus actual responses and (D) Box-Cox plot for power transformation for floating lag time of RIF microspheres.

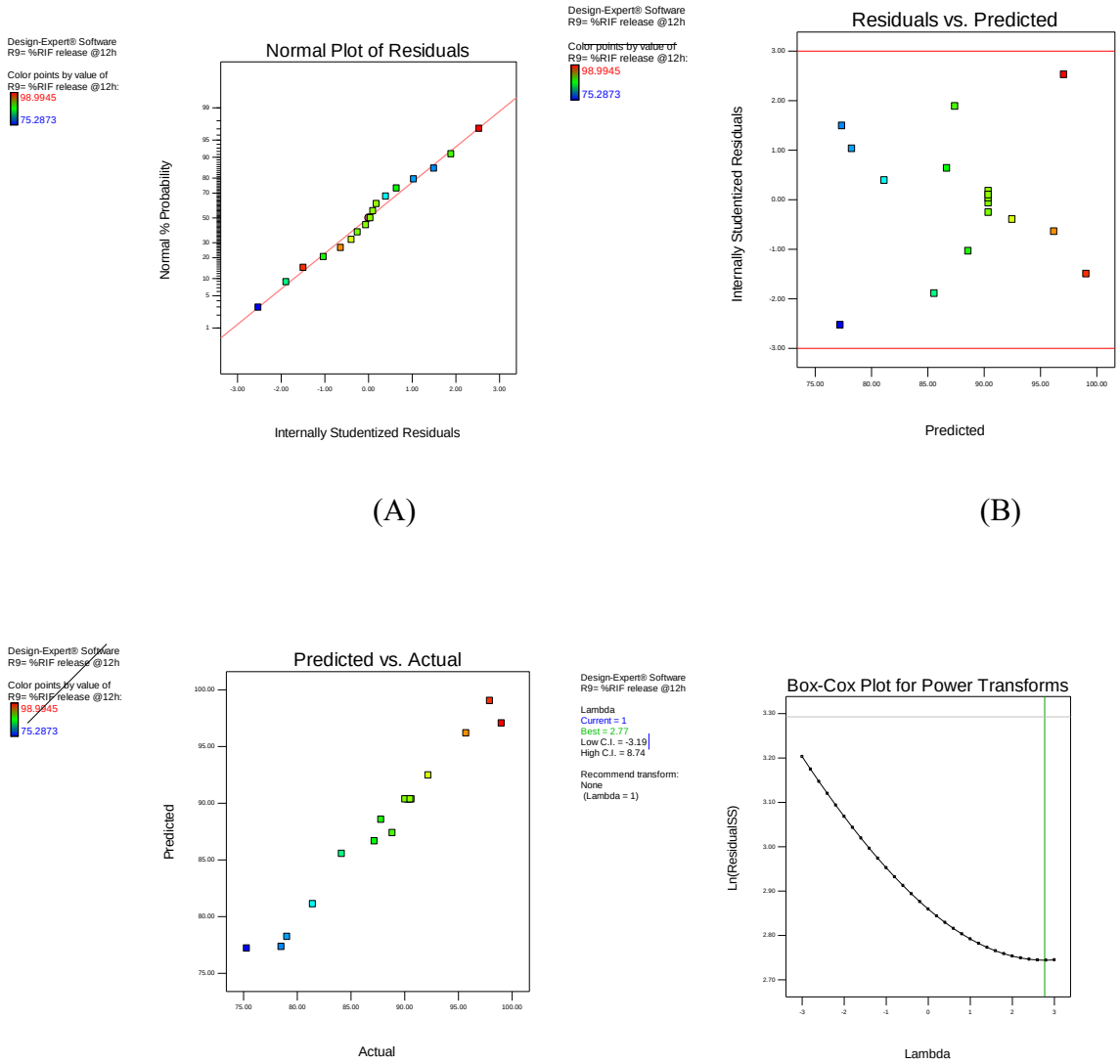

Figure 1.9C Plots of (A) normal plot of residuals, (B) residuals versus predicted responses, (C) predicted versus actual responses and (D) Box-Cox plot for power transformation for % RIF released at 12 h.

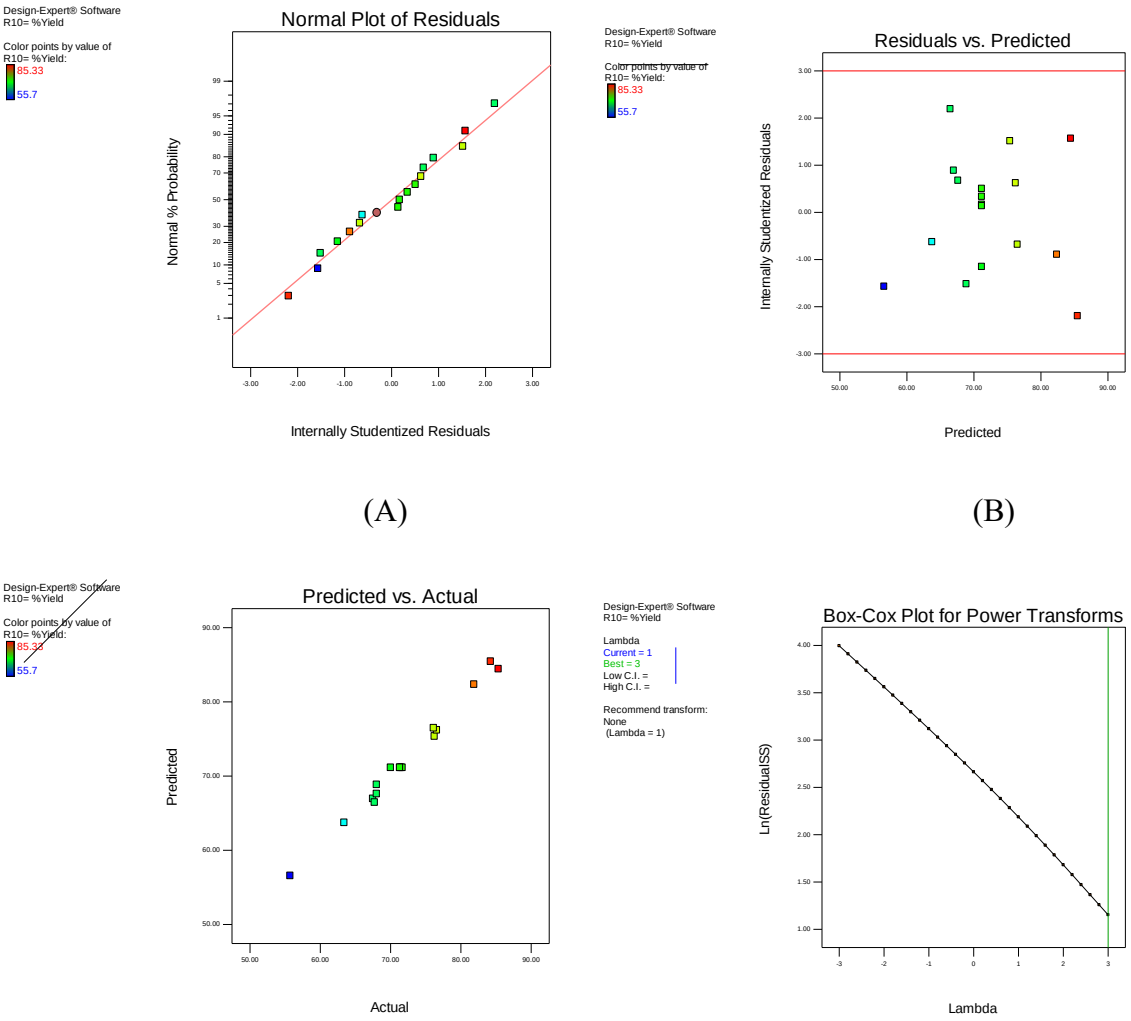

Figure 1.10C Plots of (A) normal plot of residuals, (B) residuals versus predicted responses, (C) predicted versus actual responses and (D) Box-Cox plot for power transformation for % yield.

APPENDIX 2A

BATCH SUMMARIES FOR THE MANUFACTURE OF GASTRIC RESISTANT SUSTAINED RELEASE INH MICROSPHERES

BATCH SUMMARY – Batch INH-001

Faculty of Pharmacy, Rhodes University

Formulator:	Chiluba Mwila	Batch size:	7.16 g
Product:	INH microspheres	Microencapsulation Time (start):	08:00
Batch Number:	INH-001	(end):	13:00
Date of Manufacture	Date: 30-03-2017		

Material	Amount added (g)	Rhodes RM #
INH	0.75	RM000339
HPMC-AS	3.41	RM000351
Eudragit® L100	2.0	RM000016
Avicel® PH101	1.0	RM000038
Liquid paraffin	125.0 mL	
Acetone	50.0 mL	
Span 80	1.25 mL	

Dissolution profile

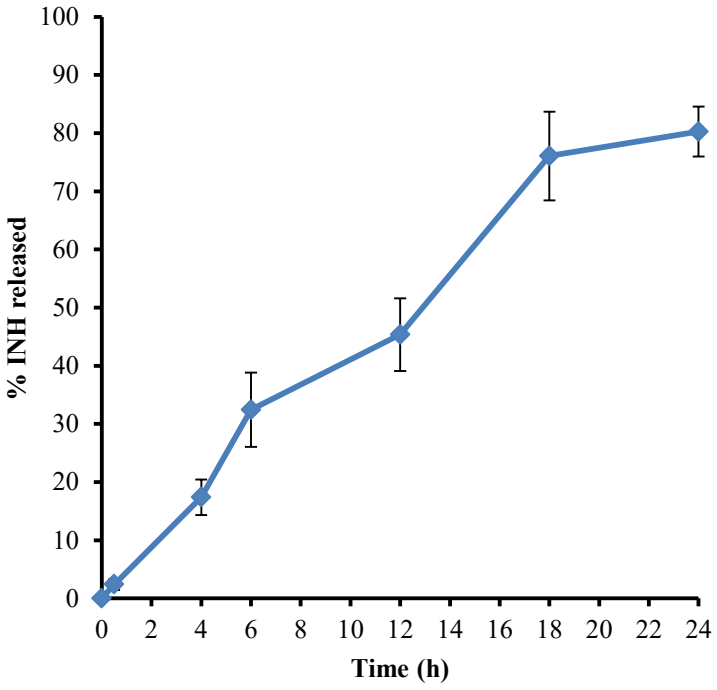

SEM

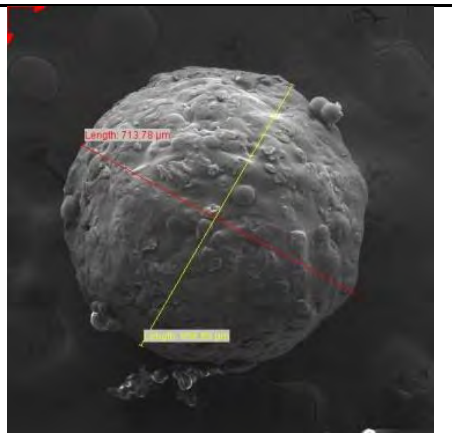

Comments

-Spherical
-rough surface
-hard/bouncy and free flowing
-% yield = 51.32
-Temperature = 22.0°C
-Drying Temperature 30.0°C
-Drying time = 18 h
-Homogenization speed = 1500 rpm

BATCH SUMMARY – Batch INH-002

Faculty of Pharmacy, Rhodes University

Formulator:	Chiluba Mwila	Batch size:	5.75 g
Product:	INH microspheres	Microencapsulation Time (start):	14:00
Batch Number:	INH-002	(end):	19:00
Date of manufacture:	02-04-2017		

Material	Amount added (g)	Rhodes RM#
INH	0.75	RM000339
HPMC-AS	2.0	RM000351
Eudragit® L100	2.0	RM000016
Avicel® PH101	1.0	RM000038
Liquid paraffin	125.0 mL	
Acetone	50.0 mL	
Span 80	1.25 mL	

Dissolution profile

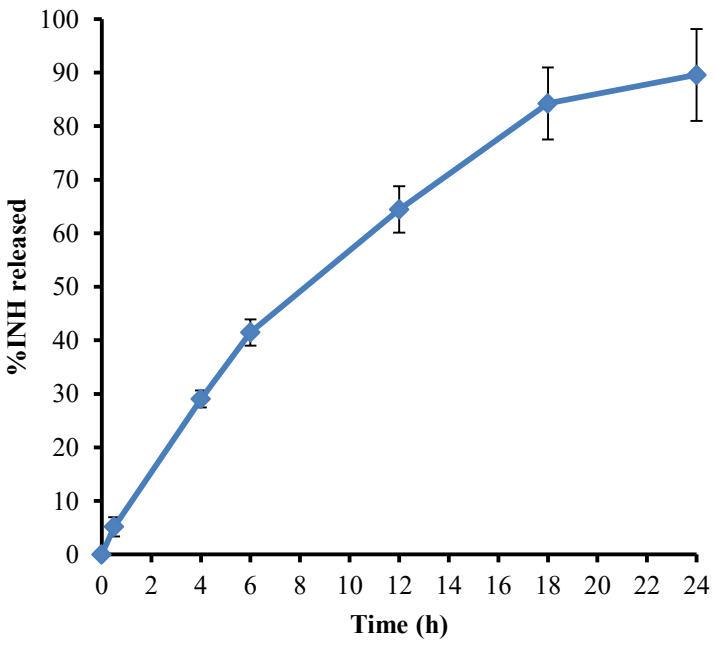

SEM

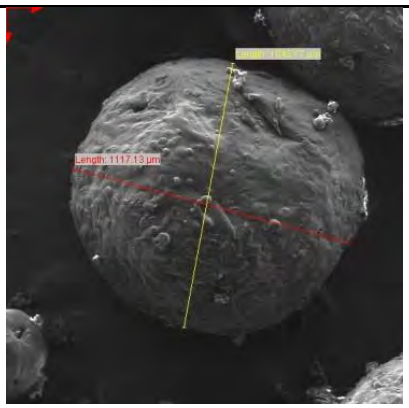

Comments

-Spherical
-rough surface
-hard/bouncy and free flowing
-%yield = 43.3
-Temperature = 22.0°C
-Drying Temperature 30.0°C
-Drying time = 18 h
-Homogenization speed = 2000 rpm

BATCH SUMMARY – Batch INH-003

Faculty of Pharmacy, Rhodes University

Formulator:	Chiluba Mwila	Batch size:	5.75 g
Product:	INH microspheres	Microencapsulation Time (start):	07:00
Batch Number:	INH-003	(end):	12:00
Date of manufacture:	03-04-2017		

Material	Amount added (g)	Rhodes RM#
INH	0.75	RM000339
HPMC-AS	2.0	RM000351
Eudragit® L100	2.0	RM000016
Avicel® PH101	1.0	RM000038
Liquid paraffin	125.0 mL	
Acetone	50.0 mL	
Span 80	1.25 mL	

Dissolution profile

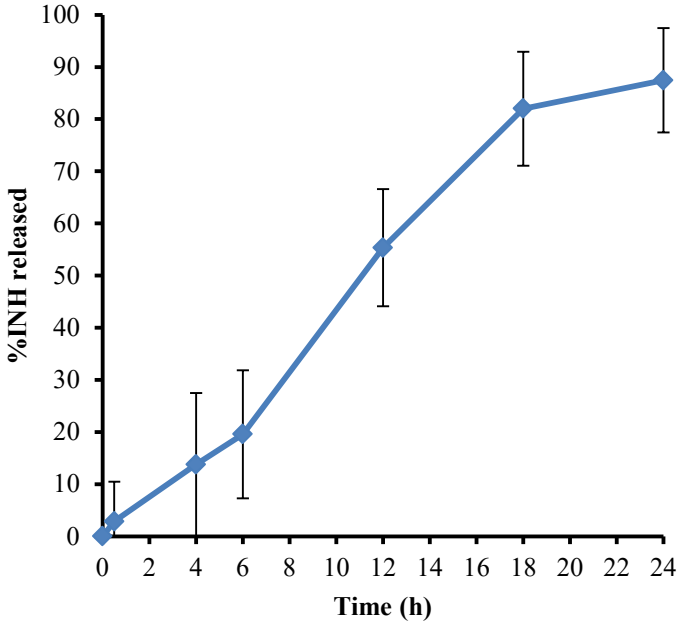

SEM

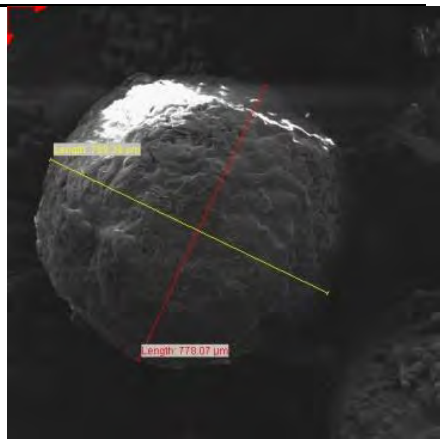

Comments

-Spherical
-rough surface
-hard/bouncy and free flowing
-%yield = 56.52
-Temperature = 22.0°C
-Drying Temperature 30.0°C
-Drying time = 18 h
-Homogenization speed = 500 rpm

BATCH SUMMARY – Batch INH-004

Faculty of Pharmacy, Rhodes University

Formulator:	Chiluba Mwila	Batch size:	7.75 g
Product:	INH microspheres	Microencapsulation Time (start):	15:00
Batch Number:	INH-004	(end):	20:00
Date of manufacture:	04-04-2017		

Material	Amount added (g)	Rhodes RM#
INH	0.75	RM000339
HPMC-AS	3.0	RM000351
Eudragit® L100	3.0	RM000016
Avicel® PH101	1.0	RM000038
Liquid paraffin	125.0 mL	
Acetone	50.0 mL	
Span 80	1.25 mL	

Dissolution profile

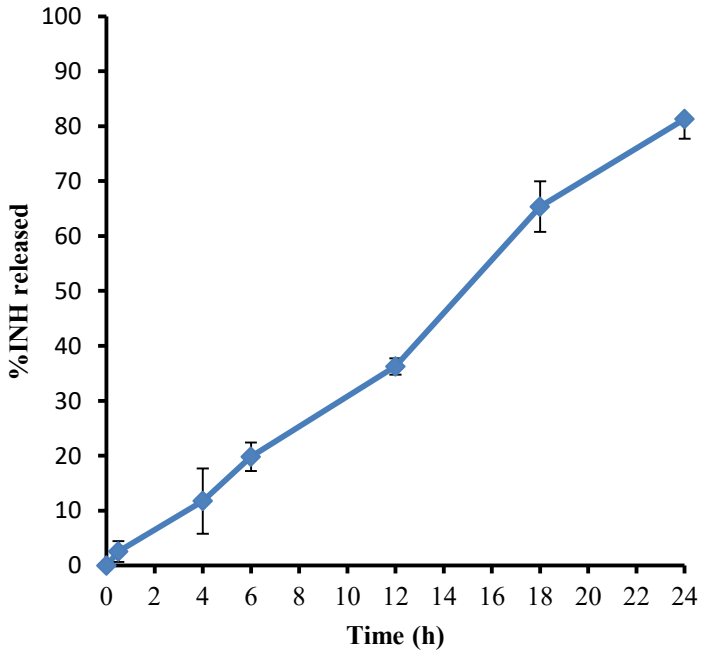

SEM

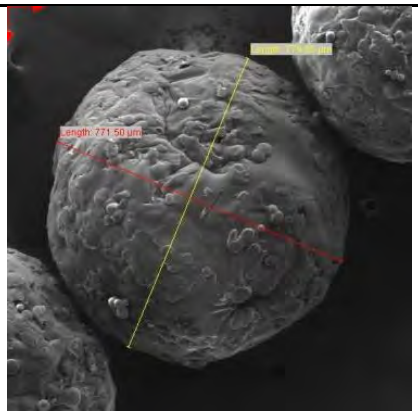

Comments

-Spherical
-rough surface
-hard/bouncy and free flowing
-%yield = 48.32
-Temperature = 22.0°C
-Drying Temperature 30.0°C
-Drying time = 18 h
-Homogenization speed = 2500 rpm
- <85% INH released after 24 h

BATCH SUMMARY – Batch INH-005

Faculty of Pharmacy, Rhodes University

Formulator:	Chiluba Mwila	Batch size:	4.325 g
Product:	INH microspheres	Microencapsulation Time (start):	08:00
Batch Number:	INH-005	(end):	13:00
Date of manufacture:	05-04-2017		

Material	Amount added (g)	Rhodes RM#
INH	0.75	RM000339
HPMC-AS	0.485	RM000351
Eudragit® L100	2.0	RM000016
Avicel® PH101	1.0	RM000038
Liquid paraffin	125.0 mL	
Acetone	50.0 mL	
Span 80	1.25 mL	

Dissolution profile

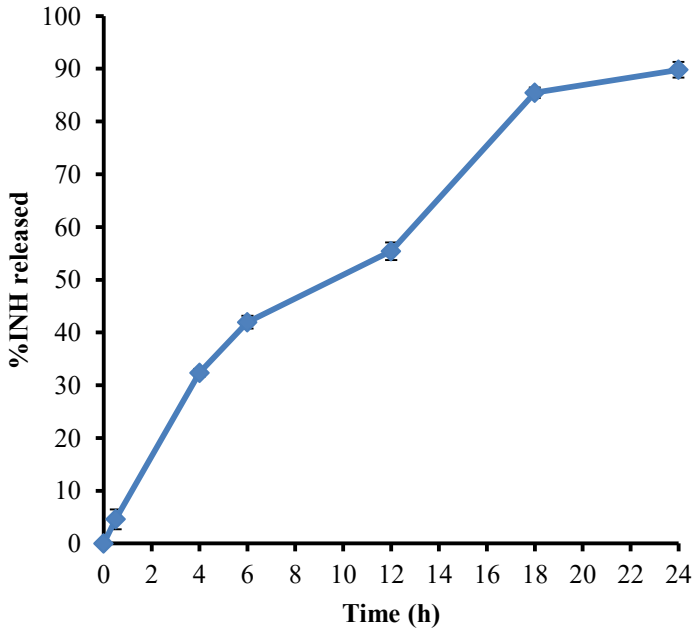

SEM

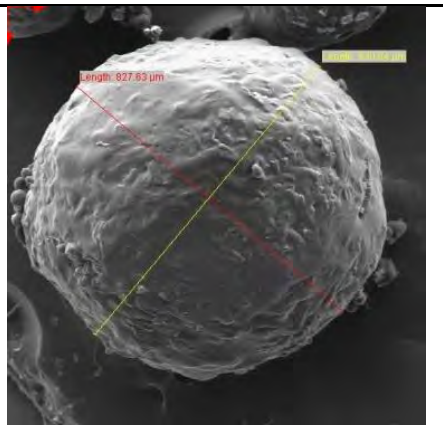

Comments

-Spherical
-slightly smooth surface
-hard/bouncy and free flowing
-%yield = 21.91
-Temperature = 22.0°C
-Drying Temperature 30.0°C
-Drying time = 18 h
-Homogenization speed = 1500 rpm

BATCH SUMMARY – Batch INH-006

Faculty of Pharmacy, Rhodes University

Formulator:	Chiluba Mwila	Batch size:	5.75 g
Product:	INH microspheres	Microencapsulation Time (start):	13:00
Batch Number:	INH-006	(end):	18:00
Date of manufacture:	08-04-2017		

Material	Amount added (g)	Rhodes RM#
INH	0.75	RM000339
HPMC-AS	3.0	RM000351
Eudragit® L100	1.0	RM000016
Avicel® PH101	1.0	RM000038
Liquid paraffin	125.0 mL	
Acetone	50.0 mL	
Span 80	1.25 mL	

Dissolution profile

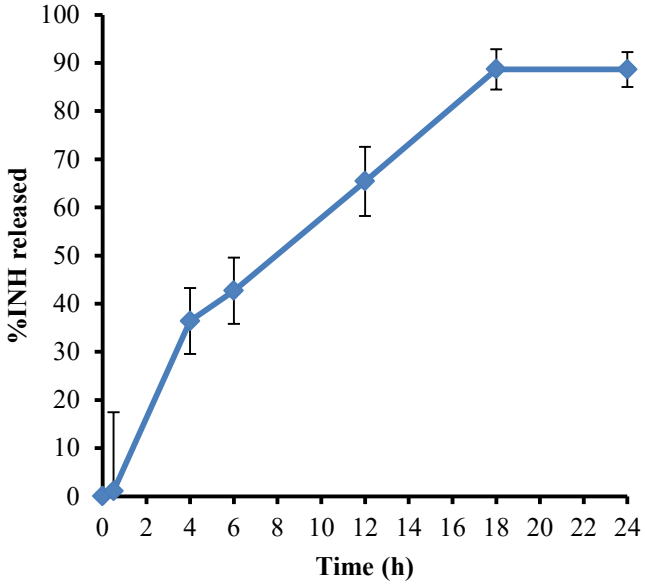

SEM

Comments

-Spherical
- rough surface
-hard/bouncy and free flowing
-%yield = 45.83
-Temperature = 22.0°C
-Drying Temperature 30.0°C
-Drying time = 18 h
-Homogenization speed = 2500 rpm

BATCH SUMMARY – Batch INH-007

Faculty of Pharmacy, Rhodes University

Formulator:	Chiluba Mwila	Batch size:	5.75 g
Product:	INH microspheres	Microencapsulation Time (start):	14:00
Batch Number:	INH-007	(end):	19:00
Date of manufacture:	10-04-2017		

Material	Amount added (g)	Rhodes RM#
INH	0.75	RM000339
HPMC-AS	1.0	RM000351
Eudragit® L100	3.0	RM000016
Avicel® PH101	1.0	RM000038
Liquid paraffin	125.0 mL	
Acetone	50.0 mL	
Span 80	1.25 mL	

Dissolution profile

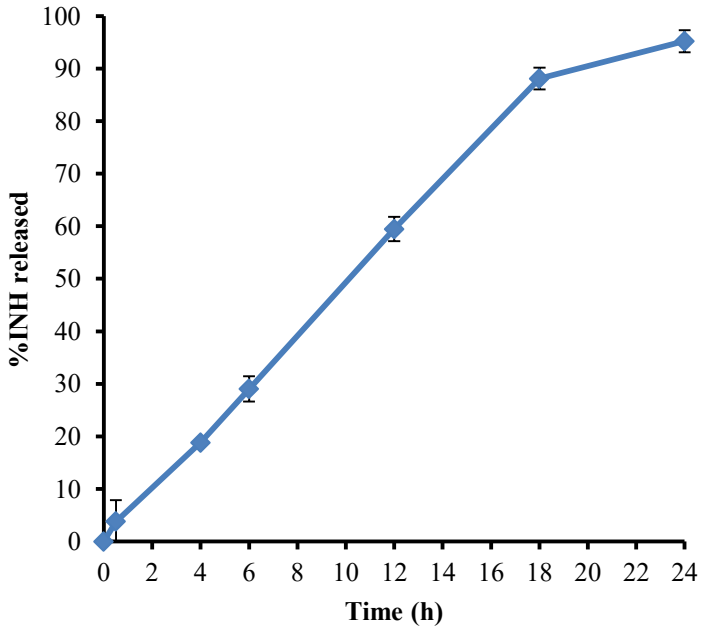

SEM

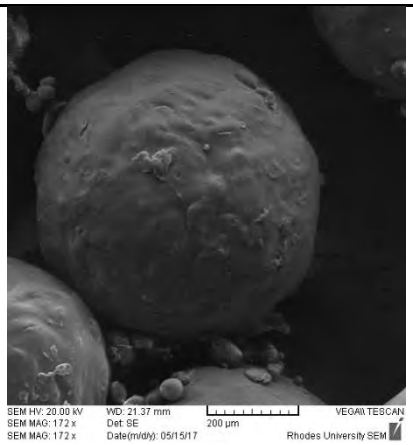

Comments

-Spherical
-smooth surface
-hard/bouncy and free flowing
-%yield = 40.00
-Temperature = 22.0°C
-Drying Temperature 30.0°C
-Drying time = 18 h
-Homogenization speed = 2500 rpm

BATCH SUMMARY – Batch INH-008

Faculty of Pharmacy, Rhodes University

Formulator:	Chiluba Mwila	Batch size:	4.235 g
Product:	INH microspheres	Microencapsulation Time (start):	08:00
Batch Number:	INH-008	(end):	13:00
Date of manufacture:	13-04-2017		

Material	Amount added (g)	Rhodes RM#
INH	0.75	RM000339
HPMC-AS	2.0	RM000351
Eudragit® L100	0.485	RM000016
Avicel® PH101	1.0	RM000038
Liquid paraffin	125.0 mL	
Acetone	50.0 mL	
Span 80	1.25 mL	

Dissolution profile

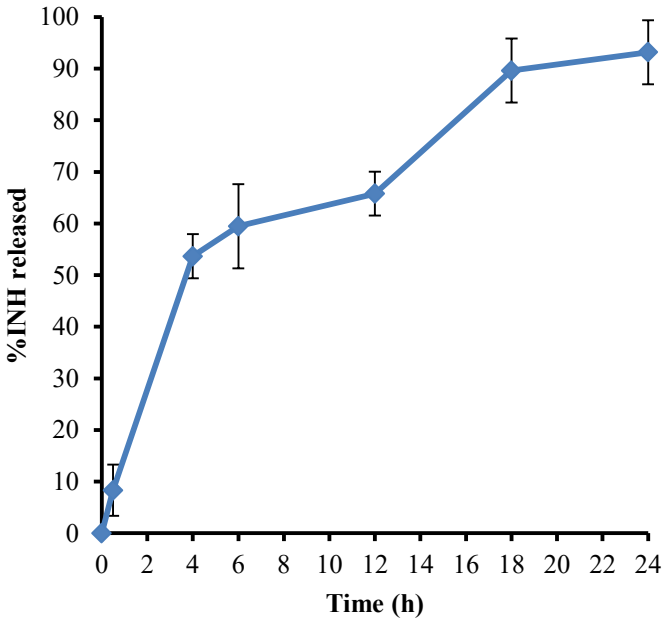

SEM

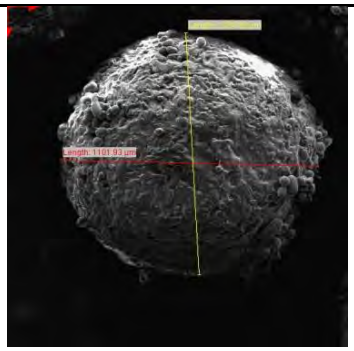

Comments

-Spherical
-rough surface
-hard/bouncy and free flowing
-%yield = 21.14
-irregularly shaped dissolution profile
-Temperature = 22.0°C
-Drying Temperature 30.0°C
-Drying time = 18 h
-Homogenization speed = 1500 rpm

BATCH SUMMARY – Batch INH-009

Faculty of Pharmacy, Rhodes University

Formulator:	Chiluba Mwila	Batch size:	5.75 g
Product:	INH microspheres	Microencapsulation Time (start):	15:00
Batch Number:	INH-009	(end):	20:00
Date of manufacture:	15-04-2017		

Material	Amount added (g)	Rhodes RM#
INH	0.75	RM000339
HPMC-AS	2.0	RM000351
Eudragit® L100	2.0	RM000016
Avicel® PH101	1.0	RM000038
Liquid paraffin	125.0 mL	
Acetone	50.0 mL	
Span 80	1.25 mL	

Dissolution profile

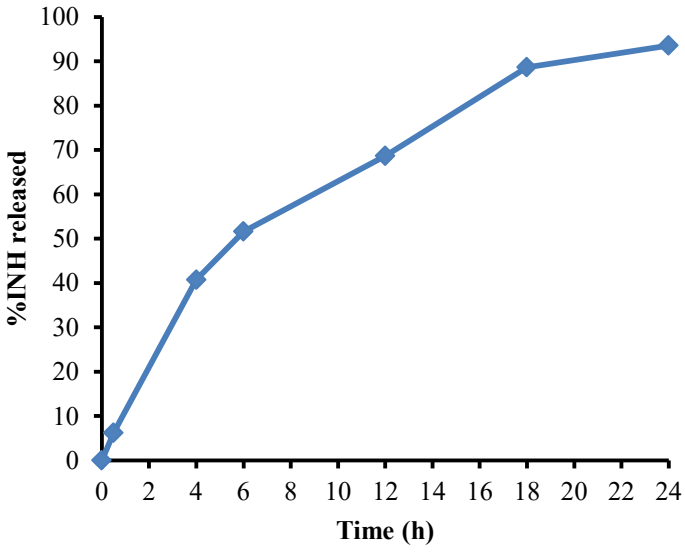

SEM

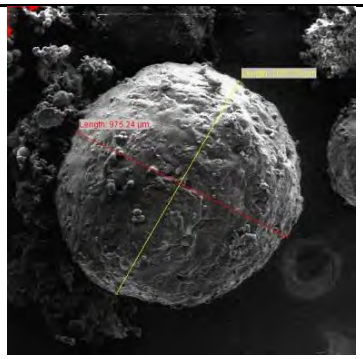

Comments

-Spherical
-rough surface
-hard/bouncy and free flowing
-%yield = 31.83
-irregularly shaped dissolution profile
-Temperature = 22.0°C
-Drying Temperature 30.0°C
-Drying time = 18 h
-Homogenization speed = 3500 rpm

BATCH SUMMARY – Batch INH-010

Faculty of Pharmacy, Rhodes University

Formulator:	Chiluba Mwila	Batch size:	3.75 g
Product:	INH microspheres	Microencapsulation Time (start):	07:00
Batch Number:	INH-010	(end):	12:00
Date of manufacture:	18-04-2017		

Material	Amount added (g)	Rhodes RM#
INH	0.75	RM000339
HPMC-AS	1.0	RM000351
Eudragit® L100	1.0	RM000016
Avicel® PH101	1.0	RM000038
Liquid paraffin	125.0 mL	
Acetone	50.0 mL	
Span 80	1.25 mL	

Dissolution profile

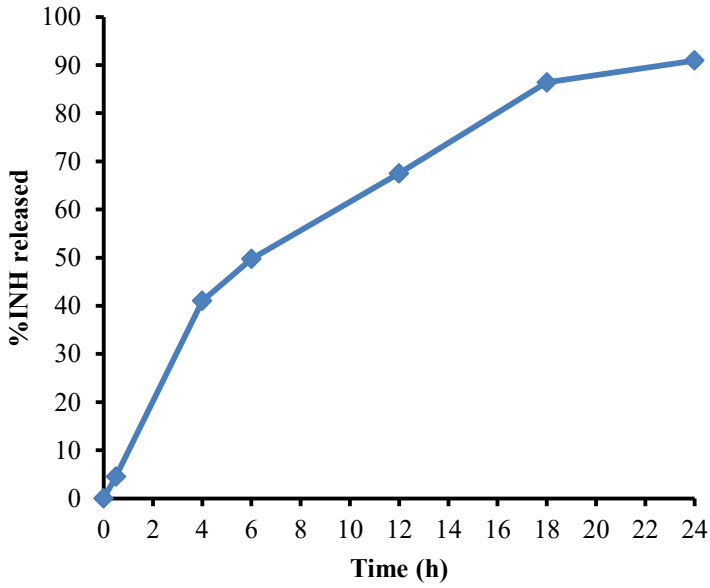

SEM

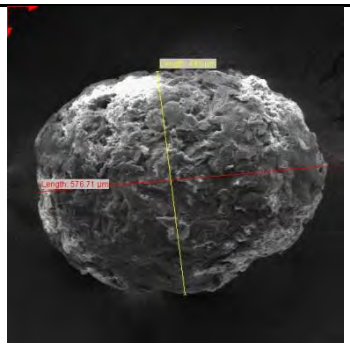

Comments

-not highly spherical
-rough surface
-hard/bouncy and free flowing
-%yield = 22.27
-irregularly shaped dissolution profile
-Temperature = 22.0°C
-Drying Temperature 30.0°C
-Drying time = 18 h
-Homogenization speed = 2500 rpm

BATCH SUMMARY – Batch INH-011

Faculty of Pharmacy, Rhodes University

Formulator:	Chiluba Mwila	Batch size:	7.16 g
Product:	INH microspheres	Microencapsulation Time (start):	14:00
Batch Number:	INH-011	(end):	19:00
Date of manufacture:	20-04-2017		

Material	Amount added (g)	Rhodes RM#
INH	0.75	RM000339
HPMC-AS	2.0	RM000351
Eudragit® L100	3.41	RM000016
Avicel® PH101	1.0	RM000038
Liquid paraffin	125.0 mL	
Acetone	50.0 mL	
Span 80	1.25 mL	

Dissolution profile

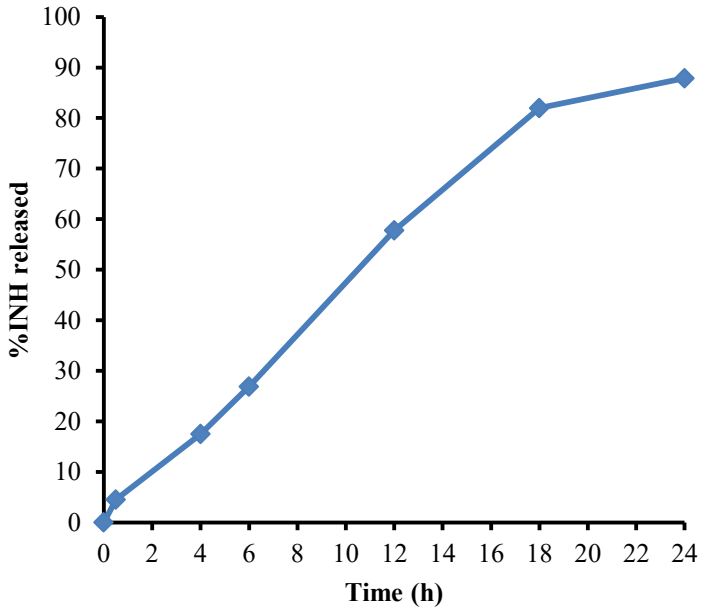

SEM

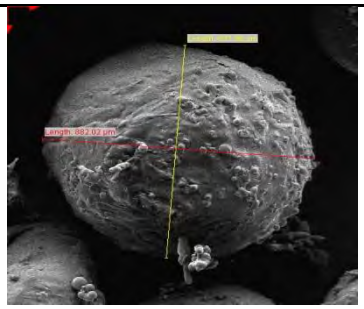

Comments

-spherical
-rough surface
-hard/bouncy and free flowing
-%yield = 47.17
-irregularly shaped dissolution profile
-Temperature = 22.0°C
-Drying Temperature 30.0°C
-Drying time = 18 h
-Homogenization speed = 1500 rpm

BATCH SUMMARY – Batch INH-012

Faculty of Pharmacy, Rhodes University

Formulator:	Chiluba Mwila	Batch size:	7.26 g
Product:	INH microspheres	Microencapsulation Time (start):	08:00
Batch Number:	INH-012	(end):	13:00
Date of manufacture:	25-04-2017		

Material	Amount added (g)	Rhodes RM#
INH	0.75	RM000339
HPMC-AS	2.1	RM000351
Eudragit® L100	3.41	RM000016
Avicel® PH101	1.0	RM000038
Liquid paraffin	125.0 mL	
Acetone	50.0 mL	
Span 80	1.25 mL	

Dissolution profile

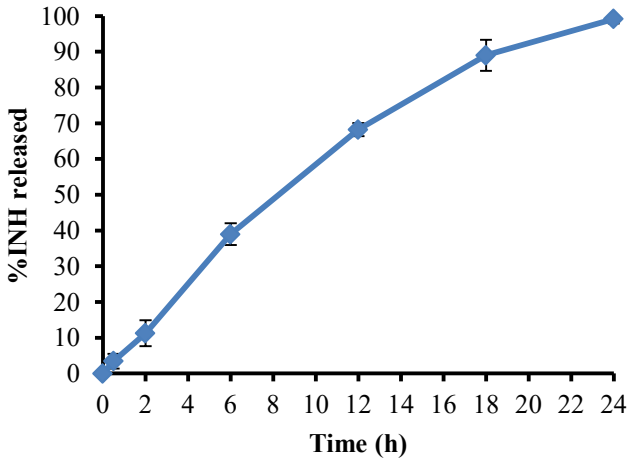

SEM

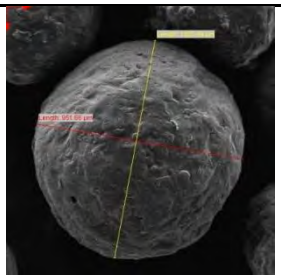

Comments

-spherical
-smooth surface
-hard/bouncy and free flowing
-%yield = 51.35
-irregularly shaped dissolution profile
-Temperature = 22.0°C
-Drying Temperature 30.0°C
-Drying time = 18 h
-Homogenization speed = 1500 rpm

APPENDIX 2B

BATCH SUMMARIES FOR THE MANUFACTURE OF MICROPOROUS FLOATING SUSTAINED RELEASE RIFAMPICIN MICROSPHERES

BATCH SUMMARY – RIF001

Faculty of Pharmacy, Rhodes University

Formulator:	Chiluba Mwila	Batch size:	7.25 g
Product:	RIF microspheres	Microencapsulation Time (start):	09:00
Batch Number:	RIF001	(end):	10:30
Microencapsulation Date:	06-11-2017		

Material	Amount added (g)	Rhodes #
RIF	1.0	RM000340
Ethylcellulose	1.5	RM000068
Eudragit® RLPO	3.0	RM000022
Avicel® PH101	1.0	RM000038
d-glucose	0.75	
Liquid paraffin	125.0 mL	
Acetone	20.0 mL	
Dichloromethane	30.0 mL	
Span 80	1.25 mL	

Dissolution profile

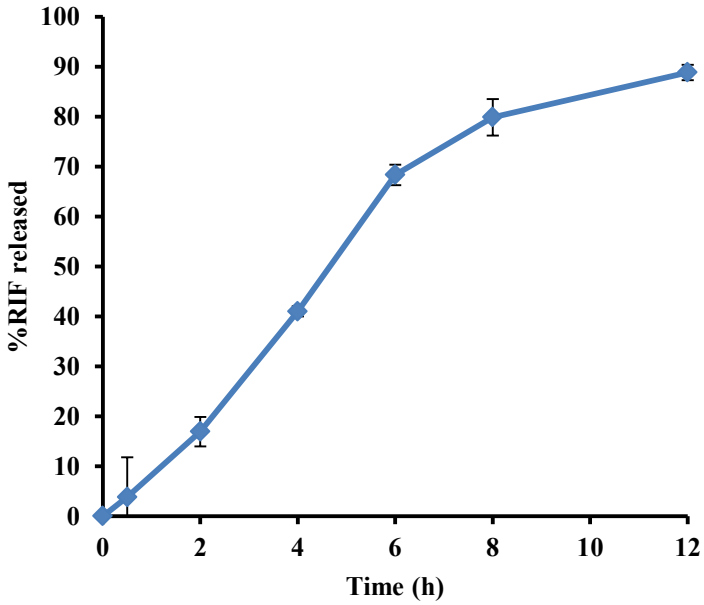

SEM

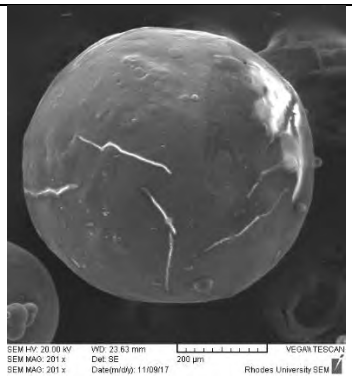

Comments

-Spherical
-Smooth surface
-Cracks
-Free flowing
-% yield = 81.86
-Temperature = 22.0°C
-Drying Temperature 22.0°C
-Drying time = 24 h

BATCH SUMMARY – RIF002

Faculty of Pharmacy, Rhodes University

Formulator:	Chiluba Mwila	Batch size:	6.5 g
Product:	RIF microspheres	Microencapsulation Time (start):	11:30
Batch Number:	RIF002	(end):	13:00
Microencapsulation Date:	06-11-2017		

Material	Amount added (g)	Rhodes #
RIF	1.0	RM000340
Ethylcellulose	1.0	RM000068
Eudragit® RLPO	3.0	RM000022
Avicel® PH101	1.0	RM000038
d-glucose	0.5	
Liquid paraffin	125.0 mL	
Acetone	20.0 mL	
Dichloromethane	30.0 mL	
Span 80	1.25 mL	

Dissolution profile

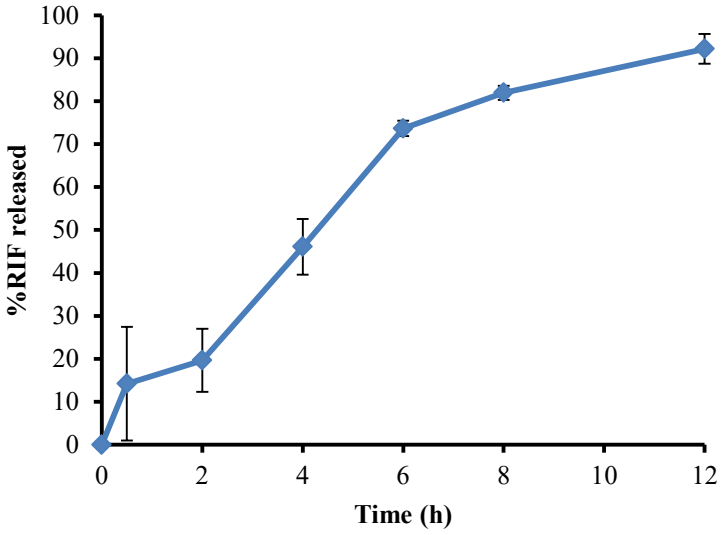

SEM

Comments

-Spherical
-Smooth surface
-Cracks
-Free flowing
-% yield = 76.23
-Temperature = 22.0°C
-Drying Temperature 22.0°C
-Drying time = 24 h

BATCH SUMMARY – RIF003

Faculty of Pharmacy, Rhodes University

Formulator:	Chiluba Mwila	Batch size:	6.0 g
Product:	RIF microspheres	Microencapsulation Time (start):	15:30
Batch Number:	RIF003	(end):	17:00
Microencapsulation Date:	06-11-2017		

Material	Amount added (g)	Rhodes #
RIF	1.0	RM000340
Ethylcellulose	1.5	RM000068
Eudragit® RLPO	2.0	RM000022
Avicel® PH101	1.0	RM000038
d-glucose	0.5	
Liquid paraffin	125.0 mL	
Acetone	20.0 mL	
Dichloromethane	30.0 mL	
Span 80	1.25 mL	

Dissolution profile

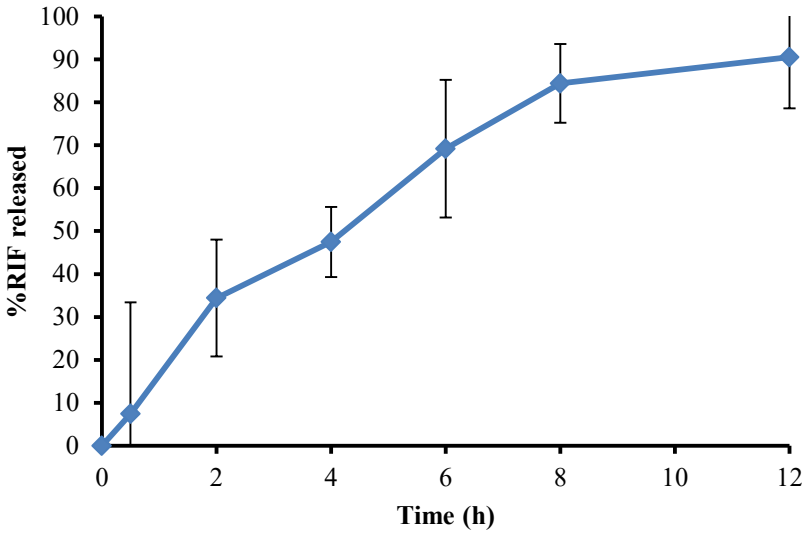

SEM

Comments

-Spherical
-Smooth surface
-Cracks
-Free flowing
-% yield = 70
-Temperature = 22.0°C
-Drying Temperature 22.0°C
-Drying time = 24 h

BATCH SUMMARY – RIF004

Faculty of Pharmacy, Rhodes University

Formulator:	Chiluba Mwila	Batch size:	6.0 g
Product:	RIF microspheres	Microencapsulation Time (start):	08:00
Batch Number:	RIF004	(end):	09:30
Microencapsulation Date:	07-11-2017		

Material	Amount added (g)	Rhodes #
RIF	1.0	RM000340
Ethylcellulose	2.0	RM000068
Eudragit® RLPO	1.0	RM000022
Avicel® PH101	1.0	RM000038
d-glucose	0.5	
Liquid paraffin	125.0 mL	
Acetone	20.0 mL	
Dichloromethane	30.0 mL	
Span 80	1.25 mL	

Dissolution profile

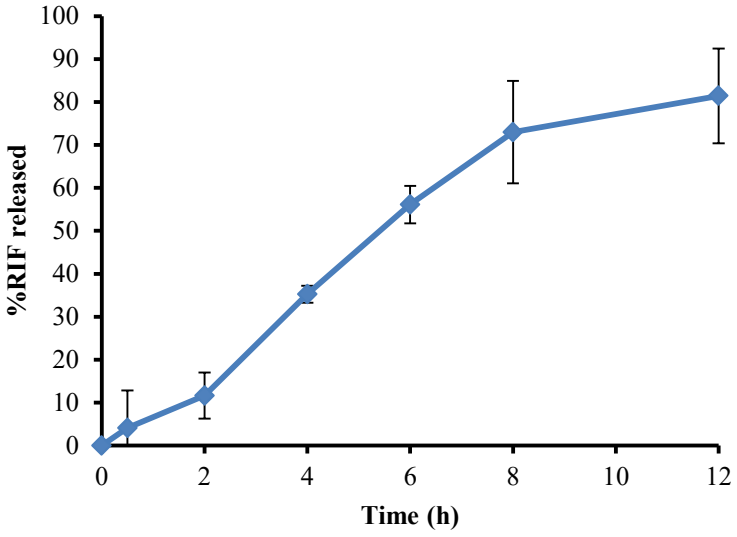

SEM

Comments

-Spherical
-Smooth surface
-Cracks/pores
-Free flowing
-% yield = 68
-Temperature = 22.0°C
-Drying Temperature 22.0°C
-Drying time = 24 h
- < 85% RIF released after 12 h

BATCH SUMMARY – RIF005

Faculty of Pharmacy, Rhodes University

Formulator:	Chiluba Mwila	Batch size:	6.0 g
Product:	RIF microspheres	Microencapsulation Time (start):	08:00
Batch Number:	RIF005	(end):	09:30
Microencapsulation Date:	07-11-2017		

Material	Amount added (g)	Rhodes #
RIF	1.0	RM000340
Ethylcellulose	1.5	RM000068
Eudragit® RLPO	2.0	RM000022
Avicel® PH101	1.0	RM000038
d-glucose	0.5	
Liquid paraffin	125.0 mL	
Acetone	20.0 mL	
Dichloromethane	30.0 mL	
Span 80	1.25 mL	

Dissolution profile

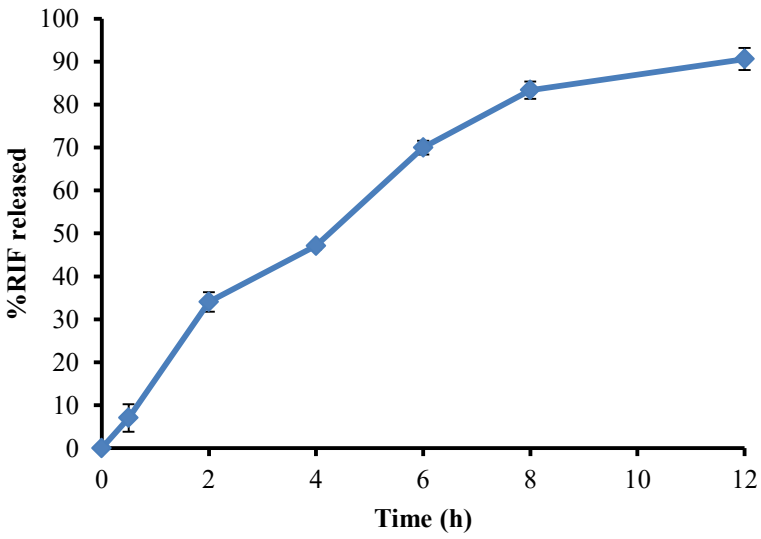

SEM

Comments

-Spherical
-Smooth surface
-Cracks/pores
-Free flowing
-% yield = 71.3
-Temperature = 22.0°C
-Drying Temperature 22.0°C
-Drying time = 24 h

BATCH SUMMARY – RIF006

Faculty of Pharmacy, Rhodes University

Formulator:	Chiluba Mwila	Batch size:	6.75 g
Product:	RIF microspheres	Microencapsulation Time (start):	11:00
Batch Number:	RIF006	(end):	12:30
Microencapsulation Date:	07-11-2017		

Material	Amount added (g)	Rhodes #
RIF	1.0	RM000340
Ethylcellulose	1.5	RM000068
Eudragit® RLPO	3.0	RM000022
Avicel® PH101	1.0	RM000038
d-glucose	0.25	
Liquid paraffin	125.0 mL	
Acetone	20.0 mL	
Dichloromethane	30.0 mL	
Span 80	1.25 mL	

Dissolution profile

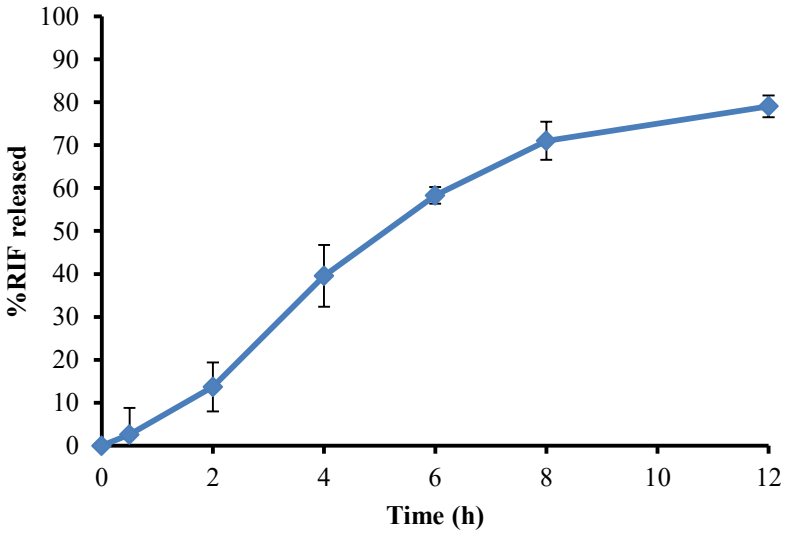

SEM

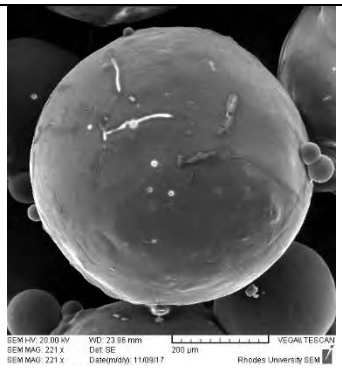

Comments

-Spherical
-Smooth surface
-Cracks/pores
-Free flowing
-%yield = 84.22
-Temperature = 22.0°C
-Drying Temperature 22.0°C
-Drying time = 24 h
- < 85% RIF released at 12h

BATCH SUMMARY – RIF007

Faculty of Pharmacy, Rhodes University

Formulator:	Chiluba Mwila	Batch size:	6.0 g
Product:	RIF microspheres	Microencapsulation Time (start):	14:00
Batch Number:	RIF007	(end):	15:30
Microencapsulation Date:	07-11-2017		

Material	Amount added (g)	Rhodes #
RIF	1.0	RM000340
Ethylcellulose	1.5	RM000068
Eudragit® RLPO	2.0	RM000022
Avicel® PH101	1.0	RM000038
d-glucose	0.5	
Liquid paraffin	125.0 mL	
Acetone	20.0 mL	
Dichloromethane	30.0 mL	
Span 80	1.25 mL	

Dissolution profile

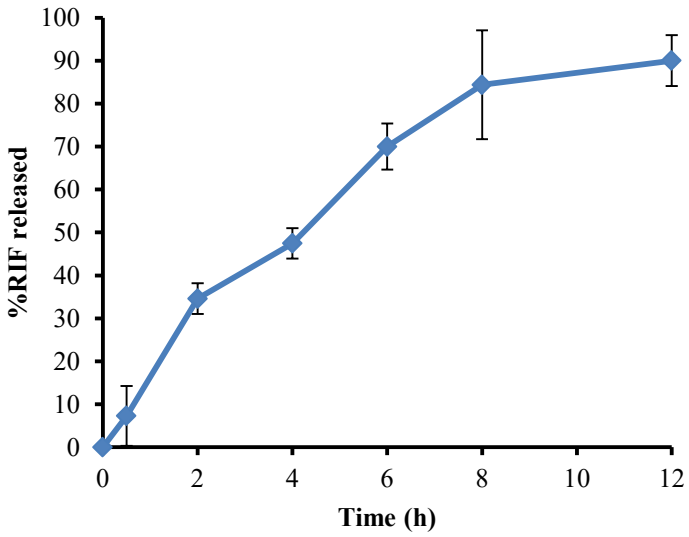

SEM

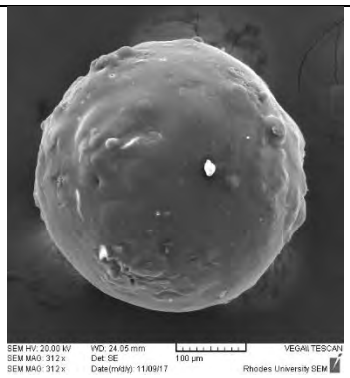

Comments

-Spherical
-Smooth surface
-Cracks/pores
-Free flowing
-% yield = 71.67
-Temperature = 22.0°C
-Drying Temperature 22.0°C
-Drying time = 24 h

BATCH SUMMARY – RIF008

Faculty of Pharmacy, Rhodes University

Formulator:	Chiluba Mwila	Batch size:	7.5 g
Product:	RIF microspheres	Microencapsulation Time (start):	17:00
Batch Number:	RIF008	(end):	18:30
Microencapsulation Date:	07-11-2017		

Material	Amount added (g)	Rhodes #
RIF	1.0	RM000340
Ethylcellulose	2.0	RM000068
Eudragit® RLPO	3.0	RM000022
Avicel® PH101	1.0	RM000038
d-glucose	0.5	
Liquid paraffin	125.0 mL	
Acetone	20.0 mL	
Dichloromethane	30.0 mL	
Span 80	1.25 mL	

Dissolution profile

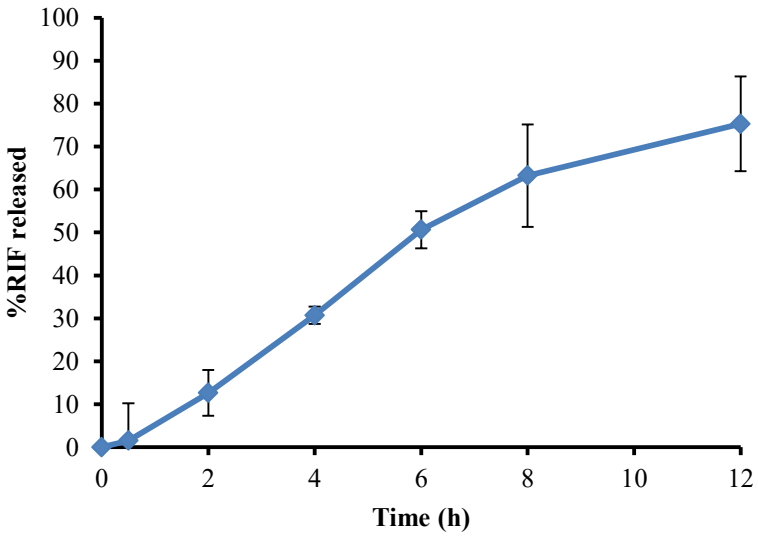

SEM

Comments

-Spherical
-Smooth surface
-Free flowing
-% yield = 85.33
-Temperature = 22.0°C
-Drying Temperature 22.0°C
-Drying time = 24 h
- < 85% RIF released at 12 h

BATCH SUMMARY – RIF009

Faculty of Pharmacy, Rhodes University

Formulator:	Chiluba Mwila	Batch size:	6.0 g
Product:	RIF microspheres	Microencapsulation Time (start):	07:00
Batch Number:	RIF009	(end):	08:30
Microencapsulation Date:	08-11-2017		

Material	Amount added (g)	Rhodes #
RIF	1.0	RM000340
Ethylcellulose	1.5	RM000068
Eudragit® RLPO	2.0	RM000022
Avicel® PH101	1.0	RM000038
d-glucose	0.5	
Liquid paraffin	125.0 mL	
Acetone	20.0 mL	
Dichloromethane	30.0 mL	
Span 80	1.25 mL	

Dissolution profile

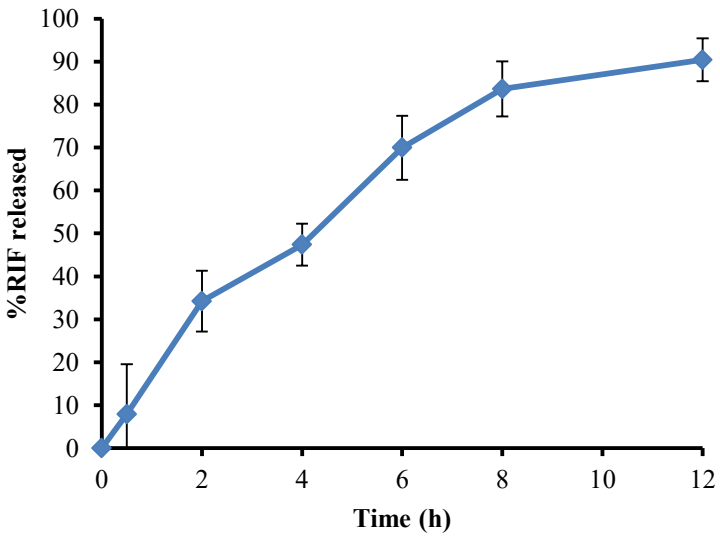

SEM

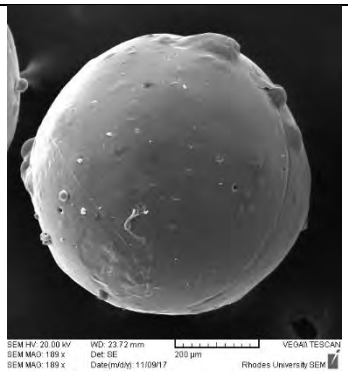

Comments

-Spherical
-Smooth surface/pores
-Free flowing
-% yield = 71.5
-Temperature = 22.0°C
-Drying Temperature 22.0°C
-Drying time = 24 h

BATCH SUMMARY – RIF010

Faculty of Pharmacy, Rhodes University

Formulator:	Chiluba Mwila	Batch size:	6.25 g
Product:	RIF microspheres	Microencapsulation Time (start):	10:00
Batch Number:	RIF010	(end):	11:30
Microencapsulation Date:	08-11-2017		

Material	Amount added (g)	Rhodes #
RIF	1.0	RM000340
Ethylcellulose	2.0	RM000068
Eudragit® RLPO	2.0	RM000022
Avicel® PH101	1.0	RM000038
d-glucose	0.25	
Liquid paraffin	125.0 mL	
Acetone	20.0 mL	
Dichloromethane	30.0 mL	
Span 80	1.25 mL	

Dissolution profile

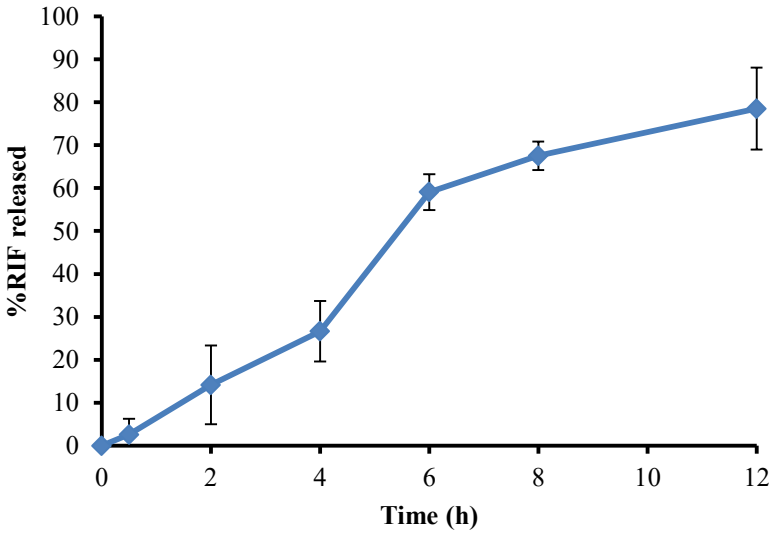

SEM

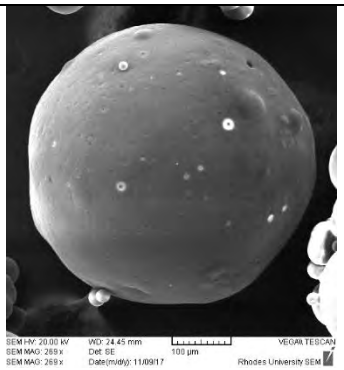

Comments

-Spherical
-Smooth surface/pores
-Free flowing
-% yield = 76.56
-Temperature = 22.0°C
-Drying Temperature 22.0°C
-Drying time = 24 h
- < 85% RIF released at 12 h

BATCH SUMMARY – RIF011

Faculty of Pharmacy, Rhodes University

Formulator:	Chiluba Mwila	Batch size:	6.0 g
Product:	RIF microspheres	Microencapsulation Time (start):	12:00
Batch Number:	RIF011	(end):	13:30
Microencapsulation Date:	08-11-2017		

Material	Amount added (g)	Rhodes #
RIF	1.0	RM000340
Ethylcellulose	1.5	RM000068
Eudragit® RLPO	2.0	RM000022
Avicel® PH101	1.0	RM000038
d-glucose	0.5	
Liquid paraffin	125.0 mL	
Acetone	20.0 mL	
Dichloromethane	30.0 mL	
Span 80	1.25 mL	

Dissolution profile

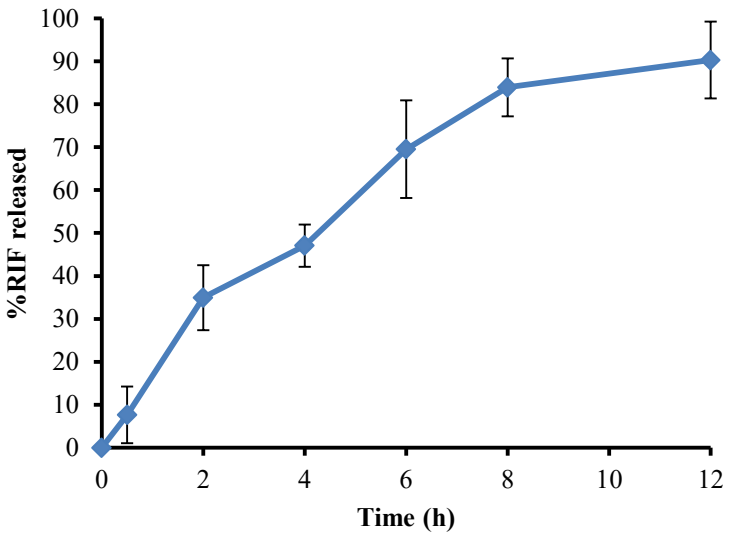

SEM

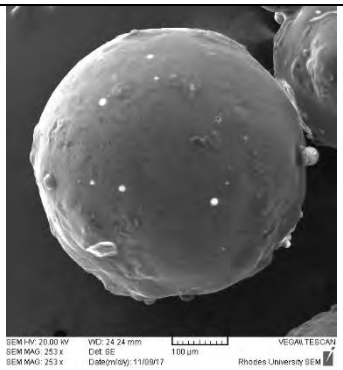

Comments

-Spherical
-Smooth surface/pores
-Free flowing
-% yield = 71.33
-Temperature = 22.0°C
-Drying Temperature 22.0°C
-Drying time = 24 h

BATCH SUMMARY – RIF012

Faculty of Pharmacy, Rhodes University

Formulator:	Chiluba Mwila	Batch size:	6.0 g
Product:	RIF microspheres	Microencapsulation Time (start):	14:00
Batch Number:	RIF012	(end):	15:30
Microencapsulation Date:	08-11-2017		

Material	Amount added (g)	Rhodes #
RIF	1.0	RM000340
Ethylcellulose	1.5	RM000068
Eudragit® RLPO	1.0	RM000022
Avicel® PH101	1.0	RM000038
d-glucose	0.75	
Liquid paraffin	125.0 mL	
Acetone	20.0 mL	
Dichloromethane	30.0 mL	
Span 80	1.25 mL	

Dissolution profile

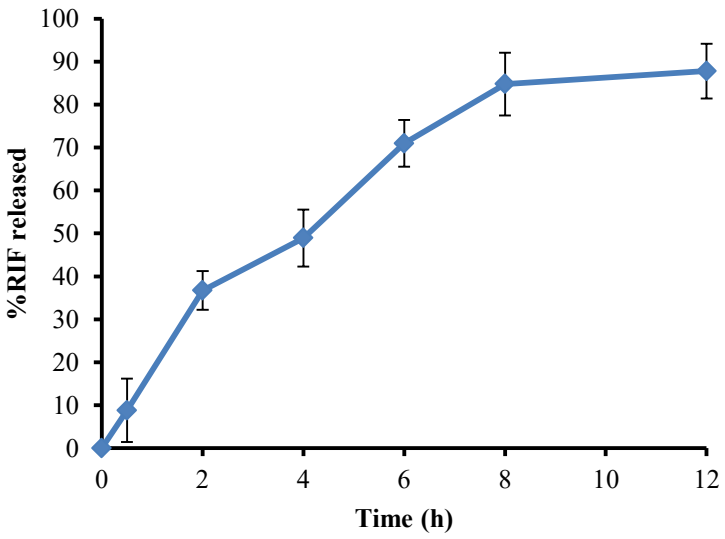

SEM

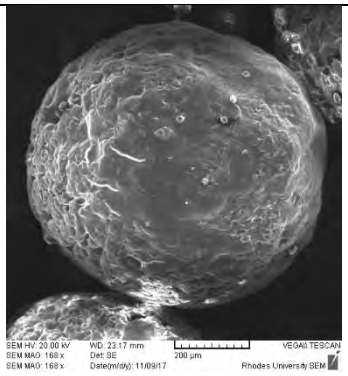

Comments

-Spherical
-Rough surface/pores
-Free flowing
-% yield = 67.71
-Temperature = 22.0°C
-Drying Temperature 22.0°C
-Drying time = 24 h

BATCH SUMMARY – RIF013

Faculty of Pharmacy, Rhodes University

Formulator:	Chiluba Mwila	Batch size:	4.75 g
Product:	RIF microspheres	Microencapsulation Time (start):	16:00
Batch Number:	RIF013	(end):	17:30
Microencapsulation Date:	08-11-2017		

Material	Amount added (g)	Rhodes #
RIF	1.0	RM000340
Ethylcellulose	1.5	RM000068
Eudragit® RLPO	1.0	RM000022
Avicel® PH101	1.0	RM000038
d-glucose	0.25	
Liquid paraffin	125.0 mL	
Acetone	20.0 mL	
Dichloromethane	30.0 mL	
Span 80	1.25 mL	

Dissolution profile

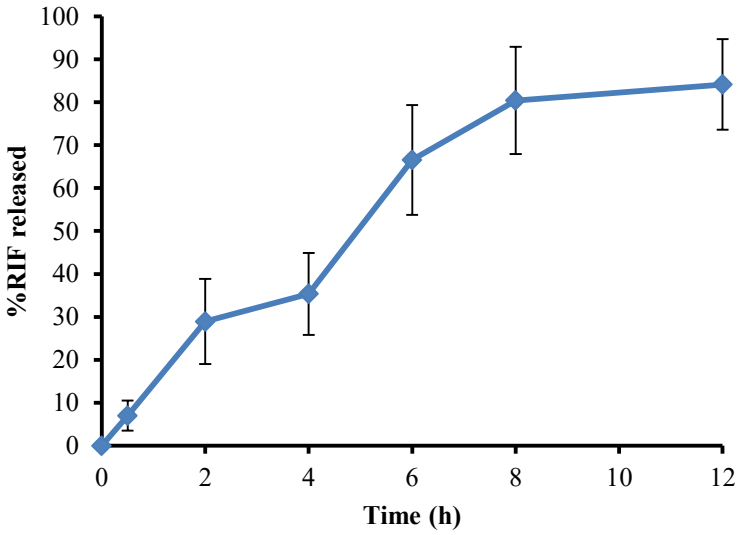

SEM

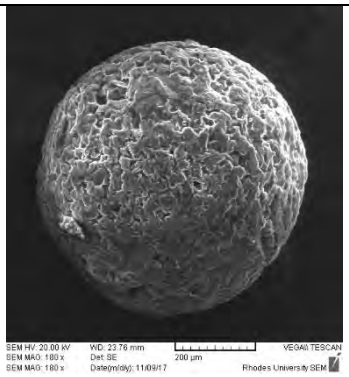

Comments

-Spherical
-Rough surface/pores
-Free flowing
-% yield = 67.47
-Temperature = 22.0°C
-Drying Temperature 22.0°C
-Drying time = 24 h
- < 85% RIF released at 12 h

BATCH SUMMARY – RIF014

Faculty of Pharmacy, Rhodes University

Formulator:	Chiluba Mwila	Batch size:	5.25 g
Product:	RIF microspheres	Microencapsulation Time (start):	17:00
Batch Number:	RIF014	(end):	18:30
Microencapsulation Date:	08-11-2017		

Material	Amount added (g)	Rhodes #
RIF	1.0	RM000340
Ethylcellulose	1.0	RM000068
Eudragit® RLPO	2.0	RM000022
Avicel® PH101	1.0	RM000038
d-glucose	0.25	
Liquid paraffin	125.0 mL	
Acetone	20.0 mL	
Dichloromethane	30.0 mL	
Span 80	1.25 mL	

Dissolution profile

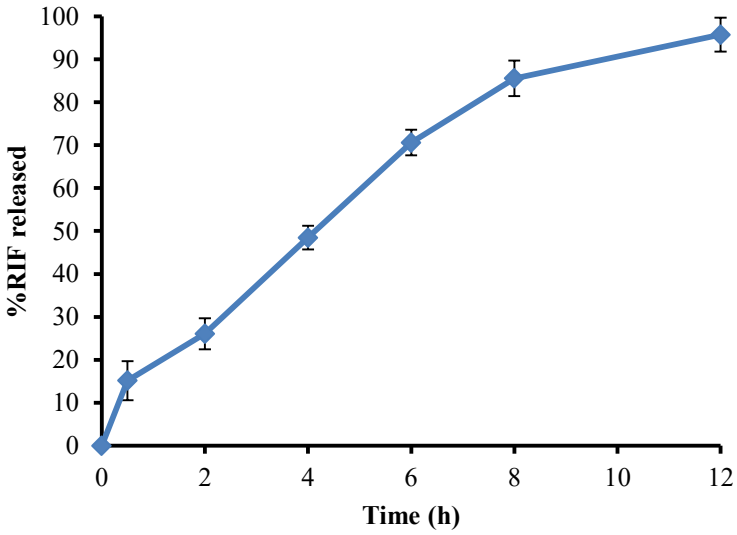

SEM

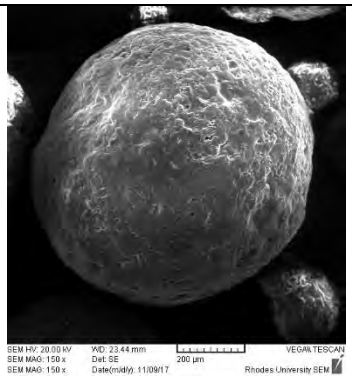

Comments

-Spherical
-Rough surface/pores
-Free flowing
-% yield = 68
-Temperature = 22.0°C
-Drying Temperature 22.0°C
-Drying time = 24 h

BATCH SUMMARY – RIF015

Faculty of Pharmacy, Rhodes University

Formulator:	Chiluba Mwila	Batch size:	5.75 g
Product:	RIF microspheres	Microencapsulation Time (start):	19:00
Batch Number:	RIF015	(end):	20:30
Microencapsulation Date:	08-11-2017		

Material	Amount added (g)	Rhodes #
RIF	1.0	RM000340
Ethylcellulose	1.0	RM000068
Eudragit® RLPO	2.0	RM000022
Avicel® PH101	1.0	RM000038
d-glucose	0.75	
Liquid paraffin	125.0 mL	
Acetone	20.0 mL	
Dichloromethane	30.0 mL	
Span 80	1.25 mL	

Dissolution profile

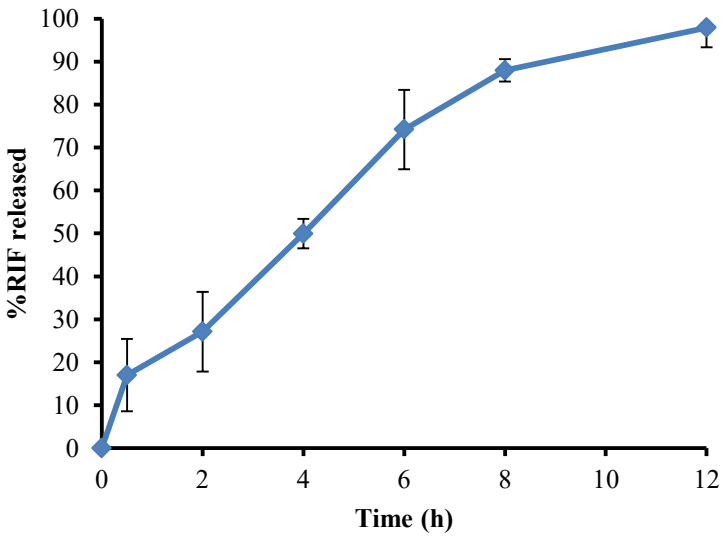

SEM

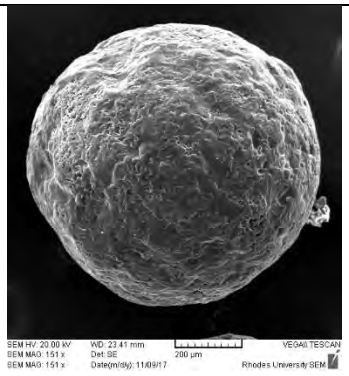

Comments

-Spherical
-Rough surface/pores
-Free flowing
-% yield = 63.39
-Temperature = 22.0°C
-Drying Temperature 22.0°C
-Drying time = 24 h

BATCH SUMMARY – RIF016

Faculty of Pharmacy, Rhodes University

Formulator:	Chiluba Mwila	Batch size:	4.5 g
Product:	RIF microspheres	Microencapsulation Time (start):	21:00
Batch Number:	RIF016	(end):	22:30
Microencapsulation Date:	08-11-2017		

Material	Amount added (g)	Rhodes #
RIF	1.0	RM000340
Ethylcellulose	1.0	RM000068
Eudragit® RLPO	1.0	RM000022
Avicel® PH101	1.0	RM000038
d-glucose	0.5	
Liquid paraffin	125.0 mL	
Acetone	20.0 mL	
Dichloromethane	30.0 mL	
Span 80	1.25 mL	

Dissolution profile

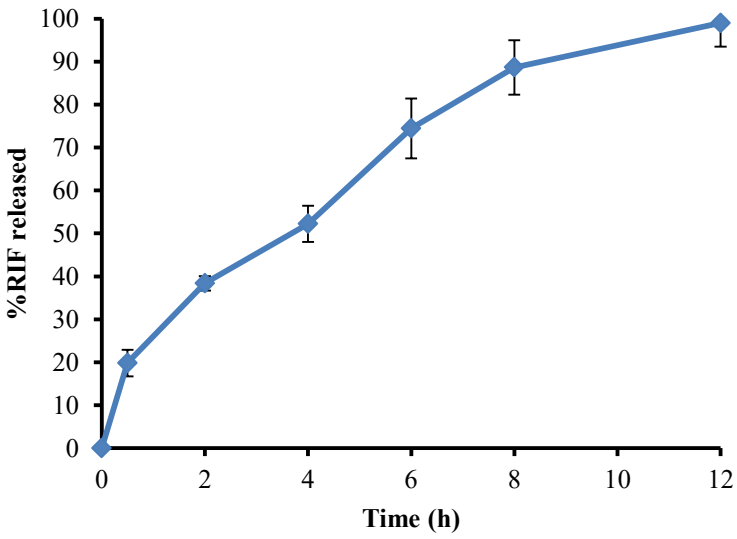

SEM

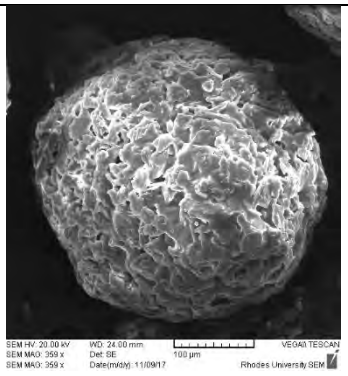

Comments

-Spherical
-Rough surface/pores
-Free flowing
-Not well formed microspheres
-% yield = 55.7
-Temperature = 22.0°C
-Drying Temperature 22.0°C
-Drying time = 24 h

BATCH SUMMARY – RIF017

Faculty of Pharmacy, Rhodes University

Formulator:	Chiluba Mwila	Batch size:	6.75 g
Product:	RIF microspheres	Microencapsulation Time (start):	23:00
Batch Number:	RIF017	(end):	00:30
Microencapsulation Date:	08-11-2017		

Material	Amount added (g)	Rhodes #
RIF	1.0	RM000340
Ethylcellulose	2.0	RM000068
Eudragit® RLPO	2.0	RM000022
Avicel® PH101	1.0	RM000038
d-glucose	0.75	
Liquid paraffin	125.0 mL	
Acetone	20.0 mL	
Dichloromethane	30.0 mL	
Span 80	1.25 mL	

Dissolution profile

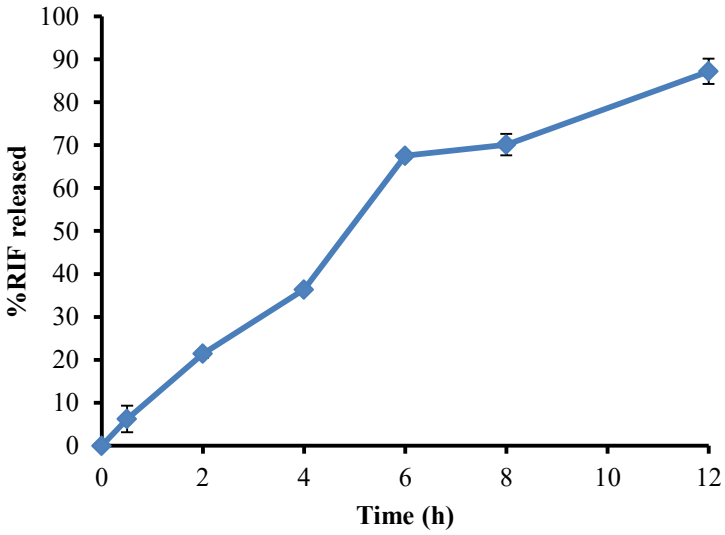

SEM

Comments

-Spherical
-Smooth surface
-Free flowing
-% yield = 76.11
-Temperature = 22.0°C
-Drying Temperature 22.0°C
-Drying time = 24 h

BATCH SUMMARY – RIF018

Faculty of Pharmacy, Rhodes University

Formulator:	Chiluba Mwila	Batch size:	6.25 g
Product:	RIF microspheres	Microencapsulation Time (start):	9:00
Batch Number:	RIF018	(end):	10:30
Microencapsulation Date:	24-11-2017		

Material	Amount added (g)	Rhodes #
RIF	1.0	RM000340
Ethylcellulose	1.5	RM000068
Eudragit® RLPO	2.0	RM000022
Avicel® PH101	1.0	RM000038
d-glucose	0.75125.0 mL	
Liquid paraffin	20.0 mL	
Acetone	30.0 mL	
Dichloromethane	1.25 mL	
Span 80		

Dissolution profile

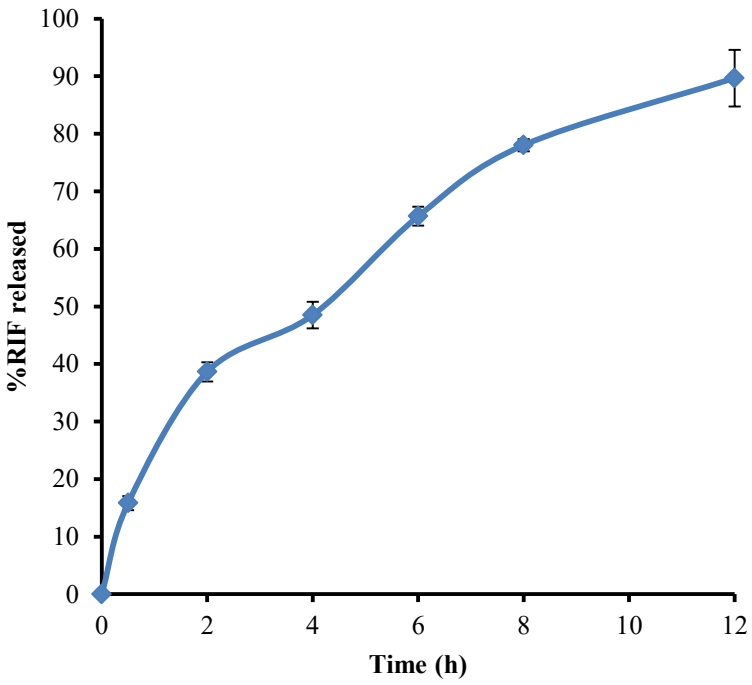

SEM

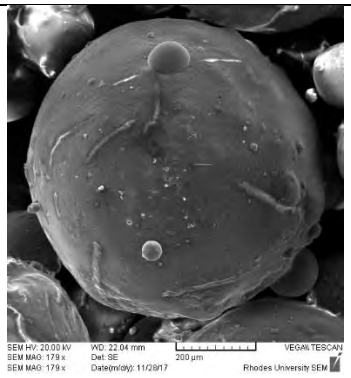

Comments

-Spherical
-Smooth surface/cracks
-Free flowing
-% yield = 76.24
-Temperature = 22.0°C
-Drying Temperature 22.0°C
-Drying time = 24 h

BATCH SUMMARY – RIF023

Faculty of Pharmacy, Rhodes University

Formulator:	Chiluba Mwila	Batch size:	8.25 g
Product:	RIF microspheres	Microencapsulation Time (start):	14:00
Batch Number:	RIF023	(end):	15:30
Microencapsulation Date:	24-11-2017		

Material	Amount added (g)	Rhodes #
RIF	1.0	RM000340
Ethylcellulose	1.5	RM000068
Eudragit® RLPO	2.0	RM000022
Avicel® PH101	1.0	RM000038
d-glucose	0.75	
Sodium bicarbonate	1.0	
Anhydrous citric acid	0.5	
Liquid paraffin	25.0 mL	
Acetone	20.0 mL	
Dichloromethane	30.0 mL	
Span 80	1.25 mL	

Dissolution profile

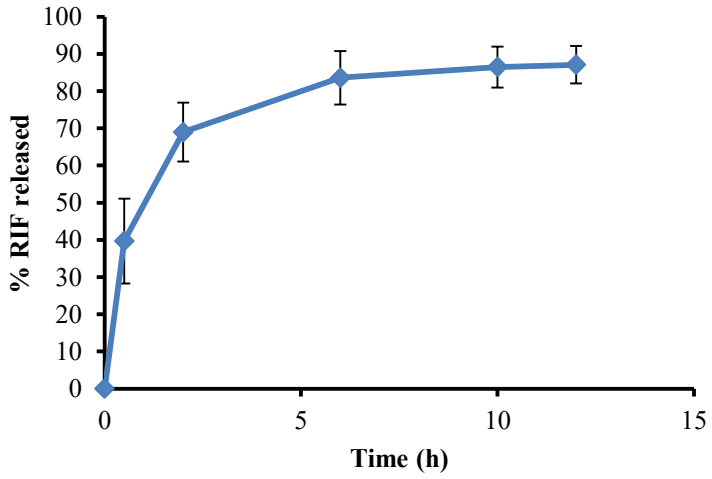

SEM

Comments

-Spherical
-Smooth surface/cracks
-Free flowing
-% yield = 76.24
-Temperature = 22.0°C
-Drying Temperature 22.0°C
-Drying time = 24 h